THE POSSIBLE IMPLICATION OF SELECTED *Fusarium* MYCOTOXINS IN THE AETIOLOGY OF BRAIN CANCER

BY

THESLA PALANEE

***B Sc* (Hons), University of Natal**

***M Med Sci.* University of Natal, Medical School**

Submitted in partial fulfilment of the requirements for the degree of Doctor of Philosophy in Medical Science in the Department of Physiology, Faculty of Medicine, Nelson R Mandela School of Medicine, University of KwaZulu-Natal, Durban

2004

ABSTRACT

The central nervous system is a potential site of action for the *Fusarium* mycotoxin Fumonisin B_1 (FB_1), and is exemplified in horses by the disease equine leukoencephalomalacia. Structurally resembling sphingoid bases, FB_1 inhibits ceramide synthase, an enzyme involved in sphingolipid metabolism, leading to accumulation of free sphinganine (Sa) and sphingosine (So). This investigation focused on FB_1, Sa, So and the *Fusarium* mycotoxins fusaric acid (FA), moniliformin (MON), zearalenone (ZEA), deoxynivalenol (DON), and T-2 toxin (T2).

Effects of the *Fusarium* mycotoxins and sphingoid bases on the N2α neuroblastoma cell line were assessed using the methylthiazol tetrazolium (MTT) and ApoGlow™ assays. The MTT assay revealed significant differences between the viability of N2α control cells and the cytotoxic effects of FB_1 ($p=0.001$), So ($p=1.1 \times 10^{-6}$), Sa ($p=1.9 \times 10^{-6}$), MON ($p=0.002$), DON ($p=0.04$) and ZEA ($p=0.003$) on N2α cells between 5-250μM. The cytotoxic effects of FA did not differ significantly from controls ($p=0.1$). The ApoGlow™ assay revealed that in N2α cells, FB_1 at $8\mu g.ml^{-1}$, FA at $128\mu g.ml^{-1}$, and (FB_1+FA) combined induced growth arrest at 2 and $4\mu g.ml^{-1}$. Assessment of the effects of FB_1 and FA on the Jurkat leukaemic suspension cell line revealed that FB_1 induced apoptosis at 1.56,12.5 and $50\mu g.ml^{-1}$, growth arrest at 100, 200 and $800\mu g.ml^{-1}$ and proliferation at $400\mu g.ml^{-1}$. Fusaric acid induced proliferation at $1.56\mu g.ml^{-1}$, apoptosis at $3.15\mu g.ml^{-1}$, growth arrest at 100 and $200\mu g.ml^{-1}$, and necrosis at $800\mu g.ml^{-1}$. Combined, (FB_1+FA) induced apoptosis at 1.56, 3.15, 12.5 and $800\mu g.ml^{-1}$.

Flow cytometry and fluorescence microscopy revealed that mycotoxins, Sa and So induced varying levels of apoptosis and necrosis in N2α cells. Acridine orange and ethidium bromide staining facilitated discrimination between viable, apoptotic and necrotic cells. Transition of the mitochondrial transmembrane potential was measured using Rhodamine 123 with propidium iodide, and the dual emission potential sensitive stain JC-1. Changes in mitochondrial membrane potential and plasma membrane integrity were expressed as increases or decreases in fluorescence intensity. An increase in mycotoxin concentration from 50 to 200μM was usually paralleled by a decrease in J-aggregate formation, suggesting a decrease in the $\Delta\psi m$. Staining with Rh123/PI indicated at specific concentrations whether N2α cells were either late apoptotic or necrotic reflected by the levels of PI uptake. No dose dependant mechanism of cell death was established using either method, as fluctuations were evident.

Immunolocalisation of T2, ZEA and FB_1 within cellular organelles that exhibited ultrastructural pathology provided correlation between mycotoxin exposure and effects. Multinucleate giant cells and retraction of cellular processes were observed. At the electron microscope (EM) level, FB_1 was immunolocalised within microsegregated and peripherally condensed nucleoli, the nucleoplasm, distorted mitochondria and dilated endoplasmic reticulum (ER). The capacity of cells to incorporate mycotoxins and effect cytological changes represents a major factor in the potential for initiation of malignant transformation.

Exposure of N2α cells to FB_1 for 72 hours increased intracellular free Sa and depleted complex sphingolipids. Using High Performance Liquid chromatography (HPLC), acid hydrolysis revealed reduction in Sa from a level of 0.6±0.12μM in control cells, to 0.2±0.1μM in cells exposed to 50μM and 100μM FB_1. Base hydrolyses revealed increase in free Sa: So ratios from 0.52±0.2 in control cells, to 1.14±0.2 and 1.4±0.3 in cells exposed to 50 and 100μM FB_1 respectively. The Sa: So ratio in the complete culture media (CCM) increased from 1.7±0.3 for control cells to 2.0±0.2 and 2.50±0.4 for cells exposed to 50 and 100μM FB_1 respectively.

Correlation coefficients between Sa: So ratios to FB_1 exposure in CCM (R=0.75) and within cells (R=0.85), imply that the free Sa: So ratio within cells appears to be a better biomarker for FB_1-induced disruption of sphingolipid metabolism *in vitro*, than the Sa: So ratio in CCM.
Optimisation of HPLC analytical procedures improved recovery of FB_1 from spiked human sera to 95.8% (n=15) and detection limits to ~5ng.ml^{-1} at a signal to noise ratio of 5:1. Optimisation of methods for recovery of Sa and So from spiked sera, led to recoveries of 77.9% and 85.0%, for So and Sa respectively at levels of spiking with 10ng per 500µl of serum. Matched sera Sa:So ratios and FB_1 levels in brain cancer and non-cancer subjects in KwaZulu-Natal were determined using these optimised methods. Fumonisin B_1 was detected in sera of non-cancer (76.7±62.2nM) and brain cancer subjects (107.38±116nM). Mean serum Sa:So ratios of 21 non-cancer subjects was 1.7±0.7. There was no correlation (R=0.26) between these variables in non-cancer subjects. The mean serum FB_1 level in brain cancer subjects was 107.4±116nM (range 10.5-298nM) (n=50) and the mean Sa:So ratio (n=50) was 1.9±1.7 (range 0.40-8.16). No correlation was found between these variables in the brain cancer subjects either (R = -0.23).

Fumonisin B_1 was immunolocalised in 49 of 76 brain tumour tissue samples analysed using immunohistochemistry (IHC). Thirty-eight of the 76 specimens had matched serum FB_1 levels and Sa: So ratios, and 23 of these were positive for FB_1 presence. Although not significantly different (p=0.11), the FB_1 sera levels in the cancer group with FB_1 within the tumour tissue had higher levels of FB_1 in sera than the IHC FB_1 negative group. Fumonisin B_1 was localised within irregular profiles of nuclei, elongated and swollen mitochondria and ER. Immunolocalisation of FB_1 within organelles in the brain showing ultrastructural cellular pathology suggests FB_1 may be implicated in the aetiology of human brain carcinogenesis.

AUTHOR'S DECLARATION

The experimental work presented in this thesis was approved by the Faculty of Medicines Ethics Committee and represents the original work by the author, and has not been submitted in any form to any other University. Where use was made of the work of others, it was duly acknowledged in the text.

The research described in this study was carried out under the supervision of Prof. AA Chuturgoon in the Departments of Physiology, Neurosurgery and Haematology and the Optics and Imaging Centre, University of KwaZulu-Natal, Nelson R Mandela School of Medicine, as well as at Nottingham Trent University, United Kingdom during the period February 1999 to July 2004.

Palanee

Miss T Palanee

I dedicate this to my Swami, who gives me strength, support, courage and guidance to persevere in every sphere of life

How does one thank the air that sustains life? Can there ever be enough words?

How then do I thank *You* Swami?

PUBLICATIONS AND PRESENTATIONS

PAPERS DELIVERED AT CONFERENCES:

Dutton MF, Chuturgoon AA, Chelule PK, Coumi N, Palanee T and Pillay D. 2001. Fungal Poisons in South African foods-Are they really killing consumers? SAAFoST 16th Biennial Congress, Durban, 2001.

Dutton MF, Chelule PK, Pillay D, Palanee T, Chuturgoon AA. The occurrence of mycotoxins in rural African people. 41st International Association of Forensic Toxicologists, Melbourne, Australia, 16-20 November 2003.

POSTER PRESENTATIONS

Palanee T, **Jithoo R**, Nathoo N, Nevines E and Chuturgoon AA. High Performance Liquid Chromatographic detection of Fumonisin B_1 in the serum of patients with brain cancer: A preliminary study. 16th Biennial Congress, Society of Neurosurgeons of South Africa, Mount Grace Country House Hotel, Magaliesburg, 15-16 September 2000.

Palanee T, Jithoo R, Nathoo N, Nevines E and Chuturgoon AA. High Performance Liquid Chromatographic detection of Fumonisin B_1 in the serum of patients with brain cancer: KwaZulu-Natal Biochemistry and Molecular Biology Symposium 2000, University of Durban Westville, Senate Chamber, 18 October 2000.

Palanee T, **Nathoo N**, Jithoo R and Chuturgoon AA. Immunolocalisation of the mycotoxin fumonisin B_1 in human brain tumour tissue: A preliminary study. The 2001 World Federation of Neurosurgical Societies Congress, Sydney, Australia.17-20 September 2001.

Palanee T, Nathoo N, Jithoo R and **Chuturgoon AA.** Immunolocalisation of the mycotoxin fumonisin B_1 in human brain tumour tissue. International Union of Biochemistry and Molecular Biology Meeting, Cape Town, 19-24 November 2001.

PUBLICATIONS SUBMITTED

Palanee T and Chuturgoon AA. Cytotoxicity of Fumonisin B_1 and the sphingoid bases, sphinganine and sphingosine on the N2α mouse neuroblastoma cell line. Mycopathologia.

Palanee T, Nevines E and Chuturgoon AA. Effects of Fumonisin B_1 on sphingolipid metabolism in the N2α neuroblastoma cell line. Toxicon.

ACKNOWLEDGEMENTS

I humbly offer my sincerest gratitude to my parents and family for their love, support, encouragement, patience and guidance through the years. Your strength and faith in me has helped me overcome many obstacles, steered me towards persevering and attaining my goals, and taught me to be true to myself. Most especially to my mother, Ma you have led by your example, been my biggest inspiration and my strongest support. You have been my friend, psychologist and source of comfort through the rough times. Thank you Ma. Thank you also to my brother Devan for your support and help with printing. To my God son Prenavin Mudaly and my nieces Micosha and Theah Palanee, thank you for the joy you bring.

I am deeply indebted to several people with whom I have had the privilege to work with and come to know in the past few years during my mycotoxin adventure. I wish to express my heartfelt appreciation and sincerest gratitude to all these people.

I extend my appreciation to my supervisor Prof AA Chuturgoon for his guidance on the preparation and presentation of this manuscript. I would also like to thank Prof. MF Dutton for the kind access to his reprints at the start of my study, and appraisal of the first draft of the chapters I sent to him.

Dr Elena Nevines, my dear friend who has taught me all I know about HPLC and helped me with the method development. You spared your time and effort to edit and help shape my HPLC work and chapters. My deepest gratitude goes to you for your unflinching support, patience and kindness.

I am grateful to all the doctors with whom I had the pleasure to collaborate with during this study. In particular, I express gratitude and appreciation to the assistance and patience of neurosurgeons Dr Nathoo, Dr Jithoo, Dr Boodhoo, Dr ST Govender, Dr Dasi, Dr PV Govender and Dr Kiratu of the Department of Neurosurgery. Your humility and dedication to your work was humbling and inspiring. I know that many of you have relocated all around the world and I wish you all the best in life and brilliant futures ahead. Your help was invaluable. Thank you also to all anaesthetists and nurses for help in obtaining samples. A sincere thank you also to the secretaries Mrs S Govender, Miss P Govender and Miss Leigh at the Department of Neurosurgery for being so accommodating of my daily calls for specimens, and Tony Singh for help with the computer generated oral presentations at WWH and with the layout and printing of the posters presented by the neurosurgeons at conferences.

I would especially like to thank all patients and volunteers that participated in this study. Without you this study would not have been possible.

Thank you to the staff of the department of Anatomical Pathology for allowing me access to Pathology reports and for histological classification of the tumours collected and analysed. Dr Priya Pillay (Pathology) for help in obtaining wax embedded tissues of brain tumours and Dr Batitang (Forensic Medicine) for assistance in obtaining normal brain tissue at autopsies. I am also sincerely grateful to Mrs Roshilla Reddy and Mrs Seetha Harinarain, Chief Medical Technologists of the Department of Anatomical Pathology who helped me in wax-embedding specimens. Your warmth and kindness will always be remembered and appreciated.

Thank you to Dr Anita Naicker for assistance with Image Analysis and electron microscopy. For being a good friend and helping me with all immunohistochemical techniques and for the critique of the immunohistochemical chapter. A sincere thank you as well to Mrs Priscilla Maartens for the unselfish guidance, patience and assistance during my sessions at the Electron Microscope Unit. To Trevor Doorasamy and Vinogran Dorsamy for the use of, guidance and assistance with Flow cytometry. Trevor, your help and patience were invaluable in helping me venture into this new exciting technique and ignited my interest in Flow cytometry. This knowledge helped me secure my

first job at the Africa Centre and I thank you sincerely for helping and encouraging me to persevere in this study.

Thank you to Prof. Marasas and Dr Gelderblom for the rat liver and kidney tissue you kindly gave us to optimise the immunochemical techniques presented herein.

Thank you to Prof. Martin Griffin and Anne Cox of Nottingham Trent University, staff at Nottingham City hospital and students at NTU who made my stay memorable and enjoyable, and for your hospitality and kindness. Prof Griffin, thank you for the opportunity to study in an established scientific environment, and Anne thank you for your unselfish guidance, encouragement and for teaching me the exciting cell culture techniques and assays. Thank you also to Prof. Maggie Manson and Paul Atherfold for the help during my brief visit to Leicester University.

Thank you to Logan Naidoo of Microbiology for assistance in cell culture, and Strinivasen Naidoo of Clinical and Applied Pharmacology for use of the Bio-Rad plate reader. Also to Mr John Sydney for assistance throughout this study in obtaining interlibrary loans, your encouragement was sincerely appreciated.

Thank you to staff and students of the Department of Physiology who were encouraging. To Theresa Makhubela, Ronnie Naicker, Ganas and Nisha Perumal and thank you for being so loving, caring and supportive of me. To Mr Arthur Peterson, thank you for having arranged to retrieve my HPLC data when the hard drive crashed. Thank you also for all the help with accessing the HPLC printer as a part-time student. Your help will always be remembered and valued. Thank you also Mrs Valencia the general assistant who ensured my lab was clean and had an ever-ready giggle to pep me up.

To Jith the hard drive doctor who recovered all my HPLC data when the hard drive on the system crashed. Those were worrying days and I thank you sincerely for the months of effort that ensured you retrieved my data and rebuilt the programme to analyse the data. Without your help, half this thesis would be non-existent today.

To my friends Kavidha Reddy, Thiroshini Govender and Sureshnee Pillay thank you for being my couriers of chapters to and from Anil while I worked at the MRC. To you and Karly Naidoo, Enba Dorsamy, Krina Reddy, Donella Wright and Hlengiwe Mbongwa for the friendship and warmth that you guys have shown me, and for the constant help and support. Thank you for the encouragement through the years and the best cups of tea a girl could ask for ☺.

To Sarvesh Moodley, thank you for your support while we were together. To my friends Nikki Coumi, Kanthi Mudaly, Inbarani Naidoo, and Thivani Naidoo thank you for being my loving and sincere support. Without you I certainly would have gone completely cuckoos. I would need a book to tell of the times you have stood by me and been strong for me. Thank you for the laughter and joy you bring to my life and all the memories. Thank you also to Desigan Subroyen for your friendship in those early days, for the pep talks, and for your support. I could not have survived the trying times without all of you. May each of you succeed in all your dreams and endeavours.

I would like to thank the Foundation for Research and Development and Kennedy Potts Research grant for financial support that enabled me to study further. Thank you for giving me the opportunity to pursue laboratory techniques that would have otherwise not been within my reach.

Finally and most importantly, I would like to thank my Swami, Sai Baba, for the guidance and wisdom that He brings to my life, for courage, determination and helping me every day, every step of the way. For all the tests (and there were many), for inspiration, and for showing me that the longest of journeys begins with that first step. For all you bring to my life, I thank you.

LIST OF FIGURES

Chapter 2

Chapter 3

Chapter 4

Chapter 5

Chapter 6

Chapter 7

Chapter 8

Chapter 9

Chapter 10

LIST OF TABLES

Chapter 8

Chapter 9

Chapter 10

LIST OF ABBREVIATIONS

AA	arachidonic acid
AcO	acridine orange
ADP	adenosine diphosphate
AEC	aminoethyl carbozole
Ag-Ab	antigen-antibody
AIDS	Acquired Immune Deficiency Syndrome
AMP	adenosine monophosphate
AP_1	aminopentol
aPKB	activated protein kinase B
ATA	alimentary toxic aleukia
ATP	adenosine triphosphate
ATPase	adenosine triphosphatase
AUC	area under the curve
BBB	blood brain barrier
BHK	baby hamster kidney
BSA	bovine serum albumin
$CaCl_2$	calcium chloride
CANSA	Cancer Association of South Africa
CCD	charged couple device
CCM	complete culture medium
CDK	cyclin-dependent kinase
CER	ceramide
$CHCl_3$	chloroform
CHO	Chinese hamster ovary fibroblast cells
CNP	2', 3'-cyclic nucleotide 3'-phosphohydrolase
CNS	central nervous system
CoA	coenzyme A
cPLA2	cytoplasmic phospholipase A2
CSF	cerebrospinal fluid
Cu^{2+}	copper ion
DA	dopamine
DAB	3,3 diaminobenzidine tetrahydrochloride
DEN	diethylnitrosamine
DIV	days *in vitro*
DL-*erythro*-dihydrosphingosine	sphinganine
DMEM	Dulbecco's Modified Essential Medium
DMF	N,N'-dimethylformamide
DMPC	dimyristoylphosphatidyl-choline
DMS	N,N,-dimethyl sphingosine
DMSO	dimethylsulphoxide
DNA	deoxyribonucleic acid
DON	deoxynivalenol
D-sphingosine	sphingosine
EDG	endothelial differentiation gene
EDTA	ethylenediamine tetraacetic acid
EGF	epidermal growth factor
ELEM	equine leukoencephalomalacia
EM	electron microscopy
ER	endoplasmic reticulum
ESR	electron spin resonance
EtBr	ethidium bromide

EtOH	ethanol
EYPC	egg yolk phosphatidylcholine
FA	fusaric acid
FA_1,	fumonisin A_1
FA_2	fumonisin A_2
FA_3	fumonisin A_3
FAK_1	fumonisin AK_1
FB_1	fumonisin B_1
FB_2	fumonisin B_2
FB_3	fumonisin B_3
FB_4	fumonisin B_4
FC_1	fumonisin C_1
FC_2	fumonisin C_2
FC_3	fumonisin C_3
FC_4;	fumonisin C_4
FCM	flow cytometry
FCS	foetal calf serum
FFPE	formalin fixed paraffin embedded
FITC	fluorescein isothiocyanate
FL-1	fluorescence channel 1
FL-2	fluorescence channel 2
FM	fluorescence microscopy
FP_1	fumonisin P_1
FP_2	fumonisin P_2
FP_3	fumonisin P_3
FSC	forward scattered
Gal C	galactocerebroside
GFAP	glial fibrillary acidic protein
GGT	gamma-glutamyl transferase
GGTP	gamma-glutamyl-transpeptidase positive
GIT	gastrointestinal tract
GPI	glycosylphosphatidylinositol
GSK-3β	glycogen synthase kinase 3 β
GSLs	glycosphingolipids
H & E	haematoxylin and eosin
H_2O	water
H_2O_2	hydrogen peroxide
HBSS	Hank's balanced Salt solution
HIV	Human Immunodeficiency Virus
IARC	International Agency for Research on Cancer
IC_{50}	approximate concentration giving 50% inhibition of cell proliferation
ICC	immunocytochemistry
IHC	immunohistochemistry
IL-β	interleukin β
ISP-1	Myriocin
JC-1	5,5',6,6'-tetrachloro-1,1',3,3'-tetraethylbenzimidazol-carbocyanine iodide
KCl	potassium chloride
K_m	Michaelis-Menten constant
KOH	potassium hydroxide
KS 300	Kontron Elektronik Imaging System 300 software programme

KZN	KwaZulu-Natal
LM	light microscopy
Magn.	Magnification
MAPK	mitogen-activated protein kinase
MBP	myelin basic protein
MEF	mouse embryo fibroblasts
MeOH	methanol
min.	minutes
$\Delta\psi m$	mitochondrial transmembrane potential
MM	McCoy mouse fibroblast cells
Mn^{2+}	manganese ion
MOG	myelin oligodendrocytes glycoprotein
MON	moniliformin
MRC	Medical Research Council
mRNA	messenger ribonucleic acid
MTAs	microculture tetrazolium assays
MTT	3-{4,5-dimethyl thiazol-2-yl}-2,5-diphenyltetrazolium bromide
MVA	motor vehicle accident
NA	noradrenalin
NaCl	sodium chloride
NADH	reduced nicotinamide adenine dinucleotide
NADPH	reduced nicotinamide adenine dinucleotide phosphate
NaOH	sodium hydroxide
NCR	National Cancer Registry
NGF	nerve growth factor
NGS	normal goat serum
$-NH_2$	amine group
NH_4OH	ammonium hydroxide
NMR	nucleotide monitoring reagent
NOAEL	no-observed-adverse-effect level
NRF	National Research Foundation
NRR	nucleotide releasing reagent
NTD	neural tube defects
NTU	Nottingham Trent University
OC	oesophageal cancer
OD	optical density
OPA	*o*-phthaldialdehyde
OSCC	oesophageal cancer squamous cell carcinoma
PAP	peroxidase-anti-peroxidase
PBS	phosphate buffered saline
PCT	proximal convoluted tubules
PDBu	phorbol dibutyrate
PDGF	platelet-derived growth factor
PDH	pyruvate dehydrogenase
PDI	probable daily intake
PE	phyocoerythrin
PGST	placental glutathione S-transferase
PI	propidium iodide
PKA	protein kinase A
PKC	protein kinase C
PMA	phorbol 12 myristate-13 acetate
PMT	photomultiplier tube
PND	post-natal development day

PNETs	primitive neuroectodermal tumours
PNS	peripheral nervous system
ppm	parts per million
PPO	porcine pulmonary oedema
PROMEC	Programme on Mycotoxins and Experimental Carcinogenesis
PS	phosphotidylserine
PT	permeability transition
R	correlation coefficient
rER	rough endoplasmic reticulum
RH	rat hepatoma tumour
Rh123	Rhodamine 123
RLUs	relative light units
RNA	ribonucleic acid
ROS	reactive oxygen species
RT	room temperature
Rti	retention times
SA	South Africa
Sa	sphinganine
SAX	strong anion exchange
SD	standard deviation
sec.	seconds
SER	smooth endoplasmic reticulum
SM	sphingomyelin
SMase	sphingomyelinase
So	sphingosine
So-1-phosphate	sphingosine -1- phosphate
SOD	superoxide dismutase
SPE	solid phase extraction
sphinganine	DL-erythro-dihydrosphingosine
sphingosine	D-sphingosine
SPT	serine palmitoyltransferase
SSC	side scattered
T2	T-2 toxin
TB	Tuberculosis
TCA	tricarballylic acid
TEM	transmission electron microscopy
TMP	transition of the mitochondrial transmembrane potential
TMS	N,N,N-trimethyl So
TNF	tumour necrosis factor
TNF-α	tumour necrosis factor α
Tris	Tris-[hydroxymethyl]-aminomethane
TUNEL	terminal uridine triphosphate nick-end labelling
UK	United Kingdom
UKZN	University of KwaZulu-Natal
USA	United States of America
UTP	uridine triphosphate
UV	ultraviolet
v/v	volume per volume
V_{max}	maximal velocity
w/v	weight per volume
WWH	Wentworth Hospital
ZEA	zearalenone
Zn^{2+}	zinc ion

TABLE OF CONTENTS

CHAPTER 1

Introduction

1.1 THE DIET-CANCER RELATIONSHIP

Food is one of the ultimate complex mixtures to which man is exposed. Research indicates that dietary variables, anti-carcinogenic substances, and exposure to carcinogens that occur in foods or are induced during its' preparation, are relevant determinants in the diet-cancer relationship (Institute of Food Technologists, 1993). Given the popular misconception that the natural human diet is "safe", and that such risks are due to contamination by pesticides, xenobiotics and other "chemical" residues, there is a need for continual evaluation of the avenues open to investigators to reduce disease incidence. Well-structured studies would ultimately wield meaningful results enabling medical and scientifically based advice to be given to the public with regard to improving dietary habits.

Numerous hypotheses on cancer causation exist. Their diversity and variety often reflect the paucity or conflicting, often over-abundance of experimental and epidemiological evidence on which they are based. Correlation is not necessarily causation, and hypotheses, however plausible, require unbiased evaluation. Although the complete web of cancer is complex, medical science is concerned with effective action, and this firstly requires no more than the identification of the relevant proximate influence, which, if removed, would lead to a substantial reduction in the risk of disease. On this empirical basis, what is diagnosed as a causal relation may turn out to be a predisposing, carcinogenic or co-carcinogenic factor. These factors may be several degrees away from those immediately responsible for carcinogenesis, but their discovery would help disclose the chain of causality, whose precise links could then be ascertained (Oettle', 1965).

1.2 MYCOTOXINS

Food-borne illnesses are of global importance. Among the factors that may induce these illnesses, mycotoxins that are defined as secondary metabolites synthesised by fungi under certain environmental conditions, have received considerable attention (International Agency for Research on Cancer, 1993a). Mycotoxins are potentially

carcinogenic compounds produced by fungi mainly in the genera *Aspergillus*, *Penicillium* and *Fusarium*.

Mycotoxins of importance in human health include the aflatoxins, ochratoxin A, fumonisins, trichothecenes and zearalenone (Pitt *et al.*, 2000). The interest they generate stems from their high toxicity and potency in producing tumours in laboratory animals (Institute of Food Technologists, 1993). Consumers of foods contaminated by fungi are vulnerable to acute toxicity and to chronic long-term mutagenic and immunosuppressive effects of mycotoxins, which exacerbate primary infections or interact with inter-current diseases. The present study focuses on the *Fusarium* mycotoxins fusaric acid (FA), moniliformin (MON), zearalenone (ZEA), deoxynivalenol (DON), and T-2 toxin (T2), with specific emphasis being placed on Fumonisin B_1 (FB_1).

1.3 EXPOSURE TO *Fusarium* FUNGI AND FUMONISINS IN SOUTH AFRICA

Exposure to FB_1 and other *Fusarium* metabolites is a public health hazard where mass food production and improper storage conditions are conducive to mould spoilage and subsequent mycotoxin production. Between 1984 to 1993, over 1600 samples of agricultural commodities comprising maize, compound animal feeds, oil seeds, soy bean, fish meal and forage in KwaZulu-Natal (KZN), South Africa (SA) were examined using a multi-mycotoxin screen. Aflatoxin had the highest incidence with over 14% of all samples examined followed by trichothecenes at 10%, and ZEA at 4%. Since 1989, selected maize samples with high levels of *Fusarium* species were examined for FB_1 and of these (n=20), 90% were positive in 1993. As a consequence of these results and high incidence of *Fusarium* species (32%) in maize and maize containing feeds, which was higher than either *Aspergillus* species (27%) or *Penicillium* species (12%), concern was expressed with regard to the potential presence and exposure to fumonisin in the South African food chain (Dutton and Kinsey, 1996).

As the potential for daily dietary exposure to these compounds via the ingestion of contaminated foods and feeds exists, their importance in food safety and as causes of human illness has increased. The diseases produced as a result of the consumption of contaminated foods however, remains poorly understood at the clinical level.

Fusarium fungi have been implicated in haemorrhagic, oestrogenic, emetic, and feed refusal syndromes in animals. There is considerable evidence that the central nervous system (CNS) is a potential site of action for FB_1 and is exemplified in horses by the disease equine leukoencephalomalacia (ELEM). This disease is characterised by marked neurotoxicity and liquefactive necrotic lesions in the white matter of the cerebral hemispheres of the brain of horses and other equine species (Marasas *et al.*, 1988a; Kellerman *et al.*, 1990; Wilson *et al.*, 1992; Ross *et al.*, 1993).

Studies on the pathophysiology of fumonisin toxicoses are essential in disease diagnosis, establishment of safety parameters, and development of control and prevention procedures. As the potential for dietary exposure to *Fusarium* mycotoxins exists, the human CNS is at risk of exposure to their biochemical effects and potential carcinogenicity. The data that exists on the adverse health effects of fumonisins in animals serves as the basis for concern for their effects on human health. However difficulty is inherent in the extrapolation of risk from animals to humans, and in the determination of what a significant biological exposure constitutes, due to differences in species-specific responses to a compound.

Fusarium mycotoxins have been implicated in alimentary toxic aleukia, Urov or Kashin-Beck disease, Akakabi-byo or scabby grain intoxication, and oesophageal cancer in humans (Marasas *et al.*, 1979a; 1988b; Rheeder *et al.*, 1992). However, these published studies demonstrate inconclusive associations of fumonisins with human disease. In addition, minimal work has been channelled into investigating directly the possible implication of *Fusarium* mycotoxins, especially FB_1, in the aetiology of human brain cancer, or in relation to isolated cells of the CNS and their lesions.

The selection of a single agent for investigation does not deny the complex aetiology of cancer, nor does it exclude the possibility of other factors contributing to disease causation. Over simplification in an effort to shed clarity of understanding to a problem for proper elucidation is sometimes considered better than taking the dichotomous route of complication beyond recognition. This holds true especially if the latter were to become no more than a bewildered acknowledgment of complexity that explains away anomalies and effectively hinders logical analysis.

1.4 BRAIN CANCER IN SOUTH AFRICA

The National Cancer Registry (NCR) collates information on cancer diagnosed via a network of private and public pathology laboratories in SA. The most recent available report by Sitas *et al.* (1998), provides statistics for the time-frame between 1993 to 1995, that includes frequencies by population, sex, age-group, cancer site, age standardized, cumulative incidence rates and lifetime risks of developing cancer. These statistics (Table 1) indicate that a total of 387 females and 494 males were diagnosed with brain or CNS tumours between 1993 and 1995. The Asian and White race groups seemed more susceptible to development of tumours as indicated by the calculated lifetime risk of getting these tumours, with males across all race groups at greater risk than women (Table 1). Figures A1.1 and A1.2 (Appendix 1) graphically illustrate the frequency of histologically diagnosed brain and CNS cancer, and the age specific cancer rates per 100 000 in SA between 1993 and 1995 (Sitas *et al.*, 1998).

Table 1: Summary statistics for cancer in the brain and central nervous system in South Africa, 1993-1995 (Sitas *et al.*, 1998).

	93	94	95	93 to 95	% of all cancers	No of cases/ population, Per 100 000	Age standardised incidence rate per 100 000	Cumulative incidence rate (0-74 yrs)	Lifetime risk of developing a cancer
Total female	154	135	98	387	0.57	0.72	0.85	0.09	1111
Total male	192	142	160	494	0.69	0.94	1.1923	0.11	909
Asian Female	10	7	3	20	1.21	1.75	1.58	0.12	833
Asian Male	6	5	11	22	1.91	2.03	2.34	0.24	417
Black Female	45	31	29	105	0.51	0.29	0.31	0.03	3333
Black Male	63	28	38	129	0.69	0.38	0.43	0.04	2500
Coloured Female	10	7	3	20	0.86	0.53	0.56	0.04	2500
Coloured Male	8	6	5	19	0.90	0.53	0.79	0.07	1429
White Female	69	58	38	165	0.56	7.80	2.62	0.26	385
White Male	87	62	65	214	0.61	3.78	3.57	0.34	294
Race unknown Female	20	32	25	67					
Race unknown male	28	41	41	110					

The increased incidence of brain cancer in adults and children is suspected of having a strong environmental influence (Curan and Jones, 1991). The cancers most prevalent amongst South African children follows a worldwide trend, according to the Cancer Association of South Africa (CANSA) with brain cancer ranking second amongst the most common cancers, and accounting for 21% of all cancers diagnosed. Neuroblastomas, a cancer of the sympathetic nervous system, also ranked fifth amongst most common childhood cancers (Cancer Information Services, 1998).

On the basis of racial classification, South Africans were previously subject to environments that determined their lifestyle, diet, socio-economic condition, residence, type of work and access to health care (Sitas and Pacella, 1994). These differences influenced reported cancer patterns observed among population groups. However, major socio-economic changes have occurred in SA over the past ten years that have impacted on these aspects. Were more recent statistics available, it would provide a more accurate representation of current cancer incidence across the racial groups due to increased reporting and increased access to health care for all races. The statistics presented by Sitas *et al.* (1998) are representative of cases reported within only the 1993-1995 timeframe. At that time, in socially impoverished communities, limited access to medical facilities and treatment, lack of money and knowledge on disease treatment, may have prevented people from seeking and securing help. Nevertheless, this information was helpful in providing insight into past trends of reported cancer incidence in SA.

1.5 POTENTIAL FOR FUNGAL ASSOCIATION IN NEUROLOGICAL DISEASES

The overall goal of neurotoxicological investigations is to develop and validate quantitative biomarkers of neurotoxicity and to utilize these to elucidate toxicity mechanisms. This would increase the certainty of assumptions underlying risk assessment for neurotoxicants. Advances in medical science have revolutionized understanding of brain tumours and shown that abnormal proliferation, inability of the cells to die and their potential to modify their tissue environment, result from accumulation of genetic aberrations. Understanding the potential initiators and chain of events responsible for brain tumour growth is a prerequisite for the development of effective therapeutic modalities leading to improved prognosis and cures.

In order to develop and implement methods of preventing intoxication and managing symptoms of poisoning by *Fusarium* mycotoxins known to potentially affect the CNS, identification and understanding the mechanisms whereby these toxicants exert their effects is imperative. The selection of *Fusarium* toxins for study was on the basis of their incidence in analytical surveys of commercially available SA food and feeds (Dutton and Kinsey, 1995; 1996), as well as on the requirement for further research into their potential role in CNS-associated human disease. The significant contribution of maize and maize-based foods to the diet, and therefore their potential diet-toxicity interaction, warranted the present study to ascertain whether selected *Fusarium* mycotoxins may be associated with the pathophysiology of brain cancer in the population of KwaZulu-Natal, South Africa.

Diagnosis of neurological diseases caused by fungi can be difficult as clinical signs are often ambiguous or similar to those found in other diseases, and histological lesions may be non-specific or absent. Therefore, the diagnosis of diseases caused by neurotoxic mycotoxins depends not only on history, clinical signs or finding the mycotoxin in the appropriate food and feed material (Plumlee and Galey, 1994), but also on finding the specific mycotoxin directly within lesions, in infected tissues, and/or in physiological fluids.

1.6 OBJECTIVES

This study comprised of an *in vitro* experimental, as well as a *in vivo* clinical component. The objectives of the *in vitro* component were to assess the: -

- potential for selected *Fusarium* mycotoxins to induce cytotoxicity, apoptosis, growth arrest or necrosis in the N2α mouse neuroblastoma cell line;
- structural and ultrastructural changes that occur as a result of exposure to *Fusarium* mycotoxins in N2α mouse neuroblastoma cells using immunochemical techniques; and
- *in vitro* effects of FB_1 on sphinganine (Sa) and sphingosine (So) metabolism in the N2α cells.

The objectives of the clinical component of this study were to: -

- analyse sera obtained from non-cancer subjects and brain tumour patients for levels of FB_1, Sa, So and Sa:So ratios in order to establish whether any correlation exists between these variables, and
- immunolocalise FB_1 within brain tumour tissues.

CHAPTER 2

Literature Review

2.1 STRUCTURE OF THE NERVOUS SYSTEM

The nervous system is divided into the CNS that consists of the brain contained within the cranium and spinal cord lodged in the vertebral canal, and the peripheral nervous system (PNS), made up of ganglia and peripheral nerves that lie outside the brain and spinal cord. Further subdivisions of the CNS, PNS and the associated functions are shown in Appendix 2. For the purpose of this study, discussion will specifically focus on some of the functions and parts of the brain.

2.2 STRUCTURE OF THE BRAIN

2.2.1 The meninges

The meninges are three layers of tissue made up of the dura mater, arachnoid mater, and pia mater that cover and protect the brain and spinal cord. The dura mater is made up of two layers of whitish, inelastic film or membrane. The outer layer, the periosteum and an inner layer, the dura, lines the inside of the skull and creates folds or compartments in which parts of the brain are neatly protected and secured. The second layer of the meninges, the arachnoid layer is a thin and delicate membrane made up of delicate, elastic tissue and blood vessels of different sizes, and covers the entire brain. The space between the dura and the arachnoid membranes is the subdural space. The layer of meninges closest to the surface of the brain, the pia mater, has many blood vessels that reach deep into the surface of the brain. The pia that covers the entire surface of the brain follows the folds of the brain. The major arteries supplying the brain provide the pia with its blood vessels. The space that separates the arachnoid and the pia is called the subarachnoid space and it is here that cerebrospinal fluid (CSF) flows. Cerebrospinal fluid is found within the brain and surrounds the brain and spinal cord. It is within hollow channels in the brain, called ventricles, where the fluid is produced. The choroid plexus is responsible for the majority of CSF production.

2.2.2 The cerebrum

The brain protected by the rigid, bony skull consists of the cerebrum, the cerebellum and the brain stem (Figure 2.1). The cerebrum consists of two cerebral hemispheres that are incompletely separated by the longitudinal cerebral fissure. The hemispheres consist of the cerebral cortex, which refers to the grey matter covering the cortex, the white matter under the cortex, and three deeply located nuclei. These are the basal ganglia, the hippocampal formation and the amygdala. The cerebral hemispheres are divided by the hemispheric fissure and are thought to be concerned with perception, cognition, emotion, memory and higher motor functions.

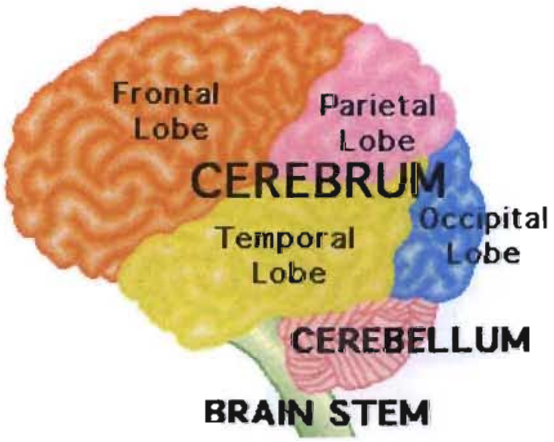

Figure 2.1: Structure of the brain (Burkitt *et al.*, 1993).

The corpus callosum connects the two halves of the brain and allows for communication between the hemispheres. The surface of the cerebrum contains billions of neurons and glia that together form the cerebral cortex. The cerebral cortex appears greyish brown in colour and is called the "grey matter". The cerebral cortex has small grooves (sulci), larger grooves (fissures) and bulges between the grooves called gyri. Beneath the cerebral cortex or surface of the brain, connecting fibres between neurons form the "white matter". The cerebral hemispheres have several distinct fissures. The brain can effectively be divided into pairs of lobes; namely the frontal, temporal, parietal and occipital lobes (Figure 2.1).

2.2.3 The cerebellum

Like the cerebrum, the cerebellum (Figure 2.1) is divided into two hemispheres and is composed of white and grey matter. The cerebellum, located at the back of the brain beneath the occipital lobes, is separated from the cerebrum by the tentorium (fold of dura).

The cerebellum fine-tunes motor activity or movement and controls balance and co-ordination.

2.2.4 The brain stem

The brain stem consists of the midbrain, pons and medulla oblongata (Figure 2.1) and extends from the base of the cerebrum and merges into the top of the spinal cord. Neurological functions located in the brainstem include those necessary for breathing, digestion, heart rate, blood pressure, for being awake and alert. It serves as a relay station, passing messages back and forth between various parts of the body and cerebral cortex.

The midbrain is the smallest part of the brain. The midbrain is an important centre for ocular motion, while the pons is involved with coordinating the eye and facial movements, facial sensation, hearing and balance. The medulla oblongata is the most caudal part of the brain stem, composed of the midbrain, pons and medulla. It controls breathing, blood pressure, heart rhythms and swallowing.

2.3 THE BLOOD BRAIN BARRIER

The blood brain barrier (BBB) (Figure 2.2) is created by the tight apposition of endothelial cells lining blood vessels in the brain, forming a barrier between the circulation and the brain parenchyma (e.g., astrocytes, microglia). Blood-borne immune cells such as lymphocytes, monocytes and neutrophils cannot penetrate this barrier. A thin basement membrane, comprising lamin, fibronectin and other proteins, surrounds the endothelial cells and associated pericytes, and provides both mechanical support and a barrier function. Thus, the BBB is crucial for preventing infiltration of pathogens and restricting antibody-mediated immune responses in the CNS, as well as for preventing disorganization of the fragile neural network. This, together with a generally muted immune environment within the brain itself, protects the fragile neuronal network from the risk of damage that could ensue from a full-blown immune response. On rare occasions, pathogens (e.g., viruses, fungi and prions) and autoreactive T cells breach the endothelial barrier and enter the brain. A local innate immune response is mounted in order to limit the infectious challenge, and pathogens are destroyed and cell debris is removed, a vital process that must precede tissue repair (Francis *et al.*, 2003).

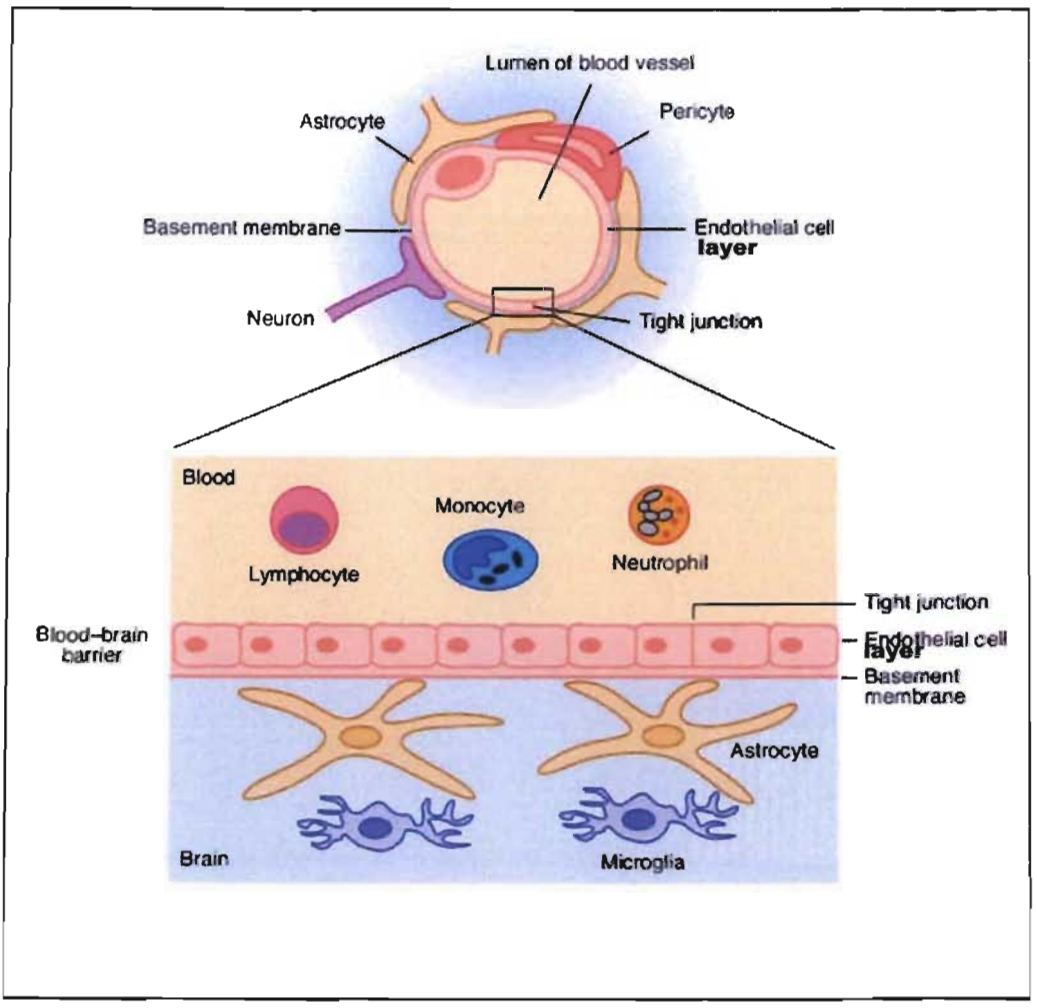

Figure 2.2: The blood brain barrier (Francis *et al.*, 2003).

The barrier is a differentially permeable structure that is partially ascribable to the presence of specialised CNS capillaries and the envelopment of capillaries by astroglial foot processes. Specialized capillaries have tight junctions between endothelial cells and a lower rate of pinocytosis than visceral capillaries. The cerebral capillary endothelial cell displays some peculiar morphologic characteristics that form the anatomic basis of the BBB. It differs from the peripheral capillary endothelial cell (referring to all non-CNS sites) in that it is not fenestrated. Cells are joined by tight junctions composed of six to eight pentalaminar structures, and actively block protein movements, hydrophilic transfer and even ionic diffusion (Burkitt *et al.*, 1993). Thus, there is very little movement of compounds between endothelial cells from the blood to the CNS.

The cerebral vascular endothelial cell possesses a transcellular lipophilic pathway, allowing diffusion of small lipophilic compounds. In addition to this route, specific receptor-mediated transport systems are present for molecules, like insulin, transferrin, glucose, purines and amino acids. The CNS endothelial cell displays a net negative charge at its endoluminal side and at the basement membrane. This provides an additional selective mechanism by impeding anionic molecules to cross the membrane. The cerebral endothelial cell has very few pinocytic vesicles, and these vesicles are not involved in any transport function (Burkitt *et al.*, 1993).

The BBB provides neurons with a relatively constant biochemical and metabolic environment, protection against endogenous and exogenous toxins and infective agents and insulates the neurons from circulating neurotransmitters and other humoural agents. The capillaries of the choroid plexus, the pituitary gland and pineal glands and the vomiting centre of the hypothalamus are, however, devoid of this barrier as befits their various functions. By virtue of this selective barrier, the CNS can preferentially regulate the extracellular concentration of certain solutes, growth factors and neurotransmitters, keep certain molecules in the CNS and isolate itself from some others, and further isolate itself from sudden systemic homeostatic changes. It is therefore an integral component of the mechanisms involved in the tight regulation of the extra-cellular homeostasis necessary to the normal CNS function (Burkitt *et al.*, 1993).

2.4 WHAT IS BRAIN CANCER?

Cancer development is a multistage process in which the summation of the steps of genetic change, clonal expansion of initiated cells and malignant conversion is required to produce a malignant tumour. Conversion from a pre-malignant phenotype to a malignant cell type is the major time-dependent stage of cancer pathogenesis, whereas tumour heterogeneity; associated with the acquisition of metastatic potential, is a relatively rapid event (Yuspa, 2000).

Tumours in the CNS resulting in an overgrowth of cells in the brain or spinal cord are potentially harmful because of the solid framework of the skull and vertebrae. The growing tumour presses against other structures in this non-expanding space, eventually causing symptoms. Various cell types make up the brain and spinal cord, and each type of cell can

give rise to a different type of tumour. Benign brain tumours can cause problems by pressing on and damaging the surrounding brain tissue, however, they can often be successfully removed. Malignant brain tumours, or brain cancers, vary widely both in the way they grow and the way they respond to treatment. In addition, both benign and malignant tumours may cause the brain tissue around them to swell. Many malignant tumours in the brain are secondary cancers that arise as a result of metastasis of a tumour from another region of the body.

There is no known cause of primary tumours of the brain and spinal cord. In certain individuals, primary tumours of the CNS may result from specific genetic diseases such as neurofibromatosis and tuberous sclerosis, or exposure to radiation or cancer-causing chemicals. Although smoking, alcohol consumption and certain dietary habits are associated with some types of cancers, they have not been linked to primary brain and spinal cord tumours. Some of the possible causes under investigation include viruses, defective genes, xenobiotics and chemicals. Studies are now investigating whether or not there is a link between dietary factors and CNS tumours.

Studying the epidemiology of CNS tumours will ensure elucidation of factors responsible for the formation of different tumours, and determination of whether certain tumours are more prevalent at certain ages or in certain people. This information may reveal environmental factors that are linked to tumours, connections between tumours and other disorders, or patterns of tumour occurrence. Analytical epidemiological studies have revealed an increased risk of human brain tumour development in association with certain occupations but, with the exception of therapeutic X-ray irradiation, attempts to identify a specific exposure or causative environmental agent have so far been unsuccessful.

2.5 NEUROTOXICOLOGY

The nervous system differs from most other body systems in the degree of selective vulnerability of its subdivisions. Neurotoxins act by affecting the basic components of the nervous system producing various clinical syndromes. Neurotoxins may be highly specific, affecting limited numbers of specialised neurons. While vulnerability to toxins can be highly specific, neurotoxins are rarely mono-specific. Differences in vulnerability are due

to anatomical, physiological, and pharmacological and biochemical specializations of neurons, their processes and supporting structures.

2.6 TYPES OF BRAIN TUMOURS

2.6.1 Gliomas

Within the brain, gliomas, tumours arising from glial cells, usually occur in the cerebral hemispheres but may also strike the optic nerve, the brain stem, and particularly among children, the cerebellum. Gliomas are classified into several groups. The types of graded astrocytomas include well differentiated, anaplastic and glioblastoma multiforme. Sometimes astrocytomas are graded on a scale of I to III; grade III being the most malignant. Gliobastoma multiforme (sometimes called high-grade or grade IV astrocytomas), grow rapidly, invade nearby tissue, and contain cells that are very malignant. Brain stem gliomas are tumours located in the bottom part of the brain that connects to the spinal cord (the brain stem). Mixed gliomas are brain tumours that occur in more than one type of brain cell, including cells of astrocytes, ependymal cells and oligodendrocytes.

2.6.2 Ependymomas

Ependymal tumours begin in the ependyma, the cells that line the passageways in the brain where CSF is made and stored. About 50% of them expand deep into the cerebellum or cerebrum, the rest are found in the spinal cord. Ependymomas usually affect children and develop from cells that line both the hollow cavities of the brain and the canal containing the spinal cord.

2.6.3 Oligodendrogliomas

Oligodendroglial tumours develop from oligodendroglia; cells that make myelin to insulate nerve fibres. Oligodendroglia also provide support and nourishment for the cells that transmit nerve impulses. Oligodendrogliomas usually develop slowly in the cerebrum, and occur most often within the brain's cerebral hemispheres in young adults.

2.6.4 Ganglioneuromas

Ganglioneuromas contain both glial cells and mature neurons. Mixed gliomas contain more than one type of glial cell, usually astrocytes and other glial cell types. Brain stem gliomas are named by their location at the base of the brain, rather than the cells they contain. Optic nerve gliomas are found on the optic nerve and are particularly common in individuals who have neurofibromatosis.

2.6.5 Meningiomas

Meningiomas are tumours that develop from the meninges (described in section 2.2.1). Meningiomas generally do not invade surrounding normal tissue and rarely spread to other parts of the CNS or body. Malignant meningioma is a rare tumour that grows more quickly than other meningiomas. Meningeal carcinomatosis strikes when individual cells from cancer outside the CNS enter the CSF. These cells travel with the CSF and can form colonies or small tumours in many places, including the roots of nerves, the surface of the brain, the brain stem, and the spinal cord.

2.6.6 Pineal tumours

Pineal parenchymal tumours and pineal region tumours are found in or around the brain (the pineal gland). The tumours can be slow growing (pineocytomas) or fast growing (pineoblastomas). Astrocytomas may also start here. The three most common types of pineal region tumours are gliomas, germ cell tumours, and primitive neuroectodermal tumours (PNETs). Primitive neuroectodermal tumours are usually very malignant, growing rapidly and spreading easily within the brain and spinal cord. In rare cases they spread outside the CNS. Primitive neuroectodermal tumours include neuroblastomas, pineoblastomas, medulloepitheliomas, ependymoblastomas, and polar spongioblastomas.

2.6.7 Pituitary Adenomas

The pituitary gland releases hormones that help control the body's other glands and influences growth, metabolism, and maturation. Pituitary adenomas are classified into two groups, secreting and non-secreting. Secreting tumours release unusually high levels of

pituitary hormones triggering a constellation of symptoms, which can include impotence, amenorrhoea, abnormal body growth, Cushing's syndrome, or hyperthyroidism, depending on which hormone is involved.

2.6.8 Medulloblastomas

Medulloblastoma is a rapidly growing tumour that develops in the cerebellum. This type of cancer may spread from the brain to the spine. It accounts for about 20% of the brain tumours found in children less than 15 years, and may also develop in adults. Cells from this type of tumour can travel through the CSF to start new tumours in other parts of the brain and spinal cord.

2.6.9 Choroid plexus tumours

The choroid plexus is located in the spaces inside the brain ventricles and makes the fluid that fills the ventricles and surrounds the brain and spinal cord. Tumours of the choroid plexus can grow slowly (choroid plexus papilloma) or rapidly (anaplastic choroid plexus papilloma). The rapidly growing tumours are more likely to spread to other places in the brain and spinal cord. The choroid plexus tumour is a rare, benign tumour most common in children under the age of 12. Choroid plexus papillomas grow slowly and eventually block the flow of CSF. This causes hydrocephalus and increased intracranial pressure. Choroid plexus carcinoma is the rare inoperable or malignant form of this tumour.

2.7 ENVIRONMENTAL TOXICOLOGY

Various environmental toxicants are known to affect the CNS, and in order to facilitate development of methods of preventing intoxication and managing symptoms of poisoning, it is imperative to understand their mechanisms of action. These mechanisms can be discussed at the level of the action on organs and tissues, on cells and membranes, and at the molecular level. Documentation of pathways for metabolic activation and detoxification of carcinogens explain the specificity of carcinogen-macromolecule interactions, illuminate important genetic determinants of cancer risk, and lead to the development of methods to detect carcinogen-macromolecule adducts in human populations. Marked variability in animal species focus attention on the search for

susceptibility determinants in human populations. These insights and methods help to explain organ specificity to certain carcinogens.

2.8 HYPOTHESES AND THEORIES OF CANCER INDUCTION

In the evaluation of human health risks, sound human data, whenever available, are preferred to animal data. Animal and *in vitro* studies however do provide support, and are used to supply evidence missing from human studies. When epidemiological studies indicate that environmental factors are major causes of human cancer, research expands into a more mechanistic era. Cancer research has played a critical supporting role in validating hypotheses developed from population studies. Experimental studies have been predictive of cancer risks. The modifying influence of nutrition on cancer induction and the identification of environmental contaminants that contribute to cancer incidences, are examples of hazards identified through model systems designed to study chemical carcinogenesis (Yuspa, 2000).

Human cancers do not result from a single mutation, but develop through stages reflecting the accumulation of several genetic changes. Given the involvement of several rather than one genetic event in many, if not all cancers, epidemiologice efforts to identify human dietary carcinogens may succeed under the following limited circumstances: -

- there may be some cancers that require a single, rate-limiting event, or
- the cancer may involve multiple events, but all (or most) can be elevated by a single aetiological agent to which the high incidence population is chronically exposed; or
- the final progressive event (e.g., the p53 mutation) for a cancer can be traced to a recent carcinogen exposure, or
- the high- and low-incidence populations must not be differentially exposed to an unknown and hence uncontrolled chemo-protective agent.

When further considering the multi-step nature and mechanisms involved in cancer development, it becomes clear that genetic changes, cellular adaptive reactions and responses and/or dynamic interaction between cells and tissues are important factors that underline the entire system (Farber *et al.*, 1989; 1990). The latter considerations form part of the epigenetic way of cancer development, an aspect that is largely ignored when the mechanism of cancer induction by chemicals is considered. Furthermore, recent investigations indicate that an increasing number of non-genotoxic chemicals in the

spectrum of chemical carcinogenesis remain an open one. In this context, it has to be realized that the chemical and/or biological basis of cancer induction, whether via genotoxic or non-genotoxic systems still remains unknown.

2.9 MYCOTOXINS

Mycotoxins are a diverse group of compounds produced by a taxonomically wide range of filamentous fungi that contaminate foods and feeds. On exposure to animals or man via inhalation, ingestion or skin contact; mycotoxins may initiate both acute (short-term) and chronic (medium/long-term) toxicities ranging from death to chronic interferences with the function of the CNS, cardiovascular and pulmonary systems, and the alimentary tract (Smith and Moss, 1985; Bennet, 1987).

Mycotoxins are produced for a variety of reasons that include facilitating entry or attack of hosts by helping to dissolve cell membranes, or as protective measures against encroaching organisms. Structurally diverse, mycotoxins are capable of reacting with molecular receptors including deoxyribonucleic acid (DNA), ribonucleic acid (RNA), functional proteins, enzyme co-factors and membrane constituents. Toxicological action depends on the nature of the mycotoxin, dose, entrance route, time of exposure, and species susceptibility (Pitt *et al.*, 2000). The relative significance of a molecular receptor of a mycotoxin is determined by its affinity to the active form of the toxin, its role in vital biochemical processes, the persistence of the lesion it bears, and the severity of the consequence of the lesion (Hsieh, 1987).

When considering the above arguments concerning the mechanisms of cancer developments, this review will focus on fumonisin related biological effects that could provide information on the possible mechanism involved in the toxic and carcinogenic effects of these apparently non-genotoxic compounds.

2. 10 *Fusarium* SPECIES OF FUNGI AND THEIR ASSOCIATED MYCOTOXINS

Individual *Fusarium* species are known to produce several mycotoxins of which the fumonisins, ZEA, DON, FA, nivalenol, HT-2 toxin, and T2 are considered among the most important. In order to develop methods of preventing intoxication and managing symptoms of poisoning by *Fusarium* mycotoxins known to potentially or adversely affect the CNS;

identification of, and understanding the general mechanisms whereby these toxicants exert their effects is essential. The International Agency for Research on Cancer (IARC) reviewed the toxicity of *Fusarium moniliforme* derived toxins, and classified FB_1 and fumonisin B_2 (FB_2) as "possible" human carcinogens (Group 2B) (IARC, 1993b). It was concluded that there was inadequate evidence in humans for carcinogenicity, whereas there was limited evidence (FB_1) or inadequate evidence (FB_2) for carcinogenicity in experimental animals. In addition, IARC (1993b) found that FB_1 was neither mutagenic nor genotoxic.

Studies available were considered largely inconclusive, and quantitative data enabling a risk assessment on human studies were unavailable. Numerous studies have focussed on aspects of the possible role of FB_1 in cancer.

These studies include the mechanism of action of FB_1 in cultured human cells, *in vivo* rodent studies, and the tumorigenicity of FB_1 in rats and mice. To determine the overall human cancer risk from exposure to a particular mycotoxin, one needs to understand the exposure, bioavailability and mechanism(s) of action. This must occur prior to reviewing the carcinogenic potential of this compound in representative animal bioassays or cell culture models, and epidemiological studies that show the potential for implication of this mycotoxin in the aetiology of cancer.

2.11 FUMONISINS

2. 11. 1 Occurrence and production of fumonisins

Fusarium moniliforme is a soil and seed-borne fungal pathogen of maize (*Zea mays*) (Figure 2.3) (Nelson *et al.*, 1991; Bacon *et al.*, 1992; Munkvold, 1996).

Figure 2.3: Typical *Fusarium* ear rot (Munkvold, 1996).

Infection of the maize plant and kernel varies depending on the point(s) of entry by the fungus into the developing maize plant (Bacon and Nelson, 1994; Munkvold *et al.*, 1997). In addition, the extent of fumonisin contamination varies with geographical location, agricultural practices, and the maize genotype, which determines the susceptibility of the plants to fungal invasion. Fumonisin production is further influenced by temperature, humidity, drought stress, rainfall during the pre-harvest and harvesting periods, as well as by the storage of the maize kernels under improper moisture conditions (Bacon and Nelson, 1994).

The fumonisins are a class of polar metabolites, originally isolated from *Fusarium moniliforme [*now known as *F. verticillioides]* (Bezuidenhout *et al.*, 1988) and later, from *F. proliferatum*, *F. nygamai*, and *F. napiforme*. The worldwide occurrence of fumonisins in maize and maize-based products has been well documented and reviewed (Doko and Visconti, 1994; Pohland, 1994; Marasas, 1996; Bullerman, 1996; Shephard *et al.*, 1996a; Patel *et al.*, 1997; Castelo *et al.*, 1998; de Nijs, 1998; de Nijs *et al.*, 1998a; 1998b). Also reported are the sporadic natural occurrence of fumonisins in sorghum, rice and navy beans (Tseng *et al.*, 1995; Patel *et al.*, 1996; Munibazi and Bullerman, 1996; Bhat *et al.*, 1997).

The polarity of the fumonisin molecule (Figure 2.4) determines its level of carcinogenicity (Gelderblom *et al.*, 1993), i.e., the more polar a molecule, the greater the cytotoxic response. In addition to polarity, the presence of a free amino group and the location of the hydroxyl group could also affect the biological activity of these compounds. Thus, both the amino group and the intact molecule play an important role in the toxic and cancer promoting activity of fumonisins. This would explain the associations of FB_1 with soluble and insoluble portions of cells (Cawood *et al.*, 1994).

Feed-derived fumonisins are poorly absorbed by farm animals therefore fumonisin residues in milk (Scott *et al.*, 1994; Maragos and Richard, 1994; Becker *et al.*, 1995; Richard *et al.*, 1996), eggs (Vudathala *et al.*, 1994), and meat (Prelusky *et al.*, 1994; Prelusky *et al.*, 1996; Smith and Thakur, 1996) are either undetectable or detected at extremely low levels. Due to the heat stability (Dupuy *et al.*, 1993; Howard *et al.*, 1998), light stability (IARC, 1993b), water solubility (United States National Toxicology Program, 1999), poor absorption and metabolism, as well as rapid excretion by animals, most fumonisin will

eventually be recycled into the environment in a manner that will concentrate its spatial distribution.

2.11.2 Structure, physical and chemical properties of fumonisins

Fumonisin B_1 (FB_1) has the empirical formula $C_{34}H_{59}NO_{15}$ and is the diester of propane-1,2,3-tricarboxylic acid and 2-amino-12,16-dimethyl-3,5,10,14,15-pentahydroxyeicosane (relative molecular mass: 721) (Figure 2.4). It is the most prevalent of fumonisins, a family of toxins with at least 15 identified members. The pure substance is a white hygroscopic powder, which is soluble in water, acetonitrile-water or methanol, is stable in acetonitrile-water (1:1), at food processing temperature and in light, but is unstable in methanol. The 15 fumonisins reported have been grouped into four main categories (Plattner, 1995; Musser and Plattner, 1997; Abbas *et al.*, 1998):

- fumonisin A_1 (FA_1), fumonisin A_2 (FA_2), fumonisin A_3 (FA_3), fumonisin AK_1 (FAK_1);
- FB_1, FB_2, fumonisin B_3 (FB_3), fumonisin B_4 (FB_4);
- fumonisin C_1 (FC_1), fumonisin C_2 (FC_2), fumonisin C_3 (FC_3), fumonisin C_4 (FC_4); and
- fumonisin P_1 (FP_1), fumonisin P_2 (FP_2) and fumonisin P_3 (FP_3).

Fumonisin B_2, FB_3 and FB_4 differ from FB_1 in that they lack hydroxyl groups present in FB_1; FA_1, FA_2 and FA_3 are like FB_1, FB_2 and FB_3, but are N-acetylated; FAK_1 is like FA_1 but is 15-keto functionalised; the fumonisin 'C's are like the fumonisin 'B's but lack the methyl group adjacent to the amino group; and the fumonisin 'P's have a 3-hydroxypyridium group instead of the amine group in the fumonisin 'B's (Gelderblom *et al.*, 1992; Plattner *et al.*, 1992; Branham and Plattner, 1993).

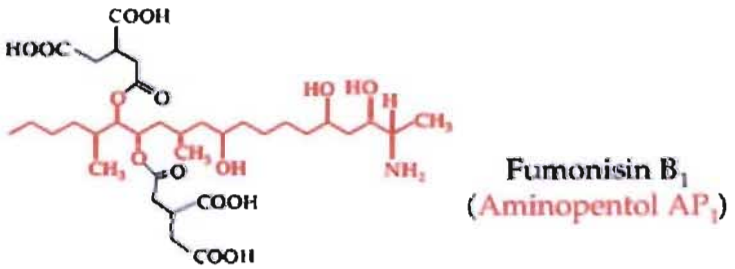

Figure 2.4: The Chemical structure of Fumonisin B_1 and aminopentol (Merrill, 2002).

The "B" series are believed to be the most abundant and toxic naturally occurring analogues (Sydenham *et al.*, 1992; Thiel *et al.*, 1992). Because of the four free carboxyl

groups and the amine group, the compounds are water soluble, but insoluble in non-polar organic solvents. Three dimensional minimum energy conformation for FB_1, FB_2, FB_3 and FB_4 were calculated (Beier *et al.*, 1995), and it was found that the amine and carboxylic acid groups are spatially related, suggesting that they have chelating properties, and hence, could cause membrane ion leakage (Abbas *et al.*, 1992).

2.11.3 Fumonisins and sphingolipids

Fumonisins bear structural resemblance to Sa (Figure 2.5), an intermediate in the biosynthesis of complex sphingolipids (Sweeley, 1991; Bell *et al.*, 1993). This structural similarity led to the hypotheses that the mechanism of action of these mycotoxins might be via disruption of sphingolipid metabolism; via interaction with enzyme(s) of sphingolipid metabolism, or a combination of both these factors (Merrill *et al.*, 1996a; 1996b). The fumonisins have been shown to inhibit ceramide (CER) synthase, the key enzyme in sphingolipid biosynthesis. Since sphingolipids play critical roles in the regulation of cell growth, cell differentiation and transformation (Merrill, 1991), disruption of the metabolism of these bioactive molecules may be the mechanism for toxicity and carcinogenicity of these mycotoxins (Yoo *et al.*, 1992; Merrill *et al.*, 1993a; 1993b; 1993c). The implication that several human and animal diseases arise from defects in sphingolipid hydrolysis increased interest in the study of sphingolipid metabolism.

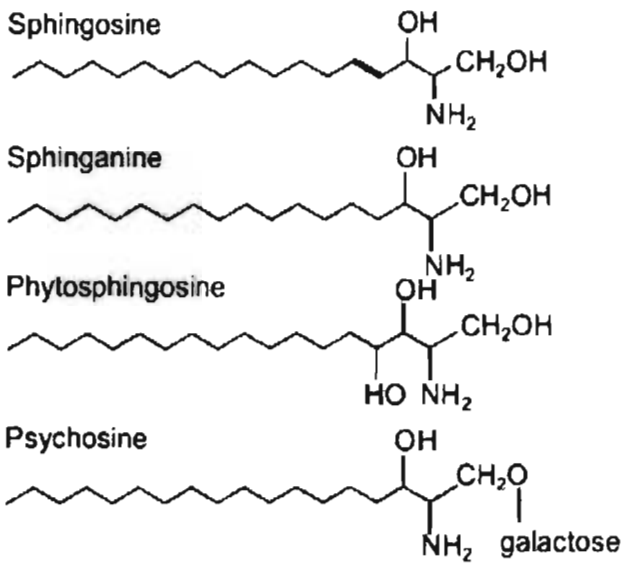

Figure 2.5: Chemical structures of select sphingolipids.

2.12 SPHINGOLIPIDS

2.12.1 Structure and occurrence of sphingolipids

Sphingolipids are components of the plasma membrane of eukaryotic cells. These compounds are the most structurally diverse class of membrane lipids, being composed of over 70 long-chain (sphingoid) bases, dozens of amide-linked fatty acids, and more than 300 head groups (Merrill and Sweeley, 1996).

Sphingolipids are composed of a long chain sphingoid base, an amide linked fatty acid and a polar head group at the 1-position (Figure 2.5). Sphingolipids contain a CER backbone, which anchors them in the outer leaflet of the lipid bilayer. The CER backbone can be modified by attachment of phosphorylcholine to form sphingomyelin (SM), or by attachment of one or more sugar residues to form glycosphingolipids (GSLs). Except for CER, which has a hydroxyl at the 1-position, and for SM, which has a phosphorylcholine head group; all other sphingolipids contain carbohydrate head groups and hence are designated GSLs (Hannun and Bell, 1989).

The first classes of sphingolipids were named according to the tissue from which they were isolated (e.g., SM, cerebrosides, psychosine) (Figure 2.5) leaving the false impression that these compounds are unique to neuronal tissues. Sphingolipids are present in all eukaryotic cells where they primarily occur in cell membranes and related intracellular membranes, such as Golgi and lysosomal membranes, as well as in some prokaryotic organisms (Merrill *et al.*, 1997). In addition to biosynthesis, catabolism of sphingolipids also occurs. In the intestines, SM and other complex GSLs are digested, and the gut cells absorb CER and So.

There have been a few analyses of the amounts and types of sphingolipids in foods (Ohnishi and Fujino, 1982; Blank *et al.*, 1992; Jensen and Newburg, 1995); and as a result relatively little is known about the role that these components of the diet may contribute to, or protect against disease.

2.12.2 Fate and significance of sphingolipids

Sphingolipids serve as structural molecules in membranes (Hannun and Bell, 1989; Hakomori, 1990; Merrill, 1991) and as regulators of cell growth, differentiation and

neoplastic transformation through participation in cell-cell communication, cell receptors and signalling systems, and endothelial cell permeability (Merrill, 1991; Wang *et al.*, 1991). Ceramides derived from sphingolipid metabolism affect DNA synthesis. The role of CER as an intracellular second messenger for tumour necrosis factor -α (TNF-α), interleukin β (IL-β) and other cytokines; as well as So, So-1-phosphate among other sphingolipid metabolites, have been demonstrated to modulate cellular calcium homeostasis, cell cycle progression and apoptosis. Carcinogens and toxins may act via unscheduled initiation or inhibition of these pathways leading to disruption of metabolism of these molecules, and leading, ultimately, to the toxicity and carcinogenicity of these mycotoxins (Yoo *et al.*, 1992; Merrill *et al.*, 1993b).

2.13 SPHINGOLIPIDS AND THEIR METABOLISM

Sphingosine is a component of complex sphingolipids. The maintenance of a low concentration of free So and free Sa is important because these compounds have intrinsic biological activity (Hannun and Bell, 1989; Merrill and Stevens, 1989; Merrill, 1991; Riley *et al.*, 1994a). The regulated metabolism of complex sphingolipids result in the formation of lipid "second messengers" (hormones being the "first messengers") (Merrill and Jones, 1990; Ballou, 1992) that modulate cellular processes, including expression of genes and activation or inactivation of specific proteins (Ballou, 1992).

The major toxic effects of fumonisins are based on their disruptive effects on sphingolipid biosynthesis and accumulation of sphingoid bases leading to cell membrane damage (Wang *et al.*, 1996). Since long-chain sphingoid bases may be growth inhibitory, cytotoxic, induce apoptosis (Merrill, 1983; Stevens *et al.*, 1990; Nakamura *et al.*, 1996; Sweeney *et al.*, 1996; Yoo *et al.*, 1996) but can stimulate growth under certain conditions (Zhang *et al.*, 1990; 1991; Schroeder *et al.*, 1994); the accumulation of Sa and So might account for the aforementioned effects of fumonisins.

2.13.1 Biochemical pathways and compartmentalization of *de novo* sphingolipid biosynthesis

Essential to the understanding of how disruption of sphingolipid metabolism contributes to the diseases associated with consumption of fumonisins, is the understanding of sphingolipid biosynthesis. Studies on the kinetics of *de novo* sphingolipid biosynthesis are

usually conducted by following the incorporation of radiolabelled serine or fatty acids into long chain base components of complex sphingolipids such as SM and GSLs. The earliest effect of fumonisin on sphingolipid metabolism *in vitro* is the decrease in serine incorporation into CER (Figure 2.6), followed by an increase in free Sa concentration (Yoo *et al.*, 1992). Large increases in free Sa concentration in cells are observed within a few hours after exposure to fumonisins. Some of the Sa is metabolised to other bioactive intermediates, and some released from cells. In animals, free Sa accumulates in tissues and appears in blood and urine, with a concentration dependent decrease in more complex sphingolipids (Yoo *et al.*, 1996).

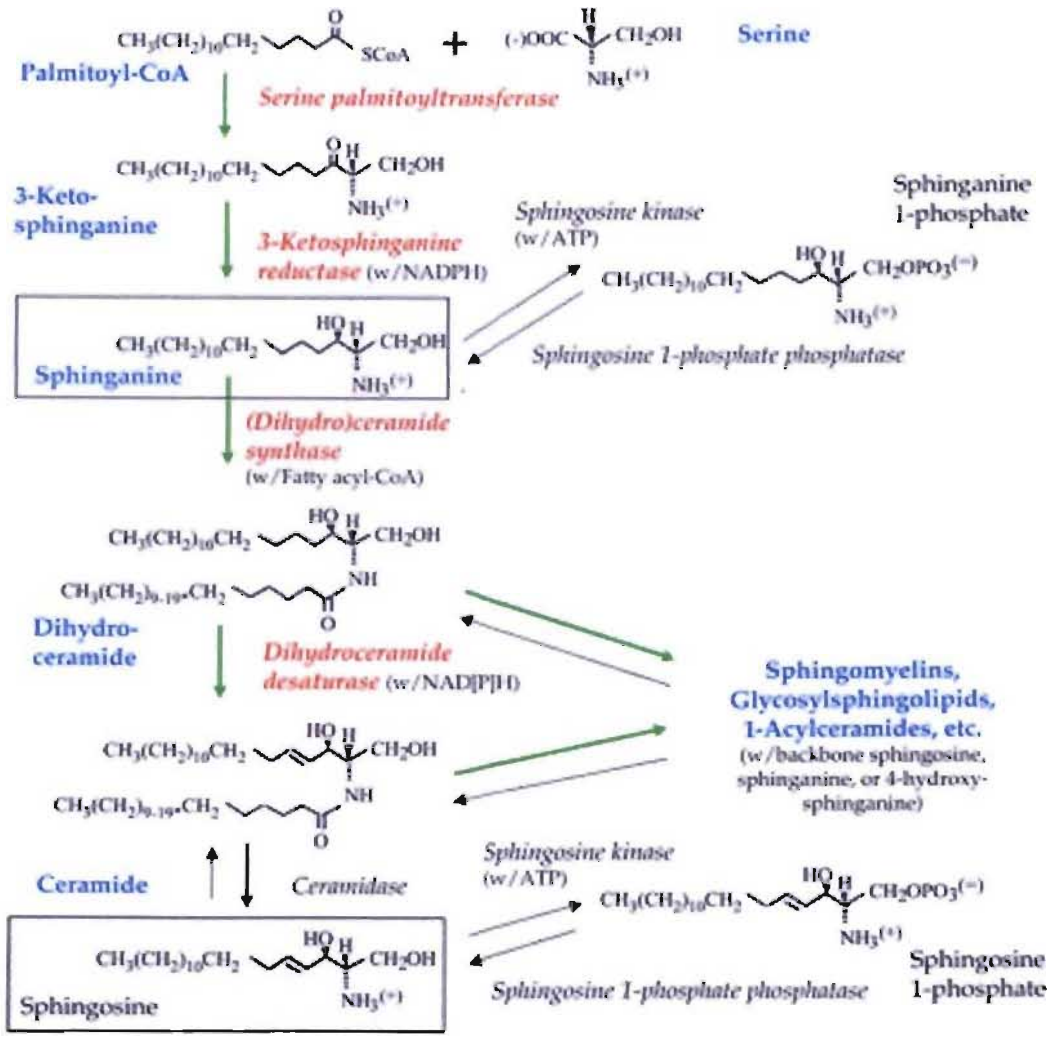

Figure 2.6: ***De novo*** **biosynthetic pathway for sphingoid bases and complex sphingolipids. The colour coding distinguishes the biosynthetic enzymes (with common names in *red* and *green* arrows for the reactions catalysed) and intermediates in *blue*) from additional reactions that occur with these intermediates (in *black*) (Merrill, 2002).**

De novo biosynthesis of GSLs is coupled to intracellular vesicular transport of the growing molecules through the cisternae of the Golgi apparatus and to the plasma membrane. Typically, *de novo* sphingolipid biosynthesis (Figure 2.6) proceeds via the following reactions (Merrill and Jones, 1990; Sweeley, 1991; Bell *et al.*, 1993): -

- The condensation of the amino acid L-serine with a fatty acyl-coenzyme A, usually palmitoyl-coenzyme A (palmitoyl-coA), to 3-ketoSa is catalysed by the enzyme serine palmitoyltransferase (SPT), a pyridoxyl 5'-phosphate-dependent enzyme.
- In the following reduced nicotinamide adenine dinucleotide phosphate (NADPH)-dependent reaction, 3-ketoSa is reduced to D-erythro-Sa by the enzyme 3-keto Sa reductase.
- Sphinganine is acylated to dihydroceramide (N-acyl Sa) by the CER synthase using various fatty acyl CoAs.
- Head-groups are subsequently added to the 1-hydroxyl group.
- The 4,5-trans-double bond of the So backbone is added after acylation of the amino group of Sa by the enzyme dihydroceramide desaturase (Merrill and Wang, 1986; Michel *et al.*, 1997).
- Both dihydroceramide and dihydrosphingomyelin are substrates for the enzyme. Thus, free sphingosine is not an intermediate of *de novo* sphingolipid biosynthesis (Merrill, 1991; Rother *et al.*, 1992).

The endoplasmic reticulum (ER) (and possibly the Golgi, mitochondrial associated membranes, and the nuclear membrane) is the primary site of *de novo* synthesis of CER, and several lines of evidence point to roles for this CER in mediating apoptosis. At the organelle level in animal cells, the initial steps from the condensation of serine and palmitoyl-CoA, through to the formation of CER takes place in the ER (Figure 2.7). Subsequent biosynthesis of GSLs and SM takes place in the Golgi apparatus. Ceramide is processed in the Golgi apparatus, and complex sphingolipids are packaged, sorted and transported to all cell membranes (Simons and van Meer, 1988; Schwarzmann and Sandhoff, 1990). The catabolism of complex sphingolipids occurs in the lysosomes, endosomes and the plasma membrane.

Sphingolipid turnover involves the hydrolysis of complex sphingolipids to ceramides, then to So. Free So released as a consequence of either regulated turnover or catabolism is quickly reacylated to CER (Wilson *et al.*, 1988) or is phosphorylated in the cytosol

and cleaved to a fatty aldehyde and ethanolamine phosphate in the ER (Van Veldhoven and Mannaerts, 1991), which is incorporated into phosphotidylethanolamine. The fatty aldehyde and ethanolamine phosphate can be redirected into the biosynthesis of glycerophospholipids and other fats with degradation of free sphingoid bases occurring in the cytosol.

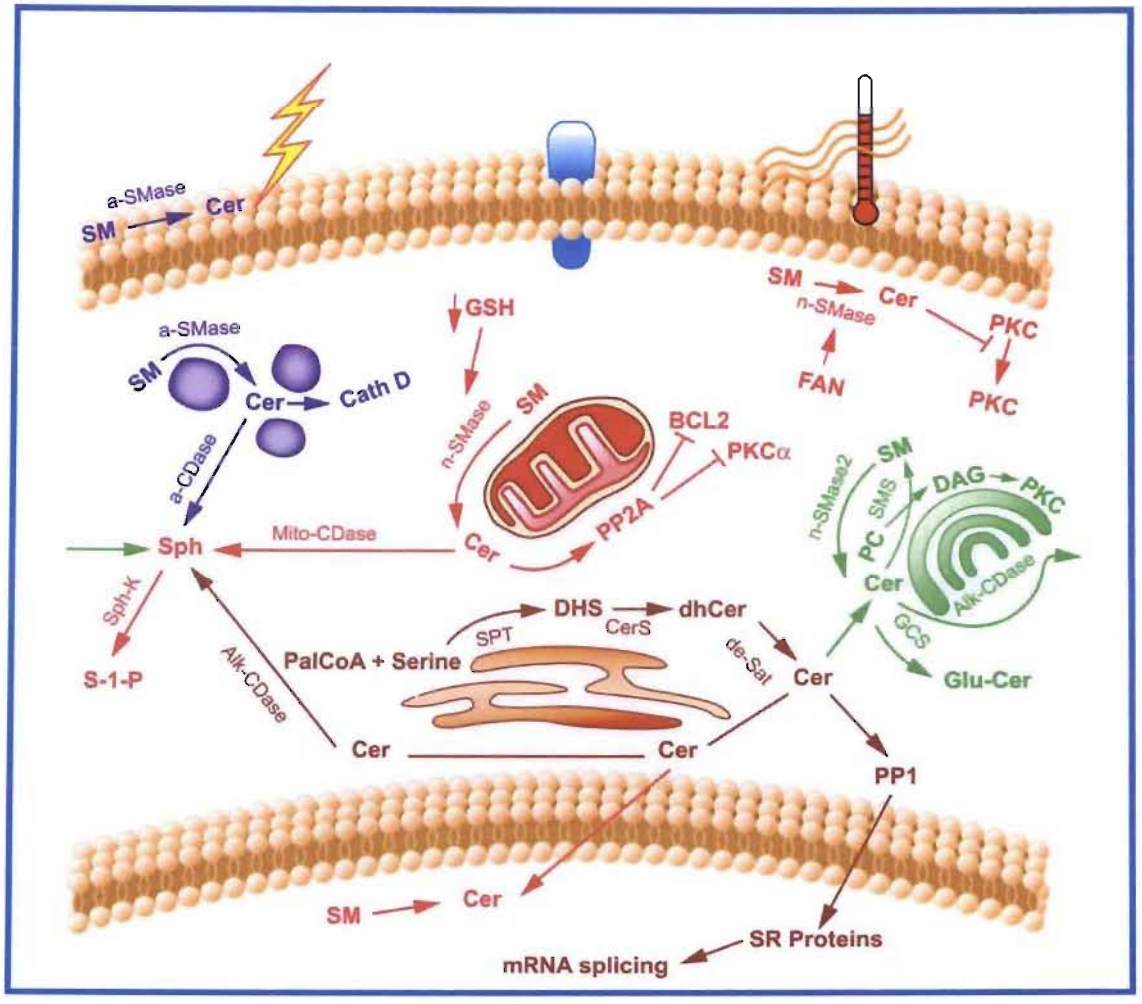

Figure 2.7: Compartmentalization of ceramide metabolism and function. Shown are several distinct compartments of ceramide metabolism and function. Abbreviations in the figure are Cer, ceramide; DHS, dihydrosphingosine, Cath D, cathepsin D, Sph, sphingosine, Sph-K, sphingosine kinase, Alk, alkaline, PalCoA, palmitoyl-CoA, SR, sarcoplasmic reticulum; dhCer, dihydroceramide, CerS, ceramide synthase, de Sat, desaturase, PC, phosphotidylcholine, SMS, SM synthase (Hannun and Obeid, 2002).

2.13.2 Functions of sphingolipids and their breakdown products in cellular regulation

The maintenance of a low level of free sphingoid bases in tissues is important, as these compounds are biologically active and cytotoxic in high concentrations. Elevation of

intracellular free sphingoid bases disrupts the regulatory mechanisms within cells. Complex sphingolipids such as gangliosides, interact with growth factor receptors, the extracellular matrix, and neighbouring cells, whereas the backbones, So and other sphingoid bases, ceramides, and sphingosine-1-phosphate (So-1-phosphate); activate or inhibit protein kinases and phosphatases, ion transporters, and other regulatory machinery. Tumour necrosis factor α, IL-β and nerve growth factor (NGF), for example, induce SM hydrolysis to CER. Other agonists, such as platelet-derived growth factor (PDGF), trigger further hydrolysis of CER to So, and activate So kinase to form So-1-phosphate. These metabolites either stimulate or inhibit growth, and may be cytotoxic in some cases via induction of apoptosis, depending on which products are formed or added exogenously, the cellular levels, intracellular localization, and the cell type. Ceramide and So-1 phosphate are second messengers with opposing roles in mammalian cell growth arrest and survival, their relative cellular level being proposed to be a rheostat that determines the fate of cells (Mandala *et al.*, 1998). Therefore, fumonisin disruption of sphingolipid metabolism and deregulation of lipid biosynthesis might impact many of these processes, and will likely have a variety of effects depending on cell type and other factors.

2.14 THE SPHINGOMYELIN PATHWAY, APOPTOSIS AND CERAMIDE

The SM pathway is a ubiquitous signalling system that links specific cell surface receptors and environmental stresses through to the nucleus (Hannun, 1994). Enzymes of CER metabolism show distinct subcellular localization. The plasma membrane (Figure 2.7) harbours a fraction of acid sphingomyelinase (SMase) and possibly a caveolar-associated neutral SMase (Andrieu-Abadie *et al.*, 2001), and generation of CER at the plasma membrane exerts distinct and specific functions, such as inhibition of protein kinase C (PKC) translocation, and aggregation of the *Fas* receptor (Hannun *et al.*, 2001; Paris *et al.*, 2001), but not other effects mediated by endogenous CER (apoptosis and cell cycle arrest (Hannun *et al.*, 2001). Activation of the apoptotic pathway by TNF-α, *Fas* and ionising radiation was mediated through the SM signal transduction pathway (Obeid *et al.*, 1993; Jarvis *et al.*, 1994; Cifone *et al.*, 1995) that is initiated by hydrolysis of SM by SMases to generate CER. The specificity of CER as a second messenger for apoptosis was demonstrated when cell permeable CER analogues were able to recapitulate the effects of TNF-α, *Fas* and ionising radiation and induce apoptosis directly (Obeid *et al.*, 1993; Jarvis *et al.*, 1994; Cifone *et al.*, 1995).

2.14.1 Ceramide in Apoptosis

Apoptosis is an inducible pre-programmed pathway of sequential biochemical events leading to activation of calcium and magnesium dependent endonucleases that cleave the nuclear chromatin at selective inter-nucleosomal linker sites (Wyllie, 1980; Vaux, 1993). Bose *et al.* (1995) demonstrated that CER synthase activity can be regulated in eukaryotes and constitutes definitive evidence for a requirement for CER elevation in the induction of apoptosis. Signals generated at the membrane of affected cells activate neighbouring intact cells and infiltrating macrophages to phagocytose dying cells and disintegrating nuclei (Duvall *et al.*, 1985).

The biosynthesis of sphingomyelin is approximately 10-fold more sensitive to inhibition by FB_1 than that of GSLs. This is also the case for other inhibitors of CER synthesis, such as ß-fluoroalanine (Medlock and Merrill, 1988; Merrill *et al.*, 1993b). Although excessive amounts of CER are often toxic and results in apoptosis of many cell types (Jarvis and Grant, 1998), a basal level of this messenger is required for cell proliferation and differentiation. Decreasing the steady-state CER leads to growth arrest and loss of differentiation (Spiegel and Merrill, 1996; Merrill *et al.*, 1997). Therefore, a delicate balance in CER levels is needed for maintenance of proper cell function.

2.14.2 Ceramide metabolism and disease

Deregulation in intracellular CER levels also has been implicated in diabetes, Acquired Immune Deficiency Syndrome (AIDS) and autoimmunity (Mathias *et al.*, 1998; Sandhoff *et al.*, 1998). Increasing evidence points to the roles of disruption of these pathways in disease pathogenesis. For example, the primary mutation responsible for hereditary neuropathy has been mapped to the LCB1 subunit of SPT, and it has been suggested to induce apoptosis of susceptible sensory neurons (Bejaoui *et al.*, 2001; Dawkins *et al.*, 2001). Ceramide levels have been shown to be elevated in a number of neurodegenerative disorders such as Batten's disorder, and two of the genes responsible for subtypes of this disorder, CLN3 and protein palmitoyl thioesterase, have been shown to attenuate ceramide levels in response to apoptotic stimuli, suggesting a role for the CER pathway in mediating cell dysfunction and death in these disorders (Puranam *et al.*, 1999; Cho *et al.*, 2000).

The absence of CER in specialized areas of the brain like the nigro-striatal neurons is believed to result in the death of these neurons leading to Parkinson's disease (France-Lanord *et al.*, 1997; Hunot *et al.*, 1997; Larocca *et al.*, 1997). C2-ceramide has been shown to protect hippocampal neurons from death induced by amyloid b-peptide, suggesting that a basal level of CER is required for the delay of Alzheimer's disease (Goodman and Mattson, 1996; Mattson *et al.*, 1997). Increases in CER are therefore notably beneficial for delaying the onset of neurodegenerative diseases.

This increase in CER may be manipulated to assist in limiting uncontrolled cell growth. High amounts of CER usually lead to apoptosis, and this property can be used as a powerful weapon for killing tumour cells. Ceramide has potential for eliminating aberrant cells in circumstances when they are not desired. Given the pleotropic functions of CER in a plethora of signalling systems and its involvement in the aetiology of many diseases, it is possible that new approaches to treat diseases could be initiated by modulating CER levels, either through reduction in *de novo* CER synthesis or CER release through blockade of neutral SMase and acidic SMase activity (Spiegel and Merrill, 1996; Merrill *et al.*, 1997).

2.14.3 Ceramide synthase and fumonisins

All fumonisins of the "B" series inhibit CER synthase at low or submicromolar concentrations (Wang *et al.*, 1991; Merrill *et al.*, 1993b; 1993c; 1996b). In assays of FA_1, less than 2% inhibition of CER synthase at 10μM was found. Acetylation therefore appears to reduce the potency by more than 50 fold. Removal of the tricarballylic acid (TCA) side chains (Figure 2.4) reduces the potency *in vitro* by approximately ten fold (Merrill *et al.*, 1993c).

In order to determine whether fumonisins inhibit other enzymes aside from CER synthase, that interact with either long chain bases or fatty acyl-CoA's, FB_1 was tested with So kinase (the enzyme initiating sphingoid base disposal) and SPT (the regulatory enzyme for sphingoid base synthesis) (Wang *et al.*, 1991). Neither enzyme was inhibited by the levels of fumonisins that result in complete inhibition of CER synthase (Merrill *et al.*, 1993b; 1996b).

Norred *et al.* (1997) assessed the relative potency of analogues of FB_1 to inhibit CER synthase. Fumonisin B_1, FB_2, FB_3, FB_4, FC_4, and TA toxin (a structurally similar mycotoxin produced by the tomato pathogen, *Alternaria alternata* f. sp. *lycopersici*) were approximately equipotent inhibitors. Hydrolysed FB_1, FB_2 and FB_3 were only 30-40% as potent as the parent toxins. Fumonisin A_1 did not block CER synthase, suggesting that FA_1 is non-toxic. Inhibition of CER synthase by fumonisin analogues did not appear to be related to the lipophilicity of the compounds. The ability of relatively high doses of other mycotoxins that bear no structural similarity to fumonisins, including aflatoxin B_1, cyclopiazonic acid, beauvericin, T2, sterigmatocystin, luteoskyrin, verrucarin A, scirpentriol, and ZEA to block CER synthase was also determined. All of the toxins tested were negative in the bioassay with the exception of fumonisins, indicating that disruption of sphingolipid metabolism is a specific cytotoxic response (Norred *et al.*, 1997).

Fumonisin B_1 inhibits CER synthase with either Sa or So as the substrate, and with a variety of fatty acyl-coenzyme As as the co-substrate (Wang *et al.*, 1991; Merrill *et al.*, 1993b; 1993c). The inhibition is competitive with both sphingoid bases and fatty acyl-CoA (Merrill *et al.*, 1993c) which indicates that fumonisin may inhibit CER synthase by interacting with both the binding site for Sa or So, and the site for the fatty acyl-CoAs (Merrill *et al.*, 1996b). Ceramides also affect DNA synthesis. The inhibition of CER synthase by fumonisins causes Sa to accumulate, and at least a portion of Sa undergoes phosphorylation and cleavage (Merrill *et al.*, 1993c).

2.15 FUMONISIN INDUCED DISRUPTION OF SPHINGOLIPID METABOLISM

The term "fumonisin-induced disruption of sphingolipid metabolism" includes the inhibition of So and CER biosynthesis, depletion of more complex sphingolipids, increase in free Sa, decrease in reacylation of So derived from complex sphingolipid turnover and degradation of dietary sphingolipids, increase in sphingoid base degradation products (i.e., So-1-phosphate, Sa-1-phosphate, ethanolamine phosphate and fatty aldehydes), and increase in lipid products derived from the increase in the sphingoid base degradation products (Merrill *et al.*, 1996b).

2.15.1 Fumonisin-induced disruption of sphingolipid metabolism in cell systems

To fully understand the ways that disruption of sphingolipid metabolism could account for the cell damage caused by fumonisins, it is necessary to consider: -

- the multitude of functions of complex sphingolipids (Bell *et al.*, 1993),
- the potent bioactivity of Sa and its metabolites (Merrill *et al.*,1993a), and
- the parallel or branch metabolic pathways that can be affected by disruption of sphingolipid metabolism (Riley *et al.*,1996; Merrill *et al.*, 1997).

Sphingolipids have been associated with many facets of cellular regulation (Merrill *et al.*, 1993a; Bell *et al.*, 1993; Ballou *et al.*, 1996; Merrill *et al.*, 1997; Kolesnick and Krönke, 1998; Perry and Hannun, 1998). Such associations could contribute to or modify the expression of fumonisin-associated diseases. Based on existing knowledge about some of the systems regulated by sphingolipids, mechanisms can be proposed whereby disruption of sphingolipid metabolism by fumonisins could account for the toxicity and carcinogenicity of these mycotoxins (Bose *et al.*, 1995; Strum *et al.*, 1995; Witty e*t al.*, 1996; Suzuki *et al.*, 1997).

Ceramide signalling is mediated by SM hydrolysis via enzymes that are not inhibited by fumonisin (Perry and Hannun, 1998). When fumonisins are added to cells for the purpose of inhibiting *de novo* CER generation, there is potential for accumulation of free sphingoid bases and their downstream sphingoid base-1-phosphates. Considerable data supports the hypothesis that fumonisin-induced disruption of sphingolipid metabolism is an important event in the cascade of events leading to cellular deregulation (Table 2.1). Several biochemical modes of action have been proposed to explain all, or some, of the fumonisin-induced animal diseases. Some invoke disruption of sphingolipid metabolism as the initial site of action, and there are also studies that hypothesize fumonisin-induced changes in key enzymes involved in cell cycle regulation, differentiation and/or apoptosis as initial or secondary sites of action (Merrill *et al.*,1995; 1996b; Riley *et al.*, 1996; Norred *et al.*, 1996; Merrill *et al.*, 1997; Norred *et al.*, 1998; Wang *et al.*, 1999). Fumonisins may effect/affect carcinogenesis by altering sphingolipid metabolism. Cellular regulatory processes modulated by sphingolipids are known to be important in the control of normal cell growth, differentiation, apoptosis and immune response (Table 2.1). Fumonisins impact many of these processes and have a variety of effects depending on cell type and other factors.

The two most likely explanations for the increased cell death after inhibition of sphingolipid biosynthesis by fumonisins are that the accumulation free Sa (or a Sa degradation product) are growth inhibitory and cytotoxic for the cells (Stevens *et al.*, 1990; Hannun *et al.*, 1991; Sweeney *et al.*, 1996), that complex sphingolipids are required for cell survival and growth, and loss of complex sphingolipid biosynthesis would be expected to alter cell behaviour, and lead to cell death. These hypotheses are based on findings with mutants of SPT, the initial enzyme of sphingolipid biosynthesis (Hanada *et al.*, 1990; 1992; Riley *et al.*, 1999) and in studies with specific inhibitors of GSL biosynthesis (Radin, 1994; Nakamura *et al.*, 1996).

Table 2.1: Mechanisms for cell behaviour changes, growth inhibition and cytotoxicity induced by fumonisin via disruption of sphingolipid metabolism.

Repression of expression of PKC, stimulation of a cyclic adenosine monophosphate (AMP) response element in CV-I African green monkey kidney cells (1-10μM FB_1, 3 to 16 hours)	Huang *et al.*, 1995
Decreased phorbol dibutyrate binding, increased cytosolic PKC activity, with both exogenous Sa and FB_1 to J774A1 cells	Smith *et al.*, 1997
Inhibition of phorbol dibutyrate binding in short-term incubations using crude cerebrocortical membrane preparation and both FB_1 and exogenous So	Yeung *et al.*, 1996
Activation of the mitogen-activated protein kinase (MAPK) in Swiss 3T3 cells with FB_1	Wattenberg *et al.*, 1996
Over-expression of nuclear cyclin D1 and increased cyclin-dependent kinase (CDK) 4 activity in rat livers obtained from a long-term feeding study and a 21-day feeding study with FB_1	Ramljak *et al.*, 2000
Dephosphorylation of the retinoblastoma protein, repression of CDK 2, and induction of two CDK inhibitors in CV-1 cells with FB_1	Ciacci-Zanella *et al.*, 1998
Apoptosis inhibitor and protease inhibitor protection of CV-1 cells and primary human cells from FB_1-induced apoptosis	Ciacci-Zanella and Jones, 1999
Increased TNF secretion in lipopolysaccharide-activated intra-peritoneal macrophages from FB_1-treated mice	Dugyala *et al.*, 1998
Glutathione depletion and lipid peroxidation in cultured cells	Kang and Alexander, 1996; Lim *et al.*, 1996; Abado-Becognee *et al.*, 1998; Abel and Gelderblom, 1998; Sahu *et al.*, 1998; Yin *et al.*, 1998

2. 15.2 Mutagenicity of fumonisin B_1 and related end-points

Fumonisin B_1, FB_2 and FB_3 were shown to be non-mutagenic in the *Salmonella* assay against the tester strains TA 97a, TA 98, TA 100 and TA 102, either in presence or absence

of the S9 microsomal preparation at a range of concentrations from 0 to 10 mg/plate (Gelderblom and Snyman, 1991). The non-mutagenicity of FB_1 to *Salmonella* tester strain TA 100 at concentrations up to 100mg per plate was supported by Park *et al.* (1992). Similar negative results were reported in gene mutation assays with FB_1 in *Salmonella* TA98 and TA100, as well as in SOS chromotest in *Escherichia coli* strain PQ37 (5, 16, 50, 166, 500μg/assay) in the presence and absence of metabolic activation, and differential DNA repair assays with *E. coli* K12 strains (343/753, uvrB/recA and 343/765, uvr^+ rec^+) (Knasmüller *et al.*, 1997).

In contrast, Sun and Stahr (1993), using a commercial bioluminescent bacterial (*Vibrio fischeri*) genotoxicity test, claimed that FB_1 showed genotoxic activity without the metabolic activation of S9 fraction at a range of 5-20 μg/ml. Fumonisin B_1 and FB_2 were non-genotoxic in an *in vitro* rat hepatocyte DNA repair assay at concentrations of 0.04-80μM/plate (and FB_2 at 0.04-40μM/ plate), as well as *in vivo* at 100 $mg.kg^{-1}$ of FB_1 or FB_2 (Gelderblom *et al.*, 1989; 1992). The finding that FB_1 does not induce unscheduled DNA synthesis was confirmed in an *in vitro* assay in primary hepatocytes at concentrations from 0.5-200μM (Norred *et al.*, 1990; 1992a; 1992b).

Gelderblom *et al.* (1988a; 1988b) found that fumonisins are complete carcinogens capable of inducing gamma-glutamyl-transpeptidase positive (GGTP) foci in the livers of both non-initiated and diethylnitrosamine (DEN) initiated rats. At low doses in rats, fumonisins appear to act primarily as tumour promoters (Gelderblom *et al.*, 1995a) and induce increased apoptosis (Tolleson *et al.*, 1996a). Single gavage doses of 50, 100 and 200 mg FB_1/kg body weight significantly ($p=0.05$) inhibited hepatocyte proliferation in partially hepatectomized male Fischer rats (Gelderblom *et al.*, 1995a). Inhibition of hepatocyte proliferation was also observed after dietary exposure to FB_1 (>50mg/kg diet) (Gelderblom *et al.*, 1996a). However, when evaluating the genotoxicity of several toxins to rat, FB_1 also inhibited DNA synthesis induced by epidermal growth factor (EGF) in primary rat hepatocytes (Gelderblom *et al.*, 1995a; 1995b).

Norred *et al.* (1992a) found FB_1 at 0.5-250 μM, to have no effect on unscheduled DNA synthesis. Sheu *et al.* (1996) on the basis of results in studies of FB_1 (10-1000μg/ml) in BALB/3T3 A31-1-1 mouse embryo cells concluded that FB_1 lacks *in vitro* transforming

activity. In these cells, FB_1 treatment produced transforming activity at 500 μg/ml, but not at lower or higher concentrations.

Intraperitoneal injection of FB_1 induced an increased frequency of micronuclei in mouse bone marrow polychromatic erythrocytes at 25 and 100 $mg.kg^{-1}$ (Aranda *et al.*, 2000). Micronuclei form when chromosomal fragments behave independently of remaining chromosomes during the division of cells damaged by genotoxic agents, and the frequency of micronuclei is considered to reflect genotoxic damage to cells. It was concluded that FB_1 induces *in vivo* genotoxicity in the absence of *in vitro* mutagenicity in *Salmonella* (Aranda *et al.*, 2000). Sahu *et al.* (1998) showed that FB_1 induced DNA strand breaks in isolated rat liver nuclei.

On the basis of negative genotoxicity data from experiments covering several endpoints using the Ames test and *in vitro* and *in vivo* assays (Gelderblom *et al.*, 1989; 1992; 1995a; Norred *et al.*, 1990; 1992a; Gelderblom and Snyman, 1991; Park *et al.*,1992) and positive results in a non-validated type of bacteria test (Sun and Stahr, 1993), the overall conclusion is that there is inadequate evidence that FB_1 is genotoxic.

More recently however, Bever *et al.* (2000) reported that the incubation of methanolic extracts of *Fusarium* cultures with DNA in the presence of rat liver S9 proteins resulted in the formation of DNA adducts. The chromatographic characteristics of these unidentified DNA adducts suggest they are hydrophobic. Therefore, the possibility exists that compounds present in *Fusarium* fungi might alkylate DNA and participate in the induction of *Fusarium* induced tumours (Bever *et al.*, 2000; Howard *et al.*, 2001).

2.15.3 Lipid peroxidation

Lipid peroxidation normally occurs at low levels in all cells and tissues, whereby free oxygen radicals attack the double bonds of polyunsaturated fatty acid side chains in phospholipid membranes. These fatty acids are then converted to lipid peroxides. Lipid peroxides and oxygen free radicals stimulate peroxidation reactions that are toxic to cells and membranes (Walsh, 1994). Some of their effects include endothelial cell injury and dysfunction, increased uptake of low-density lipoproteins into vessel walls (Hennig *et al.*, 1984), alterations in membrane fluidity (Halliwell and Gutteridge, 1990),

altered membrane permeability to ions and proteins, stimulation of mitogens and growth factors, modification and destruction of proteins (Rice-Evans and Burbon, 1993), decreased protein synthesis (Machlin and Bendich, 1987), DNA strand breakage (Floyd, 1990) and inactivation of enzymes, increased production of toxic aldehydes, increased intracellular calcium leading to activation of calcium dependent enzymes, such as proteases and phospholipases (Walsh, 1994).

The effects of FB_1 on lipid peroxidation were studied in Vero monkey kidney cells. Fumonisin B_1 was found to be a potent inducer of malondialdehyde, a secondary product formed during lipid peroxidation (Abado-Becognee *et al.*, 1998). Fumonisin B_1 also induced lipid peroxidation and DNA strand breaks in isolated rat liver nuclei at concentrations ranging from 40 to 300 μM (Sahu *et al.*, 1998). Fumonisin treatment has also been shown to increase the extent of lipid peroxidation in Fischer-344 rat primary hepatocytes, and in liver *in vivo* in a concentration and dose-dependent manner (Abel and Gelderblom, 1998).

2.15.4 Endothelial cell damage

Healthy endothelial cells maintain vascular integrity, prevent adhesion and influence the tone of underlying vascular smooth muscle (Flavahan and Vanhoutte, 1995). This interface between intra and extra-vascular compartments simultaneously allows transport of nutrients, waste products, regulatory molecules, and phagocytic cells across basement membranes (Jaffe, 1987). Damaged endothelial cells are unable to function, leading to increased capillary permeability, platelet thrombosis and increased vascular tone (Flavahan and Vanhoutte, 1995). Increased permeability of endothelial cell membranes in the systemic circulation to proteins could explain oedema.

Ramasamy *et al.* (1995) established that FB_1 alters sphingolipid metabolism in endothelial cells from porcine pulmonary arteries, and that FB_1 and D-erythro Sa interfere with their permeability barrier function. Ramasamy *et al.* (1995) showed that FB_1 increased the rate of albumin transfer across endothelial cell monolayers derived from pulmonary artery, and elevated Sa levels, the latter possibly explaining the loss of endothelial barrier function. By 24 hours, incubation of endothelial cells with 50μM FB_1 resulted in the Sa:So ratio, which is a frequently used indicator of exposure to this mycotoxin, increasing significantly from

approximately 0.19 to 6.8 (Ramasamy *et al.*, 1995).The blockage of *de novo* sphingolipid synthesis might therefore have weakened intercellular interactions, making the barrier "leaky". In addition, complex sphingolipids, as well as So and Sa, affect numerous signal transduction pathways, some of which have been implicated in the control of endothelial permeability (Hoek, 1992). Identification of the process/es that are affected could be complex, because there is evidence for both transcellular and paracellular pathways for macromolecule transport.

A simple explanation for the reduction in the permeability barrier may be that the FB_1 (and/or the Sa that accumulates) killed a substantial portion of the cells. Yoo *et al.* (1992) showed that in the LLC-PK_1 pig renal epithelial cell line, there was a close association between the inhibition of sphingolipid biosynthesis by FB_1 and growth inhibition and toxicity. However, Ramasamy *et al.* (1995) found no evidence of cytotoxicity based on using trypan blue exclusion and morphology in the porcine pulmonary artery endothelial cells at any of the concentrations of FB_1 tested. Therefore, cytotoxicity does not appear to account for the increase in albumin transfer in this cell model. Studies with fatty acids (Hennig *et al.*, 1984; Ramasamy *et al.*, 1991) also showed increased albumin transfer without significant loss of cell viability (Ramasamy *et al.*, 1995).

Accumulation of Sa may play a role in the disruption of barrier function by FB_1, but this is unlikely to account for all of the effects of this mycotoxin. The concentrations of FB_1 that affected the endothelial cells were similar to the amounts toxic to the pig renal epithelial line LLC-PK_1 (Yoo *et al.*, 1992), and that were mitogenic for Swiss 3T3 cells (Schroeder *et al.*, 1994). They are much lower than the concentration that was toxic for cultured hepatocytes (>100μM) (Gelderblom *et al.*, 1995b). Since fumonisins are nephrotoxic and hepatotoxic *in vivo* (Riley *et al.*, 1994b), this implies that vascular endothelium may be as sensitive as these known target organs. Effects of fumonisin (and/or Sa) on endothelial cells (Ramasamy *et al.*, 1995), might contribute to the pathogenesis of diseases caused by these mycotoxins. A disrupted or damaged endothelium will allow increased penetration of plasma components into underlying tissues. Based on these findings regarding the ability of FB_1 to affect the endothelial cells in culture, the possibility exists that this mycotoxin may affect vascular function *in vivo*.

2.15.5 The role of fumonisins in mitogenesis

At low doses, fumonisins appear to be mainly tumour promoters (Gelderblom *et al.*, 1988a). Tumour promoters are often mitogens, which is intriguing since Spiegel *et al.* (1993) have shown that So and So 1-phosphate can induce DNA synthesis in growth arrested Swiss 3T3 cells (Zhang *et al.*, 1990; Zhang *et al.*, 1991). The amount of free Sa that accumulates in cells is a function of the extent of inhibition of CER synthase, concentration of essential precursors (serine, palmitoyl-CoA), and growth rate of cells, the rate of Sa degradation, and the rate of elimination from cells.

Using Swiss 3T3 cells, Schroeder *et al.* (1994) demonstrated that addition of FB_1 to cells elevated Sa and induced an increase in [^{3}H] thymidine incorporation into DNA. Furthermore, fumonisin-induced accumulation of free Sa was blocked by addition of an inhibitor of SPT, β-fluoroalanine, which blocks the initial step of sphingolipid biosynthesis. β-fluoroalanine which reduces the fumonisin induced accumulation of free Sa, but not the inhibition of complex sphingolipid biosynthesis, prevented the fumonisin-induced stimulation of DNA synthesis, but had no effect on mitogenesis when added alone. This indicates that FB_1 did not cause accumulation of Sa 1-phosphate, and that sphingoid bases *per se* can stimulate DNA synthesis. Schroeder *et al.* (1994) suggest that disruption of sphingolipid metabolism by fumonisins might cause cancer due to the mitogenic potential of these compounds, and hypothesised that fumonisin might induce DNA synthesis via the accumulation of Sa.

2.16 MOLECULAR MECHANISM OF ACTION OF FUMONISINS, SIGNAL TRANSDUCTION PATHWAYS, SPHINGOLIPIDS AND FUMONISIN B_1

Fumonisins cause compositional or oxidative damage to cellular lipids, which in turn cause molecular events culminating in oxidative damage to DNA and other critical macromolecules (Gelderblom *et al.*, 1996b; 1997; Abado-Becognee *et al.*, 1998; Abel and Gelderblom, 1998; Sahu *et al.*, 1998; Yin *et al.*, 1998). Wang *et al.* (1991) discovered that fumonisins inhibit CER synthase leading to disruption of *de novo* sphingolipid biosynthesis. The immediate consequences are accumulation of Sa and So, an increase in the Sa:So ratio, and depletion of complex sphingolipids. Recognizing the importance of sphingolipids in cell regulatory processes, including those related to proliferation and apoptosis, investigators proposed that the critical mechanistic step in fumonisin toxicity

was inhibition of CER synthase, starting a cascade of molecular events leading to cytotoxicity or neoplasia (Merrill, 1991; Riley *et al.*, 1994a; Hannun and Obeid, 1995; Merrill *et al.*, 1997),.

Different hypotheses on the ability of FB_1 to alter signal transduction pathways and its potential role in carcinogenesis exist. Protein kinase C is a pivotal enzyme in cell regulation and signal transduction. Sphingosine is a potent and reversible inhibitor of PKC. Based on the ability of free sphingoid bases to inhibit PKC, it is possible that fumonisin repression of PKC activity is secondary to fumonisin-disruption of sphingolipid metabolism. Huang *et al.* (1995) treated green monkey kidney cells with FB_1 and found that fumonisin represses expression of PKC and AP-1 dependent transcription. In contrast, fumonisin stimulated a simple promoter containing a single cyclic AMP response element. Since fumonisin did not alter protein kinase A (PKA) activity, it appears that cyclic AMP response element activation was independent of PKA. Huang *et al.* (1995) concluded that altered signal transduction pathways played a role in the carcinogenesis of fumonisins. Similar results were found for baby hamster kidney cells treated with FB_1 (Abeywickrama and Bean, 1992).

The activation of MAPK results in the modulation of transcription and activation of enzymes involved in signal transduction such as cytoplasmic phospholipase A2 (cPLA2), which releases arachidonic acid (AA) from membrane phopholipids. Arachidonic acid is the precursor of prostaglandins and leukotrienes, two inflammatory mediators that regulate gene expression and protein kinase activity among other effects. Fumonisin B_1 increases PKC translocation and stimulates MAPK. Pinelli *et al.* (1999) in an investigation on effects of FB_1 on the AA cascade in the W126 VA human bronchial epithelial cell line, found that FB_1 stimulated cPLA2 activity and increased AA release by a mechanism independent of PKC activation. The activation of cPLA2 was found to be a two-step process: the first being its phosphorylation by MAPK, and the second was a consequence of the increase in So inside and outside the cells after two hours, which is known to induce a rise in intracellular free calcium. Overall, this suggests that the effect of FB_1 on cells is partially dependent on the action of FB_1 on the enzymes involved in the cell cycle, such as MAPK and PKA, and on bioactive fatty acids, such as the prostaglandins and leukotrienes, and on disruption of sphingolipid metabolism (Pinelli *et al.*, 1999).

In a study by Ramljak *et al.* (2000), which suggested the mechanism by which FB_1 acts as a carcinogen, the over-expression of cyclin D1 protein was shown in both pre-neoplastic and neoplastic liver specimens obtained from a long-term feeding study of FB_1 in rats. In rats fed FB_1 short-term, cyclin D1 protein levels in liver were increased up to five-fold in a dose-responsive manner. Northern blot analysis demonstrated no increase in messenger ribonucleic acid (mRNA) levels of cyclin D1. Two-dimensional electrophoresis of cyclin D1 protein in FB_1-treated samples showed a distinct pattern of migration (presence of less negatively charged form of the protein) that differed from controls. Recently, it has been shown that phosphorylation of cyclin D1 by glycogen synthase kinase 3 β (GSK-3β) on a single threonine residue (Thr-286) positively regulates proteosomal degradation of cyclin D1. In FB_1-treated samples, GSK-3β phosphorylated on serine 9 was detected. Activated protein kinase B (aPKB) appeared to be responsible for this inhibitory phosphorylation. These findings suggest that over-expression of cyclin D1 results from stabilization due to a lack of phosphorylation mediated by GSK-3β. An increase in CDK4 complexes with cyclin D1 in FB_1-treated samples was also observed. This study showed that the activation of aPKB leads to increased survival, inhibition of GSK-3β activity and post-translational stabilization of cyclin D1, all events responsible for disruption of the cell cycle G1/S restriction point in hepatocytes (Ramljak *et al.*, 2000).

2.17 APOPTOSIS BY FUMONISINS

2.17.1 *In vivo* studies with rodents

Fumonisin B_1 administered to different animal species increased apoptosis in various tissues (Lim *et al.*, 1996; Tolleson *et al.*, 1996a; Voss *et al.*, 1996a; Sharma *et al.*, 1997; Bucci *et al.*, 1998; Haschek-Hock *et al.*; 1998; Ciacci-Zanella and Jones, 1999; Lemmer *et al.*, 1999; United States National Toxicology Program, 1999). Increased apoptosis seems to play a role in toxic effects including tumour induction by FB_1. In most studies, apoptosis is one of the observations on which the no-observed-adverse-effect level (NOAEL) is based. The dose level causing apoptosis depends on the duration of exposure, and can vary in rodents from 0.9 to 12mg FB_1/kg body weight (respectively in long-term and short-term experiments). Oxidative damage has also been indicated in the aetiology of toxic effects (Abel and Gelderblom, 1998).

Studies with rats have shown fumonisin-induced apoptosis in both liver and kidney. Male and female F344 rats were fed FB_1 (99, 163, 234, and 484 parts per million (ppm)) for 28 days and the organs examined histologically. Apoptosis was seen in hepatocytes at the lowest dose level, and the prevalence and severity increased with increasing dose. There was a dose dependent decrease in liver and kidney weights in the rats. The liver weight loss was accompanied by the induction of apoptosis and hepatocellular and bile duct hyperplasia in both sexes, with the female rats being more responsive at lower doses. The induction of tubular epithelial cell apoptosis was the primary response of the kidneys to dietary FB_1. Apoptosis was present at all doses in the kidneys of male rats, and occurred in females only at 163, 234 and 484ppm FB_1 (Tolleson *et al.*, 1996a).

In a study on Fischer rats and B6C3F1 mice, FB_1 caused renal carcinomas in male rats and liver cancer in female mice. In male BD-IX rats, FB_1 caused hepatic toxicity and hepatocellular carcinomas. An early effect of FB_1 exposure in these target organs was apoptosis. However, there was also some evidence of oncotic necrosis following FB_1 administration, especially in the liver. Induction of apoptosis may be a consequence of CER synthase inhibition and disruption of sphingolipid metabolism by FB_1. Dragan *et al.* (2001) hypothesise that FB_1 may be the first example of an apparently non-genotoxic agent producing tumours through a mode of action involving apoptotic necrosis, atrophy, and consequent regeneration.

Sharma *et al.* (1997) administered subcutaneous injections (0 to 6.25 $mg.kg^{-1}$) of FB_1 daily for five days to male BALB/c mice. Their liver and kidneys were sampled one day after the last injection, and a decrease in kidney weight was observed. An evaluation of stained sections revealed dose-dependent FB_1-associated hepatic and renal lesions in all groups. Terminal uridine triphosphate (UTP) nick-end labelling (TUNEL) in liver and kidney sections confirmed the presence of dose-related apoptotic cells, at all treatment levels. Thus, FB_1 produced apoptosis after a brief exposure to relatively low doses. The toxicity of FB_1 was greater than previously found in studies on oral toxicity (Sharma *et al.*, 1997).

2.17.2 Apoptosis in *in vitro* models

Increased apoptosis has been reported following *in vitro* exposure to FB_1 in turkey lymphocytes (Dombrink-Kurtzman *et al.*, 1994), human keratinocytes, fibroblasts,

oesophageal cells and hepatoma cells (Tolleson *et al.*, 1996b), and CV-1 monkey kidney cells (Wang *et al.*, 1996). Tolleson *et al.* (1996b) found that FB_1 inhibited incorporation of [^{3}H] thymidine by cultured neonatal human keratinocytes and HepG2 human hepatocarcinoma cells at 10^{-7} and 10^{-4}M, respectively. Fumonisin B_1 also inhibited clonal expansion of normal human keratinocytes and HET-1A human oesophageal epithelial cells at 10^{-5}M and growth in mass culture of normal human fibroblasts at 10^{-7}M. The clonogenicity of normal human keratinocytes decreased to 45.5% of controls after exposure to 10^{-4}M FB_1 for two days. However, no differences in the cell cycle distribution of cultured keratinocytes were noted after exposure to 10^{-5}M FB_1 for 40 hours. The viability of normal human keratinocytes and HET-1A cells decreased as a result of FB_1 treatment, as determined by a fluorescein diacetate and propidium iodide (PI) flow cytometric cell viability assay. Fumonisin B_1 treated keratinocytes released nucleosomal DNA fragments into the medium 2-3 days after exposure to 10^{-4}M FB_1 and more DNA strand breaks were detected in attached keratinocytes exposed to 0-10^{-4}M FB_1 using a terminal deoxynucleotidyl transferase-based immunochemical assay system. Furthermore, FB_1-treated keratinocytes and HET-1A cells developed morphological features consistent with apoptosis, shown by phase contrast microscopy, fluorescent microscopy of acridine orange (AcO) stained cells, and electron microscopy (EM) (Tolleson *et al.*, 1996b).

Tolleson *et al.* (1999) further examined the role of sphingolipid changes in FB_1-stimulated apoptosis. Sphinganine accumulated rapidly, So levels remained unchanged, and CER decreased during FB_1 exposure. Increased DNA fragmentation, decreased viability, and apoptotic morphology were observed in cells exposed to FB_1, Sa or N-acetyl So. Co-exposure to N-acetyl So or β-chloroalanine, which blocks Sa accumulation, partially protected cells from FB_1-induced apoptosis. These results illustrate three sphingolipid-dependent mechanisms for inducing apoptosis; accumulation of excess CER, accumulation of excess Sa, and depletion of CER or complex sphingolipids derived from CER.

Incubation of human colonic HT29 cells, with FB_1 or the aminopentol (AP_1) caused a significant reduction in cell number. The AP_1 was less potent with 50μM AP_1 causing the same reduction in cell number (~30% after 24 hr) as 10μM FB_1. The reduction in cell number reflected increases in DNA fragmentation, and the percentage of apoptotic cells. Both FB_1 and AP_1 caused the accumulation of Sa (25 and 35-fold by 10μM FB_1 and 50μM AP_1, respectively); thus, concentrations of FB_1 and AP_1 that caused comparable reductions

in cell number were also similar with respect to elevation of Sa, which is growth inhibitory and cytotoxic. Inhibition of the first step of sphingolipid biosynthesis with myriocin (ISP-1) prevented the elevation in Sa, DNA fragmentation, and apoptosis induced by FB_1. Therefore, these effects of FB_1 on HT29 cells can be attributed to the accumulation of Sa (Schmelz *et al.*, 1998).

Wang *et al.* (1996) established that FB_1-induced apoptosis, or cell cycle arrest, in CV1 African green monkey kidney fibroblasts, by assessing the appearance of apoptosis, cell cycle regulation, and putative components of signal transduction pathways involved in apoptosis. The addition of FB_1 to CV1 cells induced formation of DNA ladders, compaction of nuclear DNA, and appearance of apoptotic bodies. Fumonisin B_1 also induced cell cycle arrest in the G1 phase in CV1 cells (Wang *et al.*, 1996).

In a subsequent study, Jones *et al.* (2001) identified genes that inhibit FB_1-induced apoptosis in CV1 cells and two mouse embryo fibroblast (MEF) lines. A baculovirus gene p53, and inhibitor of apoptosis, CpIAP, protected these cells from apoptosis. CpIAP blocks apoptosis induced by the tumour necrosis factor (TNF) pathway, as well as via other mechanisms. Further support for the involvement of the TNF signal transduction pathway in FB_1 induced apoptosis, was the cleavage of caspase 8. Inhibition of caspases by the baculovirus gene p35 also inhibited FB_1-induced apoptosis. The tumour suppressor gene p53 was not required for FB_1 induced apoptosis because p53-/- MEF undergoes apoptosis following FB_1 treatment. Furthermore, Bcl-2 was not an effective inhibitor of FB_1-induced apoptosis in CV1 cells or p53+/+ MEF. These results provide information to understanding the mechanism by which FB_1 induces apoptosis (Jones *et al.*, 2001).

2. 18 APOPTOSIS BY SPHINGOID BASES

Sphingosine induces apoptosis in neutrophils (Ohta *et al.*, 1994). Jarvis *et al.* (1996) also documented the ability of sphingoid bases to induce apoptosis in HL60 and U937 cells. Exposure to either So or Sa for six hours promoted apoptotic degradation of genomic DNA. The DNA damage correlated directly with reduced cloning efficiency, and was associated with the appearance of apoptotic cytoarchitectural traits. At sub-lethal concentrations (≤750nM), however, sphingoid bases synergistically augmented the apoptotic capacity of CER (10μM), producing both a leftward shift in the CER concentration-response profile and a pronounced increase in the response to maximally

effective levels of CER. Thus, So and Sa increased both the potency and efficacy of CER (Jarvis *et al.*, 1996).

Sweeney *et al.* (1996) reported that So and its methylated derivative N,N,-dimethyl So (DMS) induced apoptosis in cancer cells of both haematopoietic and carcinoma origin. In human leukaemic cell lines CMK-7, HL60 and U937, treatment with 20μM So for six hours caused apoptosis in up to 90% of cells. Human colonic carcinoma cells HT29, HRT18, MKN74 and COLO205 were shown to be more susceptible to apoptosis upon addition of DMS (>50%) than of So (<50%), yet were weakly or not sensitive to N, N, N-trimethyl So (TMS). Under the same conditions in the presence of serum, neither So-1-phosphate nor CER analogues C2-, C6- or C8-CER were able to induce apoptosis in any cell lines. However, in the absence of serum, CER analogues induced apoptosis in leukaemic cell lines after 18 hours, yet much less so than So or DMS. Furthermore, apoptosis induced by So or DMS could not be inhibited by FB_1. Apoptosis was not induced by sphingolipids in primary culture cells, such as HUVEC or rat mesangial cells, but was apparent in transformed rat mesangial cells. Additionally, apoptosis induced by So, DMS or C2-CER were inhibited by protease inhibitors. These data support evidence that the catabolic pathway of SM involving So and other metabolites is an integral part of the apoptosis pathway (Sweeney *et al.*, 1996).

Gennero *et al.* (2002) studied the apoptotic effect of So-1-phosphate and increased So-1-phosphate hydrolysis on mesangial cells, and found that So-1-phosphate stimulated proliferation of rat mesangial cells and phosphorylation of MAPKs at sub-confluent cell density. Mesangial cells expressed several So-1-phosphate receptors of the endothelial differentiation gene (EDG) family: EDG-1, -3, -5, and -8. Conversely, So-1-phosphate induced apoptosis at low cell density ($2x10^4$cells/cm^2), which was demonstrated by flow cytometry and Hoechst staining. Apoptosis was observed also in quiescent or growing cells. Incubation with [^{33}P] So-1-phosphate, [^{3}H] So-1-phosphate and [^{3}H] So demonstrated increased So-1-phosphate hydrolysis, resulting in enhanced intracellular So levels and decreased So-1-phosphate levels. Therefore, Gennero *et al.* (2002) suggested that So and decreased So-1-phosphate are primarily responsible for So-1-phosphate-induced apoptosis, and that incubation of low density mesangial cells with So-1-phosphate results in apoptosis, presumably due to increased So-1-phosphate hydrolysis.

2.19 INHIBITION OF *DE NOVO* SPHINGOLIPID BIOSYNTHESIS IN CULTURED CELLS

Theoretically, the balance between the intracellular concentration of effectors that protect cells from apoptosis, and those that induce apoptosis, determine cellular responses. As the balance between the rates of apoptosis and proliferation are important in tumorigenesis, cells sensitive to the proliferative effect of decreased CER and increased So-1-phosphate may be selected to survive and proliferate when free sphingoid base concentration is not growth inhibitory. Conversely, when the increase in free sphingoid bases exceeds a cell's ability to convert Sa:So to dihydroceramide/CER, or their sphingoid base 1-phosphate, then free sphingoid bases will accumulate. In this case, cells that are sensitive to sphingoid base-induced growth arrest will die, and non-sensitive cells will survive. If the cells selected to die are of normal phenotypes, and the cells selected to survive are abnormal, then cancer risk will increase (Riley *et al.*, 2001).

The potential for fumonisins to inhibit *de novo* sphingolipid biosynthesis was examined in cultures of hepatocytes obtained from male Sprague-Dawley rats and in rat liver microsomes. Fumonisin B_1 caused almost complete inhibition of [^{14}C] So formation by hepatocytes. Similar inhibition occurred when [^{14}C] serine and FB_1 were added together for 2 or 16 hours, and when the cells were incubated for 16 hours with FB_1 before addition of [^{14}C] serine. Fumonisin B_2 produced a comparable degree of inhibition. Wang *et al.* (1991) speculated that similarities between the fumonisins and sphingoid bases allowed their recognition as substrate (or transition state or product) analogues of CER synthase. It was further speculated that the absence of a hydroxyl group at carbon 1 may have altered their orientation in the active site of the enzyme and precluded acylation or, if acylated, resulted in an inhibitory CER that could not be removed by addition of a sphingolipid headgroup at that position.

Wang *et al.* (1991) conducted further *in vitro* assays of So N-acyltransferase using rat liver microsomes, and followed the conversion of [^{3}H] So to [^{3}H]CER by rat hepatocytes. Results showed that 0.1μM of FB_1 caused 50% inhibition in So N-acyltransferase activity. When rat hepatocytes were incubated with 1μM FB_1 and 1μCi of [^{3}H] So for one hour, the conversion of [^{3}H] So to CER was significantly inhibited ($p<0.05$) compared to that of untreated control cultures, with an approximate concentration giving 50% inhibition of cell proliferation (IC_{50}) of 0.1μM. These results provide identification of a biochemical target

for the action of fumonisins and imply that inhibition of *de novo* sphingolipid biosynthesis *in vitro* may underlie the hepatotoxicity and hepatocarcinogenicity of this mycotoxin *in vivo* (Wang *et al.*, 1991).

Cytotoxicity studies in primary rat hepatocytes and binding studies using subcellular fractions indicate that [^{14}C] FB_1 binds tightly to hepatocytes and microsomal and plasma membrane fractions (Cawood *et al.*, 1994).

Investigations on pig kidney epithelial cells showed that the fumonisins were potent inhibitors of sphingolipid biosynthesis in the cells, killing the renal cells after three days at 70μM of FB_1 (Yoo *et al.*, 1992). Fumonisin B_1 and FB_2 between 10 and 35μM inhibited cell proliferation in the LLC-PK_1 cells, whereas higher concentrations (>35μM) killed cells. Inhibition of cell proliferation and cell death were preceded by a lag period of at least 24 hours during which cells appeared to be functioning normally. Inhibition of *de novo* sphingolipid biosynthesis occurred before inhibition of cell proliferation or cytotoxicity, and the dose response for decrease in [^{3}H] So:[^{3}H] Sa ratio at seven hours closely paralleled the dose response for effects on proliferation and cytotoxicity at three-five days. In addition, the level of free Sa and to a lesser extent So, increased in fumonisin treated-cells in a dose dependent manner. The fact that Sa accumulated to a much greater extent than So, suggested that the *de novo* pathway was the primary target for inhibition, and as a result of this differential inhibition, the Sa:So ratio increased after exposure to fumonisin. These increases occurred long before any indication of cytotoxicity. These results support the hypothesis that inhibition of *de novo* sphingolipid biosynthesis is an early event in the toxicity of fumonisins to LLC-PK1 cells (Yoo *et al.*, 1992).

Other consequences of fumonisin inhibition of CER synthase include increase in degradation products from catabolism of free sphingoid bases (Merrill *et al.*, 1993a;1993b), increase in lipid products derived from increases in sphingoid base degradation products (Smith and Merrill, 1993), and increase in free So presumably from inhibition of reacylation of So derived from either the diet or catabolism of complex sphingolipids (Yoo *et al.*, 1992; Merrill *et al.*, 1993b).

Fumonisin B_1 stimulates Sa-dependent DNA synthesis in Swiss 3T3 cells, but is mitoinhibitory and growth inhibitory in many cell systems (Merrill, 1983;

Stevens *et al.*, 1990; Zhang *et al.*, 1990). Schroeder *et al.* (1994) found that free sphingoid bases can act as mitogens, however that the critical concentration of cellular sphingoid bases necessary to stimulate mitogenesis is within a range and the effects were cell-type specific. Fumonisins that cause sphingoid base accumulation can therefore be regarded as tumour promoters, possibly by stimulating cell proliferation. The exogenous addition of So and So-1-phosphate to Swiss 3T3 cells was also shown to stimulate DNA synthesis (Zhang *et al.*, 1990; Spiegel *et al.*, 1993). In contrast, other studies indicate that accumulation of sphingoid bases and depletion of complex sphingolipids were contributing factors to growth inhibition and increased cell death (Spiegel and Merrill, 1996).

While So has little difficulty in crossing cell membranes (Hannun *et al.*, 1991), the half-life of Sa inside LLC-PK1 cells is much longer than that of FB_1 in LLC-PK1 cells (Riley *et al.*, 1998), which suggests either that the inhibition of Sa N-acyltransferase is persistent, that Sa does not easily diffuse out of cells, or that Sa degradation is slow relative to its biosynthesis. Studies with LLC-PK1 cells also indicate that a low, but persistent pool of [^{14}C] labelled material is retained inside cells long after the rapidly diffusible pool of [^{14}C] fumonisin has exited the cells (Riley *et al.*, 1998). This retained pool appears to be capable of maintaining the elevation of cellular free sphingoid base concentration, a biomarker of fumonisin exposure (Solfrizzo *et al.*, 1997; Riley *et al.*, 1998; Wang *et al.*, 1999). Riley *et al.* (1999) using the same cell system showed that fumonisin inhibition of cell proliferation and increased cell death (apoptosis) are prevented by >90% using the SPT specific inhibitor, ISP1 (Riley *et al.*, 1999). Similar results were obtained with the HT29 human colonic cell line (Schmelz *et al.*, 1998).

Fumonisin B_1 elevated intracellular free Sa levels in both LLC-PK1 and Chinese hamster ovary fibroblast (CHO) cells (Yu *et al.*, 2001). However, CHO cells were resistant to fumonisin cytotoxicity at 50μM, while LLC-PK1 cells were sensitive at concentrations >35μM. Adding exogenous Sa to the CHO cells along with 50μM FB_1 treatment for 72 hours caused both necrosis and apoptosis. It was concluded that elevated endogenous Sa acts as a contributing factor to fumonisin-induced cell death (Yu *et al.*, 2001).

2. 20 THE EFFECT OF FUMONISIN B_1 ON OXYGEN TRANSPORT

Yin *et al.* (1996a) used electron spin resonance (ESR) spin label oximetry to study the effect of FB_1 on oxygen transport in phosphotidylcholine bilayers. Moreover, the use of

spin label attached to different carbons of fatty acids facilitated structural and oximetric determinations with the same test sample. The incorporation of 10 mol %FB_1 increased the oxygen transport properties of both saturated and unsaturated membranes at 37°C by approximately 30% and decreased the ordering of the hydrocarbon chains near the surface of the membranes. Concomitantly, oxygen transport near the centre of bilayers was diminished slightly, and the relative oxygen diffusion-concentration product profile curves were markedly flattened.

Yin *et al.* (1996b) used ESR spectroscopy and spin label techniques further to study the effects of FB_1 and AP_1 on the structural and dynamic properties of phosphatidylcholine membranes at the molecular level. Multilamellar liposomes consisting of dimyristoylphosphatidyl-choline (DMPC) and egg yolk phosphatidylcholine (EYPC) were used. In the fluid phase membrane, FB_1 significantly increased the fluidities of *n*-doxylstearic acid spin labels attached to carbons 5 and 7, which disordered the alkyl chains and perturbed the surface region of the bilayer. By comparison, minimal effects were detected near the middle of the bilayer. In the gel phase, FB_1 and AP_1 decreased membrane fluidity, which further enlarged the change in ordering on the phase transition. Fumonisin B_1 also restricted the mobility of the rigid cholestane spin label. A reduction in mobility of the temp-stearate spin label suggests that the TCA moieties of FB_1 might mimic the structure of polar head groups in phospholipids. These results that show fumonisins disturbed the ordering of membranes, provide additional mechanisms to elucidate toxicological activities of fumonisins.

Subsequently Yin *et al.* (1998) studied the effects of FB_1 on lipid peroxidation in membranes. In this study of the interaction between FB_1 and lipid bilayers, fumonisins disturbed the ordering of membranes, enhanced oxygen transport in membranes, and also increased membrane permeability. The results provided the first evidence that fumonisin appears to increase the rate of oxidation, promote free radical intermediate production and accelerate the chain reactions associated with lipid peroxidation. The disruption of membrane structure, enlargement of relative oxygen diffusion-concentration products, and enhancement effects on membrane permeability, provide additional insights into potential mechanisms by which fumonisins could enhance oxidative stress and cell damage.

2.21 FUMONISIN-INDUCED DISRUPTION OF SPHINGOLIPID METABOLISM *IN VIVO*

Free So and Sa are present in tissues and cells in trace amounts (Merrill *et al.*, 1988). Free Sa is a metabolic intermediate of the sphingolipid biosynthetic pathway, and free So is generated primarily as a consequence of sphingolipid turnover or degradation. Thus, neither should accumulate under normal conditions (Merrill, 1991; Rother *et al.*, 1992; Michel *et al.*, 1997). The hypothesis was that if fumonisin inhibition of CER synthase *in vivo* resulted in accumulation of free Sa in the liver, at least some of the Sa that accumulates in cells treated with fumonisins would leave the cells and appear in blood, and if the kidney was affected, some would leave in the urine (Wang *et al.*, 1992; Merrill *et al.*, 1996b). This was reasonable since Sa is a hydrophobic compound that can enter and presumably cross cell membranes. It was hypothesised that disruption of sphingolipid biosynthesis in liver (or other organs) of animals consuming fumonisins or fumonisin-contaminated feeds could be detected by an increase in free Sa concentration, and an increase in the free Sa:So ratio in serum (Riley *et al.*, 1994a). This hypothesis was tested by a number of retrospective studies using serum and tissue obtained from feeding studies with ponies, pigs, chickens and rats.

2.21.1 Tissue and species specificity

Fumonisin B_1 has low acute oral toxicity in several animal species (Eriksen and Alexander, 1998). There are several sub-acute toxicity studies performed with animal species (poultry, rabbits, hamsters, non-human primates, lamb, mink, cattle) not directly useful for quantitative dose response assessment. Many of these studies were performed with contaminated feed, rather than pure fumonisin (Bryden *et al.*, 1987; Weibking *et al.*, 1993; Javed *et al.*, 1995; Kuiper-Goodman *et al.*, 1996; Norred *et al.*, 1996). Differences in tissue and species specificity may be due to varying susceptibility to the cellular effects of disrupted sphingolipid metabolism (Voss *et al.*, 1996b). Fumonisin induced free sphingoid bases or their metabolites in serum may affect the function of the vasculature, and thus indirectly affect tissues that are not directly affected by fumonisin inhibition of CER synthase (Ramasamy *et al.*, 1995; Smith *et al.*, 1996).

2.21.2 Fumonisins as cancer initiators and promoters in rats, mice and rabbits

Fumonisin B_1 appears to be non-genotoxic based on *in vitro* assays (Gelderblom and Snyman, 1991; Norred *et al.*, 1992a), and is a complete carcinogen (Gelderblom *et al.*, 1991) in that it effects the different stages of cancer development in rat liver, including cancer initiation, promotion and progression. Studies with other carcinogens have uncovered a basic pattern that is characteristic for initiation and promotion in rat liver. This pattern represents induction of rare "resistant" hepatocytes (resistant to negative regulation or sensitive to growth stimuli), the outgrowth of which can be selectively stimulated during the process of cancer promotion, to generate hepatocyte nodules. A subset of nodules, the persistent or late nodules, is one site of origin for hepatocellular carcinoma (Farber and Sarma, 1987; Farber *et al.*, 1989).

Fumonisins are slow initiators because prolonged exposure (up to 14 days) at a relatively high dosage is required to effect cancer initiation (Gelderblom *et al.*, 1992; 1994). Creation of an environment conducive to expansion of initiated cells by inhibition of normal hepatocyte proliferation is often observed with genotoxic hepatocarcinogens (Farber, 1990). Selective proliferation of resistant hepatocytes results in clonal expansion of these initiated cells. It is not known whether the characteristic enzyme phenotype induced by genotoxic carcinogens is also induced by fumonisins (Roomi *et al.*, 1985; Riley *et al.*, 1994a; 1994b).

Gelderblom *et al.* (1994) showed that prolonged exposure of rats to FB_1 or even a single gavage dosage, inhibited compensatory hepatocyte proliferation following partial hepatectomy. In this regard, FB_1 resembles many other carcinogens that are potent inhibitors of normal proliferation, as typically seen even after hepatectomy and chemically induced necrosis, is sometimes a pre-requisite for cancer initiation (Cayama *et al.*, 1978). The inhibitory effect of FB_1 could explain why FB_1 is a slow cancer initiator (Gelderblom *et al.*, 1992; 1994). It can also be reasoned that a threshold level for cancer initiation by fumonisins exists in rat liver which, as a function of time, will be determined by the dosage used, induced effects, and inhibitory effects on the resultant compensatory cell proliferation (Gelderblom *et al.*, 1994). The rate-limiting step for cancer induction may be the induction of cell death and resultant compensatory cell proliferation. Superimposed on this is the inhibitory effect on cell proliferation, which could further delay or inhibit

cancer initiation, and therefore the apparent carcinogenic potential of this mycotoxin (Riley *et al.*, 1994a; 1994b).

Fumonisins also serve as promoters. The cancer promoting activity by *F. moniliforme* culture material and pure FB_1 in DEN-initiated rats is associated with its hepatotoxic effects (Gelderblom *et al.*, 1988a; 1988b; 1994). Long-term feeding studies have indicated that hepatotoxicity of FB_1 plays a determining role in carcinogenicity of this mycotoxin in rat liver. In the absence of a promoting regimen, FB_1 is a promoter and is continuously present during long term feeding studies (Gelderblom *et al.*, 1992). When considering these properties of FB_1, it would appear that cancer promotion by this mycotoxin proceeds via the induction of a growth differential because it has the potential to serve both to increase the growth rate of abnormal (pre-cancerous) cells and arrest growth (and be toxic) for normal cells. This data suggests that the fumonisins are complete carcinogens because they are potent selecting agents.

2.21.3 Fumonisin-induced disruption of sphingolipid metabolism and cancer

Given the close correlation between the elevation in free sphingoid bases and the severity and extent of liver and kidney ultrastructural alterations in rats fed pure FB_1 for four weeks (Riley *et al.*, 1994b), it seems likely that disruption of sphingolipid metabolism occurred in animals fed fumonisins for longer periods to produce cancer. *In vivo*, fumonisin acting as a mitogen could increase the probability, or irreversibly lock in a spontaneous genomic error. Mitogenesis increases cancer risk by increasing the probability of DNA damage being converted to mutations, making DNA more sensitive to being damaged, increasing gross chromosomal alterations, and increasing the expression of oncogenes (Ames and Gold, 1990). Cancer is a proliferative disorder, thus the fact that different cell types might respond in a differential fashion to elevated intracellular free sphingoid bases is not consistent with either the multistage model of carcinogenesis or the genotoxic/non-genotoxic classification scheme of Cohen and Ellwein (1990). Cohen and Ellwein (1990) hypothesised that non-genotoxic carcinogens act by increasing cell proliferation by direct mitogenic stimuli, toxicity and consequent regeneration, or through interruption of physiological processes.

Livers from rats fed *F. moniliforme* culture material containing fumonisins at concentrations which caused focal necrosis and hepatocellular hyperplasia, also contained free sphingoid bases and elevated free Sa:So ratios (Voss *et al.*, 1990). Focal necrosis and hepatocellular hyperplasia is indicative of ongoing repair and regeneration. The observation of mitotic figures in these tissues indicate that the presence of high concentrations of free sphingoid bases in these livers do not preclude cell division, and thus tissue repair processes may have been suppressed. Alternatively, clonal selection may have selected for cells sensitive to the mitogenic effects of elevated free sphingoid bases. Changes in pool size of specific sphingolipids (e.g., SM and CER) that are associated with cellular signalling systems could alter the way extracellular messages are transduced. Systems which are important control points for cellular growth and differentiation could be disrupted during the interval when repair processes and thus mitogenesis are rapidly proceeding. The mitogenic, cytostatic and cytotoxic potential of fumonisin induced disruption of sphingolipid metabolism, may all play some role in the increased cancer risk in rats (Riley *et al.*, 1994a; 1994b).

In short-term studies with rats, rabbits and mice, disruption of sphingolipid metabolism occurred at, or below the fumonisin dosages that cause liver or kidney lesions (Riley *et al.*, 1994b; Martinova and Merrill, 1995; LaBorde *et al.*, 1997; Tsunoda *et al.*, 1998; Voss *et al.*, 1998). In rats and rabbits, the fumonisin concentration that causes nephrotoxicity and an increase in kidney free Sa concentration is lower than the fumonisin dose that causes hepatotoxicity (Voss *et al.*, 1993; 1996b; 1998; Gumprecht *et al.*, 1995; LaBorde *et al.*, 1997).

2.21.4 Short and long term cancer initiation studies

Short-term studies in a cancer initiation/promotion model in rat liver provide important information about the possible mechanisms involved during the initial stages of cancer development by this apparently non-genotoxic mycotoxin. The short-term assays have mainly used rat liver nodules as the end-point, assessed either using microscopy or histochemical analysis of different enzyme activities such as gamma-glutamyl transferase (GGT) or placental glutathione S-transferase (PGST). In these assays, different stages of the multistage carcinogenesis model were investigated by combining FB_1 treatment with classical promotion assays. In these studies, FB_1 or a *Fusarium* extract was administered alone, before a promoting treatment, or after an initiating treatment. These studies

indicated that a cytotoxic/proliferative response is required for cancer induction, and that a no-effect threshold exists for cancer induction. The mechanisms proposed for cancer induction include the possible role of oxidative damage during initiation, the disruption of lipid metabolism, integrity of cellular membranes, and altered growth-regulatory responses as important events during promotion (Gelderblom *et al.*, 2001).

Short term *in vivo* studies have shown that FB_1 mimics genotoxic carcinogens with respect to the induction of resistant hepatocytes in rat liver (Gelderblom *et al.*, 1992; 1994). This was substantiated by observations that FB_1 induces GGT and PGST, which are accepted histological markers for putative pre-neoplastic lesions initiated by genotoxic carcinogens. It is unclear whether the characteristic enzyme phenotype that is associated with the fumonisins in rats indicated an increase in cell proliferation is also likely to play a role in the induction of the "resistant phenotype" as hepatotoxicity, and resultant regenerative cell proliferation is a prerequisite for initiation (Gelderblom *et al.*, 1994). The only difference noticed thus far in the induction of the resistant phenotype between the fumonisins and other genotoxic carcinogens, lies in the kinetics of the cancer initiation step.

2.22 ANIMAL DISEASES ASSOCIATED WITH CONSUMPTION OF FUMONISIN B_1

2.22.1 Equidae

Fumonisin B_1 and FB_2 are causative agents of ELEM. The name is somewhat misleading since the grey matter may also be involved (Marasas *et al.*, 1988a). The disease has been recognised as 'mouldy corn poisoning' and has been experimentally reproduced by feeding horses with corn naturally contaminated with fumonisins (Wilson *et al.*, 1992), as well as by the administration of purified FB_1 (Kellerman *et al.*, 1990). Wilson and Maronpot (1971) succeeded in establishing the causative agent when they isolated *F. verticillioides* as the predominant contaminant of mouldy maize that had caused cases of ELEM in Egypt, and reproduced ELEM by feeding culture material of the fungus on maize to two donkeys. Subsequently, investigators in SA confirmed the ability of *F. verticillioides* (MRC 826) culture material to induce the characteristic clinical signs and pathological changes of ELEM, as well as hepatosis in horses and donkeys (Kellerman *et al.*, 1972; Marasas *et al.*, 1976; Kriek *et al.*, 1981; Marasas *et al.*, 1988a).

The horse appears to be the species most sensitive to fumonisins, and ELEM is the most frequently encountered disease associated with *F. moniliforme* and *F. proliferatum*

(Kellerman *et al.*, 1990; Wilson *et al.*, 1992; Ross *et al.*, 1993). Equine leukoencephalomalacia is characterised by liquefactive necrosis of the cerebral hemispheres, causing damage to vascular endothelium of the CNS and, in some cases, hepatocellular necrosis and vacuolisation. The clinical signs associated with the neurologic form of ELEM in horses include apathy, lethargy, head pressing, drowsiness, pharyngeal paralysis, blindness, staggering, hyper-excitability, seizures and eventual recumbency. Once animals show the neurological signs, death usually occurs within 48-72 hours. If an animal survives the acute syndrome, neurological deficits are observed. The signs associated with the hepatic form include petechial or ecchymotic haemorrhages of the mucous membranes, icterus, oedema of the head and neck, decreased appetite, depression, lingual paralysis, clonic convulsions, and coma. On post-mortem examination, the classic finding is grey to brown areas of malacia and cavitation of the white matter of the cerebral hemisphere. It is usually unilateral, but may be asymmetrically bilateral. Histologically, there is marked, multifocal, liquefactive necrosis, multifocal vascular congestion, and perivascular haemorrhage throughout the white matter of the cerebrum.

Equine leukoencephalomalacia concurrent with significant liver disease was observed in horses and ponies fed feeds naturally contaminated with fumonisins at low concentrations (Wilson *et al.*, 1992; Ross *et al.*, 1993). The development of brain lesions in the absence of major liver lesions does not preclude biochemical dysfunction in non-brain tissue from contributing to the brain lesions. The length of exposure, levels of contamination, individual animal differences, previous exposure, or pre-existing liver impairment contribute to incidence of clinical disease (Ross *et al.*, 1993). Elevated serum enzyme levels indicative of liver damage (Wilson *et al.*, 1992) are preceded by elevation in the serum Sa: So ratio (Wang *et al.*, 1992; Riley *et al.*, 1997). Serum enzyme levels often return to near normal concentrations, but usually increase markedly immediately prior to, or at the onset of behavioural changes (Kellerman *et al.*, 1990; Wang *et al.*, 1992; Wilson *et al.*, 1992; Ross *et al.*, 1993; Riley *et al.*, 1997). Marasas *et al.* (1988a) have suggested that high dosage levels of fumonisins induce fatal hepatotoxicity with mild brain lesions, whereas low dosage levels cause mild hepatotoxicity and severe brain lesions.

The causes of ELEM after FB_1 dose may be divided into direct and indirect effects. Direct action may be mediated by the presence of Sa in brain. An indirect effect of FB_1 is also possible because FB_1-induced hepatotoxicity and nephrotoxicity in rats, disruption of

barrier function of cultured endothelial cells, and damage to the cerebral blood vessels have been reported. Alteration of blood vessels in the CNS and/or disruption of the BBB may have effects on the transfer of FB_1 or Sa in brain tissue (Kwon *et al.*, 1997a).

Leukoencephalomalacia was induced in two horses by the oral administration of FB_1. A filly received 59.5 $mg.kg^{-1}$ of a 50% preparation of FB_1 isolated from corn cultures of *F. moniliforme* MRC 826, administered in 21 doses of 1.25-4 $mg.kg^{-1}$ over 33 days (the other 50% was inorganic matter that co-eluted during purification), and a colt received 44.3 $mg.kg^{-1}$ of 95% pure FB_1 in 20 doses of 1-4 $mg.kg^{-1}$ in 29 days. Gross necropsy of the filly revealed a sunken area (2cm in diameter) in the lateral part of the anterior frontal lobe of the left cerebral hemisphere. The white matter on the cut section of this focus was softer than normal and reddish-brown. Microscopic examination revealed necrosis of the white matter, numerous macrophages, aggregates of mineralisation, and small haemorrhages. At the periphery of the necrotic area, the blood vessels showed hypertrophy and hyperplasia of endothelial cells, fibrinoid changes of their cell walls, and perivascular mononuclear cell infiltration. The white matter close to the focal lesion had mild status spongiosis and mild to moderate proliferation of astrocytes. Necropsy of the colt showed swelling of the cerebral hemisphere and flattening of the gyri. A yellowish-brown focus was seen in the subcortical white matter of the left dorsal frontal lobe, and extended posteriorly to the occipital lobe. A smaller, gelatinous focus was found in the white matter of the right occipital lobe. Microscopic examination of the lesions revealed partial loss of cellular detail of the white matter, swelling and proliferation of astrocytes, infiltration of macrophages, and swelling of axons. The blood vessels around the foci had hyperplasia and hypertrophy of endothelial cells, as well as perivascular oedema. The white and grey matter of the rest of the left side of the brain showed moderate oedema, and the right side showed only a mild oedema. These authors concluded that these results unequivocally prove that FB_1 can induce LEM in horses (Kellerman *et al.*, 1990). There is no specific therapy for ELEM. By the time clinical signs are noted, it is usually too late in the course of the disease. Removal of the contaminated feed from susceptible animals is very important and avoidance is the only way to prevent the disease.

2.22.2 Porcine pulmonary oedema syndrome

Kriek *et al.* (1981) were the first to report porcine pulmonary oedema (PPO) syndrome.

When culture material of *F. verticillioides* (MRC 826) was fed to horses, pigs, sheep, rats and baboons; lung oedema occurred only in pigs. Clinical signs of PPO typically occur two to seven days after pigs consume diets containing large amounts of fumonisins over a short period of time. Clinical signs include dyspnoea, weakness, cyanosis and death (Kriek *et al.*, 1981; Osweiler *et al.*, 1992; Casteel *et al.*, 1993; 1994; Diaz and Boermans, 1994; Rotter *et al.*, 1996; Fazekas *et al.*, 1998; Gumprecht *et al.*, 1998). At necropsy, the animals exhibit varying degrees of interstitial and interlobular oedema, with pulmonary oedema and hydrothorax (Colvin and Harrison, 1992; Colvin *et al.*, 1993). It has been hypothesised that cardiovascular alterations are a consequence of sphingoid base induced inhibition of L-type calcium channels (Smith *et al.*, 1996), and that cardiovascular dysfunction in pigs, subsequent to increased free sphingoid base concentration in the heart, is the cause of PPO (Haschek *et al.*, 1995; Smith *et al.*, 1996; 1999; Haschek-Hock *et al.*, 1998).

2.22.3 Vervet monkeys

Riley *et al.* (1996) recommended that quantitative detection of high concentrations of free Sa in urine, serum or tissues be used in conjunction with other clinical tools in situations where toxicity to animals resulting from exposure to fumonisins is suspected. Shephard *et al.* (1996b) studied the Sa:So ratio in serum of Vervet monkeys over 60 weeks. These animals consumed diets such that their total daily fumonisin intake was ~0.3 and 0.8 $mg.kg^{-1}$ bodyweight per day of *F. moniliforme* culture material. Serum Sa levels in the experimental groups (mean of 219nM and 325nM, respectively) were significantly elevated above the levels in controls (mean 46nM; $p=0.02$). The Sa:So ratio was significantly elevated from a mean of 0.43 in the control group to 1.72 and 2.57 in the experimental groups, respectively ($p=0.003$). Hence, the disruption of sphingolipid biosynthesis in vervet monkeys induced by fumonisins in their diet, can effectively be monitored in the serum as an elevation of the Sa: So ratio (Shephard *et al.*, 1996b).

2.23 HUMAN STUDIES

Studies have suggested potential developmental effects, such as neural tube defects (NTD), could be associated with exposure to fumonisins (Flynn *et al.*, 1996; 1997; Collins *et al.*, 1997). By what mechanism could fumonisin induce NTDs? Folate is needed

for biochemical reactions involving one carbon metabolism, such as the biosynthesis of purines and thymidine, the regeneration of methionine from homocysteine and histidine metabolism. The folate receptor is found in membrane domains enriched in cholesterol and sphingolipid, and is a glycosylphosphatidylinositol (GPI) anchored protein (Lacey *et al.*, 1989). This receptor is responsible for transport of folate into cells with elevated folate requirements, such as placenta, kidney and breast. By the time of organogenesis, the foetus is dependent on maternally derived folic acid. This continuous requirement for folic acid is not usually a problem because the placenta concentrates this water-soluble vitamin 3:1 in favour of the foetus (Henderson *et al.*, 1995). It has been shown that treatment of Caco-2 cells with FB_1 inhibits folate receptor mediated transport of 5-methyltetrahydrofolate in both a time and concentration dependent fashion (Stevens and Tang, 1997). It is not unreasonable to assume that blocking the placental uptake of this water-soluble vitamin for a few critical days might induce a NTD.

Coumi (2000) dealt with the possible role of FB_1 in pre-eclampsia, and immunolocalised FB_1 in placental tissue obtained from normotensive and pre-eclamptic patients. Image analysis indicated that the intensity of staining for FB_1 was higher in the pre-eclamptic group than in the normotensive group. Serum obtained from both maternal and cord blood samples taken from the same patients as the placental samples were analysed for FB_1 presence using high performance liquid chromatography (HPLC). Fumonisin B_1 was detected in the maternal and cord blood serum samples of the pre-eclamptic group. Fumonisin B_1 was also detected in three normotensive maternal serum samples, but was not detected in any of the cord serum samples of those pregnancies. *In utero* exposure to FB_1 is suggested by the presence of this mycotoxin in the placental samples, and in the maternal and cord serum samples obtained from pre-eclamptic pregnancies (Coumi, 2000).

Chelule *et al.* (2000) analysed 20 stool samples of rural school children of Vulamehlo in SA for FB_1, as well as 23 urban control stool samples obtained from various households within the Durban metropolitan area. The rural (35%) and urban samples (9%) showed the presence of FB_1 ranging from 790 to 19 560ng per gram of freeze dried stool. Clearly, the rural population have greater exposure as they consume locally produced maize that is often contaminated with FB_1. Considering the losses due to degradation during digestion, recovery, dilution effects and the time interval to when food was consumed, the quantities detected might be equivalent to considerable amounts of fumonisins in food. Children from

rural areas, who were not regarded as suffering from any disease, are clearly routinely exposed to FB_1 which is resident in their gastrointestinal tract (GIT) for considerable periods of time, depending upon personal habits. If positive results were found, it was initially predicted these would be from the rural population where maize is the staple food. However, two volunteers from Durban were positive at levels in the higher range of contamination (3.5 and 16.2 $mg.g^{-1}$ respectively). Fischer's exact test showed that the rural population was six times more at risk to FB_1 exposure than the urban group. It is usual however for urbanized black people to eat maize products, presumably from urban stores, and therefore may be complacent about its quality (Chelule *et al.*, 2000).

Subsequently, Chelule *et al.* (2001) surveyed households in rural (in villages of Mphise and Ngcolisis) and urban (Durban Metro) areas of KZN, SA. Analysing stored maize, plate ready food and faeces enabled assessment of the exposure of the inhabitants to FB_1. Of the 50 rural maize samples examined 32% had levels of FB_1 ranging from 0.1-22.2 $mg.kg^{-1}$, whereas 29% of the 28 cooked maize (phutu) samples contained FB_1 ranging from 0.1-0.4 $mg.kg^{-1}$. The incidence and levels of FB_1 in faeces were 33% and 0.5-39 $mg.kg^{-1}$ respectively. Of the 49 urban maize samples analysed, 6.1% had a range of 0.2-0.5 $mg.kg^{-1}$ FB_1, whereas 3 of 44 faecal samples (6%) ranged between 0.6-16.2$mg.kg^{-1}$. No FB_1 was detected in urban phutu samples. Because these levels are lower than those published from regions in SA with high incidence of oesophageal cancer (OC), it may be concluded that the risk of OC from FB_1 exposure is lower in the KZN region (Chelule *et al.*, 2001).

Several possibilities present themselves; either FB_1 is highly potent or its absorption is aided by other dietary factors such as alcohol or fat. Previous data indicates that it is improbable that in the digestive tract toxin is modified into a more accessible form e.g., by esterification, or that there are transport systems that assist in passage, either present in an active or latent form. An alternative approach is to measure Sa and So levels, which are elevated, however, hold out some hope for exposure studies. However detailed work will be needed to correlate exposure levels with dose and time periods.

2.24 HUMAN EXPOSURE ESTIMATES

2.24.1 Environmental levels and human exposure

The occurrence of FB_1 in maize intended for human consumption is common worldwide. Considerable differences are evident in the extent of human exposure between maize-growing regions in the developed and developing countries. For example, although FB_1 can occur in maize products in the United States of America (USA), Canada and Western Europe, human consumption of those products is modest. In parts of Africa, South-Central America and Asia where FB_1 contamination may be high, some populations consume a high percentage of their calories as maize meal. Maize contaminated naturally by FB_1 can be simultaneously contaminated with *F. verticillioides* or *F. proliferatum* toxins, or with other mycotoxins including DON, ZEA, aflatoxin and ochratoxin.

Human exposure estimates have been made for fumonisins in Canada, SA, USA and the Netherlands (Kuiper-Goodman *et al.*, 1996; Humphreys *et al.*, 1997; Marasas, 1997; de Nijs, 1998). For Canada during the period 1991 to early 1995, human exposure estimates of 0.017-0.089 $\mu g.kg^{-1}$ bodyweight per day were reported (Kuiper-Goodman *et al.*, 1996). In the Netherlands, the exposure estimates ranged from 0.006 to 7.1 $\mu g.kg^{-1}$ bodyweight per day (based on the daily average intakes of maize and maize products of 3g (general population average), 42g (regular maize product eaters) and 162g (individuals with gluten intolerance) in the Netherlands, the respective population groups had an estimated daily intake of 4, 57 and 220 μg FB_1 per person respectively, based on a mean FB_1 content of 1.36 $mg.kg^{-1}$ maize produced (de Nijs *et al.*, 1998a; 1998b).

Thiel *et al.* (1992) estimated that human exposures in the Transkei region in SA are 14 and 440μg FB_1 per kilogram body weight per day for healthy and mouldy corn respectively. More recent estimates of the probable daily intake (PDI) of South Africans are summarized in Table 2.2. These vary from 1.2-to 355 $\mu g.kg^{-1}$ bodyweight per day in rural blacks in Transkei (Marasas, 1997). These exposure estimates vary considerably according to the source and extent of maize in the diet, as well as the extent of *Fusarium* kernel rot prevalent in the harvested crop.

Table 2.2: Probable daily intake of fumonisin in South Africa (Marasas, 1997).

Product	Country of Origin	Number of Samples	Mean FB_1+FB_2 concentration (µg/kg)	Probable daily intake (µg/kg body weight per day)	
				Rural population	Urban population
Commercial maize	SA [a]	68	400	2.6	1.6
Commercial maize	SA [a]	209	300	2.0	1.2
Maize meal	SA [a]	52	200	1.3	0.8
Home-grown maize	SA [b]	18	7100	46.6	28.0
Home-grown maize	SA [c]	18	54 000	354.9	212.9
Imported maize	USA [d]	1682	1100	7.2	4.3
Maize consumption					
gram/70 kg body weight per day				460	276
a From: Marasas (1997)					
b Transkei, from individual farms in high OC area, healthy maize					
c Transkei, from individual farms in high OC area, mouldy maize					
d Imported in 1993					

Maize examined by Dutton *et al.* (1993) was found to have a 50% incidence of FB_1 contamination. During the period 1984-1993, just over 1600 samples of agricultural commodities comprising maize, compound animal feeds, oil seeds, soybean, fish meal and forage were examined in KZN in SA for fungi and over 20 mycotoxins using a multiscreen augmented with individual assays (Dutton and Kinsey, 1996). Aflatoxin occurred most commonly at over 14% of all samples examined followed by trichothecenes at 10%, and then zearalenone at 4%. Since 1989, selected maize samples with high levels of *Fusarium* species have been examined for FB_1 and of these (n=20) in 1993, 90% were positive. Because of this result and high incidence of *Fusarium* species (32%) in maize and maize containing feeds that were higher than either *Aspergillus* species (27%) or *Penicillium* species (12%), concern was expressed with regard to the potential presence of fumonisin in the SA food chain (Dutton and Kinsey, 1996).

In 1994, 417 samples of agricultural commodities, comprising maize, compound animal feeds, oil seeds, soybean, fish meal and forage were examined in KZN in SA for fungi and over 20 mycotoxins, using a multiscreen augmented with individual assays. The majority of samples examined were maize (198; 47.9%) reflecting the agricultural importance of this cereal in SA. Feeds were the next most important, as this cereal was the usual energy

source in them. Trichothecenes occurred most commonly of over 19% in all samples received and zearalenone at 3%. Selected samples (73) were analysed for FB_1 and of these 69 (94%) were found to be positive. Because of this result and high incidence of *Fusarium* species (over 70% in maize and maize containing feeds, attention was drawn to the actual and potential presence of fumonisin in the food chain in SA (Dutton and Kinsey, 1995).

2.25 OESOPHAGEAL CANCER IN HUMANS

2.25.1 Transkei, South Africa

The high incidence of OC among the black population of Transkei, SA has been reported in several surveys (Jaskiewicz *et al.*, 1987; Makaula *et al.*, 1996), and reviewed by IARC. The only studies available were correlation studies, most of which indicated some relationship between OC rates and occurrence of *F. verticillioides* (IARC, 1993a; 1993b). Contamination of homegrown maize in Transkei by a number of toxigenic *Fusarium* species, particularly *F. verticillioides*, has been observed since the early 1970's (Marasas *et al.*, 1979a; 1979b; 1981; 1984; 1988a; 1988b; 1993; Marasas, 1993; 1994; 1996; 1997). Another *Fusarium* species associated with maize in Transkei *is F. graminearum*, and the mycotoxins DON and ZEA produced by this fungus occur in homegrown maize intended for human consumption (Marasas *et al.*, 1979a).

In rural communities in SA, the chief component of the staple diet is maize. An association has been suggested between high levels of fumonisin-producing moulds on maize used to make alcoholic beverages and OC in human subgroups in Transkei. Transkeians deliberately favour and frequently use visibly mouldy maize in the making of home brewed beer because of the unique flavour the mould imparts (Norred, 1993). This maize has been found to contain up to 118 $mg.kg^{-1}$ fumonisins (Rheeder *et al.*, 1992). Based on experiments conducted on beer made from wort containing added FB_1 (Scott and Lawrence, 1995), such beers could contain fumonisin concentrations of 30mg/litre beer.

The incidence of OC was higher in both sexes in the south (Butterworth and Kentani Districts) compared to the northern parts of the Transkei region (Bizana and Lusikisiki Districts). Both areas depend on homegrown maize for around 50-100% of the year's

supply, the remaining being purchased from commercial sources or imports. Maize porridge is the staple diet (up to 100% of calories). The occurrence of *F. graminearum* in maize kernels was found to be greater in low-risk than in high-risk areas for OC in later studies (Marasas *et al.*, 1981; 1988b). Sydenham *et al.* (1990a) confirmed that DON and ZEA levels were significantly higher in homegrown maize from areas with low rates of OC than from those with high rates. In contrast, the occurrence of *F. verticillioides* in maize kernels was significantly correlated to OC rates. However, the rules for selection of families were different between the two populations. The prevalence of *F. verticillioides* was greater in homegrown maize collected in 12 households in the high-incidence area compared to a similar collection in a low-incidence area. Households in the high-incidence area were selected on the basis of cytological examination of cells collected from the oesophagus (Marasas *et al.*, 1988b). Subsequent studies conducted after the chemical characterization of the fumonisins in 1988, also found significantly higher levels of *F. verticillioides* and fumonisins (20 times higher) in areas with high rates of OC in Transkei than in areas with low rates (Sydenham *et al.*, 1990a; 1990b; Rheeder *et al.*, 1992).

The fungi *F. verticillioides* and *F. graminearum* cause maize ear disease under different ecological conditions. The environmental conditions that prevail in the areas in the Transkei with high rates of OC clearly favour colonization of maize ears by *F. verticillioides*. Significant fumonisin accumulation in maize occurs periodically in all such environments examined so far, primarily in relation to drought and other environmental stresses. Taking this into account, SA studies have shown that the level of fumonisin in home-grown maize has been consistently high in the areas in the Transkei with high rates of OC. Cancer registry data have shown these areas to have consistently high rates of OC since 1955 (Jaskiewicz *et al.*, 1987; Makaula *et al.*, 1996). However, these studies were limited by the lack of controlled conditions, particularly for established confounding risk factors (e.g., alcohol consumption), and therefore do not allow any definitive conclusions to be made about cancer causation in humans.

The incidence of OC in the Transkei region averages about 50 per 100 000, but can be as high as 200 per 100 000 compared with less than five per 100 000 in most parts of the world. Other parts of the world with high OC include the Linxian region of China (100-150/100 000) and North Eastern Iran (>100/100 000) (Nair, 1998).

2.25.2 China

Maize is also consumed as a staple in a number of areas in China, including Linxian and Cixian counties in Henan province (Chu and Li, 1994; Yoshizawa *et al.*, 1994). Mortality rates for males in the high-risk areas ranged from 26 to 36 per 100 000 in the low-risk counties and from 76 to 161 per 100 000 in the high-risk counties. The incidence of *F. verticillioides* has been reported to be higher in maize in high- than low-risk areas. Maize samples from Linxian and Cixian counties were analysed for FB_1 by Chu and Li (1994). All 31 samples contained FB_1 at levels ranging from 18 to 155 $mg.kg^{-1}$.

2.25.3 Charleston, South Carolina

Both FB_1 and FB_2 were detected in commercial maize-based samples obtained from Charleston, South Carolina in 1989. This city has one of the highest incidences and mortality rates of OC in the USA. The mean levels of FB_1 (detected in 7/7 samples) and FB_2 (detected in 6/7 samples) were 635 and 182 $ng.g^{-1}$, respectively. Even though these levels were lower than those determined in homegrown maize samples from the Transkei, Sydenham *et al.* (1991) stated that the presence of these mycotoxins in commercial foodstuffs is cause for further investigation of the role of fumonisins in OC aetiology.

2.26 EFFECTS OF FUMONISINS ON THE BRAIN AND BRAIN CELLS

Long-term exposure to low levels or non-cytotoxic concentrations of certain environmental pollutants may lead to neurodegeneration through specific patterns of neural cell reactivity. This section of the literature review deals with data relating to the potential effects of fumonisins on the brain and brain cells.

2.26.1 Effects of fumonisins on the brains of animals

The developing nervous system in rats is vulnerable to perturbations by environmental toxicants (Spyker, 1975; Vorhees, 1992). In the rat, the rate of the brain is most rapid during post-natal development day (PND) 7 (Dobbing and Sands, 1979). The immature brain has a greater passive permeability of lipid soluble molecules between blood and brain tissue or CSF than does the mature brain (Saunders and Mollgard, 1984). In rat cerebral cortex, the maximal proliferation of capillary cells occurs between PND 5 to 9

(Robertson *et al.*, 1985), and some drugs (e.g., phenobarbital, phenytoin) can permeate the neonatal brain more readily than the adult (Cornford *et al.*, 1983). Therefore, it appears that the developing rat may be a more sensitive model to study FB_1 effects than is the adult rat, because FB_1 is a hydrophilic, lipid soluble compound possessing a relatively large molecular weight (721.8 daltons).

The question of toxicity to the neonate is of concern since neonates may be more sensitive to fumonisins than adults. Kwon *et al.* (1997b) indicated that subcutaneous injection of FB_1 in neonatal rats caused elevation in the Sa:So ratio in brain tissue and reduced myelin deposition. Kwon *et al.* (1997b) further demonstrated that FB_1 treatment altered Sa levels and significantly increased Sa: So ratios in two regions of the brain, namely in the forebrain and brainstem. In the same regions of the CNS, rats with limited nutrition did not demonstrate altered Sa levels or Sa: So ratios. These data suggest that sphingolipid metabolism in the CNS of developing rats is vulnerable to FB_1 exposure. The elevated Sa level was the result of a direct effect on the neonate brain, indicating that FB_1 can cross the BBB (Kwon *et al.*, 1997a). When toxicity to the dam was minimal, evidence of toxicity to the rat neonate was minimal or absent (Ferguson *et al.*, 1997).

Since FB_1 exposure is associated with alteration of sphingolipid metabolism, Kwon *et al.* (1997a) investigated the effects of FB_1 treatment on BBB transfer in developing rats in order to elucidate whether blood Sa levels affect brain Sa levels. Sphinganine and So levels in brain tissue and plasma were analysed by HPLC. Area under the curve (AUC) $^{0\text{-}24\text{hour}}$ ratios of brain Sa to plasma Sa levels were about 40 after a single 0.8 to 8 $mg.kg^{-1}$ subcutaneous dose of FB_1. The AUC $^{0\text{-}12\ \text{hour}}$ ratio of brain FB_1 to plasma was 0.02. Sphinganine levels in brain and plasma show dose dependent increases, and brain Sa $AUC^{0\text{-}24\ \text{hour}}$ was higher than plasma Sa $AUC^{0\text{-}24\text{hour}}$ at both the 0.8 and 8 $mg.kg^{-1}$ dose. These data indicate that small amounts of FB_1 entered brain tissue and increased Sa levels in the developing rats. This was supported by HPLC detection of FB_1 in the brain tissue. The data also suggest that plasma Sa elevation due to FB_1 exposure probably did not contribute to the elevation of brain Sa levels. Fumonisin B_1 effects on increasing Sa levels continued to 24 hours in both brain and plasma after the 8 $mg.kg^{-1}$ dose. However, in the 0.8 $mg.kg^{-1}$ dose, the alteration of brain Sa levels was transient and plasma Sa levels were not elevated. The fact that FB_1 alters brain Sa levels and Sa: So ratios indicates that sphingolipid metabolism in the CNS of developing rats is vulnerable to FB_1 exposure

(Kwon *et al.*, 1997a). These data suggest that even low levels of FB_1 in brain were sufficient to increase endogenous Sa levels in the brain. It seems that the accumulation of Sa was due to a direct effect of FB_1 on brain tissue rather than passive accumulation of peripheral Sa into the brain from the blood (Kwon *et al.*, 1997a). This data supports the hypothesis that alterations of the brain Sa levels are related to the direct action of FB_1 on the brain rather than the transport of peripheral Sa to the brain.

Kwon *et al.* (1997b) further determined whether FB_1 alters Sa levels and myelin synthesis in the CNS of developing rats. Fumonisin B_1 administration (subcutaneous 0.4 or 0.8 $mg.kg^{-1}$ per day) from PND3 to PND12 resulted in a significant reduction of body weight and decreased survival rates. Both Sa levels and Sa:So ratios were significantly increased in the brain of rats given 0.8 mg FB_1/kg/day or treated by limited nutrition when compared to those in saline controls. Sphinganine levels and Sa:So ratios were significantly higher in the 0.8 mg FB_1/kg/day treated, but were not altered in the limited nutrition group. Myelin deposition in the corpus collosum and 2', 3'-cyclic nucleotide-3'-phosphorylase (CNP) activities were decreased significantly in both nutritionally limited and FB_1 exposed rats (Kwon *et al.*, 1997b). This data indicates that sphingolipid metabolism in the CNS of developing rats is vulnerable to FB_1 exposure, and that the hypomyelination associated with FB_1 treatment may be mediated by limited nutrition.

Alterations of sphingolipid metabolism and myelin synthesis in the CNS may be caused by FB_1 exposure and the direct disruption of brain enzyme activity involved in sphingolipid synthesis and/or damage to myelinating cells. In support of this theory it has been reported that 35% of the myelin lipid in both rat and human brain are GSLs (cerebrosides and sulphatide) and SM, key components in the myelination of axons in the brain and spinal cord. In addition, sphingolipid biosynthesis and axonal growth in cultured hippocampal neurons are inhibited by FB_1 (Harel and Futerman, 1993).

The transfer of FB_1 into rat brain may become one of the principal factors involved with the assumption of direct action of FB_1 on brain. However, bioavailability of FB_1 in brain tissue was not high according to kinetic data of Kwon *et al.* (1997b). The low transfer of FB_1 to the brain was probably due to the low lipid solubility and a large molecular weight of FB_1. Alteration of blood vessels in the CNS and/or disruption of the BBB, may have effects on the transfer of FB_1 or Sa in brain tissue (Kwon *et al.*, 1997b).

Goel *et al.* (1995) reported that brain Sa levels, but not Sa:So ratios, were significantly elevated in horses that developed ELEM. Fumonisin B_1 elevates free sphingoid levels in developing rats as does the phenomena of Niemann-Pick disease (type A) in the human foetus (gestational ages, 16-20 weeks). The latter condition, however, causes much more accumulation of So that Sa in cerebral cortex, liver and spleen (Rodriguez-Lafrasse *et al.*, 1994), while the former increased Sa in the brain of developing rats without affecting So levels (Goel *et al.*, 1995). This suggests that alterations of brain sphingolipid metabolism may be related to the outcome of human or animal diseases. Disruption of sphingolipid metabolism by FB_1 in liver and kidneys may directly cause tissue damage, whereas the damage in the brain and lung may be indirect due to disruption of endothelial functions (Gumprecht *et al.*, 1995; Ramasamy *et al.*, 1995; Riley *et al.*, 1996; Eriksen and Alexander, 1998; Tsunoda *et al.*, 1998).

Two of five pregnant rabbits gavaged with purified FB_1 at 1.75 $mg.kg^{-1}$/day died, one after nine doses and the other after 13 doses. Microscopic examination revealed focal small haemorrhages in cerebral white matter in both animals, with malacia and haemorrhage also present in the hippocampus of one. The lesions were bilateral. Haemorrhage and degeneration were also present in the choroid plexus of the lateral ventricle, with perivascular oedema in the temporal cerebral cortex. Haemorrhagic and leukomalacic lesions similar to those associated with fumonisin exposure in equidae were observed (Bucci *et al.*, 1996).

2.26.2 Effects of fumonisins on myelin synthesis

Since sphingolipids are major constituents of myelin, and activators of PKC are known to induce demyelination (Pouly *et al.*, 1997), effects on myelin formation and integrity may be expected as a consequence of FB_1 exposure. Recent reports support such a hypothesis. Pre-natal treatment of rats with FB_1 alter the functional development of the nervous system (Ferguson *et al.*, 1997), while myelin synthesis was reduced in pups treated post-natally with this mycotoxin (Kwon *et al.*, 1997a; Kwon *et al.*, 1997b). These authors' indicate that multiple subcutaneous dosing of developing rats with FB_1 significantly reduces body and brain weights, and also causes hypomyelination accompanied by altered sphingolipid metabolism in the CNS. Kwon *et al.* (1997b) showed that a single injection of FB_1 ($8mg.kg^{-1}$) resulted in FB_1 concentrations in the brain equivalent to 0.42μM at

30 minutes (min.) and 0.06μM at 12 hours after injection, whereas plasma concentrations were 58.6μM and 0.3μM respectively.

2.26.3 Effects of fumonisin B_1 on tissue slices

Protein kinase C consists of a family of isozymes that are differentially localized in various cells (Nishizuka, 1988; Nishizuka *et al.*, 1991). Among these, γ-PKC exists at high concentrations in various brain regions (Tanaka and Saito, 1992). Yeung *et al.* (1996) evaluated whether FB_1 affects PKC activation, and its redistribution in response to FB_1 exposure in rat cerebrocortical slices. Similar to the tumour promoting phorbol ester, phorbol 12 myristate-13 acetate (PMA), PKC is also catalytically activated by FB_1. Cytosolic and membranous PKC activities were determined by histone phosphorylation in the presence of [γ-^{32}P] adenosine triphosphate (ATP), phosphotidyl-L-serine, PMA, and calcium ions. Distribution of γ-PKC isozyme in the presence of FB_1 was assessed by immunoblotting using affinity purified anti-peptide antibodies. Similar to PMA, FB_1 added to rat cerebrocortical slices facilitated PKC translocation from cytosol to membrane in a concentration dependent manner. This FB_1-induced PKC translocation was inhibited by incubation with the inactive 4α-phorbol-12,13-didecanoate. The effects of FB_1 and PMA were neither additive nor synergistic. In addition, PMA and FB_1-induced PKC enzyme redistribution were inhibited by pre-treating tissues with So. A concentration-related FB_1 attenuation of specific phorbol dibutyrate (PDBu), [^{3}H] PDBu, binding was also observed when cortical membranes were incubated with either PMA or So (Yeung *et al.*, 1996). This was the first report of FB_1-induced PKC translocation via a direct action on the diacylglycerol site that also binds phorbol esters. Because phorbol esters are well-known tumour promoters, this study provides a plausible mechanism to explain the carcinogenicity of FB_1.

Interference with sphingolipid metabolism in response to sustained FB_1 exposure is a plausible mechanism by which these mycotoxins induce mitogenesis (Yoo *et al.*, 1992; Merrill *et al.*, 1993a; 1993b; Schroeder *et al.*, 1994). Given the differences in duration of FB_1 exposure that are required to activate PKC and inhibit sphingolipid metabolism, it is possible that mycotoxin-induced mitogenesis involves two phases. Thus, upon chronic exposure to FB_1, PKC activation seems to be a dominant mechanism in the early stage, followed by FB_1-mediated disruption of sphingolipid biosynthesis and accumulation of

sphingoid bases or their metabolites (Wang *et al.*, 1991; Riley *et al.*, 1994b). In the later phase, profound reductions in PKC activation may be due to the additive actions of FB_1-induced translocation followed by proteolytic degradation of the translocated enzyme, as well as inhibition of enzyme activation by the sphingoid bases or their metabolites (Hannun *et al.*, 1986; Vaccarino *et al.*, 1987; Kharlamov *et al.*, 1993). The mechanism FB_1 uses to elicit its mitogenic activity are complex and these findings provide an additional cellular mechanism to further define the effects.

2.26.4 Fumonisin B_1 in isolated brain cells

2.26.4.1 Fumonisin B_1 inhibits ceramide synthase and *de novo* sphingolipid biosynthesis in cultured neurons *in situ*

van Echten *et al.* (1990) and Mandon *et al.* (1991) showed that the addition of So to cultured mouse cerebellar neurons caused a decrease in the incorporation of [^{14}C] serine into sphingolipids, apparently due to the down regulation of SPT. Since FB_1 caused cellular Sa to accumulate, it was thought that FB_1 might induce a secondary inhibition of the first step of the pathway, as well as at CER synthase. However, in experiments in which cells were treated overnight with 25μM FB_1 and the microsomes were isolated and assayed for SPT activity, the activity of the fumonisin treated cells was not significantly different from controls. This effect was further studied in neuroblastoma cells (Rother *et al.*, 1992), where it was shown that FB_1 specifically inhibited the conversion of Sa to dihydroceramides.

Incorporation of [^{14}C] serine into SM and GSLs was examined to evaluate how this affects the distribution of newly synthesised CER, among different complex sphingolipids in cultured mouse cerebellar neurons (Merrill *et al.*, 1993b). Fumonisin B_1 inhibited CER synthase in mouse brain microsomes with a competitive-like kinetic behaviour with respect to both Sa and stearoyl-CoA. This suggests that CER synthase recognizes both the amino group (sphingoid binding domain) and the TCA side-chains (fatty acyl-CoA domain) of FB_1 (Merrill *et al.*, 1996b). The reduced inhibition by the hydrolysed derivatives of the fumonisin B series (Norred *et al.*, 1997; van der Westhuizen *et al.*, 1998) supports this hypothesis. Humpf *et al.* (1998) have shown that CER synthase acylates hydrolysed FB_1, AP_1, to form N-palmitoyl-AP_1. The product was found to be an inhibitor of CER synthase, and to be 10 times more toxic than FB_1 in the HT29 human colonic cell line.

Fumonisin B_1 inhibited sphingolipid biosynthesis in the cultured cerebellar neurons and this was reflected by accumulation of free Sa, a reduction in the mass of total sphingolipids, reductions in the incorporation of [^{14}C] serine into glucosylceramide, lactosylceramide, SM and gangliosides (G_{M1}, G_{D3}, G_{D1a}, G_{D1b}, G_{T1b}, G_{Q1b}), and inhibition of the incorporation of [^{14}C] galactose and [^{3}H] Sa into complex sphingolipids (Merrill *et al.*, 1993b). Dose response studies revealed that the labelling of SM (IC_{50} of 0.7μM) was more sensitive to inhibition by FB_1 than was glycolipid formation (IC_{50} of ~7μM) in these cells. A similar effect was seen when β- fluoroalanine was added to inhibit the activity of SPT, the first enzyme of the pathway. The inhibition of complex sphingolipid synthesis was reversible, and nearly normal labelling products were obtained 48 hours after removing the mycotoxin. These studies establish that FB_1 inhibits *de novo* sphingolipid biosynthesis by neuronal cells, and moreover, that limiting CER synthesis differentially affects the formation of SM versus GSLs.

Fumonisin B_1 had a more potent effect on SM formation than on glycolipid biosynthesis Merrill *et al.* (1993b). This was considered due to a greater sensitivity of SM synthesis to a reduction in CER formation, because it was also seen with another inhibitor of *de novo* CER biosynthesis (β-fluoroalanine). Such selectivity may be due to a number of causes:-

- The Michaelis-Menten constant (K_m) for CER of glucosylceramide synthase may be lower than that of SM synthase, thus a decrease in CER synthesis will not affect GSL formation until the CER concentration decreases to below the K_m.
- The intracellular localisation of SM and GSL biosynthesis (Hoekstra and Kok, 1992) might account for these differences. For example, GSL synthesis may begin in a cellular compartment that is more proximal to the site of CER synthesis; therefore these enzymes would have first access to CER. This explanation agrees with evidence that CER synthesis is on the cytoplasmic surface of the ER (Mandon *et al.*, 1992) whereas SM synthase is thought to be on the luminal side of the *cis*-Golgi (Jeckel *et al.*, 1990; 1992), although some cells appear to have more than one intracellular site for SM synthesis.
- The inhibitors (FB_1 and β-fluoroalanine) may inhibit a CER "flipase" that moves this substrate from the cytosolic to the luminal side of the Golgi membrane.
- The inhibitors may affect SM synthase and glycosyltransferase(s) directly but more potently inactivate the former.

Merrill *et al.* (1993b) however further postulated that similar findings with two very structurally different compounds, FB_1 and β-fluoroalanine, make these last two explanations less likely. Thus, the greater sensitivity of SM synthesis is probably due to the differences in the K_m and/or subcellular localisation of the pertinent enzymes (Merrill *et al.*, 1993b). This study demonstrated that FB_1 blocks sphingolipid formation from [^{14}C] serine, [^{3}H] galactose, and [^{3}H] Sa in neuronal cells, that Sa accumulates in cells treated with this mycotoxin, and that SM biosynthesis from [^{14}C] serine is differentially affected at fumonisin concentrations that only partially inhibit CER synthesis. These studies establish FB_1 inhibits *de novo* sphingolipid biosynthesis by neuronal cells and moreover, that limiting CER synthesis differentially affects the formation of SM versus sphingolipids.

Fumonisin B_1 may have two modes of interaction with CER synthase. The 'Sa-like' domain may interact with the Sa binding-site, and the negatively charged TCA groups may interact with the fatty acyl-CoA binding site by mimicking the polyanionic phosphate groups of the CoA. The latter interaction is probably not the most important, because FB_1 does not inhibit another CoA-dependent enzyme (i.e., SPT) or labelling of glycerolipids (Wang *et al.*, 1991), and removal of the TCA groups increases the IC_{50} only about 10-fold (Merrill *et al.*, 1993b). The ability of FB_1 to interact with both the binding sites however might account for its potency.

Sphingolipid biosynthesis was studied in cultured murine cerebellar neurons (van Echten *et al.*, 1990) in the absence or presence of exogenous So homologues with different alkyl chain lengths (12,18,24 carbon atoms). Labelling of cells with [^{14}C] serine for 24 hours indicated that endogenous So biosynthesis with incorporation of radiolabelled serine was inhibited by these long chain bases (0.5-50μM) in a concentration-dependent manner. The inhibition was fully reversible after removal of the long chain bases from the culture medium. Metabolic labelling of neurons with [^{14}C] galactose provided strong evidence that the cells were able to use the exogenous So homologues, irrespective of their alkyl chain length, as substrates for the biosynthesis of GSLs. When the biosynthetically inert sphingoid, azidosphingosine (5-50μM) was fed to the cells, *de novo* So and GSL biosynthesis were both strongly inhibited (van Echten *et al.*, 1990).

El Bawab *et al.* (2001) characterised the reverse activity of a purified rat brain membrane bound ceramidase. Fumonisin B_1 was shown to inhibit the CoA dependent CER synthase activity in rat brain microsomes, and was also found to not inhibit the reverse ceramidase activity purified from rat brain. These results clearly indicate that the two activities represent different enzymes and further attest to the specificity of FB_1.

2.26.4.2 Fumonisin B_1 impairs myelin formation in aggregating brain cell culture

The effects of subchronical applications of FB_1 were analysed *in vitro*, using cultures of rat telecephalon as a model. As cells in the aggregates develop from an immature state to a highly differentiated state with synapse and compact myelin formation, it is possible to study the effects of FB_1 at different developmental stages. The results showed that FB_1 did not cause cell loss and it had no effect on neurons. At all developmental stages tested, FB_1 caused neither cell death nor apoptosis. It also did not induce microglial reaction, which is considered an early marker of neurotoxicity (Monnet-Tschudi *et al.*, 1995; 1996).

Fumonisin B_1 delayed oligodendrocyte maturation, as suggested by the slight decrease of the differentiation marker galactocerebroside (Gal C), without affecting the number of myelinating cells, since no change in the enzymatic marker CNP was found (Espinosa de los Monteros *et al.*, 1988). Since the myelin basic protein (MBP) content was not significantly decreased in highly differentiated cultures, mature myelin appeared to be more resistant to FB_1 treatment. However, at 40 μM FB_1, the MBP immunoreactivity was decreased in myelinating, as well as in highly differentiating cultures. These data indicate that at high concentrations, FB_1 may affect both the synthesis and the deposition of MBP. Furthermore, FB_1 may also interfere with the compaction of the myelin sheath in differentiated cultures, since the myelin oligodendrocytes glycoprotein (MOG) was decreased in differentiated cultures. This marker, localized essentially at the external surface of the myelin sheath, appears late in the compacting myelin sheaths (Brunner *et al.*, 1989). This could explain why no effect on MOG was detected earlier in development.

The other effect observed after FB_1 treatment in differentiated cultures, was a loss of the astrocytic marker, glial fibrillary acidic protein (GFAP), while the enzymatic marker glutamine synthetase was not modified. These data indicate that FB_1 did not interfere with maturation of astrocytes or with their viability. It is known that sphingolipids bind to

cytoskeletal proteins leading to stabilization of the cytoskeleton. Therefore a deficit of sphingolipids due to a block on CER synthase by FB_1 could explain this loss of GFAP. Since GFAP is largely distributed in astrocytic foot processes, FB_1 could disrupt their structural organisation. The content of GFAP was decreased in differential astrocytes exclusively, while neurons were not affected by 40μM of FB_1 applied continuously for 10 days. In summary, FB_1 selectively affected glial cells while neurons were spared. In particular, FB_1 delayed oligodendrocyte development and impaired myelin formation and deposition. At high concentrations, FB_1 affected mature compact myelin. The relevance of this data to humans, and the relationship between the observations and the known actions of FB_1 require further investigation (Monnet-Tschudi *et al.*, 1999).

2.26.4.3 Effects of fumonisins on myelin synthesis

Kwon *et al.* (2000) assessed short-term consequences of direct FB_1 exposure on astrocytes and oligodendrocytes in primary cultures of rat cerebrum, to determine the effects of FB_1 on myelin and sphingolipid metabolism. Beginning at five days *in vitro* (DIV), the cultures were exposed to FB_1 at five concentrations (between 0.5-75 μM). The cultures were evaluated after exposure to the toxin for five (10 DIV) and ten days (15 DIV) respectively. The levels of the sphingolipid associated constituents So and Sa were determined with HPLC. Relative to untreated cultures, exposure to FB_1 diminished the levels of So at 15 DIV, whereas FB_1 exposed cultures showed significantly increased Sa levels and Sa:So ratios. In addition, FB_1 exposed cultures exhibited a two fold increase in the number of process bearing cells by 15 DIV. Also the activity of CNP was increased in FB_1-treated cultures. Overt cytotoxicity to FB_1 was not observed in this study. Even at the highest FB_1 concentration (75μM), exposure of glial cultures continuously for 10 DIV did not result in FB_1-associated changes in protein or DNA. This finding is consistent with previous reports that FB_1 did not change protein content or cell number in cultured hippocampal neurons or aggregating brain cell cultures (Harel and Futerman, 1993; Monnet-Tschudi *et al.*, 1999).

However, Kwon *et al.* (2000) reported that protein and DNA content were inconsistently increased after exposure to FB_1 for 15 DIV. Previous cell culture studies have yielded seemingly divergent results perhaps due to differences in cell type or metabolic status. For instance, FB_1 and Sa are cytotoxic to proliferating cultured CHO cells (Stevens *et al.*, 1990) and a line of kidney cells (Yoo *et al.*, 1992). In contrast, FB_1 or Sa

stimulates DNA synthesis in fibroblasts (Schroeder *et al.*, 1994). The saturating effects of FB_1 on the Sa levels may be due to either the inhibitory action of FB_1 on target enzymes or saturating of FB_1 transport across cell membranes. When administered experimentally, FB_1 exposure results in reduced brain growth, hypomyelination and changes in sphingolipid metabolism that are evident from increases in both the Sa level and the Sa: So ratio of brain tissue (Kwon *et al.*, 1997a).

Fumonisin B_1 exposure for a long period may result in decreased So levels due to the reduction of sphingolipids. Kwon *et al.* (2000) reported that Sa levels were significantly increased at both 10 DIV and 15 DIV in FB_1-treated cultures. Kwon *et al.* (2000) concluded that there was indication that the direct cellular exposure to FB_1 does not inhibit cell growth as assessed by DNA or protein content. Furthermore, the FB_1 related increases in both CNP activity and number of process bearing cells suggests that FB_1 may be mitogenic for cells in the oligodendrocytes/astrocyte lineage as it is for cultured fibroblasts. Thus, the white matter defects in animals exposed to FB_1 may not result directly from glial cytotoxicity. However, because the changes observed in the Sa levels and Sa:So ratios of FB_1 exposed cultures quantitatively resemble those previously found *in vivo* (Kwon *et al.*, 1997a; 1997b), subtle FB_1 related changes in sphingolipid metabolism may impair oligodendrocytes differentiation and the formation of myelin. The study of Kwon *et al.* (2000) suggests that short-term exposure to FB_1 may modify the proliferation of glial cells.

2.26.4.4 Effects of fumonisin B_1 on glycosphingolipids and gangliosides

Sialic-acid containing GSLs, gangliosides, are principal constituents of cell membranes and enriched in mature neurons. Sphingolipids are strong candidates as regulators of growth since they are enriched in neurons, and their levels and types, particularly gangliosides change significantly during development and differentiation. Furuya *et al.* (1995) observed an aberrant growth of dendrites of Purkinje cells depleted of membrane GSLs by FB_1 treatment. Fumonisin B_1 treatment resulted in less complex patterns of dendritic arborisation, suggesting a role of GSLs in neurite branching. Endogenous sphingolipids are required for the normal growth of cultured cerebellar Purkinje neurons and SM is present abundantly in the somatodendritic region of these cells. Furuya *et al.* (1998) in a subsequent study investigated the effects of depletion of sphingolipids on the phenotypic

growth and survival of immature Purkinje cells and the ability of CER or other sphingolipids to antagonize these effects. Inhibition of CER synthesis by ISP-1, decreased cellular levels of sphingolipids, decreased cell survival accompanied by an induction of apoptotic cell death, and aberrant dendritic differentiation of Purkinje cells with no detectable changes in other cerebellar neurons (Furuya *et al.*, 1998). These observations suggest that CER is a requisite for survival and dendritic differentiation of Purkinje cells.

SHSY5Y $_{trk\text{-}A}$ neuroblastoma cells are a cell clone transfected with NGF-receptor gene $p140^{trk\text{-}A}$. Addition of FB_1 (30-50μM) to $SHSY5Y_{trk\text{-}A}$ human neuroblastoma cells resulted in a 40% decrease of the ganglioside content, and in a reduction of NGF-induced outgrowth of neuritic processes within four days. A comparable effect of FB_1 was found in a neuronal tissue culture system, resulting in a dose dependent inhibition of neurite outgrowth from embryonic chicken spinal cord explants. The effective concentrations were in the range of 20-50μM FB_1. Similar concentrations have been reported to reduce axon elongation and branching of rat hippocampal neurons during a defined period of cell culture (Harel and Futerman, 1993; Schwarz *et al.*, 1995), as well as serum deprivation-induced neurite outgrowth of murine neuroblastoma cell lines.

Since FB_1 did not impair neurite growth, newly synthesised GSLs are not essential for axonal growth. This finding is in accordance with the study by Schwarz *et al.* (1995), in which incubation of cultured hippocampal neurons with FB_1 dramatically reduced the amount of cell surface gangliosides, as early as 24 hours after the initiation of treatment. Schwarz *et al.* (1995) analysed the relationship between neuronal growth and sphingolipid metabolism by analysing the effect of FB_1 on neuronal development. Inhibition of GSL synthesis did not affect the formation of the parent axon during its emergence from the cell body. In hippocampal neurons, the most significant effect of inhibition of GSL synthesis was impairment of formation or stabilization of collateral axonal branches. Inhibition of sphingolipid synthesis results in a decrease in the number of axonal branch points/cell, whereas inhibition of sphingolipid degradation results in an increase in the number of axonal branch points (Schwarz *et al.*, 1995).

Schwarz and Futerman (1998) demonstrated that dendritic growth in hippocampal neurons also requires ongoing sphingolipid synthesis. With continuous incubation with FB_1, dendritic growth rates were ~25% slower than control cells, resulting in neurons with

shorter dendritic arbors and less dendritic branch points per cell, and readily apparent differences in morphology compared to control cells after 10-14 days in culture. In contrast, FB_1 had no effect on the initial growth of minor processes, which were destined to become dendrites, even in cells in which FB_1 affected the rate of axon growth. These data demonstrate that normal dendrite growth in hippocampal neurons requires sphingolipid biosynthesis, although the molecular requirements for sphingolipid synthesis may differ from those in axons.

de Chaves *et al.* (1997) presented evidence that FB_1 inhibits GSL synthesis in cultured primary rat sympathetic neurons by showing that FB_1 inhibited incorporation of [^{3}H] palmitate into several gangliosides in rat sympathetic neurons indicating that it inhibits GSL synthesis. The findings also indicate that newly synthesized GSLs are not essential for neurite growth, but that the lipid second messenger CER negatively regulates neurite growth.

2.26.4.5 Effect of fumonisin B_1 on cell viability, protein synthesis and cell cycle

The involvement of lipid peroxidation on FB_1 induced cytotoxicity was investigated in the C6 glioma cell line to establish any relationship between cell viability, genotoxicity and cell division (Mobio *et al.*, 2000). The study showed that FB_1 induced a reduction in cell viability, which was prevented by the antioxidant vitamin E, thus confirming the involvement of lipid peroxidation in the cytotoxicity induced by this toxin. Rat C6 glioma cell viability was not affected significantly up to 5-6μM of FB_1, then decreased to 60-65% with 9-30 μM FB_1. Viability was never lower than 50% even with higher concentrations of 30-50 μM FB_1. The reduction in C6 glioma cells viability induced by FB_1 was prevented by vitamin E at 25μM when cells were pre-treated before the addition of the toxin ($p=0.01$). Protein synthesis as determined by the incorporation of [^{3}H] leucine in C6 glioma cells was inhibited in a dose dependent manner by FB_1 after 24hour incubation. The inhibition was strong and linear ($r=0.987$) up to 10μM. The IC_{50} concentration was 6μM. For higher concentrations of FB_1, the percentage of inhibition reached a plateau at about 75-80%. After 48hour incubation, FB_1 inhibited DNA synthesis exactly as after 24hour incubation. A residual DNA synthesis was still going on. Protein synthesis was slightly less inhibited after 48 hours, as compared to percentage inhibition after 24 hours. This applied also to the C6 cells viability.

Using flow cytometry, the distribution of cells within the different cell cycle phases in control C6 cells was 36±2% for the G_0/G_1 phase, 18.5±3% for S phase and 46±0.5% in G_2/M phase. When C6 glioma cells were incubated with FB_1, the distribution of cells into the different cell cycle phases was modified. The number of cells in S phase decreased significantly, ($p \leq 0.05$), but not in a dose-dependent manner, from six up to 18μM FB_1. The number of cells in G_2/M phase increased significantly ($p \leq 0.05$), but not in a dose-dependent manner from 3μM of FB_1. The reason for this lack of dose dependency is not clear, however it is striking that low concentrations of FB_1 that are not highly cytotoxic are capable of inducing the cell cycle arrest. This effect could be closely related to genotoxicity or some epigenetic effects. This suggests that even low concentrations of FB_1 that do not affect cell viability are already capable of inducing cell cycle arrest in the G_2/M phase (Mobio *et al.*, 2000).

The synthesis of DNA as determined by [^{3}H] thymidine incorporation in C6 glioma cells was not significantly inhibited up to 5μM. With 10, 20 and 50μM of FB_1, the inhibition of the DNA synthesis was of 27±4%, 37±4% and 27±0.5% respectively. Concerning the epigenetic effects, the results of Mobio *et al.* (2000) show that FB_1 induces significant hypermethylation in the DNA of C6 glioma cells in the concentration range of 9 to 18μM. The lack of hypermethylation with FB_1 concentrations above 18μM could be related to an extreme cytotoxicity and also as a consequence of DNA damage. The extent of DNA damage induced by concentrations of FB_1 in the range of 6-18μM could favour the hypermethylation of DNA. In addition, methylated CpG sites can bind specific nuclear proteins such as MeCp1 and MeCp2 (Nan *et al.*, 1993), which could conceivably block or modify the repair process (Tornaletti and Pfeifer, 1995).

The apparent discrepancy between the percentage of FB_1-induced inhibition of DNA synthesis and protein synthesis in the C6 glioma cells, as related to the concentrations of the mycotoxin, could tentatively be explained by assuming that protein synthesis is the first target of FB_1, thus confirming previous results (Abado-Becognee *et al.*, 1998). This could consequently decrease the intracellular level of DNA synthesis with the 48-hour incubation time. C6 cell viability was not modified while the protein synthesis inhibition was slightly lower. All these results reflect consequences of the residual DNA synthesis, and may allow cell multiplication to a new generation, which at its turn is being inhibited by FB_1. Such a

pathway could generate mutated cell types due to possible DNA base modification induced by FB_1 in the previous cell generation.

2.26.4.6 Effects of fumonisin B_1 on neuron extension and synapse formation

Neuronal growth is regulated by both extracellular and cellular determinants and proceeds by the addition of new membrane material at the growth cone. To determine whether lipid synthesis is necessary to maintain neuronal growth, Harel and Futerman (1993) examined the effect of FB_1 on the development of cultured hippocampal neurons. Ganglioside synthesis and content was reduced after FB_1 treatment, ganglioside GD1b was not detectable at the cell surface by immunofluorescence, and in fumonisin-treated cells no increase in axon length was observed. Addition of a fluorescent derivative of CER together with FB_1 reversed the effect, confirming that FB_1 acts via inhibition of CER synthase. Normal axonal growth was restored by addition of exogenous CER derivative suggesting that depletion of GSLs directly caused the reduced axonal growth. The ability to restore normal function by CER replacement shows that these effects of fumonisins are due to loss of biosynthesis of a key sphingolipid (or sphingolipids). However, fumonisin induced disruption of sphingolipid metabolism causes numerous biochemical changes that could affect cellular regulation. It is difficult therefore to clearly demonstrate that a single biochemical perturbation could account for any specific effect on cell behaviour. This study showed that sphingolipid synthesis is necessary to maintain neuronal growth by demonstrating that in hippocampal neurons, inhibition of CER synthesis by FB_1 disrupted axonal outgrowth.

Using primary cultures of hippocampal neurons in a study on the regulatory roles for sphingolipids in the growth of polarised neurons, Futerman *et al.* (1998) found that sphingolipids play at least three distinct roles in regulating neuronal development. These are namely that CER enhances the formation of minor neuronal processes from lamellipodia, that glucosylceramide synthesis is required for both normal and accelerated axon growth, and that at both of these stages of development, CER induces apoptotic cell death at high concentrations. These observations are consistent with the possibility that minor process formation and apoptosis are both regulated by CER-dependent signalling pathways, whereas axonal growth may require glucosylceramide synthesis to support an intracellular transport pathway (Futerman *et al.*, 1998).

Meivar-Levy and Futerman (1999) demonstrated that inhibition of CER synthesis by FB_1 for five days, resulted in up-regulation of the activities of three enzymes in the pathway of Gb3 synthesis; namely glucosylceramide, lactosylceramide and Gb3 synthases. Up regulation of the activities is due to an increase in maximal velocity (V_{max}), with no change in K_m values.

Aggregating brain cell cultures exposed to FB_1 (3-40 μM) for 10 days show decreases in both the total content of MBP and immunoreactivity of the oligodendrocyte membrane marker Gal C in the absence of general cytotoxicity (Monnet-Tschudi *et al.*, 1999).

2.26.4.7 Effects of ceramide, sphinganine and sphingosine on neuronal cells

The effect of six structurally modified So analogues on biosynthesis of sphingolipids was studied in primary cultured murine cerebellar neurons. Treatment of cells with *cis*-4-methylsphingosine at micromolar levels resulted in a markedly decreased sphingolipid biosynthesis, whereas the other compounds examined; *trans*-4-methyl-So, *cis*-5-methyl-So, *trans*-5-methyl-So, *cis*-So, and 1-deoxy-So inhibited sphingolipid biosynthesis less efficiently. The inhibition of sphingolipid biosynthesis by the various compounds was paralleled by a decrease of SPT activity *in situ*. The activity of other enzymes of sphingolipid biosynthesis, as well as phospholipid and protein biosynthesis was not affected. Except for 1-deoxysphingosine, the other five So analogues were shown to be substrates for So kinase *in vitro*. The inhibitory effect of the So analogues on SPT was mediated by their respective 1-phosphate derivatives and the pronounced effect of *cis*-4-methyl-So was caused by a high intracellular concentration of *cis*-4-methyl-So 1-phosphate. *cis*-4-methyl-So, in addition, caused drastic changes in cell morphology of primary cerebellar neurons, which were not observed when these cells were treated with one of the other So analogues examined (van Echten-Deckert *et al.*, 1997).

Sphingosine has been found to inhibit neutrite outgrowth in PC-12 cells in response to NGF (Hall *et al.*, 1988). 1-Methylthiodihydroceramide (10μM) decreased *de novo* CER biosynthesis by about 90% in primary cultured cerebellar neurons. Accordingly, *de novo* formation of SM and of GSLs, all of which contain CER in their backbone, was reduced in a time and concentration-dependent manner by up to 80%. Complex sphingolipid synthesis was restored upon addition of dihydroceramide or CER, in micromolar concentrations, to

the culture medium, suggesting that none of the glycosyltransferases involved in GSL biosynthesis is inhibited by this analogue (van Echten-Deckert *et al.*, 1998).

Riboni *et al.* (1995) showed that CER plays a mediator role in the regulation of cell differentiation in N2α neuroblastoma cell line. Fumonisin B_1 blocked So-induced differentiation, which established that conversion of So to CER is required. Fumonisin B_1 also diminished retinoic acid induced differentiation, showing that *de novo* CER synthesis is important in differentiation of this cell line.

2.26.4.8 DNA damage in astrocytes exposed to fumonisin B_1

Galvano *et al.* (2002) exposed rat astrocytes to FB_1 with the aim of evaluating the involvement of oxygen free radicals and some other biochemical pathways such as caspase-3 activity and DNA damage. Their results indicated that FB_1 treatment (48 hours, 72 hours and 6 DIV, and 10, 50, and 100μM) does not affect cell viability. Conversely, after 72 hours of treatment, 50 and 100μM FB_1 induced DNA damage and enhancement of caspase-3 activity compared to controls. The authors conclude that the DNA damage of apoptotic type in rat astrocytes is caused by FB_1, and that the genotoxic potential of FB_1 should be reconsidered as it has probably been underestimated.

2.27 OTHER *Fusarium* MYCOTOXINS

Included in the *in vitro* component of the work in this study are the mycotoxins FA, ZEA, T2, and DON. Brief summarises of their characteristics are listed below.

2.27.1 Zearalenone

Zearalenone is a non-steroidal oestrogenic mycotoxin produced by several *Fusarium* species (Figure 2.8). It is a stable compound, both during storage/milling and the processing/cooking of food, and does not degrade at high temperatures. Zearalenone has been implicated in numerous mycotoxicoses in farm animals, especially in pigs (European Commission, 2000a).

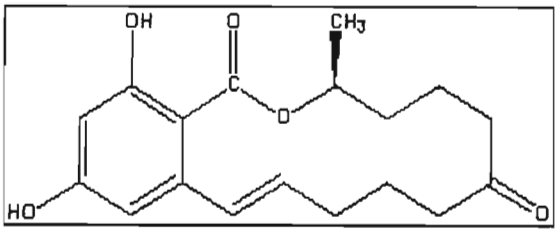

Figure 2.8: **Chemical structure of zearalenone.**

Consumption of ZEA by swine at more than 0.1 to 5ppm causes an oestrogenic syndrome, characterised in females by a swollen vulva with enlarged mammary glands, and in young males by a shrinking of the testes. Oestrogenism in swine is usually more prevalent in the early spring because, once the fungus is established in the grain, it generally requires a period of relatively low temperatures to produce significant amounts of ZEA (Jacobsen *et al.*, 1993).

Zearalenone has shown a DNA damaging effect in recombination tests with *Bacillus cereus*, and further experiments revealed DNA adduct formation in the kidney, ovaries and livers of female mice. In contrast, DNA adducts were not observed in rats after treatment with ZEA. Zearalenone was not carcinogenic to rats of either sex but was carcinogenic in mice, as observed by the increased proportion of male and female mice with pituitary adenomas and by the increased proportion of female mice with hepatocellular adenomas after feeding these animals ZEA (United States National Toxicology Program. 1982).

Further research is also needed with regard to human toxicity. Zearalenone was suspected to be the causative agent in an epidemic of pubertal changes in young children in Puerto Rico between 1978 and 1981 and it has been suggested that zearalenone may have a possible involvement in human cervical cancer. Currently, IARC classifies zearalenone as a Class 2A carcinogen, the highest possible classification when categorical human epidemiology is absent (Leatherhead Food Research Association, 2002).

2.27.2 T-2 Toxin

T-2 toxin belongs to the trichothecenes type A group that are produced by *Fusarium*

species of fungi (Figure 2.9). The trichothecenes share a tricyclic nucleus and usually contain an epoxide at C-12 and C-13. This epoxide is essential for toxicity. Trichothecenes are in general very stable compounds, both during storage/milling and the processing/cooking of food and do not degrade at high temperatures (Desjardins, 1993).

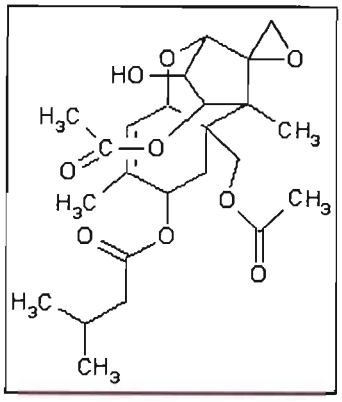

Figure 2.9: Chemical structure of T-2 toxin.

Trichothecenes are sesquiterpene epoxides that inhibit eukaryotic protein synthesis and thereby impair human and animal health (Desjardins *et al.*, 1993). T-2 toxin has been implicated in two outbreaks of acute human mycotoxicoses. The first occurred in Siberia, during the Second World War, producing a disease known as "alimentary toxic aleukia" (ATA) where thousands of people, who were forced to eat grain that had over-wintered in the field were affected. The symptoms of ATA included fever, vomiting, and acute inflammation of the alimentary tract, anaemia, circulatory failure and convulsions. T-2 toxin poisoning also occurred in Kashmir in India in 1987, and was attributed to the consumption of bread made from mouldy flour from which T2 was isolated.

The major symptom was abdominal pain together with inflammation of the throat, diarrhoea, bloody stools and vomiting. This mycotoxin has also been implicated with the occurrence of haemorrhagic toxicoses in farm animals, especially in poultry. T-2 toxin is a potent skin-damaging agent and is absorbed slowly (12-24 hours) via intact skin, but rapidly through abraded skin. The rapid appearance of symptoms after respiratory exposure in humans, along with the results of animal inhalation studies, indicates rapid absorption and high retention of aerosolised T2, with the respiratory tree retaining small amounts (Augerson, 2000). The many mechanisms by which T2 produces toxicity are varied and their relative importance in producing illness is not fully understood. These mechanisms

include inhibition of protein, DNA and mitochondrial protein synthesis, as well as induction of single strand breaks in DNA (European Commission, 2000b).

Dietary levels of T-2 toxin as low as 0.5ppm were found to cause a reduction in feed intake in pigs (Rafai *et al.*, 1995). T-2 toxicoses are due to elevation of tryptophan in the brain. Tryptophan is a precursor of serotonin, a mediator of appetite (Smith and Seddon, 1998). The relative toxicities of the type A (isovaleryl, hydrogen or hydroxyl at the C8 position, (e.g., T2, Figure 2.9) and the type B (carbonyl group at the C8 position e.g., DON, Figure 2.10) trichothecenes have been studied in a number of cell and animal systems. While the ranking of toxicity is similar, the range of toxicity varies dramatically with the system used. The difference in toxicities between the most (T2 toxin) and the least (3-acetyl DON) toxic trichothecenes was 1300-fold for Vero cells (Thompson and Wannemacher, 1986), 23 000 fold for MIN-GL1 cells, 2000 fold for K562 cells (Visconti *et al.*, 1991), and 1500 for BHK-21 cells (Rotter *et al.*, 1993).

Holt and Deloach (1988) found that bovine cells were the most sensitive to T2 (50% inhibition at 2.2ng.ml^{-1}) while hamster cells were the least sensitive (50% inhibition at 26.2ng.ml^{-1}). Murine cells exhibited intermediate sensitivity (50% inhibition at 10.9ng.ml^{-1}). Lymphocytes were three fold more sensitive to T2 inhibition than comparable tissue culture cell lines. Mirocha *et al.* (1992) found that T-2 toxin was toxic to five rat hepatoma cell lines (H4TG, H4-II-E, H4-II-E-C3, Fao and MH1C1) and one dog kidney cell line (MDCK). The IC_{50} values for T2 were between 1.5-5ng.ml^{-1} for the rat hepatoma lines and 0.5ng.ml^{-1} for the dog kidney cell line.

2.27.3 Deoxynivalenol

Deoxynivalenol is produced by *F. culmorum* and *F. graminearum*, which are abundant in cereal crops (wheat, maize, barley, oats, and rye) and processed grains (malt, beer and bread) (Figure 2.10). Chemically, it belongs to the class of tricothecenes. In contaminated cereals 3- and 15-acetyl DON can occur in significant amounts (10-20%) concomitantly with DON. Deoxynivalenol is a very stable compound, both during storage/milling and the processing/cooking of food (Rotter *et al.*, 1996; Ehling *et al.*, 1997; Eriksen and Alexander, 1998).

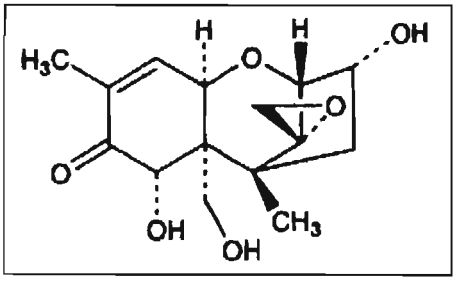

Figure 2.10: Chemical structure of 4-deoxynivalenol (DON; vomitoxin, dehydronivalenol, RD-toxin).

The IARC (1993a) classified DON in Category 3, i.e., not classifiable as to its carcinogenicity to humans. At that time however, the negative chronic study in mice was not available (Iverson *et al.*, 1995). Deoxynivalenol inhibits the synthesis of DNA and RNA and protein synthesis at the ribosomal level, and has a haemolytic effect. An acute dose of DON can induce vomiting in pigs, whereas at lower concentrations in the diet it reduces growth and feed consumption. Both effects, which are also seen with other trichothecene toxins, are possibly mediated by modifying the serotonergic activity in the CNS or via peripheral actions on serotonin receptors (Rotter *et al.*, 1996; Eriksen and Alexander, 1998).

Deoxynivalenol showed neither mutagenic activity in Ames tests with *Salmonella typhimurium*, both with and without S-9 activation systems, nor in an *in vitro* unscheduled DNA synthesis test using rat primary hepatocytes. Deoxynivalenol enhanced cell transformation in mouse embryo cells *in vitro*, and induced clastogenic effects and inhibited gap-junctional intercellular communication in Chinese hamster V79 cells. Deoxynivalenol inhibited the protein synthesis in CHO cells *in vitro* in the same dose range as that inducing clastogenic effects. There are indications for a suppression of humoral and cellular immunity, resulting in an increased susceptibility for infectious diseases (Hsia *et al.*, 1988; IARC, 1993a; 1993b; Leatherman and Middlebrook, 1993; Eriksen and Alexander, 1998). Regarding this increased susceptibility for infectious diseases, a NOAEL of 0.25 $mg.kg^{-1}$ body weight per day (Tryphonas *et al.*, 1986) and a lowest-effect level of 0.22 $mg.kg^{-1}$ body weight per day were reported in studies with male Swiss-Webster and male Balb/C mice, respectively (Baars *et al.*, 1999). Studies are needed to cover the trichothecenes group as a whole, to confirm that there are no neurotoxic effects at doses below those causing effects on growth and body weight, focusing on the known target for tricothecenes, the CNS serotonergic system.

2.27.4 Fusaric acid

Fusaric acid (5-butylpicolinic acid, FA) (Figure 2.11) is a phytotoxin produced mainly by *F. moniliforme*. Fusaric acid selectively inhibits the enzyme dopamine β-hydroxylase, both *in vitro* and *in vivo* (Nagatsu *et al.*, 1970) leading to an increased concentration of dopamine (DA) and its metabolites with concomitant reduction in brain noradrenalin (NA) concentrations. Dopamine-β hydroxylase catalyses the final step in the biosynthesis of norepinephrine. Fusaric acid does not influence the activity of tyrosine hydroxylase, monoamine oxidase or aldehyde dehydrogenase (Nagatsu *et al.*, 1970) nor does it affect the release or uptake of catecholamines. In man, FA was shown to increase CSF DA metabolites, while reducing NA metabolites (Sack and Goodwin, 1974). Disease symptoms observed includes loss of appetite, vomiting, gastrointestinal lesions, lethargy, immunosuppression and loss of muscle co-ordination.

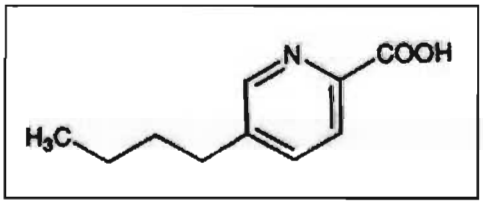

Figure 2.11: Chemical structure of fusaric acid (5-butylpicolinic acid, FA).

Fusaric acid is mildly toxic to mice and has several important pharmacological properties in that both brain and pineal neurotransmitters and metabolites are affected (Porter *et al.*, 1995). Fusaric acid was growth inhibitory and cytotoxic *in vitro* (Fernandez-Pol *et al.*, 1993; Vesonder *et al.*, 1993) and inhibited DNA synthesis in WI-38 fibroblasts (Fernandez-Pol *et al.*, 1993). It is a hypotensive agent and by inhibiting β-hydroxylases (Hidaka *et al.*, 1969), alters tissue levels of catecholamines and indolamines in rats (Porter *et al.*, 1995; Rimando and Porter, 1997). Fusaric acid was not overtly toxic to rats (Voss *et al.*, 1999) and enhanced vomiting and feed refusal in pigs given trichothecenes (Smith and MacDonald, 1991; Smith *et al.*, 1997). Bacon *et al.* (1995) found enhanced toxicity when FA and FB_1 were administered simultaneously to developing chicks *in ovo*, providing direct evidence of FA and FB_1 synergism.

Swine are particularly sensitive to the presence of *Fusarium* mycotoxins in feedstuffs. Deoxynivalenol and FA act in a synergistic manner to reduce growth rates and production efficiency in swine. *Fusarium* mycotoxicoses are known to affect appetite regulation in swine, with suppression of appetite being an economically significant factor. It has been proposed that the loss of appetite is associated with elevated brain tryptophan concentrations. Large doses of tryptophan can cause vomiting in swine. Fusaric acid has a relatively low toxicity in animals, however it has been demonstrated that acute doses of FA administered to rats can elevate brain tryptophan and serotonin levels. Seddon *et al.* (1997) have shown that orally dosing swine with FA can trigger vomiting and lethargy with accompanying increases in brain tryptophan and serotonin. Deoxynivalenol triggers similar responses in swine. The ability of tryptophan to be taken up by the brain across the BBB is a limiting factor in determining brain tryptophan concentrations. Large neutral amino acids such as leucine, isoleucine, valine, phenylalanine and tyrosine compete with tryptophan for uptake into the brain. Therefore, dietary supplementation of these amino acids or the feeding of feedstuffs rich in these amino acids might overcome the feed refusal due to *Fusarium* mycotoxins and would facilitate increased use with *Fusarium*-contaminated grains in swine production.

2.27.5 Moniliformin

Moniliformin is formed in cereals by a number of *Fusarium* species that include *F. avenaceum, F. subglutinans*, and *F. proliferatum* and occurs as the sodium or potassium salt of 1-hydroxycyclobut-1-ene-3, 4-dione.

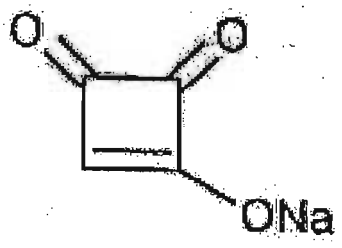

Figure 2.12: Chemical structure of moniliformin.

There is a limited amount of data on the effects of MON on mammalian species. It is a potent inhibitor of mitochondrial pyruvate and ketoglutarate oxidation. In a few studies MON caused chromosomal aberrations. In humans, MON has been linked to Keshan disease which is endemic to certain areas of China.

2.28 CONCLUSION

Research on the occurrence, toxicity, and mechanism of action of *Fusarium* mycotoxins has provided information essential to establishing the degree of exposure of humans and animals to these toxins, and the extent to which they pose a threat to human and animal health. Further studies on the human pathophysiology of fumonisin toxicoses are essential in diagnosis of the disease, establishment of safety parameters and development of control and prevention procedures. Currently, the available information on human health effects associated with fumonisins is inconclusive. However, based on the information on the animal health effects associated with fumonisins, human health risks associated with fumonisins are possible and require investigation. Unless systems other than sphingolipid metabolism are discovered affected by fumonisins, the inhibition of CER synthase would be considered the initial step in the toxicity and carcinogenicity of these mycotoxins. This represents only the starting point for understanding the pathology of these compounds. More must be learned about the cellular consequences of elevations in Sa and various Sa metabolites, and the reductions in key complex sphingolipids caused by fumonisins. Such investigations should provide insight into, not only the mechanism of diseases caused by fumonisins, but also into the biological role of sphingolipids.

This review has highlighted that a vast amount of work has been directed into *in vitro* and *in vivo* analyses of the effects of fumonisins. Due to interspecies differences between structure and cell composition in the CNS of humans and animals, the consequent varying cytotoxic effects of fumonisin are not easy to extrapolate to the human situation. Although research has been directed into the effects of fumonisins on selected cells in the human CNS, no direct links have been established between fumonisins and human brain cancer. This study aims to address this gap in knowledge by screening brain tumour tissue and matched serum samples using immunohistochemical techniques and HPLC to establish whether FB_1 is associated with the pathogenesis of human brain cancer.

CHAPTER 3

Cytotoxicity of selected *Fusarium* mycotoxins and sphingoid bases on the N2α mouse neuroblastoma cell line

3.1 INTRODUCTION

The development of ideal *in vitro* models contribute significantly to the knowledge of cytotoxic and genotoxic mechanisms of chemical procarcinogens. Although the complexity of a whole organism can never be represented or mimicked *in vitro*, there are a number of toxicological questions that may be addressed in these systems. For the understanding of basal mechanistic aspects, and for the screening of compounds for specific toxic effects, such simplified systems are often preferable, facilitating reduction in the number of compounding variables (Horbach and De Groene, 1995). Furthermore, due to the advantages of *in vitro* cytotoxicity assays in terms of convenience, direct detection of toxicity, cost and duration, these assays may well be suited for risk assessment in general.

Toxic compounds may present a potential risk to neuronal function by directly or indirectly affecting the nervous system via interference with biochemical processes. Neuronal cell lines represent homogenous cell populations that may be maintained indefinitely in culture, providing experimental systems with relatively constant characteristics (Walum *et al.*, 1990; Bonsi *et al.*, 1996). Furthermore, different cell lines express specific neuronal phenotypes. Such experimental models would permit the identification of specific cellular targets of toxins within the nervous system, and facilitate the study of the mechanism of their cytotoxic action (Bonsi *et al.*, 1996).

The N2α cell line is a transformed cell line derived from a mouse neuroblastoma tumour of the PNS and arises from cells of the neuroectoderm. *In vivo*, this tumour subtype arises from neuroblasts forming the adrenergic component of the sympathetic nervous system, so the most common sites of presentation are the adrenal medulla and sympathetic ganglia running along the spinal cord from the neck to the abdomen (Kemshead, 1985).

Rapid and accurate assessment of viable cell number and cell proliferation are important requirements in experiments involving *in vitro* studies. Microculture tetrazolium assays (MTAs) are used to measure cell proliferation, and in cytotoxicity assays; to probe the

relationships between cell survival, cytotoxicity and viability, as well as investigate associations between compromised cell metabolism, oxidative stress, and programmed cell death. Slater *et al.* (1963) described the staining reactions of four tetrazolium salts caused by the intact respiratory chains of rat liver mitochondria, the main point being the applicability of these observations for measuring the mitochondrial activity of living cells. Mossman (1983) further described a colorimetric cell culture assay based on this study, using the tetrazolium salt 3-{4,5-dimethyl thiazol-2-yl}-2,5-diphenyltetrazolium bromide (MTT) to measure cell proliferation and survival. This assay depends upon the reduction of the yellow-coloured MTT salt to purple formazan crystals by the succinate tetrazolium reductase system that belongs to the respiratory chain of mitochondria in viable cells (Altmann, 1976; Slater *et al.*, 1963). Berridge *et al.* (1996) showed that the reduction is intracellular, and is catalysed predominantly by microsomal enzymes that require reduced nicotinamide nucleotides, and that succinate can also act as an electron donor in MTT reduction, through mitochondrial succinate dehydrogenase. This reduction through mitochondrial succinate dehydrogenase is slow however, and contributes little to total cellular MTT reduction. Both cell viability and cell proliferation may be monitored by this colorimetric assay. Increased total enzymatic activity, including that for mitochondrial dehydrogenases, accompanies cell proliferation.

Based on these principles, MTT assays have been used for numerous medical, microbiological and toxicological tests (Cole, 1986; Gerlier and Thomasset, 1986; Hanelt *et al.*, 1994). Reubel *et al.* (1987) and Reubel *et al.* (1989) reported the suitability of the MTT assay for the cytotoxic evaluation of the mycotoxins DON, ZEA and ochratoxin A using monolayers, as well as floating cells. Similar studies were carried out by Holt *et al.* (1988), Holt and Deloach (1988) and Holt *et al.*(1989) studying the cellular effects of T2 on different cell lines. The MTT assay has also been used for testing other *Fusarium* mycotoxins on many cell lines (Visconti *et al.*, 1991).

The objective of the present investigation was to assess the cytotoxicity of selected water-soluble (FB_1, MON and FA) and ethanol soluble (ZEA, T2 and DON) *Fusarium* mycotoxins on the N2α mouse neuroblastoma cell line. In addition, the cytotoxic effects of the exogenously added sphingoid bases, Sa and So, were also assessed.

3.2 MATERIALS AND METHODS

3.2.1 Materials

Cell culture materials, media, antibiotics, and sterile disposable consumables were purchased from Adcock Ingram (SA) unless otherwise indicated. Pre-sterilised Corning plastic tissue culture flasks ($75cm^2$) were used as culture vessels, and sterile 96-well microtitre plates were used for the cytotoxicity assays. All mycotoxins were obtained from the Mycotoxin Research Group at the University of KwaZulu-Natal (UKZN). The MTT salt, DL-erythro-dihydrosphingosine (sphinganine) and D-sphingosine (sphingosine) were purchased from Sigma Aldrich Chemical Company (SA).

The N2α mouse neuroblastoma cell line was purchased from Highveld Biologicals, SA. A strict aseptic protocol was adhered to with regard to the culture environment and apparatus used.

3.2.1.1 Cell culture media

Dulbecco's Modified Essential Medium (DMEM) (pH 7.2-7.4) balanced salt solution (without L-glutamine and with a combination of inorganic salts, glucose, amino acids and vitamins) was purchased pre-sterilized for cell culture. L-glutamine (200mM) (10ml) was added to DMEM (500 ml). Foetal calf serum (FCS) was used as an additional nutrient source. Pre-sterilised, heat- inactivated filtered FCS was aliquoted into sterile vials (25ml) and stored at -20°C until use. Foetal calf serum was added (10%) (volume per volume (v/v)) to DMEM (500ml) to make complete culture medium (CCM) required for growing cells. The CCM (500ml) was also supplemented with sodium pyruvate (100mM) (5 ml).

The antibiotic Penstrep-Fungizone (5ml) was added to CCM (500ml) routinely. Hank's Balanced Salt solution (HBSS) (2ml) was used routinely to wash and remove dead cells and cell debris prior to supplementing cells with fresh CCM (5ml). Ethylenediamine tetraacetic acid [(EDTA), 0.1% in distilled water] was used for trypsinising the N2α cells. Dimethylsulphoxide (DMSO) was used at concentrations of 5%-10% (v/v) in 10%CCM as the freezing medium for cells stored at -70°C. High FCS concentrations are used in freezing because FCS does not crystallise, and surrounds cells preventing water from entering and crystallising within the cells.

3.2.2 Methods

Descriptions of all cell culture techniques employed, including environment, trypsinisation, cell counting, viability assessment, storage, and preservation of cells were applied as previously documented in Palanee (1998).

3.2.2.1 Preparation of the mycotoxins, sphingoid base stock solutions, and MTT salt

Fumonisin B_1, FA, and MON (1mg per mycotoxin) were dissolved directly in CCM (1ml), with CCM as the comparative control for this set of mycotoxins. Zearalenone, T2, DON, Sa, and So (1 mg each) were dissolved in ethanol (100 µl) and CCM (900 µl) to a stock solution of $1 mg.ml^{-1}$. The control was made up of EtOH (100µl) and CCM (900µl). All stock solutions were vortexed thoroughly to ensure complete dissolution of the toxins. Each stock solution was then used in the preparation of a range of concentrations (5, 10, 25, 50, 100, 150, 200 and 250 µM) in CCM.

The MTT salt (5 mg) was dissolved in HBSS (1ml) to a concentration of $5mg.ml^{-1}$. This suspension was filtered through a 0.45µm filter to remove insoluble residues of the MTT salt. The sterile stock solution was prepared immediately before use and stored in the dark at room temperature (RT) until required.

3.2.2.2 The MTT bioassay

The MTT bioassays on the N2α cell line were carried out according to Hanelt *et al.* (1994). Briefly, a culture flask (75 cm^2) of confluent N2α cells was trypsinised and the cells resuspended in CCM to give a cell number of 4×10^6 $cells.ml^{-1}$. Aliquots of the cell suspension (10µl) were dispensed in each of the 96 wells of the microtitre plate to give a final cell count of 40 000 cells/well.

The diluted mycotoxins and sphingoid bases were mixed thoroughly and an aliquot (200 µl) of the test compound at each of the above-mentioned concentrations was transferred to individual wells of the microtitre plate. There were five replicates at each test concentration for each compound and the respective controls. Following the assays 48 hour incubation

period, all test compounds and media were aspirated from the wells, and the cells in the wells were supplemented with fresh CCM (100 µl) and MTT salt solution (10 µl of a 5 $mg.ml^{-1}$ MTT salt solution in HBSS), followed by a further four hour incubation period at 37°C in the dark. The media and MTT salt solution were then aspirated, and the formazan crystals solubilised with DMSO (100 µl) for 1 hour at 37°C. The optical density (OD) of the cells was measured spectrophotometrically, at a dual wavelength of 595nm and 610nm, on a Bio-Rad Microplate Reader. Dose response graphs were drawn using the mean absorbance values obtained in relation to increasing mycotoxin or sphingoid base concentration (Figures 3.1; 3.2 and 3.3).

3.2.3 Statistical analyses

All data were presented as means±standard deviation (SD). The results of the cytotoxicity assay were analysed using the paired 2-tailed Student's t test. A p value <0.05 was considered statistically significant. Mean absorbance values of cells treated with each mycotoxin/sphingoid base at each concentration in the range was used to determine the percentage cell viability in comparison to the control cells at each concentration (Equation 1).

Equation 1:

$$\textit{Cell viability (\%)} = \frac{\textit{mean absorbance of toxin treated cells}}{\textit{mean absorbance of control cells}} \times 100$$

p Values <0.05 were taken as an indication of significant difference from controls. $p<0.05$=♦, $p<0.01$ = ■, $p<0.001$ • indicating significant difference from controls are illustrated on Figures 3.1; 3.2 and 3.3.

3.3 RESULTS AND DISCUSSION

3.3.1 The MTT cytotoxicity assays

The MTT assays were performed to monitor cell viability by measuring the conversion of tetrazolium salts to yield formazan, the amount of which was considered proportional to the number of living cells.

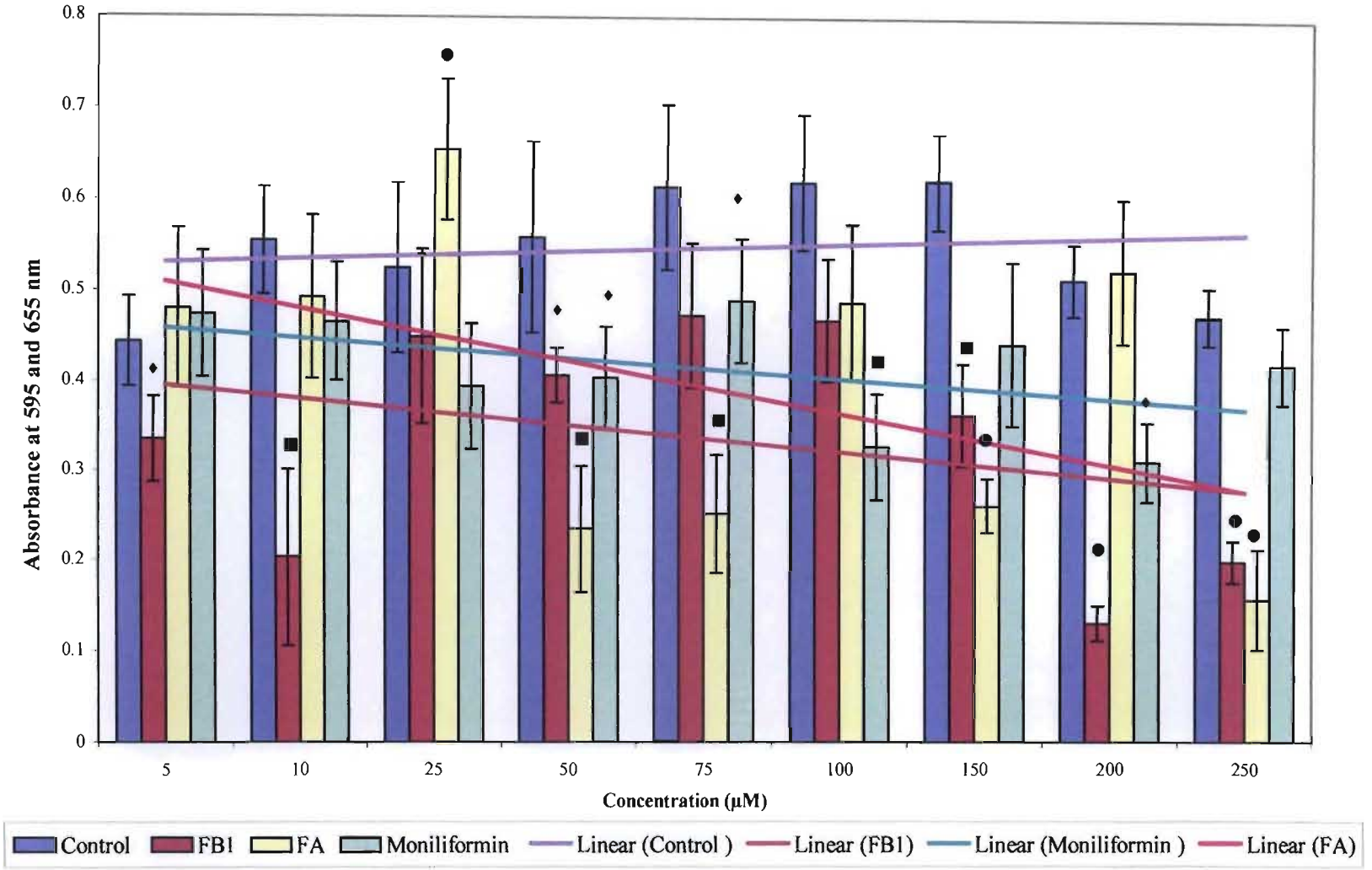

Figure 3.1: **Dose response graphs of the effects of Fumonisin B_1, Moniliformin and Fusaric acid on the N2α cell line. p values <0.05 were taken as an indication of significant difference from the controls. p<0.05=♦, p<0.01 = ■, p <0.001= • , using Student's t-test are illustrated.**

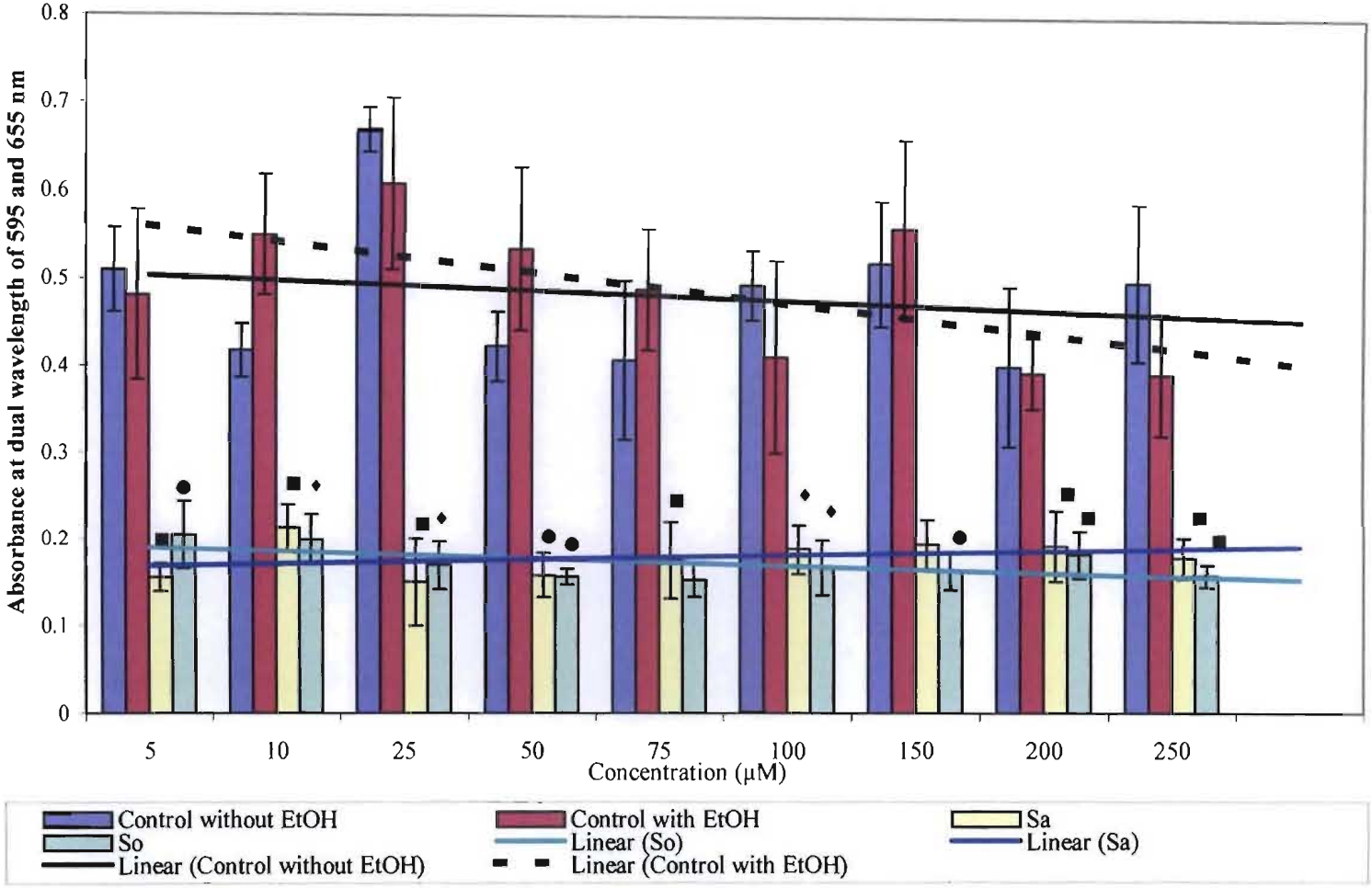

Figure 3.2: **Dose response graphs of the effects of sphinganine and sphingosine on the N2 α cell line. p values <0.05 were taken as an indication of significant difference from controls. $p < 0.05$=♦, $p<0.01$ = ■, $p <0.001$= • using Student's t-test are illustrated.**

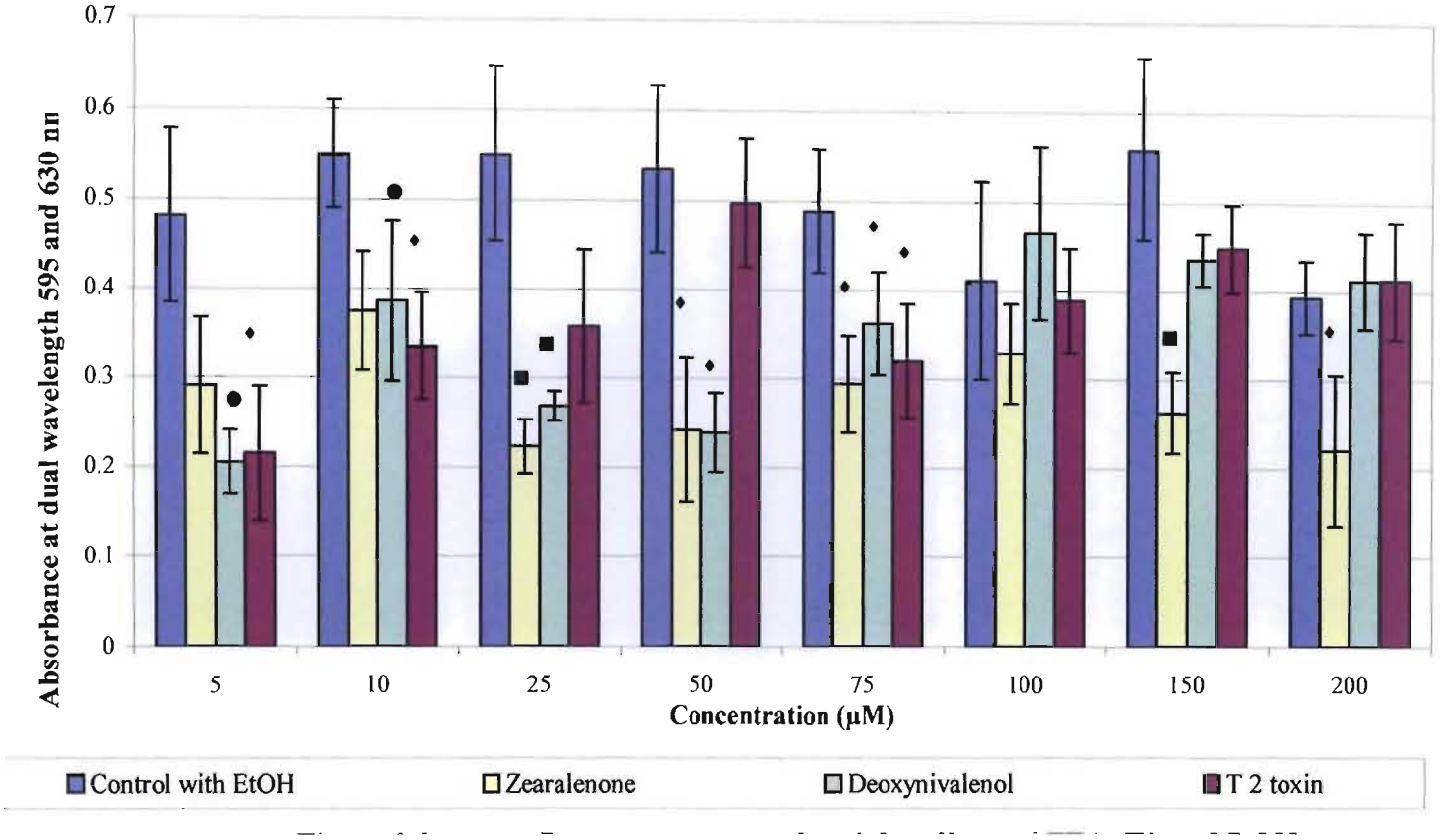

Figure 3.3: **Dose response graphs of the effects of Zearalenone, Deoxynivalenol and T-2 toxin on the N2α cells. p values <0.05 were taken as an indication of significant difference from the controls. $p< 0.05=^{\blacklozenge}$, $p<0.01=^{\blacksquare}$, $p <0.001=^{\bullet}$ using Student's t-test are illustrated .**

The results of the MTT cytotoxicity assays and the comparative effects of FB_1, MON and FA on the N2α neuroblastoma cell line, are shown in Figure 3.1. The effects of the sphingoid bases Sa and So, as well as ZEA, DON, T2 on the same cell line are illustrated in Figures 3.2 and 3.3, respectively.

The exposure time of 48 hours was selected for the MTT assays on the basis of a dose response curve carried out over several time intervals. This helped determine a reasonable length of time that N2α cells could be cultured in the microtitre plates with minimal levels of control cell death, taking into account the standard doubling rate of these cells in the volume of media per well. Support for selection of the 48 hour exposure time, comes from studies of Yoo *et al.* (1992) who showed that FB_1 inhibited cell proliferation (between 10 and 35μM), and cytotoxicity (>35μM FB_1) in LLC-PK1 cells was preceded by a lag period of at least 24 hours during which cells appeared to be functioning normally. Although it is acknowledged that cytotoxicity is cell-type specific, in this study the 48-hour exposure period was considered appropriate for the MTT assays on the N2α neuroblastoma cell line. To remove any bias in interpretation, all treated cells were assessed in parallel to their respective controls.

Most mycotoxins are difficult to dissolve in CCM, and in order to obtain a homogenous test solution, organic solvents are usually added to the media. Many studies have used FB_1 dissolved in methanol and/or acetonitrile: water (1:1) for *in vitro* studies. However, based on the data of the United States National Toxicology Program (1999) that FB_1 is soluble in water to at least 20 $mg.ml^{-1}$, FB_1 was resuspended directly in the CCM in this study to ensure that all effects seen were the direct result of exposure to this mycotoxin, and not by exposure to the organic solvent.

Statistical analyses of the MTT bioassay results using Student's t-test indicate that there were significant differences between the overall effects of FB_1 (p=0.00095) in comparison to untreated N2α control cells across the concentration range (Figure 3.1; Table 3.1). Statistically significant differences (p<0.01) were also noted specifically at 5, 50, 150, 200 and 250μM FB_1 in comparison to controls. The FB_1 trend line in Figure 3.1 indicates that there is a decrease in N2α cell viability with increasing FB_1 concentration (Figure 3.1). Cell viability decreased from 75.7% at 5μM to 42.1% at 250μM FB_1 (Table 3.1). This decrease however was not strictly dose-dependent (Table 3.1). These results are supported

by studies by Norred *et al.* (1991), Shier *et al.* (1991) and Yoo *et al.* (1992) who have shown that FB_1 inhibits cell proliferation and is cytotoxic to many cell types. Inhibition of cell proliferation by FB_1 exposure usually occurs at concentrations that are lower than those which cause cytotoxicity.

Table 3.1: Mean percentage of N2α cell viabilities (p value) following 48 hours exposure to fumonisin B_1, fusaric acid and moniliformin in comparison to untreated N2α control cells[1].

Conc (μM)	% Cell viability (p value)		
	FB_1	FA	MON
5	75.7 (0.01)	108.4 (0.48)	106.9 (0.5)
10	36.7 (0.006)	88.9 (0.25)	83.9 (0.09)
25	85.6 (0.3)	134.1 (0.0009)	77.3 (0.13)
50	72.8 (0.028)	42.1 (0.006)	69.4 (0.04)
75	79.9 (0.06)	41.1 (0.004)	69.5 (0.02)
100	86.3 (0.11)	91.4 (0.3)	61.4 (0.002)
150	71.6 (0.003)	51.6 (0.0004)	87.2 (0.14)
200	29.8(0.0001)	115.4 (0.13)	68.7 (0.013)
250	42.1(0.0001)	33.2 (0.0003)	86.6 (0.08)

[1] Statistical analyses were done with comparison to matched controls. p values<0.05 were taken as an indication of significant difference from controls. p values < 0.05=•, p<0.01 = ■, p <0.001 • are indicated in Figure 3.1.

In an earlier study, Riboni *et al.* (1995) showed that FB_1 blocked So-induced differentiation of the N2α neuroblastoma cell line. These authors established that conversion of So to CER was required and that *de novo* CER synthesis was important, as CER played a mediator role in the regulation of differentiation in these cultured cells. The structural similarity of the polyhydric alcohol moiety of FB_1 to So and Sa (Figures 2.4 and 2.5), allow FB_1 to be recognised as a substrate for CER synthase (Merrill *et al.*, 1996b). Merrill *et al.* (1993b) using microsomal preparations from cultured mouse cerebellar neurons showed that FB_1 was competitive with both sphingoid base and fatty acyl-CoA for CER synthase. Merrill and Sweeley (1996) further suggested that CER synthase recognized both the amino group (sphingoid binding domain) and the TCA side-chains (fatty acyl-CoA domain) of FB_1. Spiegel and Merrill (1996) also showed that inhibition of the enzyme induced a consequent intracellular accumulation of biologically active sphingoid bases and depletion of complex sphingolipids. These factors require consideration in the present study as compounding variables that may have initiated or exacerbated impairment of cellular transduction processes, cell differentiation, growth inhibition, cell mortality and/or mitogenicity of FB_1 on the N2α cells.

In this study, ~63% cytotoxicity was induced in the N2α cells at 10 μM FB_1 (Figure 3.1), and at 200μM, FB_1 induced ~70% cell death following the 48 hour exposure period (Table 3.1). It is likely that the levels of cytotoxicity of FB_1 indicated by the MTT assay are related to the FB_1-induced inhibition of So-induced differentiation of the N2α cells in culture. Tolleson *et al.* (1996b) found that the growth of keratinocytes and epithelial cells were inhibited by 42% when exposed to 10μM FB_1. More recently, Mobio *et al.* (2000) reported that in the C6 glioma cells, FB_1 induced 10 ± 2% and 47 ± 4% cell death following 24-hour incubation period with 3μM and 54μM FB_1 respectively. In contrast, Galvano *et al.* (2002) exposed rat astrocytes to FB_1, and found that FB_1-treatment (48 hours, 72 hours and six days *in vitro*, at 10, 50 and 100μM FB_1) did not affect cell viability. These results highlight that the cytotoxic effects of FB_1 vary with cell type and duration of exposure and there are variable cellular responses.

Variable toxin susceptibility and the cytotoxic responses of cell types to FB_1 may be explained by the following. Although glial cells, astrocytes and neuroblasts are components of the CNS, the variability in cytotoxic response after exposure to FB_1 by the N2α neuroblastoma cell line in comparison to glioma cells and astrocytes are potentially due to cellular, structural and biochemical differences. Reubel *et al.* (1987), Von Milczewskis (1987) and Holt *et al.* (1988) suggest that the varying cytotoxic responses of different cell types to particular mycotoxins may be due to the different metabolic activity of the target cells. The three most commonly encountered explanations for cell to cell variability in toxin sensitivity are differences in the amounts of target enzymes or other cellular functions which interacts with the toxin, the amounts of metabolic enzymes which activate a non-toxic precursor molecule into a metabolite with non-specific toxicity, and the efficiency of detoxification mechanisms that protects the cells and tissues that are less susceptible to toxic agent (Shier *et al.*, 1991).

Thompson and Wannemacher (1984) suggest that the cytotoxic effects of a mycotoxin may also be influenced by the ability of a mycotoxin to bind to cellular receptors and/or penetrate cell membranes. This is dependent on the size, structural conformation of the toxin molecule, and its polarity. Furthermore, the relative significance of a molecular receptor of a mycotoxin is determined by its affinity to the active form of the toxin, its role in vital biochemical processes, the persistence of the lesion it bears, and the severity of the consequence of the lesion.

Inhibition of CER synthase by FB_1 causes the intracellular Sa levels to increase (Wang *et al.*, 1991; Yoo *et al.*, 1992). The two most likely explanations for the increased cell death after inhibition of sphingolipid biosynthesis by fumonisins are that the accumulating free Sa (or a Sa degradation product) is growth inhibitory and cytotoxic to the cells (Stevens *et al.*, 1990; Hannun *et al.*, 1991; Sweeney *et al.*, 1996), and/or that more complex sphingolipids are required for cell survival and growth (Hanada *et al.*, 1992; Radin, 1994; Nakamura *et al.*, 1996). There is therefore the potential for misinterpretation of results of experiments using fumonisins as an inhibitor of CER biosynthesis, unless the effects of these sphingoid bases are also considered.

Ethanol was used as the solvent vehicle for Sa and So in combination with CCM in the MTT assays. Figures 3.2 and 3.3 show that although the viability of the N2α neuroblastoma cells decreased with exposure to the ethanol containing control serial dilutions, no significant differences were detected between any of the test concentrations. This is indicated in Figure 3.2 by the control trend line, which indicates a gradual decrease in cell viability, with an increase in the percentage of ethanol in the CCM. To illustrate that the amount of ethanol used (100 µl) to dissolve the mycotoxins did not induce an acute cytotoxic response in these cells, an ethanol-free control was run against the ethanol-containing CCM treated cells. The lack of a significant difference between the control and (control plus ethanol) treatment (p=0.99) indicate that the cytotoxicity induced by the ethanol solvent was negligible on this cell line.

Elevations of sphingoid bases disrupt normal regulatory mechanisms within cells, and are cytotoxic as indicated by exposure of the N2α cells to exogenous Sa and So (Figure 3.2). The results of the MTT assay indicate that Sa and So were extremely cytotoxic at all the concentrations tested on the N2α cell line (Figure 3.2). Statistical analyses and comparison of So and Sa against their ethanol containing controls across the entire range, indicate statistically significant differences with $p=1.1 \times 10^{-6}$ and $p=1.9 \times 10^{-6}$ for So and Sa respectively. Comparison of the effects of Sa to So revealed that they did not differ significantly ($p=0.51$). At each concentration tested however, statistically significant differences were noted ($p<0.01$) in comparison to the controls within the range. In addition, at all test concentrations cell viabilities were below 50% of the controls (Table 3.2).

Table 3.2: Mean percentage of N2α viabilities (p value) following 48 hours of exposure to sphinganine and sphingosine in comparison to ethanol treated N2α controls[2].

Concentration (μM)	% N2α cell viability (p value)	
	Sa	So
5	32.3 (0.003	42.6 (0.0009)
10	38.7 (0.002)	36.2 (0.002)
25	27.4 (0.004)	30.7 (0.0012)
50	29.5 (0.0003)	29.3 (0.0007)
75	36.0 (0.001)	31.27 (0.0007)
100	45.8 (0.013)	40.72 (0.014)
150	34.8 (0.003)	29.26(0.0008)
200	49.1 (0.001)	46.45 (0.004)
250	45.5 (0.002)	40.22 (0.003)

[2] Statistical analyses were done with comparison to controls run in parallel. p values <0.05 were taken as an indication of significant difference from controls. p values < 0.05=♦, p<0.01 = ■, p <0.001 • are indicated in Figure 3.2.

These results are supported by findings of previous studies on the N2α cell line by Hall *et al.* (1988) and Riboni *et al.* (1995), who reported that addition of exogenous So rapidly elevated cellular CER levels in the N2α cells, suggesting that some effects of So may be mediated by its conversion to CER. The role of CER as an intracellular second messenger for TNF-α, IL-β and other cytokines; So, So-1-phosphate among other sphingolipid metabolites, has been demonstrated to modulate cellular calcium homeostasis, cell cycle progression and apoptosis (Yoo *et al.*, 1992; Merrill *et al.*, 1993b). Elevated So and Sa in the N2α cells may therefore have acted via unscheduled initiation or inhibition of these pathways leading to disruption of metabolism of these endogenous molecules, leading to cytotoxicity and cell death. The maintenance of a low level of free sphingoid bases in cells is important because these compounds have considerable intrinsic biological activity and can be cytotoxic in high concentrations.

Another potential mechanism of action leading to decreased cell viability in the N2α cells exposed to Sa and So, may be via a mechanism similar to that proposed by van Echten *et al.* (1990) and Mandon *et al.* (1991). These authors showed that adding So to cultured mouse cerebellar neurons caused a decreased incorporation of [^{14}C] serine into sphingolipids, apparently due to a down regulation of SPT in a time-and concentration dependent manner. A maximum decrease of 80% in this enzymes activity was achieved with doses as high as 50μM So homologues (Mandon *et al.*, 1991). At this concentration of Sa and So added to the N2α cell line in the present study on the N2α cells, approximately

70% cell cytotoxicity was induced following the 48-hour exposure period (Figure 3.2 and Table 3.2).

Chapter 8 in this dissertation documents the quantitative HPLC analyses of intra and extracellular levels of Sa and So in the N2α cells prior to and following exposure to FB_1, and provides an indication of baseline levels of these sphingoid bases. *In vitro* and *in vivo* Sa and So levels are usually in the nanomolar range whereas in this MTT assay, they were tested at levels multifold higher; hence this level of cytotoxicity was not unexpected. However, concentrations below 5μM Sa and So were not tested on the N2α cell line as this was a comparative study with the effects of the mycotoxins, and the dilution range to which the cells were exposed was standardised for both mycotoxins and sphingoid bases. Future studies on these cells however will endeavour to establish the effects of exposure to exogenous Sa and So at concentrations below 5μM.

Given that FB_1 inhibits CER synthase resulting in an increase in free Sa and So, and that the toxicity of FB_1 may be exacerbated via accumulation of these endogenous sphingoid bases, a point of interest in this study was that the equivalent amount of cell cytotoxicity was induced at 250μM FB_1 (Figure 3.1) and 5μM So (~42%) (Figure 3.2). In addition, 32% cell viability was noted with 5μM Sa. This is relevant, in that FB_1 may have induced inhibition of sphingolipid metabolism in these cells over the 48 hours leading to an increase in Sa and So, resulting in FB_1 initiating indirectly the equivalent levels of cell cytotoxicity. This hypothesis is supported by Gelderblom *et al.* (1995b; 1996b) where in fumonisin-treated primary rat hepatocytes, Sa: So ratios were maximally elevated at 1μM FB_1, whereas cytotoxicity was observed at >250μM FB_1.

Exposure to FA (Figure 2.11) at a concentration of 25μM, induced proliferation of the N2α cells with viabilities of 134% being detected, i.e., viabilities 34% above controls (Figure 3.1). Fusaric acid may act on cytosolic copper ion/zinc ion (Cu^{2+}/Zn^{2+}) and/or mitochondrial manganese ion (Mn^{2+}) - containing superoxide dismutase (SOD) enzymes that may be important for growth and survival of cancerous cells (Fernanadez-Pol *et al.*, 1982) or it may act by binding zinc which is a structural component of certain zinc finger DNA binding proteins that are involved in cell proliferation (Johnson and McKnight, 1989; Fernandez-Pol, 1991; Fernandez-Pol, 1992). Enhanced levels of formazan may therefore be interpreted as increased metabolic activity (Hanelt *et al.*, 1994)

and proliferation as observed with the N2α cells treated with FA. This hypothesis is supported by elevated cell viabilities of 108% and 134.1% detected at 5μM and 25μM FA in this study respectively (Table 3.1, Figure 3.1).

At higher concentrations of FA exposure (50, 75, 150 and 250μM; $p<0.001$), higher levels of cell death were recorded, e.g., 41.1% viability at 75μM FA and 33.2% viability at 250μM FA. However, using Student's t-test, when assessed across the entire range of concentrations, the effects of FA on the N2α cells were not significantly different to that of control cells ($p=0.1$), or to cells treated with MON ($p=0.9$) (Figure 3.1). Fernandez-Pol *et al.* (1993) reported similar findings with the human colon adenocarcinoma LoVo cells. In that study, within 24 hours of exposure to 500μM FA, most of the cells were blocked at random in the cell cycle and approximately 80% of the cells were dead after 30 hours. Vesonder *et al.* (1993) also found that FA was cytotoxic to the MDCK dog kidney fibroblast cell line, McCoy mouse fibroblast cells (MM), rat hepatoma tumour (RH) and CHO cell lines. Three human colorectal adenocarcinoma cell lines, SW 48, SW 480 and SW 742 were also sensitive to the inhibitory and cytotoxic effects of FA.

The cytotoxicity of FA may be attributed to the 5-butyl side chain (Figure 2.11), which because of its lipid solubility may allow better cellular penetrability of this mycotoxin. At 50μM and 200μM FA, 42.1% and 33.2% cell viability was detected in the N2α cell line respectively, following the 48hour exposure period. Telles-Pupulin *et al.* (1998) showed that FA affects mitochondrial energy metabolism by at least three modes of action, namely inhibition of succinate dehydrogenase, inhibition of oxidative phosphorylation, and inhibition of α-ketoglutarate dehydrogenase. The inhibition of oxidative phosphorylation seems to be the result of a direct action on the ATP synthase/adenosine triphosphatase (ATPase) without significant inhibition of the ATP/adenosine diphosphate (ADP) exchange. In isolated perfused rat liver, FA inhibits oxygen uptake and gluconeogeneis from pyruvate, the latter being strictly dependent on intra-mitochondrially generated ATP. In the present study, cell viability is partially reflected by conversion of the MTT salt by succinate dehydrogenase enzymes of mitochondria of viable N2α cells. Lower cell viabilities may have been as a consequence of the inhibition of these enzymes by FA.
In this study, statistically significant differences were noted between MON-treated ($p=0.002$) and control N2α cells across the range of the mycotoxin test concentrations. Cell

viabilities were between 61% and 69.5% with exposures between 50-200μM MON (Figure 3.1). Similar levels of cytotoxicity were noted in the RH, CHO and MDCK cell lines (Vesonder *et al.*, 1993).

Thiel (1978) reported that the principal mechanism of action of MON is believed to involve selective inhibition of mitochondrial pyruvate dehydrogenase (PDH) and α-ketoglutarate dehydrogenase. Thiel (1978) reported that a 5μM concentration of MON caused a 50% inhibition of oxygen uptake by rat liver mitochondria with pyruvate as the substrate. Burka *et al.* (1982) showed that MON binds to PDH preventing entry of pyruvate into the TCA cycle, therefore decreasing mitochondrial respiration. Support for direct binding of MON to PDH was also provided by Burka *et al.* (1982), who showed that rat brain transketolase and pyruvate dehydrogenase were inhibited by 59% by 100μM MON. More recently, decreased protein synthesis and induction of oxidative damage have also been ascribed to MON (Norred *et al.*, 1990).

The MTT assay uses reduced nicotinamide adenine dinucleotide (NADH) as a marker of cell viability. There are two main sources of NADH in cells catabolising carbohydrates; namely glycolysis and the TCA cycle. The former is in the cytosol and the latter in mitochondria. Of these, the TCA cycle produces 10 times more NADH, so essentially the MTT assay measures this. If MON blocks the entry of pyruvate into the TCA cycle, it decreases mitochondrial respiration and therefore NADH production, and this would be reflected by decreased cell viabilities using the MTT assay. Following 48hour exposure to 50 μM and 100 μM MON, viabilities of 69.4% and 61.4% were noted for the mycotoxin treated N2α cells respectively.

In this study, sodium pyruvate supplementation of the CCM was essential to ensure N2α cell proliferation and survival; cells grown in CCM without sodium pyruvate ceased growing. This was considered significant in that it is possible that MON and the pyruvate supplement may have competed for the binding site on PDH. By adding high levels of MON as a suicide substrate of PDH, it may have potentially blocked or decreased mitochondrial respiration causing cell death. The data in the present study concur with earlier findings by Gathercole *et al.* (1986) who showed that pyruvate supplementation resulted in decreased MON-induced inhibition of PDH function. However in the present study, sodium pyruvate was added to the CCM for the N2 α cells at a concentration of

2mM. The higher concentration of pyruvate than MON in the CCM may be the reason why cell viability never dropped below 61% in these cells. At the lowest concentrations of 5μM and 10μM MON, viabilities of 106 % and 83% were determined respectively which indicated the potential negligible proliferative capacity of 5μM MON, and ~20% cytotoxic capacity at 10μM MON. Even at the highest concentration of 250μM MON, 86.6% cell viability was noted which indicates that the levels of sodium pyruvate in the CCM may have protected N2α cells from the toxic effects of this water-soluble mycotoxin.

Statistically significant differences were noted for N2α cells treated with DON ($p=0.04$) and ZEA ($p=0.003$) when the entire range of mycotoxin test concentrations were compared to their controls (Figure 3.3, Table 3.3). With the cytotoxicity of T-2 toxin on the N2α cells there was a tendency towards significance ($p=0.07$). The entire range of concentrations of ZEA when assessed against that of DON ($p=0.09$), were not significantly different from each other either, nor were there significant differences between the effects of DON and T2 ($p=0.4$). However, the effects of ZEA compared to that of T2 toxin did differ significantly ($p=0.04$).

In the T2-treated N2α cells, viability increased with increasing toxin concentration from 45.5% viability at 5μM, to 80.2% viability at 200μM T2. A similar trend was noted in cells treated with DON, with cell viabilities increasing from 42.6% at 5μM DON to 104.8% at 250 μM. Deoxynivalenol and T2 either induced growth arrest or minimal mitogenic effects at the higher levels of the exposure (e.g., at 200 μM), in contrast to the levels of cytotoxicity induced at lower concentrations (e.g., at 10 μM, Table 3.3, Figure 3.3), as indicated by the higher percentage of viable cells in both sets of treated N2α cells. At the lower range of concentrations (i.e., 5 and 50μM), ZEA induced between 40-60% cell-death. At the 200μM ZEA however, 56.1% cell viability was indicated. For these mycotoxins, a distinct dose-dependent effect for cytotoxicity was not established.

The trichothecenes are directly toxic without activation. T-2 toxin is an amphipathic molecule that can enter the cell membrane, disrupt membrane function (Khachatourians, 1990), and induce cell membrane injury via a free-radical mechanism (Coulombe, 1993). In this study on the N2α cells, >50% cell death was induced between 5 and 10μM T2 after the 48 hours, but cell viabilities were close to controls at the higher

range of concentrations. Beasley (1989) reported that trichothecenes inhibit the peptidyltransferase reaction by binding to the 60S ribosomal subunit in eukaryotic ribosomes and their anti-proliferative activity has been presumed to be a consequence of inhibition of protein synthesis in the initiation phase. This concurs with findings in this study on the N2α neuroblastoma cells, where at concentrations of 100 and 200μM, DON seemed to have induced proliferative effects in the N2α cells with cell viabilities of 113% and 104% in comparison to controls (100%). This hypothesis was further supported by lack of a significant difference to controls at these test concentrations.

Table 3.3: Mean percentage of N2α cell viabilities (p value) following 48 hours of exposure to zearalenone, deoxynivalenol and T-2 toxin in comparison to ethanol treated N2α controls[3].

Concentration (μM)	% Cell viability (p value)		
	ZEA	DON	T2
5	60.5 (0.06)	42.6 (0.0007)	45.5 (0.02)
10	68.2 (0.05)	70.2 (0.001)	44.9 (0.02)
25	40.5 (0.002)	48.8 (0.004)	61.02 (0.07)
50	45.3 (0.01)	44.7 (0.004)	65.1 (0.4)
75	60.3 (0.02)	74.2 (0.04)	93.0 (0.02)
100	80.0 (0.4)	113.0 (0.7)	65.6 (0.3)
150	47.0 (0.007)	77.9 (0.09)	94.5 (0.06)
200	56.1 (0.04)	104.8 (0.9)	80.2 (0.8)

[3]Statistical analyses were carried out with comparison to controls using Student's t-test. p values <0.05 were taken an indication of significant difference from controls. p values < 0.05=♦, p<0.01 = ■, p <0.001 • are indicated in Figure 3.3 .

Holt and Deloach (1988) have shown using the toxin sensitive MDCK canine kidney cell line and in toxin-resistant CHO cells, that T-2 toxin mediates a number of effects on the cell membrane, on protein synthesis, and probably mitochondrial reduction of MTT. Using the MTT assay, Holt *et al.* (1988) further showed that the inhibitory effects of T-2 toxin on MTT cleavage in L929 cells was comparable to that observed for protein and DNA synthesis (50% inhibition at 6-8ng.ml^{-1}). T-2 toxin also inhibits the mitochondrial electron transport system by inhibiting succinate dehydrogenase (Khachatourians, 1990) and inhibits gap-junctional intercellular communication in Chinese Hamster V79 cells (IARC, 1993a).

It is possible in the N2α cell line, that at the lower range of concentrations, T2 may have inhibited succinate dehydrogenase in these cells. As was suggested for the effects of FA, cell viability is partially reflected by the conversion of the MTT salt by the succinate

dehydrogenase enzymes of the mitochondria of viable N2α cells. Lower cell viabilities may have been detected as a result of the inhibition of this enzyme by T2 in the N2α cell line. In contrast, using this system to analyse the lethal effects of T2 on cells from various animal species (Holt and Deloach, 1988), it was found that the concentrations that induced 50% cell death were much lower than those used in this study on the N2α cells, highlighting further that a mycotoxins effects are cell type specific.

The N2α cells treated with DON followed a similar trend to the T2-treated cells, with viabilities increasing from 42.6% at 5μM DON to 104.8% at 200μM. Similar findings were reported by Abbas *et al.* (1984), Visconti *et al.*(1991) and Rotter *et al.*(1993), where DON was found to be cytotoxic to a variety of cells including fibroblasts and lymphocytes. Effective concentrations ranged from 0.1 to 2μg.ml^{-1} (5-10 μM) DON. At the cellular level, the key toxic event was related to inhibition of protein synthesis at the ribosomal level during the elongation-termination step (Ueno, 1983). Mekhancha-Dahel *et al.* (1990) showed that DON inhibited the synthesis of DNA, RNA and protein synthesis at the ribosomal level, as well as inhibited DNA synthesis in murine splenic lymphocytes and human peripheral blood lymphocytes.

At 25, 50μM and 200μM ZEA, 40.5, 45.4 and 56.1% cell viabilities were reported respectively for the N2α cells following the 48-hour exposure period. Abeywickrama and Bean (1992) studied the cytotoxic effects of ZEA on the baby hamster kidney cell line (BHK)-21, and on the human epidermoid cell line HEP-2. Zearalenone was highly cytotoxic to BHK-21 cells at 2μg.μl^{-1}, and HEP-2 cells were less susceptible even at a level of 1μg.μl^{-1}. The concentrations of ZEA to which Abeywickrama and Bean (1992) exposed the cells, were equivalent to the millimolar range. This may be considered extremely high since micromolar concentrations were used in this study on the N2α cells, and although significantly lower concentrations of mycotoxin were tested, high percentages of cell death were reported in this study (Table 3.3).

Reubel *et al.* (1987) evaluated the effect of DON and ZEA on the human erythroleukaemia cell line K562, and on porcine lymphocytes and granulocytes. After 24-hour exposure, concentrations of DON as low as 4μg.ml^{-1} (2-5μM) were found to inhibit significantly the cleavage activity of K562. Cytotoxicity in lymphocytes and granulocytes were observed at concentrations of 0.4-0.8μg.ml^{-1} (~1-3μM) DON. Reubel *et al.* (1987) reported that 25 to

12.5μg.ml^{-1} (~50-75μM) ZEA inhibited mitochondrial cleavage activity of lymphocytes and K562 cells significantly, whereas in granulocytes none of the concentrations tested were toxic. Shelby *et al.* (1995) reported that when using the brine shrimp bioassay, the concentration of ZEA that caused 50% mortality was ~75μM. These results are similar to that of the present study, where following 48-hour exposure to 75μM ZEA, 60% cell mortality was noted in the N2α cell line.

3.4 CONCLUSION

The MTT assay was efficient in providing an indication of the levels of cytotoxicity or mitogenicity induced by the *Fusarium* mycotoxins FB_1, FA, MON, DON, T2 and ZEA, as well as the sphingoid bases, Sa and So in the N2α neuroblastoma cells at the range of concentrations comparatively assessed after the 48 hour exposure period. Dead cells were unable to metabolise various tetrazolium salts, and this factor facilitated the use of the colorimetric assay to measure cell survival.

Different levels of susceptibility were determined and indicate that the test compounds were able to traverse or interact biochemically with cellular organelles or cell membranes and induce toxicity due to often negligible differences in their molecular structures (e.g., DON and T2; and FB_1, Sa and So) that effected differences in bioactivity and the cellular responses. At the concentrations tested, the sphingoid bases were clearly more cytotoxic to this cell line than any of the mycotoxins tested, with viabilities as low as 29% being reported. Based on studies presented later on in this dissertation (i.e., in Chapter 8), it is clear (in retrospect) that the levels of Sa and So added to the cells were multifold higher than those that a cell would normally be exposed to, and therefore these levels of cell death were natural. Sphingoid bases are endogenous compounds found in cells, unlike the xenobiotic mycotoxins, and are known to play important roles in cell regulatory processes. This factor highlights further the importance of the regulation of levels of free sphingoid bases in cells, and the need for intervention with regards to exposure to compounds such as FB_1 that disrupt biochemical pathways that regulate levels of sphingoid bases in cells.

Findings that neuronal function may be impaired by the presence of *Fusarium* mycotoxins and elevated Sa and So, even if at a negligible level, require consideration *in vivo*. The use of the MTT assay can only provide information on the cytotoxic properties that are

characteristic of certain, but not all compounds. This colorimetric assay possibly underestimates cellular damage, and detects cell death only at the later stages of apoptosis when the metabolic activity of the cells is reduced. Regardless of this disadvantage, this colorimetric assay was useful for quantifying factor-induced cytotoxicity within a 24 to 48 hour period of cell culture, and opened avenues to pursue further more comprehensive analyses of the effects of these compounds on the N2α neuroblastoma cell line.

CHAPTER 4

Bioluminescent determination of apoptosis and necrosis using adenylate nucleotide measurements to analyse the effects of fumonisin B_1 and fusaric acid on the N2α neuroblastoma and Jurkat cell lines

4.1 INTRODUCTION

Apoptosis and necrosis are conceptually and morphologically distinct forms of cell death (Wyllie *et al.*, 1980). However, these two types of cell demise can occur simultaneously in tissues and cultured cells exposed to the same stimulus (Ankarcrona *et al.*, 1995; Shimizu *et al.*, 1996a). Often the intensity of the initial insult decides the prevalence of either apoptosis or necrosis (Bonfoco *et al.*, 1995). This suggests that while some early events may be common to both forms of cell death, a downstream controller may be required to direct cells towards the organized execution of apoptosis (Leist *et al.*, 1997).

Numerous pathways of apoptosis have been identified, the activation of which ultimately has an effect upon the cells' mitochondria. The mitochondrion consists of the outer membrane, intermembrane space, inner membrane, and matrix (Figure 4.1). Oxidative phosphorylation occurs across the inner mitochondrial membrane and results in the synthesis of ATP. Energy is released as electrons flow through the complexes of the inner mitochondrial membrane, and fall to a lower energy state, where the release of energy actively transports hydrogen ions from the matrix to the intermembrane space, thus making the matrix negatively charged, and the intermembrane space positively charged. This distribution of protons across the inner membrane generates the mitochondrial transmembrane potential ($\Delta\psi m$) (Figure 4.1). The transient opening of the megachannels or permeability transition (PT) pores, which span the inner to the outer mitochondrial membrane is necessary for the equilibration of essential ions between the cytosol and mitochondrial matrix. These PT pores open irreversibly during apoptosis. This disruption in PT is believed to be the cause of the collapse in the transmembrane potential, and brings about the release of *cytochrome c* from the inner mitochondrial membrane to the cytosol (Simmons, 1999; Bradbury *et al.*, 2000). It has recently been suggested that not all mitochondria are responsible for the release of *cytochrome c*, and that a proportion maintain the transmembrane potential and ATP production continues

(Lemasters *et al.*, 1998; Bradbury *et al.*, 2000). The loss of the transmembrane potential is also thought to precede the exposure of phosphotidylserine (PS) residues on the outer plasma membrane leaflet, which is usually confined to the inner leaflet of the plasma membrane in healthy cells.

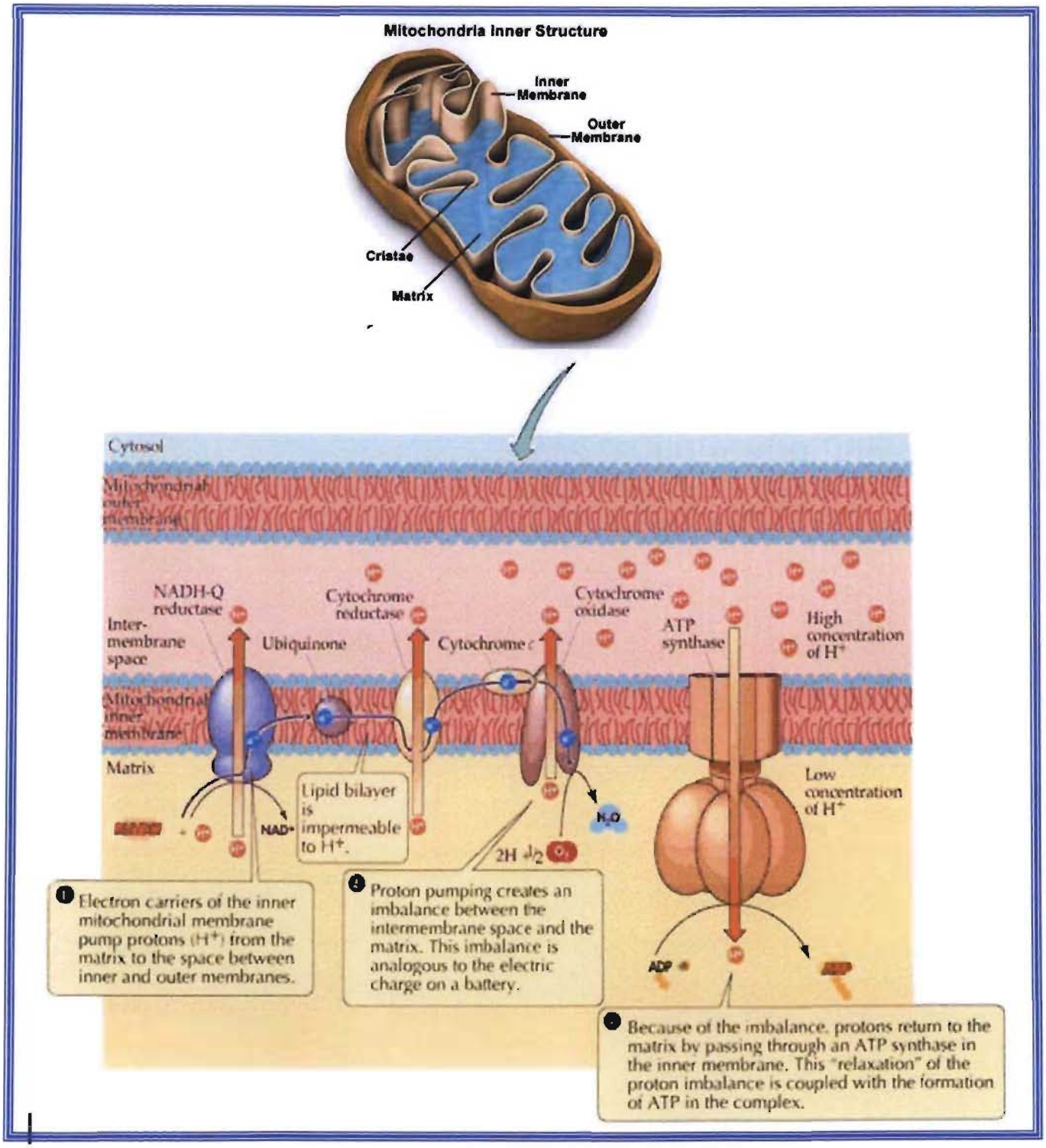

Figure 4.1: Mechanism of distribution of essential ions between inner and outer mitochondrial membranes (with modification of Simmons, 1999).

4.1.1 Determination of Apoptosis by cellular ADP:ATP ratios

Observations have been made regarding depletion of intracellular ATP during apoptosis, with various ATP depleting chemotherapeutic agents causing tumour regression. This led to a hypothesis that ATP depletion is a significant factor, making it a worthy therapeutic marker (LumiTech™, 1999). Exposure of different cell lines to apoptosis-inducing drugs causes cells to halt their normal proliferative cycle, and this can be detected as a drop in measured ATP in cell populations. When cells go into growth arrest, they maintain the same ATP levels, but when measured against a proliferating sample, there are obviously less cells to measure and thus, the overall amount of ATP per sample size is less. When the cell starts to undergo apoptosis, the ATP levels drop as the cell uses energy to organize the process, and in this case the drop of ATP levels is due to less ATP contributed per cell.

Early events in apoptosis are initiated in those cells sensitive to the agent. These cells show an increase in cellular ADP, without an appreciable drop in ATP. On exposure to either higher concentrations or longer incubation with a drug, ADP levels continue to rise and ATP levels continue to drop. The result being that in a population of cells exposed to death inducing conditions, the ratio of ADP to ATP increases as the cells become more compromised (Bradbury *et al.*, 2000). As ATP levels fall to a point where the cell can no longer perform basic metabolic functions, the cell will die. In necrosis, ATP levels fall rapidly, as a result of exposure to high concentrations of toxic agents (secondary necrosis) or mechanical damage/lyses (primary necrosis). These changes in the ATP levels brought about by apoptosis may be early indicators of apoptotic changes within cells.

4.1.2 The ApoGlow™ assay

Bioluminescent measurements of ATP have been used to assess cell proliferation and cytotoxicity since all cells have an absolute requirement for ATP to maintain viability (Crouch *et al.*, 1993). Measurement of ATP is an established method to test the chemosensitivity of cell lines and tumours, and to determine tumour growth inhibition by cytotoxic agents in primary cultures of ovarian and breast cancer cells (Andreotti *et al.*, 1995; Cree *et al.*, 1995; Kravtsov *et al.*, 1998; Kurbacher *et al.*, 1998).

Until recently, it has been difficult to measure relatively small amounts of ADP in the presence of larger quantities of ATP (Bradbury *et al.*, 2000). The ApoGlow™ Kit was designed to detect these subtle changes in adenylate nucleotide levels in cells cultured in 96 well microtitre plates. The assay facilitates the sequential measurement of ATP and ADP in each well of the microplate leading to the generation of an ADP: ATP ratio. This ratio correlates with apoptosis and necrosis, and a division can be seen between apoptosis and necrosis. By comparison of data from untreated control wells, it is also possible to determine if an agent induces death by either mechanism, or promotes cell proliferation. Proliferation results in an increase in the ATP readings, as cell numbers increase, while the ratios remain constant. From a single test, it is therefore possible to determine all possible outcomes resulting from cell viability modifying treatments.

4.1.2.1 Principles of the ApoGlow™ assay

Bioluminescent detection of adenylate nucleotides is extremely sensitive, with a detection limit of 100 cells per microwell. The ApoGlow™ kit uses bioluminescence catalysed by the enzyme luciferase to measure these intracellular nucleotides in a stepwise reaction, to give a rapid detection of cell death or proliferation that results in the emission of light at 562nm, according to the following scheme:

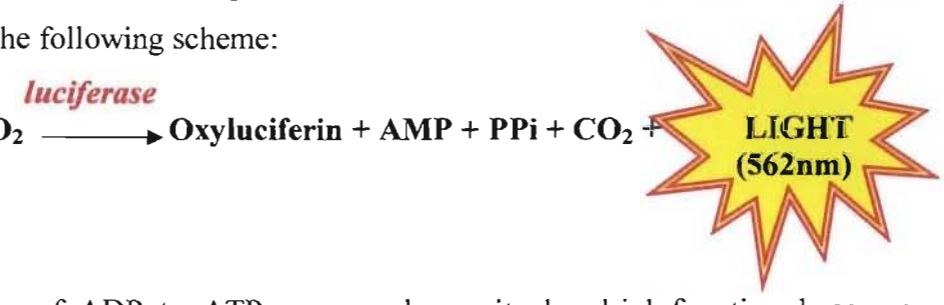

(Higashi *et al.*, 1985).

A change in the ratio of ADP to ATP occurs when mitochondrial function becomes compromised in apoptosis, and that specifically cells in the early stages of apoptosis show an increase in ADP without an appreciable drop in ATP. When all components of the reaction remain constant, the emitted light intensity is linearly related to the ATP concentration and is measured using a luminometer. The ADP is measured by its conversion to ATP, and the ADP:ATP ratio is then calculated, and used to differentiate between the different modes of cell death. The ApoGlow™ kit uses patented technology to allow for easy ADP detection in microplates (Bradbury *et al.*, 2000).

Ceramide plays a pivotal role in neural cell death and development (Merrill *et al.*, 1997). Monnet-Tschudi *et al.* (1999) have demonstrated that FB_1 selectively affected glial cells,

interfered with oligodendrocytes development, and impaired myelin formation and deposition. Another effect observed after FB_1 treatment in astrocyte-differentiated cultures was a loss of the astrocyte cytoskeletal marker GFAP due to deficit of sphingolipids by the inhibition of CER synthase (Monnet-Tschudi *et al.*, 1999). In this latter case, FB_1 could even act as a protective agent by inhibiting CER synthesis, given that in particularly stressed conditions, such as in hypoxia-injured LLC-PK1 cells, increased CER synthesis induces DNA fragmentation and apoptosis (Ciacci-Zanella *et al.*, 1998). Analogous results have been observation with chicken embryo astrocytes (Mangoura and Dawson, 1998).

Since numerous studies have demonstrated that, besides inhibition of CER synthesis, FB_1 causes DNA damage and membrane lipid peroxidation (Sahu *et al.*, 1998), the aim of this study was to determine using the ApoGlow™ assay, the potential for FB_1 and FA, individually and in combination, to induce apoptosis, necrosis, growth arrest, or proliferation in the adherent N2α neuroblastoma, as well as the Jurkat suspension cell line. The Jurkat cell line, a human acute T-lymphoblastic leukaemic suspension cell line is $CD95^+$ and has a mutated p53 gene. The Jurkat cell line was included in this study, as it would provide some insight into the effects these mycotoxins may have on circulating white blood cells *in vivo*.

4.2 MATERIALS AND METHODS

The experimental work presented in this chapter was carried out at Nottingham Trent University (NTU), Faculty of Health Sciences, United Kingdom (UK), with supervision and guidance from Mrs Anne Cox, Dr Claire Scholfield and Professor Martin Griffin (July-September 1999) in collaboration with LumiTech™ at the Nottingham City Hospital. Financial support was kindly provided by the National Research Foundation (NRF), SA. Only the effects of FB_1 and FA were assessed in this international collaborative study, the reason being that this work was part of the initial experiments carried out and the other mycotoxins included in the assessments in Chapters 3, 5, and 6 were added in later in the time line of work presented in this dissertation.

4.2.1 Materials

Cell culture materials, media, antibiotics and sterile disposable consumables were purchased from Sigma Chemical Company (UK). Pre-sterilised Corning tissue culture flasks ($75cm^2$) were used as culture vessels, sterile clear 96-well microtitre plates (CoStar) and 96 well white-walled clear-bottomed luminometer plates (Wallac) were used for the assays. Aseptic protocols were adhered to. The N2α cell line was obtained from the cell culture facility at NTU, and the Jurkat cell line from the cell culture facility at Leicester University, UK. A Lucy 1 Anthos Luminoskan Labsystems microplate luminometer equipped with reagent dispensers capable of injecting 20µl volumes was used, enabling full automation of the assay.

The Jurkat cell line was cultured in RPMI-1640 cell culture media containing 10% FCS, 2mM L-glutamine, 2% Penstrep and $2mg.ml^{-1}$ gentamicin sulphate. The N2α cell line was cultured in DMEM supplemented with 10% FCS (v/v), 2mM L-glutamine, 2mM sodium pyruvate and 2% (v/v) penicillin streptomycin.

4.2.2 Methods

4.2.2.1 The ApoGlow™ assay

ATP contamination can be a source of error for the ApoGlow™ assay. The surface of the skin contains significant levels of ATP, therefore gloves were worn when performing the assay, and ATP-free microtitre plates and tubes were also used to minimize errors.

The N2α cells were cultured in $75cm^2$ culture flasks until confluent, trypsinised, and following a cell count, 2.5×10^4 cells were dispensed into each well of the microtitre plates. The Jurkat cell line, being a suspension cell line, did not require trypsinisation. To minimize dilution of the mycotoxins by the media in the pure cell suspension, cells were concentrated in small volumes of CCM (~10-15 µl).

4.2.2.2 Preparation of the mycotoxin stock solutions

Fumonisin B_1 and FA (1mg) were dissolved in 30µl DMSO and 970µl CCM (using the defined media required for each cell line), to a stock solution of 1 $mg.ml^{-1}$. The control solution for each toxin was made up of 30µl DMSO and 970µl CCM. A range of dilutions of both the mycotoxin stocks and controls were assessed as shown in Figures 4.2- 4.3. In addition, the cells were exposed to equal volumes of a combined solution of FB_1 and FA at each concentration. For example, at 100µg.ml^{-1} (FB_1+FA), if 10µl of cell suspension was used to obtain 2.5 x 10^4 cells per well, this volume was topped up to a total of 100µl per well with 45µl of FB_1 and 45µl of FA using separate stock solutions of 100µg.ml^{-1} of each mycotoxin. Duplicate testing of each mycotoxin was carried out on both cell lines. The final volume of cell suspension and diluted mycotoxins together was 100µl according to the manufacturers' instructions. The culture plates were then incubated at 37°C for between 22.5-24 hours, after which the ApoGlow™ assay was carried out.

4.2.2.3 Outline of the method

Before cellular adenylate nucleotides were measured by bioluminescence, they were first extracted from the cell. For the N2α adherent cells, 100µl of nucleotide releasing reagent (NRR) was added to each well of the microtitre plate using a multi-channel pipette, and extraction was allowed to occur for five minutes at RT. The extracts were transferred to an opaque white microtitre plate and loaded into the luminometer. Where the cells were cultured in white walled clear-bottomed tissue culture plates, extraction and measurement of adenylate nucleotides was carried out in the same plate. The assay procedure differed slightly between the N2α adherent and the Jurkat non-adherent cells. With the Jurkat non-adherent cells, one bottle of nucleotide monitoring reagent (NMR) (20ml) was reconstituted in one bottle of NRR (20ml), enabling simultaneous release and measurement.

4.2.2.4 Equipment

The assay was fully automated using the Lucy 1 Anthos Luminoskan Labsystems microplate luminometer. The data was expressed as relative light units (RLUs).

Dispenser 1 was primed with NMR and set to dispense 20µl in the case of the N2α adherent cells, and 100µl for the Jurkat non-adherent cells. The instrument was programmed to dispense into each well and take an immediate one-second integrated reading before moving on to the next well. Dispenser 2 was primed with ADP converting reagent, and also programmed to dispense 20µl into selected wells and take an immediate one-second integrated reading before moving on to the next well. At all times the luminometer dispensing lines were kept scrupulously clean. Any residual luciferase in the dispensing line was removed using a cleaning reagent that neutralised the enzyme.

The specifically formulated luminescence cocktail (NMR) was automatically added to the wells and an ATP reading **(A)** was taken. After 10 minutes, the second injector added the ADP Converting Reagent and a second reading was taken (**B**; baseline ADP levels). After a further 5 minutes, the final converted ADP reading was taken **(C)**. These three values were then used to calculate the ADP:ATP ratio.

4.2.2.5 Interpretation of results

The ADP:ATP ratio was then calculated from measurements A, B and C as follows:-

(C-B)/A

Interpretation of different ratios obtained within each experimental situation varied according to the cell type and conditions used. However, the following criteria, provided by the manufacturers of the assay were used as guidelines: -

1. If a test gives markedly elevated ATP values (compared to seeding cell densities) with no significant increase in ADP levels, this indicates **proliferation**. Stimulation with growth/mitogenic factors will induce proliferation, and thus lead to an increase in ATP readings.
2. If a test gives considerably lower ATP levels than control but greatly increased ADP, this indicates **necrosis**.
3. If a test gives similar or slightly higher levels of ATP, and with little or no change in ADP compared to control, this indicates that the **treatment arrests proliferation but does not kill cells**.

4. If a test gives lower levels of ATP to control but shows an increase in ADP, this indicates **apoptosis**. These ratios vary according to the degree of apoptosis in the cell population.

According to the manufacturers guidelines and the LumiTech™ representative (Scholfield *pers comm.*, 2002), as a further guide on interpretation of data, ratios greater than twice the control values, but less than four times control values, were an indication that cells were undergoing apoptosis. Ratios four times greater than the control values were an indication of necrotic cell death. Ratios slightly lower than the ADP: ATP ratio of control cells were indicative of cells undergoing growth arrest, and those with ratios significantly lower, as an indication of cell proliferation.

The experiments presented were performed in duplicate and the results are presented as means ± SD.

4.3 RESULTS AND DISCUSSION

Interpretation of the ApoGlow™ assay results is based on a comparison of the ATP readings and ADP:ATP ratios with values from treatment-free control wells. The ADP:ATP ratios obtained within each experiment vary according to the cell line or cell type being assessed, the experimental and exposure conditions, and the equipment used. Although an experiment may be repeated according to a defined method, intra- and inter-laboratory variability in results often occurs. To remove this level of variability, when comparisons are made in assays such as this, treated cells are always compared to control cells of the same origin, such that each assay has its own internal control. In general, if a test gives considerably lower ATP levels than the control, but greatly increased ADP levels it would indicate necrosis. Whereas if the test gives slightly lower levels of ATP to control, but shows an increase in ADP it would point to apoptosis. These ratios vary according to the degree of apoptosis in the cell population. It is the relationship between the treated cells ratios and the control cell ratios, that is the key to the indication of the mode of cell death.

In this study, the control cells, as well as the FB_1 and FA-treated cells were exposed to a maximum concentration of 3% DMSO, with subsequent decreases in the percentage of DMSO across the dilution range in CCM. The control cells in the Jurkat assay exhibited a small, but gradual increase in viability with a decrease in the DMSO content (Figure 4.2).

These results indicate that DMSO may have induced some level of cytotoxicity on the Jurkat cells. No significant differences however were noted between concentrations in the range for the control cells, which implies that exposure to DMSO as the solvent vehicle for the mycotoxins, had negligible effects on these cultured cells.

The volume of media per well (i.e., 100 µl) was sufficient to sustain the cells for 24 hours prior to changes being induced as a result of nutrient deficiency, and therefore both assays did not exceed 24 hours. This limitation of a maximum volume of 100µl CCM per well in the microtitre plate may be considered a drawback of the test, as some compounds require longer interaction with cells for biochemical changes to become apparent. However, the assay has a sensitive detection limit with as few as 100 cells per well. In cases where longer incubation times may be required for a particular compound, the cell count per well may be decreased in order to enable a longer incubation time.

The measurement of ATP alone shows cytotoxic effects, but it is not sufficient for determining apoptosis, or for distinguishing primary and secondary necrosis. LumiTech™ have tested 15 different cell lines and four primary cell types for the induction of apoptosis/secondary necrosis and primary necrosis. In all cell types tested for apoptosis by flow cytometry and ADP: ATP ratio, there was a significant correlation ($p<0.001$) between the two methods (LumiTech™, 1999).

The results of the ApoGlow™ assays on the Jurkat and N2α neuroblastoma cells are shown in Figures 4.2 and 4.3, respectively. The results are presented as ADP:ATP ratios obtained against the concentrations of FB_1, FA, and (FB_1+FA) to which cells were exposed. The results of the 22.5 hour exposure of the Jurkat cell line to FB_1 and FA, individually as well as in combination (Figure 4.2) were interpreted as suggested in section 4.2.2.5, and by comparison of the ADP: ATP ratios of treated to untreated control cells.

Comparative analyses of the effects of FB_1, FA and (FB_1+FA) exposure on the Jurkat and N2α cells were carried out against matched controls at each test concentration (Appendices 3 and 4), since although the effects of DMSO as the diluent were considered negligible, these differences needed to be taken into account. In theory, in a population of cells exposed to death inducing conditions, the ratio of ADP to ATP increases as cells become more compromised. Analyses of the ADP: ATP ratios indicate that FB_1 induced apoptosis

in the Jurkat human suspension cell line at concentrations of 1.56, 12.5 and 50 $\mu g.ml^{-1}$, (i.e., ~2μM, 20μM, 70μM respectively) (Appendix 3).

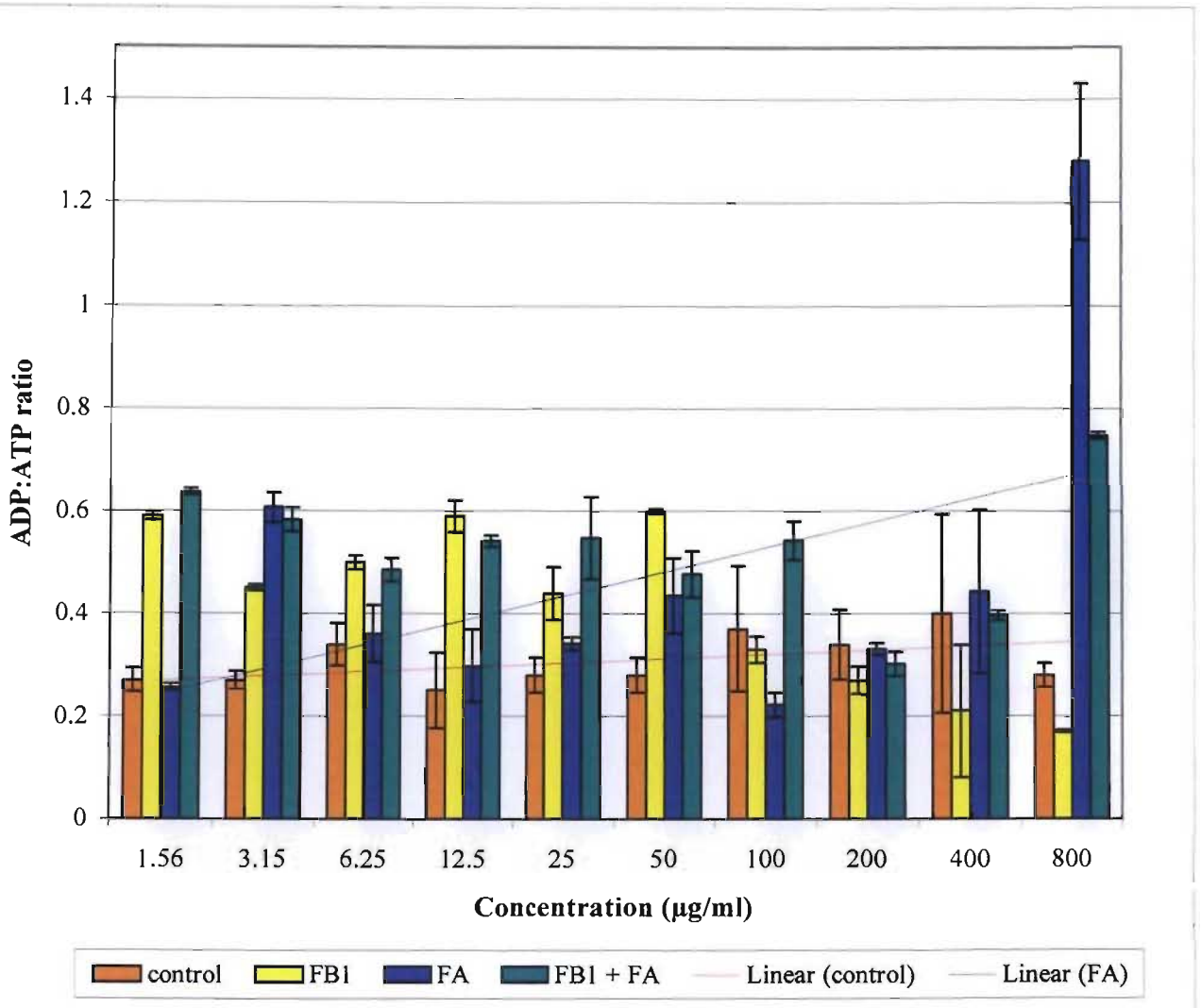

Figure 4.2: Effects of FB_1, FA and (FB_1+FA) on the Jurkat cell line as determined by the ApoGlow assay following 22.5 hour exposure period

Qureshi and Hagler (1992) reported that in primary cultures of chicken peritoneal macrophages following exposure to 2.8μM FB_1, significant cytotoxicity and morphological features consistent with apoptosis (nuclear fragmentation and membrane blebbing). Similarly, Schmelz *et al.* (1998) showed that incubation of the HT29 human colonic cell line with FB_1 caused a significant reduction in cell number, reflected by increases in DNA fragmentation and percentage of apoptotic cells, and that exposure to 10μM FB_1 caused the accumulation of Sa. These biochemical disruptions may also have occurred and contributed

to apoptosis in the Jurkat cells following the 22.5-hour exposure period at the mycotoxin concentrations used in this study. Increased apoptosis in turkey lymphocytes following *in vitro* exposure to FB_1were also reported by Dombrink-Kurtzman *et al.* (1994). In those studies, induction of apoptosis was considered a consequence of CER synthase inhibition, and disruption of sphingolipid metabolism by FB_1. In addition, at concentrations similar to those assessed in the present study, Tolleson *et al.* (1996b) found that FB_1 inhibited incorporation of [^{3}H]-thymidine by cultured neonatal human keratinocytes and HepG2 human hepatocarcinoma cells at 0.1μM (0.072μg.ml^{-1}) and 100μM (72.18μg.ml^{-1}) FB_1, respectively. The results of the present study support the hypothesis that cells responses to a mycotoxin are dose and cell type specific. The three most commonly encountered explanations for cell to cell variability in toxin sensitivity are, cell to cell variability in the amount of target enzymes or other cellular functions which interacts with the toxin, the amount of metabolic enzymes which activate a non-toxic precursor molecule into a metabolite with non-specific toxicity, and the efficiency of detoxification mechanisms that protects the cells and tissues that are less susceptible to the toxic agent (Shier *et al.*, 1991).

In the present study, FA also induced apoptosis in the Jurkat cells at a concentration of 3.15μg.ml^{-1}, and in combination, (FB_1+FA), induced apoptosis at 1.56, 3.15, 12.5 and 800μg.ml^{-1} following the 22.5 hour exposure period. At 6.25μg.ml^{-1} FB_1 and (FB_1+FA), ADP: ATP ratios of the mycotoxin-treated cells approached apoptotic levels. Fumonisin B_1 induced proliferation in the Jurkat cells at 400μg.ml^{-1} FB_1, but initiated growth arrest at concentrations of 100, 200 and 800μg.ml^{-1} FB_1 (Figure 4.2, Appendix 3). These results are in keeping with Tolleson *et al.* (1996b) who reported that FB_1 inhibited clonal expansion of normal human keratinocytes and HET-1A human oesophageal epithelial cells at 10μM (7.2μg.ml^{-1}) and inhibited growth in mass culture of normal human fibroblasts at 0.1μM.

Riley *et al.* (2001) have reported that the balance between the apoptotic and proliferative rates are critical determinants in the process of tumour genesis. In cells exposed to fumonisins, those cells sensitive to the proliferative effect of decreased CER and increased So 1-phosphate should survive and proliferate, when the conditions under which the cells are exposed to fumonisins are such that increased intracellular free sphingoid base concentration is not growth inhibitory. Conversely, when the increase in free sphingoid bases exceeds a cell's ability to convert Sa:So to dihydroceramide/CER, or their sphingoid base 1-phosphate, then the free sphingoid bases will accumulate. In this case, cells that are

sensitive to sphingoid base-induced growth arrest will die, and non-sensitive cells will survive. If the cells selected to die are of normal phenotypes, and those selected to survive are abnormal, the risk of cancer would increase (Riley *et al.*, 2001). Another condition that would promote apoptosis would be if the inhibition of CER synthase was either ameliorated or if CER synthesis increased while free Sa levels were still high.

Fusaric acid induced proliferation in the Jurkat cells at 1.56μg.ml^{-1}, but induced growth arrest at concentrations of 100 and 200μg.ml^{-1} following the 22.5hour exposure period. The combination of (FB_1+FA) also induced growth arrest at 200μg.ml^{-1}, and FA induced necrosis at a concentration of 800μg.ml^{-1} in the Jurkat cell line (Appendix 3). A possible explanation for the ability of FA to induce proliferation in these cells is provided by Johnson and McKnight (1989) and Fernandez-Pol (1991; 1992), who propose that FA may act by binding Zn^{2+}, which is a structural component of certain zinc-finger DNA-binding proteins. In addition, FA may act on cytosol Cu^{2+}/Zn^{2+}-containing and/or mitochondrial Mn^{2+}-containing SOD; these enzymes may be important for growth and survival of cancerous cells (Fernanadez-Pol *et al.*, 1982). A potential explanation for the growth-arrest inducing ability of FA is provided by Fernandez-Pol *et al.* (1993) who has demonstrated that FA was a potent inhibitor of DNA synthesis in the MDA-MB-468 human mammary cell line. Thompson and Wannemacher (1984) suggest that the different cytotoxic effects of a mycotoxin might be influenced by the ability of the mycotoxin to bind to cellular receptors and/or penetrate cell membranes. This is dependent on the size, structural conformation of the toxin molecule, and its polarity. Furthermore, the relative significance of a molecular receptor of a mycotoxin is determined by its affinity to the active form of the toxin, its role in vital biochemical processes, the persistence of the lesion it bears, and the severity of the consequence of the lesion.

There seems to be a dose-dependent response of an increase in the ADP: ATP ratio with an increase in concentration for cells treated with FA alone (Figure 4.2, linear FA trend line). Fumonisin B_1 seemed to induce apoptosis successfully at the lower doses, and then lost this effect at the higher concentrations. Scholfield *pers comm.* (2002) indicated that LumiTech™ noted this previously in some cell models, and when analysed by flow cytometry, a resistant population of cells was seen emerging which were actively proliferating, and therefore affected the ratios indicative of proliferation. The combination of (FB_1+FA) does produce an apoptotic effect, but this could be due primarily to the effects

of FB_1. At the very high doses, the combination seems to be limited in its effect suggesting some antagonistic mycotoxin-mycotoxin interaction.

The results of the exposure of the N2α neuroblastoma cells to FB_1 and FA, individually and in combination are shown in Figure 4.3. Consistent with the findings in the Jurkat cell line, a decrease in DMSO induced minor increases in cell viability in the N2α cell line, as indicated by the linear control trend line (Figure 4.3). Distinct apoptotic ADP: ATP ratios were not reached with the N2α cells when treated with FB_1. However, at the higher range of concentrations between 512 to 1000μg.ml^{-1} FB_1, ratios started to approach values indicative of apoptosis (Appendix 4). The trend in the ADP: ATP ratios however indicate the potential for exposure to higher FB_1 concentrations than those used in this study to induce apoptosis in the N2α cells. These results correlate well with the MTT assay results (Chapter 3, Table 3.1) where at 200 and 250μM FB_1 (i.e., 144.36μg.ml^{-1} and 180.45μg.ml^{-1}), 29.8% and 42.1% cell viabilities were observed in the N2α cells respectively. Although the MTT assay was carried out over 48 hours and the ApoGlow™ assay over 24 hours, both sets of result show similar response patterns for the N2α cell line.

A similar trend to that of the FB_1-treated N2α cells response was noted with both the FA-treated and (FB_1+FA)-treated N2α cells (Figure 4.3). At the higher range of concentrations (i.e., between 256 and 1000μg.ml^{-1}), the ADP: ATP ratios of the FA-treated N2α cells started to approach apoptotic levels. In the (FB_1+FA) treated N2α cells, this effect started at the lower doses of 8μg.ml^{-1} and 32μg.ml^{-1}, going up to 512 μg.ml^{-1} with the combination of the mycotoxins (FB_1+FA) potentially acting together to induce apoptosis in the cells following the 24 hour exposure period (Appendix 4). These results also correlate with the MTT assay results where on exposure to 250μM FA, 33.2% cell viability was noted indicating high levels of cell death (Chapter 3, Table 3.1).

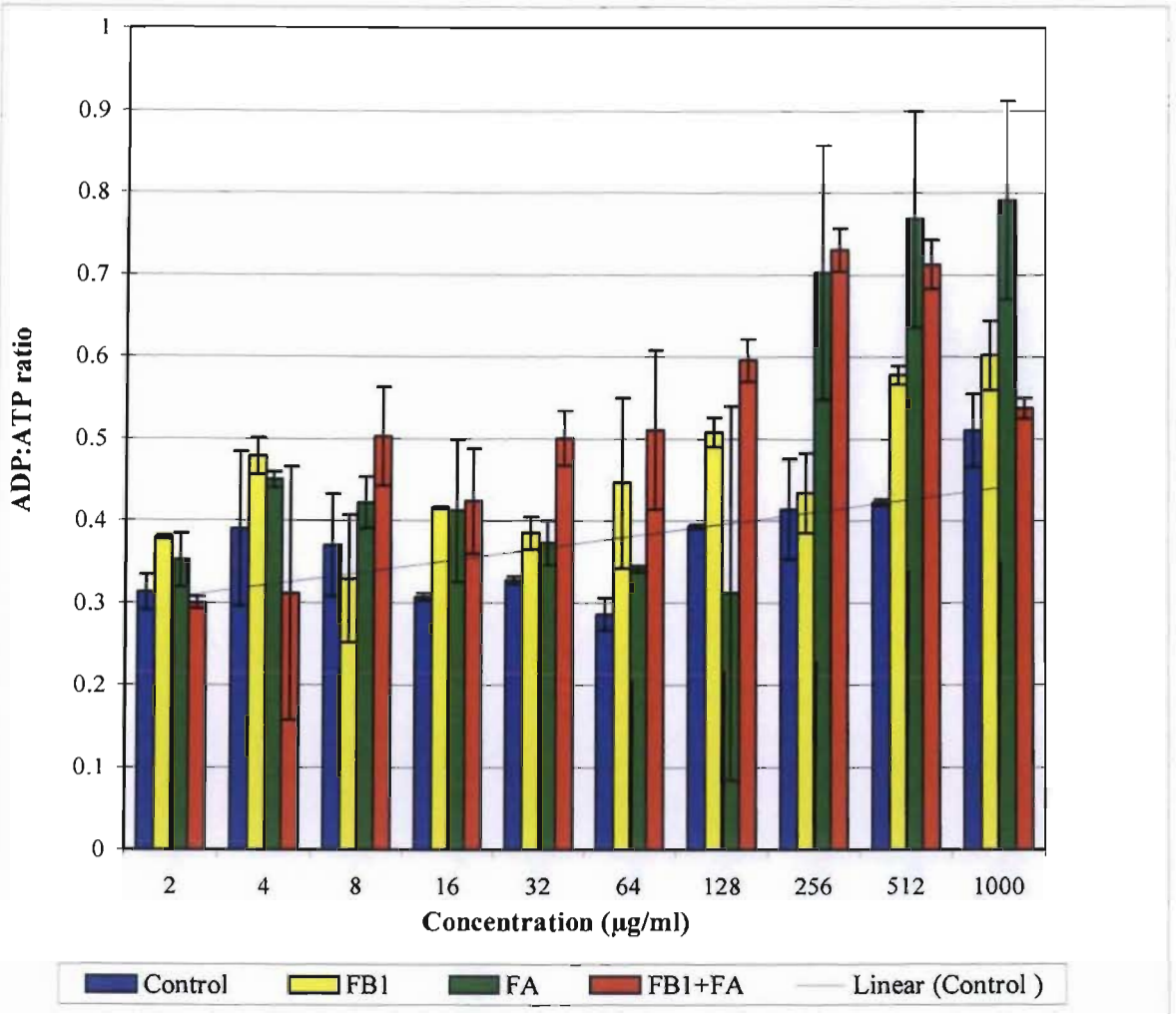

Figure 4.3: Effects of FB_1, FA, and (FB_1+FA) on the N2α mouse neuroblastoma cell line as determined by the ApoGlow assay following 24 hour exposure

Consistent with the interpretation of results for Jurkat cells, N2α cells with ADP: ATP ratios slightly lower than that control cells were interpreted as being in a state of growth arrest induced by exposure to the mycotoxins. Fumonisin B_1 at 8µg.ml^{-1}, FA at 128µg.ml^{-1}, and (FB_1+FA) in combination at 2 and 4µg.ml^{-1} induced growth arrest. Necrosis was not induced in the N2α cell line at any of the mycotoxins test concentrations according to the results reported for the ApoGlow™ assay (Figure 4.3). Fernandez-Pol *et al.* (1993) exposed WI-38 fibroblasts to 500µM (90µg.ml^{-1}) FA, and reported that cell proliferation ceased. Anti-proliferative effects of FB_1 have also been reported in a panel of rat hepatoma cell lines (namely, H4TG, H4-II-E-, H4-IIE-C3, Zfao, MH1C1, McA-RH777 and McA-RH8994), LLC-PK1 cells and MDCK cells, with IC_{50} values ranging from 2.5µM FB_1 (~2µg.ml^{-1}) and 50µM FB_1 (~37µg.ml^{-1})

(Shier *et al.*, 1991; Yoo *et al.*, 1992; Abbas *et al.*, 1998). Counts *et al.* (1996) also reported that rabbit renal epithelial cells are also very sensitive to fumonisin-induced inhibition of cell growth.

Further support for the growth arresting effect of FB_1 are provided by Mobio *et al.* (2000), who reported that after 24 hour incubation of rat C6 glioma cells with 3 to18μM of FB_1 (~2-16μg.ml^{-1}), the number of cells in phase G_2/M increased significantly as compared to the control ($p<0.05$) from 45.7±0.4% to 54.8±1.1% for 9μM FB_1 (~7μg.ml^{-1}), whereas no change occurred in the number of cells in the phase G_0/G_1. This indicates that cytotoxic concentrations of FB_1 induce cellular cycle arrest in phase G_2/M in rat C6 glioma cells possibly in relation with genotoxic events.

The cytotoxicity of FA may be attributed to the 5-butyl side chain, which because of its lipid solubility may allow better cellular penetrability of this agent. Telles-Pupulin *et al.* (1998) using isolated rat mitochondria showed that FA affects mitochondrial energy metabolism by inhibition of succinate dehydrogenase (in the 10^{-3}-10^{-2}M range), inhibition of oxidative phosphorylation (in the 10^{-5}-10^{-4}M range) and inhibition of α-ketoglutarate dehydrogenase (in the 10^{-5}-10^{-4}M range). The inhibition of oxidative phosphorylation seems to be the result of a direct action on the ATP synthase/ATPase without significant inhibition of the ATP/ADP exchange. In the present study, cell viability is partially reflected by the higher ADP: ATP ratios. These high ratios may have been a consequence of the inhibition of oxidative phosphorylation, as a result of exposure to FA.

From the analyses of the Jurkat and N2α cell lines in this study, the major factors affecting modes of cell death are the concentrations of the compounds tested and the cell types being tested. A mycotoxin may induce apoptosis at low concentrations, but kills cells by necrosis at higher concentrations probably due to the rapid collapse of cellular integrity, including plasma membrane disruption, a large calcium influx, as well as intracellular ATP depletion (Tsujimoto, 1997). Apoptosis and necrosis were detected in the cell lines assessed in this study on exposure to FB_1 and FA at various concentrations.

From the analyses, it would appear that FA is more toxic to the Jurkat and N2α cells than FB_1. However, this assay was carried out using mass-based concentrations, and not

molarity-based concentrations as in Chapter 3. The molecular weight of FB_1 is 721.8 and that of FA is 179.2. This implies for example that 7.218μg FB_1 in 1ml of CCM is equivalent to 10μM FB_1, whereas 1.792μg FA in 1ml is equivalent to 10μM FA. This implies that on a mass-to-mass comparison, all cells were exposed to comparatively higher molarities of FA in these assays.

Studies have indicated that the effects of FB_1 on different cell lines vary depending on cell type. The effects on FB_1 and FA on the Jurkat and N2α cells differ with more pronounced effects being evident in the Jurkat suspension cell line. A possible hypothesis for varying susceptibility may be due to the greater surface area of exposure to the mycotoxins in the CCM that the Jurkat suspension cells are bathed in, in comparison to the adherent N2α cells, providing an additional explanation for the lower susceptibility of these cells to the mycotoxins.

4.4 CONCLUSION

The ApoGlow™ assay was used successfully in this study to determine the effects FB_1, FA and (FB_1+FA) on the N2α neuroblastoma cell line and the Jurkat leukaemic suspension cell line. Interpretation of the data revealed at specific concentrations whether these mycotoxins individually, or in combination induced proliferation, apoptosis, necrosis, or growth arrest. Apoptosis was induced by FB_1 in the Jurkat cell line at 1.56, 12.5 and 50μg.ml^{-1}, and FB_1 induced growth arrest at 100, 200 and 800μg.ml^{-1} in these cells. Only at 400μg.ml^{-1} did FB_1 induce proliferation of the Jurkat cells. Fusaric acid however induced proliferation at the lower end of the concentration range at 1.56 μg.ml^{-1} and apoptosis at 3.15 μg.ml^{-1}. At 100 and 200μg.ml^{-1}, FA induced growth arrest in the Jurkat cells, with necrosis at 800μg.ml^{-1}. In combination, (FB_1+FA) induced apoptosis at 1.56, 3.15, 12.5 and 800μg.ml^{-1}, while at 200μg.ml^{-1}, this combination of mycotoxins induced growth arrest in the Jurkat leukaemic suspension cell line. These results have bearing on the potential effects of these mycotoxins on white blood cells in the circulatory system of humans and requires further consideration.

In the N2α cell line, necrosis and proliferation were not detected at any of the concentrations of FB_1 or FA assessed in this study. Instead, FB_1 at 8μg.ml^{-1}, and FA at

128μg.ml^{-1}, induced growth arrest after 24 hour exposure to these mycotoxins. In combination (FB_1+FA) also induced growth arrest at 2 and 4μg.ml^{-1}. Fusaric acid alone and in combination with FB_1, at 256 and 512μg.ml^{-1} induced apoptosis in the N2α cells. In addition, FA at 1000μg.ml^{-1} also induced apoptosis in the N2α cells. The effects noted on the N2α cells are important because it provides some insight as to how neural cells would respond *in vivo* on exposure to these mycotoxins. No distinct trends were noted in the responses of the N2α neuroblastoma and the Jurkat suspension cell line on exposure to these mycotoxins. However, depending on the cell line analysed and the concentrations of exposure, the mycotoxins acted either antagonistically, in synergism, or induced some level of cytotoxicity by disrupting normal cellular metabolism.

Although the ApoGlow™ assay does provide a range of results that are useful, it is not widely used as it is expensive and requires specialized equipment such as the luminometer, for the analysis of treated cells. The purchase of such specialised equipment and its maintenance is not feasible in resource poor settings. Instead, assays that do not require such specialised equipment are opted for, and at a lower cost provide similar information.

CHAPTER 5

Fluorescent microscopic and cytofluorometric analyses of N2α neuroblastoma cells exposed to selected *Fusarium* mycotoxins and sphingoid bases

5.1 INTRODUCTION

The ordered sequence of biochemical and cellular events that exemplify apoptosis and necrosis are paralleled by specific changes in the morphological and physical properties in both the cell nuclei and cytoplasm (Wyllie, 1980; Vaux, 1993; Bradbury *et al.*, 2000). These changes provide features that permit recognition of apoptotic or necrotic cell death by various methods, and for apoptosis include the loss of $\Delta\psi m$, loss of plasma membrane asymmetry, and the condensing and eventual fragmentation of chromatin into internucleosomal fragments. Necrosis, in contrast, is characterised by cell and nuclear swelling, patchy chromatin condensation, swelling of mitochondria, vacuolisation of cytoplasm, and plasma membrane rupture, leading to the formation of 'ghost-like' cells and finally, dissolution of DNA. Apoptotic and necrotic cell death are different from a mechanistic point of view, because necrosis is the passive result of cellular injury, and apoptosis forms an integral part of normal physiological cell processes (Kerr *et al.*, 1972; Vermes *et al.*, 2000).

Flow cytometry (FCM) facilitates quantitative analyses of components or structural features of cells primarily by optical means, allowing characterisation of several cell parameters and functions (Dolbeare *et al.*, 1983; Shapiro, 1985; Cossarizza *et al.*, 1991; Nicoletti *et al.*, 1991; Barbieri *et al.*, 1992; Darzynkiewicz *et al.*, 1992). Advantages of FCM techniques include the ability to analyse large numbers of living or fixed cells in a few minutes, providing a statistically significant picture of the cells physical and biochemical make-up. Cells are passed single-file through a laser beam by continuous flow of a fine stream of the suspension. When cells pass through the laser beam, they disrupt and scatter the laser light, which is then detected as forward scattered (FSC) and side scattered (SSC) light, that are related to cell size or diameter, and to the cells internal complexity or granularity, respectively. In addition to scatter, a flow cytometer measures fluorescence parameters. Cells exhibit a change in light scatter characteristics when they

die, or when their membranes become permeabilised. On a flow cytometer, this manifests as a reduction in the FSC signal and an initial increase in the SSC signal, partly due to a change in the refractive index of the cells cytoplasm. As the majority of the events that characterize apoptotic death, can be revealed by multiparameter FCM, methods have been proposed to analyse and quantify the apoptotic process through evaluation of light scattering parameters of cells. Since no single parameter defines programmed cell death, a combination of techniques is recommended for reliable detection of apoptosis and/or necrosis.

In this study, fluorescent probes for studying apoptosis and necrosis were organized into categories based on the identification of different aspects of these cellular processes. A crucial event in the mitochondrion is the formation of permeability transition pores (mitochondrial megachannel) in its outer membrane leaflet allowing flux of mitochondrial proteins into cytosol (Marchetti *et al.*, 1996; Susin *et al.*, 1998). Opening of megachannels results in collapse of asymmetric distribution of protons on both sides of the inner mitochondrial membrane, known as transition of the mitochondrial transmembrane potential (TMP) (Martinou, 1999) and will be measured using Rhodamine 123 (Rh123) and the dual emission potential sensitive probe 5,5', 6, 6'-tetrachloro-1,1',3,3'-tetraethylbenzimidazol-carbocyanine iodide (JC-1). The transition of the mitochondrial transmembrane potential is an early and universal event in apoptosis. These probes facilitated analysis of changes in mitochondrial membrane potential and plasma membrane integrity, following treatment with the selected mycotoxins and sphingoid bases. The cytofluorometric study of mitochondria in their physical environment within intact cells presents several advantages in that it is possible to evaluate at a single cell level, potential variation in mitochondrial transmembrane potential. This is of fundamental importance when coping with heterogeneous cell populations.

Robb *et al.* (1990) showed that after incubation with 20 mycotoxin standards and extracts of fungi and feedstuffs, fluorescent FCM was successfully used to measure viability of the suspension NS-1 mouse melanoma cell line, and compared well to microscopic assessment of cytotoxicity on Hep-11 monolayers. Both methods gave essentially the same results, but the cytometric analysis using Rh123 offered a more quantitative approach. In the present investigation the effects of FB_1, MON, FA, ZEA, T2, DON, Sa and So on the N2α cell line were assessed following a 48-hour exposure period, qualitatively using fluorescence

microscopy (FM) and quantitatively using FCM. The principle of FM is based on the ability of a fluorescent compound to absorb ultraviolet (UV) light and re-emit the energy as visible light. The advantage of this technique is that by using light of short wavelength as the illuminating beam, there is an increase in the detail observed, and the light of long wavelength given off, amplifies the label. Rhodamine 123 was used in conjunction with PI, to measure cell viability and permeability on unfixed cells. Ethidium bromide (EtBr) and AcO were used to indicate the presence of apoptosis and loss of plasma membrane integrity. Analyses included fluorescent microscopic detection, cytofluorometric identification and quantitation of apoptotic or necrotic cells, based on interaction with these fluorochromes.

5.2 MATERIALS AND METHODS

Techniques reported in this chapter were studied under the supervision of Mrs Anne Cox, Dr Dawn Bradbury, and Professor Martin Griffin (July-September 1999), NTU, UK, and applied in the Departments of Physiology and Haematology, and the Optics and Imaging Centre, UKZN (December 2001).

5.2.1 Materials

Cell culture materials, media, antibiotics and sterile disposable consumables were purchased from Adcock-Ingram, SA, unless otherwise indicated. Pre-sterilised Corning plastic tissue culture flasks ($25cm^2$) were used as culture vessels. Sterile centrifuge tubes (15ml) were purchased from Continental Laboratory Suppliers. N, N'-dimethylformamide (DMF), D-sphingosine, DL-erythro-dihydrosphingosine, PI, Rh123, AcO, EtBr and phosphate buffered saline (PBS) tablets were purchased from Sigma-Aldrich Chemical Company, SA. The JC-1 probe was purchased from Molecular Probes, UK. All mycotoxins were obtained from the Mycotoxin Research Group, UKZN.

A Nikon E600 fluorescence microscope fitted with a camera was used at the Optics and Imaging Centre, UKZN. A Beckman Coulter EPICS XL flow cytometer fitted with a 488nm argon laser was used in King Edward VIII Hospital, Department of Haematology, UKZN. Blue tubes for FCM analysis and Isoflow sheath fluid was purchased from

Beckman Coulter, SA. The instruments were set up according to standard operating procedures.

5.2.2 Precautions

Since $\Delta\psi m$ is sensitive to both temperature and pH, all reagents were brought to RT prior to use, to ensure that pH 7.4 was maintained. As the fluorochromes used were light sensitive, all staining procedures and incubation times were carried out in the dark.

5.2.3 Preparation of the mycotoxin and sphingoid base stock solutions

The mycotoxins FB_1, FA, MON were dissolved directly into CCM ($1mg.ml^{-1}$), with CCM as the control solution for these mycotoxins. Zearalenone, T2, DON, Sa and So were dissolved in ethanol (EtOH) (100µl per mg) and CCM (900µl per mg) to a total stock solution of $1mg.ml^{-1}$. The control for this set of compounds was made up of EtOH (100µl) and CCM (900µl). All stock solutions were vortexed thoroughly to ensure complete resuspension of the compound in the solvent vehicle and CCM, and then used to prepare dilutions of 50, 100 and 200µM of each compound in CCM.

5.2.4 Preparation of N2α cells for fluorescence microscopy

Flasks of confluent N2α cells were incubated (37°C) in each test or control solution (2ml) for 48 hours prior to analysis. As FM involved qualitative analysis of the N2α cells, tests for the effects of each compound were carried out in duplicate at the 100µM concentration only. However, as cells were analysed using FM for three separate combinations of fluorochromes, namely AcO/EtBr, Rh123/PI, and JC-1, three replicates for each test compound at the 100µM concentration were prepared in duplicate. Following the 48-hour incubation period, all flasks were removed from the incubator, and gently rinsed with HBSS (5ml) to remove the detached dead cells and test solutions. The washes were discarded and the cells replenished with either fresh CCM or PBS as detailed below.

5.2.4.1 Acridine orange and ethidium bromide staining of N2α cells for assessment by fluorescence microscopy

A 2.5ml aliquot of PBS (pH 7.4) was added to the first set of confluent N2α cells

in flasks, followed by 100µl each of a mixture (1:1) of AcO (100µg.ml^{-1} in PBS) and EtBr (100µg.ml^{-1} in PBS). The flasks were shaken gently to ensure proper mixing of the solutions, and incubated at RT for between two to five minutes with checking. The staining solution was discarded and the top half of the flask was cut off using a heated wire. The cells were immediately bathed in PBS (1ml) to prevent drying out, prior to analysis on the Nikon E600 fluorescence microscope.

5.2.4.2 Rhodamine 123 and propidium iodide uptake by N2α cells assessed by fluorescence microscopy

To the second set of flasks of N2α cells, following rinsing with HBSS (5ml), the cells were supplemented with CCM (1ml) and Rh123 (20µl of 10µg.ml^{-1} in PBS, pH 7.4) was added and gently mixed. Following a five minute incubation at 37°C, PI (20µl of 10µg.ml^{-1} in PBS) was added to the flask, gently mixed and incubated at RT for a further five minutes prior to analysis.

5.2.4.3 Measuring the mitochondrial transmembrane potential of N2α cells with JC-1

The JC-1 fluorescent probe was dissolved in DMF (2.5mg.ml^{-1}), dispensed into 10-20µl aliquots, and stored at -20°C in the dark, until use. The third set of flasks of treated N2α cells were rinsed in HBSS (5ml), and replenished with CCM (2ml). The cells were stained with 2.5µg JC-1 per ml CCM (i.e., 2µl of JC-1 stock to 2ml CCM) and shaken well until the dye was well dissolved giving a uniform red-violet colour. The flasks were incubated for 15-20 min. at 37°C in the dark with gentle shaking every five minutes. After incubation, cells were rinsed twice with HBSS (5ml) and supplemented with 2ml CCM prior to analysis on the FM (with modification from Cossarizza *et al.*, 1993).

5.2.5 Preparation of N2α cells for cytofluorometric analyses

Flasks of confluent N2α cells were incubated (37°C) in each test or control solution (2 ml) at 50, 100 and 200µM for 48 hours prior to analysis.

5.2.5.1 Measuring N2α cell viability and permeability with propidium iodide and mitochondrial transmembrane potential with rhodamine 123

Following the 48-hour incubation period, cells from duplicate flasks of N2α cells were trypsinised and pooled into CCM (5ml) in sterile centrifuge tubes (15ml). The cells were pelleted by centrifugation (250g, 5min.). The supernatant was discarded and the cell pellet resuspended in CCM (500µl). Cell clumping was avoided with gentle tapping of the sample tube every 30 seconds (sec.). A single non-stained N2α cell sample was retained to establish where the cells would lie in the quadrants, and determine the light scattering properties of N2α cells. To the rest of the cell suspensions, Rh123 (10µl of 10µg.ml^{-1} stock solution in PBS, pH 7.4) was added. After a five minute incubation at 37°C, PI (10µl of 10µg.ml^{-1} stock solution in PBS, pH 7.4) was added, and the N2α cell suspension was incubated for a further five minutes at RT, prior to immediate analysis on the FCM, where between 1000-2000 events were counted on the EPICS XL (with modification from Simmons, 1999). The primary gate was set on cells on the FSC and SCC histogram, and this gate was used in all the analyses.

5.2.5.2 Measuring the mitochondrial transmembrane potential of cells with JC-1

When staining cells with this dye, speed was critical as JC-1 is essentially insoluble in aqueous solution, and precipitates out in a matter of minutes. Due to this limitation, it was easier when working with the cells in suspension to do the staining using 1 ml volumes, as these could be sedimented quickly using a centrifuge.

Control and treated of N2α cells were trypsinised using 0.1% EDTA, pooled into sterile centrifuge tubes (15ml), pelleted by centrifugation (250g, 5 min.) and resuspended in CCM (1 ml). The N2α cell suspensions were stained with 2.5µg.ml^{-1} JC-1, and shaken well until the dye was well dissolved, giving a uniform red-violet colour. To do this, it is also possible to vortex vigorously the suspension immediately after the addition of the probe. The cell suspensions were then incubated for 15-20 minutes at 37°C with gentle agitation every five minutes. After the incubation period, the cells were washed twice by vortexing, then pelleted by centrifugation at 250g for 5 min. with a double volume of PBS (2ml per wash). The cells were then resuspended in 0.5ml PBS and analysed immediately on the FCM (with modification from Cossarizza *et al.*, 1993).

In the flow cytometer, the value of the photomultiplier tube (PMT) detecting the signal in fluorescence channel 1 (FL-1) was set at about 390V, and fluorescence channel 2 (FL-2) PMT at 320V. With regards to the detector configuration, when excited simultaneously by 488nm argon-ion laser sources, the JC-1 monomer and J-aggregates were detected separately in the conventional flow cytometer FL-1 (green) and FL-2 (red) channels, respectively. The same channels were used for Rh123 and PI detection as well.

5. 3 RESULTS AND DISCUSSION

The use of EtBr/AcO, Rh123/PI and JC-1 in the N2α cellular analyses in this study was preferred as an alternative over that of the commercially available Annexin V and TUNEL assays. Although convenient, the use of commercially available kits is not always feasible. The limitation of reagents for a specified number of tests per kit, as well as their high cost, coupled with the need to assess the effects of six mycotoxins, two sphingoid bases and their matched controls with duplicate testing and multiple test runs on the cells for FM and FCM, was not financially feasible in this study. Using the Annexin V and TUNEL assays in the assessment of apoptosis in this study would have meant purchase of multiple kits and inflated experimental costs. Boehringer Mannheim (1998) also outlined other disadvantages associated with the use of the Annexin V and TUNEL kits. Annexin V was documented as not being specific for apoptosis since Annexin V can stain the inner membrane of ruptured cells, and an additional DNA stain must be used to distinguish between necrotic and apoptotic cells. With the TUNEL assay, Boehringer Mannheim (1998) outlined that it is labour intensive, time consuming, only a few tests may be performed simultaneously, that there was undefined cell loss during fixation, and uncertainty with regards to loss of a specific cell population. With all this room for error, and the fact that the objectives could also be assessed using the fluorochromes used in this study with very similar confounding variables, it was considered unnecessary to purchase an expensive kit with the restriction of a limited number of tests when a larger amount of a more economical fluorochrome could provide similar findings. Although not an objective, this study aimed to establish an alternative cheaper method that could be used in resource poor settings.

5.3.1 Acridine orange and ethidium bromide staining assessed by fluorescence microscopy

Acridine orange and EtBr were initially used to determine whether apoptosis, and loss of plasma membrane integrity occurred in the mycotoxin and sphingoid base-treated N2α neuroblastoma cells. In growing cells that are active in protein synthesis, RNA is responsible for cytoplasmic basophilia, i.e., the tendency of the cytoplasm to stain with basic dyes such as AcO (Vermes *et al.*, 2000). Acridine orange fluoresces green and EtBr fluoresces orange/red when bound to DNA. Acridine orange was permeable to the cell membrane, whereas EtBr was excluded from cells with intact plasma membranes (Figures 5.1 and 5.2). According to Gorman *et al.* (1997), AcO is taken up regardless of plasma membrane integrity and stains all cells to give green fluorescence, whereas EtBr is only taken up by late apoptotic and necrotic cells, i.e., cells that have become permeable, to give orange fluorescence. Even though apoptotic cells are beginning to die, their plasma membrane continues to exclude special dyes, and their chromosomal DNA fragments remain contained within the cell membrane until late in the process (Wyllie *et al.*, 1980; Darzynkiewicz *et al.*, 1992; Migliorati *et al.*, 1993). Necrotic cells are metabolically compromised, and vital dyes therefore readily penetrate their plasma membranes. However, because the plasma membrane of necrotic cells are leaky, the protein content of these cells is also reduced, and as a result have very faint staining with dyes such as AcO (Figure 5.3).

Using AcO and EtBr in combination, made it possible to differentiate between viable cells (green fluorescence with intact nuclei), early apoptotic (green fluorescence with chromatin condensation), late apoptotic (orange fluorescence with chromatin condensation) and necrotic cells (orange fluorescence with intact nuclei) following treatment with the mycotoxins, Sa and So (Figures 5.1-5.4). Cells at various stages from live (green), dead (red/orange) and those that were dying were observed by loss of cell membrane integrity, and either dye exclusion or inclusion (Figures 5.1-5.4). The live cells remained green, the dead cells red/orange and the transient or dying cells, showed staining with both dyes at various levels. Figures 5.1 and 5.2 illustrate the staining typical of control cells, where there was a predominance of green staining AcO in healthy cells, and very low levels of orange/red staining in apoptotic cells. Apoptosis is characterised by the maintenance of an intact plasma membrane during a significant part of its time course (Wyllie *et al.*, 1980;

Vermes *et al.*, 1998) and is a normal physiological process. Low levels of apoptotic cells were therefore expected in the control N2α cells as well.

Following the 48-hour exposure period, the six mycotoxins, as well as Sa and So induced varying levels of apoptosis and necrosis in the cultured N2α cells. As confluent flasks of N2α cells were used at the initiation of the 48-hour exposure period, the large intercellular gaps (Figure 5.3 and 5.4) were considered a reflection of the level of cell death induced by the treatment regimen. A feature of cells that lose viability in culture is the loss of their ability to adhere to the culture substrate. These dead cells consequently float off, and are removed in the washes prior to staining cells.

Significant differences in the staining intensities were apparent by comparison of control N2α cells (Figure 5.1) with the FB_1-treated (Figure 5.3) and T2-treated N2α cells (Figure 5.4). There was a notable inversion in the ratio of green to red/orange staining, with a high proportion of apoptotic and necrotic cells detected following exposure to these mycotoxins. In relation to the MTT data generated subsequent to 48-hour exposure to these mycotoxins (Chapter 3, Table 3.1 and 3.3), T2 induced ~35% cytotoxicity and FB_1 ~15% cytotoxicity. Comparable patterns of staining were seen following exposure of the N2α cells to the six mycotoxins, as well as Sa and So, although the intensity of staining varied.

As a result of its basic property, AcO has the ability to accumulate in lysosomes, which, due to an ATP-dependent proton pump have a low pH. Once inside, the dye is protonated and becomes entrapped in these organelles. The supravital cell staining with a low concentration, which appears as red fluorescence, is the reflection of the activity of the proton pumps of lysosomes (Darzynkiewicz *et al.*, 1992). The ability of lysosomes to accumulate AcO remains intact during the initial stages of apoptosis whereas it is immediately lost during necrosis. This difference can be exploited for discrimination between apoptosis and necrosis. The monomeric binding of AcO to the cellular DNA results in green fluorescence, while polymeric binding of AcO to lysosomes results in red fluorescence. During apoptosis, the red fluorescence is not changed because of the intact lysosomal membrane, while the green fluorescence may diminish due to DNA breakdown, resulting in a net increase of the red signal in apoptotic cells, and a decrease of the red signal in necrotic cells, due to ruptured and leaky lysosomes, while the green DNA fluorescence remains stable at least during the initial stage of apoptosis. In apoptosis, after

loss of the mitochondrial transmembrane potential, the lysosomal pumps lose their function (Vermes *et al.*, 2000).

Visually, it was difficult to differentiate between the red-staining lysosomes (Figure 5.1) and the orange-staining chromatin within cells in this study (Figure 5.3). Quantitative assessment of the cells following staining with AcO and EtBr on the FM was omitted, as the red and orange staining were difficult to separate due to their closeness in the colour spectrum, and hence spectral overlap on the image analysis system. An attempt to quantify this type of staining would have led to inaccurate values being obtained if used as a gauge of the level of necrosis/apoptosis that occurred.

5.3.2 Rhodamine 123 and propidium iodide staining assessed by fluorescence microscopy

The $\Delta\psi m$ results from the asymmetric distribution of protons and other ions on both sides of the inner mitochondrial membrane (Chapter 4, Figure 4.1). The matrix side of this is negatively charged; consequently cationic lipophilic fluorochromes distribute to the mitochondrial matrix (Kroemer *et al.*, 1997). An early event of apoptosis is TMP, which is reflected by a loss of the cells' ability to accumulate these fluorochromes. Disruption of TMP occurs before cells exhibit nuclear DNA fragmentation or exposure of phosphotidylserine on the outer cell membrane leaflet (Marchetti *et al.*, 1996). Rhodamine 123 and JC-1 serve as probes for TMP. Viable cells incubated in their presence, accumulate the probes in their mitochondria, and the efflux of the fluorochrome measured by intensity of cellular fluorescence is considered to reflect TMP.

Rhodamine 123 is a cationic fluorochrome, that fluoresces green when actively taken up due to the $\Delta\psi m$. When membrane integrity is compromised, cells take up PI that binds to DNA or double stranded RNA and fluoresces red. When Rh123 was applied together with PI, intact cells stained with Rh123 (green fluorescence and no PI staining because of intact membrane function). Healthy control N2α cells with functioning mitochondria and intact cell membranes accumulated the Rh123 to give fluorescence in the green wavelength, and as PI was excluded, no fluorescence in the red wavelength (Figure 5.5). Rhodamine 123 was taken up by the mitochondria of these cells resulting in cells with brightly staining green cytoplasm, while non-viable cells exhibited a diffuse, pale-green fluorescence due to

compromised mitochondrial function (Figures 5.6-5.7). Rhodamine 123 in combination with PI, facilitated discrimination between live cells and dying cells (necrotic or late apoptotic cells), whose plasma membrane integrity was compromised and consequently stained with PI as well. Necrotic and apoptotic cells are shown in Figures 5.6 and 5.7 where the N2α cells were treated with Sa and So (100μM), respectively.

N2α cells with intact membranes (e.g., viable and early apoptotic cells) excluded PI, preventing its intercalation into intracellular nucleic acids. Thus, these cells did not exhibit enhanced DNA dependent fluorescence due to the absence of PI-DNA complex formation. The early apoptotic cells however, in contrast to viable cells had markedly diminished staining capacity for Rhl23, and stained with faint green fluorescence, due to fewer viable mitochondria than in the viable cells. Apoptotic cells retained their membrane integrity, and thus excluded PI. As apoptosis progressed however, the permeability of cell membranes gradually increased in discrete stages, resulting in late apoptotic cells staining with PI. Furthermore, necrotic N2α cells were intensely labelled with PI, since their damaged membranes were incapable of excluding the stain. Overall, cells with compromised plasma membranes, namely the necrotic and late apoptotic N2α cells stained with PI, showing red fluorescence.

In this study, optical separation and identification of necrotic and late apoptotic N2α cells were complicated to assess using FM, as illustrated in Figures 5.6 and 5.7. Rhodamine 123 was taken up by the mitochondria of live N2α cells resulting in cells with brightly staining cytoplasm, while non-viable N2α cells displayed diffuse fluorescence. The ZEA-treated N2α cells shown in Figure 5.8 displayed features of cytoplasmic condensation and cell shrinkage that are consistent with the late apoptotic stage. In addition, cells with relatively intact cell membranes are noted in comparison to the DON-treated N2α cells shown in Figure 5.9. The DON-treated N2α cells were swollen and displayed compromised plasma membrane integrity indicative of possible necrosis. The N2α cells treated with DON also displayed characteristic features of apoptosis such as membrane blebbing.

Propidium iodide uptake was a reflection of the extent of membrane damage and permeability of these unfixed N2α cells. Propidium iodide was not excluded by necrotic cells and after entering the cell, and intercalating with intracellular nucleic acids, induced bright red fluorescence of the necrotic DON-treated N2α cells nuclei (Figure 5.9). Cells

with their membrane integrity compromised incorporated PI (red fluorescence), with a decrease in the green fluorescence reflective of cells whose mitochondria were not functioning optimally, or at all (Figure 5.7). Cells with decreased Rh123 fluorescence and that were PI positive included necrotic cells (Figure 5.9), indicated by cellular swelling, and loss of plasma membrane integrity shown in comparison to control N2α cells that stained purely with Rh123 and excluded PI (Figure 5.5).

5.3.3 Measuring the mitochondrial transmembrane potential of cells with JC-1

Variations in mitochondrial membrane potential were detectable at the single cell level by staining N2α cells with the lipophilic cation JC-1. This dye fluoresces green in its monomeric form. Active mitochondria with high transmembrane potentials, capable of accumulating the JC-1 at concentrations greater than 100nM, formed J-aggregates that fluoresced red. JC-1 binding to mitochondria was therefore detected by the shift in fluorescence from green to orange/red, which reflected its aggregation in mitochondria driven by the $\Delta\psi m$. The change in binding of JC-1 was reflected by the loss of orange fluorescence and a decrease in the green fluorescence, although to a lesser degree than the orange. The ratio of green to orange/red fluorescence was dependent only on the membrane potential, and not on other factors such as mitochondrial size, shape and density that influence single component fluorescence signals.

As JC-1 was light sensitive, speed was critical in capturing the images under the FM once exposed to light. During apoptosis there was a marked decrease in orange fluorescence, and to a lesser degree, in the green fluorescence of JC-1. The uptake of this cationic probe depends not only on the $\Delta\psi m$, but also on transport of these molecules through the plasma membrane, cytoplasmic loading which is dependent upon plasma membrane potential, and mitochondrial loading which is dependent upon ER loading, that theoretically can take place after the fall in $\Delta\psi m$. In the case of JC-1, aggregates are present no longer when the dye is released from mitochondria. Cells with high transmembrane potential were those forming J-aggregates, thus showing high red fluorescence and cells with low transmembrane potential were those in which JC-1 maintained (or reacquired) monomeric form, thus showing only green fluorescence. Polarized mitochondria were marked by punctate orange-red fluorescent staining in the control N2α cells stained with JC-1 (Figures 5.10 and 5.11).

In the N2α cells exposed to FA (100 μM) for 48 hours, J-aggregate formation was elevated in N2α cells that were large and apparently unaffected by mycotoxin exposure, in comparison to those N2α cells in the centre of the micrograph, that had decreased staining and showed cytoplasmic condensation (Figure 5.12). These were likely apoptotic cells. On depolarisation, the orange-red punctate staining was replaced by the diffuse green monomer fluorescence. From Figure 5.12, is also evident that large numbers of cells were killed as a result of exposure to FA, since large intercellular gaps were evident. All flasks of N2α cells utilized in these experiments were confluent prior to addition of the mycotoxins or sphingoid bases, and the duration of exposure to the mycotoxins was sufficient to have induced cell death at a detectable level. Dead cells would have been rinsed out prior to staining, creating the large intercellular gaps between the cells (Figure 5.12).

In the N2α cells exposed to MON (100μM), a decreased cytotoxicity was apparent in comparison to the FA-treated cells by the noticeably higher number of cells with intensely coloured J-aggregates (Figure 5.13). These results are supported by findings of the MTT assay, (Chapter 3, Table 3.1) where following 48-hour exposure to 100μM MON, 61.4% cell viability was noted in comparison to the untreated N2α controls. In the cells exposed to FB_1 (100μM) for 48-hours, fluorescent J-aggregates were visible in the remaining adherent cells, but as with FA, large intercellular spaces were noted indicative of the proportion of cell death that occurred as a consequence of FB_1 exposure (Figure 5.14).

5.3.4 Flow cytometric analysis of cells stained with rhodamine 123/ propidium iodide and JC-1

Although qualitative analysis of Rh123/PI and JC-1 incorporation was done using FM, quantitative analyses of apoptotic and necrotic cells was facilitated on the FCM, using Rh123/PI uptake as a measure of cell permeability, and determination of $\Delta\psi m$ using JC-1. The results these probes provided were expressed as increases or decreases in fluorescence intensity. Consequently, variations of membrane potential were usually expressed as the shift of the mean peak channel of a single fluorescence.

Flow cytometry was a comparatively more expensive technique in terms of requiring higher cell numbers, which involved culturing multiple flasks of N2α cells for treatment and analysis. Higher concentrations of mycotoxins and sphingoid bases in larger volumes of CCM were also used in comparison to *in vitro* micro-culture assays to ensure uniform exposure of N2α cells to these test compounds during the exposure periods. A further requirement was the use of specialized equipment, i.e., the flow cytometer and technical expertise to operate the FCM and guide interpretation of data. These drawbacks were however considered a trade-off when taking into account the ability to quantitatively analyse the effects of a treatment regime on the N2α cultured cells.

JC-1 is a marker of mitochondrial activity, and it changes reversibly its colour from green to orange/red as membrane potentials increase (over values of about 80-100mV). This property is due to the reversible formation of JC-1 aggregates upon membrane polarization that causes shifts in emitted light from 530nm (i.e., emission of JC-1 monomeric form) to 590nm (i.e., emission of J-aggregate) when excited at 490nm, the colour of the dye changes reversibly from green to greenish orange as the mitochondrial membrane becomes more polarized. Normally, green fluorescence of depolarised cells is a little higher than that of polarized ones, simply because of the presence of a higher amount of JC-1 monomers. Consequently, mitochondrial depolarisation is indicated by a decrease in the red/green fluorescence intensity ratio. The potential-sensitive colour shift is due to concentration-dependent formation of red fluorescent J-aggregates. Both colours were detected using the filters commonly mounted in all flow cytometers, so that green emission was analysed in FL-1 and reddish orange emission in FL-2.

Use of the fluorescence ratios of cells in each channel allowed comparative measurements of membrane potential and determination of the percentage of mitochondria within a population that were affected by exposure to the mycotoxins or sphingoid bases (Table 5). Subtle heterogeneity in cellular responses was discerned in this way. The method using JC-1 is both qualitative, as shown by fluorescence microscopic detection, considering the shift from green to orange JC-1 fluorescence emission, and quantitative, considering the pure fluorescence intensity, which was detected in both FL-1 and FL-2 channels. These characteristics were useful in the study of mitochondrial membrane potential variation in living N2α cells. For the analysis of cells stained with JC-1, results were represented as the proportion of total cells that displayed high red J-aggregate

formation, against those that showed a predominance of the monomeric green fluorescence (Table 5). Those cells with red J-aggregates were indicative of viable cells and those with green monomers only, indicative of apoptotic and necrotic cells with compromised mitochondria.

Rhodamine 123 also served as a marker of decreased mitochondrial transmembrane potential, and was used in conjunction with PI to measure cell viability and permeability on unfixed cells, for cytometric discrimination of viable versus dying cells. Healthy cells with functioning mitochondria and intact cell membranes accumulated the Rh123 to give fluorescence in FL-1, the green wavelength fluorescence channel on the FCM, and no fluorescence in the red wavelength fluorescence channel, FL-2. Cells with their membrane integrity compromised, took up PI to give a population of cells in FL-2, and if their mitochondria were not functioning, a decrease in the FL-1 fluorescence was detected.

Apoptotic cells retained their membrane integrity and thus excluded PI. As apoptosis progressed, the permeability of cell membranes increased in discrete stages. Cells with compromised plasma membranes (necrotic and late apoptotic cells) stained only with PI, showing red fluorescence. Early apoptotic cells, in contrast to viable cells, had markedly diminished staining capacity with Rhl23 and less green fluorescence. Cells with intact membranes (e.g., viable and early apoptotic cells) excluded PI. Thus, these cells did not exhibit enhanced DNA-dependent fluorescence due to PI-DNA complex formation, which was detected in the FL2 channel of the FCM. Furthermore, necrotic cells were labelled with PI, since damaged membranes were incapable of excluding the stain. Thus, necrotic cells exhibited very strong PI fluorescence.

JC-1 seems to be a more reliable indicator of the true $\Delta\psi m$ than Rh123 alone as there have been a few problems associated with staining with Rh123. Typically, the signal coming from cells whose mitochondria had a low potential was much lower than that of control samples, and in a classical histogram depolarised populations go to the left. However, after the shift to the left the peaks (i.e., that of controls and treated cells) are not always perfectly separate, the operator has to decide "by eye" where the population of cells with depolarised mitochondria begins. In addition, Rh123 binding to mitochondria is difficult to calculate when the cells present certain mitochondrial heterogeneity due, for example, to a high number of mature or immature mitochondria, as in a continuously growing cell line

(Lopez-Mediavilla *et al.*, 1989) as used in this study. Moreover, different mitochondrial binding sites for Rh123 exist, i.e., sites which are freely accessible whatever the energy status of the mitochondria, and sites which are hidden in the energized state and freely accessible in the de-energized form of the organelle. This has been attributed to different maturative states of the organelle. Thus, in a single cell the organelles can have different Rh123 mitochondrial binding sites with consequent different binding emissions, and it is very difficult to ascertain whether or not mitochondria strongly bind Rh123 in an energy dependent or independent manner. However, the probe is considered more reliable when used in association with PI, as this combination allows a clear distinction between dead and living cells. JC-1 is however considered more specific for mitochondrial versus plasma membrane potential, and more consistent in its response to depolarisation, than Rh123.

The flow cytometric analyses of the staining of the treated N2α cells stained with Rh123 and PI are also summarised in Table 5. Cells with green fluorescent Rh123 uptake were taken as an indication of the percentage of viable and early apoptotic cells, and those with PI uptake as late apoptotic or necrotic cells. As FCM using the specified probes is unable to discriminate between necrotic and late apoptotic cells definitively, for this study, cells in these two subpopulations were defined as non-viable cells (according to Tolleson *et al.*, 1996b).

Good correlation was found between both methods for the assessment of N2α control cells. JC-1 staining is unaffected by agents that depolarise the plasma membrane, whilst strongly affected by drugs/compounds that dissipate $\Delta\psi m$ (Simmons, 1999). The ratio of red to green JC-1 fluorescence is dependent only on the mitochondrial membrane potential and not on other factors, such as mitochondrial size, shape, or density that may influence single-component fluorescence signals.

Table 5: **Flow cytometric analyses of the mycotoxin and sphingoid base treated N2α cells following staining with JC-1, rhodamine 123 and propidium iodide.**

		JC-1 stained N2α cells		Rh123/PI stained N2α cells	
Treatment	Conc. (μM)	% Red J-aggregates	% Green monomers	% Rh 123 uptake	% PI uptake (late apoptotic /necrotic cells)
Control		94.2±3.8 (n=4)	5.8±3.8 (n=4)	90.1±3.7(n=2)	9.9±3.6(n=2)
FB_1	50	67.5±3.3(n=3)	32.2±3.7(n=3)	70.2±2.8(n=2)	30.3±2.1(n=2)
	100	64.2±8.9 (n=3)	34.0±8.0(n=3)	69.1±24.3(n=2)	30.7±24.0 (n=2)
	200	63.4±12.3(n=3)	36.1±12.4(n=3)	73.4±2.4(n=2)	26.55±2.3(n=2)
FA	50(n=3)	83.5±5.8	16.5±5.8	42.7±4.1	57.1±3.9
	100(n=3)	70.8±15.4	29.2±15.5	62.26±1.6	37.7±1.5
	200(n=3)	75.2±11.1	24.6±11.3	41.5±4.0	58.4±3.8
MON	50	78.9±16.1(n=3)	20.5±15.7(n=3)	84.3±6.0(n=2)	14.8±4.6(n=2)
	100	70.7±1.1(n=2)	26.7±3.7(n=2)	85.3±2.3(n=2)	14.7±2.3(n=2)
	200	89.5±3.8(n=2)	10.1±3.5(n=2)	86.9±1.8(n=2)	13.4±2.1(n=2)
Control with EtOH		88.5±13.2(n=2)	11.5±13.2(n=2)	85.16±2.2(n=3)	14.63±1.9(n=3)
Sa	50	59.4±19.3(n=4)	40.7±19.3(n=4)	16.8±1.3(n=3)	83.2±1.3(n=3)
	100	53.4±9.7(n=4)	46.0±7.6(n=4)	27.4±9.2(n=3)	72.56±9.2(n=3)
	200	53.1±16.2(n=4)	45.3±15.5(n=4)	23.5±6.6(n=3)	76.4±6.7(n=3)
So	50	51.1±13.9(n=3)	48.5±14.2(n=3)	35±4.5(n=3)	63.8±6.3(n=3)
	100	77.6±4.2 (n=3)	22.4±4.2 (n=3)	4.9±2.1(n=3)	95±2.1(n=3)
	200	75.7±1.5 (n=3)	24.1±1.5 (n=3)	3.0±0.3(n=3)	96.9±0.3(n=3)
T2	50	63.1±2.8 (n=3)	36.9±3.2 (n=3)	0.3±0.2(n=3)	99.6±0.2(n=3)
	100	55.3±4.4 (n=3)	44.8±4.4 (n=3)	0.96±0.4(n=3)	99.0±0.4(n=3)
	200	57.8±11.1(n=3)	41.4±10.6(n=3)	15.6±25.8(n=3)	82.3±25.8(n=3)
DON	50	51.8±6.1 (n=3)	47.5±7.1 (n=3)	3.5±0.1 (n=2)	96.5±0.2 (n=2)
	100	82.6±4.0 (n=3)	16.7±4.7 (n=3)	1.3±0.3 (n=3)	98.7±0.3 (n=3)
	200	52.8±22.6(n=3)	47±22.4 (n=3)	1.95±1.2 (n=2)	98.1±1.2 (n=2)
ZEA	50	60.0±41.4(n=3)	32.9±40.2(n=3)	22.2±0.3 (n=2)	77.8±0.3 (n=2)
	100	68.6±1.4 (n=3)	31.1±1.8 (n=3)	55.4±1.8 (n=2)	44.5±1.6 (n=2)
	200	45.8±9.6 (n=3)	52.3±8.7 (n=3)	7.5±0.4 (n=2)	92.6±0.4 (n=2)

Figure 5.15 is a FCM acquisition report showing how the unstained cells were used to set the cells into region C3 in Histogram 3 for the analyses. To briefly discuss how the data was interpreted, Histogram 1 illustrates how the primary gate A was derived from the cells when using FSC against SSC on the X and Y axes respectively. Histogram 2 is the same as Histogram 1 except that the FSC and SSC parameters are presented in the log function. The gate B was drawn around the events in this Histogram 2. In Histograms 3 and 4, Fluorescein isothiocyanate (FITC) (green fluorescence channel 1) and Phycoerythrin (PE) (red fluorescence channel 2) were on the X and Y-axes respectively. In Histogram 3, the gate A was imposed and region C2 shows the percentage of cells from gate A with red J-aggregates that display the double stain, i.e., that fluoresce green and red, and region C4 shows those cells that fluoresce green only. Green fluorescence was indicative of compromised mitochondria with a low transmembrane potential. Histogram 4 has the gate B imposed from Histogram 2, and region D2 also shows the percentage of cells from gate B with the double stain. In addition, as seen in Histogram 7, all unstained cells (illustrated by the peak of cells) were set to lie before the first log position in the PE FL-2.

Figure 5.16 is an example of a FCM acquisition report showing N2α controls cells stained with JC-1. Histogram 7 serves more as an internal reference check, as the approximate number of events in linear gate E in the red fluorescence channel of PE should correspond with those events in C2 and D2. Note the shift in the peak of unstained cells in Figure 5.15 in Histogram 7 to the position after the first log of the X-axis after staining with JC-1 in Histogram 7 in Figure 5.16.

For the N2α control cells stained with JC-1, a mean (n=4) percent viability of 94.2±3.7% was established, in comparison to 5.75±3.75% of the cells that showed the green monomer fluorescence only. Controls were run on 4 separate occasions with between 1000-3000 events per FCM analysis. The number of events analysed was considered sufficient, as all results presented are a mean of between two to four replicates of the same experiments with the N2α cells (Doorasamy *pers comm.*, 2004). In addition, the fact that two confluent flasks of N2α cells were pooled for each analysis at each concentration due to the significant levels of cell death and cell losses that occurred as a consequence of exposure to these mycotoxins and sphingoid bases, as well as when staining and washing the cells prior to analysis, these results were considered valid and representative.

In comparison to the JC-1 staining, when staining with Rh123/PI, 90.1±3.67% viable N2α cells with intact mitochondrial transmembrane potential (indicated by Rh123 uptake) and 9.85±3.6% late apoptotic or necrotic cells (indicated by the PI uptake) were analysed. For both the JC-1 and Rh123/PI analyses, these levels of apoptotic cells were not unexpected, as apoptosis is a normal physiological response, and usually occurs in cultured cells where the rate of cell turnover is very high. The N2α line is primarily a transformed cell line and can therefore be cultured continuously for prolonged periods. This, however, raises concerns with respect to normal cell function, for example, with respect to apoptosis. Indeed, transformation can be likened to a process of 'dedifferentiation'. Nevertheless, experience with a variety of transformed cell lines that retain specialised, differentiated functions has indicated that although such cell lines are the exception (most transformed cell lines show little functional dedifferentiation), those functions that are expressed are likely to reflect accurately the *in vivo* functions of the parent cell type (Sato *et al.*, 1970; Dannies and Tashjian, 1973). It is clear however, that observations made in such systems must be confirmed in untransformed cells, in tissues, and ultimately *in vivo*.

In the control N2α cells treated with EtOH, in keeping with the results of the MTT assay (Chapter 3) where the use of EtOH as a solvent vehicle was shown to induce a comparatively minor, but higher proportion of cell death in comparison to EtOH-untreated controls; staining with JC-1 indicated that 88.5±13.15% of the cells showed J-aggregate formation, with 11.5±13.15% showing monomeric green fluorescence. In addition, staining with Rh123 revealed 85.16±2.18% viable cells with intact mitochondrial transmembrane potential, and 14.63±1.92% compromised cells with PI uptake. Figure 5.17 is an FCM acquisition report showing higher percentage of green Rh123 stained cells in region C4 of Histogram 3, and a small percentage of cells that have taken up PI in quadrant C2. Once these controls were run, the FCM was then set to compensate for this known proportion of non-viable cells within each control population when analysing all the treated N2α cells.

In the N2α cells exposed to FB_1, an increase in toxin concentration from 50 to 200μM was paralleled by a decrease in red J-aggregate formation from 67.5±3.3% to 63.4±12.3% (n=3) (Table 5), suggesting a decrease in the $\Delta\psi m$. Similar levels of cell viability were also obtained using the MTT assay in Chapter 3, where 72% cell viability was reported for those cells exposed to 50μM FB_1. With Rh123/PI staining however, although this trend was not as evident, approximately the same levels of cell viability were reported

(Table 5). Increased apoptosis has been reported following *in vitro* exposure of turkey lymphocytes (Dombrink-Kurtzman *et al.*, 1994), human keratinocytes, fibroblasts, oesophageal and hepatoma cells (Tolleson *et al.*, 1996b), as well as CV-1 monkey kidney cells to FB_1 (Wang *et al.*, 1996). The FB_1-induced inhibition of CER synthase results in an increase in the accumulation of Sa within the cell, and may indirectly be responsible for increased cell death from exposure to FB_1 (Merrill *et al.*, 1993a). Inhibition of sphingolipid metabolism leads to compromised cell membrane integrity, and may have increased N2α cell membrane permeability to PI. The results of this study on the N2α cells are also supported by findings of Galvano *et al.* (2002) who exposed rat astrocytes to FB_1, and after 72 hours treatment found that FB_1 (50 and 100μM) induced DNA damage of apoptotic type in the astrocytes.

JC-1 staining revealed that following treatment with FA, at the highest concentration of 200μM, 24.56±11.31% of the N2α cells had compromised mitochondria. Staining with Rh123/PI indicated that at this concentration, 58.4±3.83% of the N2α cells were either late apoptotic or necrotic as indicated by the uptake of PI. Figures 5.18 (a-c) are FCM histograms showing the N2α cells treated with 50, 100 and 200μM FA for 48 hours, and then stained with Rh123/PI. The results summarised in Table 5 indicate that staining the cells with Rh123/PI shows a higher proportion of cells that are compromised at all concentrations. In this treatment set, the JC-1 and Rh123/PI staining results did not correlate.

Telles-Pupulin *et al.* (1998) using isolated rat mitochondria reported that FA affects mitochondrial energy metabolism by inhibition of succinate dehydrogenase, oxidative phosphorylation and α-ketoglutarate dehydrogenase. The inhibition of oxidative phosphorylation seems to be the result of a direct action on the ATP synthase/ATPase without significant inhibition of the ATP/ADP exchange. In the present study, cell viability was partially reflected by the maintenance of the $\Delta\psi m$, and the lower cell viabilities may have been detected as a result of the FA induced inhibition of these enzymes in the N2α cell line, and subsequent loss of TMP. As apoptosis is an active process requiring energy, ATP may be generated by glycolysis in cells where mitochondrial membrane potential has been compromised. It has been reported that malignant cells are able to change their energy production from oxidative phosphorylation to glycolysis (Chen, 1988). This shift to glycolysis may enable the apoptotic process to

continue in cells in which oxidative phosphorylation has been impaired by a reduction in the number of functioning mitochondria.

Shimizu *et al.* (1996a) measured intracellular ATP levels during cell death and showed that intracellular ATP levels remain unchanged until the very end of the apoptotic process. As disruption of plasma membrane potential that halts mitochondrial energy production is an early step in apoptosis (Zamzami *et al.*, 1995a; Shimizu *et al.*, 1996a), intracellular ATP required for the rest of apoptosis must be provided by glycolysis. When glucose is provided in culture medium, respiratory chain inhibitors induce apoptosis or necrosis (Shimizu *et al.*, 1996b). According to Tsujimoto (1997), this distinction is due to the cells dependence on respiration to maintain intracellular ATP levels. Cells depending more on mitochondria for ATP, die by necrosis because of an energy crisis and cells with a larger contribution of glycolysis, die by apoptosis because of lowered intracellular ATP levels which are still sufficient for apoptosis (Tsujimoto, 1997).

Results of the treatment of the N2α cells with MON for 48 hours were similar when assessed using both JC-1 and Rh123/PI staining, with viabilities not falling below 70% across the tests range of concentrations (Table 5). These results are also similar to those of the MTT assay where at 50 and 200μM MON, viabilities of ~70% were reported (Chapter 3, Table 3.1). Although decreased protein synthesis and oxidative damage have been ascribed to MON (Norred *et al.*, 1990), Thiel (1978) reported that the principal mechanism of action of MON is believed to involve selective inhibition of mitochondrial PDH and α-ketoglutarate dehydrogenase. Moniliformin binds to PDH, preventing entry of pyruvate into the TCA cycle, therefore decreasing mitochondrial respiration (Burka *et al.*, 1982). Rat brain transketolase and PDH were inhibited 59% by 10^{-4}M MON (Burka *et al.*, 1982). Thiel (1978) also reported that a 5μM concentration of MON caused a 50% inhibition of oxygen uptake by rat liver mitochondria with pyruvate as the substrate.

As was previously indicated the N2α cell line also required sodium pyruvate in the CCM to ensure cell proliferation. Cells grown in CCM without sodium pyruvate ceased growing and died. It is possible that MON and the added pyruvate may have competed for the binding site on PDH. By adding MON as a suicide substrate of PDH, it is likely to have caused a block on, or decreased mitochondrial respiration causing cell death. This hypothesis is supported by Gathercole *et al.* (1986) who showed that supplementation with pyruvate resulted in decreased MON-induced inhibition of PDH function. However, in the

present study, sodium pyruvate was added at a concentration of 2mM. The higher concentration of pyruvate than MON in the CCM may explain why cell viability never decreased below 70% in these cells. Even at the highest concentration of 200μM MON, ~90% cell viability was noted with JC-1 staining which indicates that the high concentration of sodium pyruvate in the media may have protected cells from the toxic effects of MON. These results are in keeping with the results of MON treatment of N2α cell using the MTT assay (Chapter 3).

The results of the Sa, So, T2, ZEA and DON treatments appear discrepant when comparing JC-1 staining to Rh123/PI results (Table 5). However, apoptosis is a sequential process of variable duration, depending on inducer and cell type. As a result, any method has an optimal 'time-window' for analysing the apoptotic process, and it is possible that the percentage of apoptotic cells in the same population may not be identical when two methods are utilized (Cossarizza *et al.*, 1993).

Using JC-1 staining, viabilities for the Sa-treated cells were reported to be between 53-60% (Table 5). Using Rh123/PI staining however, necrotic and late apoptotic cells were established to comprise between 72 to 83 % of the total cell population. Figure 5.19 show the analyses of the cells treated with 50μM Sa and then stained with Rh123/PI, and Figure 5.20 shows the FCM analyses of N2α cells treated with 200μM So. The linear gate E in Histogram 7 of Figure 5.20 shows the good correlation between the gating strategy and the linear gate E indicating the percentage of cells stained with PI.

Ohta *et al.* (1994) reported that So induced apoptosis in neutrophils. Jarvis *et al.* (1996) also reported that So induced apoptosis in HL-60 and U937 cultured cells. In this study, So induced high levels of apoptosis and/ or necrosis in N2α cells following the 48 hours exposure period as indicated by the high proportion of PI uptake reported in 62-97% of the N2α cells analysed (Table 5). The accumulation of free Sa has also been shown to be growth inhibitory and cytotoxic (Merrill *et al.*, 1983; Stevens *et al.*, 1990; Hannun *et al.*, 1991; Sweeney *et al.*, 1996). The Sa results on the N2α cells correlate well with the MTT assay data, where viability of Sa-treated cells after 48-hour exposure at 50, 100 and 200μM was found to be 29, 46, and 50%, respectively (Chapter 3, Table 3.2).

With the N2α cells exposed to T2 and DON, staining with Rh123/PI, revealed that the late apoptotic and necrotic N2α cells comprised greater than 80% of the N2α cell population (Table 5). Staining with JC-1 however showed that a potential toxin-dependent decrease in viability was evident from 63 to 57% for T2, with larger standard deviations evident at the highest concentration of 200μM with many of the compounds tested. The viabilities of the N2α cells exposed to DON also varied considerably when the methods were compared. No dose dependent mechanism of cell death was established using either method, with fluctuations from 51.8% at 50 μM, up to 82% at 100μM, and then a decrease back to 53% at 200 μM (Table 5). Using Rh123/PI cell viabilities were consistently below 5% at all three levels of exposure.

Trichothecenes produce toxicity via inhibition of protein synthesis (Ueno, 1983; Kiessling, 1986), inhibition of DNA synthesis (Thompson and Wannemacher,1984; Kiessling, 1986), impairment of ribosome function (Coulombe, 1993), inhibition of mitochondrial protein synthesis (Pace, 1983) and induction of reparable single strand breaks in DNA. The variable potency at the cellular level is probably due to the rate of transport into the N2α cells, the metabolism of mycotoxins by cytosolic enzymes, changes in affinity for the active binding site or reduced capacity to interfere with protein synthesis. Metabolism may be more important in detoxification than in producing toxicity, as the trichothecenes are directly toxic without activation.

T-2 toxin inhibited the mitochondrial electron transport system in yeast by inhibiting succinate dehydrogenase (Khachatourians, 1990), and induced cell membrane injury with haemolysis, apparently via a free-radical mechanism (Coulombe, 1993). T-2 toxin also affected the permeability of cell membranes *in vitro* at concentrations of $0.4 pg.ml^{-1}$ (Bunner and Morris, 1988). The fact that T2 is able to increase permeability of cell membranes may explain why PI was detected in such a high proportion of N2α cells, and its effects on mitochondrial electron transport may be responsible for the disruption of the mitochondrial transmembrane potential.

With the ZEA-treated N2α cells, the results seemed more reliable as there was a decrease in J-aggregate formation from 60 to 46%, with an increase in PI uptake by the N2α cells from 78 to 92%. The Rh123/PI method of staining gave consistently higher levels of compromised cells than the JC-1 staining method. With the ZEA-treated N2 α cells, the

JC-1 staining method gave viability levels similar to those obtained using the MTT assay (Chapter 3, Table 3.3).

There are many criteria that require consideration for the unbiased interpretation of these results. Flow cytometric measurement of apoptosis, regardless of the method used, is associated with selective loss of apoptotic cells during sample preparation. The inherent setback of JC-1 staining is that in the cell preparation procedure, following staining, cells have to be pelleted and washed twice prior to analysis on the flow cytometer to remove this probe. Its' use nonetheless, was considered more accurate than the staining with Rh123/PI when compared with the MTT assay results in Chapter 3. With Rh123/PI, there was no washing step prior to analysis on FCM. In cases where a course of treatment results in induction of a major proportion of cellular damage via apoptosis or necrosis, washing the cells is responsible for the loss or removal of these damaged, fragmented populations of cells. This is evident from the visible decrease in the cell pellet size between washing stages, and the lower number of cells available for analysis on the flow cytometer when compared to controls. Intact cells are easily pelleted and retained in a greater proportion following centrifugation, and a large proportion of fragmented and damaged cells are discarded in the washes. This presents a problem as a major percentage of treated compromised cells are removed and not included in the absolute analysis. This problem is unavoidable however as JC-1 is insoluble in water and crystallizes out quickly, and needs to be removed from the cell suspension prior to FCM analysis.

The major advantage of FCM is that it offers the possibility of multi-parametric analysis of several cell attributes. On the other hand, the major drawback of FCM methods stems from the fact that identification of apoptotic or necrotic cells is not based on morphology and cannot be correlated with morphological classification. Rather, it relies on a single parameter reflecting the change in biochemical or molecular attributes of the cell, presumed to represent either apoptosis or necrosis. In addition, most FCM methods do not allow for a clear distinction between late apoptotic and necrotic cells. In cases such as this, it becomes clear why more than one method of analysis is required for determination of apoptosis, why unbiased interpretation of results is necessary, and why microscopical analysis of cells remains the gold standard for apoptotic measurements. Apoptosis in an individual cell is a rapid event but the time that the cells take to display the characteristics that identify them vary, and it must not be assumed that signs of apoptosis by enabling FCM analyses, will be quantifiable at all times. There is no single feature that will

discriminate between cells that have died by apoptosis and those that have died by necrosis. Therefore, it is still important to use FCM in conjunction with other methods especially where cell morphology can be assessed, such as in this study with FM.

5.4 CONCLUSION

Using FM in conjunction with FCM facilitated an investigation that enabled quantitative correlation between the structural and biochemical changes in the N2α cells. Following the 48-hour exposure period, the six mycotoxins, as well as Sa and So induced varying levels of apoptosis and necrosis in these cells, the features of which were identified by microscopic examination. Using AcO/EtBr staining in combination with FM, facilitated identification of viable, early apoptotic, late apoptotic, and necrotic cells following treatment. Cells at various stages from live (green), dead (red/orange) and those that were dying were observed by loss of cell membrane integrity, and either dye exclusion or inclusion. The live cells remained green, the dead cells red/orange and the transient or dying cells, showed staining with both dyes at various levels. Significant differences in the staining intensities were evident by comparison of the mycotoxin (e.g., FB_1-treated and T2-treated cells) and sphingoid base-treated cells to N2α control cells. There was an inversion in the ratio of green and red/orange staining, with a predominance of apoptotic and necrotic cells being detected following exposure to these compounds.

The TMP was measured using Rh123 and the dual emission potential sensitive probe JC-1, and facilitated analysis of changes in mitochondrial membrane potential and plasma membrane integrity, following treatment with the sphingoid bases and mycotoxins. The results were expressed as increases or decreases in fluorescence intensity, and consequently, variations of membrane potential were usually expressed as the shift of the mean peak channel of a single fluorescence. Rhodamine 123 in combination with PI, facilitated discrimination between vital N2α cells and dying cells (necrotic or late apoptotic cells), whose plasma membrane integrity was compromised and consequently stained with PI as well. N2α cells with intact membranes (e.g., viable and early apoptotic cells) excluded PI, preventing its intercalation into intracellular nucleic acids. The early apoptotic N2α cells had markedly diminished staining capacity for Rhl23, and stained with faint green fluorescence, due to fewer viable mitochondria than in viable cells. Apoptotic cells retained their membrane integrity, and excluded PI. Overall, N2α cells with

compromised plasma membranes, namely the necrotic and late apoptotic cells stained with PI, showing red fluorescence. Optical separation of necrotic and late apoptotic N2α cells was difficult to assess using FM (e.g., in the ZEA and DON-treated N2α cells). Cells with decreased Rh123 fluorescence and that were PI positive included necrotic cells, indicated by cellular swelling and loss of plasma membrane integrity, in comparison to control N2α cells that stained with Rh123 and excluded PI.

Although qualitative analysis of Rh123/PI and JC-1 incorporation was done using FM, quantitative analyses of apoptotic and necrotic cells was facilitated on the FCM, using Rh123/PI uptake as a measure of cell permeability, and determination of $\Delta\psi m$ using JC-1. Variations in mitochondrial membrane potential were detectable at the single N2α cell level by staining cells with JC-1 that fluoresced green in its monomeric form. Active mitochondria with high transmembrane potentials capable of accumulating the JC-1 formed J-aggregates that fluoresced red. These were assessed using both FM and FCM.

In this study, the FCM results of the JC-1 and Rh123/PI staining did not correlate consistently. However, both the FM and FCM results showed that the mycotoxins and sphingoid bases at the 50, 100 and 200μM test concentrations induced varying levels of apoptosis, necrosis, and cytotoxicity on the N2α neuroblastoma cell line. As FCM was unable to discriminate between necrotic and late apoptotic cells definitively using Rh123/PI, cells in these two subpopulations were defined as non-viable. The FCM results indicated that Rh123/PI staining showed a higher proportion of compromised cells at all concentrations. Overall the FM and JC-1 FCM results correlated well with the results of the MTT assays. The Rh123/PI method of staining gave consistently higher levels of compromised cells than the JC-1 staining method for FCM analyses. JC-1 was considered more specific for mitochondrial versus plasma membrane potential, and more consistent in its response to depolarisation, than Rh123.

This *in vitro* study also highlights the importance of microscopic assessment of cells in combination with quantitative analyses in order to gauge the direct effects of a mycotoxin or sphingoid base on cellular organelles, cellular metabolism, and hence on their influence on mechanisms of cell death be it via cytotoxic, apoptotic or necrotic pathways.

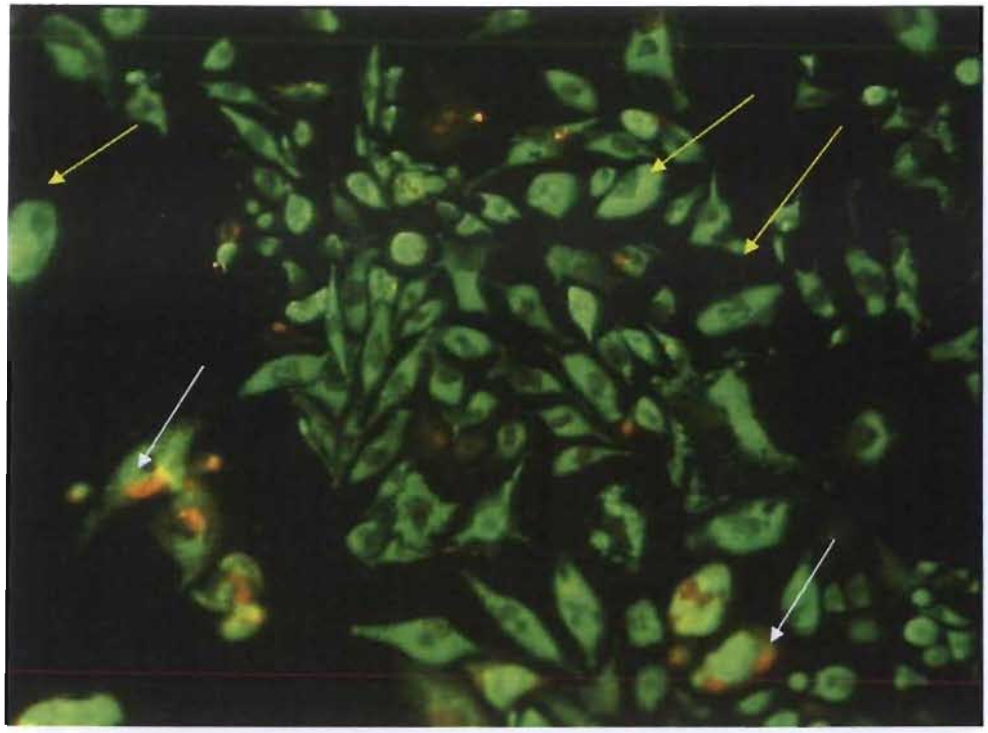

Figure 5.1: Fluorescence micrograph of control N2α neuroblastoma cells stained with AcO and EtBr. Vital cells with intact cell membranes are characterised by intense green fluorescence (yellow arrows) and red staining lysosomes (white arrows) (Magnification (Magn.) X 100).

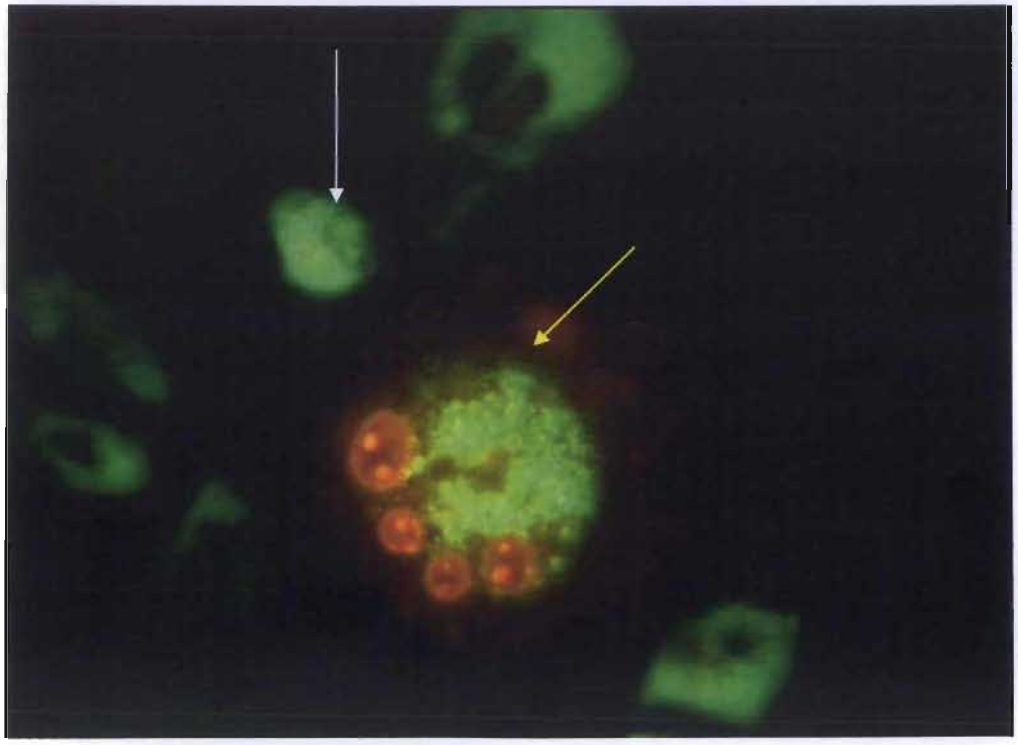

Figure 5.2: Fluorescence micrograph of control N2α neuroblastoma cells stained with AcO and EtBr, showing vital cells characterised by the intense green fluorescence (white arrow). A potentially apoptotic or necrotic giant cell is shown containing red staining multiple nuclei (yellow arrow)(Magn. X 1000).

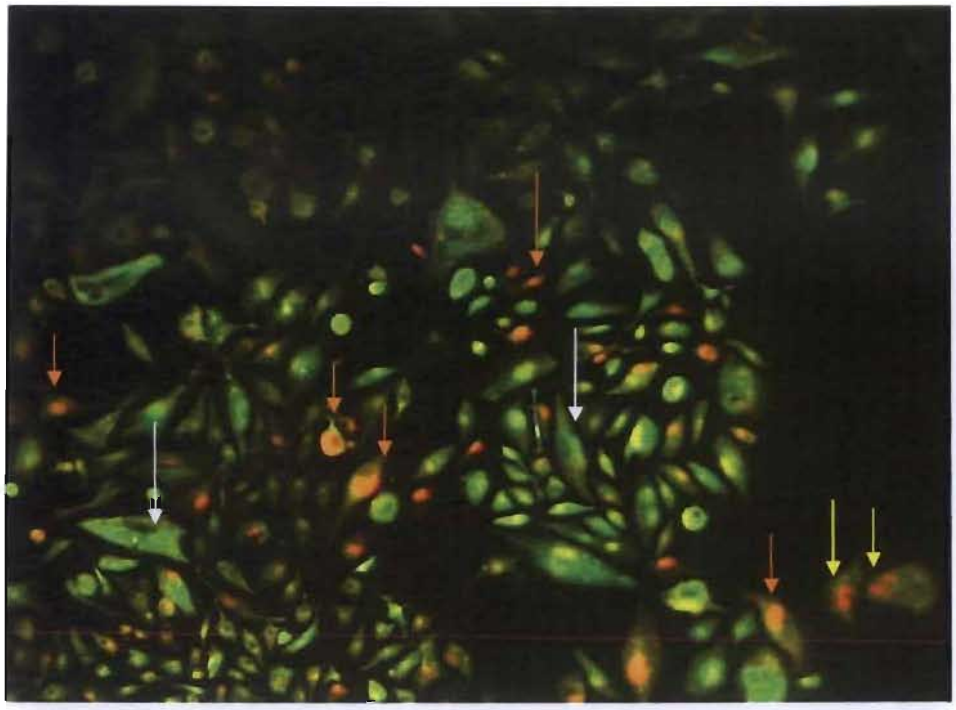

Figure 5.3: Fluorescence micrograph of 100μM FB_1-treated N2α neuroblastoma cells following staining with AcO and EtBr. Vital cells are indicated by the intense green fluorescence (white arrows). Red stained lysosomes are shown within possibly early apoptotic cells coupled with diminished green fluorescent cytoplasm (yellow arrows). Late apoptotic or necrotic cells are characterised by bright orange and diffuse green fluorescence (orange arrows) (Magn. X 100).

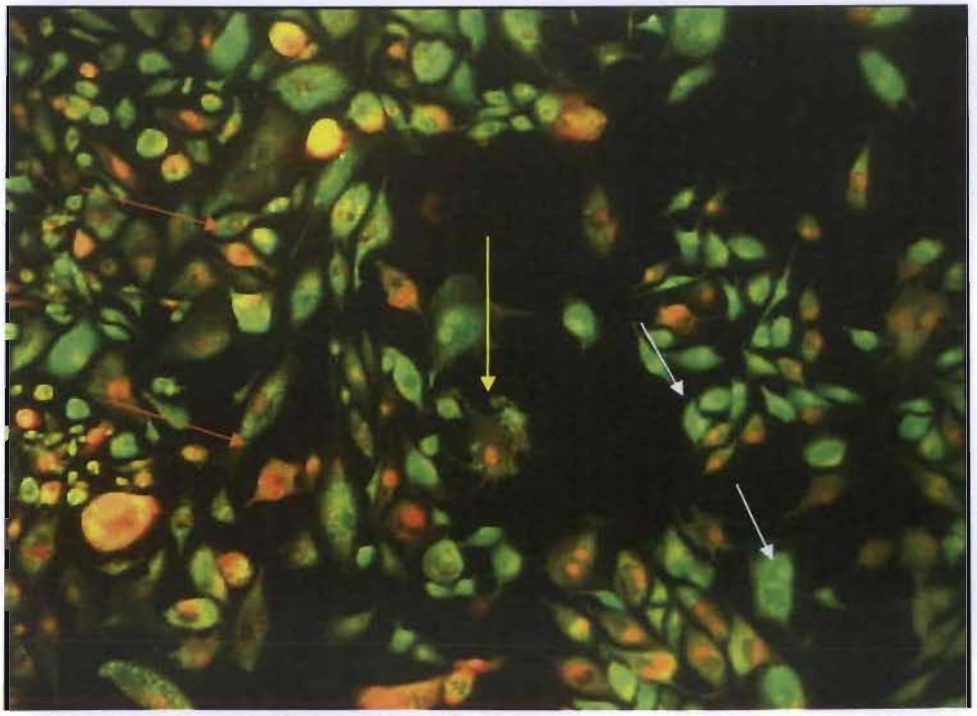

Figure 5.4: Fluorescence micrograph of 100 μM T-2 toxin-treated N2α cells stained with AcO and EtBr. Vital cells are characterised by intense green fluorescence (white arrows), early apoptotic cells by diminished green fluorescence with orange staining within cell cytoplasm (yellow arrow), and late apoptotic or necrotic cells by orange fluorescence (orange arrows) (Magn. X 400).

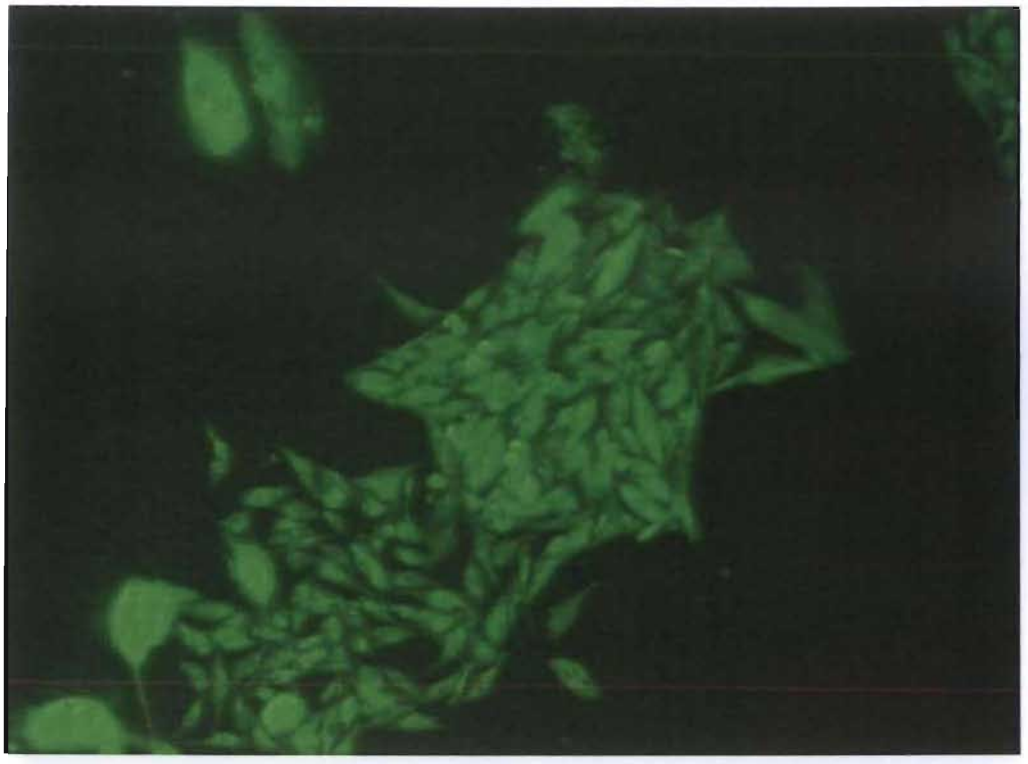

Figure 5.5: Fluorescence micrograph of control N2α cells stained with Rh123 and PI. Intact vital cells are characterised by intense green fluorescence and absence of PI staining (Magn. X 400).

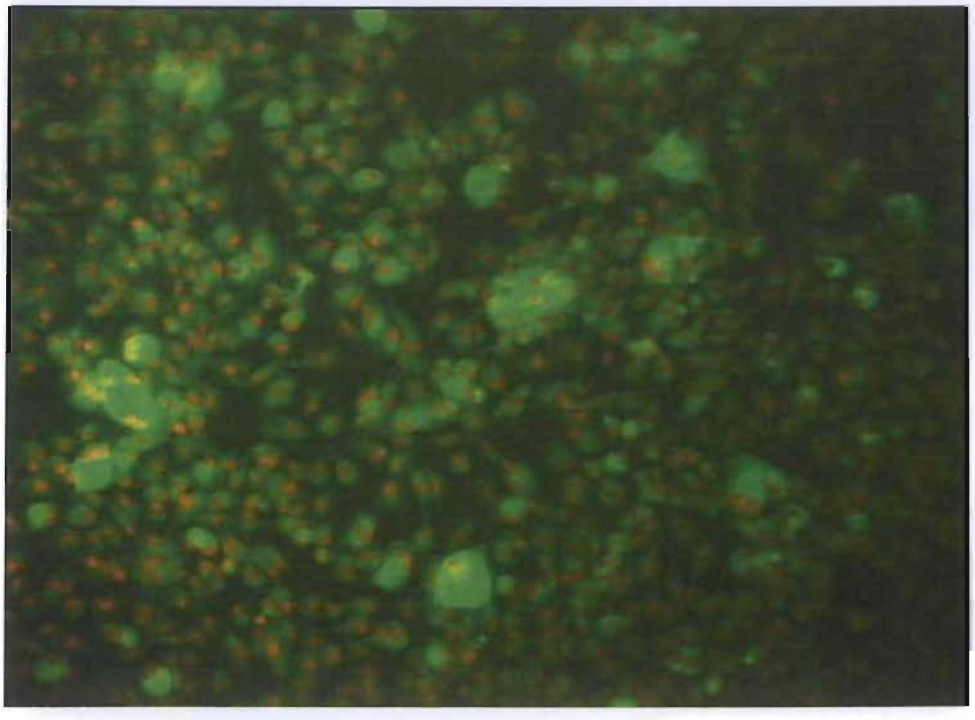

Figure 5.6: Fluorescence micrograph of N2α cells exposed to 100μM sphinganine and then stained with Rh123 and PI. Compromised N2α cells are characterised by diminished green fluorescence and red PI stained nuclei (late apoptotic or necrotic cells) (Magn. X 100).

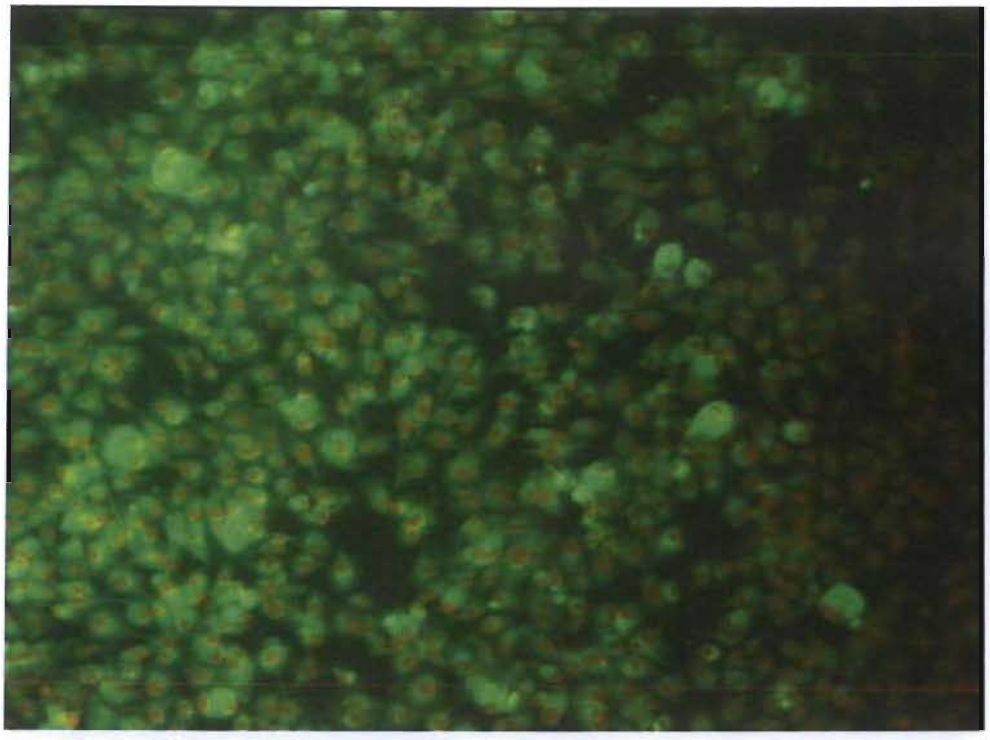

Figure 5.7: Fluorescence micrograph of sphingosine-treated (100μM) N2α cells stained with Rh123 and PI. Compromised N2α cells are characterised by diminished green fluorescence and red PI stained nuclei (late apoptotic or necrotic cells) (Magn. X 100).

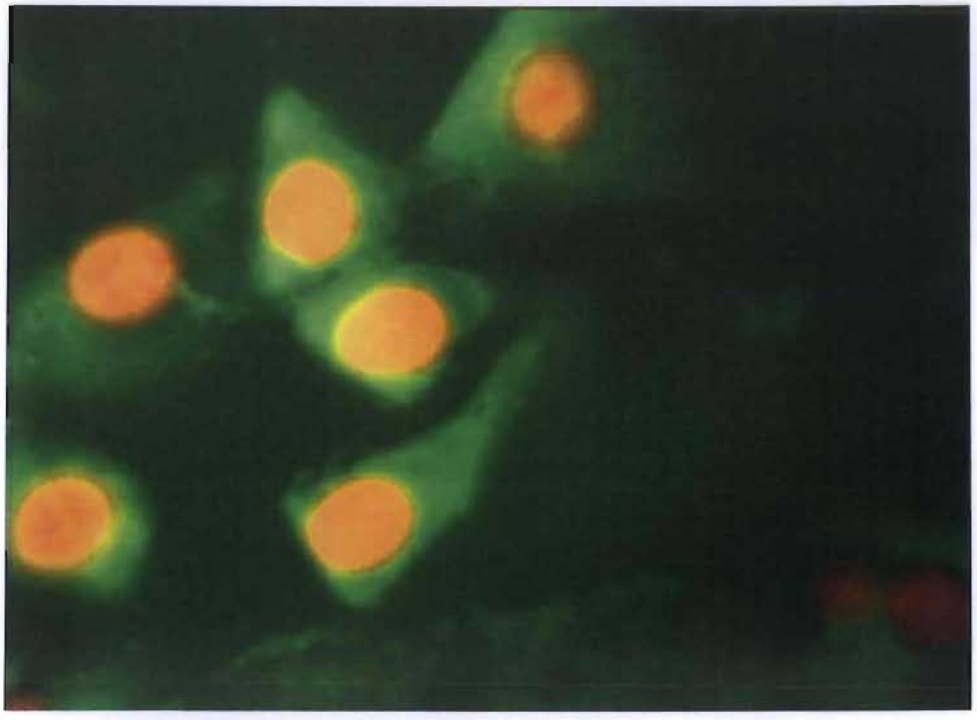

Figure 5.8: Fluorescence micrograph of ZEA-treated (100μM) N2α cells stained with Rh123 and PI. Necrotic cells are characterised by diminished green fluorescence with red/orange staining nuclei and cytoplasmic condensation (Magn. X 1000).

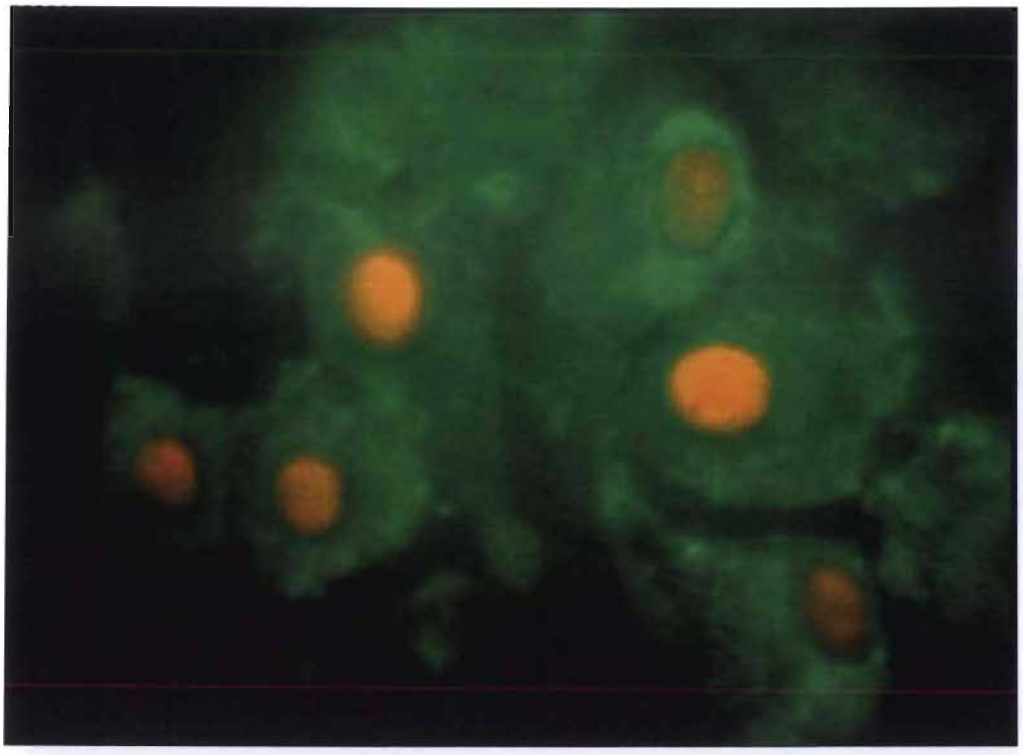

Figure 5.9: Fluorescence micrograph of DON-treated (100μM) N2α cells stained with Rh123 and PI. Cells were characterised by their compromised plasma membrane integrity and diminished green fluorescence, with PI staining nuclei, cellular swelling and membrane blebbing (Magn. X1000).

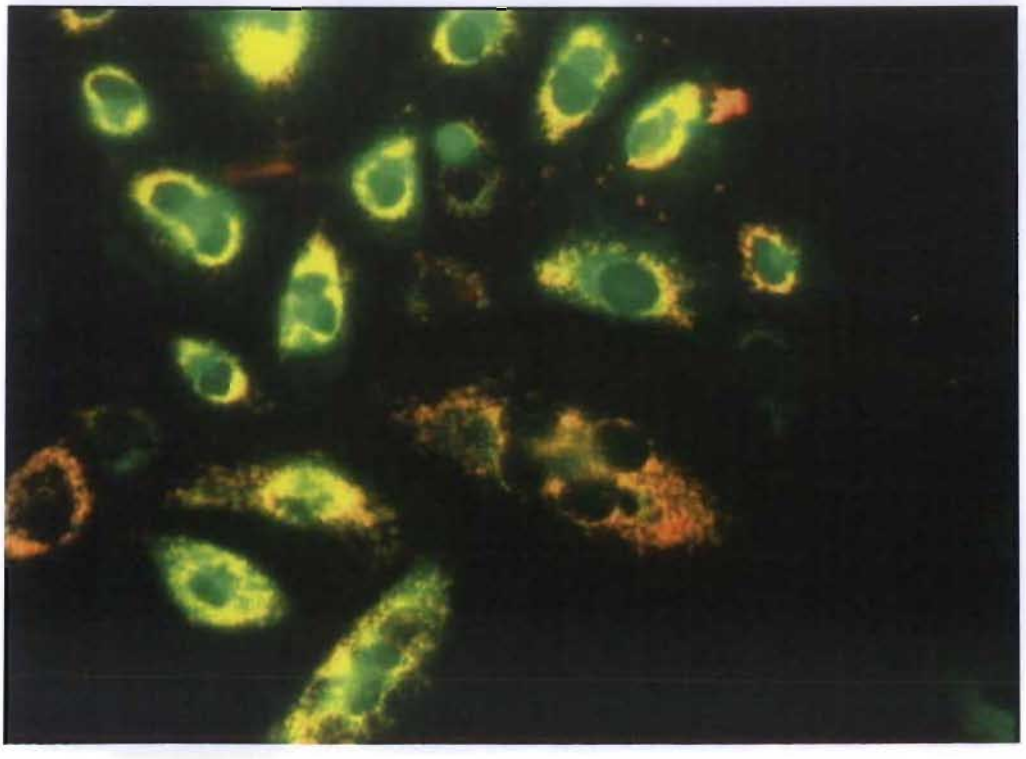

Figure 5.10: Fluorescence micrograph of N2α cells control JC-1 stained cells showing intracellular distribution of J-aggregates. The stain in its monomeric form is shown by green fluorescence and red/orange staining J-aggregates (Magn. X 400).

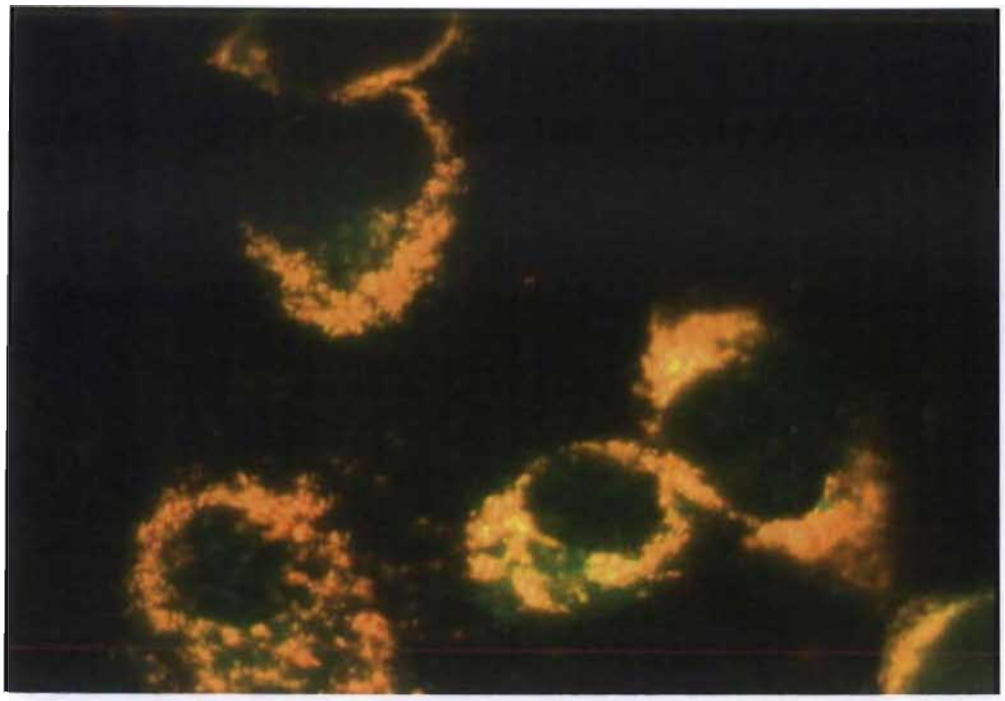

Figure 5.11: Fluorescence micrograph of control JC-1 stained N2α cells showing intracellular distribution of red/orange J-aggregates that are indicative of functioning mitochondria (Magn. X 1000).

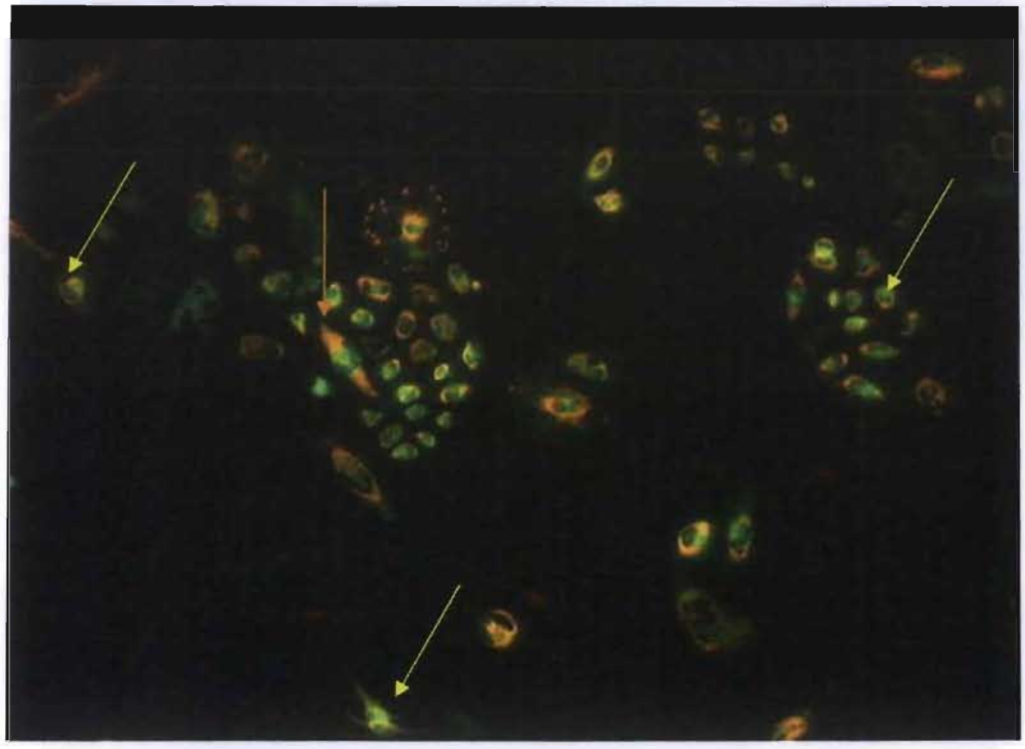

Figure 5.12: Fluorescence micrograph of FA-treated (100μM) N2α cells stained with JC-1 showing cellular distribution of high levels of orange/red J-aggregates in viable cells (orange arrow), and cells with cytoplasmic condensation with very low levels of J-aggregates (yellow arrows) (Magn. X 40).

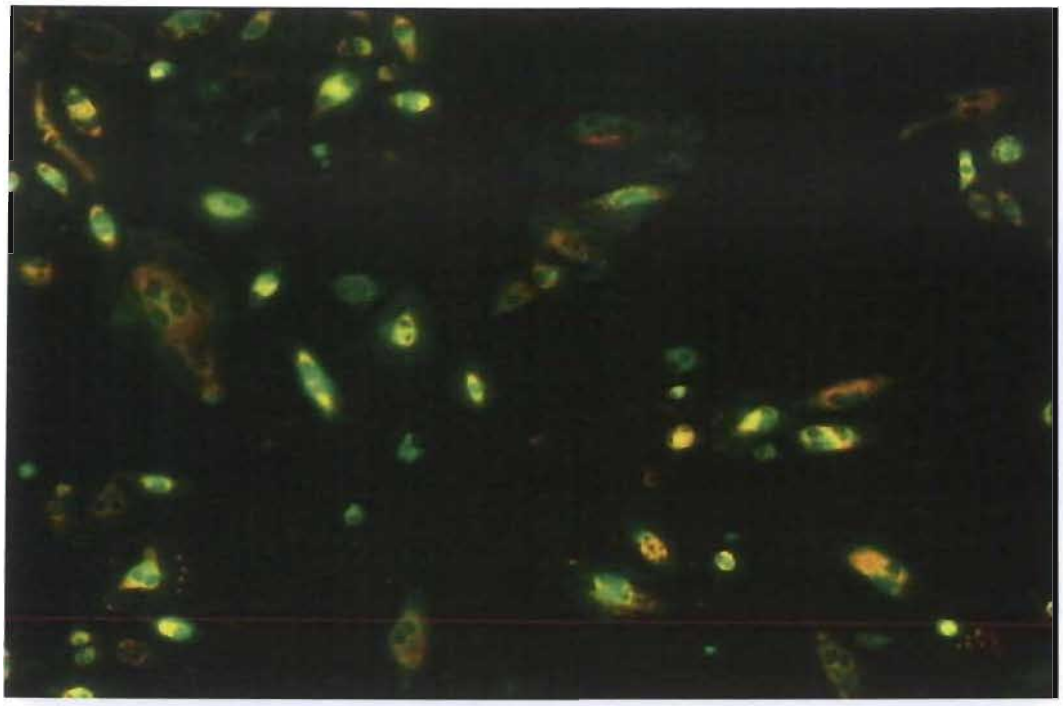

Figure 5.13: Fluorescence micrograph of MON-treated (100μM) N2α cells stained with JC-1 showing variable levels of intracellular distribution of orange/red J-aggregates (Magn. X 40).

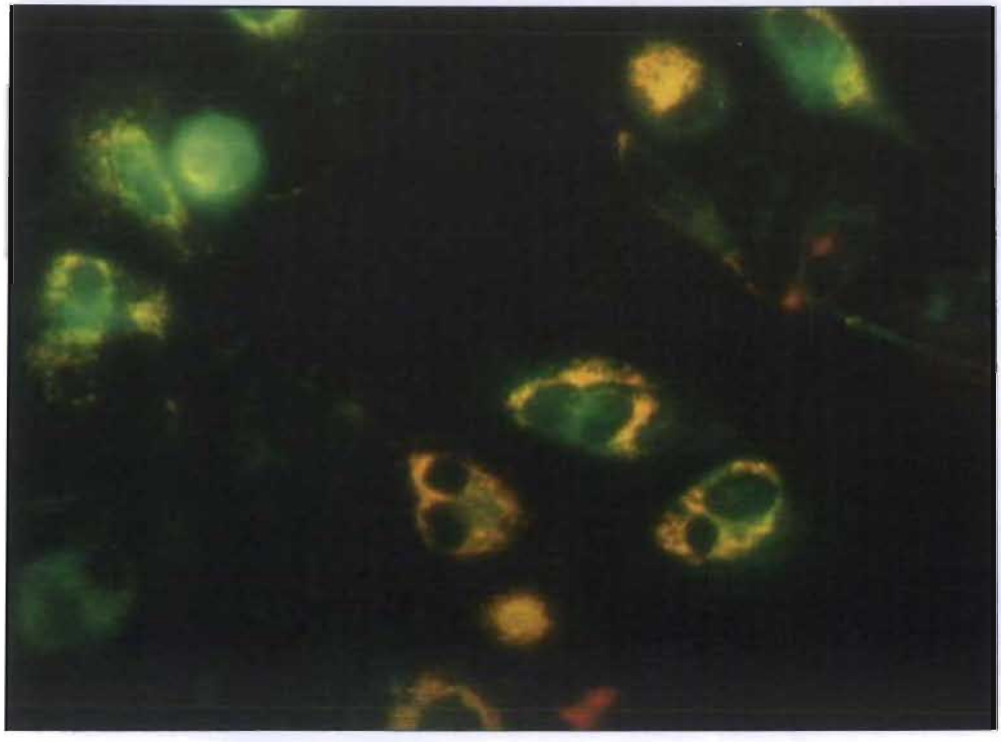

Figure 5.14: Fluorescence micrograph of FB_1 -treated (100μM) N2α cells stained with JC-1 showing intracellular distribution of orange/red J-aggregates and large intercellular gaps between remaining adherent cells (Magn. X 400).

CELLS-CONT

tosett. from prot. RHODAMINE/PI 50 seconds. 1126 events

Manual Stop

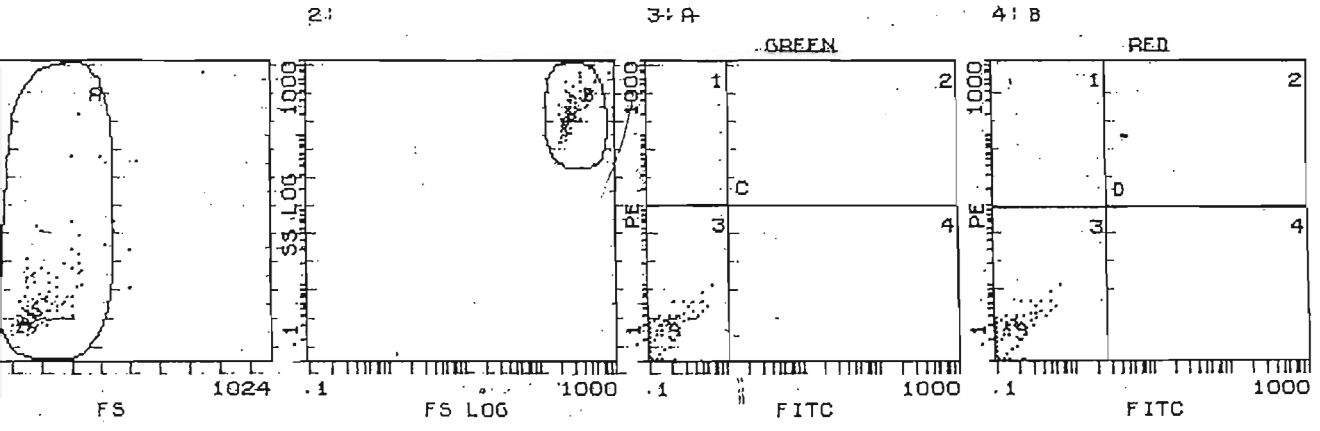

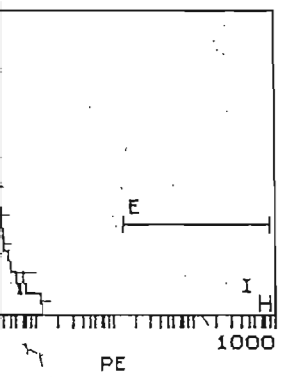

Normalized, Listgating: Disabled

Region	ID	%	Count	Mn X	Mn Y	PkPosX	PkPosY	PkCnt	FPCVX	FPCVY
A	A	89.4	1007	293.1	213.1	248.0	152.0	9	24.46	55.46
B	B	94.0	1059	289.2	192.9	242.8	146.7	24	27.25	50.57
C1	C	0.0	0	****	****	****	****	**	**	**
C2	C	0.0	0	****	****	****	****	**	**	**
C3	C	99.7	1004	0.153	0.214	0.102	0.102	118	50.16	54.80
C4	C	0.3	3	3.24	5.11	1.47	2.80	1	60.51	47.56
D1	D	0.0	0	****	****	****	****	**	**	**
D2	D	0.0	0	****	****	****	****	**	**	**
D3	D	99.8	1057	0.155	0.220	0.102	0.102	119	51.11	56.15
D4	D	0.2	2	4.81	6.89	3.74	5.36	1	25.25	25.25

Region	ID	%	Count	Mn X	Md X	PkPosX	PkCnt	HPCV	Min	Max
E	E	0.0	0	****	****	****	**	**	13.9	927.5
I	I	0.0	0	****	****	****	**	**	689.3	927.5

Figure 5.15: Flow cytometry acquisition report showing how the unstained control N2α cells where used to determine the N2α cells light scattering properties and to establish where the cells would lie in the quadrants.

CONT-STAINE

l cytosett. from prot. TESS/JC1/5/12 54 seconds. 1383 event

Manual Sto

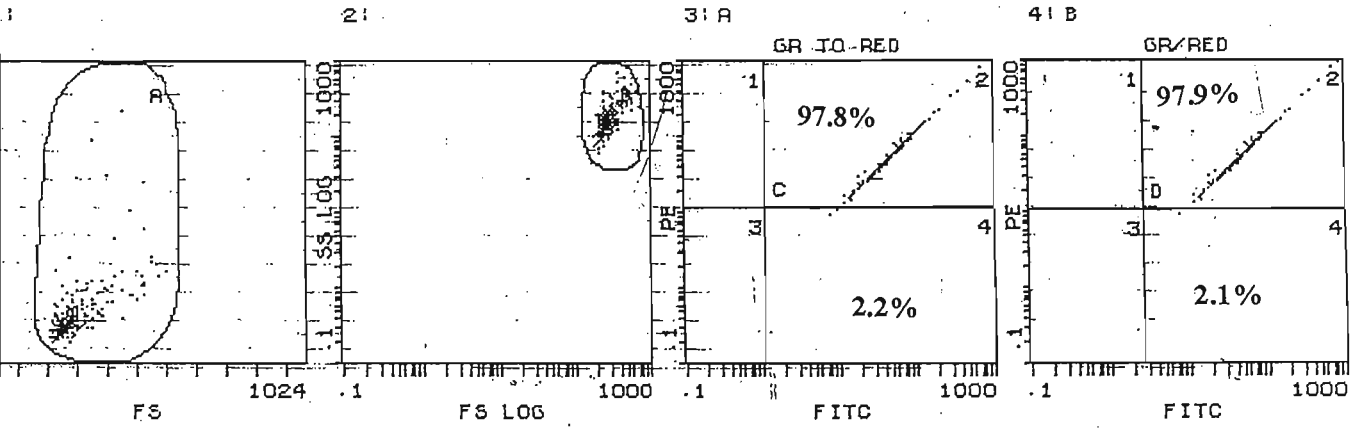

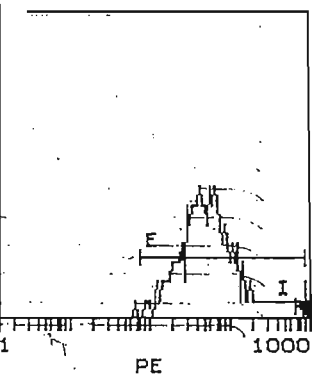

s: Normalized, Listgating: Disabled

t	Region	ID	%	Count	Mn X	Mn Y	PkPosX	PkPosY	PkCnt	FPCVX	FPCVY
	A	A	93.7	1296	303.6	197.8	224.0	88.0	9	29.02	71.5
	B	B	94.6	1309	289.3	167.0	260.9	146.7	22	27.82	52.0
	C1	C	0.0	0	****	****	****	****	**	**	**
	C2	C	97.8	1267	52.0	56.1	40.2	43.2	26	86.15	85.1
	C3	C	0.0	0	****	****	****	****	**	**	**
	C4	C	2.2	29	7.25	7.89	8.87	9.53	4	25.94	23.6
	D1	D	0.0	0	****	****	****	****	**	**	**
	D2	D	97.9	1281	51.9	56.0	40.2	43.2	26	84.40	83.4
	D3	D	0.0	0	****	****	****	****	**	**	**
	D4	D	2.1	28	7.16	7.78	8.87	9.53	4	25.54	22.8

t	Region	ID	%	Count	Mn X	Md X	PkPosX	PkCnt	HPCV	Min	Ma
	E	E	99.1	1371	63.1	57.3	911.0	16	0.38	7.96	927.
	I	I	2.3	32	834.5	898.8	911.0	16	0.38	689.3	927.

Figure 5.16: Flow cytometry acquisition report showing the analysis of the JC-1 stained control N2α cells.

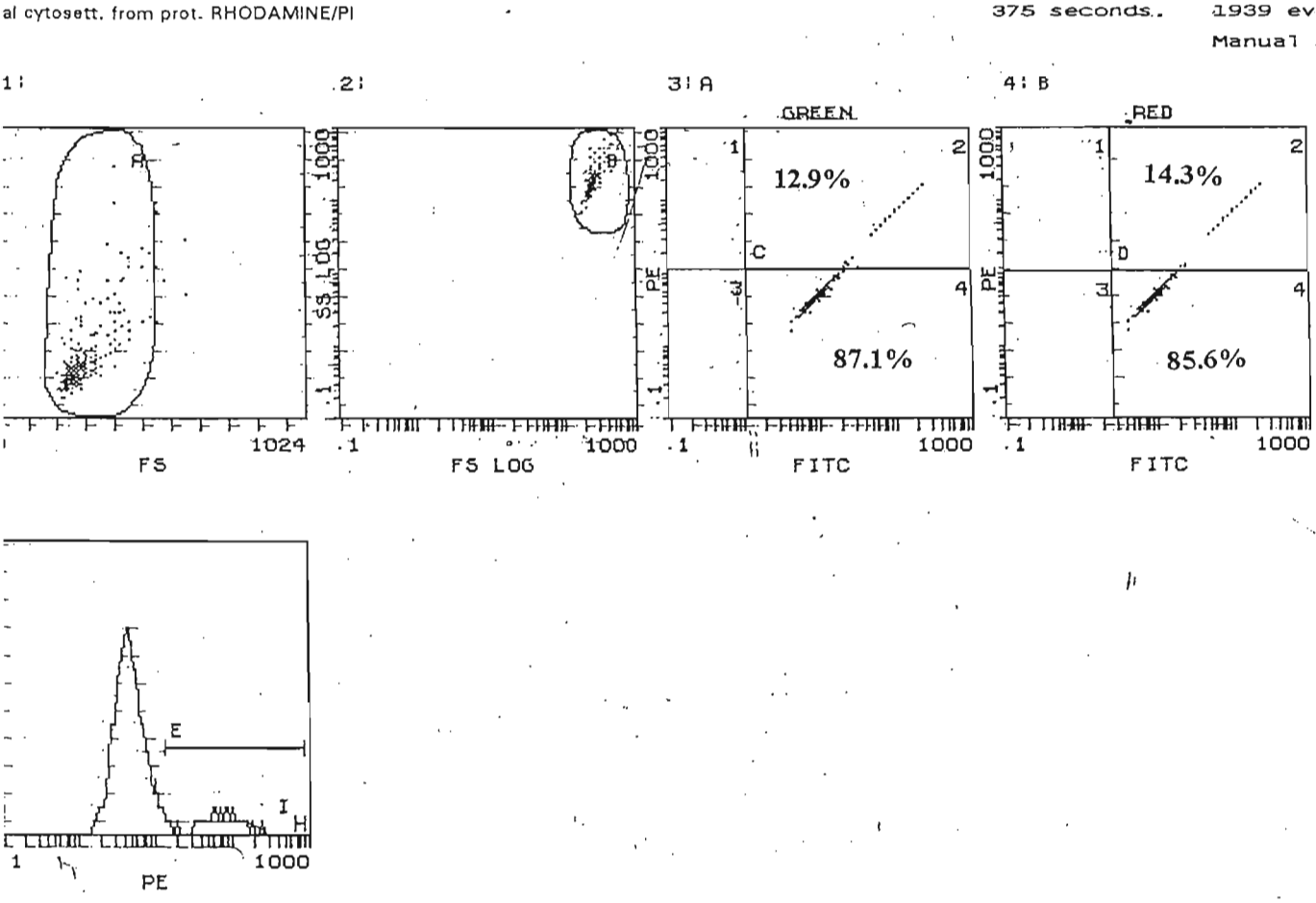

ta: Normalized, Listgating: Disabled

st	Region	ID	%	Count	Mn X	Mn Y	PkPosX	PkPosY	PkCnt	FPCVX	FPCVY
1	A	A	95.8	1858	278.9	209.5	216.0	120.0	23	23.41	59.26
2	B	B	97.7	1895	270.5	185.1	226.0	127.1	44	28.45	50.08
3	C1	C	0.0	0	****	****	****	****	**	**	**
	C2	C	12.9	240	79.1	50.7	127.1	88.7	9	65.27	72.58
	C3	C	0.0	0	****	****	****	****	**	**	**
	C4	C	87.1	1618	9.05	4.40	8.87	4.64	42	36.46	40.77
4	D1	D	0.0	0	****	****	****	****	**	**	**
	D2	D	14.3	271	74.0	46.7	127.1	88.7	9	72.64	81.38
	D3	D	0.1	1	2.10	0.768	2.10	0.768	1	0.00	0.00
	D4	D	85.6	1623	9.08	4.41	8.87	4.64	42	36.38	40.37

st	Region	ID	%	Count	Mn X	Md X	PkPosX	PkCnt	HPCV	Min	Max
7	E	E	14.2	275	66.6	71.2	71.5	4	0.45	13.9	927.5
	I	I	0.0	0	****	****	****	**	**	689.3	927.5

Figure 5.17: Flow cytometry acquisition report showing the analysis of the Rh123/PI stained ethanol-treated control N2α cells.

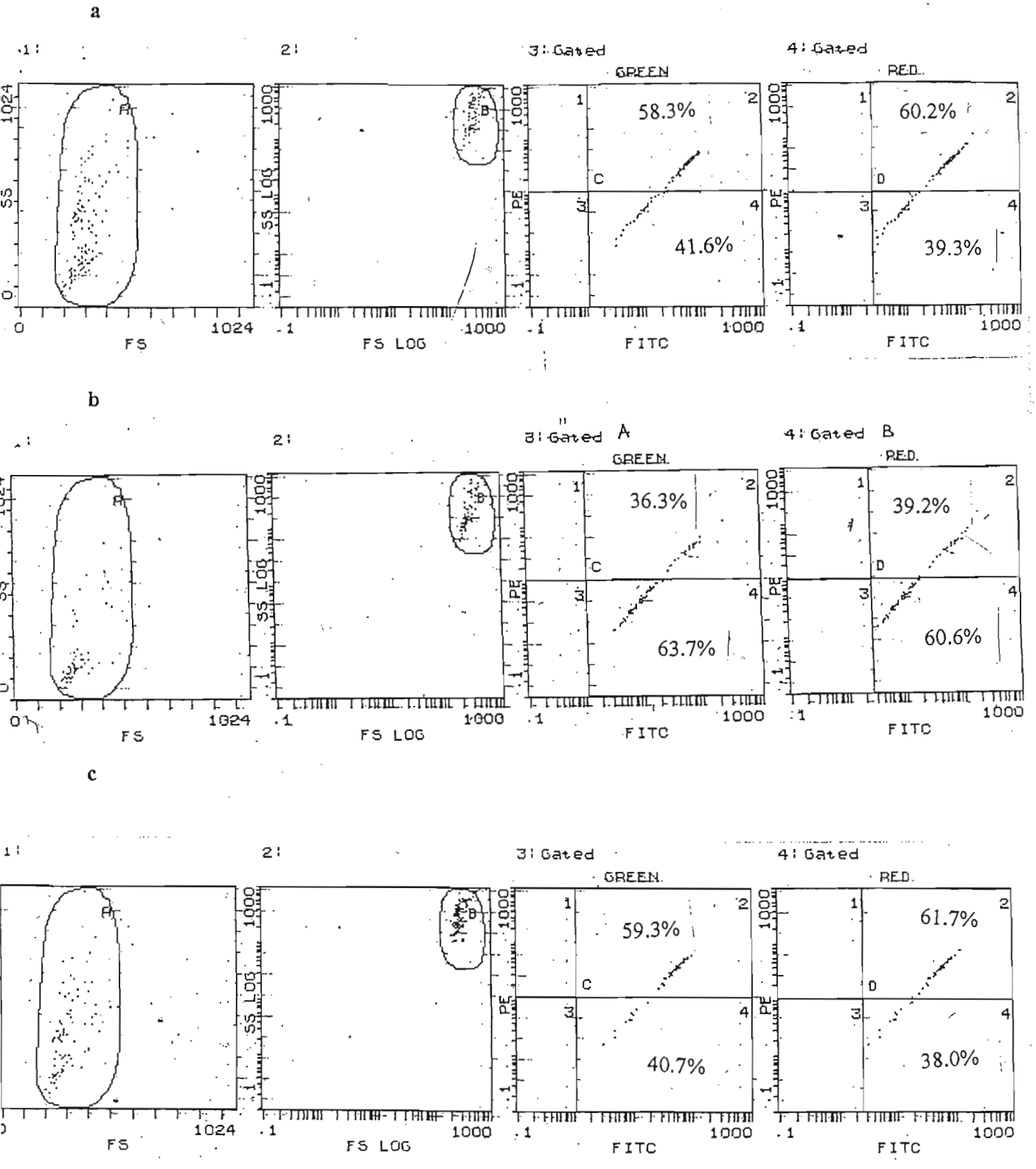

Figure 5.18: Flow cytometry histograms of N2α cells analysed after staining with Rh123/PI following 48 hour exposure to 50μM (a), 100μM (b) and 200μM (c) fusaric acid.

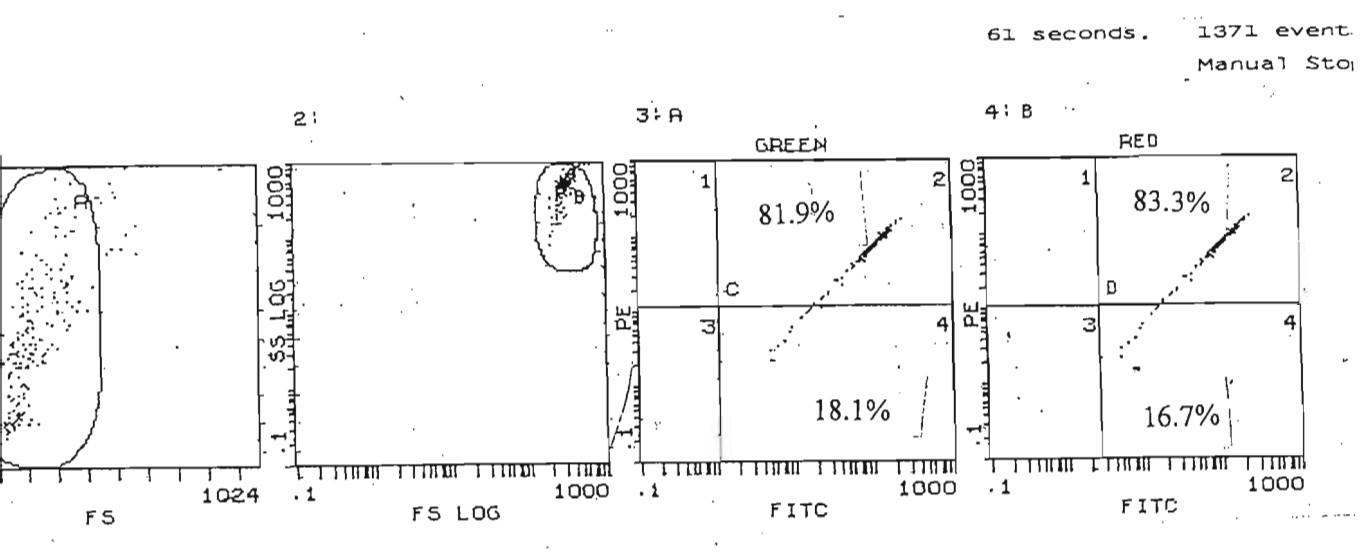

Figure 5.19: Flow cytometry acquisition report showing N2α cells analysed after staining with Rh123/PI following 48-hour exposure to 50μM sphinganine.

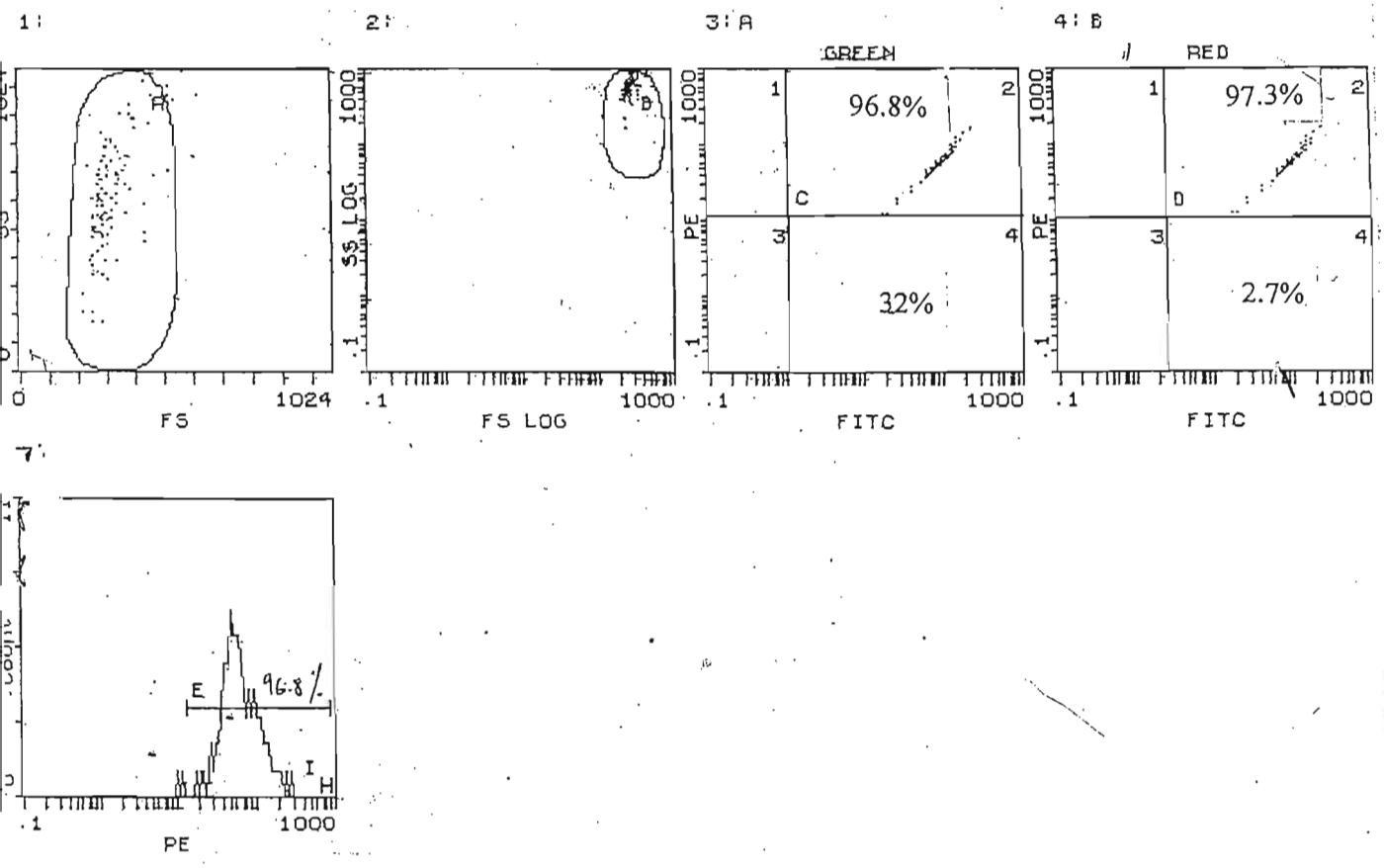

Figure 5.20: Flow cytometry acquisition report showing N2α cells analysed after staining with Rh123/PI following 48-hour exposure to 200μM sphingosine.

CHAPTER 6

An Immunochemical study into the effects of fumonisin B_1, zearalenone and T-2 toxin on the N2α neuroblastoma cell line

6.1 INTRODUCTION

Light and EM are complementary techniques used in structural and ultrastructural studies of cells. Immunological advancements and improved technology have impacted on histological procedures, leading to the incorporation of immunological techniques into microscopy, increasing use of antibodies as laboratory reagents and accelerating research on cellular components. To confirm presence of known antigens in altered cellular organelles, antibodies raised for use in their detection, have expanded knowledge of an antigens effects on internal structure and function of cells (Goers, 1993). The availability of immunoglobulin fractions, monoclonal and polyclonal antibodies to clinically relevant mycotoxins has expanded immunohistology. Mycotoxins within cells may be identified and localised by chemical high-affinity interactions. The binding of antibodies to the antigens (i.e., mycotoxins) within cells can be labelled by either insoluble coloured compounds observable at the light microscope level, or electron scattering gold particles that may be seen with the electron microscope.

Immunocytochemistry (ICC) facilitates identification and localisation in a biological system of any constituent or inclusion to which an antibody may be raised and marked by a microscopically visible label. Its potential for localising various types of molecules, provides a correlation between structure and function (Snyman, 1993). Immunohistochemistry (IHC) in this study was used in the detection of FB_1, ZEA and T2 at the light microscope level by specific antigen-antibody (Ag-Ab) interactions labelled with the chromogen 3,3-diaminobenzidine tetrahydrochloride (DAB). The peroxidase-anti-peroxidase (PAP) method of immunochemical detection was utilised.

At the electron microscope level, gold probe labelled monoclonal antibodies was used to tag FB_1 within cellular organelles and components. The indirect method of immunochemical analysis was used to identify antigenic sites due to its increased sensitivity. The primary antibody was not labelled and was identified by a labelled

secondary antibody raised to the immunoglobulin of the species providing the primary antibody.

When using light and EM in combination with immunochemical techniques, an investigation in cell culture allows one to construct a probable sequence of events to account for the effects of a mycotoxin in a biological system. This *in vitro* investigation aimed to monitor the effects of FB_1, ZEA, and T2 on the structure and ultrastructure of cultured N2α cells, and to evaluate the sites of action of these environmental xenobiotics. Immunohistochemical techniques were carried out on ZEA, FB_1 and T2-treated N2α neuroblastoma cells, as these were the only mycotoxin antibodies available at the time. Immunoelectron microscopy analyses were also carried out on FB_1-treated N2α cells, as this was the mycotoxin of fundamental importance in this study.

6.2 MATERIALS AND METHODS

6.2.1 Materials

Cell culture media and consumables were purchased from Adcock-Ingram, SA. All reagents, solvents, bovine serum albumin (BSA), normal goat serum (NGS), and chemicals were purchased from MERCK, SA. All light and EM materials, copper and nickel grids (200μm mesh size), Araldite and Spurr epoxy resin kits, and the DAB Peroxidase Substrate Tablet set, and Tris-(hydroxymethyl)-aminomethane (Tris) salt were purchased from Sigma-Aldrich, SA. Antibodies used for IHC and ICC, were purchased from Sigma-Aldrich, SA, unless otherwise indicated. Neogen supplied the primary monoclonal mouse anti-FB_1 antibody. The secondary antibody was goat anti-mouse IgG. The PAP complex used was developed in mouse and purchased in its non-conjugated form. For the detection of ZEA and T2, the polyclonal anti-ZEA primary antibody developed in rabbit fractionated serum and the polyclonal anti-T-2 toxin primary antibody developed in rabbit fractionated serum were used respectively. The secondary antibody used for both T2 and ZEA, was anti-rabbit IgG whole molecule peroxidase conjugate developed in goat.

A Reichert Ultracut ultramicrotome was used to cut 50nm sections whilst a Nikon Optiphot photomicroscope was used to digitise images at the Optics and Imaging Centre, UKZN. The JEOL 1010 TEM was used at the Electron Microscope Unit, UKZN for ultrastructural examination and electron micrographs.

6.2.2 Methods

Descriptions of all cell culture techniques employed were as previously documented in Palanee (1998).

6.2.2.1 Growth and preparation of N2α neuroblastoma cells for light microscopy

Using aseptic techiques, N2α neuroblastoma cells were trypsinised and plated onto 25cm^2 sterile Corning tissue culture flasks as described previously (Palanee, 1998). Cells were grown in culture flasks for all analyses, because N2α neuroblastoma cells did not adhere successfully to glass coverslips. The N2α cells were cultured at 37°C for 24 to 72 hours, or until confluency was reached.

6.2.2.2 Haematoxylin and eosin staining of control N2α neuroblastoma cells

An untreated flask of confluent N2α neuroblastoma cells was rinsed in HBSS (2ml), fixed in 1% glutaraldehyde in HBSS (5ml) (37°C for 30min.), rinsed again in HBSS (2ml) and then rinsed thoroughly in distilled water (2x5ml) prior to staining routinely with Mayer's haematoxylin and eosin stain (H&E) (5%) (2ml) (Humason, 1972; Drury and Wallington, 1980). The stained cells were viewed and photographed on a Zeiss photomicroscope using a Nikon FX camera.

6.2.3 Preparation of the mycotoxin stock solutions

Fumonisin B_1 was dissolved directly in CCM (1mg.ml^{-1}), with CCM as the control solution for this mycotoxin. Zearalenone and T2 were dissolved in EtOH (100µl per mg) and CCM (900µl per mg) to a stock solution of 1mg.ml^{-1}. The control for this set of compounds was made up of a combination of EtOH (100µl) and CCM (900µl). All stock solutions were vortexed thoroughly to ensure complete resuspension of the mycotoxins in the solvent vehicle and CCM, and then used to prepare a dilution series of 50,100 and 200µM in CCM.

6.2.4 Preparation of N2α neuroblastoma cells for microscopy

Flasks of confluent cells were incubated (37°C) in each mycotoxin or control solution (2 ml) for 48 hours prior to analysis. As IHC involved qualitative analysis of the cells only, testing was carried out for each compound at 50,100 and 200μM in duplicate flasks for ZEA and T2. An additional set of flasks of FB_1-treated cells was also prepared for ICC analysis.

Following the 48-hour incubation period, flasks of N2α neuroblastoma cells were removed from the incubator, and gently rinsed with HBSS (5ml) to remove detached dead cells and all CCM containing mycotoxin. The washes were discarded and the cells fixed as outlined below (in section 6.2.6).

6.2.5 Preparation and dilution of the fumonisin B_1 monoclonal antibody

The FB_1 primary antibody stock solution was prepared by diluting the lyophilised antibody (1mg) in 0.01M PBS (pH 7.4) (100μl). Aliquots of this stock solution were further diluted (1:100) in PBS containing 1% BSA (pH 7.4) prior to use.

6.2.6 Preparation of cells for immunohistochemical staining for light microscopy

The immunostaining procedures using the PAP technique on the FB_1, ZEA and T2-treated N2α cells in culture flasks are outlined in Table 6.1.

Method controls were used in all immunohistochemical analyses to ensure that the staining detected was the result of immunological interaction between the primary antibody and the antigen. The primary antiserum was omitted in the method controls and replaced with the antibody diluent buffer. Positive staining in method controls was considered caused by non-specific binding of the secondary antibody and the chromogen to cellular components. The negative controls consisted of the untreated N2α cells, and the positive controls were those N2α cells that were exposed either to FB_1, ZEA or T-2 toxin. The primary antibodies were added to these cells to verify specificity of the methods used.

Table 6.1: Immunostaining procedures using the PAP technique on treated N2α cells in culture flasks.

PROCEDURE	TIME (min.)	
	FB_1-treated N2α cells	T2 and ZEA treated N2α cells
Washed 25cm^2 flasks of N2α cells thrice in HBSS (2 ml per rinse)	10	
Fixed cells in 1% glutaraldehyde in HBSS (3 ml)	30	
Washed N2α cells in HBSS (3 ml)	3	
Washed flasks of N2α cells in distilled water (10 ml)	5	
Incubated N2α cells in 5% H_2O_2 in methanol (2 ml)	30	
Poured off methanol	2	
Washed flasks of N2α cells in PBS (pH 7.4)(10 ml)	20	
Incubated in NGS (1ml)(1:20 in 1%BSA in PBS)	20	
Incubated in primary antibody [anti-FB_1 (1:100), anti-ZEA (1:200) or anti-T2 (1:500)], diluted in PBS containing 1% BSA (pH 7.4) (1ml). The primary antibody was replaced with PBS (pH 7.4) (1ml) on the method controls	60	
Washed flasks of N2α cells with PBS (2x5 ml)	5	5
For FB_1-treated cells: Incubated in secondary antibody i.e., goat anti-mouse IgG (1:200) in 1% BSA in PBS (pH 7.4)	45	Omitted step
Rinsed flasks of N2α cells with PBS (pH 7.4) (2x5 ml)	5	Omitted step
For FB_1-treated cells: Incubated in PAP enzyme developed in mouse (1:400) in PBS containing 1% BSA (pH 7.4)	45	Omitted step
For T2 and ZEA-treated cells: Incubated in secondary antibody i.e., anti-rabbit IgG (whole molecule peroxidase conjugate, antibody developed in goat) diluted (1:400) prior to use in 1% BSA in PBS (pH 7.4)	Omitted step	60
Rinsed flasks of N2α cells with PBS (pH 7.4) (2 x 5ml)	5	
Used heated wire to remove the top cover of flasks of N2α cells		
Stained with DAB chromogen (prepared according to manufacturers instructions)	3-5 with checking	
Washed the adherent N2α cells with distilled water (2 x 5 ml)		
Stained N2α cells with haematoxylin (2 ml)	~3 with checking	
Washed N2α cells in distilled water (2 x 5ml)	1	
Blued N2α cells in ammonia water (1% v/v) or hot water (60 °C)	5	
Coverslipped N2α cells using glycerol jelly		
Viewed and photographed immunostained N2α cells on a Zeiss photomicroscope fitted with a Nikon FX camera		

6. Preparation of flasks of treated and control N2α neuroblastoma cells for transmission electron microscopy and immunocytochemistry

A flask of untreated N2α neuroblastoma cells was fixed for transmission electron microscopy (TEM). Transmission electron microscopy allowed characterization of cellular detail facilitated by infiltration of the cells with osmium tetroxide in the processing. Cellular detail is

not as preserved in specimens fixed for ICC as osmium is omitted since it masks antigenic sites. The remaining control flask of N2α cells and all FB_1-treated cells were fixed for ICC as outlined in Table 6.2 (Robinson and Gregory, 1977).

Table 6.2: Processing of N2α neuroblastoma cells for transmission electron microscopy and immunocytochemistry.

Procedure	Time (min.)	
	TEM	ICC
Fixed confluent N2α cells in 1% glutaraldehyde in HBSS (3 ml)	45	
Rinsed in HBSS (3 ml x 2)	5	
Osmicated (4°C) (3 ml)	60	Omitted step
Rinsed in HBSS (3 ml)	2 x 5	Omitted step
Dehydrated in 70% EtOH (3 ml)	20	
90% EtOH (3 ml)	20	
100% EtOH (3 ml)	20	
100% EtOH (3 ml)	20	
Infiltrated with EtOH: Araldite resin (1:1) (2 ml)	30	Omitted step
Infiltrated with Araldite resin (60°C)	2 x 90	Omitted step
Embedded in Araldite resin (60°C)	24 hours	Omitted step
Infiltrated with EtOH: Spurr resin (1:1) (2 ml)	Omitted step	30
Infiltrated with Spurr resin (60°C)	Omitted step	2 x 90
Embedded in Spurr resin (60°C)	Omitted step	24 hours

The embedded flasks of N2α cells were cut into 5-10mm blocks using a heated wire. The blocks, which comprised of cells sandwiched between the resin and the plastic flask, were trimmed and vertically sectioned on a Reichert Ultracut ultramicrotome. Sections (50nm) cut for TEM were picked up on 200 mesh copper grids, stained with uranyl acetate followed by Reynolds' lead citrate (1963), then viewed and photographed on the JEOL 1010 TEM transmission electron microscope. Sections (50nm) cut for ICC were picked up on 200μm mesh-size nickel grids, stained as outlined in Table 6.3, then viewed and areas of interest photographed on the JEOL-TEM 100S transmission electron microscope.

Table 6.3: Staining procedure using immuno-gold on resin sections for electron microscopy.

Procedure	Time
Etched non-osmicated sections on nickel grids by placing in 5% H_2O_2 (20µl)	5min.
Placed grids on droplet of distilled water. Jet-washed with distilled water (10ml) and dried on fibre-free filter paper with specimen-side up	
Submerged grids at RT in NGS (20µl) (1:20 in 50mM Tris buffer) (pH 7.2)(Appendix 5)*	30min.
Drained on fibre free paper	
Placed in monoclonal mouse anti-FB_1 (10µl) (1:100) in 1% BSA in 50mM Tris buffer (Appendix 5). Placed method controls in Tris buffer only (pH 7.2)(10µl)	3-18 hours
Placed grids in Tris buffer (pH 7.2) (20µl). Jet washed with 20ml/grid Tris buffer (pH 7.2)	5min.
Placed grid in droplet Tris containing 0.2% BSA weight per volume (w/v) (pH 7.2) then jet washed with 5ml per grid (Appendix 5)	5min.
Placed grid in droplet of 50mM Tris containing 1% BSA (w/v) (pH 8.2) (Appendix 5)	5 min.
Placed in droplet of mouse anti-rabbit IgG conjugated to 10nm gold (1:15 in 50mM Tris containing 1%BSA (pH 8.2) centrifuged at 2000g for 20 min.)	1hour
Placed in droplet of Tris containing 0.2% BSA (w/v), pH 7.2. Jet washed using: 50mM Tris containing 0.2% BSA (w/v), pH 7.2 (10 ml per grid), 50mM Tris, pH 7.2 (5 ml/grid) and distilled water (10 ml per grid)	
Counterstained with 2% uranyl acetate (20µl), then jet washed with distilled water (10ml) (Appendix 6.1).	3min.
Counterstained with Reynolds' lead citrate (20µl), then jet washed in distilled water (10ml) (Appendix 6.2).	3min.

* Methods for preparation of buffers and stains used in the ICC run are outlined in Appendix 5.

6.3 RESULTS AND DISCUSSION

6.3.1 Light microscopy with haematoxylin and eosin stained N2α cells

The N2α cell line grew as a monolayer culture with a doubling time of between 48-72 hours. Conventional light microscopy in combination with H&E staining revealed that N2α cells were epithelioid in morphology, characteristically large with centrally located large nuclei and multiple nucleoli (Figure 6.1). The cellular processes of control N2α cells extended over a large surface area and were firmly attached to the culture substrate (Figure 6.2). The cytoplasm surrounding the nucleus of the majority of control N2α cells were uneventful, in terms of the absence of cytoplasmic lyses or vacuolation.

Even in untreated N2α cell populations, a percentage of cells showing features characteristic of apoptosis were identifiable (Figures 6.1, 6.2 and 6.3). This was not unexpected, as apoptosis is a normal physiological process, and usually occurs in cultured cells where the

rate of cell turnover is high. The N2α cell line is primarily a transformed cell line and can therefore be cultured continuously for prolonged periods. This, however, raises concerns with respect to normal cell function, for example, with respect to apoptosis. Indeed, transformation can be likened to a process of 'dedifferentiation'. Nevertheless, experience with a variety of transformed cell lines that retain specialised, differentiated functions has indicated that although such cell lines are the exception (most transformed cell lines show little functional dedifferentiation), those functions that are expressed are likely to reflect accurately the *in vivo* functions of the parent cell type (Sato *et al.*, 1970; Dannies and Tashjian, 1973). It is clear however, that observations made in such systems must be confirmed in untransformed cells, in tissues, and ultimately *in vivo*.

The morphological criterion on which recognition of apoptosis is based still remains the gold standard of analysis of this mode of cell death. Cells showing two characteristic morphological features of reduced size due to cell shrinkage, and cytoplasmic condensation (Arends *et al.*, 1990; Arends and Wyllie, 1991) that are typical of the apoptotic process, are seen in cells shown in Figures 6.1 and 6.2. Control cells that have completely retracted cytoplasmic processes, cytoplasmic condensation, and plasma membrane undulations or 'blebbing', i.e., features typical of apoptosis are also indicated (Figure 6.3). In control N2α cells, this apoptotic population constituted a negligible percentage of the entire cultured cell population, whereas in treated cells there was a distinct increase in the proportion of cells that displayed this mechanism of cell death due to exposure to an exogenous cytotoxic compound.

6.3.2 Immunohistochemical analysis of mycotoxin treated N2α cells

The PAP method of immunochemical detection was applied, and is based on the combination of anti-peroxidase with peroxidase before applying it to a specimen of interest. The combination produces a very stable cyclic complex with three peroxidase molecules to two antibody molecules. The complex is separated from non-reacted antibody and peroxidase before use.

The criteria for the selection of the mycotoxin concentrations to which the N2α cells were exposed in this study, was based on the results of the MTT assay (Chapter 3). Using the MTT assay, at concentrations of 50, 100 and 200μM FB_1, approximately 27%, 13%, and 70% N2α cell mortalities were reported following the 48 hour exposure period. For the

ZEA-treated cells, 55%, 19%, and 44%, and for T-2 toxin, 35%, 34% and 20% cell mortalities were reported following exposure to 50, 100 and 200μM of these mycotoxins respectively. These concentrations were selected and standardised across all mycotoxin treatments involving microscopic assessments. It was accepted that a proportion of N2α cells would be damaged and lost at all test concentrations, since dead cells retract processes completely, float off the substrate, and are removed in the washes. Using these exposure levels, a proportion of N2α cells that were compromised at various stages would still be attached to the culture substrate for microscopic assessments.

6.3.2.1 Immunohistochemical analyses of the fumonisin B_1-treated N2α cells

Method controls were used in all immunohistochemical analyses to ensure that the staining detected was the result primarily of immunological interaction between the primary antibody and the antigen. A significant advantage of a monoclonal antiserum is that it contains a population of antibodies that recognise only one epitope on the antigen, reducing the likelihood of non-specific binding.

The method specificity for the FB_1 immunohistochemical staining procedure was verified by the absence of DAB chromogen adhesion to cellular components of N2α cells that were treated with 50μM FB_1, but where the primary antibody was omitted and replaced with PBS (Figure 6.4). A further confirmation of the method specificity was provided by the absence of chromogen adhesion to untreated control N2α cells, where all antibodies were applied as for the treated N2α cells (Figure 6.5). This provides further support for the specificity of the Ag-Ab interaction since potential exists for non-specific immunological complexes to bind to cellular components, leading to false positive staining of cells with chromogen.

The steady-state concentration of many biologically active lipid intermediates and end products are usually altered by fumonisin-induced disruption of sphingolipid metabolism. As there are many potential molecular sites that may be affected by fumonisin exposure, a diversity of cellular and structural alterations were expected in the FB_1-treated N2α cells.

Untreated control N2α cells exhibited a high degree of confluence, with characteristic epithelioid morphology and well-defined cellular processes (Figure 6.5). The presence of

comparatively more cellular processes in FB_1-treated N2α cells than in the control cells, may indicate the absence of a toxicological stress in their environment. This ensured that cell growth was unimpeded and cells consequently adhered tightly to the flask surface. The FB_1-treated N2α cells however tended to retract from the culture substrate as more mycotoxin was incorporated from the surrounding medium, and cells gradually rounded up (Figures 6.6-6.10). Some N2α cells had irregular shapes, and the cell monolayers exhibited a number of intercellular gaps, as with retraction, more cellular processes became apparent as different regions of the cells progressively detached from the culture substrate (Figure 6.10).

Fumonisin B_1 bears structural similarity to sphingoid bases, and because sphingoid bases inhibit cell growth, differentiation, transformation, and apoptosis, FB_1 can also alter growth of certain mammalian cells. Riboni *et al.* (1995) showed that CER plays a mediator role in the regulation of cellular differentiation of the N2α cell line. Fumonisin B_1 blocked So-induced differentiation, which established that conversion of So to CER was required, and that *de novo* CER synthesis was important in the differentiation of the N2α cells.

The biochemical consequences of FB_1 exposure and subsequent disruption of sphingolipid metabolism most likely to have altered cell regulation are, increased intracellular levels of free sphingoid bases and their 1-phosphates, alterations in complex sphingolipids, and decreased CER biosynthesis. Because free sphingoid bases and CER can induce cell death, the fumonisin inhibition of CER synthase can inhibit cell death induced by CER, but promote free sphingoid base induced cell death. Exposure to FB_1 potentially blocks sphingol acylation, and should therefore result in the loss of CER, and may also stimulate growth and prevent apoptosis. However, studies of this inhibitor have shown that Sa and So accumulate. Sphinganine and So compounds are active as growth inhibitors and growth stimulators, and may possibly undergoing rapid phosphorylation to form sphingol phosphates. Unfortunately, most studies have made the simplistic assumption that the observed changes were due to slowing the ceramide synthase enzymatic step. Little thought has been given to the concept that depleting an enzyme leads to depletion of it's products due to the normal catabolism of those products. In addition, there can be accumulation of the enzymes substrates and diversion of these precursors to other bioactive products.

Continuous signalling by cell-cell contacts and cell-matrix interactions are necessary for cells to refrain from undergoing apoptosis. Aberrations in cell death signalling in membranes or cytoplasmic receptors, or alterations in genes that govern apoptosis are involved in the pathogenesis of congenital malformation and many acquired diseases (Vermes *et al.*, 2000). In this study, it is likely that these interactions were affected in the N2α cells on exposure to, and incorporation of FB_1 (Figure 6.6), as FB_1 is known to affect membrane integrity. Sphingolipids serve as important structural molecules in membranes (Hannun and Bell, 1989; Hakomori, 1990; Merrill, 1991) and related intracellular membranes, such as Golgi and lysosomal membranes (Merrill *et al.*, 1997). Complex sphingolipids are required for cell survival and growth, and the loss of complex sphingolipid biosynthesis and membrane biogenesis would be expected to alter cell behaviour, and lead to cell death. Therefore, those N2α cells that were most sensitive for survival signals would stay alive, and cells that could not compete with their more avid sister cells would have apoptosed due to relative shortness of survival factors.

Yin *et al.* (1998) studied the effects of FB_1 on lipid peroxidation in membranes and showed that fumonisins disturb the ordering of membranes, enhances oxygen transport in membranes, and also increases membrane permeability. The study provided evidence that incorporation of FB_1 in test samples made the membranes highly susceptible to oxidation, and that fumonisin appears to increase the rate of oxidation, promote free radical intermediate production, and accelerate the chain reactions associated with lipid peroxidation. The disruption of membrane structure, the enlargement of the relative oxygen diffusion-concentration products, as well as the enhancement effects on membrane permeability, provide additional insights into potential mechanisms by which fumonisins could enhance oxidative stress and cell damage.

In addition, Beier *et al.* (1995) reported that the amine and carboxylic acid groups of FB_1 were spatially related, suggesting that they have chelating properties, and hence, could cause membrane ion leakage. These characteristics may have also contributed to membrane damage in the N2α cells treated with FB_1. Fumonisin B_1 was immunolocalised within cytoplasmic organelles, the cytoplasm (Figure 6.6) and in cell nuclei and provides data that highlights the ability of FB_1 to traverse N2α neuroblastoma cell membranes.

Incorporation of FB_1 into N2α cells was visualized by the binding of the brown DAB chromogen with the peroxidase-labelled mycotoxin within the cells exposed to 50μM FB_1 (Figure 6.6). This low power light micrograph illustrates cells that have incorporated FB_1 are distinctly larger than the blue haematoxylin stained N2α cells, and hence that toxin incorporation may be associated with their formation (Figure 6.7). The primary site of action of FB_1 is distinctly cytoplasmic as indicated by the absence of DAB staining within the nuclei of the majority of N2α cells exposed to 100μM FB_1 (Figures 6.8 and 6.9). Extensive areas of cytoplasmic lyses or swelling of the ER were also characteristic of the DAB stained N2α giant cells, and were visualised as white clearings (indicated by the arrows) within the cells (Figure 6.7).

Fowler *et al.* (1989) have indicated that the effects of toxicants on cells are mediated via damage to one or more of the specialised subcellular compartments, and that formation of giant cells may be a consequence of organelle damage as a consequence of toxicant exposure. Specific organelle systems become damaged if the organelle plays a primary role in the metabolism of the toxicant, when a toxicant is stored intracellularly, or as a result of an inherent sensitivity of some essential biochemical pathway in the organelle (Fowler *et al.*, 1989).

Fumonisin B_1 disrupts sphingolipid metabolism by inhibition of CER synthase that is localized in the ER. This inhibition results in an accumulation of intracellular cytotoxic sphingoid bases and a decrease in the production of complex sphingolipids. In cultured hippocampal neurons, FB_1 inhibited sphingolipid synthesis and axonal growth, and also decreased cellular sphingolipids (Harel and Futerman, 1993). Schwarz *et al.* (1995) further showed that FB_1 affected the formation of axonal branches in these cells, and that this inhibition could be reversed by addition of CER with FB_1. In this study on the N2α cells, FB_1-induced inhibition of CER synthase may have lead to the formation of the giant cells. As the ER plays a crucial role in facilitating metabolic processes, its alteration due to the effects of FB_1 may have hindered cell growth and decreased cellular viability. As the areas of cytoplasmic clearing in these FB_1-treated N2α cells are not clearly distinguishable, they may potentially be either swollen ER or swollen Golgi complexes (Figure 6.7). These cellular abnormalities may have arisen as a consequence of the combined exposure to FB_1 and increased sphingoid bases, as well as the compromised membrane integrity of these cells.

Free s ingoid bases are growth inhibiting and cytotoxic at micromolar concentrations (Steve *et al.*, 1990; Merrill 1991; Hanada *et al.*, 1992) and reduced complex sphingolipid biosyn sis reduces cell proliferation (Hanada *et al.*, 1992; Yoo *et al.*, 1992; Radin *al.*, 1993). Altering levels of sphingolipids may affect the physical properties of the pla na membrane and may also affect cytoskeletal structures disrupting cell growth (Spieg *et al.*, 1986; Fentie and Roisen, 1993). The cellular uptake of certain compounds such a itamins is enabled by the action of membrane-anchored receptors. If however, the build u of the membrane is impaired by the action of fumonisins, the vitamin uptake will also be fected. If these compounds are essential for cytosolic metabolism and their uptake is imp l, this may lead to, or contribute to cell death (Wang *et al.*, 1996). These effects of FB_1 y have compromised the integrity of the cell membranes facilitating entry of FB_1 into th ells.

The F reated N2α cells displayed features of progressive damage leading from gradual retract of processes, to loss of cytoplasmic volume and complete rounding. All these are consis with progression to cell death (Figure 6.8). Cell rounding could be attributed to a loss of rgidity and subsequent perturbation of the cytoplasm. The attachment of cells to the su rate and to each other is also mediated by cell surface glycoproteins, as well as calciu d magnesium ions. The loss of cell viability would imply a loss of production of these i and the glycoproteins that facilitate cell adhesion (Freshney, 1983).

Yoo *e* (1992) reported similar findings in the LLC-PK1 renal epithelial cell line, and showe t that there was a concentration-dependent association between the inhibition of sphing id biosynthesis by FB_1, and growth inhibition and cell death. After 24hour expos FB_1, many cells developed fibroblast-like appearance, with loss of cell-cell contac d an elongated, spindle shape. In this present study, a proportion of FB_1-treated N2α were reduced in size due to cell shrinkage and displayed cytoplasmic conde n, which are features consistent with the apoptotic mechanism of cell death. (Figur). Cells at different stages of the cell cycle with varying maturative states of cellula ganelles metabolise, incorporate, and respond differently to an exogenous xenobi such as FB_1. By visual comparison, a positive correlation seemed to exist betwe α cells that displayed high intensity of chromogen adhesion or incorporation, and c that appeared more compromised by FB_1 exposure, indicating higher conce ons of toxin incorporation.

As these *in vitro* experiments were initiated with confluent flasks of N2α cells, at the exposure level of 200μM FB_1 a significant proportion of cell death was indicated by the gaps between remaining adherent cells (Figure 6.10). These results are supported by the data of the MTT assay (Chapter 3, Table 3.1) where only 29.8% cell viability was noted after exposure to FB_1. Cell detachment suggests a loss of viability, as anchorage dependency is a characteristic feature of cultured cells (Freshney, 1983). Cell division requires an appropriate substrate, and partial or complete cell detachment from the substrate would suggest an inhibition of mitosis and cell growth.

Hidari *et al.* (1996) reported that FB_1-induced inhibition of biosynthesis of GSLs disrupted cell substratum adhesion in mouse melanoma cells, and concur with the findings on the N2α cells. Other studies have also shown that FB_1 altered the manner in which glycosyl-phosphatidylinositol-anchored proteins, such as the folate receptor, are organized and function in membranes (Hanada *et al.*, 1993; Stevens and Tang, 1997). Fumonisin B_1 inhibition of galactosylceramide biosynthesis has also been documented to disrupt assembly and disassembly of cytoskeletal proteins responsible for lipid transport and maintenance of the subcellular architecture in the human adrenal carcinoma SW13 cell line (Gillard *et al.*, 1996). The findings on the N2α cells also support earlier findings by Merrill *et al.* (1993b) who showed that in cultured neuronal cells *de novo*, SM biosynthesis appeared to be more sensitive to fumonisin inhibition than biosynthesis of GSLs. The loss of complex sphingolipids would also have contributed to the abnormal behaviour and altered morphology of the FB_1-treated N2α cells. Taken altogether, these documented findings (Gillard *et al.*, 1996; Merrill *et al.*, 1993b) may have similarly influenced the level of cytotoxicity noted in the N2α cell line.

6.3.2.2 Immunohistochemical analyses of the zearalenone-treated N2α cells

A polyclonal antibody was used for the immunolocalisation of ZEA within the N2α cells. The method specificity for the IHC staining procedure for this mycotoxin was established by the absence of chromogen adhesion to cellular components in the N2α cells treated with 50μM ZEA, but where the ZEA primary antibody was omitted and replaced with PBS.

Exposure of the N2α cells to ZEA (50μM) seemed to have accelerated cell growth at the foci indicated by the multi-layering of the cells in combination with concentrated DAB

staining demonstrating ZEA incorporation (Figures 6.11a and 6.11b). Exposure to ZEA (100μM) also induced giant cell formation (Figures 6.11 and 6.12), nuclear condensation (Figure 6.12), peripheral location of nuclei and intense nuclear and cytoplasmic staining. Additional effects of ZEA exposure in the N2α cells included loss of cell membrane integrity and membrane blebbing (Figure 6.13). The MTT assay results on the N2α cell line indicate that 50μM ZEA induced cytotoxicity in 55% of the cell population following a 48-hour exposure period (Chapter 3).

Based on the staining pattern of ZEA-treated N2α cells, it appears that the primary cellular target of ZEA was cytoplasmic (Figure 6.13), although nuclear staining was also evident (Figure 6.12). Zearalenone mimics oestrogenic compounds and seemed to promote mitogenesis when compared to untreated N2α controls (Figures 6.11a and 6.11b). Natural oestrogens at a physiological level promote cellular proliferation. Oestrogens diffuse in and out of cells, but are retained with high affinity and specificity in target cells by an intranuclear receptor. Zearalenone has shown a DNA damaging effect in recombination tests with *Bacillus cereus* and DNA adduct formation in mice. Zearalenone also induced pituitary adenomas in mice following consumption of a ZEA-spiked diet (United States National Toxicology Program. 1982), indicating that the CNS may be a target for the effects of this mycotoxin *in vivo*. Other *in vitro* studies have shown that ZEA induced sister chromatid exchange, chromosomal aberrations and polyploidy in CHO cells in the absence of exogenous metabolic activation

6.3.2.3 Immunohistochemical analyses of the T-2 toxin-treated N2α cells

A polyclonal antibody was used for the immunolocalisation of T2 within the N2α cells. As with both FB_1 and ZEA, the specificity of the IHC staining procedure for this mycotoxin was demonstrated in the method control by the absence of chromogen adhesion to cellular components in N2α cells treated with 50μM T2, but where the T2 primary antibody was omitted and substituted with PBS. As with the previous two mycotoxins (i.e., FB_1 and ZEA) exposure, induction of giant cell formation was a feature of T2 exposed N2α neuroblastoma cells (Figure 6.14).

The susceptibility of a cell to the adverse effects of a mycotoxin may be a reflection of its ability to incorporate the toxicant (Holt and Deloach, 1988). T-2 toxin inhibits the

mitochondrial electron transport system, with succinic dehydrogenase as one site of action (Khachatourians, 1990). The most prominent effects of T2 at the biochemical and cellular level are the strong inhibitory effect on protein synthesis by binding to ribosomes, the inhibitory effect on RNA and DNA synthesis, and the toxic effects on cell membranes (Eriksen and Alexander, 1998).

To gain access to the cytoplasm and cellular organelles, trichothecenes must pass through the plasma membrane. T-2 toxin is an amphipathic molecule that diffuses into the membranes and disrupts their function. Susceptibility to lysis is species dependent and correlates with the presence of phosphatidylcholine. Owing to their amphipathic nature T2 and other trichothecenes could exert their cytotoxicity by acting on cell membranes (Khachatourians, 1990). T-2 toxin is known to increase lipid peroxidation and membrane damage (Rizzo *et al.*, 1994). Visual comparison of the immunostaining intensity among the three mycotoxin treatments assessed in this study, indicate that T-2 toxin appeared to traverse the cell membranes more easily than either FB_1 or ZEA, by the comparatively higher intensity of DAB staining in these cells. This may be attributed to its high lipophilicity. In this study, the N2α neuroblastoma cells grew as a monolayer with no barrier interface, and this may have rendered the cells more susceptible to the cytotoxic effects of this mycotoxin.

T-2 toxin induced extensive cytoplasmic lyses and membrane damage in the N2α cells, evident by the high level of DAB-stained cellular debris, which increased progressively with exposure to higher concentrations of this mycotoxin (Figures 6.14-6.19). Full receptor occupancy is a good candidate as the first step towards the expression of T-2 toxin toxicity, and this idea is consistent with the suggestion that the cell membrane is involved in and may modulate T2 cytotoxicity (Gyongyossy-Issa and Khachatourians, 1984). As T2 is an amphipathic molecule, it tends to partition into cell membranes. This differential permeability would be subject to constraints of parameters influencing the partition coefficient, as well as factors influencing the state of the cells membrane (Gyongyossy-Issa and Khachatourians, 1984). In Figure 6.16, disintegration of the N2α cell membrane is indicated, and this would have led to impairment of the cell's ability to maintain homeostasis, causing swelling and rupture of the cell membrane, and subsequent cytoplasmic leakage into the surrounding media. These results concur with studies by Bunner and Morris (1988) who reported that T2 affected multiple cell membrane functions.

Blebbing of the cell membrane and condensation of the nucleus are markers of apoptosis, and result in the fragmentation of the cell into apoptotic bodies, which swell and finally lyse (Figures 6.19 and 6.20). Support for the apoptotic effects of T2 are provided by studies of Ueno *et al.* (1995) where 40nM T2 induced apoptosis in HL-60 human promyelotic leukaemic cells within two to six hours without significant cytotoxicity. Shifrin and Anderson (1999) reported that 10μM T2 caused apoptosis in Jurkat cells, and Yang *et al.* (2000) also reported that 40nM T2 caused apoptosis in Raw 264.7 cells. In this study, >50% cell death was reported between 5 and 10μM T2 after the 48hour exposure period in the N2α cells using the MTT assay (Chapter 3). In the flow cytometric analyses, T2 treated N2α cells that were stained with Rh123/PI, showed ~ 15% viability, with ~82% of the cells taking up PI, indicating compromised membrane structure (Chapter 5).

In vivo, T2 caused dilation and swelling of microvessels, damage to the plasma membrane and tearing of the blood vessel wall, compromised endothelial cells in the capillaries of the BBB, and altered amino acid transport into the brain (Yarom and Yagen, 1986). In this *in vitro* cell study, intracytoplasmic swelling (Figure 6.18), as well as damage to the cell membranes were evident in the N2α cells following exposure to T2. Although T2 was concentrated in the CCM bathing the cells membranes for a limited period, this time was sufficient to provide T2 ample opportunity to exert its noxious effects. Pace and Watts (1989) examined subcellular distribution of [^{3}H] T2 in perfused rat liver, noting that after five minutes the plasma membrane fraction contained 38% of the labelled T2; a concentration greater than that observed from the smooth ER (27%), mitochondria (10%) and nuclear fractions (7%). The data in this present study concurs with these earlier findings where high levels of T2 were incorporated into the cells. T-2 toxin also induces cell membrane injury with haemolysis, apparently via a free-radical mechanism (Coulombe, 1993). As the IHC staining for T2 seemed predominantly cytoplasmic, it may have altered mitochondrial function in the N2α cells, as in the study by Pace and Watts (1989). Khachatourians (1990) have indicated that T2 inhibited the mitochondrial electron transport system by inhibiting succinate dehydrogenase, and Jone *et al.* (1987) reported that T2 inhibited gap-junctional intercellular communication in Chinese Hamster V79 cells.

A notable feature in the T2-treated N2α cells was the intensity of the immunoreactivity of T2 around the nuclear membrane of multiple nuclei in cells exposed to 50μM T2

(Figure 6.16). At this concentration, it was unclear whether T2 traversed the nuclear membrane. The nuclei in these N2α cells appeared intact apart from the peripheral condensation of the chromatin. However the N2α cells treated with the higher concentrations of T2 (i.e., 100 and 200μM) showed incorporation of this mycotoxin into nuclei (Figures 6.17-6.20).

Inhibition of DNA synthesis by T2 has been demonstrated *in vitro* (Thompson and Wannemacher, 1984), but evidence exists that this response is probably secondary to protein synthesis (Cundliffe *et al.*, 1974; Munsch and Muller, 1980). Studies by Oldham *et al.* (1980) have indicated that T2 (0.005-0.5μg.ml^{-1}) induced unscheduled DNA synthesis in cultured human fibroblasts, and at the highest doses, protein and DNA synthesis were strongly inhibited. Trusal and O'Brien (1986) also reported that T2 could inhibit nucleic acid and protein synthesis and disrupt cytoplasmic membrane function.

Yike *et al.* (1999) demonstrated 50% cell death in porcine kidney cells following treatment with 0.0091μM T2. However in the N2α cells, much higher concentrations of T2 were used, but based on the MTT assay data (Chapter 3), cell viability was reported to be ~65% at the 50μM exposure level. This reinforces that different cell types have varying cytotoxic responses to mycotoxins due to the differing metabolic activity of the target cells. The most commonly encountered explanations for cell to cell variability in toxin sensitivity are cell to cell variability in the amount of target enzymes, other cellular constituents or functions that can interact with the toxin, and the efficiency of detoxification mechanisms that protect the cells and tissues (Reubel *et al.*, 1987; 1989; Holt *et al.*, 1989; Palanee *et al.*, 2000;).

Biochemically, the trichothecene compounds cytotoxicity is predominantly due to the potent inhibitory effect on protein synthesis (Ueno, 1983). Cundliffe *et al.* (1974) have documented that T2 inhibits protein synthesis by suppressing peptidyltransferase activity, and Rosenstein and Lafarge-Frayssinet (1983) subsequently showed that T2 inhibited synthesis of DNA and RNA *in vitro* (>0.1-1ng.ml^{-1} in suspensions of rat hepatocytes caused 75% inhibition). T-2 toxin also inhibits protein synthesis in the initiation phase. It has been suggested that trichothecenes trigger a ribotoxic stress response causing the activation of MAPK. Such activation may signal either cell survival or induce cell death in

various cell types depending on the conditions such as the length of signal, and concurrent protein inhibition; the latter appears to favour cell death (Shifrin and Anderson, 1999).

6.3.3 Transmission electron microscopy and immunocytochemistry of FB_1-treated N2α cells

At the EM level, gold probe labelled monoclonal antibodies tagged FB_1 within cellular organelles. The indirect method of immunochemical analysis was used to identify antigenic sites due to its higher sensitivity. The primary antibody was unlabelled and was identified by a labelled secondary antibody raised to the immunoglobulin of the species providing the primary antibody. Because at least two secondary antibody molecules can bind to each primary antibody molecule, this method is considered more sensitive than the direct method, i.e., smaller amounts of antigen were detected, or a stronger signal was given for the same number of bound primary antibody molecules (Polak and van Noorden, 1986).

Transmission electron microscopy revealed that control cells were characterised by an elongated (since transverse sectioned) nucleus of medium density (Figure 6.21) The perinuclear space was narrow and many nuclear pores were observed. Regular distribution of heterochromatin aggregates appearing adjacent to the nuclear envelope between the nuclear pores was typical. The presence of large centrally located nucleoli in nuclei of control N2α cells was consistent with the findings of light microscopy (LM) (Figure. 6.5).

Microsegregation and peripheral condensation of the nucleoli were typical features of the FB_1-treated N2α cells (Figures 6.22, 6.23a-6.25). Gold-labelled FB_1 was immunolocalised within the nucleoli, nucleoplasm and in swollen cellular processes of the N2α cells (Figures 6.23b-6.25). These findings support the IHC analyses that indicated the ability of FB_1 to traverse the nuclear membrane. The exposure to FB_1 may have compromised the integrity of the nuclear membranes of N2α cells thus facilitating its passage into nuclei (Figures 6.24 and 6.25).

Ramasamy *et al.* (1995) have shown that FB_1 increases the rate of albumin transfer across endothelial cell monolayers in addition to elevation of Sa levels, the latter possibly explaining the loss of endothelial barrier function. Changes in the N2α cell membranes were characterised by focal disappearance of membrane structure and partial loss of

continuity. These findings support the results on the N2α neuroblastoma cells since there were disruptions and clear discontinuity of the cell and nuclear membranes in these cultured cells (Figures 6.24 and 6.25).

Further immunocytochemical analysis of FB_1-treated N2α cells revealed gold-labelled FB_1 in association with discontinuous nuclear membranes, as well as within the nucleoplasm (Figure 6.26). The N2α cells exposed to FB_1 also displayed nucleoli with single or double distinctive fibrous centres which are features associated with inhibition of protein synthesis (Ghadially, 1982). The presence of nucleoli with an enlarged fibrillar component is reported to be characteristic of an inhibition of nucleolar RNA synthesis. These results are supported by studies of Norred *et al.* (1990) where FB_1 was shown to inhibit protein synthesis and the secretion of CER into very low-density lipoprotein. Monnet-Tschudi *et al.* (1999) also showed that FB_1 selectively affected glial cells by decreasing the total content of MBP in cell cultures of foetal rat telencephalon. From the ultrastructural differences between the nuclei of control and FB_1-treated cells, along with the immunolocalisation of toxin within FB_1-treated cells, nuclear function appears to be affected by FB_1 exposure. The filamentous component of the nucleolus is the site of precursor ribosomal RNA synthesis, while the granular component of the nucleolus represents a pool of accumulating partially completed ribosomal precursor particles (Daskal *et al.*, 1974). An enlarged nucleolus is indicative of an active process of synthesis of ribosomal RNA and hence, ribosomes and proteins (Ghadially, 1985). The feature of microsegregation was accompanied by that of peripheral clumping of chromatin (Figure 6.23b) at the nuclear membrane, a feature indicative of an inhibition of protein synthesis. Margination of the chromatin appears to be an early event that occurs in the nucleus after irreversible injury leading to death (Ghadially, 1982).

Mobio *et al.* (2000) showed that nine to18μM FB_1 induced significant hypermethylation in the DNA in C6 glioma cells. Hypermethylation is involved in regulation of DNA replication and gene expression, in cell division and differentiation processes. In addition, methylated CpG sites can bind specific nuclear proteins (Nan *et al.*, 1993), which could conceivably block or modify the DNA repair process (Tornaletti and Pfeifer, 1995). Hypermethylation of CpG islands in the region of genes like those involved in tumour suppression have been associated with decreased gene expression (Rouleau *et al.*, 1995).

Sahu *et al.* (1998) reported that at concentrations ranging from 40 to 300μM, FB_1 induced lipid peroxidation concurrently with DNA strand breaks in isolated rat liver nuclei. Although FB_1 is considered a non-genotoxic carcinogen, Sun and Stahr (1993) using a bioluminescent bacterial (*Vibrio fischeri*) genotoxicity test, further claimed that FB_1 showed genotoxic activity without the metabolic activation of S9 fraction at the concentration range of 5-20$\mu g.ml^{-1}$. The results of these studies concur with findings in the present study where FB_1 was directly immunolocalised within nuclei of N2α neuroblastoma cells, indicating interaction with nuclear DNA.

Transmission electron microscopy revealed that the cytoplasm of control N2α cells contained moderately large Golgi apparatus, several ovoid mitochondria and long profiles of rough ER (rER). Innumerable polyribosomes were also seen in the cytoplasm. The cytoplasm was of medium density, and the cellular margin was regular with some cytoplasmic projections/cellular processes. The mitochondria of control N2α cells showed well developed and ordered cristae, whereas mitochondrial distortion was a common feature of FB_1-treated N2α cells (Figure 6.28-6.31).

Fumonisin B_1 was immunolocalised within myelin figures, which are considered an indication of degenerating mitochondria, and of an increase in mitochondrial turnover (Figure 6.28). In addition, the internal architecture of the mitochondria was highly disintegrated (Figures 6.29-6.31), with the cristae being distorted, dilated and decreased in number. Mitochondria of the FB_1-treated N2α cells showed irregular multiple masses of electron dense material (Figures 6.29 and 6.30), as well as mitochondria that were distorted (Figure 6.31), swollen, elongated, dough-nut or C-shaped. Other mitochondrial abnormalities included clearing of the mitochondrial matrix (Figure 6.30), as well as distortion or disruption of the outer mitochondrial membrane The disorientation of the cristae from the usual transverse to longitudinal arrangement was an additional alteration occasionally observed in N2α cells exposed to FB_1. The distortion of mitochondria in FB_1-treated N2α cells with abnormalities such as mitochondrial matrix condensation (Figure 6.27), disorientation of the cristae and occasional swelling due to a flooding of the matrix chamber with water were also evident (Figure 6.28). Gold-labelled FB_1 immunolocalisation within elongated and distorted mitochondria, as well as on the cristae of mitochondria (Figures 6.27 and 6.31) of the treated N2α cells, indicate direct association of this mycotoxin with the organelle where

these ultrastructural changes were observed. Structural irregularities observed in the mitochondria of FB_1-treated N2α cells were therefore attributed to FB_1 exposure.

Mitochondrial protein synthesis, independent of nuclear control, is almost exclusively directed to production of the cristae and the inner membrane of the mitochondrial envelope. The synthesis of the outer membrane of the mitochondrial envelope is controlled by nuclear DNA-dependent RNA synthesis (Nass *et al.*, 1965; Leduc *et al.*, 1966; Anderson, 1969; Bergeron and Droz, 1969). If the outer mitochondrial membrane that is involved in phospholipid biosynthesis is dependent on the complex sphingolipids produced via sphingolipid metabolism, the altered sphingolipid metabolism may have been a factor in the disruption of normal mitochondrial structure. Coupled with these structural changes would have been the functional disruption, which then could be considered a consequence of FB_1-induced inhibition of sphingolipid biosynthesis.

It is widely accepted that there is a positive correlation between the metabolic activity of cells, the number and size of the mitochondria and the concentration of the cristae (Ghadially, 1982). The disorientation of cristae from the usual transverse to a longitudinal arrangement in the FB_1-treated N2α cells indicates a deficiency of cytochrome oxidase activity (Figure 6.30). Cytochrome oxidase is the terminal component of the chain of respiratory carriers (electron transport chain) found in mitochondria, and is therefore responsible for the reaction where electrons coming from the oxidation of NADH and $FADH_2$ by dehydrogenases, are transferred to their final acceptor, oxygen. A disruption in the electron transport chain, leads to a decrease in ATP production and ultimately leads to a decline in the functional activity of cells.

Condensation of the mitochondrial matrix is another feature associated with the loss of respiratory control, and at least partial uncoupling (Trump *et al.*, 1978). The swelling of mitochondria and the clearing the mitochondrial matrix in this investigation may be associated with both uncoupling and an inhibition of oxidative phosphorylation in FB_1-treated cells. Mitochondrial damage suppresses ATP production, which in turn leads to a failure of the ATP-dependent sodium/potassium pump at the cell membrane resulting in cellular compartments flooding with water (Ghadially, 1982). Meldolesi *et al.* (1967) reported a positive correlation between swollen mitochondria and low levels of ATP.

Oxidative phosphorylation occurs across the inner mitochondrial membrane and results in the synthesis of ATP. As discussed in Chapters 4 and 5, the transient opening of the PT pores, which span the inner to the outer mitochondrial membrane, are necessary for the equilibration of essential ions between the cytosol and mitochondrial matrix. These PT pores open irreversibly during apoptosis (Simmons, 1999; Bradbury *et al.*, 2000). Fumonisin B_1 has been shown in earlier chapters to have the ability to induce apoptosis at various concentrations in the N2α cells. This disruption in PT is believed to be the cause of the collapse in the $\Delta\psi m$, and brings about the release of *cytochrome c* from the inner mitochondrial membrane to the cytosol (Simmons, 1999; Bradbury *et al.*, 2000).

Mitochondrial damage suppresses ATP production, which in turn leads to a failure of the ATP-dependent sodium/potassium pump at the cell membrane resulting in cellular compartments flooding with water (Ghadially, 1982). Zamzami *et al.* (1995b) also suggest that swelling of mitochondria may be attributed to the production of reactive oxygen species (ROS). Reduction in the transmembrane potential as reportedly induced by FB_1 in the N2α cell line (Chapter 4 and Chapter 5), concomitant with uncoupling of oxidative phosphorylation caused by FB_1 exposure, may have caused increased generation of ROS, which in turn are important mediators of apoptosis. With an inhibition of mitochondrial DNA replication and inhibition of the respiratory chain, there could be an induction of mitochondrial ROS generation that may induce apoptosis in cells.

In this study, control N2α neuroblastoma cells contained an extensive system of rER, with long profiles often seen in association with mitochondria. The ER profiles of the FB_1-treated N2α cells however were shorter and discontinuous (Figure 6.32) in comparison to control cells, showing features of dilation with occasional vesiculation of the cisternae of the ER, seen in association with immunolabelled FB_1 (Figures 6.33 and 6.34). Swelling of the ER was also associated with a loss of ribosomes and accompanied by dissolution of the cisternae. The results of the present study concur with that of Cawood *et al.* (1994), where cytotoxicity and binding studies using subcellular fractions revealed that ^{14}C-labelled FB_1 bound tightly to microsomal and plasma membrane fractions of hepatocytes.

In several models of cell injury, changes in the ER have been considered one of the earliest cytological changes (Trump *et al.*, 1978). Dilatation of ER is also a feature of apoptosis (Arends *et al.*, 1990; Arends and Wyllie, 1991). The swollen, shorter strands of ER reported

for FB_1-treated N2α cells were an indication of a disruption or inhibition of protein synthesis, whereas in control N2α cells, the well-developed ER indicates increased functional activity and the potential for cell differentiation. The swelling of the ER may be linked to the storage of secretory products and/or the influx of water due to defects in the enzymatic or mechanical defects in the rER (Ghadially, 1982).

Numerous mitochondria in association with an extensive network of ER are an indication of increased protein synthesis. Biochemical alterations induced by FB_1 may have affected the integrity of the membrane leading to an influx of fluid, and retardation of protein synthesis. The initial steps from the condensation of serine and palmitoyl-CoA, through to the formation of CER in sphingolipid metabolism, takes place in the ER. The ultrastructural observations of the N2α cells treated with FB_1, together with direct immunolocalisation of FB_1 in association with the ER, provide further support for the mechanism of action of FB_1 to be via inhibition of sphingolipid metabolism.

Phospholipids are synthesised in the smooth ER (sER). Transport vesicles pinch off from the smooth ER and become absorbed into the Golgi complex, carrying the phospholipids with them. Phospholipid synthesis is completed on the cytosolic side of the membrane lipid bilayer. This bilayer fuses with cisternae of the Golgi complex, which buds off to yield vesicles that fuse with the plasma membrane and with membranes of other organelles. It seems likely that this is a route not only for extracellular secretion, but also for transport of membrane lipids to the plasma membrane (Mathews and van Holde, 1990). As CER synthase is localised in the ER, it is likely that this cycle was inhibited by FB_1 and accompanied by the swelling of the ER, may have lead to altered sphingolipid biosynthesis.

De novo biosynthesis of GSLs is coupled to intracellular vesicular transport of the growing molecules through the cisternae of the Golgi apparatus and to the plasma membrane. Biosynthesis of SM also takes place in the Golgi apparatus. Ceramide is processed in the Golgi apparatus, and complex sphingolipids are packaged, sorted and transported to all cell membranes (Simons and van Meer, 1988; Schwarzmann and Sandhoff, 1990). Golgi complexes were not clearly apparent in both the untreated and FB_1-treated N2α cells, as they seemed morphologically indistinguishable with areas of cytoplasmic lysis. In the untreated cells, the mimimal Golgi bodies seen may be due to the fact that confluent

culures were used and *de novo* biosynthesis of GSLs was minimal at that stage of cell growth.

In the FB_1-treated N2α cells the sparseness of the Golgi complexes may further be attributed to the inhibition of sphingolipid metabolism, since the presence of a well-developed Golgi complex is indicative of the active process of packaging of secretory material. The reduced number of Golgi in the FB_1-treated N2α treated cells may indicate an inhibition of the modification, condensing and packaging of secretory material, as well as a decrease in the turnover of glycosaminoglycans and/or sphingolipids. Figure 6.22 illustrates the difficulty in distinguishing between areas of cytoplasmic swelling and that which appears to be swollen Golgi complexes. A disruption induced by FB_1 on the normal functioning of Golgi complexes would lead to degradation of the cell membrane as well, since complex sphingolipids would no longer be directed to the cell membranes.

Areas of cytoplasmic lysis were also noted in the FB_1-treated N2α cells and may be considered a consequence of the disintegration of swollen ER (Figure 6.29). Gold-labelled FB_1 was localised within areas of cytoplasmic lysis and in the surrounding cytoplasm (Figure 6.34). The cellular processes of FB_1-treated N2α cells were numerous and swollen (Figures 6.28 and 6.29) with FB_1 immunolocalised within, providing good correlation with the results of LM.

6.4 CONCLUSION

These immunohistochemical and immunocytochemical microscopic analyses highlight variability that exists with regards to the cellular sensitivity, and consequences of exposure to a specific mycotoxin. The immunolocalisation of T2, ZEA and FB_1 within N2α cellular organelles that exhibit structural and ultrastructural pathology provided good correlation between potential cause and effects of exposure to these mycotoxins.

At the LM level, FB_1-treated cells displayed features of progressive damage leading from gradual retraction of processes, to loss of cytoplasmic volume and complete cell rounding. Some N2α neuroblastoma cells were reduced in size due to cell shrinkage and displayed cytoplasmic condensation; features consistent with the apoptotic mechanism of cell death. A positive correlation existed between cells that displayed increased intensity of

chromogen adhesion, and cells that appeared more compromised by toxin exposure. Prior to cell death however, cells that incorporated FB_1 were larger. The primary site of action of FB_1 was distinctly cytoplasmic, and extensive areas of cytoplasmic lysis or swelling of the ER were characteristic of FB_1-treated N2α giant cells.

At the EM level, microsegregation and peripheral condensation of the nucleoli were typical features of the FB_1-treated N2α cells. Gold-labelled FB_1 was immunolocalised within the nucleoli, nucleoplasm and in swollen cellular processes of the N2α cells. These findings support the IHC analyses that indicate that FB_1 is able to traverse the nuclear membrane. Further immunocytochemical analysis of FB_1-treated cells revealed the presence of gold-labelled FB_1 in association with the discontinuous nuclear membrane, as well as within the nucleoplasm. Alterations of mitochondrial morphology included markedly swollen mitochondria with circular arrangement of the cristae, disintegration of the internal architecture of mitochondria, and distorted cristae, clearing of the mitochondrial matrix, as well as distortion or disruption of the outer mitochondrial membrane. The distortion of mitochondria in FB_1-treated N2α cells with mitochondrial matrix condensation, disorientation of the cristae from the usual transverse to longitudinal arrangement and occasional swelling, due to a flooding of the matrix chamber with water, were also observed. Gold-labelled FB_1 immunolocalisation within elongated and distorted mitochondria, as well as on the cristae of mitochondria of the treated cells, indicate direct association of FB_1 with this organelle where these ultrastructural changes were observed. Structural irregularities observed in the mitochondria of FB_1-treated cells were therefore attributed to FB_1 exposure.

The ER profiles of FB_1-treated N2α cells were short and discontinuous, dilatated or swollen with occasional vesiculation of cisternae of the ER, in association with immunolabelled FB_1. Swelling of the ER was associated with a loss of ribosomes and accompanied by dissolution of the cisternae. Sparseness of the Golgi complexes in FB_1-treated cells may be attributed to the inhibition of sphingolipid metabolism, and may indicate an inhibition of the modification, condensing and packaging of secretory material. Disruption induced by FB_1 on functioning of Golgi apparatus would lead to degradation of the cell membrane, since complex sphingolipids would no longer be directed to the cell membranes. Areas of cytoplasmic lysis were also seen in the FB_1-treated N2α cells, and were considered a consequence of the disintegration of swollen ER. Gold-labelled FB_1 was localised within areas of cytoplasmic lysis, as well as in the surrounding cytoplasm.

Treatment of the N2α cells with ZEA accelerated cell growth at foci indicated by the multi-layering of the cells. Exposure to ZEA (100μM) induced giant cell formation, nuclear condensation, peripheral location of nuclei, membrane blebbing and intense nuclear and cytoplasmic staining, and loss of cell membrane integrity. Based on the staining pattern of ZEA-treated cells, it appears that the primary cellular target of ZEA was cytoplasmic, although nuclear staining was also evident.

Induction of giant cell formation was also a feature of T2-treated N2α cells. T-2 toxin induced extensive cytoplasmic lysis and membrane damage in N2α cells. Disintegration of N2α cell membranes caused swelling, cell membrane rupture, and subsequent cytoplasmic leakage of contents into the surrounding media. As the IHC staining for T2 seemed predominantly cytoplasmic, it may have altered mitochondrial function in the N2α cells. The N2α cells treated with the higher concentrations of T2 (i.e., 100 and 200μM) however showed incorporation of toxin into the nuclei.

The capacity of the N2α cells to incorporate these mycotoxins and effect cytological changes as a result of this exposure represents a major factor in the initiation of malignant transformation. The immunolocalisation of FB_1, ZEA and T2 in association with cellular degeneration highlights the potential toxic effects of these mycotoxins on cells in the nervous system, and draws attention to the cytotoxic effects that may be induced *in vivo* and lead to, or exacerbate malignant transformation.

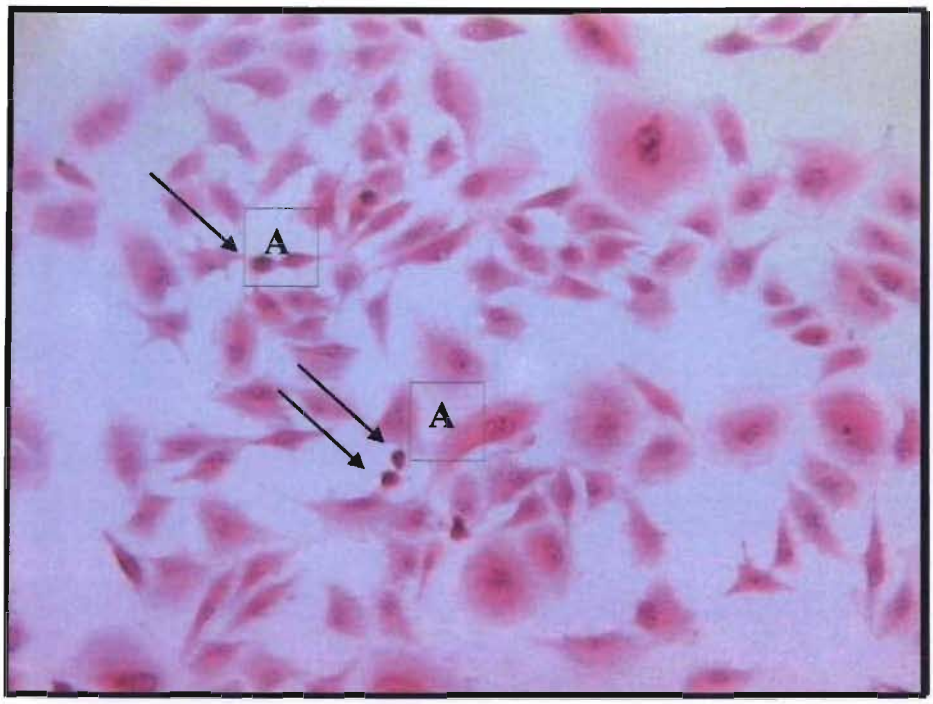

Figure 6.1: Light micrograph of untreated N2α cells displaying epithelioid morphology. Potentially apoptotic (A) cells are indicated with the arrows with reduced cell size due to cell shrinkage and cytoplasmic condensation (H&E, Magn. X 100).

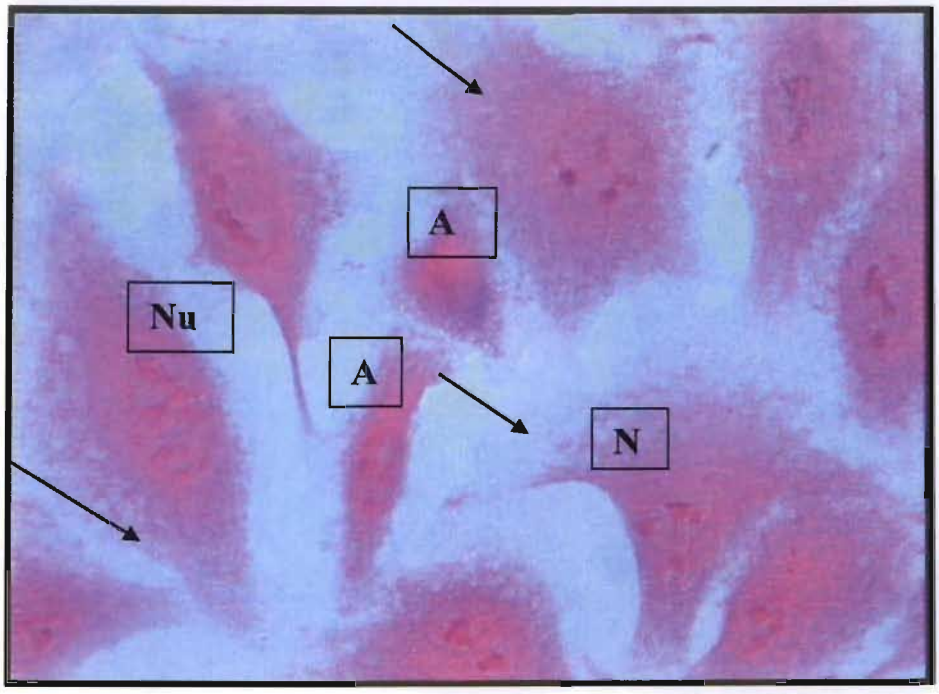

Figure 6.2: Light micrograph of untreated N2α cells with large, centrally located nuclei (N) with multiple nucleoli (Nu), cellular processes extending over a large area (black arrows). Cells in the initial stages of apoptosis (A) are characterised by reduced cell size, cell shrinkage and cytoplasmic condensation (H&E, Magn. X 1000).

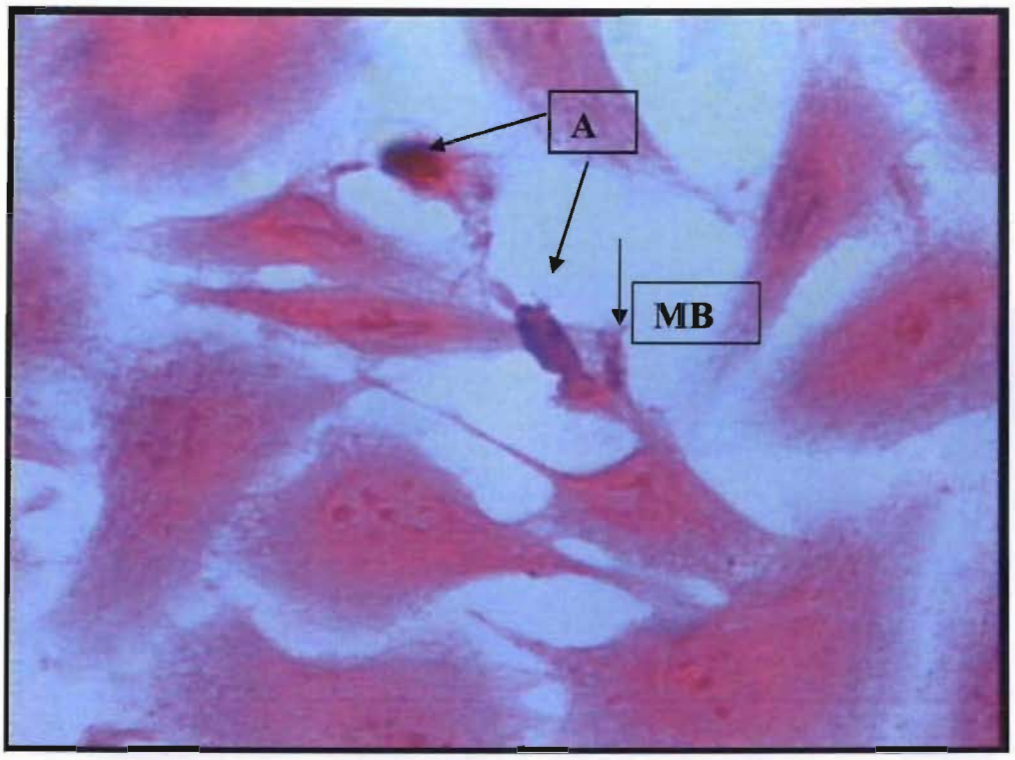

Figure 6.3: Light micrograph of control N2α cells with cells in the final stages of apoptosis (A) characterised by reduced cell size, cell shrinkage, cytoplasmic condensation, as well as membrane blebbing (MB) (H&E, Magn. X 1000).

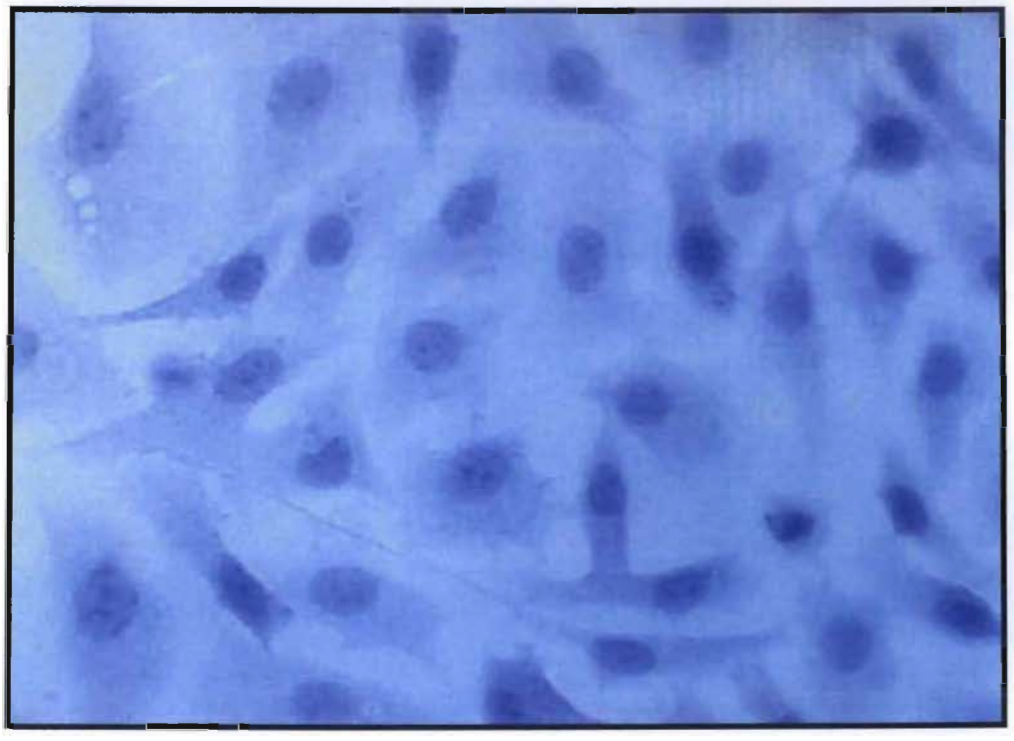

Figure 6.4: Light micrograph of 50μM FB_1-treated N2α cells used as the method control in an IHC run. The absence of DAB chromogen adhesion is an indicator of the method and antibody specificity (Haematoxylin, Magn. X 400).

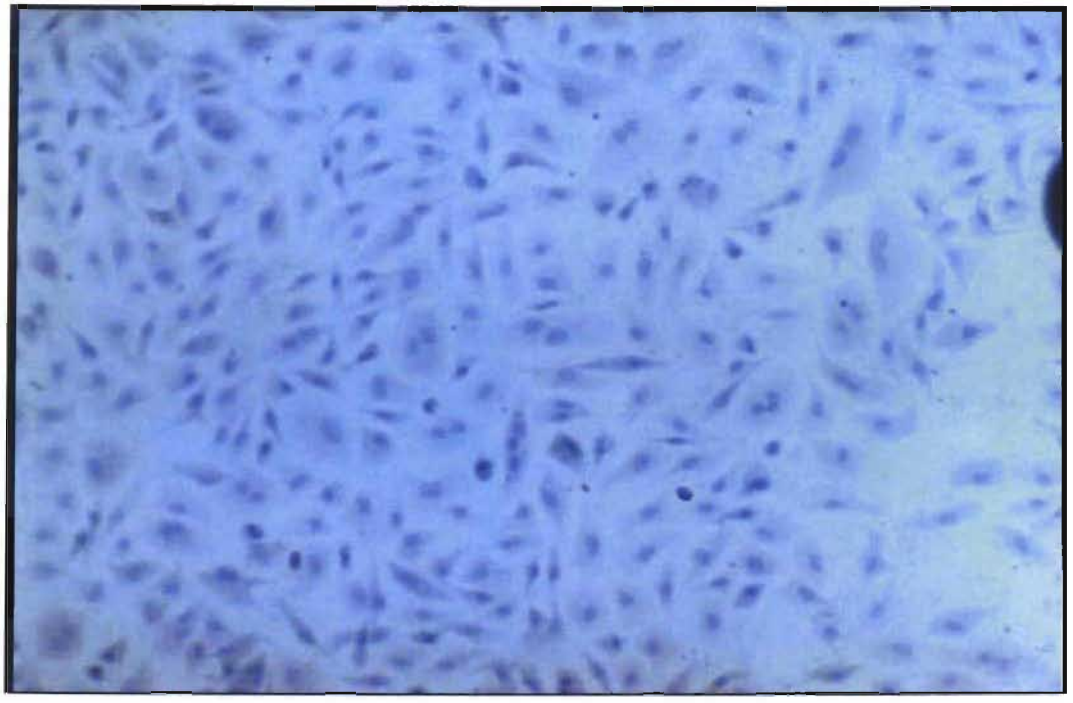

Figure 6.5: Light micrograph of N2α control cells stained in an IHC run. Absence of the DAB staining highlights the immunospecificity of the antibodies used (Haematoxylin, Magn. X 100).

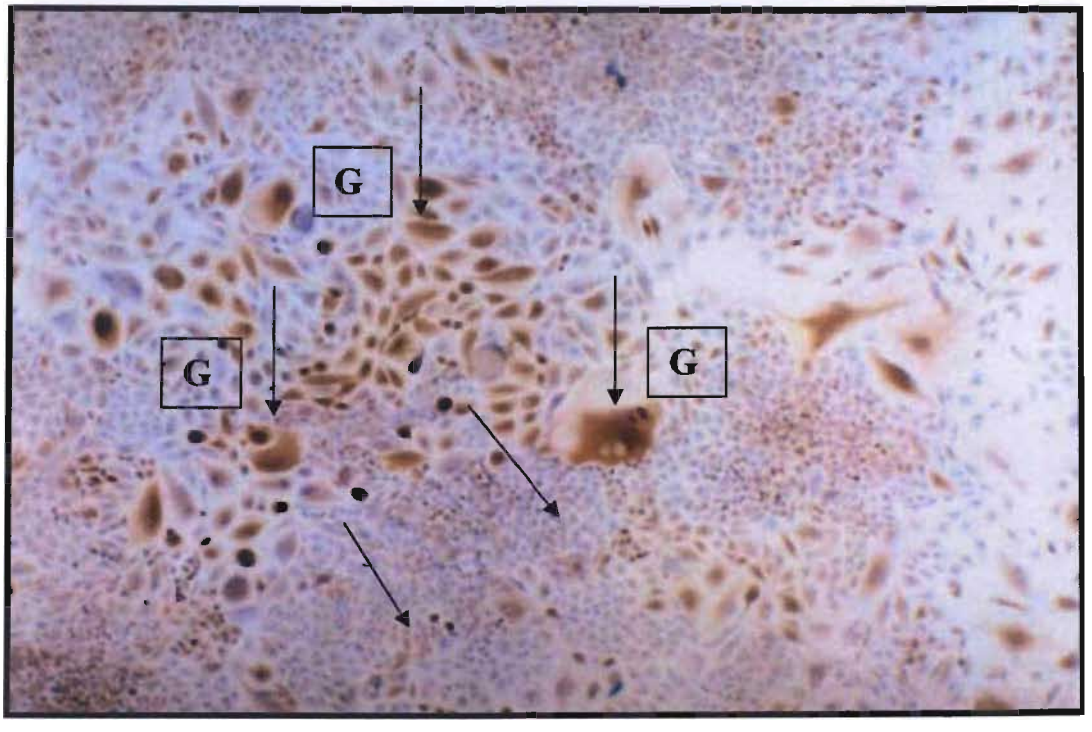

Figure 6.6: Light micrograph of 50μM FB_1-treated N2α cells with DAB-labelled FB_1 immunolocalised within cells indicating mycotoxin incorporation. Giant cell (G) formation is a consequence of FB_1 incorporation as indicated by the selective staining of these cells (Haematoxylin, Magn. X 100).

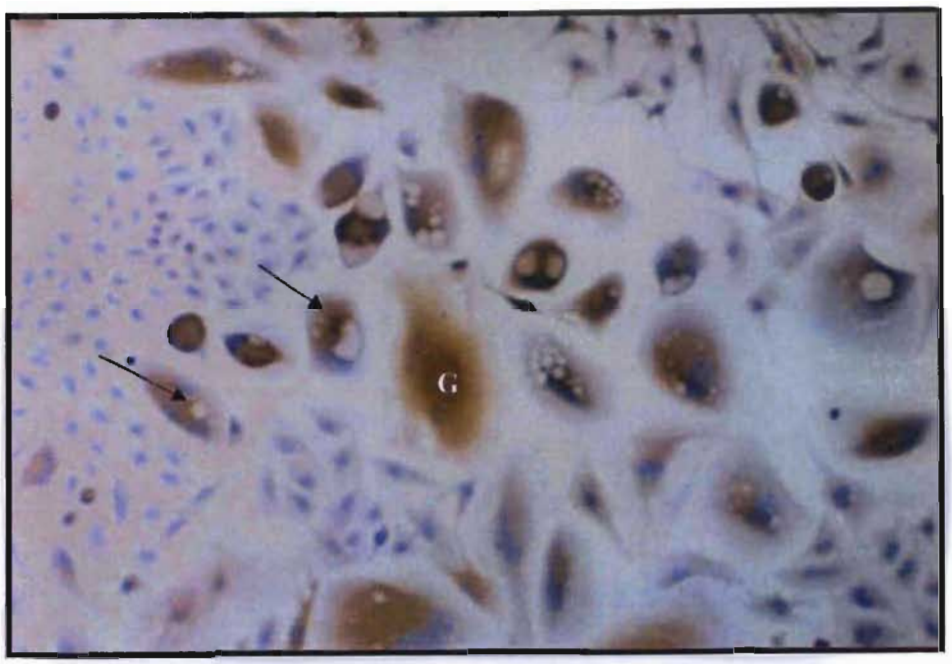

Figure 6.7: Light micrograph of 50μM FB_1-treated N2α cells with DAB-labelled FB_1 immunolocalised within giant cells (G) with extensive areas of cytoplasmic swelling, lysis or vacuolation (black arrows) (Haematoxylin, Magn. X 400).

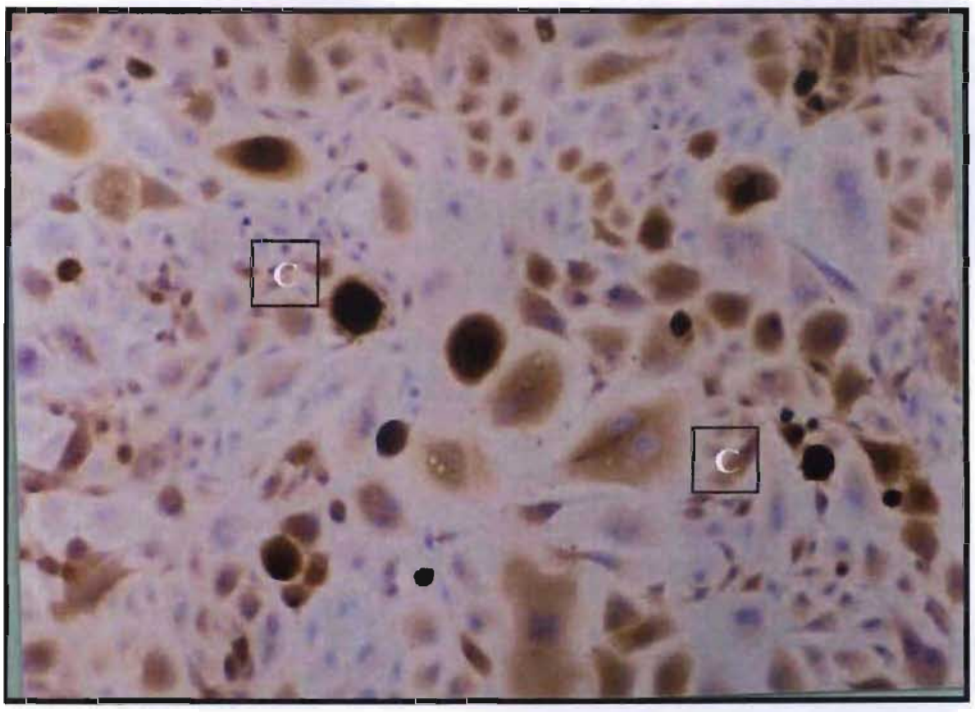

Figure 6.8: Light micrograph of 100μM FB_1-treated N2α cells with DAB-labelled FB_1 immunolocalised in cells showing reduced cell size due to cell shrinkage and cytoplasmic condensation (C) (Haematoxylin, Magn. X 400).

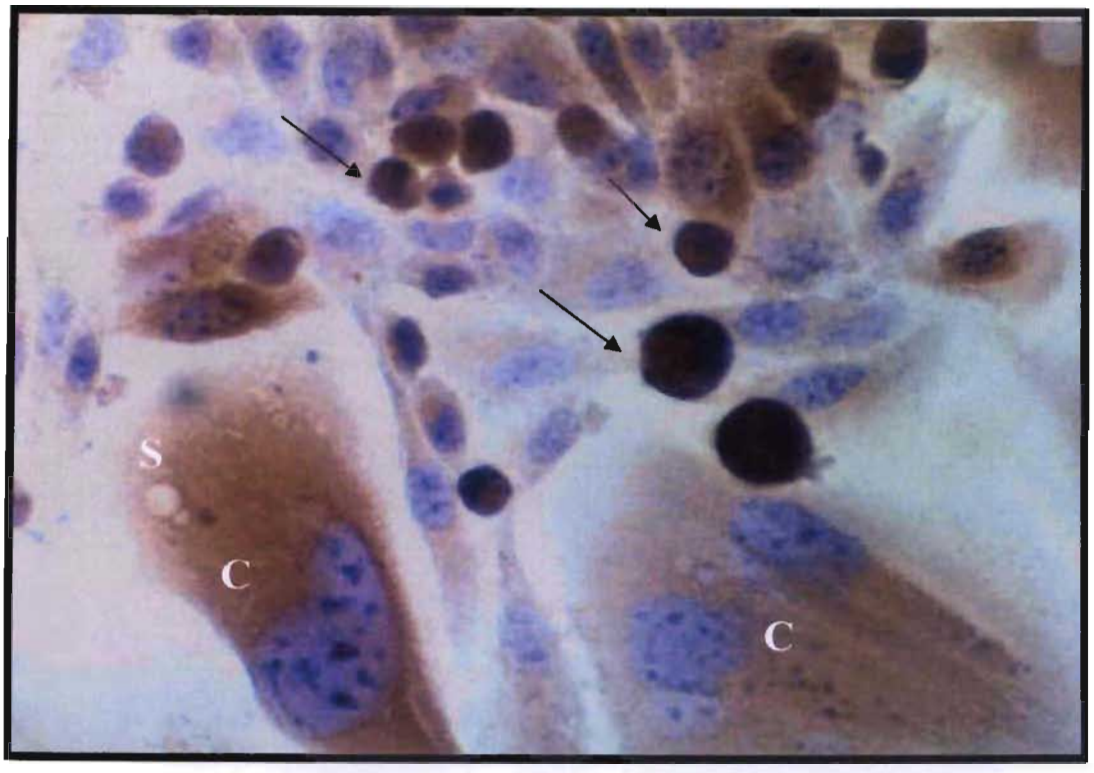

Figure 6.9: Light micrograph of 100μM FB_1-treated N2α cells with DAB-labelled FB_1 immunolocalised in rounded-up dead cells (arrows) and in the cytoplasm (C) of cells that appear less compromised, but with some cellular swelling (S) (Haematoxylin, Magn. X 400).

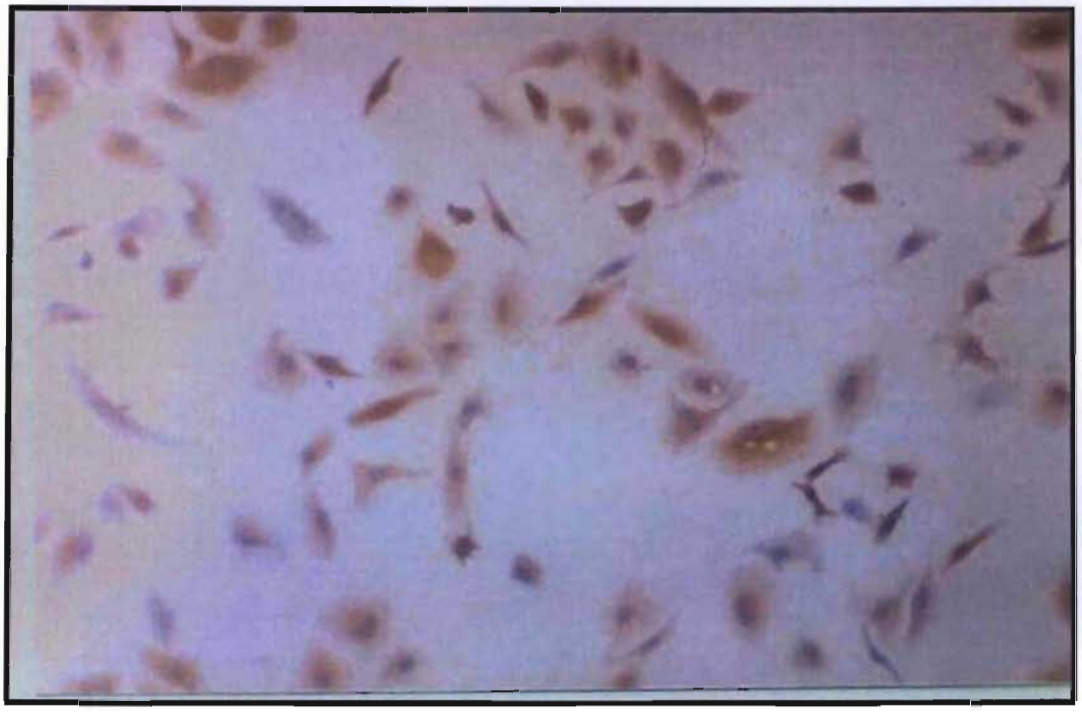

Figure 6.10: Light micrograph of 200μM FB_1-treated N2α cells with DAB-labelled FB_1 immunolocalised in the cytoplasm of cells. The large gaps between adherent cells are indicative of the proportion of cell death induced leading to cells detaching from the culture substrate (Haematoxylin, Magn. X 400).

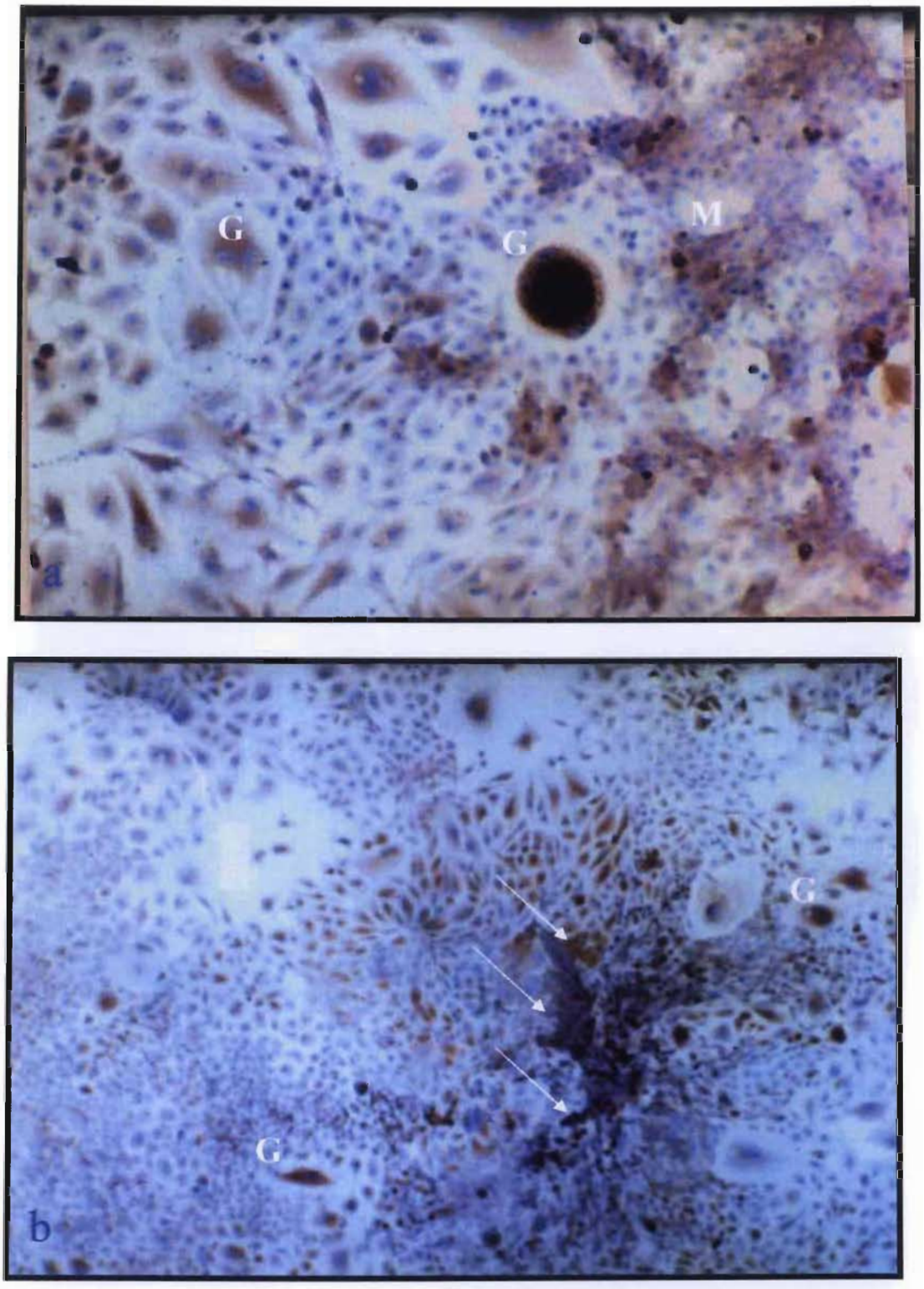

Figures 6.11a and b: Light micrographs of 50μM ZEA-treated N2α cells with DAB-labelled ZEA immunolocalised within multinucleate giant cells (G), the cell cytoplasm, condensed cells (arrows), and foci of multi-layered cells (M). (Haematoxylin, Magn. X 400 [a], X 100 [b]).

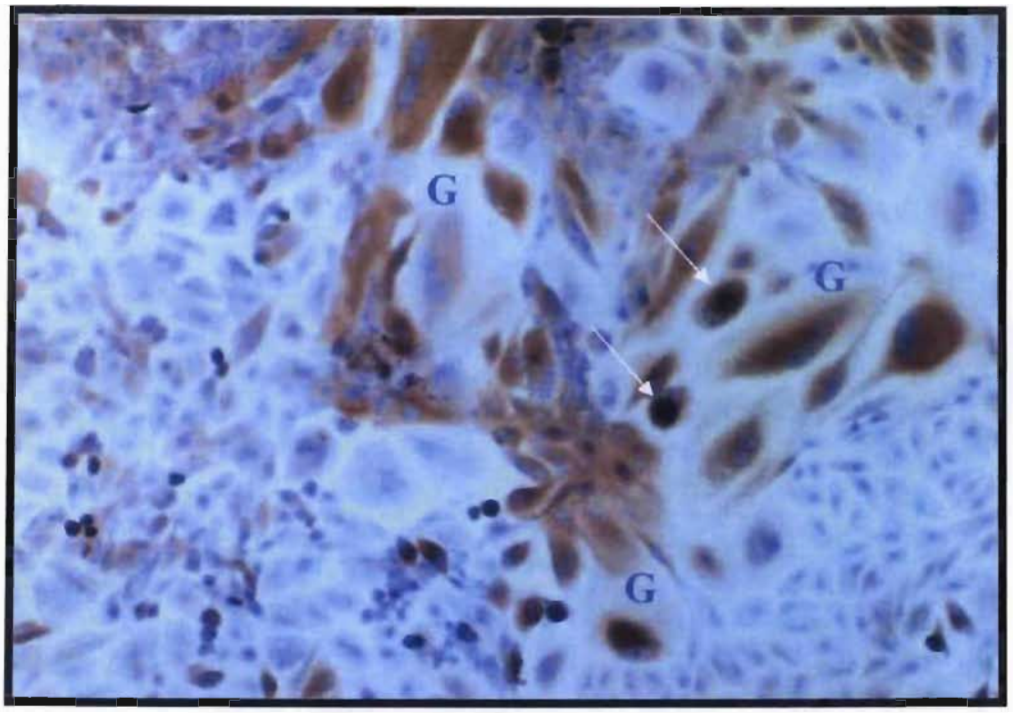

Figure 6.12: Light micrograph of 100μM ZEA-treated N2α cells with DAB-labelled ZEA immunolocalised in multinucleate giant cells (G), the cell cytoplasm, and in condensed cells (arrows) (Haematoxylin, Magn. X 400).

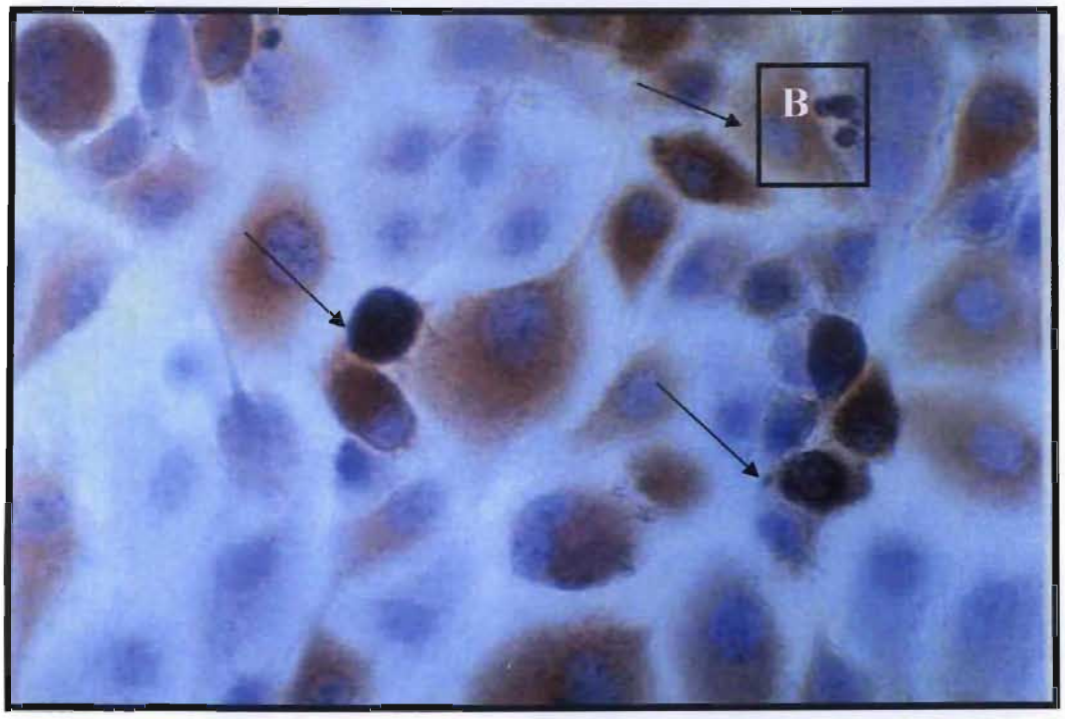

Figure 6.13: Light micrograph of 200μM ZEA-treated N2α cells with DAB-labelled ZEA immunolocalised in cell cytoplasm and rounded-up dead cells (arrows) and in cells with membrane blebbing (B) (Haematoxylin, Magn. X 1000).

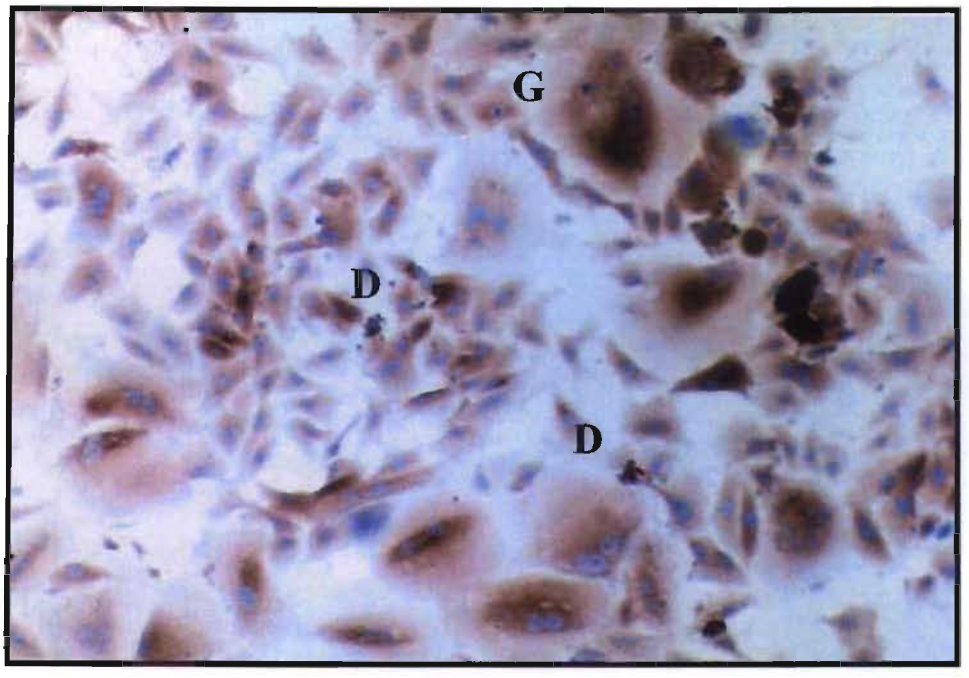

Figure 6.14: Light micrograph of 50μM T-2 toxin treated N2α cells with DAB chromogen within giant cells (G) and in the cell cytoplasm. Cellular debris (D) and remnants of dead cells are also shown (Haematoxylin, Magn. X 400).

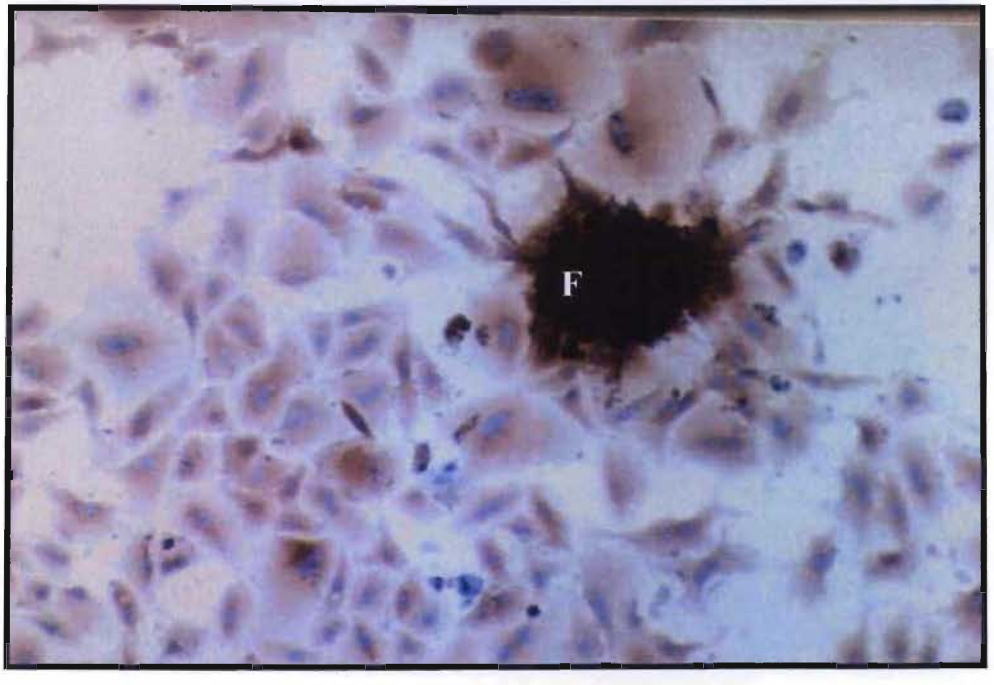

Figure 6.15: Light micrograph of N2α cells treated with 50μM T-2 toxin, immunolabelled with DAB within the focus (F) of cells. There is a predominance of cytoplasmic staining, and absence of toxin incorporation within the nuclei (Haematoxylin, Magn. X 400).

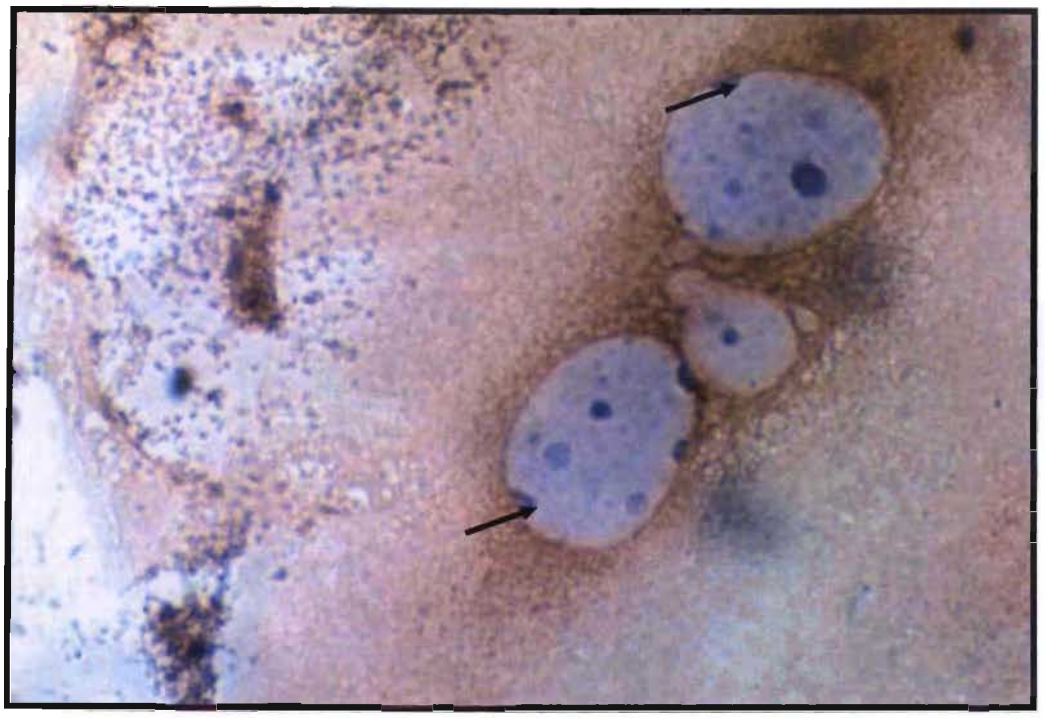

Figure 6.16: Light micrograph of 50μM T-2 toxin treated N2α cell with DAB-labelled T-2 toxin immunolocalised within the cytoplasm of a cell showing loss of cell membrane integrity, and a concentration of T2 around the nuclear membrane. Multiple nuclei and peripheral condensation of chromatin (arrows) were also features of T2-treated cells (Haematoxylin, Magn. X 1000).

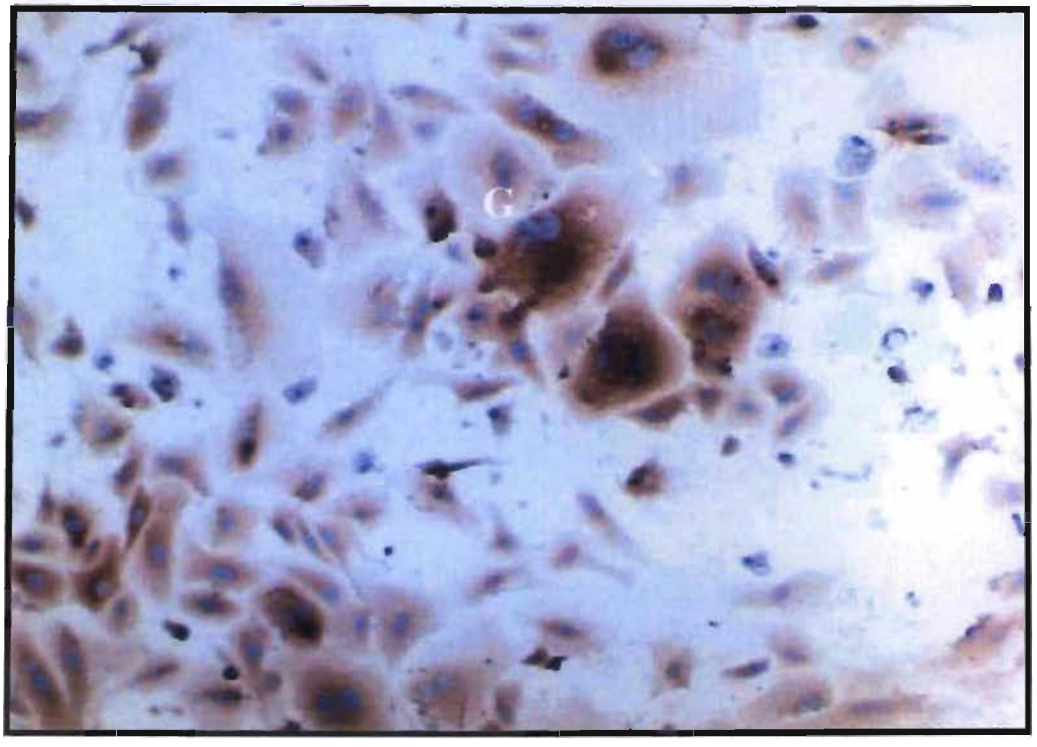

Figure 6.17: Light micrograph of 100μM T-2 toxin treated N2α cells with DAB-labelled T2 localised within giant cells (G), in the cytoplasm, as well as in rounded-up dead cells. Fragmented DAB stained cellular debris was also evident (Haematoxylin, Magn. X 400).

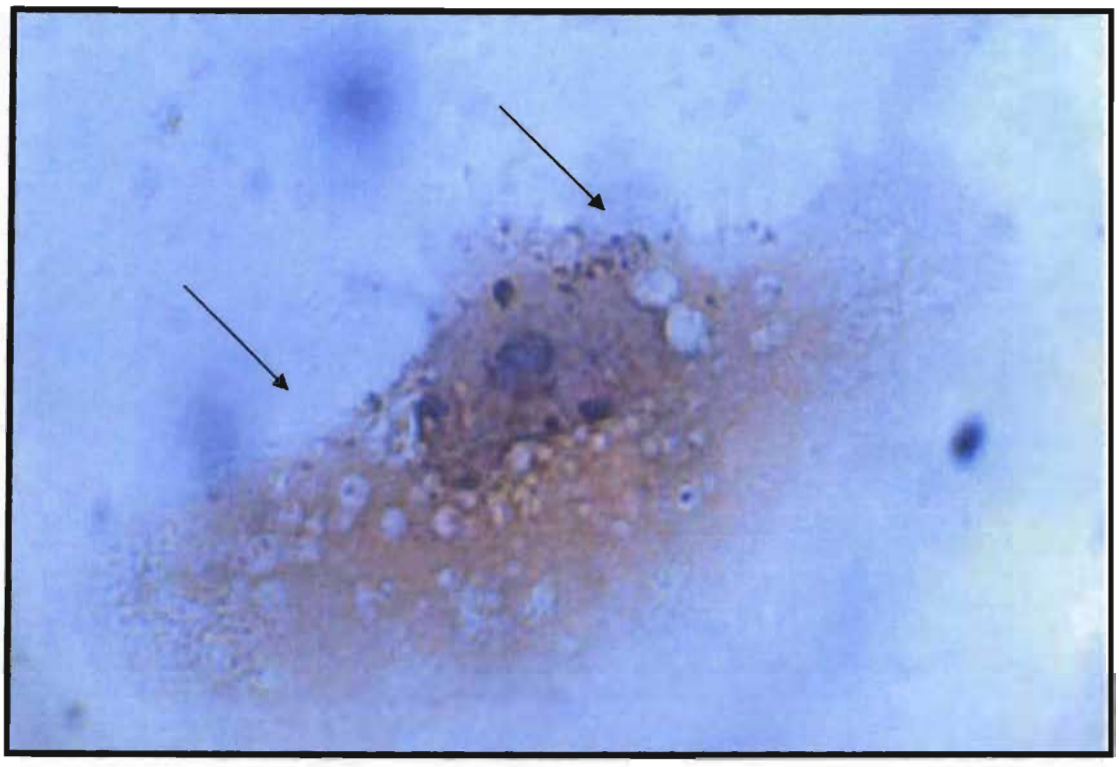

Figure 6.18: Light micrograph of 100μM T-2 toxin treated N2α cells with DAB-labelled T2 immunolocalised in the cytoplasm of a cell showing cytoplasmic swelling or lysis (arrows), and within the nucleus in association with features of peripheral condensation of chromatin. (Haematoxylin, Magn. X 1000).

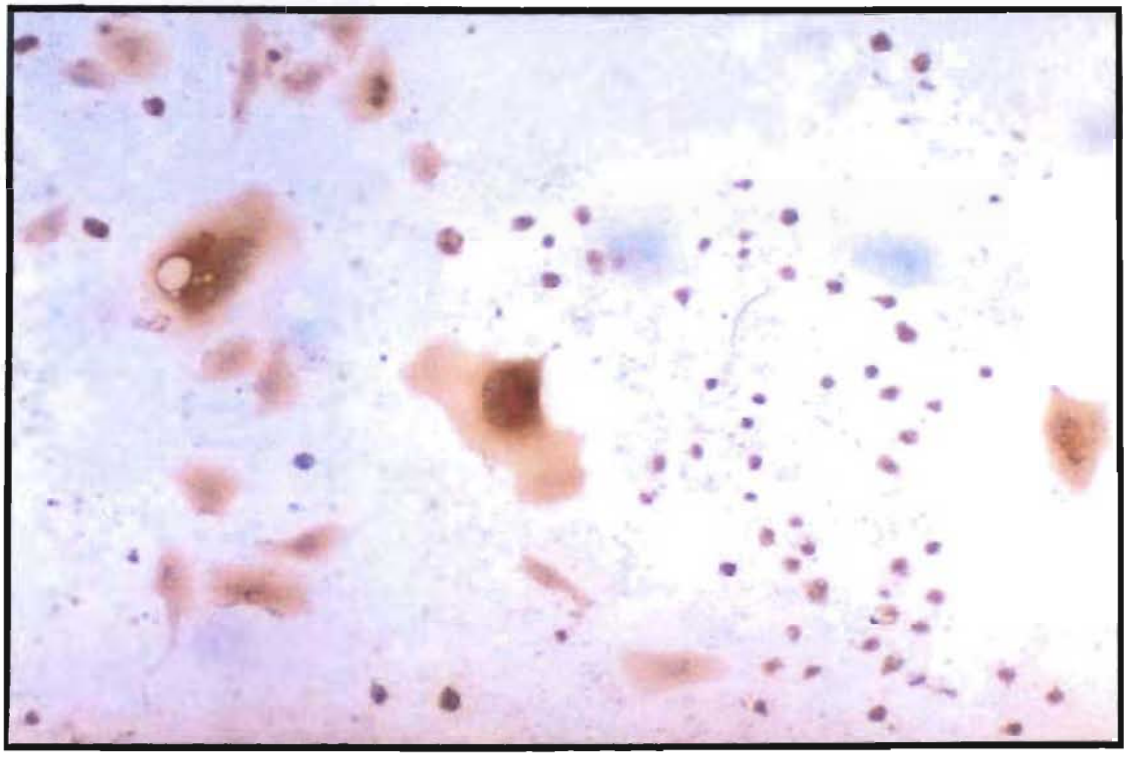

Figure 6.19: Light micrograph of 200μM T-2 toxin treated N2α cells with DAB - labelled T2 immunolocalised in the cytoplasm of giant cells and the fragments of cells lysed by exposure to T-2 toxin (Haematoxylin, Magn. X 400).

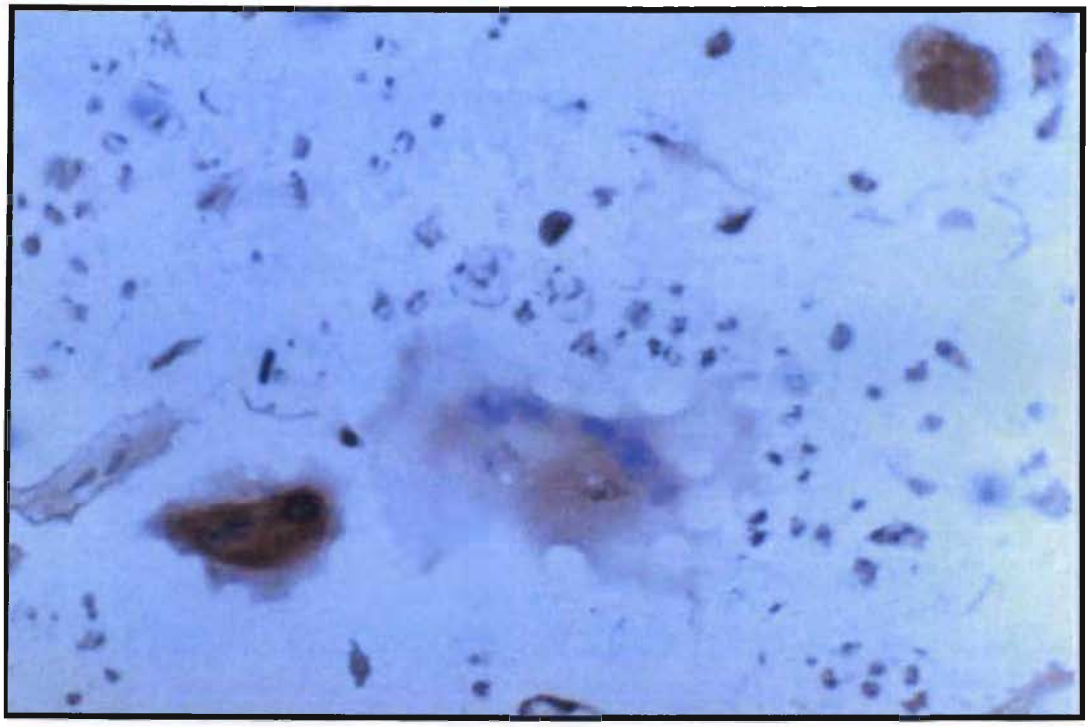

Figure 6.20: Light micrograph of 200μM T-2 toxin treated N2α cells with DAB labelled T2 localised within cells with lysed membranes and cellular debris. Large intercellular spaces between cells are indicative of the level of cell death induced (Haematoxylin, Magn. X 400).

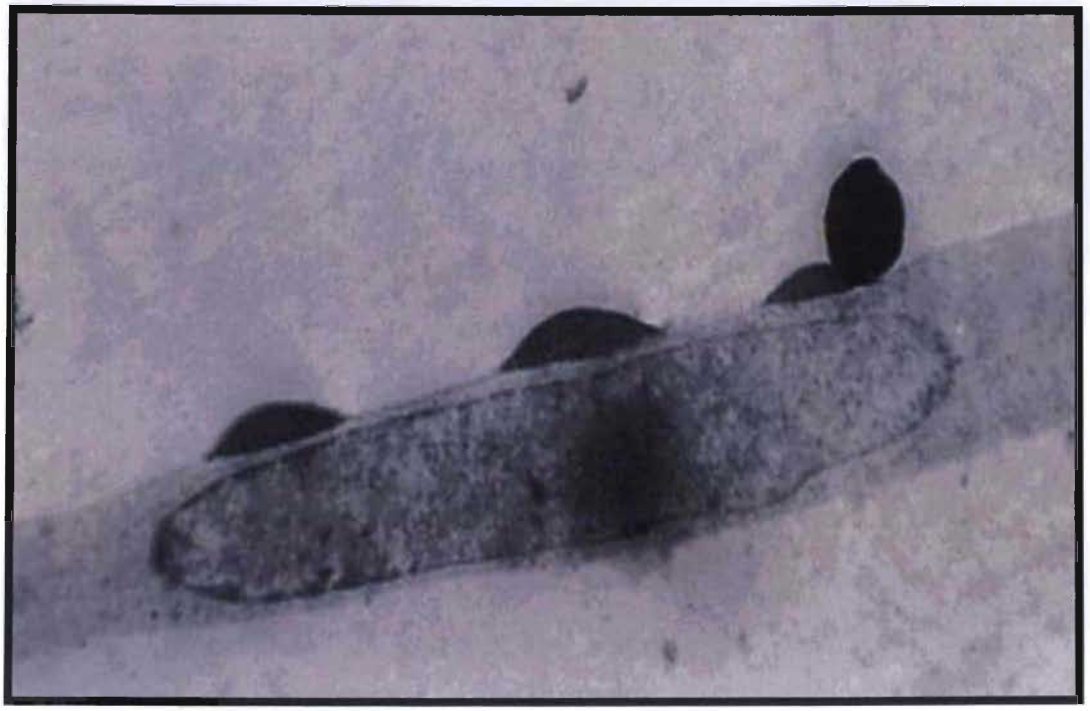

Figure 6.21: Transmission electron micrograph of a control N2α cell containing a prominent single centralised nucleolus. The area above the cell is the flask to which the cell was attached, and the area below, is the araldite resin in which the cell was impregnated and embedded (Magn. X 4000).

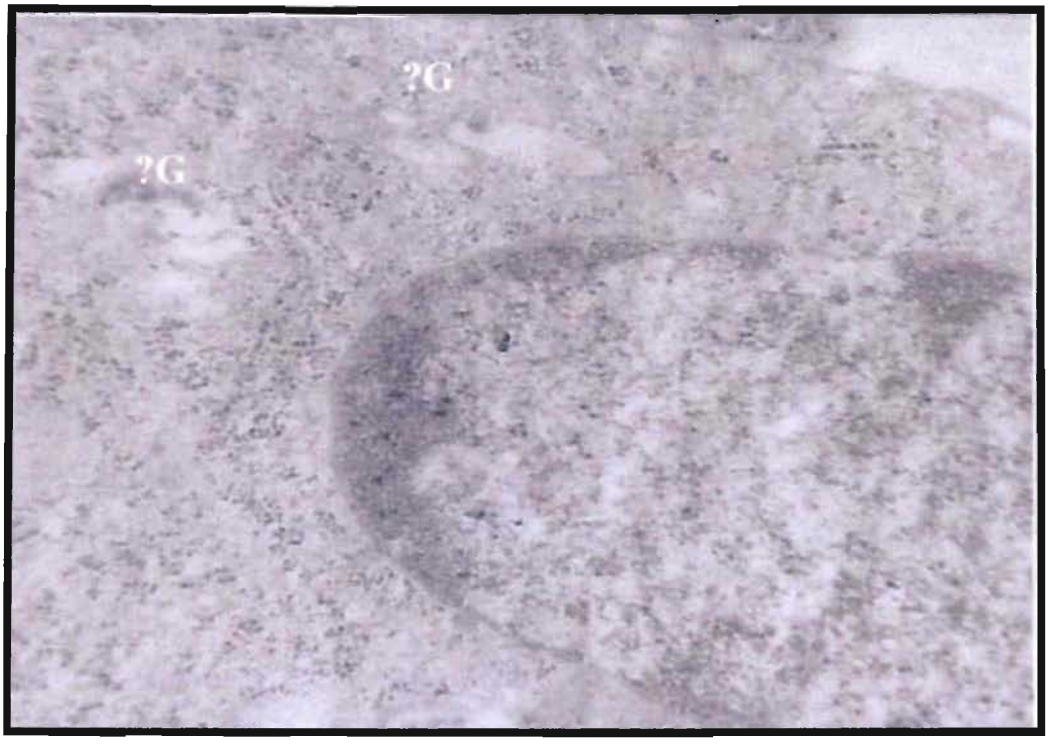

Figure 6.22: Transmission electron micrograph of a 50μM FB_1-treated N2α cell with peripheral condensation of nuclear chromatin, and areas of swelling within the cytoplasm of what appears to be the Golgi complexes (?G)(Magn. X 6 000).

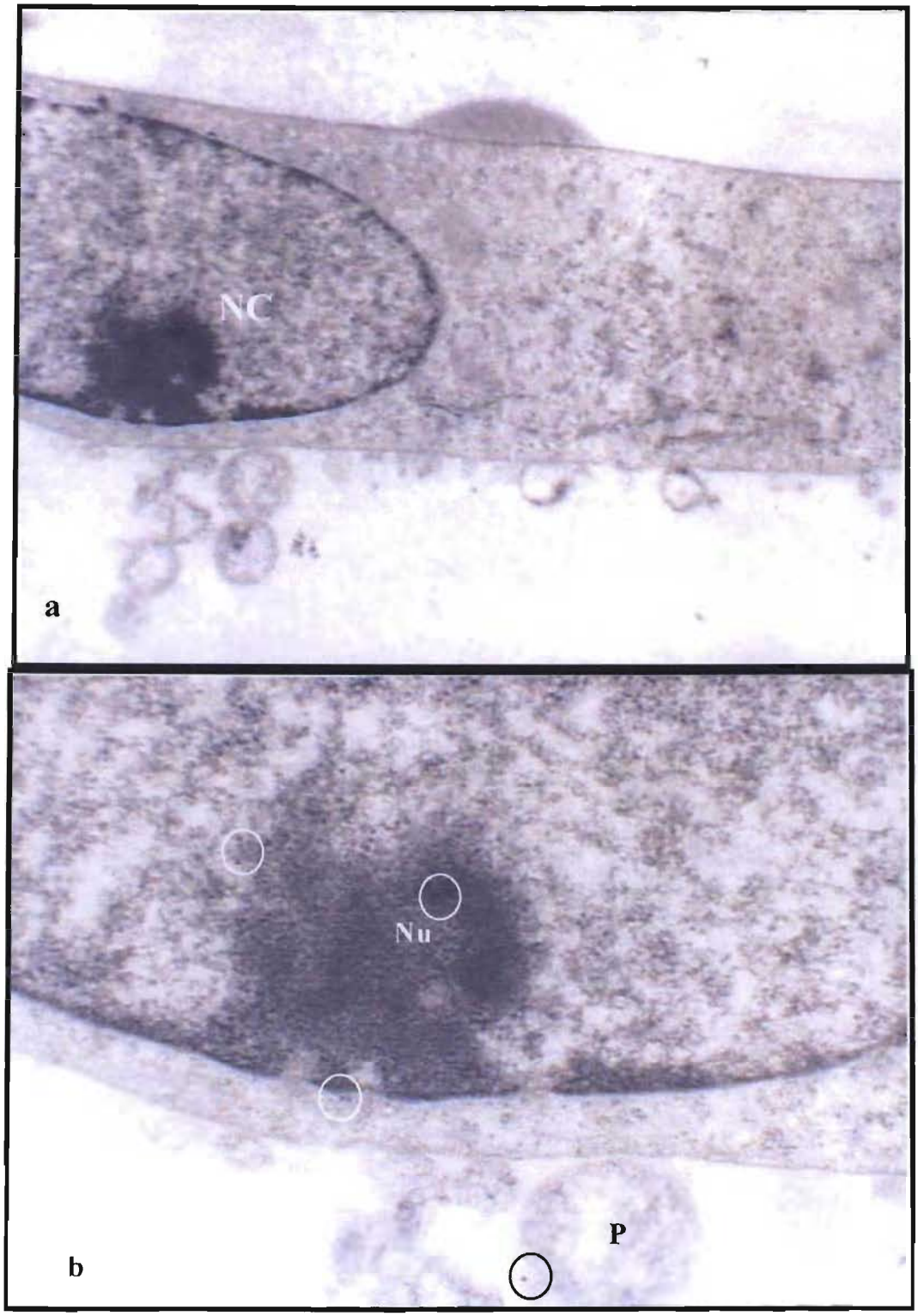

Figures 6.23a and b: Transmission electron micrographs of a 50μM FB_1-treated N2α cell with peripheral condensation of nuclear chromatin (NC) [a] (Magn. X 6 000) with FB_1 immunolocalised within the same nucleolus (Nu) and cellular processes (P) (gold probes circled) [b](Magn. X 25 000).

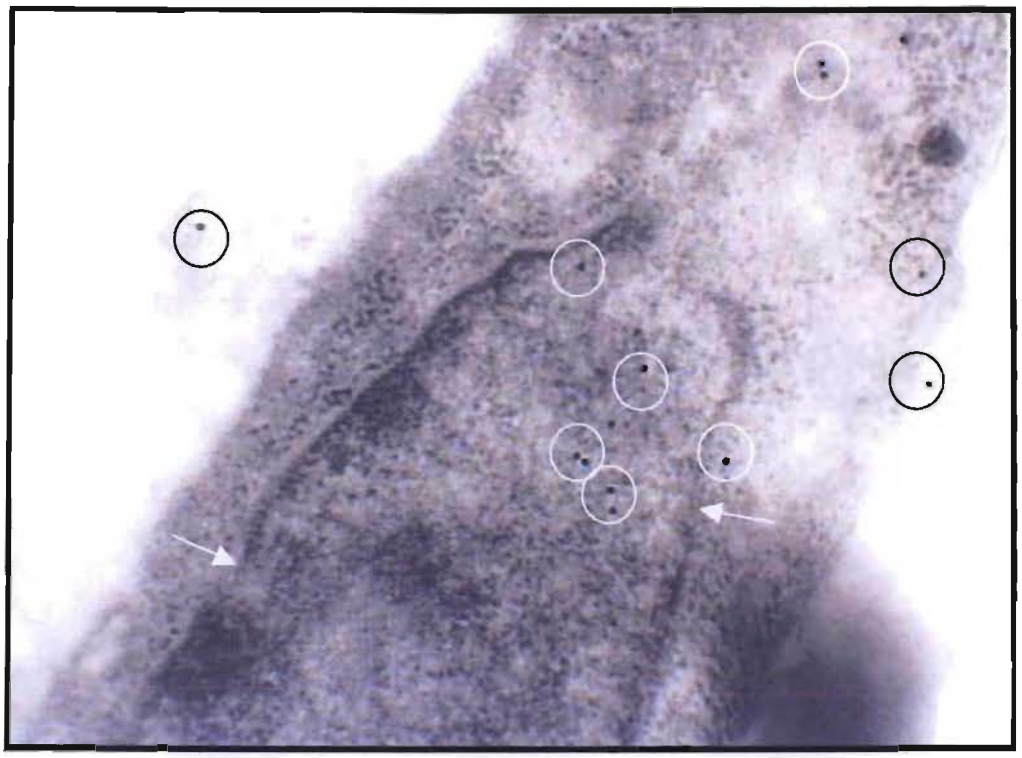

Figure 6. 24: Transmission electron micrograph of 50μM FB_1-treated N2α cell with peripheral condensation of nuclear chromatin and distinct nuclear pores (arrows) in association with immunolabelled FB_1 (gold probes circled) (Magn. X 25 000).

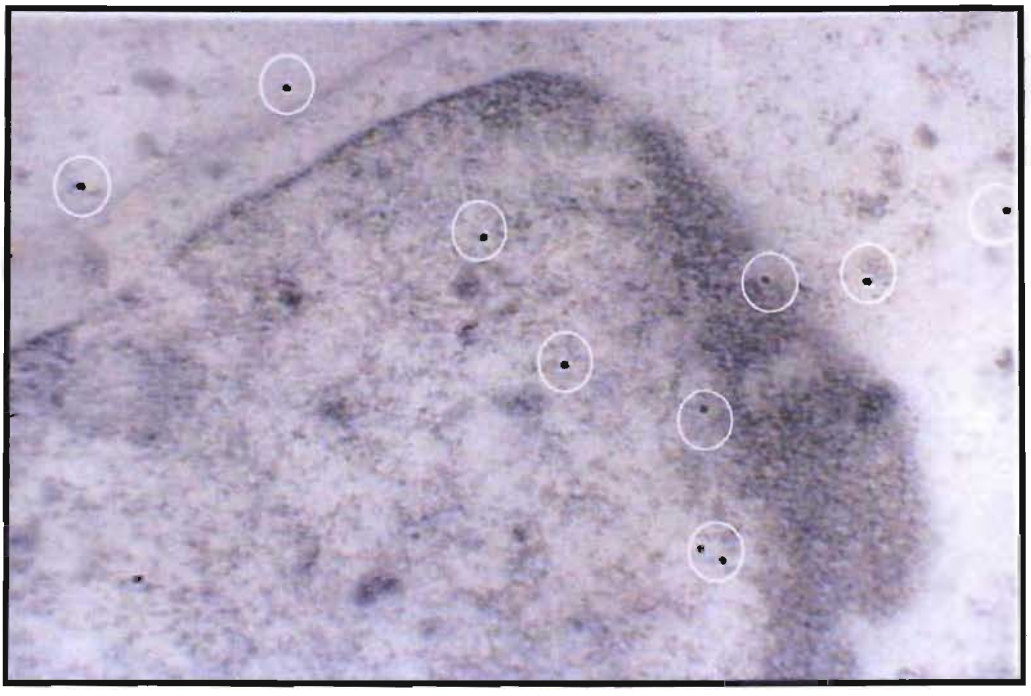

Figure 6. 25: Transmission electron micrograph of 100μM FB_1-treated N2α cell with gold-labelled FB_1 (gold probes circled) localised within the nucleoplasm and cytoplasm (Magn. X 30 000).

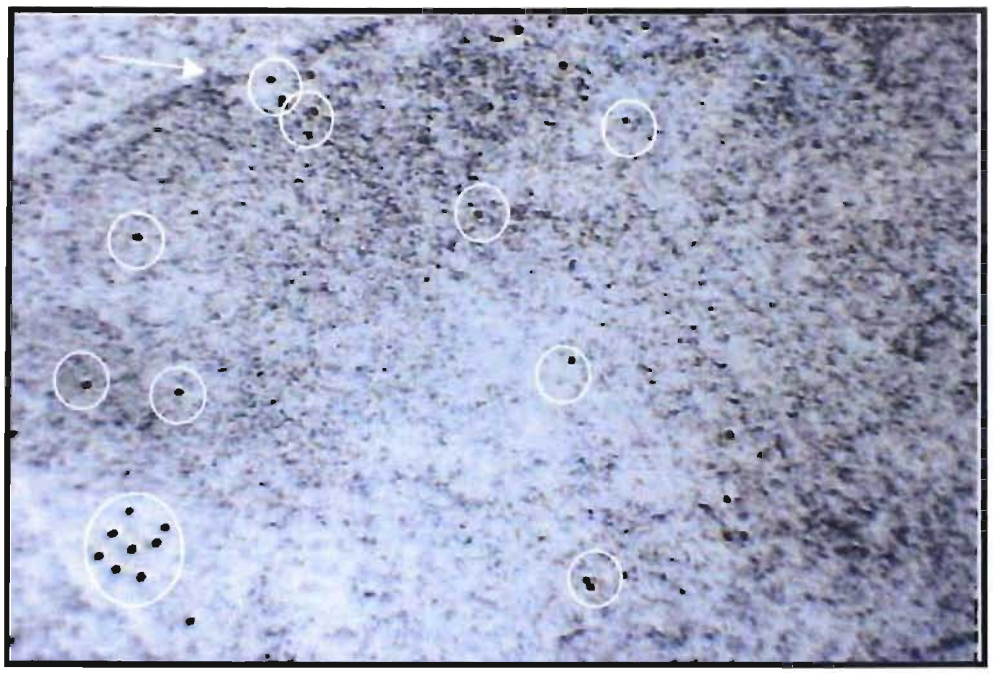

Figure 6.26: Transmission electron micrograph of 100μM FB_1-treated N2α cell with gold-labelled FB_1 (gold probes circled) localised in association with the discontinuous nuclear membrane (arrow) and the nucleoplasm of the N2α cells (Magn. X 60 000).

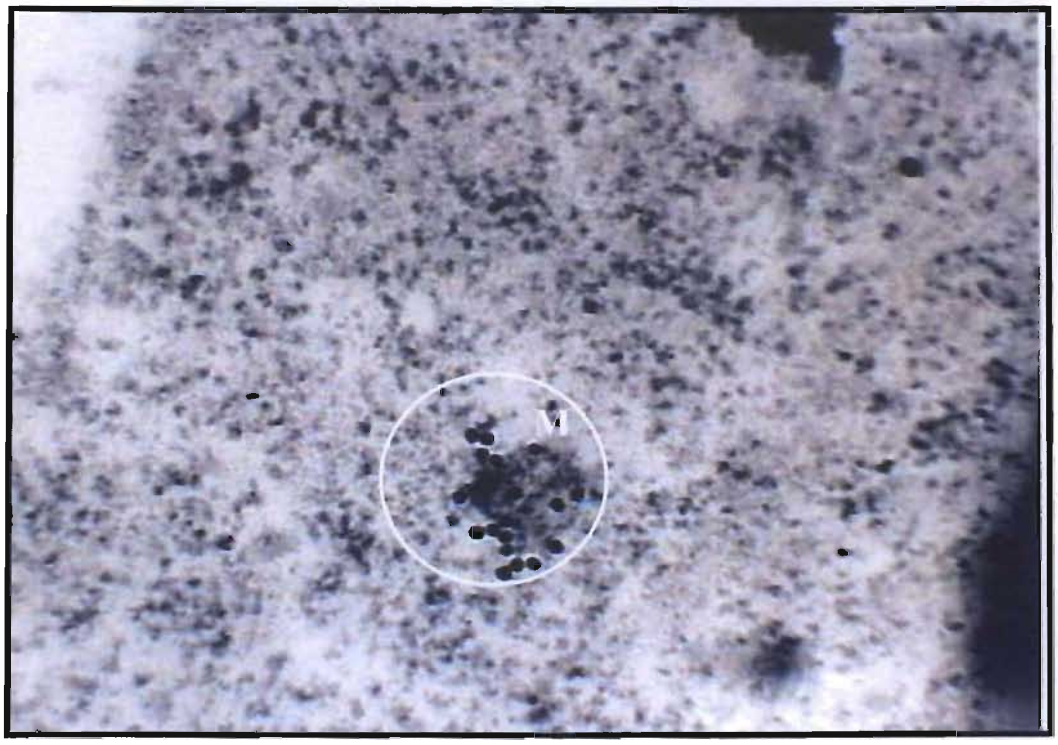

Figure 6. 27: Transmission electron micrograph of 100μM FB_1-treated N2α cell with gold-labelled FB_1 (gold probes circled) localised in association with a mitochondrion (M) (Magn. X 60 000).

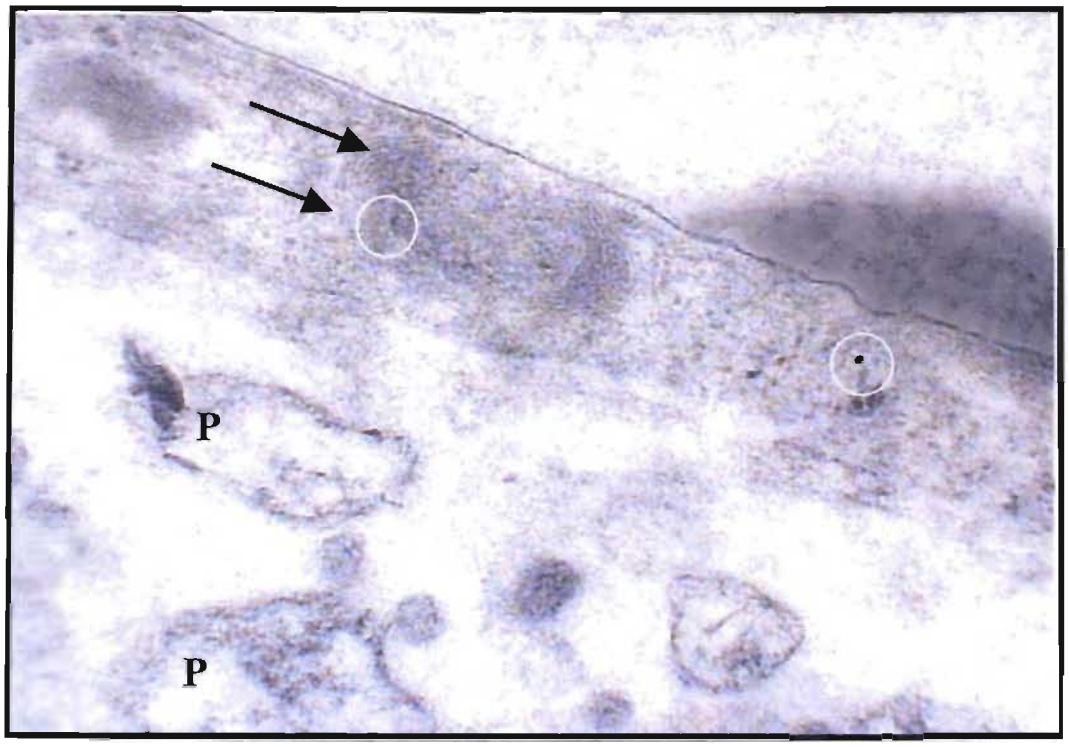

Figure 6.28: Transmission electron micrograph of 100μM FB_1-treated N2α cell within a myelin figure (arrow) in association with immunolocalised FB_1 (gold probes circled). Also note the swollen cellular processes (P) (Magn. X 25 000).

Figure 6.29: Transmission electron micrograph of 100μM FB_1-treated N2α cell with swollen mitochondria with mitochondrial matrix (M) clearing (arrow), disruption of the outer mitochondrial membrane, and swollen cellular processes (P) (Magn. X 30 000).

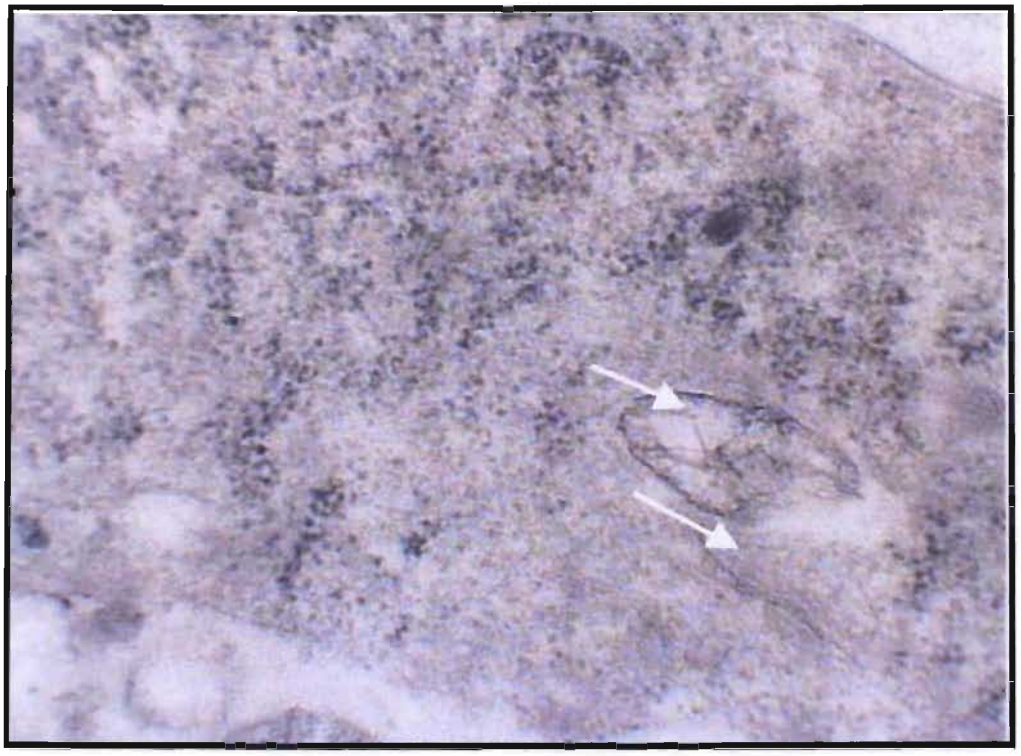

Figure 6.30: Transmission electron micrograph of 100μM FB_1-treated N2α cell with swollen mitochondria showing clearing of the mitochondrial matrix and rearrangement of the cristae (arrows)(Magn. X 35 000).

Figure 6.31: Transmission electron micrograph of 100μM FB_1-treated N2α cell with swollen mitochondria showing clearing of the mitochondrial matrix (M) and areas of cytoplasmic lysis (Magn. X 25 000).

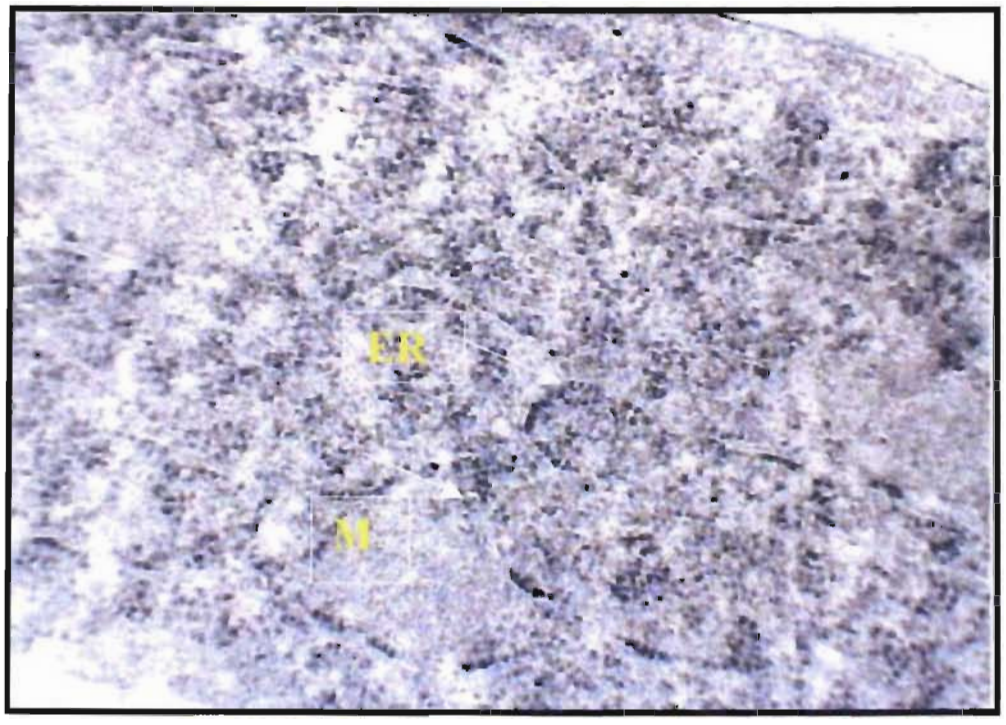

Figure 6.32: Transmission electron micrograph of 50μM FB_1-treated N2α cell with short profiles of ER (arrows) seen in association with swollen mitochondria (M) where the cristae are not clearly visible (Magn. X 30 000).

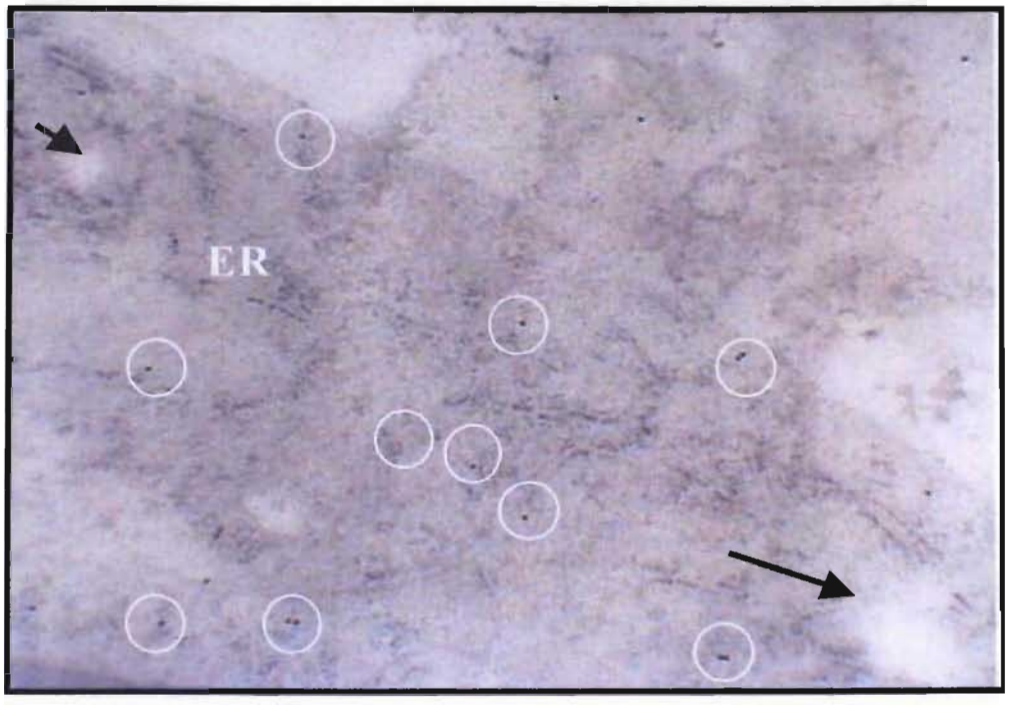

Figure 6.33: Transmission electron micrograph of 100μM FB_1-treated N2α cells with profiles of swollen ER seen in association with areas of cytoplasmic matrix clearing (arrows) and immunolocalised FB_1 (gold probes are circled) (Magn. X 30 000).

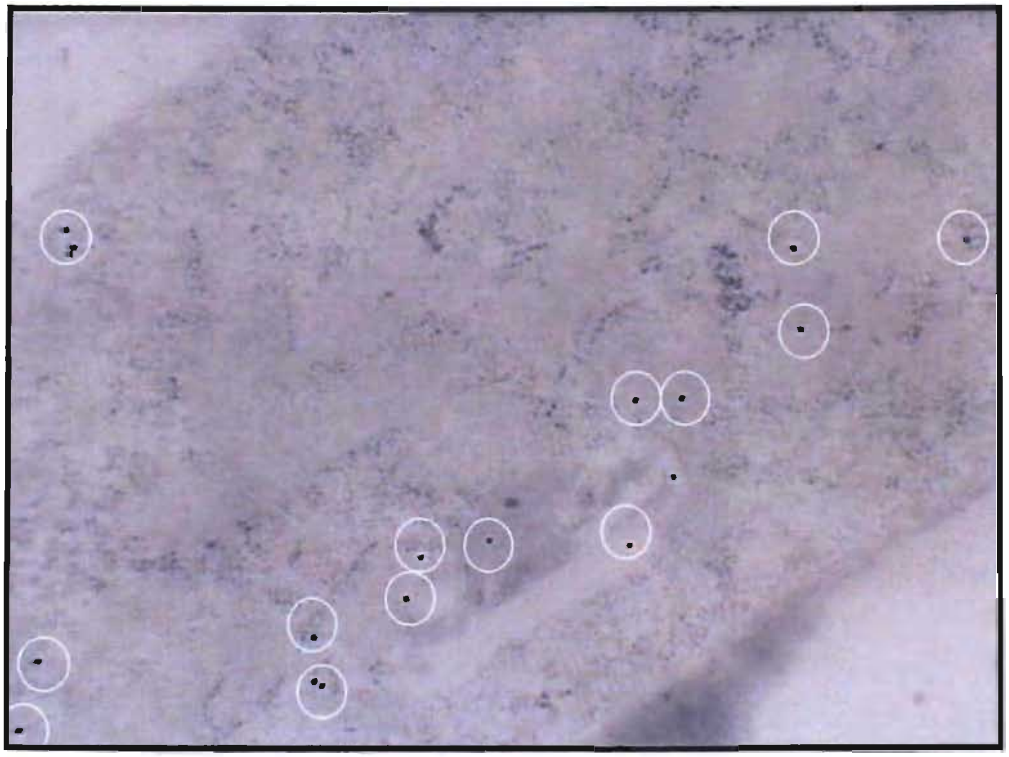

Figure 6.34: Transmission electron micrograph of 100μM FB_1-treated N2α cells with profiles of swollen ER seen in association with areas of cytoplasmic matrix clearing and immunolocalised FB_1 (Magn. X 40 000).

CHAPTER 7

Development and optimisation of methodology for isolation and quantitation of fumonisin B_1, sphinganine and sphingosine from human serum samples using high performance liquid chromatography

7.1 INTRODUCTION

The ubiquitous occurrence of FB_1 in maize and maize products presents a potential threat to human and animal health, highlighting the need for development of effective methods or biomarkers to quantitatively monitor exposure to fumonisins. Toxicokinetic experiments using oral dosing of radiolabelled FB_1 in vervet monkeys have shown that FB_1 is eliminated rapidly from serum (Shephard *et al.*, 1994a). Even though fumonisin is rapidly excreted, only 76% of the total radioactivity could be accounted for (Shephard *et al.*, 1994a), highlighting the possibility of fumonisin being sequestered into tissues or possibly into blood (Shephard *et al.*, 1994b). The estimation of free FB_1 in blood however has been considered impractical due to its poor absorption and rapid excretion from the gut leading to low serum levels (Prelusky *et al.*, 1994). This rapid elimination, low bio-availability and lack of a major metabolite, impy that direct measurement of fumonisin may not be ideal as a quantitative biomarker for exposure, but may be feasible as a qualitative biomarker.

Fumonisin induced inhibition of CER synthase leads to an elevation in the Sa:So ratio in cells. As the changes in free sphingoid bases occur before other biochemical markers of fumonisin induced cellular injury, the Sa: So ratio has been proposed as a biomarker for consumption of fumonisin contaminated feed (Riley *et al.*, 1994b). Methods based on measurement of Sa and So that accumulate due to the action of FB_1 have been developed (Riley *et al.*, 1994c). Riley *et al.* (1996) have recommended that detection of high concentrations of free Sa in serum or tissues be viewed as a clinical tool to be developed and used in conjunction with other clinical tools, in situations where animal or human toxicity resulting from exposure to fumonisin is suspected. This approach appears to give some hope to appraising human exposure to FB_1, but a disadvantage is the erratic recoveries of the sphingoid bases from physiological fluids.

The development of reproducible methods for the determination of the ratio of Sa and So in serum will enable investigations to be conducted into the suitability of this ratio as a biomarker for fumonisin exposure. Its applicability in animal studies where animals are exposed to heavily contaminated feed has already been demonstrated. Studies however are required to address its applicability in human populations that are chronically exposed to fumonisin contaminated staple food supplies (Shephard and van der Westhuizen, 1998).

High performance liquid chromatography is used for both the quantitative and qualitative analysis of compounds. Depending on the polarity of the stationary phase (polar, silica or non-polar, C_{18} modified silica), HPLC can be differentiated into normal and reverse phase, respectively. The polar fumonisin molecule is soluble in water and polar solvents, and suited for determination by reverse phase HPLC. Fumonisin B_1, as well as Sa and So lack ultraviolet chromophores, and are inherently non-fluorescent. As a result, sensitive detection of low levels of FB_1, Sa and So present in physiological samples, require derivatisation and concentration of sample extracts (Shephard, 1998). *O*-phthaldialdehyde (OPA) has proved to be a sensitive derivatisation reagent for compounds possessing a primary amine group (NH_2) and suitable for determination of FB_1 (Shephard *et al.*, 1990), Sa and So (Yoo *et al.*, 1996).

The objectives of this study were to assess established methods for FB_1, Sa and So isolation (Shephard *et al.*, 1992; Kwon *et al.*, 1998; Shephard *et al.*, 1998; Shephard and van der Westhuizen, 1998; Shephard, 1998; van der Westhuizen *et al.*, 2001), and develop optimised methods sufficiently sensitive and suitable for the quantitative detection of low levels of FB_1, as well as free Sa and So in human sera.

7.2 MATERIALS AND METHODS

7.2.1 Materials

All materials and sterile disposable consumables were purchased from Adcock Ingram, SA. Sterile polypropylene 15ml centrifuge tubes were purchased from Continental Laboratory Suppliers. Fumonisin B_1 was purchased from the Programme on Mycotoxins and Experimental Carcinogenesis (PROMEC), Medical Research Council (MRC), Tygerberg, SA. DL-erythro-dihydrosphingosine (sphinganine) and D-sphingosine (sphingosine), 2-mercaptoethanol, PBS tablets, OPA and orthophosphoric acid were

purchased from Sigma-Aldrich, SA. All analytical grade and HPLC grade reagents (acetonitrile, methanol (MeOH)), solvents, chemicals, silica 60 (40-63μm particle size), granular and powdered anhydrous sodium sulphate, sodium dihydrogen orthophosphate, potassium chloride (KCl) were purchased from MERCK, SA unless otherwise indicated. A Bond Elut vacuum system, Bond Elut strong anion exchange (SAX) solid phase extraction cartridges (10ml capacity SAX cartridges containing 500 mg sorbent) and sample microfilters, 200μl glass inserts and sample vials were purchased from Varian (Set Point Instruments, SA).

The HPLC system consisted of a Spectra Physics P200 binary pump, an AS3000 Autosampler and a FL2000 fluorescence detector (Thermo Separation Products, Set Point Instruments, SA). The analytical column was a Waters NovaPak C_{18} cartridge (4μm, 150 x 3.9mm) (Waters, Microsep, SA) preceded by a HIRPB-10C guard column (Hichrom Ltd., Set Point Instruments, SA).

Human serum was obtained from a healthy non-cancer female volunteer. All the optimisation steps outlined involved spiking the sera with known levels of Sa, So or FB_1, and establishing recoveries following application of the published methods mentioned above.

7.2.2 Methods

This chapter outlines the method development and optimisation procedures followed for FB_1, Sa and So extraction from human sera. This chapter therefore deviates from the conventional format of presentation in order to present a logical explanation of the chain of events contributing to the methodology changes.

7.2.2.1 Collection and handling of specimens

Following informed consent, blood (5ml) was collected as required from a healthy urban dwelling female volunteer into yellow-capped serum separation blood tubes. The blood samples were centrifuged at 1200g x 10 min at RT within 15 minutes of collection. Serum obtained was stored in 1ml aliquots in 1.5 ml eppendorf tubes at -70°C until processing for HPLC analyses.

7.2.2.2 The optimised method of fumonisin B_1 extraction from human serum

Prior to HPLC analyses, the serum from the subject was purified of matrix impurities (such as serum proteins) and concentrated as outlined below. The methods of Shephard *et al.* (1992), Shephard (1998) and Coumi (2000) were used after modification and optimisation.

Serum (500µl) (Figure 7.1, Step 1) was combined with 2ml PBS (pH 7.2-7.4) in a 15ml polypropylene centrifuge tube (Figure 7.1, Step 2), vortexed for 30 sec., and boiled in a water bath (100°C for 15 min.) (Figure 7.1, Step 3). The suspension was cooled to RT and ice cold MeOH (5ml) was added to precipitate the proteins (Figure 7.1, Step 4). The suspension was vortexed thoroughly and then centrifuged for 10 min. to pellet the protein precipitate (1200g, 10°C) (Figure 7.1, Step 5). The mixture of PBS and MeOH was transferred to a new 15ml centrifuge tube, and the pellet was resuspended in 5ml ice-cold MeOH. The supernatant was vortexed again to ensure extraction of any remaining FB_1 within the protein pellet, and re-centrifuged (1200g, 10°C, 10 min.) (with repetition of Steps 4 and 5 shown in Figure 7.1).The supernatant was combined with the previously retained supernatant (Figure 7.1, Step 6), and the total supernatant was then applied to a pre-conditioned SAX cartridge (Figure 7.1, Step 7).

The SAX cartridge was pre-conditioned with 5ml MeOH: water (3:1,v/v) followed by 5ml MeOH using vacuum suction. The flow rate was regulated at $1ml.min^{-1}$ through the SAX cartridge for both the application and the elution. At no stage was the cartridge allowed to run dry. Immediately after the entire sample supernatant was applied and passed through the column, the sorbent was successively washed with 5ml MeOH: water (H_2O) (3:1, v/v) and 5ml MeOH. The toxin was then eluted from the sorbent with 15ml freshly prepared 5% (v/v) acetic acid in MeOH. The eluate was evaporated to dryness at 60°C under a gentle stream of N_2 gas in a fume cupboard (Figure 7.1, Step 8) and the samples were stored at 4°C until analysis. The residue was redissolved in 100µl acetonitrile: H_2O (1:1, v/v) and incubated at RT for 5min. prior to derivatisation and HPLC analyses.

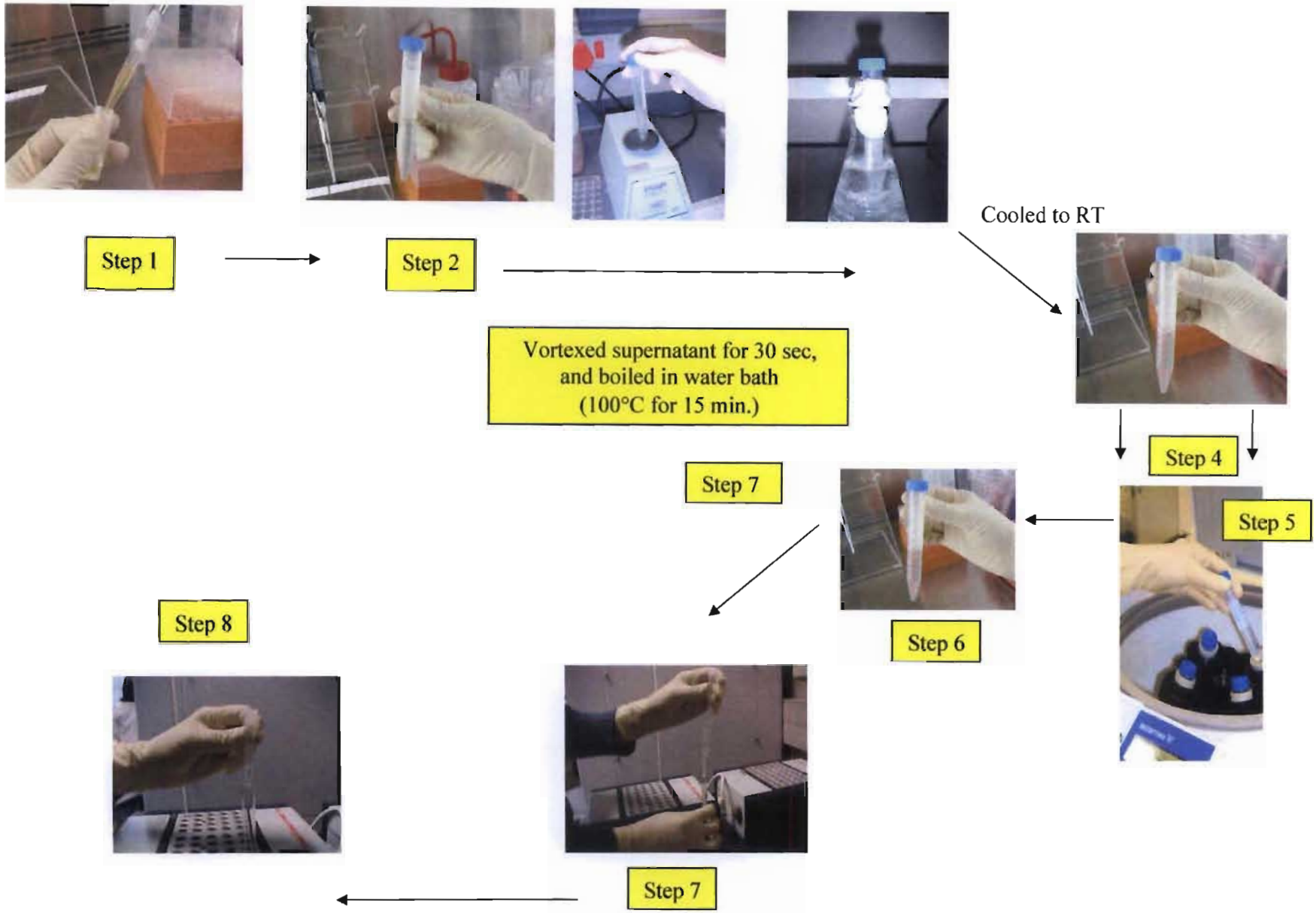

Figure 7.1 : Optimised method for Fumonisin B_1 extraction from the serum

7.2.2.3 Chromatographic analysis conditions

Reverse phase HPLC analyses of the serum samples were carried out under isocratic conditions using phosphate buffer: MeOH (29:71; v/v) as the mobile phase. The buffer was 0.1M Na_2HPO_4, adjusted to pH 3.3 with orthophosphoric acid. The buffer was filtered prior to use through a 0.45µm nylon filter. The mobile phase was degassed and pumped at a flow rate of 1 $ml.min^{-1}$ at ambient temperature.

For fluorometric detection, the excitation wavelength was set at 230nm and emission at 440nm. To avoid interference from impurities eluting at the beginning of the chromatographic run, the emission wavelength was set at 660nm for the first 4.5 min. and switched automatically to 440nm from 4.5 to 8 min. Calculations of peak area and all data collected were processed using PC1000 software (Thermo Separations Products, Set Point Instruments, SA).

The OPA reagent was prepared by dissolving 12mg of OPA in 600µl of MeOH, followed by the addition of 5ml of 0.1M disodium tetraborate (adjusted to pH 10.5 with 1M sodium hydroxide (NaOH)) and 20µl 2-mercaptoethanol. This reagent was stored in the dark at RT and prepared on the day of analysis. Derivatisation of the purified sample was achieved by addition of 40µl of the sample extract to 80µl of the OPA reagent, followed by vortexing for 15 sec. The time from derivatisation to injection did not exceed 1.5 min. Injection of 50µl of derivatised sample was performed in duplicate.

7.3 RESULTS AND DISCUSSION OF METHOD DEVELOPMENT OF FUMONISIN B_1 EXTRACTION AND ANALYSIS FROM SERUM

Numerous analytical methodologies for the determination of FB_1 in physiological fluids exist. In this study, the methods of extraction and analysis of the serum samples were based on methods of Shephard *et al.* (1992), Shephard (1998) and Coumi (2000).

The original method of Shephard *et al.* (1992) involved deproteinization of a 500µl aliquot of serum by the addition of 2.5ml methanol. The protein precipitate was centrifuged down and a 2ml aliquot of the supernatant was applied to a pre-conditioned SAX cartridge. The cartridge was then washed with 5ml of MeOH: H_2O (3:1, v/v) and 5ml methanol, and FB_1

was eluted with 5% acetic acid in methanol. Overall, the method involved solid phase anion exchange clean-up, pre-column derivatisation with OPA and reversed phase HPLC with fluorescence detection. Shephard *et al.* (1992) showed this method to be sensitive (detection limits around 50ng.ml^{-1}), reproducible (relative SD on six replicates less than 5%) and accurate (recoveries on spiked blank samples above 85%)(Shephard *et al.*, 1992). As in all quantitative analytical work however, it was important to validate this method in our laboratory with respect to reproducibility and analytical recovery of the relevant analytes from the matrix of interest. Modifications were then required and applied to the sample preparation procedure in this study to optimise the recoveries of low levels of FB_1 from serum.

The chemical nature of fumonisins makes them amenable to extraction using polar solvents. They are generally extracted using methanol/water (Sydenham *et al.*, 1996) or acetonitrile/water mixtures (Bennett and Richard, 1994).

Because fumonisins do not absorb UV and are not fluorescent, their sensitive detection required derivatisation of extracts (Pohland, 1994) to form fluorescent derivatives. The OPA method is widely used for derivatisation of primary amines, and methodology using this derivative for fumonisins has been the subject of international collaborative trials (Thiel *et al.*, 1993; Visconti *et al.*, 1993; Sydenham *et al.*, 1996).

Derivatisation of FB_1 with OPA and 2-mercaptoethanol in borate buffer is considered rapid and reproducible at RT. The method however suffers from the disadvantage of the limited stability of the fluorescent reaction products. Shephard (1998) found that these products were stable for four minutes after preparation then a decrease (5%) in fluorescence response of the FB_1 derivative was noted after eight minutes, with further decreases as time progressed. To minimise the decrease in fluorescence response, Shephard (1998) suggested standardizing the time between reagent addition and HPLC injection to approximately two minutes. In this study, significant decrease in fluorescence response of OPA derivatives of FB_1 was noted after ten minutes, and thus the time between derivatisation, and injection was not allowed to exceed 1.5 minutes.

The chromatographic method of analysis did not differ significantly from Coumi (2000). In short, isocratic elution with phosphate buffer: methanol eluant on a C_{18} column was applied

to the OPA derivatised samples. Fluorescence detection of the derivatives was achieved by setting excitation wavelength at 230nm and emission at 440nm, and significantly improved detection limits. The detection settings used by Shephard *et al.* (1992) (with excitation and emission wavelengths being 335nm and 440nm, respectively) did not allow for the detection of the toxin when present in amounts less than 0.1μg, while application of the lower excitation wavelength brought the detection limit down to 5ng.ml^{-1} with a signal to noise ratio of 5:1. However, changing the excitation wavelength reduced the specificity of the detection.

There was a marked increase in intensity of the peaks due to the polar constituents of serum samples that eluted before FB_1 leading to detector overload. In order to reduce this interference without compromising sensitivity for the FB_1, the detection parameters were modified. For the first 4.5 minutes, the emission wavelength was changed to 600nm and then returned to 440nm for the remainder of the run. The excitation wavelength remained at 230nm.

Once the method for HPLC analysis was optimised, the reproducibility of the method was tested by injection of the 200ng.ml^{-1} FB_1 standard over several days. The results of this study concur with those obtained by Coumi (2000). Reproducibility between injections of the same sample was found to be excellent as indicated with the three chromatograms of 70ng.ml^{-1} FB_1 shown in Figure 7.2.

An extensive optimisation procedure for the extraction of FB_1 from human serum samples was followed. As the matrix of human serum differs from that of rat serum, it was necessary to use a method that provided efficient clean up of the serum to reduce the amount of polar compounds that eluted. Reddy (1999) applied a method adapted from Shephard *et al.* (1992), which involved solid phase extraction (SPE) of deproteinised human sera using SAX columns, with satisfactory results. The SAX cartridges achieve superior purification over reversed phase cartridges (Bennet and Richard, 1994;

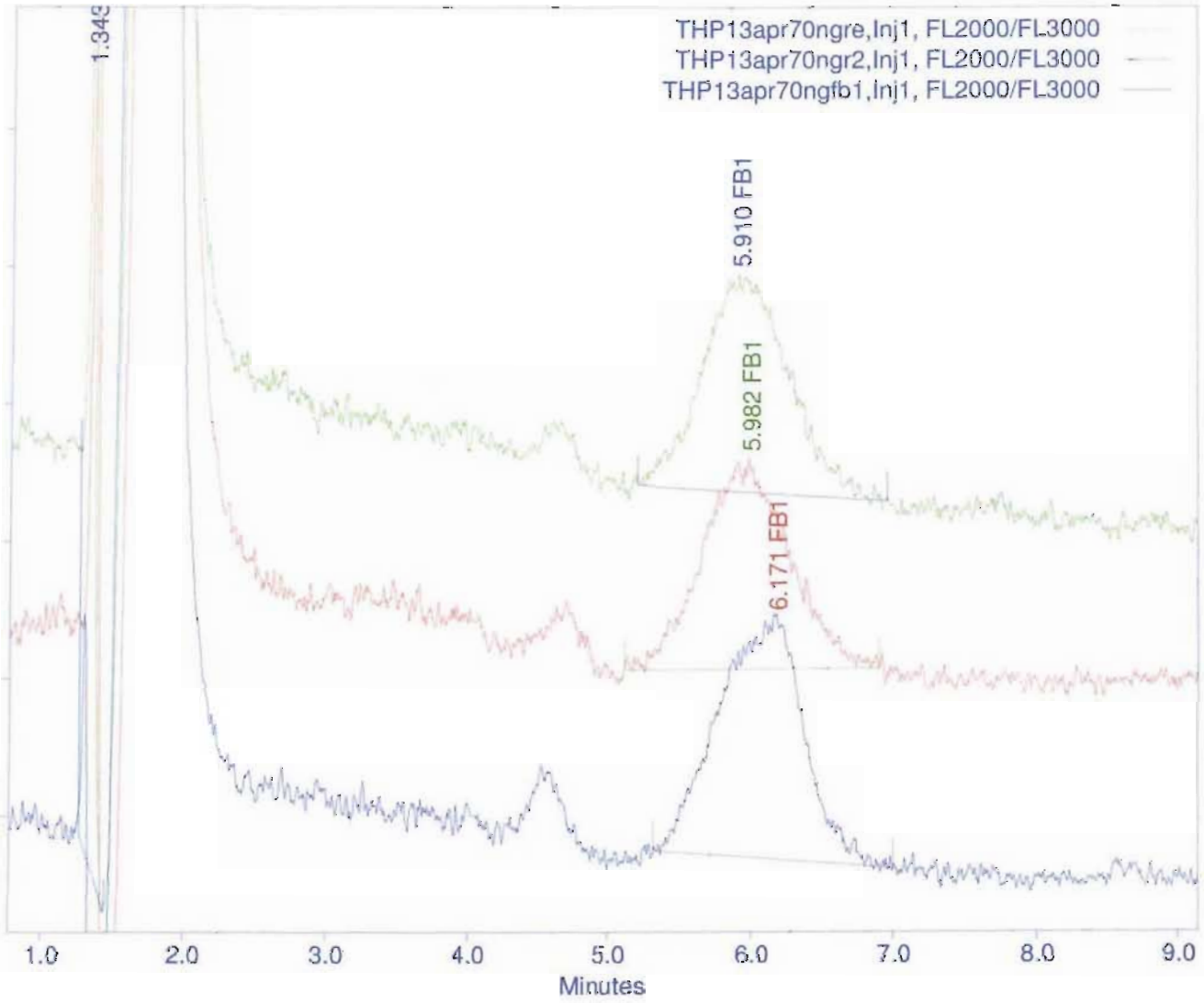

Figure 7.2: High performance liquid chromatograms of three injections of FB_1 (70 $ng.ml^{-1}$) showing reproducibility of the retention times.

Stockenström *et al.*, 1994), but require monitoring of the pH of the sample extract (above pH 5.8 for adequate retention on the SAX cartridge), and careful control of elution flow rates at less than 1ml.min^{-1} for reproducible recoveries (Sydenham *et al.*, 1992).

To optimise the method of extraction of FB_1 from human sera, the procedure outlined below was followed. Serum from a healthy female volunteer was used for determination of recoveries of FB_1 from spiked serum. Serum (500µl) was spiked with 200ng of FB_1 in acetonitrile: water (1:1, v/v) and processed according to the method of Shephard *et al.* (1992) analysed by HPLC for FB_1 and the result was used for calculation of the percent recovery.

Briefly, spiked serum samples were vortexed and incubated at RT for five minutes to ensure complete mixing of FB_1 into the sample. To the remaining 500µl aliquot of each sample, 100µl of acetonitrile: water (1:1; v/v) was added and these samples served as controls and were used to monitor baseline levels of FB_1. Both non-spiked and spiked samples were extracted and derivatised using the method described in section 7.2.2.3.

In order to determine whether the toxin was being lost or poorly retrieved, the original multi-step extraction procedure was applied with spiking of serum samples with 200ng FB_1 at various points along the isolation procedure (Figure 7.3a). All tests were done in duplicate and run parallel to non-spiked controls.

- Serum samples (Figure 7.3a, NA1 and NA2) were spiked prior to the addition of MeOH to the serum, and vortexed vigorously. This was to establish whether FB_1 was completely extracted with methanol, and whether any toxin was trapped in the protein precipitate.
- The supernatants from the serum samples were spiked following centrifugation, pelleting, and removal of the protein precipitate (Figure 7.3a, NB1 and NB2). This was to determine whether the column was efficient in binding all the FB_1 applied, and whether the elution mixture was strong enough and sufficient in volume to elute the total FB_1. Fumonisin B_1 was added directly to the supernatant and then applied to the prepared column.
- The elution reagent (i.e., 5% acetic acid in MeOH) used for serum samples (Figure 7.3a, NC1 and NC2) was spiked prior to the drying step. This was to determine

whether toxin was being degraded during heating and drying of the sample. The results of these analyses are shown in Table 7.1.

The HPLC chromatograms obtained from each of the duplicate samples (i.e., NA1, NB1, NC1 and ND1) are shown in Figure 7.3b.

Table 7.1: Quantitative determination of recoveries of fumonisin B_1 from serum samples spiked as indicated in Figure 7.3a and shown in Figure 7.3b.

Method	% FB_1 recovered (Mean ± SD)
Samples were spiked with FB_1 prior to addition of MeOH to the serum (Figure 7.3a, NA1+NA2)	33.3 ± 4.8
The MeOH supernatants from the serum samples were spiked with FB_1 prior to application to SAX column (Figure 7.3a, NB1+NB2)	94.4 ± 2.3
Sample supernatants were spiked with FB_1 after elution from the SAX column, directly into elution solvent and prior to drying on the heating block (Figure 7.3a, NC1+NC2)	98.1 ± 2.3

These results indicate that major losses (~70%) in recovery of FB_1 from samples occurred at the first step of the multi-stepped isolation procedure (Table 7.1). This implies that the protein pellet may have retained a major proportion of FB_1 that the samples were spiked with. Although there were losses in the subsequent steps of the procedure, they were minimal in comparison to the initial step. These results also indicate that the SAX cartridge was not overloaded with sample, since high recoveries were obtained in subsequent steps (Table 7.1). The next step in the optimisation procedure was therefore to increase the volume of MeOH used to extract the serum from 5ml to10ml, in an attempt to increase the recoveries of FB_1 from the sample.

In the subsequent set of analyses, duplicate serum samples (500µl) were spiked with 200ng FB_1 and a double extraction of the protein pellet was carried out. The effect of diluting the serum with an equal volume of water was also assessed as indicated in Table 7.2. The supernatant was removed after the initial pelleting stage; the pellet was re-extracted with 5ml MeOH, vortexed thoroughly and re-centrifuged. The pooled supernatant was then carried through steps 6 to 8 in the remaining unmodified method outlined in Figure 7.1.

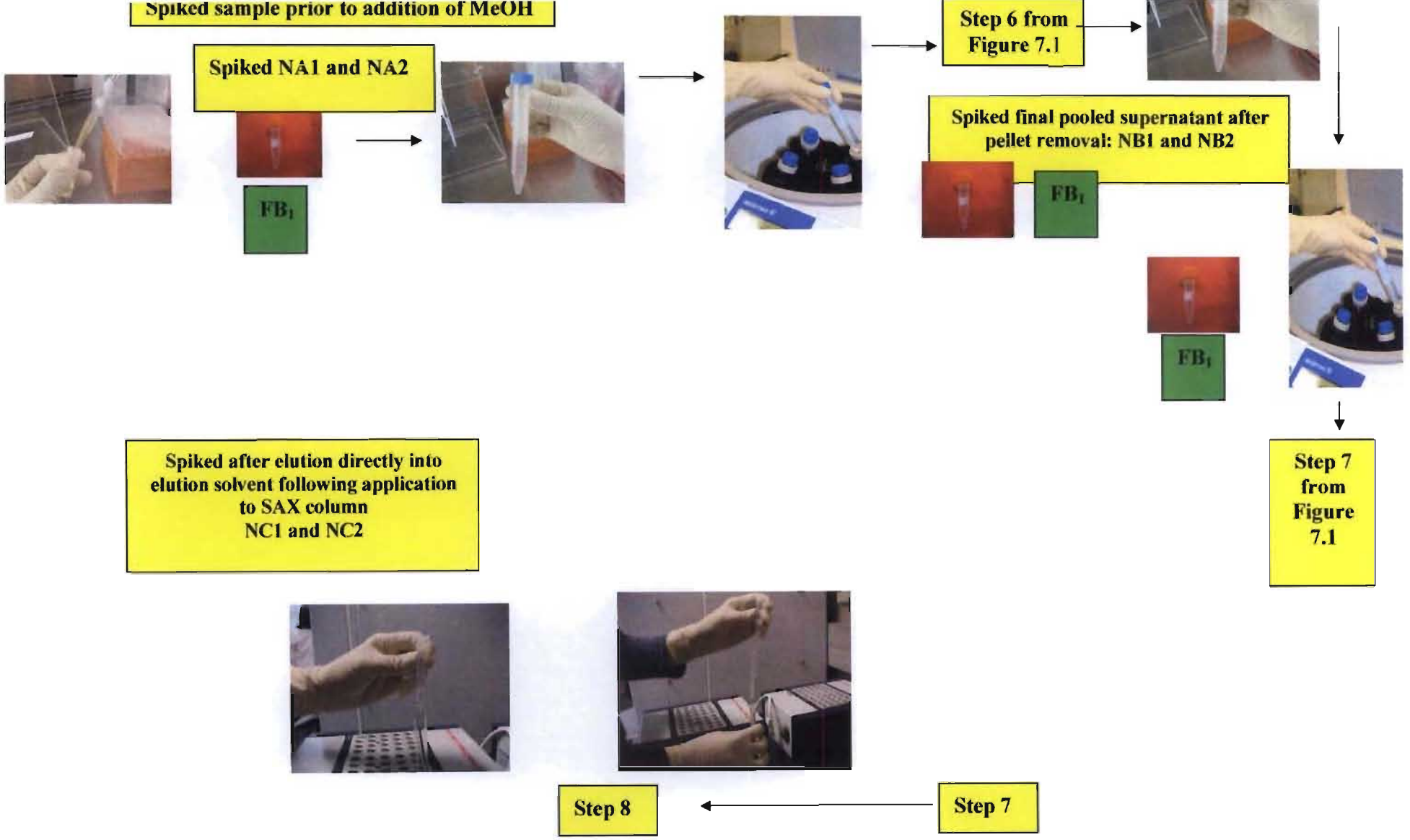

Figure 7.3a: Spiking of serum samples at selected steps for optimisation of extraction of Fumonisin B_1

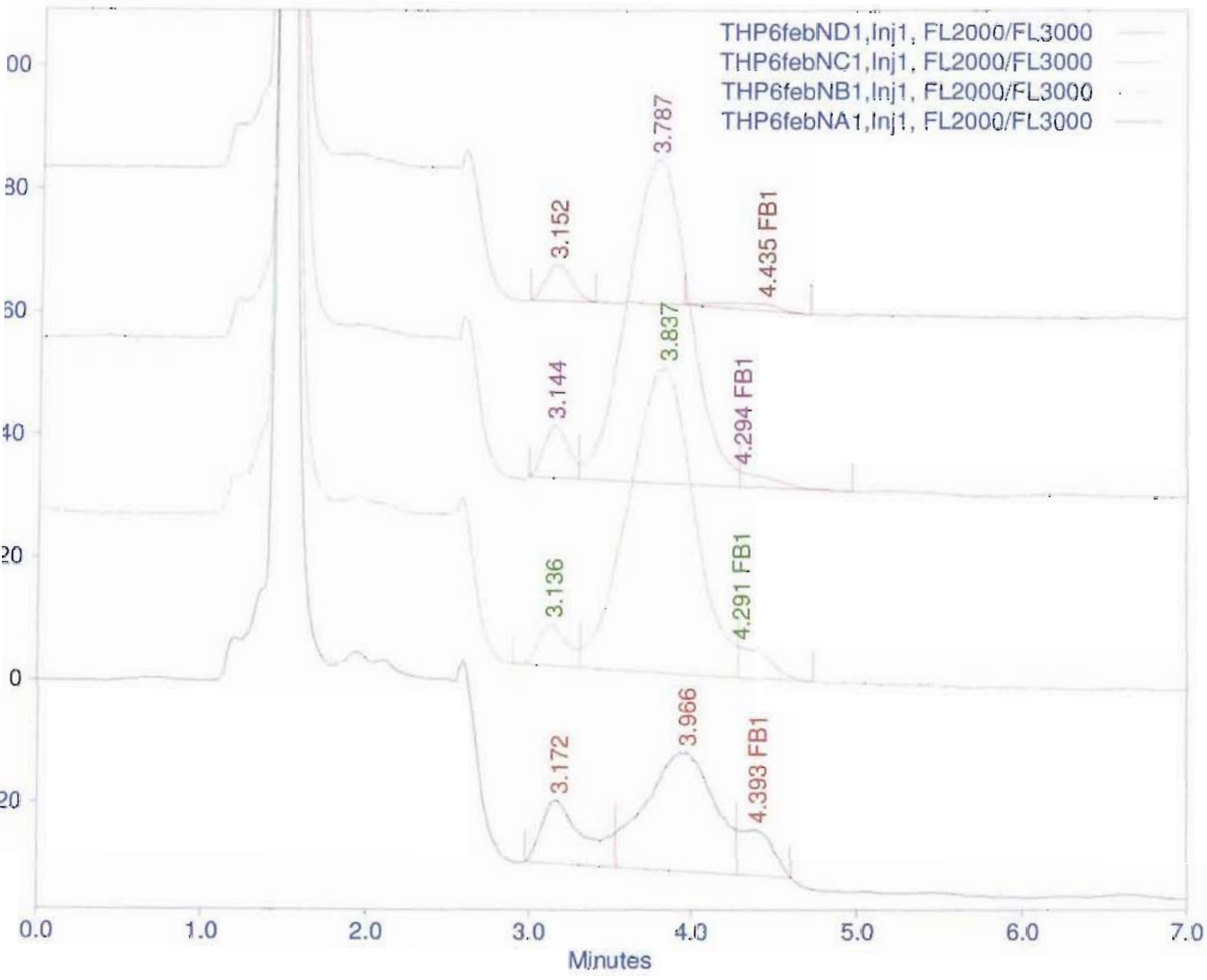

Figure 7.3b: High performance liquid chromatograms of serum samples spiked with Fumonisin B_1 shown with retention times of ~3.8-3.9 minutes.

The results in Table 7.2 and Figure 7.4 indicate that the highest recoveries of 40.2±0.1% FB_1 were obtained by dilution of the serum with 500µl deionised water, followed by extraction with two 5ml volumes of methanol. However, recoveries were only marginally above the previous recoveries of 33% (Table 7.1) and still below 50%. An additional problem with the chromatographic method was that elution of another compound close to the retention time (RTi) of FB_1 made graphical integration, and interpretation of data difficult. This is shown in Figure 7.4 by the pink trace (Sample NF1) where a compound with a RTi of 3.2 min. eluted very close to FB_1 (green trace, RTi of 3.3 min.).

Table 7.2: Quantitative determination of recoveries of fumonisin B_1 from spiked serum samples that were diluted with water.

Method	% FB_1 recovered (Mean ± SD)
500µl spiked serum samples were diluted with 500µl deionised water and extracted twice with 5ml MeOH per extraction	40.2 ± 0.1
Undiluted spiked 500µl serum samples were extracted twice with 5ml MeOH per extraction	28.8 ± 3.2
250µl serum samples were spiked with 100ng FB_1 and diluted with 250µl deionised water. The samples were extracted twice with 5ml MeOH per extraction	27.7 ± 5.3

Having established that dilution of the serum improved recoveries, further optimisation involved increasing the volume of water used in dilution of the serum (Table 7.3), and boiling the serum sample prior to extraction. As the use of two 5 ml volumes of MeOH for the extraction of FB_1 improved the recoveries from 33.3±4.8% (Table 7.1) to 40.2±0.1% (Table 7.2), this modification to the method was retained. Since decreasing the volume of serum from 500µl to 250µl, and diluting with 250µl water did not improve recoveries, the use of 500µl serum for all further analyses was kept constant.

With the next set of samples, the supernatant was removed after the initial pelleting stage, and the pellet was re-extracted with 5ml MeOH, vortexed thoroughly and re-centrifuged (Table 7.3). The supernatants were pooled and then taken through steps 6 to 8 as in the method description. The results of these modifications are shown in Table 7.3. These samples were spiked with 200ng FB_1 and vortexed thoroughly to ensure proper mixing prior to dilution of the serum (Table 7.3).

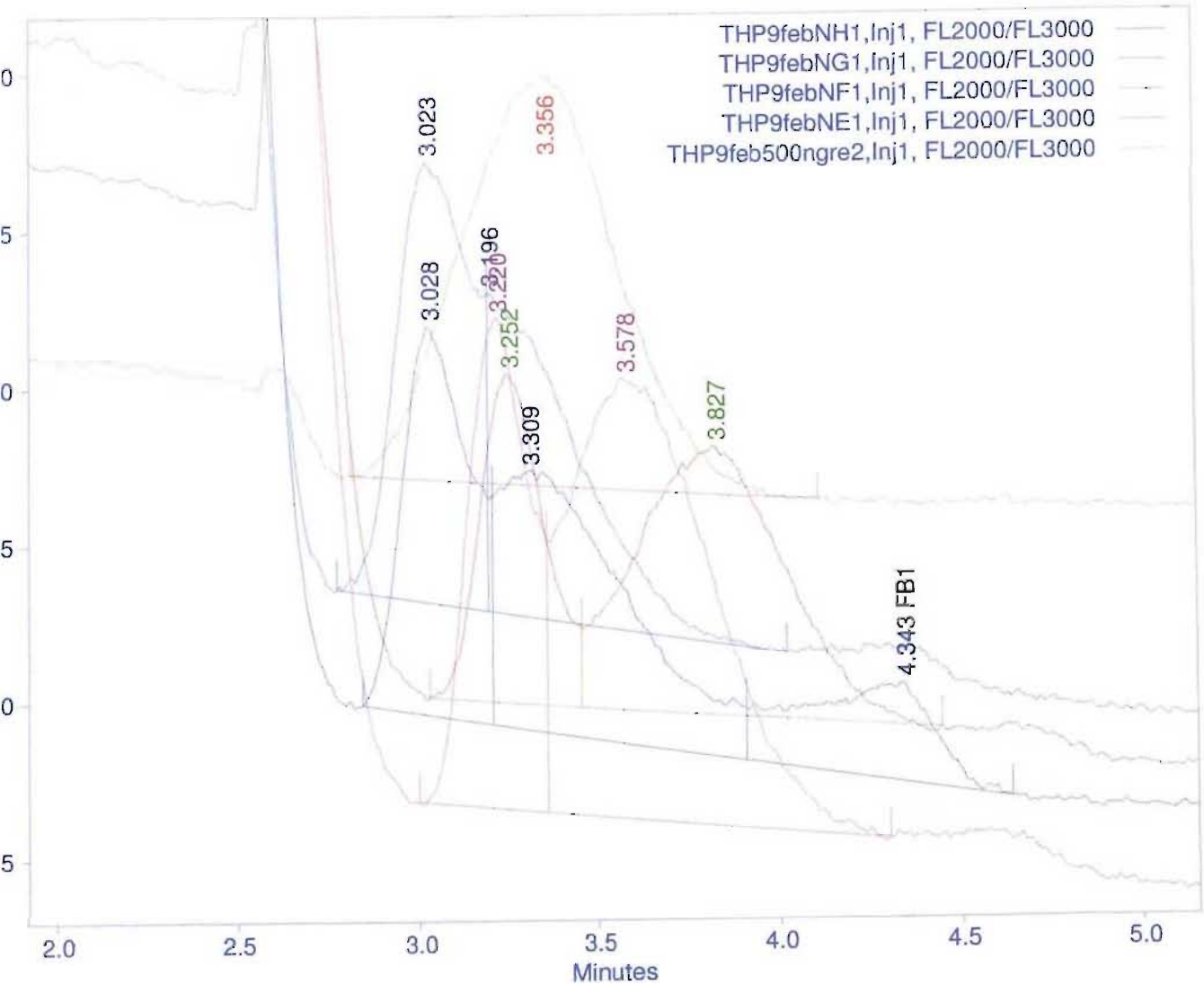

Figure 7.4: High performance liquid chromatograms of spiked serum samples showing a compound with a retention time of 3.2 min. eluting very close to Fumonisin B_1

The results in Table 7.3 and Figure 7.5 indicate that dilution of the serum sample with 2ml of water improved (shown by the green trace, sample NL1) recoveries of FB_1 to 48.8±7.4%, with further improvement to 52.0±3.0% by boiling of the sample prior to extraction (as indicated by the purple trace, sample NQ1 in Figure 7.5). Increasing the volume of water to 4ml in the dilution, prevented passage of the sample through the SAX column due to blockage of the column packing. This was possibly due to saturation of the column packing with the matrix impurities.

Table 7.3: Quantitation of recoveries of fumonisin B_1 obtained from spiked serum samples diluted with increasing volumes of water.

	Volume of diluent	% FB_1 recovered (Mean ± SD)
Dilution of 500µl spiked serum samples (n=2) with:	500µl deionised water (blue trace NJ in Figure 7.5)	38.3 ± 0.02
	1ml deionised water (red trace NK in Figure 7.5)	25.7 ± 10.8
	2ml deionised water (green trace NL Figure 7.5)	48.8 ± 7.4
	4ml deionised water	Not completed[1]
	2ml deionised water, and boiling in water bath 100°C for 15 minutes. Samples were cooled to RT and MeOH was added to precipitate proteins and extract FB_1 (purple trace NQ in Figure 7.5)	52.0 ± 3.0

[1] Samples were not completely analysed since samples blocked the SAX column. The samples were thus discarded.

In addition, it was found that the protein precipitate did not pellet well. As a result, all centrifugation stages were carried out in the refrigerated ultracentrifuge. These chromatograms also indicate the increasing difficulty experienced with graphical integration and analyses, as co-eluting compounds were evident (Figure 7.5). Fumonisin B_1 has an approximate RTi of ~3.4 min. (Figure 7.5).

To improve the precipitation of proteins out of the serum samples, ice cold MeOH was used. Following addition of MeOH, samples were refrigerated for 15 min. to maximize precipitation of serum proteins. Samples were also vortexed at five-minute intervals during the 15 minutes, to ensure more thorough extraction of FB_1 from the sample.

Biden *pers comm.* (2001) found that for antibody work, extraction of serum with PBS (pH 7.2-7.4) gave good recoveries when the serum sample was diluted with an equal volume of PBS, and then boiled for 15 minutes. The use of PBS was modified in this study by combining water and PBS in different ratios and using it in dilution of the serum samples prior to extraction (Table 7.4). In these modifications, serum (500µl) was spiked with 200ng FB_1 and then boiled in a water bath for 15 minutes in sealed polypropylene centrifuge tubes in different volumes of PBS or deionised water. The suspensions were

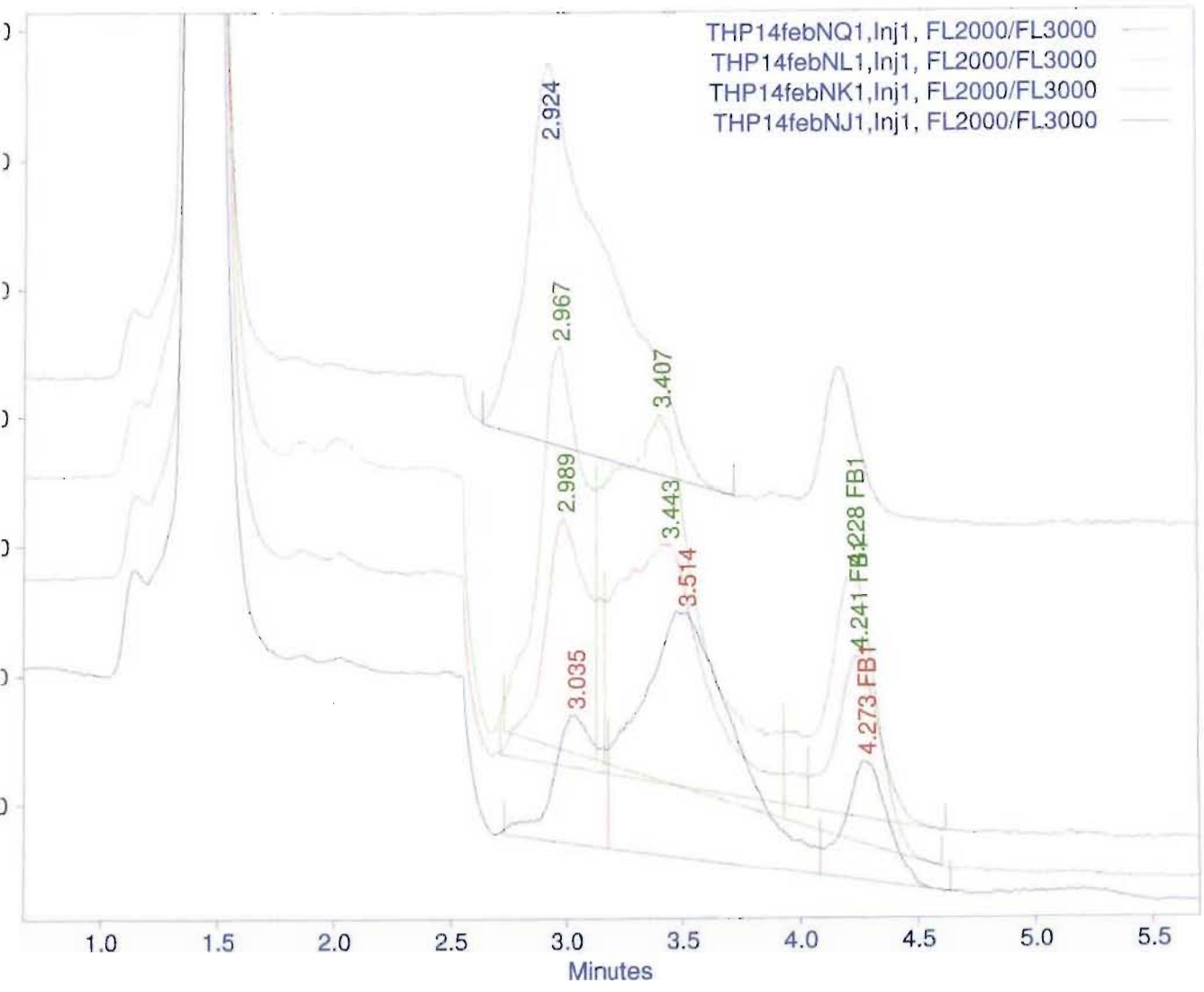

Figure 7.5: High performance liquid chromatograms of spiked serum samples indicating improved recoveries of Fumonisin B_1 following dilution and boiling of the serum samples

cooled to RT and 5ml ice-cold methanol was added to precipitate the proteins. The suspensions were vortexed thoroughly and then centrifuged to pellet the protein precipitate (1200g, 10°C, 10 min.). The PBS: MeOH supernatants were transferred to new centrifuge tubes (15ml), and the pellets were resuspended in another 5ml ice cold methanol, vortexed once more to ensure extraction of any residual FB_1 within the protein pellets and re-centrifuged (1200g, 10°C, 10min.).The supernatant was pooled with the previously retained supernatant, and this total supernatant was then applied to a pre-conditioned SAX cartridge.

Table 7.4: Recovery of fumonisin B_1 from diluted and boiled spiked serum samples.

	Volumes of diluent	% FB_1 Recovered (Mean ± SD)
Dilution of 500µl spiked serum samples (n=2) with:	1ml deionised water	58.9 ± 3.4
	1.5ml deionised water	55.9 ±10.1
	2ml deionised water	64.7 ± 6.3
	1ml PBS	55.3 ± 14.8
	1.5ml PBS	69.5 ± 9.8
	2ml PBS	89.4 ± 0.4

The results in Table 7.4 indicate that maximum recoveries of 89.4±0.4% were obtained by boiling the serum samples in PBS. Although the recoveries were greatly improved, modification and improvement on the retrieval of FB_1 brought with it the problem of compounds eluting very close to FB_1. Samples processed according to the modified method showed additional chromatographic peaks interfering with quantitation of FB_1 making graphical integration, and quantitation more difficult.

Boiling of spiked serum samples with 2ml PBS improved recoveries substantially (Table 7.4) therefore further optimisation of the extraction was not pursued. The reproducibility of the modified method was determined on replicate serum samples following spiking with 200ng, 300ng and 400ng FB_1 dissolved in MeOH. These results are summarized in Table 7.5 (Appendix 7.1). The mean recovery from the 15 serum samples spiked with FB_1 was 95.8% (Table 7.5).

Table 7.5: Recoveries of different concentrations of fumonisin B_1 used to spike 500µl serum samples.

Amount of FB_1 used	Recovery of FB_1 ($ng.ml^{-1}$)	% FB_1 Recovery (Mean ± SD)
200ng (n=4)	413.5 ± 41.1	103.4 ± 10.3
300ng (n=5)	552.1 ± 57.3	92.0 ± 9.6
400ng (n=6)	735.5 ± 52.5	91.9 ± 6.5
Mean (n=15)		**95.8%**

This method was considered suitably optimised for application to the serum of brain cancer patients and the non-cancer human subjects (data in Chapter 9). Shephard *et al.* (1992) reported recoveries of 86% for FB_1 in serum. However, the samples in that study contained much higher concentrations of fumonisins, namely 1.4µg.ml^{-1} and 6.2µg.ml^{-1} in spiked serum samples. In this study, samples were spiked with 200, 300 and 400ng FB_1 per 500µl of serum indicating improved sensitivity of this extraction method with recoveries of between 85-105% (Table 7.5). The excess 5% could be attributed to analytical error or the presence of FB_1 in the serum prior to spiking. Shephards' *et al.* (1992) method gave detection limits of about 50ng.ml^{-1} with a signal to noise ratio of 4:1. This study improved on detection limits to approximately 5ng.ml^{-1} at a signal to noise ratio of 5:1.

It is possible that boiling of the serum samples with PBS prior to deproteinization, facilitated unravelling of the coiled protein structure exposing the side groups and allowing release and hence retrieval of higher amounts of FB_1. The large amount of polar impurities detected indicated that the clean-up procedure for the serum samples was not optimally efficient. In the present study, the method of Coumi (2000) was further optimised for recoveries and purity of the samples analysed. The boiling of the serum sample with PBS, and the double extraction of the protein pellet with MeOH did improve the efficiency of recoveries of FB_1, but as with Coumi (2000) problems where still experienced with the large amount of impurities in the column. These impurities affected the analytical HPLC column by excessive absorption onto the stationary phase. It was therefore necessary to use a guard column to prevent system blockage and reduction of column efficiency. Reproducibility of RTi was dramatically affected by integrity of the guard column. Thus, the guard column had to be changed and cleaned regularly which slowed down the analytical procedure.

The identity of the FB_1 peak from serum samples was confirmed by comparison with a chromatogram of the FB_1 standard, and every three sample runs were normally bracketed by running a FB_1 standard with comparison of the RTi (±3.4 min.). Figure 7.6 shows chromatograms of serum samples from three non-cancer volunteers, as well as that of a FB_1 standard. As can be seen varying levels of FB_1 were detected in non-cancer controls. The complete quantitative data set of the analyses of sera from brain-cancer and non-cancer participants in this study are presented and discussed in Chapter 9.

7.4 METHOD DEVELOPMENT FOR DETERMINATION OF SPHINGANINE AND SPHINGOSINE LEVELS IN HUMAN SERA

The second part of this study focussed on the optimisation of methods for Sa and So isolation and analysis from sera of non-cancer and brain cancer subjects, as the Sa:So ratio has been proposed to be suitable as a biomarker for FB_1 exposure.

7.4.1 Modification and application of the method of Kwon *et al.* (1998) for extraction of free Sa and So from human sera

Firstly, the method of Kwon *et al.* (1998) originally used on brain and spinal cord tissue, was assessed for applicability to determination of Sa and So in sera. Briefly, the method involved ultrasonication of 500µl spiked serum (Table 7.6) with 2ml 50mM potassium phosphate buffer (pH 7.0; for 10 sec.) in a 15ml polypropylene screw capped vial. The samples were vortexed thoroughly and 0.5ml 0.1M borate buffer (pH 13.1) and 4ml $CHCl_3$: MeOH (9:1, v/v) were added. The solutions were vortexed and then centrifuged for 8 min. at 600g at 4°C. The $CHCl_3$ layer was transferred into a glass scintillation vial and evaporated to dryness under nitrogen gas at 37°C. The vials were shaken for five minutes, then centrifuged following addition of 0.4 M borate buffer (pH 4.4) (500µl) and 3ml n-hexane to the residue. The hexane layer was removed and discarded by suction. Potassium hydroxide (10M) (40µl), followed by 4ml $CHCl_3$: MeOH (2:1, v/v) was added to the aqueous layer, and the mixture was shaken. The organic layer was rinsed with 0.1M borate buffer (pH 10.5) and evaporated. All samples prepared according to this method and subsequent methods were derivatised prior to HPLC analysis, and analysed as described in sections 7.4.2 and 7.4.3.

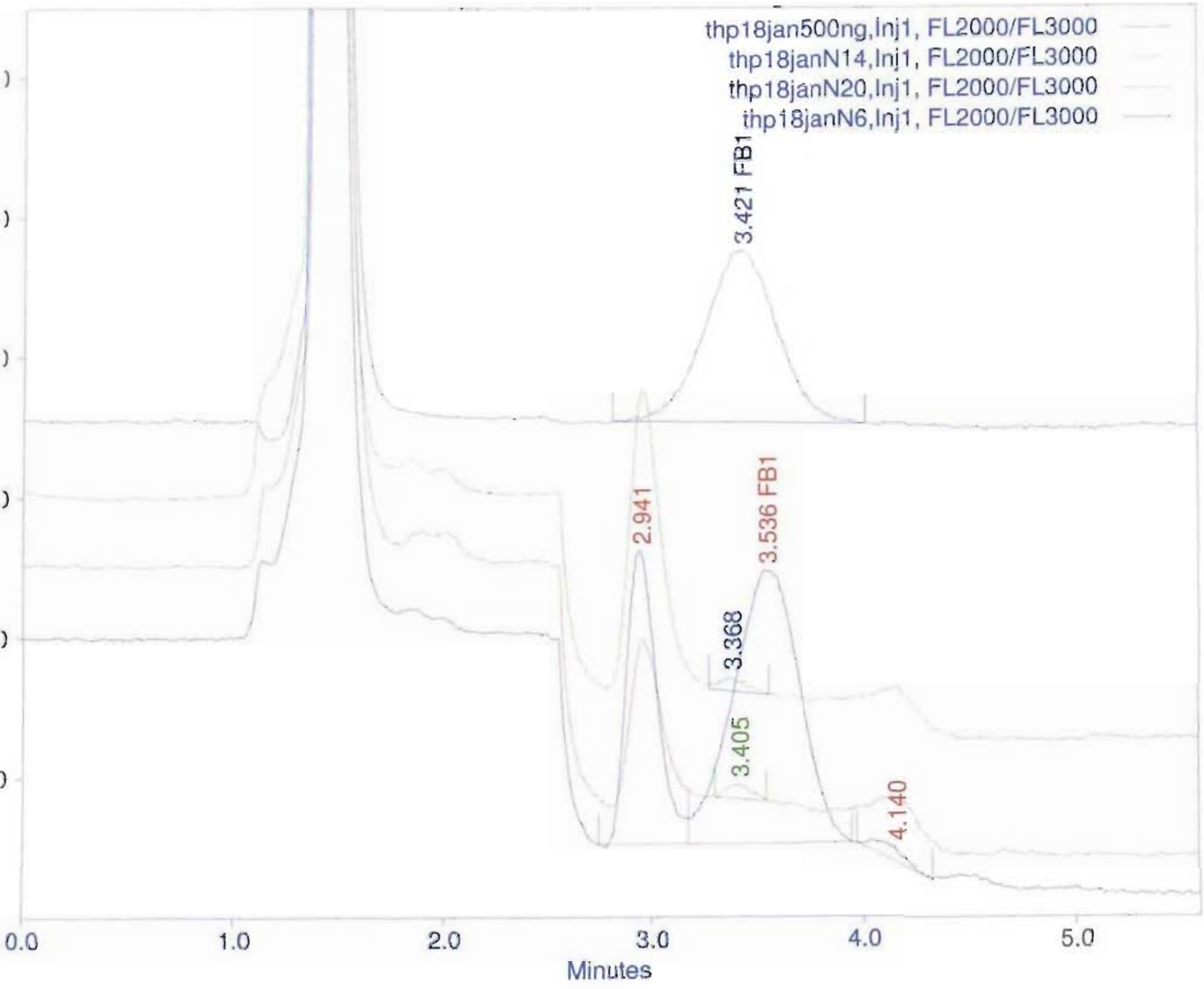

Figure 7.6: High performance liquid chromatograms of varying levels of Fumonisin B_1 isolated from the sera of non-cancer subjects (N6, N20 and N14; blue, red and green traces respectively). Also shown by the uppermost blue trace blue is the FB_1 standard at a concentration of 500ng.

7.4.2 Derivatisation of sphingoid bases for high performance liquid chromatographic analysis

The OPA reagent was prepared by dissolving 15mg of OPA in 600µl of MeOH, followed by the addition of 7.5ml of 0.1M disodium tetraborate (adjusted to pH 10.5) and 20µl of 2-mercaptoethanol. This reagent was stored in the dark at RT during use and prepared fresh daily. The sample extract was suspended in 250µl MeOH by ultrasonication for one minute and incubated for 15 min. at RT. The solution was derivatised by addition of 50µl OPA reagent, ultrasonicated for one minute, and then incubated at RT for a further 15 min. The samples were then filtered through a nylon microfilter (0.22µm pore size) into 200µl inserts placed in 2ml autosampler vials. Refrigerated samples were stable for at least 24 hours when stored in the dark.

7.4.3 High performance liquid chromatographic analysis of the sphingolipid derivatives

A Waters NovaPak C_{18} cartridge (4µm, 150 x 3.9mm) (Waters, Microsep, SA) preceded by a HIRPB-10C guard column (Hichrom Ltd., Set Point Instruments, SA), was used for separation of sphingolipids. The temperature of the column was maintained at 35°C. Fluorescence detection was employed for the analysis of the OPA derivatives, with excitation wavelength 230 nm and emission wavelength of 440nm.

Reverse phase HPLC analysis of the samples were carried out under gradient elution conditions (flow rate 1ml.min^{-1}) using 0.07M K_2HPO_4 buffer: MeOH (1:9) as Solvent A and MeOH as Solvent B. The HPLC method was based on that of Castegnaro *et al.* (1998). The gradient elution profile was modified to reduce the total run time from 1 hour to 22 minutes. The new gradient elution profile is shown in Table 7.6.

Table 7.6: Programme of gradient elution for high performance liquid chromatographic analysis of sphinganine and sphingosine.

Time (min.)	Solvent A % 0.07 M K_2HPO_4: MeOH (1:9)	Solvent B % MeOH
0	100	0.0
12.00	88	12
17.00	100	0
22.00	100	0

All solvents were degassed in the ultrasonic bath prior to use. All samples were injected in duplicate (injection volume 50µl). Standard solutions of Sa and So were run daily to verify column performance, stability of the OPA reagent, as well as the RTi and response factors for both Sa and So.

7.4.3.1 Preparation of calibration curves for both sphinganine and sphingosine

A concentration range between 75 and 1000µg.ml^{-1} gave linear area/amount responses for both Sa and So. Injections of 50µl derivatised sample standards were performed in duplicate to confirm reproducibility. Data collected was processed using PC1000 software (Thermo Separation Products, Set Point Instruments, SA). Peak area was used to quantify the concentration of Sa and So present by taking the relevant dilution factor into account.

7.4.4 Results of the extraction method of Kwon *et al.* (1998) for sphinganine and sphingosine from sera

For these analyses, two 500µl serum samples were spiked at three concentrations of Sa and So as outlined in Table 7.7. In all the analyses the Sa and So were resuspended in methanol. The samples were vortexed vigorously to ensure proper mixing and then the method outlined in 7.4.1 was followed. In the chromatographic analyses of these samples, each derivatised sample was injected in duplicate . Hence for each concentration of spiking evaluated, a mean of the 2 injections of duplicate samples was taken and these results summarized (Table 7.7). This method of evaluation was applied to all the results shown in Table 7.7 onwards unless otherwise indicated.

Table 7.7: Results of the application of the method of Kwon *et al.* (1998) for extraction of free Sa and So from spiked serum samples.

Spiking levels of the 500µl serum samples (ng)		% Recovery (Mean ± SD)	
So	Sa	So	Sa
100	100	10.4 ± 0.5	4.9 ± 0.5
200	200	6.7 ± 0.98	3.3 ± 0.2
300	300	6.0 ± 2.0	3.7 ± 1.6

Using this method, So recoveries of between 6 and 11%, and Sa recoveries of between 3 and 6% were obtained. The method did not provide reproducible results. It is possible

that this method modified the exogenous Sa and So making retrieval difficult. For these reasons, the method of Kwon *et al.* (1998) was not pursued any further.

7.5 APPLICATION OF THE METHOD OF VAN DER WESTHUIZEN *et al.* (2001) ON SERUM SAMPLES

van der Westhuizen *et al.* (2001) reported a method for the determination of Sa and So in serum and urine. Since very low recoveries were obtained with previously published methods, this method was applied to determine its suitability for adequate retrieval of Sa and So from spiked serum samples. Briefly the method described was documented as that of Riley *et al.* (1994c) with minor modifications. Lipids were extracted from the serum (500µl) by incubation with 4ml MeOH: $CHCl_3$ (2:1) (containing 0.01% butylated hydroxytoluene as an antioxidant) under nitrogen at 37°C for one hour. Thereafter, the mixture was washed twice with alkaline water (Appendix 7.2) (~pH 8.6), the phases separated by centrifugation and the $CHCl_3$ fraction dried under nitrogen gas below 40°C. The residue was hydrolysed to release the free bases by redissolving it in 0.1M methanolic potassium hydroxide (KOH): chloroform ($CHCl_3$) (4:1, v/v) and incubation at 37°C for one hour. After washing with alkaline water, the $CHCl_3$ phase was dried under nitrogen at a temperature below 40°C. The dried residues were stored at -20°C overnight. Prior to analysis, residues were redissolved in 250µl MeOH, sonicated and derivatised with 50µl OPA reagent prepared as described previously.

For these analyses, duplicate 500µl serum samples were spiked with Sa and So as outlined in Table 7.8. The samples were vortexed vigorously to ensure proper mixing, and then the method outlined above was applied. In the chromatographic analyses of these samples, each derivatised sample was injected in duplicate . The recoveries of Sa and So from these samples are shown in Table 7.8.

Table 7.8: Recoveries of sphinganine and sphingosine from spiked serum samples processed according to van der Westhuizen *et al.* (2001).

Spiking levels of the 500µl serum samples (ng)		% Recovery (Mean ± SD)	
So	Sa	So	Sa
100	100	15.3 ± 0.3	5.3 ± 0.1
200	200	17.7 ± 0.1	7.1 ± 0.2

These results indicate that using the method of van der Westhuizen *et al.* (2001) although it was an improvement from retrievals based on the method of Kwon *et al.* (1998) (Table 7.7), was not efficient based on the low recoveries of Sa and So (Table 7.8). In addition, the levels of Sa retrieved were at least three times lower than the levels of So. This indicated that separate optimisation would first be required for increasing retrieval of Sa, before the overall method could be optimised. This method was not pursued any further, and instead the method of Shephard and van der Westhuizen (1998) was applied to the next set of serum samples.

7.6 APPLICATION OF THE METHOD OF SHEPHARD AND VAN DER WESTHUIZEN (1998) FOR RETRIEVAL OF SPHINGANINE AND SPHINGOSINE FROM HUMAN SERUM SAMPLES

The method of Shephard and van der Westhuizen (1998) was investigated for the efficiency of recovery of So and Sa. Briefly, duplicate serum samples (500µl) were spiked with 100, 200 and 300ng each of Sa and So dissolved in MeOH (Table 7.9). Serum was deproteinised with 2ml MeOH in 15ml polypropylene tubes, and the protein precipitate was pelleted after vortexing in a refrigerated centrifuge (1200g, 10 min. at 10°C). An aliquot of the supernatant (2 ml) was mixed with distilled water (H_2O) (1.9 ml) and 0.35M ammonium hydroxide (NH_4OH) (1.2ml) and extracted with 4ml $CHCl_3$. After vigorous vortexing, the layers were separated by centrifugation (1200g, 10 min., 10°C) and a portion of the lower $CHCl_3$ layer (3ml) was transferred to a silica minicolumn prepared in a 6ml polypropylene cartridge with a lower layer of 0.5g of silica 60 (40-63µm particle size) and an upper layer of powdered anhydrous sodium sulphate (5g). The minicolumn was pre-conditioned with 4ml $CHCl_3$. After loading the sample, the minicolumn was washed with $CHCl_3$ (1ml), and Sa and So were eluted with $CHCl_3$: MeOH: concentrated NH_4OH (20:20:0.8, v/v), 5ml. The eluate was dried under N_2 gas at 38°C.

The dried residue was resuspended by ultrasonication in 0.125M KOH (1ml) in MeOH: $CHCl_3$ (4:1, v/v) and incubated at 37°C for 1.5 hours. After cooling on ice, $CHCl_3$ (1ml) was added and the solution was washed with alkaline water (dilute NH_4OH; ~pH 8; 5 ml). The phases were separated by centrifugation (1200g, 10 min at 10°C), and the lower $CHCl_3$ layer was dried under nitrogen gas at approximately 38°C.

The sample extract was redissolved in 250µl MeOH by ultrasonication for one minute and incubated at RT for 15 minutes. The solution was derivatised by addition of 50µl OPA reagent, ultrasonicated for one minute, and incubated at RT for a further 15 minutes. As in all previous analyses, the samples at each concentration of spiking evaluated were injected in duplicate and a mean of four injections of duplicate samples were taken. These results are summarized in Table 7.9.

Table 7.9: Recoveries of sphinganine and sphingosine from spiked serum samples prepared according to Shephard and van der Westhuizen (1998).

Spiking levels of the 500µl serum samples (ng)		% Recovery (Mean ± SD)	
So	Sa	So	Sa
100	100	10.0 ± 0.1	12.5 ± 3.1
200	200	8.9 ± 3.4	7.5 ± 1.6
300	300	13.3 ± 3.1	15.0 ± 1.9

The results in Table 7.9 show that average recoveries of between 7% and 16% for So and Sa were obtained respectively (Table 7.9). This indicates an improvement on recoveries obtained using other methods applied in this study. As relatively equal amounts of Sa and So were retrieved at this stage, separate optimisation steps for retrieval of either Sa or So individually were not required. Shephard and van der Westhuizen (1998) reported 53% and 55% recoveries of the sphingoid bases, however recoveries obtained in this study were considerably lower (Table 7.9). This was initially considered to be potentially due to use of a powdered instead of granular anhydrous sodium sulphate bed as recommended by Shephard and van der Westhuizen (1998), since this was the only variable that was inconsistent with the published method. The experiment was therefore repeated with the granular sodium sulphate bed suggested in the original method. These results were summarized in Table 7.10.

Table 7.10: Recoveries of sphinganine and sphingosine from spiked serum samples carried out according to the method of Shephard and van der Westhuizen (1998) using a granular sodium sulphate bed.

Spiking levels of the 500µl serum samples (ng)		% Recovery (Mean ± SD)	
So	Sa	So	Sa
100	100	18.6 ± 4.3	14.7 ± 2.5
200	200	23.4 ± 3.3	10.1 ± 0.8
300	300	13.7 ± 0.6	6.9 ± 1.8

The use of the granular sodium sulphate bed slightly improved recovery of So to between 13-26%, but did not significantly improve on Sa recoveries (5-17%). These recoveries however, still did not approach the 50-55% recoveries documented by Shephard and van der Westhuizen (1998). As the sodium sulphate bed improved recoveries initially, alternate beds with similar chemical properties were substituted (Table 7.11), and the remaining steps of the method were unmodified. In the first instance, a magnesium sulphate bed was substituted for the anhydrous sodium sulphate bed. These results are presented in Table 7.11.

Table 7.11: Recoveries of sphinganine and sphingosine from spiked serum samples carried out according to the method of Shephard and van der Westhuizen (1998), but using a magnesium sulphate bed.

Spiking levels of the 500µl serum samples (ng)		% Recovery (Mean ± SD)	
So	Sa	So	Sa
100	100	38.7 ± 13.8	17.6 ± 0.3
200	200	10.6 ± 4.5	4.5 ± 0.1
300	300	15.5 ± 3.5	9.9 ± 2.5

There was a negligible increase in recoveries to between 10-40% for So, and between 4-18% for Sa by substituting a magnesium sulphate bed (5 grams) for a sodium sulphate bed. However, taking the poor reproducibility between duplicate samples into consideration as indicated by the large SD, the use of this magnesium sulphate bed was not pursued further.

Subsequently, a calcium chloride ($CaCl_2$) bed was substituted for the anhydrous sodium sulphate and the method repeated. In this instance, the sample preparation was made difficult by the $CaCl_2$ bed becoming soggy, the sample clogging the bed and not passing through the column easily. Only two (of 10) samples passed through the column and were run on HPLC, clogged the guard column and prevented further running of the samples (data not shown). The use of the $CaCl_2$ bed was therefore not pursued further.

As this stage a different approach was introduced to achieve the optimal recoveries of Sa and So from serum. Taking into account the nature of the sample preparation procedure, a protocol similar to that applied for the optimisation of the FB_1 isolation was followed, and the samples were spiked at each step of the isolation procedure to establish at exactly which stage the major losses occurred (Figure 7.7, A-F; Table 7.12).

All 500µl serum samples were spiked with 200ng Sa and 200ng So at the specific stages of the isolation procedure outlined in Table 7.12 and Figure 7.7, and then processed through the rest of the isolation procedure. Duplicate samples were run for each stage of spiking, and these samples were injected in duplicate into the HPLC for analyses. The results are summarized in Table 7.12.

Addition of 2ml MeOH to 500µl serum (A) with vortexing for 30 sec.

↓

Centrifugation at 1200g for 10 min at 10°C
(B)

↓

Vortexing of 2ml aliquot of total supernatant + H_2O (1.9ml)+ 0.35M NH_4OH (1.2 ml)

↓

Extraction of total supernatant with 4 ml $CHCl_3$
(C)

Mixing/vortexing thoroughly (30 sec.)

↓

Separation by centrifugation at 1200g for 10 min at 10°C

↓

Retention of lower $CHCl_3$ layer for application to minicolumn

***

LOADING OF SAMPLE ONTO PREPARED MINICOLUMN

Loading and passing 3ml of retained $CHCl_3$ extract through column
(D)

↓

Washing column with 1ml $CHCl_3$

↓

Elution with 5 ml $CHCl_3$: MeOH: concentrated NH_4OH (20:20:0.8, v/v) (E)

↓

Drying of eluate under N_2 gas (~38°C).

↓

Ultrasonication of residue in 0.125 M KOH (1ml) in MeOH: $CHCl_3$ (4:1, v/v)

↓

Incubation at 37°C for 1.5 hours (F)

↓

Cooling on ice, $CHCl_3$ (1ml) was added

↓

Washing of solution with alkaline water (Dilute NH_4OH, ~pH 8 (5ml))

↓

Separation of phases by centrifugation at 1200g, 10 min at 10°C

↓

Drying of lower $CHCl_3$ layer under N_2 gas at 38°C in glass vial

Figure 7.7: Isolation of sphinganine and sphingosine from serum according to Shephard and van der Westhuizen (1998).

Table 7.12: Quantitative analyses of serum samples spiked with sphinganine and sphingosine at different stages of the isolation procedure to determine where losses occurred.

Methodology		% Recovery ± SD	
		So	Sa
Serum samples were spiked prior to deproteinization at Step1, Figure 7.7 **(A)**[1]		22.9 ± 1.9	16.8 ± 1.2
The supernatant was spiked after deproteinization at step **(B)**		33.9 ± 6.9	20.5 ± 8.3
The supernatant was spiked after extraction with $CHCl_3$ at step **(C)**. This supernatant was not vortexed with the sodium sulphate bed but:	passed directly through the prepared 0.5g silica bed	29.3 ± 0.7	17.3 ± 0.1
	passed through the prepared 1g silica bed	21.4 ± 3.6	11.9 ± 3.0
The supernatant was spiked after extraction with $CHCl_3$ at step **(C)**. The supernatant was vortexed with the 0.5g sodium sulphate bed, prior to passing the $CHCl_3$ layer:	through the prepared 0.5g silica bed	25.2 ± 1.1	14.4 ± 1.0
	prepared 1g silica bed	14.8 ± 6.2	11.3 ± 5.3
The supernatant was spiked after extraction with $CHCl_3$ and passing through column at step **(D)**. The sodium sulphate bed was removed completely and the column:	was not washed with $CHCl_3$. The sample was then eluted from column	12.4 ± 1.5	17.0 ± 3.1
	was washed with 1ml $CHCl_3$. The sample was then eluted from column.	14.9 ± 3.1	14.1 ± 1.9
The elution agent was spiked at step **(E)** after passing through the column.		18.5 ± 1.7	18.9 ± 0.5
The resuspended ultrasonicated residue was spiked after the 1.5 hour incubation at 37°C stage at step **(F)**		10.7 ± 7.2	14.3 ± 8.4

Spiking at each step of the isolation procedure revealed that significant losses occurred throughout the method (Table 7.12). Modification of the method involved vortexing the sample in the recommended weight of sodium sulphate directly, and following centrifugation to separate the bed and sample, the resultant supernatant was passed through the prepared silica column.

The initial steps of the procedure were targeted for optimisation. The volume of MeOH used in deproteinization and extraction of the initial serum sample was doubled from two to four millilitres in the first step. The supernatant was diluted with 1%KCl in 1.9ml water and 1.2ml 0.35M NH_4OH, or 1.9ml water and 1.2ml 0.35M NH_4OH. Following elution with 5ml $CHCl_3$: MeOH: concentrated NH_4OH solution (20:20:0.8, v/v), a further 2.5ml

[1] A-F are graphically illustrated in Figure 7.7 where the samples were spiked at a specific stages in the isolation procedure to determine where losses of Sa and So occurred.

MeOH or 2.5ml $CHCl_3$ was passed through the minicolumn (Table 7.13) to improve elution. In addition, the sodium sulphate bed was removed completely since recoveries improved in its absence. Reference has been made to steps in Figure 7.7 in Table 7.13 to aid description of the methodology.

Duplicate samples were run for each highlighted stage where the methodology was changed, and each sample was injected in duplicate into the HPLC for analyses. These results are summarized in Table 7.13.

Table 7.13: Optimisation of steps in the method of Shephard and van der Westhuizen (1998) for retrieval of sphinganine and sphingosine from spiked serum samples.

Methodology		Solvent X	% Recovery (Mean ± SD)	
			So	Sa
The supernatant was diluted in 1%KCl in 1.9ml water and:	1.2 ml 0.35M NH_4OH at step **(B).** Following elution with 5ml $CHCl_3$: MeOH: concentrated NH_4OH (20:20:0.8, v/v) at step **(E)** (Figure 7.7), **Solvent X** was passed through the column	2.5 ml MeOH.	18.4 ± 1.0	15.5 ± 0.4
		2.5 ml $CHCl_3$	30.3 ± 0.1	27.00 ± 0.1
		7ml ethyl acetate	15.8 ± 1.6	5.4 ± 0.1
The supernatant was diluted in 1.9ml water and:		2.5 ml MeOH	6.0 ± 0.001	4.3 ± 0.1
		2.5 ml $CHCl_3$	4.4 ± 0.2	3.1 ± 0.02
		7ml ethyl acetate	16.1 ± 3.2	5.1 ± 0.3

These analyses (Table 7.13) indicate that:

- increasing the volume of methanol for deproteinization of the serum from 2 to 4ml,
- dilution of the entire volume of supernatant in a solution of 1%KCl in 1.9ml water and 1.2ml NH_4OH at step **(B)** (Figure 7.7);
- and eluting Sa and So from the column with 5ml $CHCl_3$: MeOH: concentrated NH_4OH (20:20:0.8, v/v), followed by 2.5ml $CHCl_3$ improved recoveries to 30% for So, and 27% for Sa. The use of ethyl acetate as the elution reagent was not pursued further as it resulted in significantly lower levels of recoveries of So and Sa..

Because boiling the serum in PBS improved recoveries of FB_1, the effects of boiling the samples at step (A) (Figure 7.7) prior to the addition of MeOH to the serum sample was also investigated on Sa and So recoveries. All samples in Table 7.14 were boiled for 15 minutes prior to extraction. The 500µl serum samples used in these analyses were spiked only with So at three concentrations (Table 7.14), the reason being that as relatively equal amounts of Sa and So were retrieved using the method optimised to this stage, in order to minimise costs, only So was used in the spiking. References were made to steps in Figure

7.7 to aid description of the methodology. The quantitative results of the duplicate samples analysed for each highlighted stage where the methodology was changed are summarized in Table 7.14.

Table 7.14: Effects of boiling serum samples on the recovery of sphingosine.

Spiking level of the 500µl serum samples with So (ng)	Methodology	Solvent X	% So recovery (Mean ± SD)
100	The spiked serum sample was boiled at step (A) for 15 minutes prior to extraction. In addition, following elution with 5ml $CHCl_3$: MeOH: concentrated NH_4OH (20:20:0.8, v/v) at step **(E)**, (Figure 7.7), **Solvent X** was passed through the column	2.5 ml MeOH	10.6 ± 0.9
		2.5 ml $CHCl_3$	18.4 ± 0.1
200		2.5 ml MeOH	27.0 ± 1.5
		2.5 ml $CHCl_3$	6.1 ± 0.5
300		2.5 ml MeOH	15.3 ± 0.3
		2.5 ml $CHCl_3$	11.3 ± 0.2

No significant improvements on recoveries were noted. A maximum of 27% of the So was retrieved following boiling of the spiked sera. Elution with an additional volume of MeOH improved retrieval of So from samples spiked with 200 and 300ng So (Table 7.14). As boiling of sera was not pursued further in the optimised method however, this step was not included in the optimisation procedure to retrieve Sa and So.

To determine whether smaller volumes of serum could be used in these analyses, 300µl of serum was diluted with 200µl 1%KCl in distilled water, to establish whether dilution of the serum would be appropriate in the optimisation and application of this method (Table 7.15). All samples in Table 7.15 were spiked with 200ng Sa and 200ng So. To further determine whether increasing the concentration of KCl would improve recoveries, samples were incubated with 1%, 3% or 5% KCl in the required 1.9 ml distilled water and 1.2ml 0.35M NH_4OH at step (B) in Figure 7.7 for 5 minutes prior to extraction. The use of the crystalline anhydrous sodium sulphate bed was also reassessed.

Table 7.15: Effects of increasing concentrations of KCl in the sample diluent and the use of the sodium sulphate bed on retrieval of sphinganine and sphingosine from 300µl spiked serum samples.

Methodology	x % KCl		% Recovery (Mean ± SD)	
			So	Sa
The supernatant was diluted in x % KCl in 1.9ml water and 1.2 ml 0.35M NH_4OH at step (B).	1	The sample was passed through the minicolumn containing the crystalline anhydrous sodium sulphate bed	19.1 ± 0.4	16.6 ± 0.1
	3		32.3 ± 0.2	33.4 ± 0.2
	5		18.3 ± 0.2	17.9 ± 0.1
	1	The sample was passed through the pre-conditioned minicolumn where the crystalline anhydrous sodium sulphate bed was omitted	14.5 ± 0.1	16.0 ± 0.4
	3		65.6 ± 8.0	36.9 ± 4.9
	5		29.6 ± 0.7	30.4 ± 0.6

These analyses indicate that removal of the crystalline anhydrous sodium sulphate bed, dilution of 300µl serum with 200µl 1%KCl in water up to 500µl, and use of 3%KCl in the 1.9ml of water improved recoveries of So and Sa to 65.6% and 36.9%, respectively although high SDs were evident (Table 7.15). Figure 7.8 shows the chromatograms of Sa and So retrieved from a non-spiked sample (NSa 79 shown by the dark blue chromatographic trace) in contrast to the spiked sample that showed 65.6% and 36.9% recovery (shown by the NSa 84 red chromatographic trace), for So and Sa respectively.

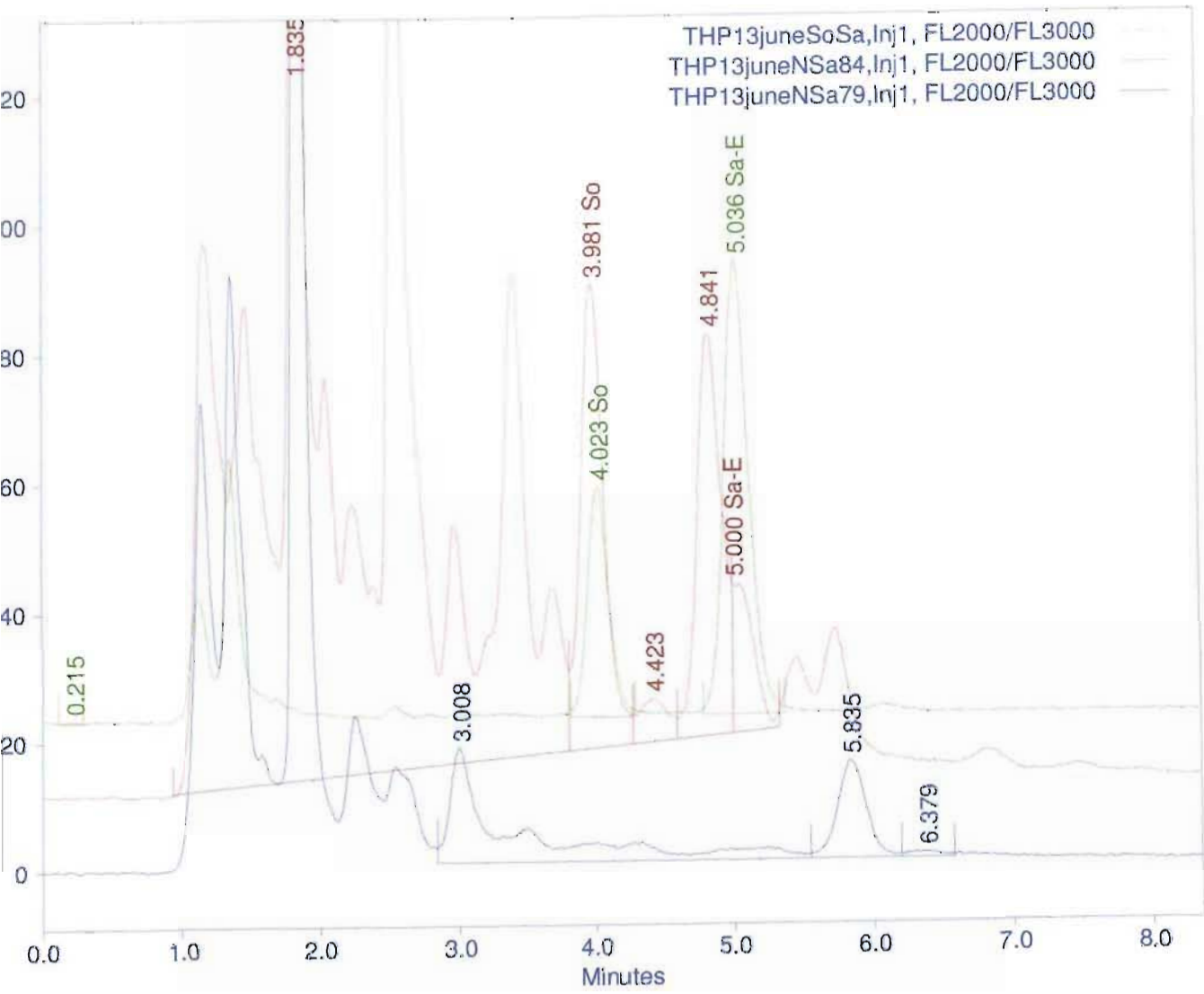

Figure 7.8: High performance liquid chromatograms of sphinganine and sphingosine isolated from the spiked sera of a non-cancer subjects (NSa 79 and 84, blue and red traces respectively) seen in association with the Sa and So standards (green trace).

For the next set of analyses, the volume of serum used reverted to 500µl (Table 7.16). All samples shown in the next table were spiked with 200ng Sa and 200ng So.

Table 7.16: Effects of 1% and 3%KCl in the sample diluent and the use or omission of the sodium sulphate bed on retrieval of sphinganine and sphingosine from spiked 500µl serum samples.

Methodology		% Recovery (Mean ± SD)	
		So	Sa
The supernatant was diluted in 1%KCl in 1.9ml water and 1.2 ml 0.35M NH_4OH at step **(B)**. The sample was passed through the pre-conditioned minicolumn:	containing the crystalline anhydrous sodium sulphate bed	7.7 ± 0.3	6.4 ± 0.3
	where the crystalline anhydrous sodium sulphate bed was omitted	23.5 ± 3.3	22.7 ± 1.7
The supernatant was diluted in 3%KCl in 1.9ml water and 1.2 ml 0.35M NH_4OH at step **(B)**. The sample was passed through the pre-conditioned minicolumn:	containing the crystalline anhydrous sodium sulphate bed.	23.6 ± 0.1	21.7 ± 1.0
	where the crystalline anhydrous sodium sulphate bed was omitted	29.5 ± 1.1	29.4 ± 0.4

The samples that were passed through the minicolumn where the anhydrous sodium sulphate bed was omitted, and 1.9ml 3% aqueous KCl was used, were found to give better recoveries of 29.5% and 29.4% of So and Sa respectively (Table 7.16).

It is likely that some level of absorption of Sa and So to the sodium sulphate bed occurred, resulting in losses of the sphingoid bases at this stage of the isolation procedure. This set of analyses led to the removal of the anhydrous sodium sulphate bed in all subsequent optimisation procedures. In the next set of samples, spiking with 200ng So only (Table 7.17) was carried out, for the same reason as given earlier in the discussion of Table 7.14. In the next set of analyses different solvent combinations were tested to determine when the maximum levels of retrieval would be achieved. Reference has been made to steps in Figure 7.7 in Table 7.17 to aid in description of methodology.

The results in Table 7.17 indicate that extraction of the sera spiked with 200ng So, with 2ml methanol and 2ml acetonitrile by successive resuspension and extraction of the pellet improved the recoveries of So to 51.2%. Large standard deviations between duplicate samples were noted however (Table 7.17). Although using 2ml acetonitrile to extract the spiked Sa and So from the serum samples did improve recoveries, it was not reproducible. For this reason, the use of 4ml methanol as an alternative step to improve recoveries was pursued, but by double extraction with 2 x 2ml portions of this solvent.

Table 7.17: Determination of the effects of different solvents extraction efficiency for sphingosine from spiked serum samples.

Methodology	Solvent X		% So recovered (Mean ± SD)
Protein was precipitated from spiked 500µl serum samples with **Solvent X** at step **(A)**.	2ml MeOH. The supernatant was removed and the pellet was re-extracted with 2ml acetonitrile to extract the So from the pellet.	The sample was recentrifuged as in step (B), the supernatants were pooled and taken through the rest of the optimised method.	51.2 ± 7.2
	4 ml acetonitrile		28.3 ± 0.7
	4 ml MeOH		39.7 ± 13.7
	4 ml isopropanol		22.6 ± 5.8

In the next set of analyses, 500µl serum samples were spiked with both 200ng So and 200ng Sa. The sample supernatants were diluted in 3.8ml 3% aqueous KCl and 2.4ml 0.35M NH_4OH at step (B) in Figure 7.7. The volumes of the KCl diluent and NH_4OH were increased to compensate for dilution effects as the volumes of the solvents used in the extraction were increased. Samples were extracted by vortexing for longer periods (~2 minutes per sample) in the methanol and acetonitrile extraction reagents being assessed. Duplicate samples were run for each highlighted stage where the methodology was changed (Table 7.18), and each sample was injected in duplicate into the HPLC for analyses. The quantitative analyses are summarized in Table 7.18.

The results presented in Table 7.18 indicate that that double extractions of the spiked serum samples with methanol increased recoveries to 67% and 34.2%, for So and Sa respectively. The inclusion of acetonitrile in the extraction procedure did not improve the extraction to any significant degree. However a concern was that the recoveries of Sa were not as consistently high as those of So indicating different affinities of the two sphingoid bases to the solvents (Table 7.18). All subsequent samples were therefore spiked with both Sa and So to monitor the recoveries of sphingoid bases.

Since the double extraction with MeOH improved recoveries, the MeOH extraction was repeated with an increased volume of MeOH to 3ml per extraction with resuspension of the pellets twice. The 500µl serum samples were spiked with 200ng So and 200ng Sa and the supernatant was diluted in 3%KCl in 3.8ml deionised water and 2.4 ml 0.35M NH_4OH, and taken through the rest of the optimised method. After elution at step (E) (Figure 7.7) 2ml

chloroform was also passed through the column. Recoveries noted were 62.6±7.8% for So and 38.1±1.6% for Sa respectively, indicating minimal improvement in recoveries.

Table 7.18: Assessment of methanol and acetonitrile as extraction reagents for sphinganine and sphingosine recoveries from spiked serum samples.

Methodology	Solvents used			% Recovery (Mean ± SD)	
	Solvent X	Solvent Y	Solvent Z	So	Sa
The 500µl spiked serum samples were extracted with 2ml MeOH at step **(A)** (Figure 7.7). The sample was re-centrifuged as in step **(B)**, the supernatant was retained and the pellet was re-extracted with **Solvent X**. The sample was re-centrifuged, the pellet re-extracted with **Solvent Y** and the supernatants pooled. The sample was re-centrifuged once more, and after a final extraction of the pellet with an additional **Solvent Z**, the supernatant was pooled. The total supernatant was diluted in 3%KCl in 3.8ml water and 2.4ml 0.35M NH_4OH at step (B), and taken through the rest of the optimised method.	2ml MeOH	-	-	67.0±0.5	34.2± 0.02
	2ml acetonitrile	2ml MeOH	-	24.1±0.4	15.4±0.2
	2ml acetonitrile	2ml MeOH	2ml acetonitrile	15.6±0.3	7.8±0.2

In the next set of analyses, duplicate 500µl serum samples were spiked with Sa and So, and extracted twice with either 3ml or 4ml volumes of methanol (Table 7.19). The total volume of supernatant was used in the extraction procedure, and mixed with distilled H_2O containing 3.8ml potassium chloride and 3.6ml 0.35M ammonium hydroxide. These results are summarized in Table 7.19.

Table 7.19: Efficiency of the double extraction of sphinganine and sphingosine from spiked serum samples with increasing volumes of methanol.

Methodology	Sa and So (ng)	Solvent (ml)	% Recovery (Mean ± SD)	
	X	Y	So	Sa
The 500µl serum samples spiked with **X**ng So and **X**ng Sa were extracted with **Y**ml MeOH at step **(A) in Figure 7.7**. The supernatant was removed and the pellet was re-extracted with **Y**ml MeOH to extract the Sa and So from the protein pellet. The sample was re-centrifuged as in step **(B)** and the supernatants pooled The total supernatant was diluted in 3%KCl in 3.8ml water and 3.6ml 0.35M NH_4OH at step **(B),** and taken through the rest of the optimised method. After elution at step **(E)**, 2ml chloroform was passed through the column.	200	3ml	50.0 ± 1.6	31.3 ± 0.4
		4ml	16.8 ± 1.9	11.4 ± 0.5
	100	3ml	55.3 ± 3.7	31.5 ± 1
		4ml	23.4 ± 1.1	13.0 ± 0.4
	150	3ml	31.2 ± 4.6	17.9 ± 1.7
		4ml	25.5 ± 0.8	12.2 ± 10.2
	50	3ml	70.6 ± 15.4	40.7 ± 4.8

These results indicate that better recoveries were consistently obtained using two 3ml volumes of MeOH at all concentrations of spiking (Table 7.19). To optimise this method further still, extraction of the serum samples with the same total volume of methanol, but decreased volumes of the solvents per extraction repeated to increase retrieval and extraction of Sa and So were used (Table 7.20). Duplicate 500µl serum samples were used, and the methanol supernatant (6ml) was mixed with distilled H_2O containing 3.8ml 3%KCl and 3.6ml 0.35M NH_4OH. The difference from the results in Table 7.19 was that instead of using two 3ml volumes of methanol in the extraction, three 2ml volumes of methanol were used. These results are summarized in Table 7.20.

These results indicate that that the triple extraction of the spiked serum samples with methanol improved retrieval of Sa and So significantly (Table 7.20). When carrying out these extractions, the time that the samples were vortexed with methanol was increased to about two minutes per sample to ensure maximal extraction. These results are an improvement on the results presented in Table 7.19 where double methanol extractions with larger volumes of methanol were used. This shows that significant losses of sphingoid bases occur during the protein extraction step.

Table 7.20: Effects of triple methanol extraction on the retrieval of sphinganine and sphingosine from spiked serum samples.

Methodology	Spiking with Sa and So (ng)	% Recovery (Mean ± SD)	
	X	So	Sa
500µl serum samples spiked with both **X**ng So and **X**ng Sa were extracted with 2ml MeOH at step **(A)(Figure 7.7).** The supernatant was removed and the pellet was re-extracted with 2ml MeOH to extract the Sa and So from the protein pellet. The sample was re-centrifuged as in step **(B) (Figure 7.7)**, the pellet was re-extracted with 2 ml MeOH and the supernatants pooled. After a final extraction of the pellet with an additional 2ml acetonitrile the pooled supernatant was diluted in 3%KCl in 3.8ml water and 3.6ml 0.35M NH_4OH at step **(B)**, and taken through the rest of the optimised method. After elution at step **(E) (Figure 7.7)**, 2ml chloroform was passed through the column	200	50.1±2.1	33.5±1.0
	150	47.4±0.8	30.3±0.1
	100	41.7±7.0	25.6±1.1
	50	72.6±12.6	41.04±3.3
	30	67.9±5.51	54.20±2.3
	20	52.5±6.7	53.2±2.2
	10	77.9±1.3	85.0±1.5

These results also indicate that with a decrease in the level of spiking of the samples to 10ng, there was an increase in recovery of sphingoid bases to 78% for So and 85% for Sa, indicating that the lower the concentration of spiking in the sample, the better the recovery (Table 7.20). This possibly indicates that the solvent volumes used during the sample isolation were insufficient at the higher concentrations of spiking with Sa and So. The chromatograms in Figure 7.9 shows the recoveries of selected samples from Table 7.20.

In Figure 7.9, the non-spiked sample is shown in comparison to spiked serum samples (i.e., trace NSa 192). Also shown are samples that were spiked with 50ng Sa and 50ng So, and then extracted with three 2ml volumes of methanol (i.e., traces NSa 189 and 190). In addition, serum that was spiked with 150ng Sa and 150ng So (i.e, trace NSa 195), and serum that was spiked with 200ng Sa and 200ng So (i.e., trace NSa 194), were extracted with two 3ml volumes of methanol is shown. Clearly, by visual comparison of the area under the peaks, there is an increase in the amount of Sa and So recovered with higher levels of spiking.

Further optimisation of this method was not pursued due to time constraints, and to the extensive costs involved in optimising the method for each specific concentration of

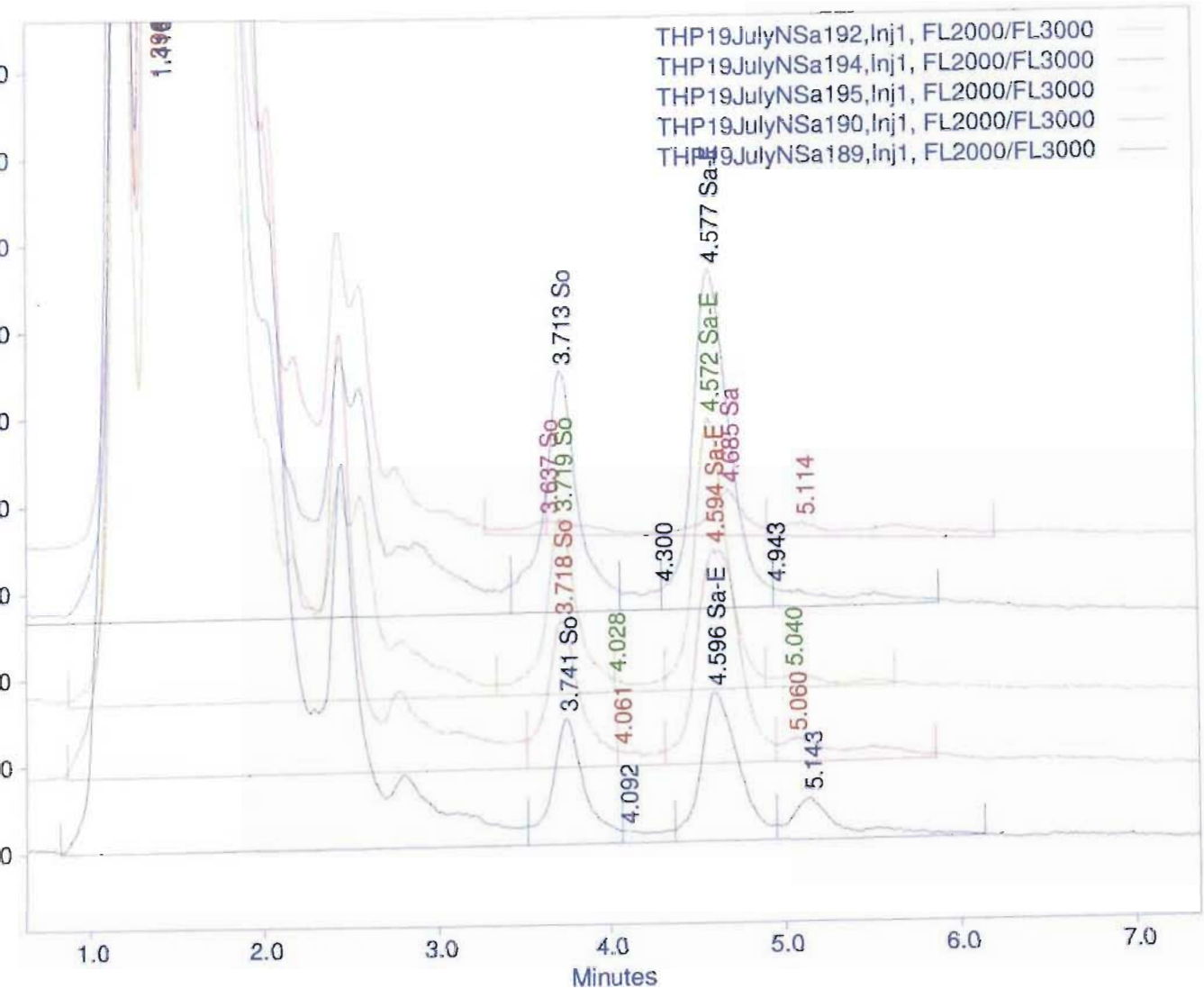

Figure 7.9: High performance liquid chromatograms of sera of a non-cancer subject spiked with increasing concentrations of recovered Sa and So standards. The traces shown are NSa 189 (blue), NSa 190 (red); Nsa 195(green), Nsa 194 (blue) and NSa 192(pink) from the bottom up.

spiking with the sphingoid bases. It was evident that there was significant improvement on the recoveries obtained at the initiation of the study (Table 7.9), where the method of Shephard and van der Westhuizen (1998) was used prior to optimisation. With the optimised method used in this study, recoveries of 72.6% and 41.0% for So and Sa respectively were obtained at a level of spiking with 50ng per 500µl of serum, and 77.9 and 85.0% at a level of spiking at 10ng per 500µl of serum.

The final optimised method applied in the isolation of Sa and So from the human serum samples is summarized below.

7.7 FINAL OPTIMISED METHOD OF RETRIEVAL OF SPHINGANINE AND SPHINGOSINE FROM HUMAN SERA

The 500µl serum sample was deproteinised with 2ml ice-cold MeOH in a 15ml polypropylene tube. The protein precipitate was pelleted by centrifugation (1200g for 10min. at 10°C) after vortexing for 2 minutes. The resultant pellet was resuspended in ice-cold 2ml methanol and re-extracted by vigorous vortexing for 2 minutes. The protein suspension was pelleted by centrifugation (1200g for 10min at 10°C), and the supernatant pooled with the retained 2ml methanol. The protein pellet was resuspended once again in 2ml ice-cold methanol and re-extracted by vortexing for 2 minutes. The centrifugation step was repeated (1200g for 10min. at 10°C) to obtain the methanol supernatant, which was then pooled with the previously retained 4ml methanol.

The 6ml methanol supernatant was combined with 3.8ml 3%KCl in distilled H_2O and 3.6ml 0.35M NH_4OH, and vortexed vigorously. This suspension was then extracted twice with $CHCl_3$ (2.5ml per extraction). Following vortexing, the layers were separated by centrifugation (1200g, 10min., 10°C) The $CHCl_3$ layers were pooled and retained for application to a minicolumn. The $CHCl_3$ layer (5ml) was transferred to a silica minicolumn prepared in a polypropylene cartridge with a layer of 0.5g of silica 60 (40-63µm particle size) that was placed on a bed of inert glass wool.

The minicolumn was pre-conditioned with 4ml $CHCl_3$. After loading the $CHCl_3$ extract, the minicolumn was washed with 1ml $CHCl_3$, and the Sa and So were eluted with 5ml $CHCl_3$: MeOH: concentrated NH_4OH (20:20:0.8,v/v). An additional 2ml $CHCl_3$ was

passed through the column into the 25ml scintillation vial. The eluate was dried in a fume cupboard under nitrogen gas at 38°C. The dried residue was redissolved by ultrasonication in 1ml 0.125M KOH in MeOH: $CHCl_3$ (4:1, v/v) and incubated at 37°C for 1.5 hours in a shaking water bath. After incubation, the samples were allowed to cool for 10min. on ice and 2.5ml $CHCl_3$ was added and vortexed thoroughly. An additional 1ml $CHCl_3$ was added and the mixture was vortexed thoroughly with 5ml alkaline water (dilute NH_4OH; ~pH 8). The phases were separated by centrifugation at 1200g for 10 min. at 10°C, and the lower $CHCl_3$ layer was removed and dried under a stream of nitrogen gas on a heating mantle (38°C). The dried residue was then ready for chromatographic analyses.

7.8 RESULTS AND DISCUSSION ON THE DEVELOPMENT OF THE METHODOLOGY FOR SPHINGANINE AND SPHINGOSINE RETRIEVAL FROM SPIKED SERUM

The applicability of published methods for the retrieval of exogenous and endogenous compounds, and hence their recoveries from physiological fluids between laboratories and within laboratories, is subjective. Under ideal conditions, one would be able to replicate an experiment under the exact conditions recommended in publications, but this is not always possible due to variability in research equipment and facilities. Often substitutions are made to create as closely as possible those ideal conditions suggested, but the standardization and calibration of machinery and purity and age of compounds used, differences in glassware and general hardware all add variability. All these factors require consideration when attempting to replicate experiments. Under ideal conditions, variation in results would be negligible and statistical differences would be minor. However, in the cases where percentage recoveries of the compounds of interest are not clearly indicated, this places a question on whether they were investigated, and on the reproducibility of methods. It was difficult to repeat published studies to an acceptable level, although as far as possible the experimental conditions were recreated and adhered to, and the routes of possible variation minimised. This part of the study dealt with the application of a few published methods to recover and quantify Sa and So from spiked sera.

As detailed in the optimisation procedures for retrieval of Sa and So above, samples were prepared using various published methods (Kwon *et al.*, 1998; van der Westhuizen *et al.*, 2001) but optimisation was primarily pursued on the method of Shephard and van der Westhuizen (1998) that was reported to yield 53-55% recoveries. The methods of

van der Westhuizen *et al.* (2001) and Kwon *et al.* (1998) on serum samples, although attempted, were not pursued due to the low recoveries obtained when applied in our labs (Tables 7.7 and 7.8).

Application of the method of Shephard and van der Westhuizen (1998) led to extensive optimisation to improve retrieval of So and Sa to an acceptable level. Unlike the published study, where an internal standard was used as a means to quantify recoveries of Sa and So, in the present investigation, quantitation was done based on external standards and by means of spiking with known quantities of Sa and So. It was believed that the use of C20 Sa internal standard could not serve as an adequate measure of recovery of So and Sa in the complex extraction procedure due to differences in solubility, and solvent affinity of all compounds. It was shown during this optimisation study that the recoveries achieved for Sa and So were often unequal depending on the extraction procedure being followed.

The optimisation procedures carried out in this present study increased the volumes of solvents, whilst omitting certain steps in the procedure. For example, the step involving passing the sample through the sodium sulphate bed was removed, as it was shown to reduce efficiency of retrieval of the sphingoid bases.

Attempts were made to reduce the suggested volume of serum used by dilution of 300µl serum with 1%KCl, since the subsequent step involved the use of potassium chloride diluted in deionised water. In many studies, obtaining adequate volumes of serum from patients for laboratory analyses usually is a problem. In this study, the attempt to minimise the volume of serum required led to large analytical errors. Dilution of samples was found to be inappropriate since although higher recoveries were initially obtained, the method was not reproducible between replicate samples. This led to subsequent standardization of the use of 500µl serum in the isolation procedure.

Optimisation of the method with extraction of the serum using smaller volumes of MeOH with repeated multiple extractions improved recoveries of Sa and So (Table 7.20). In the original method, serum samples were deproteinised with MeOH and after centrifugation, only a 2ml portion of the methanolic supernatant was used for the lipid extraction step with chloroform under alkaline conditions. Initial efforts by Shephard and van der Westhuizen (1998) to determine the ratio of the Sa and So in serum by direct application of the serum

to the silica minicolumn was unsuccessful, as the use of serum without prior deproteinization gave large chromatographic interferences. Therefore samples were deproteinised. The method in the present study differed from the method of Shephard and van der Westhuizen (1998) in that the entire volume of the methanolic supernatant was used in the subsequent steps. Although the use of the supernatant was considered to eliminate major interferences (Shephard and van der Westhuizen, 1998), these still remained.

A second step in the procedure that attempted to clean up the sample extract was the alkaline hydrolysis step of Shephard and van der Westhuizen (1998). This was placed after clean-up on the silica minicolumn, and cleaved acylglycerolipids and hydrolysed lysosphingolipids (free sphingoid bases modified at the hydroxyl group on carbon 1 of So or Sa) to release free So and Sa. The procedure yielded an extract suitable for chromatographic determinations of the ratio of the sphingoid bases.

Gaver and Sweeley (1965) documented that sphingolipid bases are extracted from hydrolysates with solvents such as diethyl ether, chloroform, ethyl acetate, or mixed solvents such as isoamyl alcohol in heptane. When a further 2.5ml $CHCl_3$ was passed through the column after the final elution stage (Tables 7.13 and 7.14); the Sa and So recoveries were improved by ~10%, in comparison to the addition of MeOH. These solvents were selected based on the fact that they were components of the elution reagent, and that Sa and So are soluble in these solvents. The use of ethyl acetate although attempted, was found to be inefficient in retrieval of Sa and So (Table 7.13).

The method was considered sufficiently optimised once recoveries of 72.6% and 41.0% for So and Sa respectively were obtained at a level of spiking with 50ng per 500µl of serum and 77.9% and 85.0% at a level of spiking at 10ng per 500µl of serum (Table 7.20). The reason that optimisation was not pursued any further was due to time constraints, and the fact that many months of work and high costs had already been invested to reach this level of recovery.

7.9 CONCLUSION

Several extraction methods for determination of FB_1, Sa and So from serum were assessed in this study. These published methods were not found to be as efficient as required in

retrieval of these compounds from spiked samples, and thus extensive optimisation procedures were pursued in order to obtain reproducible results with sufficiently high analyte recoveries. The HPLC analyses of sera described facilitated both qualitative and quantitative assessment of FB_1, Sa and So from the spiked samples. Major losses in recovery of FB_1, Sa and So occurred in the first protein extraction step and it have found that optimal retrieval was achieved with the use of smaller volumes of solvents, increased vortexing times, and triple extraction of the protein pellet with methanol for Sa and So. The recoveries observed in the individual sphingoid bases could be considered a function of the affinities for the solvents used.

With recovery of FB_1 from spiked sera, boiling of the sera followed by extraction with methanol enhanced retrieval of higher concentrations of this mycotoxin. The boiling of sera with PBS, and the double extraction of the protein pellet with MeOH improved the efficiency of recoveries of FB_1, but large amounts of impurities in the column affected the analytical HPLC column by excessive absorption onto the stationary phase. The mean recovery of FB_1 from human serum samples that was obtained in this study following optimisation was 95.8% (n=15). This study also improved on the detection limits of FB_1 to approximately $5ng.ml^{-1}$ at a signal to noise ratio of 5:1 by modifying the HPLC detection settings.

With regards to the recovery of Sa and So from spiked sera, optimisation involved increasing the volumes of solvents, whilst removing the sodium sulphate bed as this affected the efficiency of retrieval of the sphingoid bases. The method was considered sufficiently optimised once recoveries of 72.6% and 41.0% for So and Sa respectively were obtained at a level of spiking with 50ng per 500µl of serum, and recoveries of 77.9% and 85.0% at a level of spiking at 10ng per 500µl of serum.

Overall, the methods were considered adequately optimised for use in the analyses of sera obtained from non-cancer and cancer patients, to determine whether a correlation exists between FB_1 exposure, serum Sa:So ratios and brain cancer.

CHAPTER 8

Effects of fumonisin B_1 on sphingolipid metabolism in the N2α neuroblastoma cell line

8.1 INTRODUCTION

The disruption of sphingolipid metabolism has been proposed to be the initial step of the toxicity and carcinogenicity of FB_1 (Merrill *et al.*, 1996b). Ceramide synthase is responsible for acylation of Sa in the *de novo* synthesis of sphingolipids, and reacylation of So in sphingolipid turnover. Its inhibition in cells *in vitro* results in inhibition of *de novo* sphingolipid biosynthesis, an increased intracellular concentration of free Sa, and sometimes free So, depletion of complex sphingolipids, an increase in So and Sa degradation products, and an increase in lipid products derived from the increase in sphingoid base degradation products (Merrill *et al.*, 1993b; Riley *et al.*, 1994a; Yoo *et al.*, 1996).

Free sphingoid bases are growth inhibiting and cytotoxic at micromolar concentrations (Stevens *et al.*, 1990; Merrill, 1991; Hanada *et al.*, 1992), and reduced complex sphingolipid biosynthesis reduces cell proliferation (Hanada *et al.*, 1992; Yoo *et al.*, 1992; Radin *et al.*, 1993), and causes cell death (Yoo *et al.*, 1992). The two most likely explanations for the increased cell death after inhibition of sphingolipid biosynthesis by fumonisins are that the accumulation of free Sa or a Sa degradation product, such as the 1-phosphate, are growth inhibitory and cytotoxic for the cells (Stevens *et al.*, 1990; Hannun *et al.*, 1991; Sweeney *et al.*, 1996). Secondly, more complex sphingolipids are required for cell survival and growth, and the loss of complex sphingolipid biosynthesis would be expected to alter cell behaviour and also lead to cell death.

The sensitivity of cultured cells to fumonisin exposure varies. Fumonisins inhibit overall sphingolipid biosynthesis in cultured hepatocytes (Wang *et al.*, 1991) and in a renal cell line (Yoo *et al.*, 1992), but no investigations of the effects of this mycotoxin on sphingolipid metabolism on the N2α mouse neuroblastoma cell line have been pursued. The objective of this study therefore was to investigate whether the sensitivity of cultured N2α neuroblastoma cells to fumonisin exposure *in vitro* is related to the mechanistic relationship between the FB_1-induced inhibition sphingolipid metabolism, and elevated

free Sa levels. The methods of extraction and analyses of FB_1 from CCM in which these cells were cultured, was based on the optimised method detailed in Chapter 7, section 7.2.2.2. Sphingolipid extraction methods for the free sphingoid bases and total sphingolipids from the N2α neuroblastoma cells were as described in detail in Yoo *et al.* (1996) and Chapter 7, section 7.7, and were applied in this study. An additional objective was to assess this method for determination of free sphingoid bases, total sphingoid bases, and total sphingolipids in these cultured cells.

8.2 MATERIALS AND METHODS

8.2.1 Materials

Cell culture materials, media, antibiotics, and sterile disposable consumables were as described in Chapter 3, section 3.2.1. Pre-sterilised Corning plastic tissue culture flasks ($25cm^2$) were used as culture vessels. Reagents, chemicals, solvents, the HPLC system and conditions used for the analyses described in this chapter were as described in Chapter 7, section 7.2.1, unless otherwise indicated.

8.2.2 Methods to assess effects of fumonisin B_1 on the N2α neuroblastoma cells

The sensitivity of sphingolipid metabolism in cultured N2α neuroblastoma cells exposed to 50μM and 100μM FB_1 for 72hours was assessed using HPLC. A FB_1 stock solution ($1mg.ml^{-1}$ or 1.39mM in CCM) was used to prepare dilutions of 50μM and 100μM FB_1 in CCM. Complete culture media was used as the control solution.

Both extracellular and intracellular Sa and So were measured by HPLC. The original method for the determination of free sphingoid bases (base hydrolysis) was described by Merrill *et al.* (1988) and modified by Riley *et al.* (1994a), while the original method for the determination of total sphingolipids used the method of acid hydrolysis of Gaver and Sweeley (1965).

The quantitative analyses of the Sa and So levels in the CCM that the cells were cultured in were as described for serum samples in Chapter 7, section 7.7.

8.2.3 Extraction of free sphingoid bases and total sphingolipids from the N2α neuroblastoma cells

Reagents for analysis of total sphingolipids were prepared as described by Gaver and Sweeley (1965) and Yoo *et al.* (1996).

Three sets of six 25cm^2 confluent flasks of N2α neuroblastoma cells were incubated for 72 hours at 37°C in 1ml each of 50μM FB_1 in CCM, 100μM FB_1 in CCM, or CCM only, prior to analysis. The controls comprised of those flasks where the N2α cells were treated with 1ml CCM only.

All flasks of N2α cells were removed from the incubator following the 72hour incubation period. The CCM (1ml) containing cellular debris was transferred into 1.5ml polypropylene tubes and centrifuged at 4000g for 10 minutes. The cell-free media was transferred to 1.5ml polypropylene tubes, and retained for quantitative HPLC analysis of non-incorporated FB_1, and determination of Sa and So levels in the CCM. The cell pellets were retained in the 1.5ml polypropylene tubes (Pellet 1).

The remaining adherent cells in the flasks were trypsinised and pelleted at 4000g for 10 minutes (Pellet 2). The supernatant was discarded and the pellets (Pellet 1+Pellet 2) were combined and stored in 1.5ml polypropylene tubes for base hydrolysis, or 10ml glass tubes for acid hydrolysis until further processing.

8.2.3.1 Base hydrolysis and extraction of free sphingoid bases from N2α cells

The cell pellets in polypropylene tubes were base-hydrolysed with 0.125M methanolic KOH in $CHCl_3$ (4:1)(2ml) for 2 hours at 37°C in a shaking water bath to ensure complete base hydrolysis, since incomplete base hydrolysis was found to result in chromatograms with numerous peaks interfering with quantification of Sa and So. Following base hydrolysis, 2ml $CHCl_3$, 2ml alkaline water, (Appendix 7.2) and 4ml of 2M NH_4OH were added. The mixture was vortexed, centrifuged (4000g, 10 min., 10°C) and the aqueous layer then aspirated. The $CHCl_3$ phase was rinsed with 0.9ml alkaline water three times, transferred to a glass scintillation vial, and dried under a stream of nitrogen gas.

8.2.3.2 Acid hydrolysis and extraction of total sphingolipids from N2α cells

The cell pellets in screw-capped glass tubes were hydrolysed with a modified aqueous methanolic HCl solution (2ml) (Appendix 8.1) overnight (~15hr) at 65-70°C (Gaver and Sweeley, 1965). After acid hydrolysis, saturated methanolic KOH (2ml), alkaline water (2ml), 2M NH_4OH (400 µl) solution and $CHCl_3$ (2.4 ml) were added and mixed. The mixture was centrifuged (700g, 10 min.) and the aqueous layer aspirated. The chloroform layer was washed thrice with 0.9ml alkaline water. The chloroform layer was transferred to a 25ml glass scintillation vial and dried under a stream of nitrogen gas in a fume cupboard.

8.2.3.3 Determination of free sphinganine and sphingosine levels in cell culture media

The optimised method of extraction of Sa and So described in Chapter 7, section 7.7 was applied, except that instead of serum, the CCM in which the N2α cells were cultured was analysed for levels of free Sa and So.

8.2.3.4 Derivatisation of the sphingoid bases for high performance liquid chromatographic analyses

The OPA reagent was prepared and used in the derivatisation of samples for quantitative HPLC analysis of Sa and So as described in Chapter 7, section 7.4.2. The filtered samples in glass inserts were placed in the autosampler and injected in duplicate using an injection volume of 50µl.

8.2.3.5 Analysis of the sphingolipid derivatives using high performance liquid chromatography

Chromatographic analysis of the sphingolipid derivatives were carried out under the conditions as described in Chapter 7, section 7.4.3. Standard solutions of Sa and So were run daily to verify column performance, stability of the OPA reagent, as well as the RTi and response factor for both Sa and So. Derivatised samples were stable for at least 24 hours when refrigerated in darkness. The successful use of refrigerated samples for this length of time was previously documented in studies by Yoo *et al.* (1996) and was verified in this study.

8.2.4 Fumonisin B_1 extraction from the N2α cells complete culture media

The CCM containing FB_1 in which the N2α cells were cultured, was extracted, and purified for removal of matrix impurities and concentration of FB_1 prior to HPLC analysis. The method used was a modification of the method of Shephard *et al.* (1992) used for human serum samples. The method optimised in this study is outlined in detail in Chapter 7, section 7.2.2.2 as applied to human serum, but was also applied here on the CCM that the N2α cells were treated with. In this part of the study, instead of using 500µl serum, 500µl CCM was used, and FB_1 was successfully extracted. The final residue was redissolved in 100µl of acetonitrile water (1:1, v/v) and incubated at RT for 5 minutes prior to derivatisation and HPLC analysis.

8.2.4.1 Derivatisation and high performance liquid chromatographic analyses of fumonisin B_1 from culture media

The chromatographic analysis conditions used in the quantitative analysis of FB_1 from the CCM was as described in Chapter 7, section 7.2.2.3. The OPA reagent for FB_1 derivatisation was prepared as described in Chapter 7, section 7.2.2.3. The derivatised samples were injected in duplicate (50µl per injection) for determination of reproducibility and statistical viability.

8.2.5 Statistical analyses

All data were presented as means±SD. Comparative assessments were carried out using the paired 2-tailed Student's t test. A p value <0.05 was considered statistically significant. Correlation analyses were determined using Microsoft Excel.

8. 3 RESULTS AND DISCUSSION

The sensitivity of N2α mouse neuroblastoma cells to FB_1 exposure was investigated to determine whether inhibition of overall sphingolipid biosynthesis, and elevation of free Sa and So levels would occur as a result of exposure to this mycotoxin. In an earlier study Riboni *et al.* (1995) indicated that FB_1-treatment completely inhibited So-induced differentiation of the N2α cells, and also established that conversion of So to CER was

required, as CER plays a mediator role in the regulation of differentiation in these cells. This data suggests a specific bioregulatory function of CER in the control of N2α cell growth and differentiation, and poses the general hypothesis of a mediator role of CER in the differentiation of cells of neural origin.

Sphinganine is known to be a highly bioactive molecule capable of inhibiting cellular protein kinases, enzymes, and ion-transporters (Merrill *et al.*, 1993a). Sphingosine is also of interest because it influences the synthesis of DNA and interacts with DNA in competition for the binding sites with histones, some enzymes, and transcription factors (Riley *et al.*, 1994a). For these reasons, both intracellular and extracellular levels of Sa and So were also assessed quantitatively.

8.3.1 Analyses of the intracellular and extracellular levels of sphinganine and sphingosine following exposure of cultured N2α cells to fumonisin B_1

The results of the analyses of the intracellular (whole cell analyses) and extracellular levels (cell culture media analyses) of Sa and So, as well as the proportion of FB_1 remaining in the CCM are summarized in Tables 8.1 to 8.4. This is the first study where quantitative analyses of FB_1, Sa and So were concurrently carried out on N2α cultured cells.

Cell counts at the initiation of the experiments prior to addition of FB_1 indicated that there were approximately 2.5×10^5 N2α cells per flask. With this approximate cell number in mind, quantitative analysis of FB_1 remaining in the CCM following the 72hour exposure period enabled an estimation of the levels of FB_1 incorporated by the N2α cells per culture flask. These results are summarized in Table 8.1 (and Appendix 8.2) and indicate the potential for either binding (absorption) or entry of FB_1 into the N2α cells *in vitro*.

Table 8.1: Recoveries of Fumonisin B_1 from the N2α cell culture media following the 72 hours exposure period.

Treatment with FB_1 (μM)	FB_1 recovered (μM)	% FB_1 taken up by N2α cells (Mean ± SD)
50μM (n=5)	16.3 ± 4.2	67.4 ± 8.3
100μM FB_1 (n=6)	23.8 ± 1.6	76.2 ± 1.6

The limitation of the number of replicate samples throughout this *in vitro* investigation were due to the high cost of pure FB_1. A total of 20mg of FB_1 was purchased and budgeted for use in the cell culture work (presented in Chapters 3, 4, 5 and 6), optimisation of the extraction of FB_1 from serum samples for HPLC analysis (presented in Chapter 7), as well as for this *in vitro* investigation.

Figures 8.1 and 8.2 present chromatograms showing FB_1 recovered from the CCM after the $25cm^2$ flasks of confluent N2α cells (i.e., $\sim 2.5 \times 10^5$ cells) were treated with 50μM and 100μM FB_1 for 72 hours. The FB_1 content of the CCM that the N2α cells were cultured in was significantly decreased from the original concentrations that these cells were exposed to, and the proportion that was unaccounted for in the CCM was considered indicative of the level of cellular uptake of FB_1 by the N2α cells (Table 8.1). This indicates that the FB_1 that traversed the cell membranes occupied all the molecular binding sites within the cells and that at these levels of uptake, saturation was potentially reached between the intracellular levels and extracellular levels of this mycotoxin.

In the N2α cells treated with 50μM FB_1 (n=5) (Appendix 8.2), a mean of 16.3±4.2μM FB_1 was recovered from the CCM, indicating that 67.4 ± 8.3% of the FB_1 was potentially taken up by these cells. In the N2α cells treated with 100μM FB_1, a mean of 23.8±1.6μM FB_1 was recovered from the CCM, indicating that 76.2 ± 1.6% FB_1 was taken up over the 72hour incubation period. The recoveries of FB_1 from the flasks of N2α cells treated with 50μM and the 100μM FB_1 (Appendix 8.2) were significantly different ($p=0.015$) indicating that cellular uptake of FB_1 by the same number of cells per flask (i.e., $\sim 2.5 \times 10^5$ cells) N2α cells at these two concentrations differed significantly. Although the cells treated with 100μM FB_1 took up a higher percentage of FB_1 (Table 8.2), a higher SD between replicate flasks of cells exposed to 50μM FB_1 was evident. Taking the large SD into consideration, it is likely that equimolar amounts of FB_1 were metabolised at both concentrations, lending further support to the hypothesis that a saturation point was reached within the cells preventing further entry of the mycotoxins.

The results of the quantitative analyses of FB_1 in the CCM (Table 8.1) are supported by the immunohistochemical and immunocytochemical data on the N2α neuroblastoma cell line

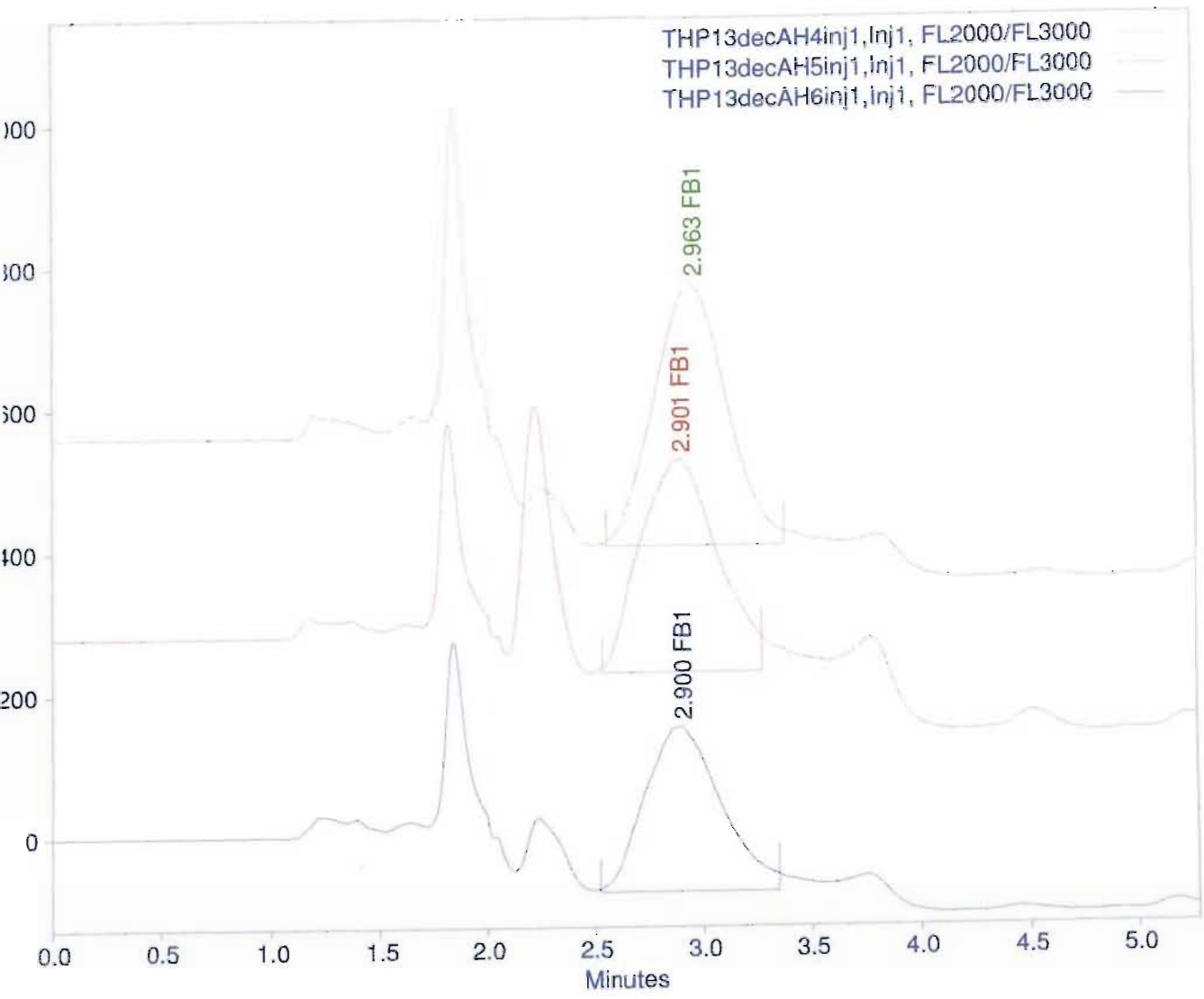

Figure 8.1: High performance liquid chromatograms showing FB_1 retrieved from the culture media after N2α cells were exposed to 50μM FB_1 for 72 hours. The traces shown are AH4, AH5 and AH6 and are green, red and blue respectively.

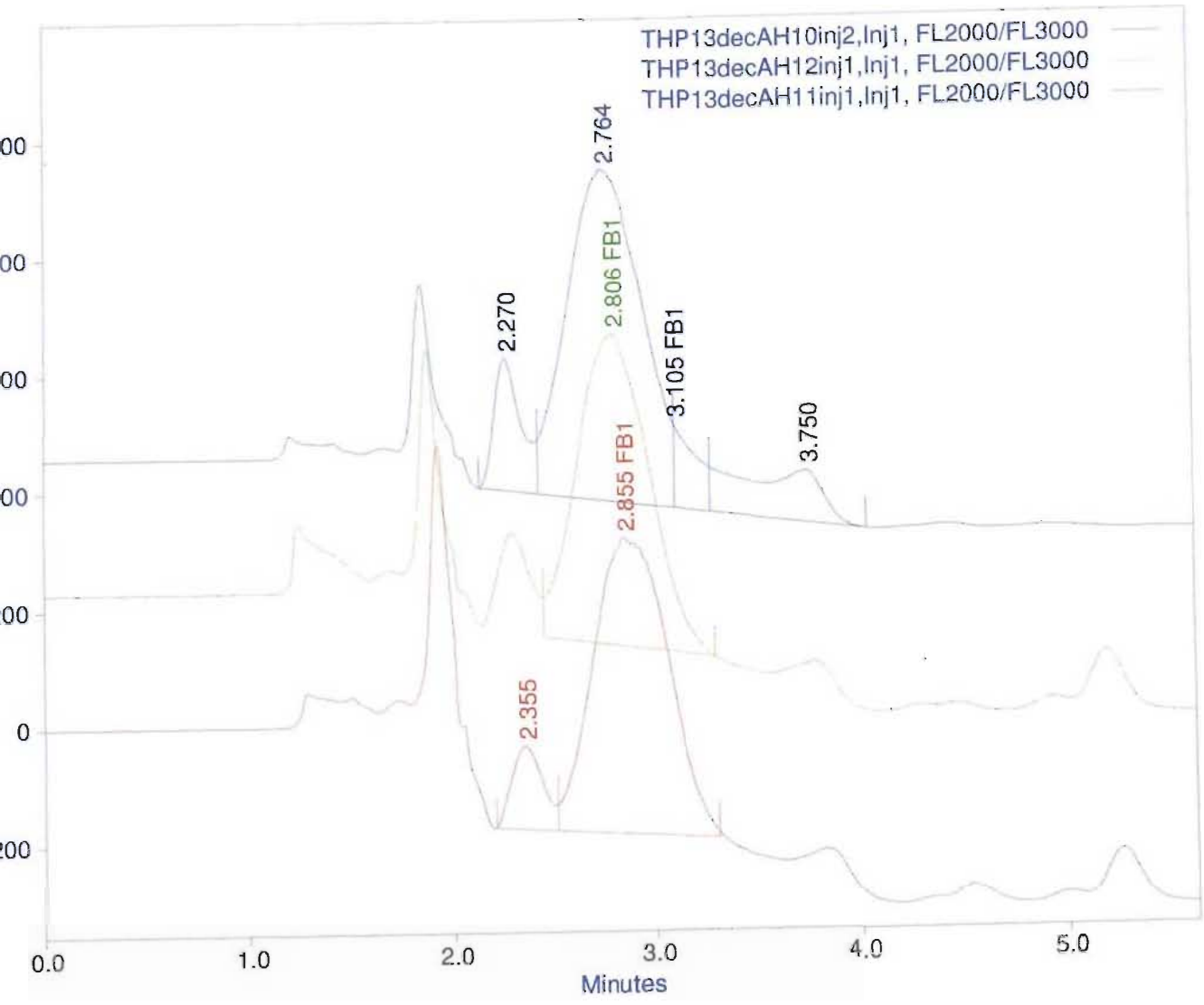

Figure 8.2: High performance liquid chromatograms showing FB_1 retrieved from the culture media after N2α cells were exposed to 100μM FB_1 for 72 hours. The traces shown are AH10, AH12 and AH11 and are illustrated in blue, green and pink respectively.

(Chapter 6) following the 48-hour exposure period, and provides further support to substantiate that FB_1 traverses the cell membranes and enters cells. The results of the MTT assay (Chapter 3) in combination with the light microscopic observation of the N2α cells treated with 50μM FB_1 and 100μM FB_1 for 72 hours prior to trypsinisation, confirmed the decrease in cell viability characterized by the high number of cells floating in the CCM. The remaining adherent cells appeared fibroblastic in morphology in comparison to untreated confluent control N2α cells. In concurrence with the findings documented in Chapter 6, the FB_1-treated cells displayed features of progressive damage leading from gradual retraction of processes to cells exhibiting loss of cytoplasmic volume and complete cell rounding; all features associated with cell death. Cell rounding could be attributed to a loss of turgidity and subsequent disruption of the cytoplasm. The attachment of cells to the substrate and to each other is also mediated by cell surface glycoproteins, as well as calcium and magnesium ions (Freshney, 1983). The loss of cell viability noted in the cells would imply a loss of production of these ions and the glycoproteins that facilitate cell adhesion.

Yu *et al.* (2001) made similar observations with the LLC-PK1 cells, with cells displaying fibroblastic morphology, as well as the presence of many floating cells following exposure to FB_1 for at least 72 hours. Taken together, these results indicate that FB_1 has the potential to affect the structure and morphology as well as adhesion capability of the N2α neuroblastoma cells following exposure and entry.

Having established the levels of FB_1 potentially taken up by these N2α cells, intracellular and extracellular levels of Sa and So levels also were assessed. The purpose of acid hydrolysis was to liberate free Sa and So from complex sphingolipids, resulting in hydrolysis of both the amide linked fatty acids and any group esterified on carbon 1 of the sphingoid base. Studies by Wang *et al.* (1992) revealed that inhibition of CER synthase in cultured cells reduced cellular levels of complex sphingolipids and increased the amounts of free Sa and So. Similar findings were noted in this study on the N2α neuroblastoma cells.

Chromatograms obtained following acid hydrolysis of the isolated control (blue trace) and FB_1-treated (pink and light blue trace) N2α cells are shown in Figure 8.3 relative to a 500ng Sa and So standard (green trace). The cellular levels of total Sa and So freed after

acid hydrolysis are summarized in Table 8.2 (Appendix 8.3). It is evident by visual comparison that the So and Sa area under the peaks are much larger in controls cells than in the FB_1-treated cells indicating decreased levels of complex sphingolipids in these cells following exposure to FB_1.

Table 8.2: Total sphingosine and sphinganine levels in N2α cells following Fumonisin B_1 treatment for 72 hours: acid hydrolysis of N2α cells.

Treatment	Mean ± SD		
	So (μM)	Sa (μM)	Sa:So ratio
Untreated controls (n=3)	4.9 ± 1.03	0.6 ± 0.12	0.13 ± 0.05
50μM FB_1 (n=3)	1.0 ± 1.4	0.2 ± 0.09	0.16 ± 0.25
100μM FB_1 (n=3)	1.8 ± 0.5	0.2 ± 0.1	0.14 ± 0.01

From Table 8.3, there was a five-fold decrease in So levels to 0.15 ± 0.09μM, and a four-fold decrease in Sa levels to 0.2 ± 0.1μM in the 50μM FB_1-treated N2α cells in comparison to untreated controls. Furthermore, a three fold decrease in both the mean Sa and mean So concentrations to 0.2 ± 0.1μM and 1.8 ± 0.5μM respectively was noted in cells exposed to 100μM FB_1 for the same length of time when compared to controls. The lowered amounts of Sa and So released from the complex sphingolipids in both sets of FB_1-treated N2α cells, indicates that FB_1 exposure decreased complex sphingolipid formation in the N2α cells. Although the Sa:So ratio in the untreated cells was the same as the 100μM FB_1-treated cells, the absolute values of the Sa and So were significantly different. These results indicate that sphingolipid biosynthesis in the N2α cells are susceptible to the inhibitory effects of FB_1 on CER synthase, and the subsequent depletion of complex sphingolipids.

Merrill *et al.* (1993a) reported similar findings with rat primary hepatocytes where as a consequence of *in vitro* inhibition of CER synthase by FB_1, there was depletion of complex sphingolipids. Complex sphingolipids have numerous functions in cell membranes, including stabilization of the membrane, sorting of lipids and proteins, binding to cytoskeletal elements and cell-cell recognition (Riley *et al.*, 1993). Depletion of complex sphingolipids in N2α cell membranes would disrupt the normal barrier function of the

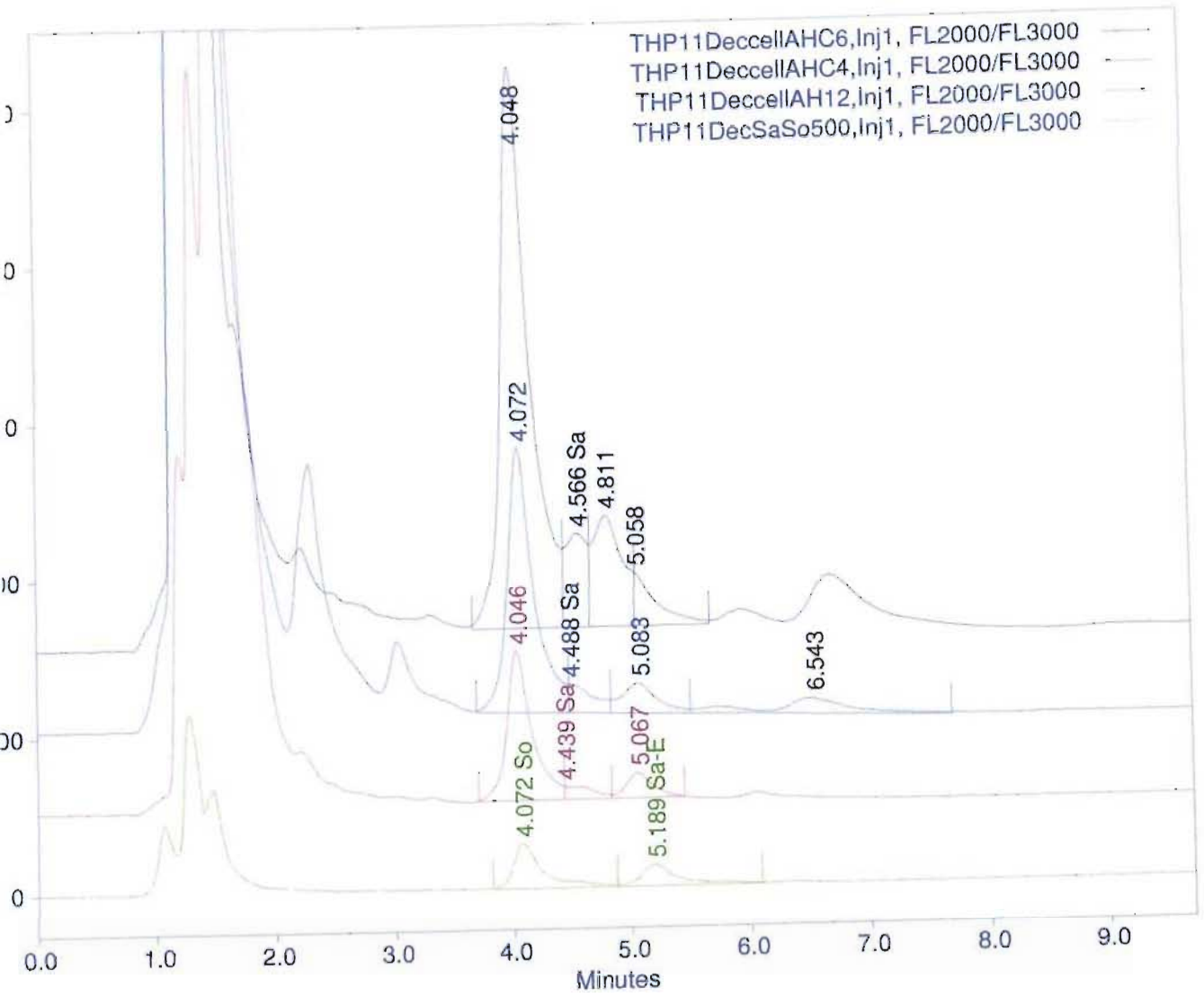

Figure 8.3: High performance liquid chromatograms of Sa and So obtained following acid hydrolysis of the isolated control (blue AHC6 trace) and FB_1-treated (pink AH12 and light blue AH4 trace) N2α cells relative to a 500ng Sa and So standard (green SaSo500 trace).

membrane leading to cellular damage as indicated by the IHC and ICC results (Chapter 6), levels of cytotoxicity indicated by the MTT assay (Chapter 3), necrosis and apoptosis indicated by the Apoglow assay (Chapter 4) as well as the flow cytometric analyses (Chapter 5) in this study.

The findings of Riboni *et al.* (1995) may be used to explain why higher concentrations of Sa and So were hydrolysed from complex sphingolipids in the untreated N2α cells in comparison to the FB_1-treated cells. Riboni *et al.* (1995) found that complex sphingolipid concentrations changed markedly with the degree of confluency and age of the N2α cells in culture. In this study, all culture flasks were confluent prior to exposure to FB_1 for the 72-hour period. However, due to the level of cytotoxicity induced by FB_1, extensive loss of cells occurred as cells lost their ability to adhere to the culture substrate, and floated into the CCM. Although these fragmented cells were pelleted by centrifugation, retained and pooled for extraction, some cells may have disintegrated due to extensive damage as a result of the cytotoxic, growth-arrest, necrotic or apoptotic effects of FB_1 in the CCM, and would have been discarded in the washes. These effects of FB_1 on N2α cells may be attributed to the depletion of complex sphingolipids, and the subsequent alterations in cell-cell and cell-matrix interactions which are known to induce apoptosis in cells (Frisch and Francis, 1994).

The purpose of base hydrolysis was to cleave acylglycerolipids and hydrolyse lysosphingolipids (free sphingoid bases modified at the hydroxyl group on carbon 1 of So or Sa) to release free So and Sa. Base treatment does not liberate sphingoid bases from complex sphingolipids (Merrill *et al.*, 1988; Yoo *et al.*, 1996). Mild base treatment followed by chloroform/methanol extraction effectively removes phospholipids (phosphotidylethanolamine and phosphotidylserine) that can react with the OPA reagent (Merrill *et al.*, 1988).

Chromatograms obtained following analysis of the base hydrolysed extracts of the isolated control and treated N2α cells are presented in Figure 8.4 along with the Sa and So standards. The quantitative results of the analysis of the base hydrolysed cells for determination of the concentration of free sphingoid bases are summarised in Table 8.4 and Appendix 8.4. In Figure 8.4 the Sa and So standard is shown by the green trace, and

control cells by the light blue trace. The cells treated with 50μM and 100μM FB_1 are shown by the pink and dark blue traces respectively.

Table 8.3: Free sphingosine and sphinganine levels in N2α cells after treatment with fumonisin B_1 for 72 hours: base hydrolysed extracts of the N2α cell line.

Treatment	Mean ± SD		
	So (nM)	Sa (nM)	Sa:So ratio
Control (n=3)	36.4 ± 6.0	19.2 ± 9.1	0.52 ± 0.2
FB_1 at 50μM (n=3)	53.6 ± 6.6	60.6 ± 5.7	1.14 ± 0.2
FB_1 at 100μM (n=3)	46.9 ± 2.9	65.1 ± 12.4	1.4 ± 0.3

In the control N2α cells where FB_1 was omitted, after the 72-hour incubation period the mean free Sa concentration of replicate flasks (n=3) was 19.17±9.14nM and the mean free So was 36.39±5.96nM (per ~$2.5x10^5$ cells per confluent $25cm^2$ flask) (Table 8.3). The mean free Sa:So ratio in the control cells was 0.52±0.19. The maintenance of a low concentration of free So and free Sa is important because these compounds have intrinsic biological activity (Merrill and Stevens, 1989; Hannun and Bell, 1989; Merrill, 1991).

As would be predicted for an inhibitor of CER synthase, FB_1 caused accumulation of free Sa in the treated N2α neuroblastoma cells, while the levels of So were not significantly affected. The amount of free Sa that accumulated in cells was considered a function of the extent of inhibition of CER synthase, the concentration of essential precursors (serine, palmitoyl-CoA), the growth rate of the cells, the rate of Sa degradation and elimination from the cells.

In N2α cells treated with 50μM FB_1, there was a 3.2 fold increase in the free Sa concentration to a mean of 60.59±5.68nM, and in those cells exposed to 100μM FB_1 over 72 hours, a 3.4 fold increase in the mean free Sa concentration to 65.10±12.43nM. Using Student's t-test and comparing the levels of free Sa in the untreated N2α control cells and the 50μM FB_1-treated N2α cells, the levels were significantly different (p=0.003). There was also a significant difference between control Sa levels and the Sa levels in the 100μM FB_1-treated N2α cells (p=0.007).

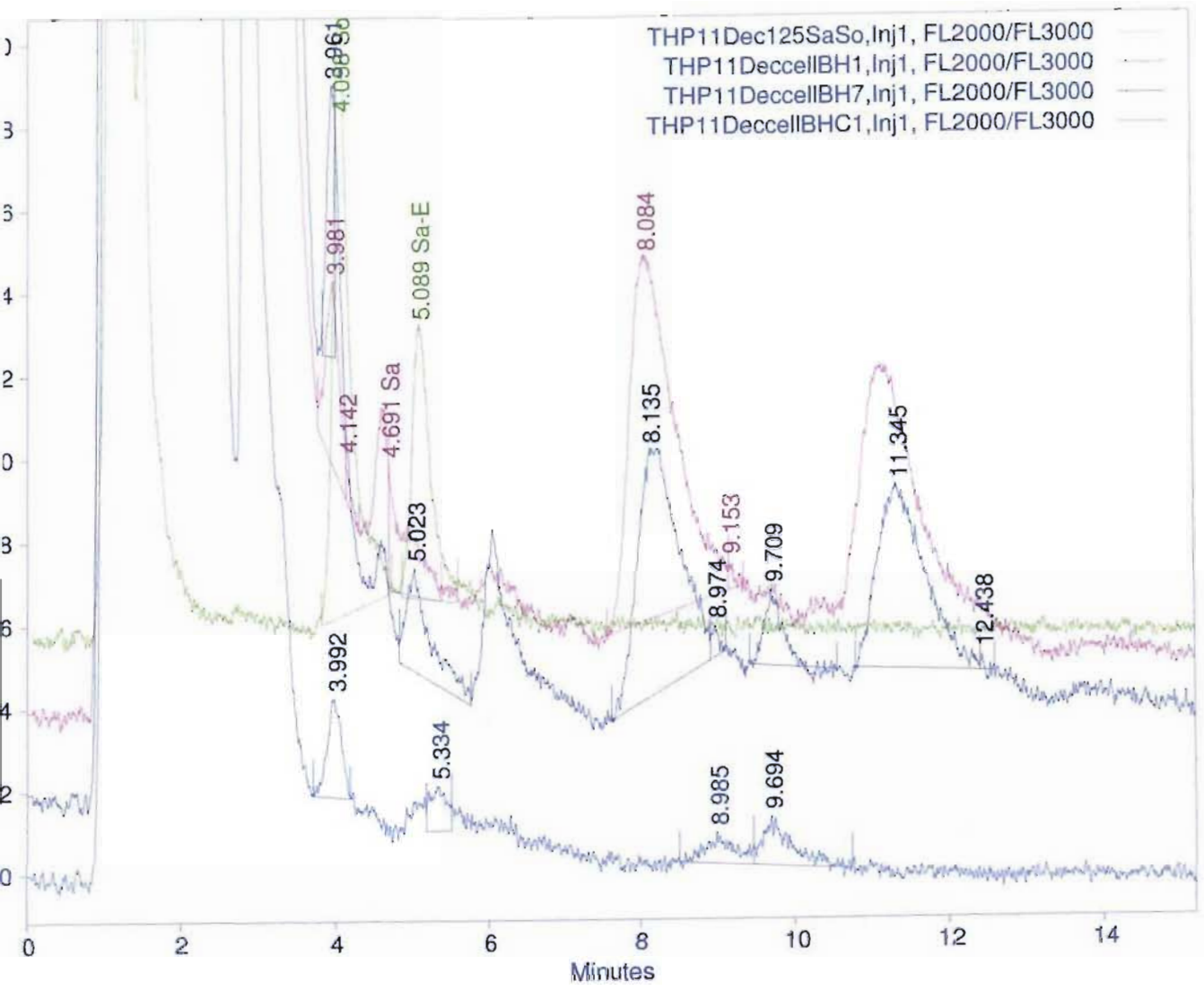

Figure 8.4: High performance liquid chromatograms of Sa and So obtained following base hydrolysis of the isolated control (light blue BHC1 trace) and FB_1-treated (pink BH1 and dark blue BH7 trace) N2α cells relative to a 125ng Sa and So standard (green 125 SaSo trace).

The free So concentration in the controls differed significantly from the 50μM ($p=0.03$) and 100μM FB_1-treated N2α cells ($p=0.05$) (Table 8.3). The occurrence of free So in mammalian cells is always as a product of catabolism of complex sphingolipids. In cell culture, there is initially little change or decrease in free So concentrations, consistent with it arising from turnover rather than *de novo* biosynthesis, and this is apparently less rapid than Sa biosynthesis. However, when cells begin to die, So would be expected to increase due to the breakdown of membrane lipids (Merrill *et al.*, 1996b). Yoo *et al.* (1992) reported that with renal epithelial LLC-PK1 cells treated with FB_1, the increase in free So occurred before any evidence of increased cell death or inhibition of cell proliferation, and although free So levels became significantly elevated, this occurred to a much lesser extent than free Sa. Studies by Zhang *et al.* (1990) and Jacobs and Kester (1993) have shown that low concentrations (below 10μM) of So stimulated the synthesis of DNA in Swiss and A7r5 cells, but a higher content of So caused cell death. In contrast, Wang *et al.* (1991) and Gelderblom *et al.* (1995b) reported that the basal levels of free So did not change significantly in primary rat hepatocytes when FB_1-induced inhibition of sphingolipid metabolism occurred. These comparative studies highlight that the response of cultured cells to FB_1 exposure are cell type specific.

The accumulation of free So is an indication that either reacylation of So derived from sphingolipid turnover, or acylation of So derived from the serum component of the culture media was also inhibited. The fact that the Sa accumulated to a much greater extent than So in the N2α cells suggests that the *de novo* pathway was the primary target for FB_1-induced inhibition.

This differential inhibition led to increased Sa:So ratios of 1.14±0.2 in the 50μM FB_1-treated N2α cells, and a further increase to 1.4±0.3 in the 100μM FB_1-treated cells, from a ratio of 0.52±0.2 in the N2α control cells. Significantly different Sa:So ratios to controls were noted with both the 50μM FB_1-treated N2α cells ($p=0.016$) and the 100μM FB_1-treated cells ($p=0.017$) in comparison to the untreated N2α cells. The intracellular elevation of free sphingoid bases is only one aspect of fumonisin disruption of sphingolipid metabolism that may cause cellular deregulation.

Merrill *et al.* (1993b) reported similar findings to that of the N2α neuroblastoma cell line when using cultured mouse cerebellar neurons. These authors reported that free Sa

increased significantly when the cells were treated with FB_1. Within 24 hours, Sa increased 20 fold, and this elevation was maintained over 168 hours of incubation with 25μM FB_1. Free So initially increased about 2 fold over the controls, however it was the same as for the controls at 96 and 168 hours (Merrill *et al.*, 1993b). In the present study on N2α neuroblastoma cells, although analyses were carried out after only 72 hours and the concentrations of FB_1 to which the cultured cells were exposed were higher, a similar trend in the response was noted. Distinct increases in Sa concentrations from 19.2±9.1nM in controls up to 60.6±5.7nM in the 50μM FB_1-treated cells, then further to 65.1±12.4nM for those cells exposed to 100μM FB_1 after 72 hours were noted (Table 8.3).

Collectively, the results of Merrill *et al.* (1993b); Riley *et al.* (1994a) and Yoo *et al.* (1996) support the findings of the acid and base hydrolyses of the FB_1-treated N2α neuroblastoma cells in this study, where FB_1 was shown to inhibit sphingolipid metabolism. Merrill *et al.* (1993b) found that FB_1 inhibited sphingolipid biosynthesis in cultured cerebellar neurons as reflected by accumulation of free Sa and a reduction in the mass of total sphingolipids. The regulated maintenance of low levels of free sphingoid bases in cells is important because these compounds have considerable intrinsic biological activity and can be cytotoxic at elevated concentrations. The results in this study are in keeping with other published studies, since the response of the N2α neuroblastoma cell line also indicates an accumulation of free Sa (Table 8.3) and a reduction in the mass of complex sphingolipids (Table 8.2).

The depletion of complex sphingolipids following exposure of the N2α neuroblastoma cell line to FB_1 (Table 8.2) concurs with findings reported for cultured CHO cells by Stevens *et al.* (1990). Complex sphingolipids have numerous important functions in cell membranes, including stabilisation of the membrane, sorting of lipids and proteins, binding to cytoskeletal elements, and cell-cell recognition. Depletion of complex sphingolipids in membranes disrupts the normal function of membranes (Riley *et al.*, 1994a). Complex sphingolipids were required for cell survival of this N2α neuroblastoma cell line, and it is likely that as with other cell lines (Hanada *et al.*, 1990; Hanada *et al.*, 1992; Radin, 1994), depletion of complex sphingolipids led to increased N2α cell death as indicated by the high number of cells floating in the CCM. These findings are supported by the results of the MTT assay (Chapter 3, Table 3.1) where ~30% cell death was observed in those N2α cells exposed to 50 and 100μM FB_1.

A further finding of this study during the base hydrolytic treatment of the N2α cells was that exposure to FB_1 caused formation of two compounds other than Sa and So that were absent in both the N2α control cells (light blue trace), and the standards solution of Sa and So (green trace) (Figure 8.4). This was taken to be an indication that these compounds that eluted were not degradation products of the Sa and So sphingoid bases, nor products of sphingolipid metabolism in the N2α cells. Figure 8.4 shows chromatograms containing two unknown compounds at approximate RTi of 8.08 and 11.35 minutes, respectively that are possibly unnatural sphingoid bases with modified backbones.

Merrill *et al.* (1993b) also reported a similar finding in the study with cultured neurons. It was reported that FB_1 caused the accumulation of a long sphingoid base that eluted after Sa on C_{18} column, but before the [C20] Sa internal standard. The nature of the compound was not known, but Merrill *et al.* (1993b) noted that they had begun to observe it in other cell lines treated with FB_1 as well. It did not appear to be one of the well known long chain bases, such as phytosphingosine (which elutes before So) nor 3-keto Sa (which was ruled out by comparison with a synthetic standard (Merrill *et al.*, 1993b). The identification of these compounds in the present study however was beyond the scope of the investigation on the N2α cell line.

8.3.2 Analysis of the culture media for free sphinganine and sphingosine

When CER synthase is inhibited by fumonisins, large quantities of Sa and So, which are lipophilic and normally occur at very low concentrations in cells accumulate, cross membranes and enter the circulatory system *in vivo*. As time progresses and as a consequence of this inhibition, Sa and So spill over and increase in the serum of affected animals and exert their biological activity. As this inhibition persists, the Sa is released from the cell and in animals, the serum may be analysed to detect any increase from baseline levels of free Sa. In *in vitro* systems, the free Sa and So are released into the extracellular fluid that *in vitro*, is equivalent to the CCM. The results of the Sa and So analyses of the culture media for the N2α cells are summarized in Table 8.4 and chromatograms are shown in Figure 8.5.

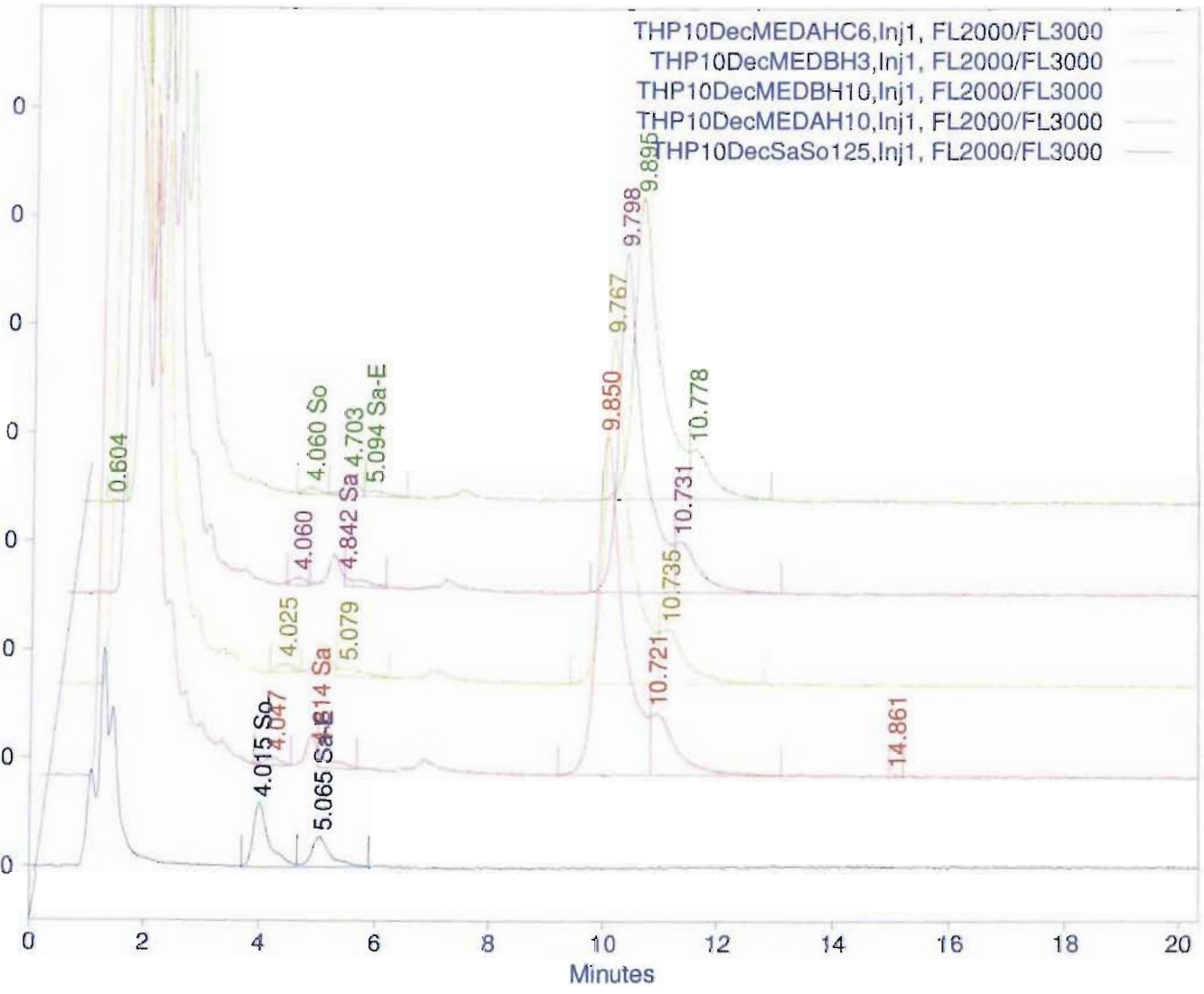

Figure 8.5: High performance liquid chromatograms of Sa and So obtained following analyses of the culture media of the control (green MEDAHC6 trace) and FB_1-treated (MED BH3, BH10 and AH10 traces) N2α cells in relation to the SaSo standard (SaSo 125 dark blue trace).

Hannun *et al.* (1991) reported that in LLC PK1 cells, So had little difficulty in crossing cell membranes, and Riley *et al.* (1998) subsequently reported that the half-life of Sa inside LLC-PK1 cells was much longer than the half-life of FB_1 in LLC-PK1 cells. This suggests that inhibition of CER synthase is persistent, that Sa does not easily diffuse out of cells, or that Sa degradation is slow relative to its biosynthesis. The saturating effects of FB_1 on the Sa levels may be due to either the inhibitory action of FB_1 on target enzymes, or saturating of FB_1 transport across cell membranes because FB_1 is an inhibitor of CER synthase, and is a hydrophilic compound with a large molecular weight. In this study on the N2α cells, the extent of the diffusion was considered a function of the concentration gradient outside and inside the cells. The results indicate that in comparison to the untreated controls that Sa seemed to diffuse out more from the FB_1-treated cells as indicated by the levels of Sa released into the culture media in comparison to So levels in all three groups (Table 8.4, Appendix 8.5).

Table 8.4: Total free sphinganine and sphingosine in CCM following N2α cell treatment with 50 and 100μM FB_1 over 72 hours.

Treatment (replicates)	Mean ± SD		
	So (nM)	Sa (nM)	Sa:So ratio
Control (n=5)	27.7±11.7	45.5±10.7	1.7±0.3
50μM FB_1 (n=5)	26.4±5.6	51.7±9.9	2.0±0.2
100μM FB_1 (n=5)	26.6±2.5	66.5±13.4	2.5±0.4

In the control cells, the mean free Sa concentration in the CCM was 45.54±10.67nM, and this increased to a mean Sa concentration 51.72±9.87nM in cells treated with 50μM FB_1. Using Student's t-test however, these values were not significantly different to each other ($p=0.18$). A further increase to 66.5±13.43nM Sa was noted for those N2α cells treated with 100μM FB_1 over the 72-hour incubation period, and this increase in Sa was significantly different to that of control N2α cell levels ($p=0.012$).

The So levels in the CCM did not increase to any significant degree, and were very close to control levels (Table 8.4, Appendix 8.5). Furthermore, the Sa:So ratio in CCM increased from 1.73±0.3 for the control cells to 2.0±0.2 (1.16 fold increase) in the N2α cells exposed

to 50μM FB_1. A further increase to a Sa:So ratio of 2.50 ± 0.40 (1.43 fold increase) was noted for the 100μM FB_1-treated N2α cells.

The Sa:So ratios of the CCM of the 50μM FB_1-treated N2α cells did not differ significantly from controls (p=0.07), while those for the N2α cells exposed to 100μM FB_1 did (p=0.004). There was clearly a FB_1-concentration-dependent increase in free Sa in those cells treated with 50 and 100μM FB_1, with no significant change in the So concentration across all three test groups (i.e., in controls and FB_1-treated cells).

In order to determine if a concentration gradient for So and/or Sa exists across the cells membranes (i.e., between intra and extracellular levels of Sa and So in these cells), the mean ratios of Sa and So from the base hydrolyses and CCM analyses from Tables 8.3 and 8.4 were analysed and presented in Table 8.5.

Table 8.5: Comparison of intracellular: extracellular levels of sphinganine and sphingosine in the control and FB_1-treated N2α cells.

Treatment	Mean intracellular So : extracellular So ratio	Mean intracellular Sa : extracellular Sa ratio
Control	1.31	0.42
FB_1 at 50μM	2.03	1.17
FB_1 at 100μM	1.76	0.98

This data indicates that there appears to be an elevation in the ratio between intracellular and extracellular levels of So from control levels in cells exposed to FB_1 (Table 8.5), but not to as distinct levels as with Sa. Sphingosine is usually elevated if there is cell death and membrane lipids are being turned over more rapidly. For Sa, the intracellular:extracellular Sa ratios increased with higher concentrations of FB_1 exposure, indicating build up of intracellular Sa as a result of inhibition of CER synthase, and its passage or diffusion out of the cells into the CCM.

Clearly, FB_1 inhibited sphingolipid biosynthesis in the cultured N2α cell line *in vitro* as reflected by the accumulation of free Sa and a reduction in the mass of total sphingolipids. These results suggest that both the elevation of free sphingoid bases and the decrease in complex sphingolipids contribute to the cytolethality of FB_1 in these cells. The fact that Sa

accumulated to a much greater extent than So suggests that the *de novo* pathway was the primary target for inhibition. As a result of this differential inhibition, the Sa:So ratio increased after exposure to FB_1.

Figure 8.6 is a correlation graph that illustrates the relationship between FB_1 exposure and Sa: So ratios in the cells and in the CCM.

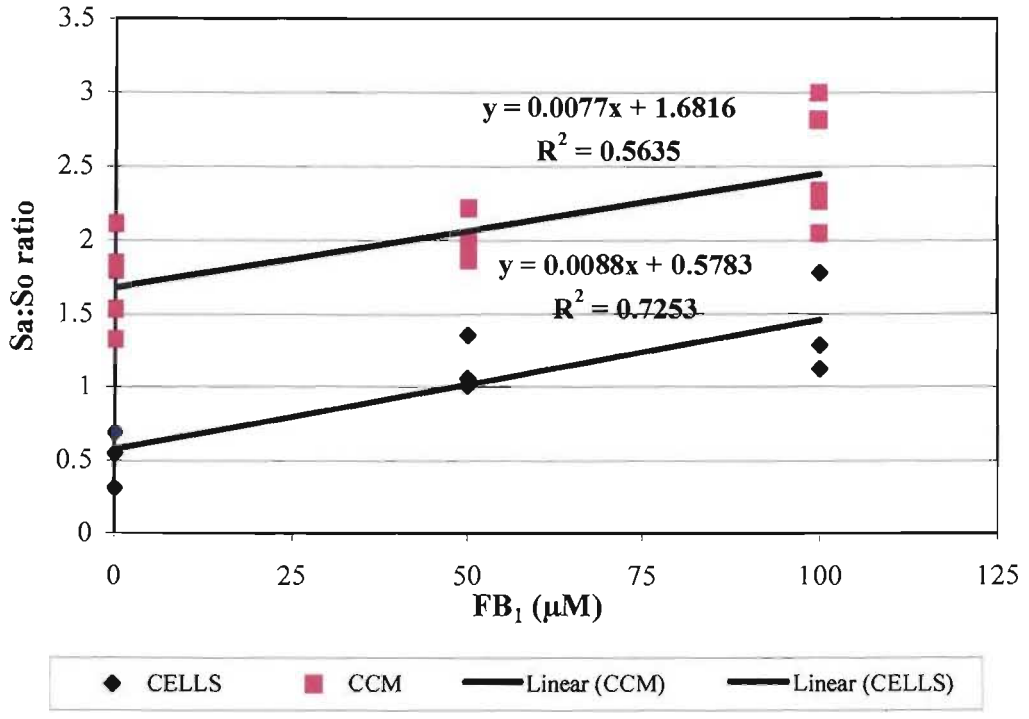

Figure 8.6: Correlation between concentrations of FB_1 exposure and intra and extracellular Sa:So ratios in the N2a cells and the CCM

From Figure 8.6, the R^2 values on the trend lines are 0.73 and 0.56 for the cells and CCM respectively. This implies that the correlation coefficients (R), for the Sa:So ratios to FB_1 in the CCM is 0.75, and that of the free Sa:So in cells is 0.85. Although both these measures provide valuable information, in this study the results indicate that the use of the free Sa:So ratio in cells appears to be a better biomarker than the Sa:So in the CCM (taking into account the large standard deviations), and may be used as a more reliable measure of exposure to fumonisins *in vitro*. These findings are supported by the hypothesis of Wang *et al.* (1992) that an elevated Sa:So ratio in serum is due to the movement of free Sa

from tissues into the blood. In this *in vitro* model, the cells are equivalent to the tissue and the CCM equivalent to the blood *in vivo*. As all cells types differ in the levels of enzyme systems and xenobiotic metabolising systems they possess, it is essential to assess each system individually. Some cells may react differently from others *in vitro* and *in vivo*, nullifying the overall effects noted here, and may not result in the expected increase in Sa: So ratios.

As in the analyses of the base hydrolysed N2α cells, analyses of the CCM revealed the presence of another compound that seemed to accumulate with the increase in concentration of FB_1 that the cells were exposed to. The compound eluted at times different from the peaks observed in the chromatograms of FB_1-treated cells after base hydrolysis (Figure 8.4). This compound eluted at ~ 9.8-10 minutes and was not present in the standards run, and to a much lower extent in the control cell extracts (Figure 8.5). The identification of this compound however, was beyond the scope of the present investigation.

8.4 CONCLUSION

It is documented that when fumonisins are added to cells, inhibition of *de novo* CER generation occurs, and there is the potential for accumulation of free sphingoid bases and their downstream sphingoid base 1-phosphates. Exposure of the N2α neuroblastoma cell line to FB_1 caused an increase in intracellular free Sa and depletion of complex sphingolipids. These results indicate that altered sphingolipid metabolism is closely associated with the effects of FB_1 on cell death. A portion of the adverse effects may be attributed to the build up Sa, which in itself is toxic. Another part of the adverse effect of FB_1 on cells may be attributed to a decrease in more complex sphingolipids that are essential for normal cell behaviour.

Chromatographic analysis of the CCM that the N2α cells were cultured in for 72hours with 50μM FB_1 and 100μM FB_1 indicate that the N2α cells took up approximately 67% and 76% of the mycotoxin, respectively. Determination of levels of total Sa and So from complex sphingolipids in the N2α cells, were facilitated by acid hydrolysis of the cultured cells. The hydrolysis procedure liberated free Sa and So from complex sphingolipids, and resulted in hydrolysis of both the amide linked fatty acids and any group esterified on

carbon 1 of the sphingoid base. The quantitative results revealed that there was a reduction in the concentrations of Sa from a level of 0.6 ± 0.12 μM in control cells, to 0.2 ± 0.09μM in those cells exposed to 50μM FB_1 and to 0.2 ± 0.1μM in those cells exposed to 100μM FB_1 over the 72 hours incubation period. In terms of So, there was a reduction from 4.9 ± 1.0μM in control cells to 1.0 ± 1.4μM and 1.8 ± 0.5μM in those cells exposed to 50μM FB_1 and 100μM FB_1 for the 72hours incubation period, respectively. These results indicate that there was as reduction in the cellular levels of complex sphingolipids

Determination of the levels of free Sa and So in the N2α cells were facilitated by base hydrolyses that cleaved acylglycerolipids and hydrolysed lysosphingolipids, and released free So and Sa. The results of the base hydrolyses of the N2α cells indicated that there was an increase in the free Sa from 19.2 ± 9.1nM in controls to 60.6 ± 5.7nM and 65.1 ± 12.4nM in those cells exposed to 50μM FB_1 and 100μM FB_1 for the 72 hours incubation period. There was an increase in the free So levels from 36.4 ± 6.0nM to 53.6 ± 6.6nm and 46.9 ± 2.9nM in the 50μM FB_1 and 100μM FB_1-treated N2α cells respectively. There was a distinct increase in the free Sa:So ratio from 0.52 ± 0.2 in control cells, to 1.14 ± 0.2 in those cells exposed to 50μM FB_1. There was also a further increase in the Sa:So ratio to 1.4 ± 0.3 in those cells exposed to 100μM FB_1 for the 72 hours incubation period.

Finally, analysis of the CCM in which the cells were cultured over the 72hour incubation period revealed that the free Sa increased from a level of 45.5 ± 10.7nM in control cells to 51.7 ± 9.9nM and further to 66.5 ± 13.4nM in those cells exposed to 50μM FB_1 and 100μM FB_1, respectively. The So levels however remained close to control levels. The Sa:So ratio in the CCM also increased from 1.7 ± 0.3 for controls cells to 2.0 ± 0.2 and 2.50 ± 0.4 for cells exposed to 50μM FB_1 and 100μM FB_1 respectively.

The data presented supports the use of the Sa:So ratio as a biomarker for a dose response of FB_1 on sphingolipid metabolism in the N2α neuroblastoma cell line. The use of the intracellular free Sa:So ratio however, appears to be more reliable biomarker than the Sa:So in the CCM. This framework is reasonably consistent with observed Sa:So ratios and FB_1 concentrations in the examined cells and culture media, as well as the current literature of FB_1 effects on sphingolipid biosynthesis in cultured cells.

CHAPTER 9

Quantitative high performance liquid chromatographic analysis of sphinganine, sphingosine and fumonisin B_1 from the serum of human brain cancer and non-cancer subjects

9.1 INTRODUCTION

On the basis of toxicological evidence, IARC has declared that *Fusarium moniliforme* toxins are possibly carcinogenic to humans (Class 2 B carcinogens) (IARC, 1993b). High levels of fumonisin contamination in homegrown maize (Rheeder *et al.*, 1992) have been correlated with the high incidence of OC among the maize consuming population in Transkei in SA (Jaskiewicz *et al.*, 1987; Makaula *et al.*, 1996), in Linxian County, China, and in KZN in SA (van Rensburg *et al.*, 1985). The ubiquitous occurrence of FB_1 in maize and its products presents a threat to human and animal health, highlighting the need for the development of effective methods and suitable biomarkers to quantitatively monitor human exposure to fumonisins.

Fumonisins exert their toxicological and carcinogenic effects via inhibition of CER synthase and the disruption of sphingolipid metabolism (Riley *et al.*, 1994c). Inhibition of CER synthase by FB_1 causes accumulation of Sa and So, which normally occur at very low concentrations in cells. As time progresses and as a consequence of this inhibition, Sa and So spill over from inside the cells and enter the circulatory system *in vivo*, increasing in the serum of affected animals (Merrill *et al.*, 2001). The Sa: So ratio appears to be a better biomarker for the consumption of fumonisin-contaminated feed than absolute levels of the individual sphingoid bases (Riley *et al.*, 1994b), and may be used to detect dietary exposure to fumonisin. If detected early enough, this Sa: So ratio may allow a response such as removal of the contaminated food before the mycotoxin causes irreversible injury. Sustained regional and global analyses of human physiological fluids for determination of levels of exposure to this mycotoxin is therefore required.

Published methods for analysis of Sa, So and FB_1 from serum samples were assessed (Shephard *et al.*, 1992; Kwon *et al.*, 1998; Shephard and van der Westhuizen, 1998; Shephard *et al.*, 1998; Shephard, 1998; van der Westhuizen *et al.*, 2001), of which some were optimised and presented in Chapter 7. These optimised methods were considered

sufficiently sensitive and suitable for the quantitative detection of FB_1, Sa and So in human sera and were applied in this study. The aim of this study was to quantitatively analyse serum samples obtained from patients presenting at Wentworth Hospital (WWH) for removal of brain tumours, as well as sera from non-cancer volunteers from KZN, Durban, SA to determine the levels of FB_1, Sa and So.

9.2 MATERIALS AND METHODS

9.2.1 Materials

Reagents, chemicals, solvents, the HPLC system and conditions used for the work described in this chapter were as described in Chapter 7, section 7.2.1, unless otherwise indicated. The specimens analysed were serum samples obtained from brain cancer patients presenting at WWH and non-cancer volunteers from KZN.

9.2.2 Methodology of sample collection

Following informed consent, blood (5ml) was collected from 50 brain cancer patients from whom brain tumour tissue was removed, and from 21 non-cancer volunteers, into yellow capped serum separation blood tubes between February 1999 to November 2001. The blood samples were transferred immediately to the laboratory and centrifuged at 1200g x 10min. at RT. The serum was stored in 1ml aliquots in 1.5 ml eppendorf tubes at -70°C until processing for HPLC analyses.

9.2.3 Fumonisin B_1 extraction and quantitation from the serum

Prior to HPLC analysis to determine the amount of FB_1 present in the sera of the human subjects, samples were purified of matrix impurities and concentrated using the optimised method outlined in detail in Chapter 7, section 7.2.2.2.

9.2.4 Derivatisation and High performance liquid chromatographic analyses of Fumonisin B_1 from human serum

The chromatographic analysis conditions used in the quantitative analysis of FB_1 from the human serum were as described in Chapter 7, section 7.2.2.3. The OPA reagent for FB_1 derivatisation was prepared as described in Chapter 7, section 7.2.2.3. The derivatised

samples were injected in duplicate (50µl per injection) for determination of reproducibility and statistical validity. The time between the injection of sample and the derivatisation was not allowed to exceed 1.5 min.

9.2.5 Determination of sphinganine and sphingosine levels in human serum

The optimised method of extraction of Sa and So from human serum described in Chapter 7, section 7.7 was applied on the cancer and non-cancer serum samples.

9.2.6 Derivatisation of sphingoid bases for high performance liquid chromatographic analyses

The OPA reagent was prepared and used in the derivatisation of samples for quantitative HPLC analysis of Sa and So as described in Chapter 7, section 7.4.2. The filtered samples in 200µl inserts were placed in the autosampler, and injected in duplicate using an injection volume of 50µl.

9.2.7 Analysis of the sphingolipid derivatives using high performance liquid chromatography

Chromatographic analyses of the sphingolipid derivatives were carried out as described in Chapter 7, section 7.4.3. Standard solutions of Sa and So were run daily to verify column performance, stability of the OPA reagent, as well as the RTi and response factor for both Sa and So. Derivatised samples were stable for at least 24-hours when refrigerated and stored in darkness. The successful use of refrigerated samples for this length of time was previously documented in studies by Yoo *et al.* (1996) and was confirmed in this study.

9.2.8 Statistical analyses

All data were presented as means±SD. Comparative assessments were carried out using the paired 2-tailed Student's t test. A p value <0.05 was considered statistically significant. Correlation analyses were determined using Microsoft Excel.

9.3 RESULTS AND DISCUSSION

Sample collection commenced in February 1999 and proceeded until November 2001. The number of cancer subjects recruited in this study was dependent upon the number of patients that presented at WWH with operable brain tumours, and on their willingness to participate in this study. Even if a patient was willing to participate, on occasion the anaesthetist decided against blood sampling. The safety of the patient was always the first priority and at times when the patient was hypotensive, blood sampling was not permissible. Due to these constraints, and although brain tumour tissue (data presented in Chapter 10) was collected from the patient at scheduled operations at WWH, matched bloods were not always obtained, or too small a volume of blood insufficient for matched FB_1, Sa and So analyses were given. Although these factors substantially decreased the number of samples in the study, a total of 50 blood samples from brain cancer patients were analysed.

The results of the extraction and HPLC analyses of serum from the non-cancer and cancer samples for Sa, So and FB_1 are summarised in Tables 9.1 and 9.2.

The wide range of the ages of the cancer patients (15 months to 67 years) posed a problem in terms of matching samples with non-cancer controls either by age or race. Due to ethical considerations and logistics, it was not possible to recruit non-cancer participants as young as those in the cancer group to obtain blood for analysis. However, 21 students at the Nelson R. Mandela School of Medicine in KZN willingly donated their blood for analysis for FB_1, Sa and So levels (Table 9.1a). These samples were used in the determination of baseline levels of FB_1, Sa and So levels in non-cancer subjects.

The presence of the FB_1 in the serum samples was confirmed chromatographically by comparison of a sample chromatogram with that of a FB_1 standard. Every three runs were normally bracketed by pure FB_1 standards, allowing accurate comparison of RTi.

The serum of 21 urban dwelling non-cancer volunteers (nine males and 12 females) were analysed for the presence of FB_1 (Table 9.1a). The mean serum concentration of FB_1 recovered was 76.7 ± 62.2nM (n=21) and the mean age of these subjects was 18.8 ± 0.6 years (Appendix 9.1). Figure 9.1 presents chromatograms of FB_1 isolated from the sera of

three non-cancer volunteers, as well as an FB_1 standard. These samples showed the presence of FB_1 at various levels, and this variation is illustrated by comparison of the areas under the FB_1 peaks in the chromatograms of the non-cancer serum samples (blue, green and pink traces) at RTi of ~3.4 minutes in Figure 9.1. The red trace is the chromatogram of the FB_1 standard at a concentration of 500ng.ml^{-1}.

The mean Sa:So ratio within these non-cancer serum samples was 1.7±0.7. Figure 9.2 presents the chromatograms obtained from serum analyses of three non-cancer volunteers (purple, blue and red traces), as well as Sa and So standards for comparison (green trace). The RTi for Sa is ~6 minutes and that for So is ~4.6 minutes (Figure 9.2, green trace) using the documented chromatographic conditions.

Table 9.1a: Determination of the serum concentrations of sphinganine, sphingosine, and fumonisin B_1 in 21 non-cancer subjects

Age	Race	Sex	FB_1 (nM)	So (nM)	Sa (nM)	Sa:So ratio
18	A	F	20.1	18	ND	ND
19	I	F	22.3	-	-	-
18	I	M	22.5	129	91	0.71
19	I	F	24.1	57.7	80	1.39
19	W	F	24.4	-	-	-
18	A	M	26	119	102	0.86
19	I	M	41.2	47.9	84	1.75
19	I	F	46.3	35.2	79	2.24
20	A	M	50.3	88.2	99	1.12
19	I	F	60.7	29.9	81	2.71
20	A	F	66	50.9	88	1.73
19	W	F	69.8	83.9	92	1.10
19	I	F	74.2	22.8	76	3.33
19	I	M	91.6	47.2	79	1.67
19	I	M	95.2	343	801	2.34
19	I	F	106	26.1	40	1.53
18	I	M	106	-	-	-
19	A	F	118	73.2	88	1.20
18	I	M	122	-	-	-
19	I	M	127	-	-	-
18	I	F	296	86.8	95	1.1
Mean ± SD						
18.8±0.6			**76.7±62.1**	**78.7±78**	**131.7±185.7**	**1.7±0.7**

Key:

A	I	W	M	F	-	ND
African	Indian	White	Male	Female	Serum in sufficient for analyses	Not Detectable

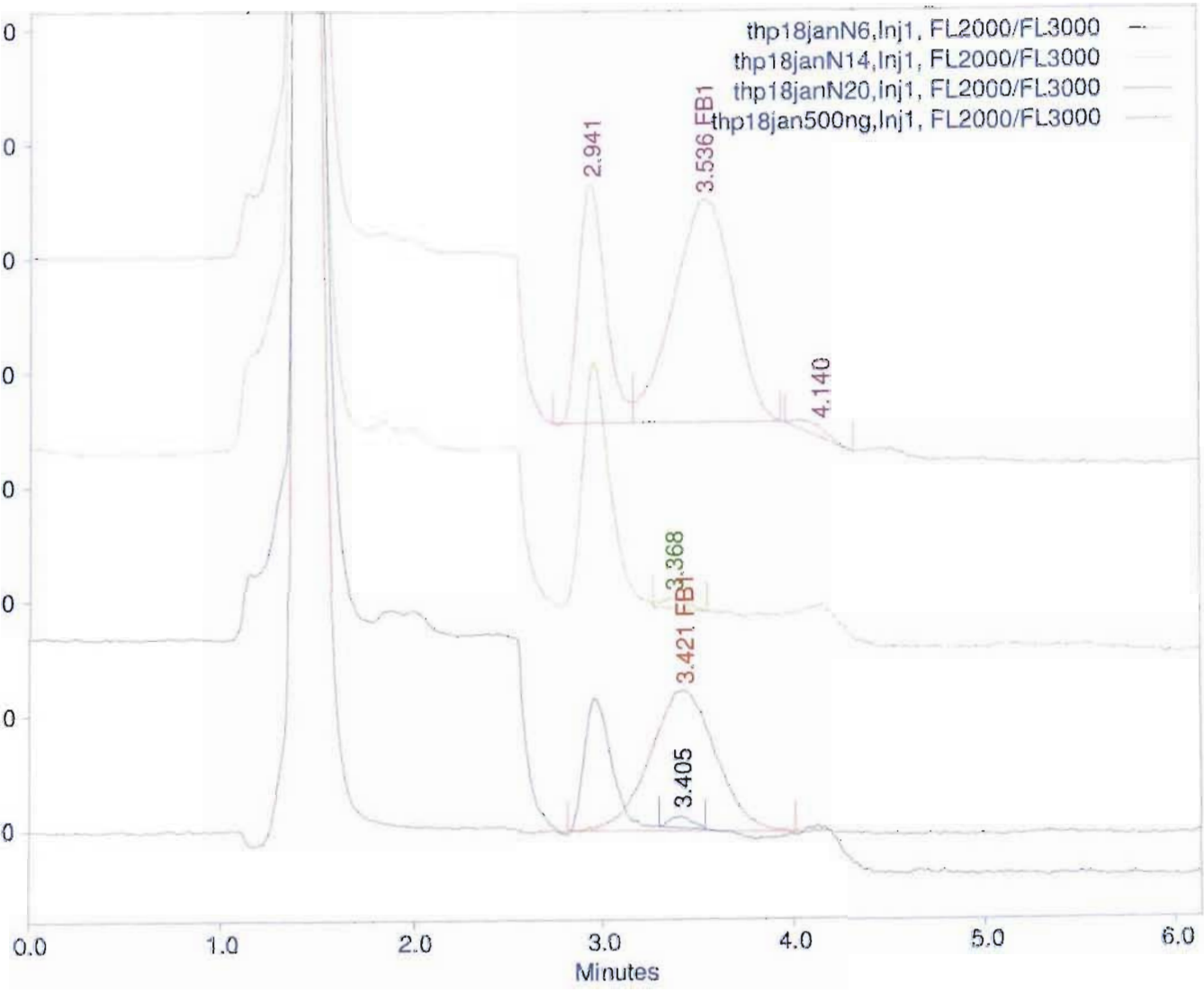

Figure 9.1: High performance liquid chromatograms showing the variable levels of FB_1 retrieved from the sera of three non-cancer volunteers (N6, N14 and N20 which are the pink, green and blue traces respectively), as well as a 500ng.ml^{-1} FB_1 standard (red trace).

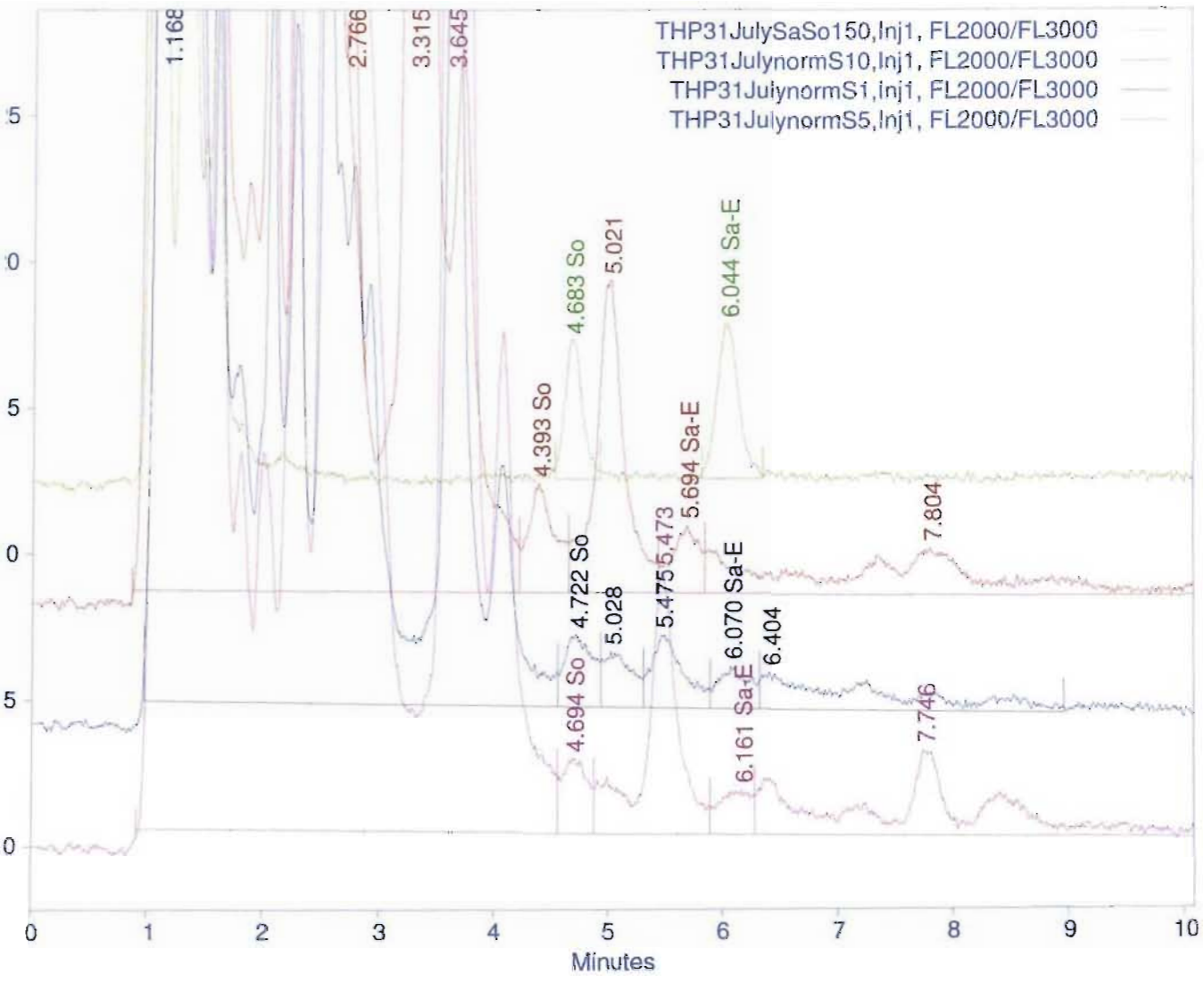

Figure 9.2: High performance liquid chromatograms showing the Sa and So bases retrieved from the serum analyses of three non-cancer volunteers (norm S10, S1 and S5, red, blue and purple traces), as well as a 150 $ng.ml^{-1}$ Sa and So standard (green trace).

These serum Sa:So ratios of urban volunteers from KZN differed markedly to those presented by van der Westhuizen *et al.* (1999) (Table 9.1b), where serum Sa:So ratios in rural male and female volunteers consuming a staple diet of homegrown maize in Transkei was 0.34±0.36 (n=154). In Kenyan volunteers, the serum Sa:So ratios were 0.28±0.07 (n=27), and in KZN, the mean serum Sa:So ratio was 0.44±0.26 (n=26) (van der Westhuizen *et al.*, 1999). The respective Sa and So levels are summarized in Table 9.1b.

Table 9.1b: Comparison of Sa: So ratios reported by van der Westhuizen *et al.* (1999) and the current study.

	Mean ± SD		
	So (nM)	**Sa (nM)**	**Sa:So ratio (range)**
This study : Urban volunteers from KZN (n=21)	78.7±78	131.7±185.7	1.7±0.7 (0.7-3.3)
van der Westhuizen *et al.* (1999)			
Transkei (n=154)	74.7±83.0	19.7±27.8	0.34±0.36 (0.01-2.97)
Kenya (n=27)	215±105	58.6±31.0	0.28±0.07 (0.17-0.50)
KZN (n=26)	128±115	66.8±88.2	0.43±0.23 (0.12-0.88)

The values reported in this study from urban non-cancer volunteers from KZN (Table 9.1b) indicate that higher levels of Sa were retrieved compared to the data reported by van der Westhuizen *et al.* (1999). This led to higher Sa:So ratios in the serum samples analysed in the present study in comparison to the Sa:So ratios obtained from serum samples of van der Westhuizen *et al.*(1999) from Kenya, KZN and Transkei.

Only 16 of the 21 serum samples were analysed for FB_1, as well as matched Sa and So levels due to the limited volume of serum obtained from the rest of the non-cancer volunteers (Table 9.1a). This group comprised White (n=1), African (n=5) and Indian (n=10) subjects (Appendix 9.2). The mean age in this group was 18.9±0.6 years, and the mean serum FB_1 was 75.5±66.3nM. The mean Sa:So ratio in these subjects was 1.65±0.7.

Analysis of the data from non-cancer volunteers according to race showed that the mean age of the Indian subjects was 18.7±0.5 years (n=14) and the mean serum FB_1 concentration was 88.2±70.3nM. The mean age of the African subjects was 19±1years (n=5) and the mean serum FB_1 concentration was 56.1±39.3nM. Comparative assessment

of the FB_1 levels detected in the Indian and African subjects using Student's t test indicated that these levels were not significantly different from each other (p=0.23). The mean age of the White subjects was 19 years (n=2) and the mean serum FB_1 concentration was 47.1 ± 32.2nM (Table 9.3). Due to the small sample size of white subjects, it was not feasible to compare or statistically analyse the data with the other race groups. The mean serum Sa: So ratios of the non-cancer volunteers was 1.0 ± 0.6 for African subjects, 1.9 ± 0.8 for Indian subjects, and 1.1 for white subjects.

The lowest level of FB_1 detected in the sera of the 21 non-cancer serum samples was 20.1nM, and in this subject the Sa level was undetectable, making it impossible to establish a serum Sa:So ratio (Table 9.1a). Cases such as this were expected since normally free So and Sa are present in tissues and cells in trace amounts (Merrill *et al.*, 1988; Riley *et al.*, 1994c). Free Sa is a metabolic intermediate in the sphingolipid biosynthetic pathway, and free So is generated primarily as a consequence of sphingolipid turnover or degradation; therefore neither should accumulate under normal conditions (Merrill, 1991; Rother *et al.*, 1992; Michel *et al.*, 1997).

Figure 9.3 correlates the serum FB_1 levels and the corresponding Sa:So ratios reported for the non-cancer volunteers. The R^2 value on the trend line is 0.0681, and the correlation coefficient (R) is 0.261 (even after removal of the outlier with a FB_1 concentration of 296nM). This indicates that there is no distinct correlation between these variables in the non-cancer volunteers recruited in this study.

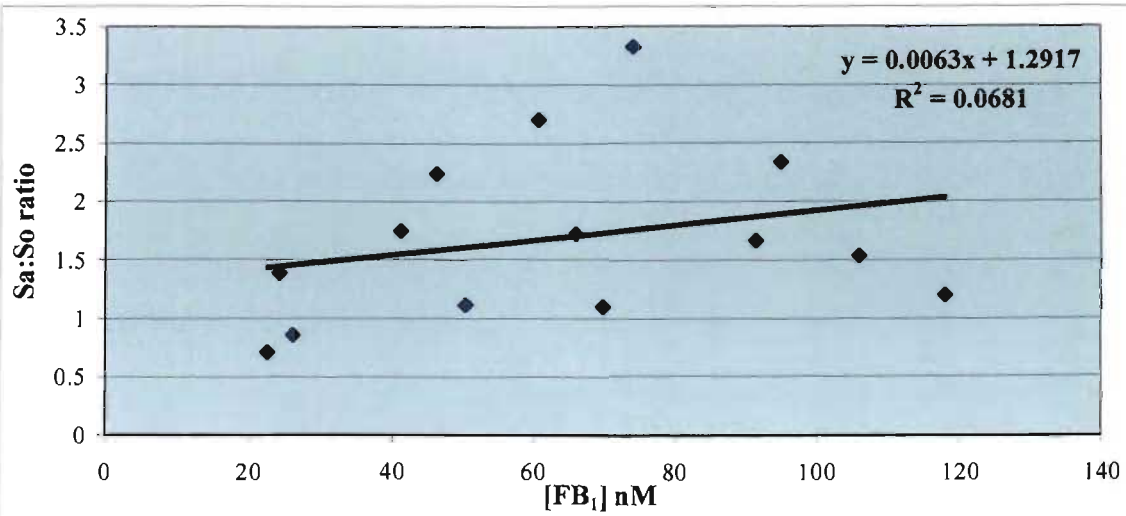

Figure 9.3: Correlation between Fumonisin B_1 concentration and the Sa:So ratio in non-cancer subjects

For example, the highest concentration of FB_1 detected in this group of urban non-cancer volunteers (n=21) was 296nM and the matched Sa: So ratio was only 1.10 (Table 9.1a). At the same time, the range of Sa: So ratios in this group varied from 0.71 to 3.3 (Table 9.1b).

It is likely that the poor correlation between serum FB_1 levels and the serum Sa:So ratio is the consequence of the rapid excretion/metabolism of FB_1 from the body into faeces and urine. Unlike cell culture models where the CCM can be retained and analysed (as in Chapter 8), drawing a defined correlation between Sa:So ratios and FB_1 levels *in vivo* are difficult. However these however indicate that the general public are exposed to varying levels of FB_1, and variation in the Sa:So ratios are evident although no correlation exists between these two variables. Clearly, there are factors, both environmental and genetic that could influence this ratio in an individual.

What then would be potential routes of exposure to FB_1 in the urban volunteers in this study? It is normal for urbanized people to eat maize products (e.g., corn flakes, pop corn. uphuthu or pap), rye, beans and other products that are infected with fumonisins presumably from urban stores, and therefore, may be unaware of its quality. Exposure to this mycotoxin was likely through the route of ingestion of commercially available food products. As documented in Chapter 2, Table 2.4 (Marasas, 1997), studies have indicated that the PDI of FB_1 from commercial maize in SA in an urban population was $1.6\mu g.kg^{-1}$ body weight per day, and this increased to $2.6\mu g.kg^{-1}$ body weight per day for rural populations. Maize examined by Dutton *et al.* (1993) showed 50% incidence of FB_1 contamination. Dutton and Kinsey (1995) analysed 417 agricultural commodities in KZN for fungi and mycotoxins. The majority of samples handled were maize (198; or 47.9%). Selected samples (73) were analysed for FB_1 and of these 69 (94%) were found to be positive. As a consequence of these results and the high incidence of *Fusarium* species (over 70% in maize and maize containing feeds), attention was drawn to the actual and potential presence of fumonisin in the SA food chain (Dutton and Kinsey, 1995). Subsequently, Dutton and Kinsey (1996) analysed over 1600 samples of agricultural commodities in KZN for fungi and mycotoxins between 1984-1993. Since 1989, selected maize samples with high levels of *Fusarium* species were examined for FB_1 and of these (n=20) in 1993, 90% were positive. These studies indicate that the general population in KZN would be exposed to varying levels of *Fusarium* mycotoxins as a result of ingesting contaminated food products.

The results of the analyses of the 50 brain cancer serum samples analysed for FB_1, Sa and So levels are shown in Table 9.2. Typical chromatograms obtained following isolation of FB_1 from sera of two cancer volunteers (green and pink traces) are presented in Figure 9.4, with a chromatogram of the FB_1 standard (dark blue trace) for comparison.

Table 9.2: Sphinganine, sphingosine and fumonisin B_1 levels in the sera of 50 brain cancer subjects.

Sex	Age	Race	Tumour	FB_1 (nM)	So (nM)	Sa (nM)	Sa:So ratio
F	22	A	Adenoma	52.8	24.0	194	8.08
M	57	A	Cerebellar hemangioblastoma	167	83.9	116	1.38
M	14	A	Choroid plexus tumour	84.7	148	115	0.78
F	17	I	Cranial pharyngioma	24.2	380	1210	3.18
F	49	A	Tumour -subtype not specified	75.7	66.3	118	1.78
M	56	A	Tumour -subtype not specified	60.0	192	147	0.77
F	55	A	Tumour -subtype not specified	66.6	74.9	117	1.56
F	17	W	Tumour -subtype not specified	105	166	665	4.01
M	1.3	A	Glioblastoma multiforme	34.7	185	521	2.82
M	23	A	Haemorrhagic lateral ventricle tumour	33.4	74.4	607	8.16
F	32	I	Left CPA tumour	39.8	194	111	0.57
M	10	A	Medulloblastoma	298	92.3	105	1.14
M	14	A	Medulloblastoma	56.4	56.4	ND	ND
M	40	A	Meningioma	65.8	58.0	83.8	1.44
F	25	A	Meningioma	283	58.1	148	2.55
F	42	A	Meningioma	25.7	229	949	4.14
F	44	A	Meningioma	312	91.6	105	1.15
F	32	A	Meningioma	49.6	422	565	1.34
F	47	A	Meningioma	101	78.9	93.6	1.19
F	29	A	Meningioma	88.8	378	205	0.54
M	50	A	Meningioma	104	124	145	1.17
M	35	I	Meningioma	23.7	29.5	ND	ND
M	25	I	Meningioma	59.7	240	456	1.9
F	64	I	Meningioma	99.6	208	182	0.88
F	51	I	Meningioma	64.2	74.4	148	1.99
M	53	W	Meningioma	329	102	96.6	0.95
M	30	W	Meningioma	58.8	203	765	3.77
M	51	W	Meningioma	23.2	207	357	1.72
F	42	W	Meningioma	32.0	389	420	1.08
F	61	W	Meningioma	52.3	214	448	2.09
F	25	W	Meningioma	83.0	87.9	103	1.17
F	53	W	Metastatic Carcinoma	140	248	325	1.31
M	59	A	Metastatic cancer- Left frontal cystic tumour	213	98.9	95.2	0.96
M	34	I	Neurilememmoma (schwannoma)	39.8	47.9	82.1	1.71
F	4	A	Occipital encephalocoele	72.5	362	391	1.08
M	11	A	Occipital tumour	31.8	162	689	4.25
M	15	A	Pilocytic astrocytomas	30.4	345	305	0.88

M	10	A	Pilocytic astrocytomas	90.3	183	251	1.37
F	5	A	Pilocytic astrocytomas	73.4	517	387	0.75
F	6	A	Pineoblastoma	24.2	297	1290	4.34
M	35	A	Pituitary adenoma	226	185	359	1.94
M	21	A	Pituitary Adenoma	NA	50.2	88.4	1.76
M	67	A	Pituitary Thoracoadenoma	420	299	120	0.40
F	34	A	Posterior fossa tumour	68.1	174	103	0.59
M	46	W	Posterior fossa tumour	602	46.8	76.0	1.62
M	4	A	Posterior fossa tumour	40.7	198	202	1.02
M	20	A	Posterior fossa tumour	79.7	271	204	0.75
M	10	I	Posterior fossa tumour	61.2	393	417	1.06
M	4	A	Posterior fossa tumour with presence of medulloblastoma	38.4	60.2	84.5	1.40
F	49	A	Transphenoidal excision of tumour	56.3	160	418	2.61
Mean ± SD							
	32.0±19			**107±116.2**	**181±121**	**316±288.4**	**1.9±1.7**

Key:

A	I	W	M	F	ND
African	Indian	White	Male	Female	Not Detectable

The 50 serum samples from brain cancer patients analysed included African (n=33; 28.9 ± 19.7 years), Indian (n=8; 33.5 ± 17.5 years), and White subjects (n=9; 42 ± 14.8 years). Their mean age was 32±19 years (Table 9.2). The absence of coloured patients in this study is supported by trends shown in Table 1 (Chapter 1). In comparison to other race groups, there are also a relatively low percentage of coloured people living in KZN. In addition, Sitas *et al.* (1998) reported that in coloured males, the lifetime risk of developing brain or CNS tumours was 1 in 1429, and in coloured females the lifetime risk was 1 in 2500. This potentially low incidence of CNS tumours in this population group may have contributed to the absence of coloured subjects in this study cohort.

The mean serum level of FB_1 in the cancer cohort was 107.4 ± 116nM (range 10.5-298nM) (Table 9.3). When analysed according to race, the mean FB_1 concentration in serum of African brain cancer subjects was 107 ± 99.2nM, 51.5 ± 25.2nM for Indian subjects, and 158.4 ± 190.5nM for White subjects (Table 9.3). Although these analyses indicate that mean serum FB_1 levels appear higher in the African and White brain cancer subjects, than in the African (56.1 ± 39.3nM FB_1) and White non-cancer subjects (47.1 ± 32.2nM FB_1), these differences were not significant (Africans, cancer versus non-cancer p=0.27; Whites,

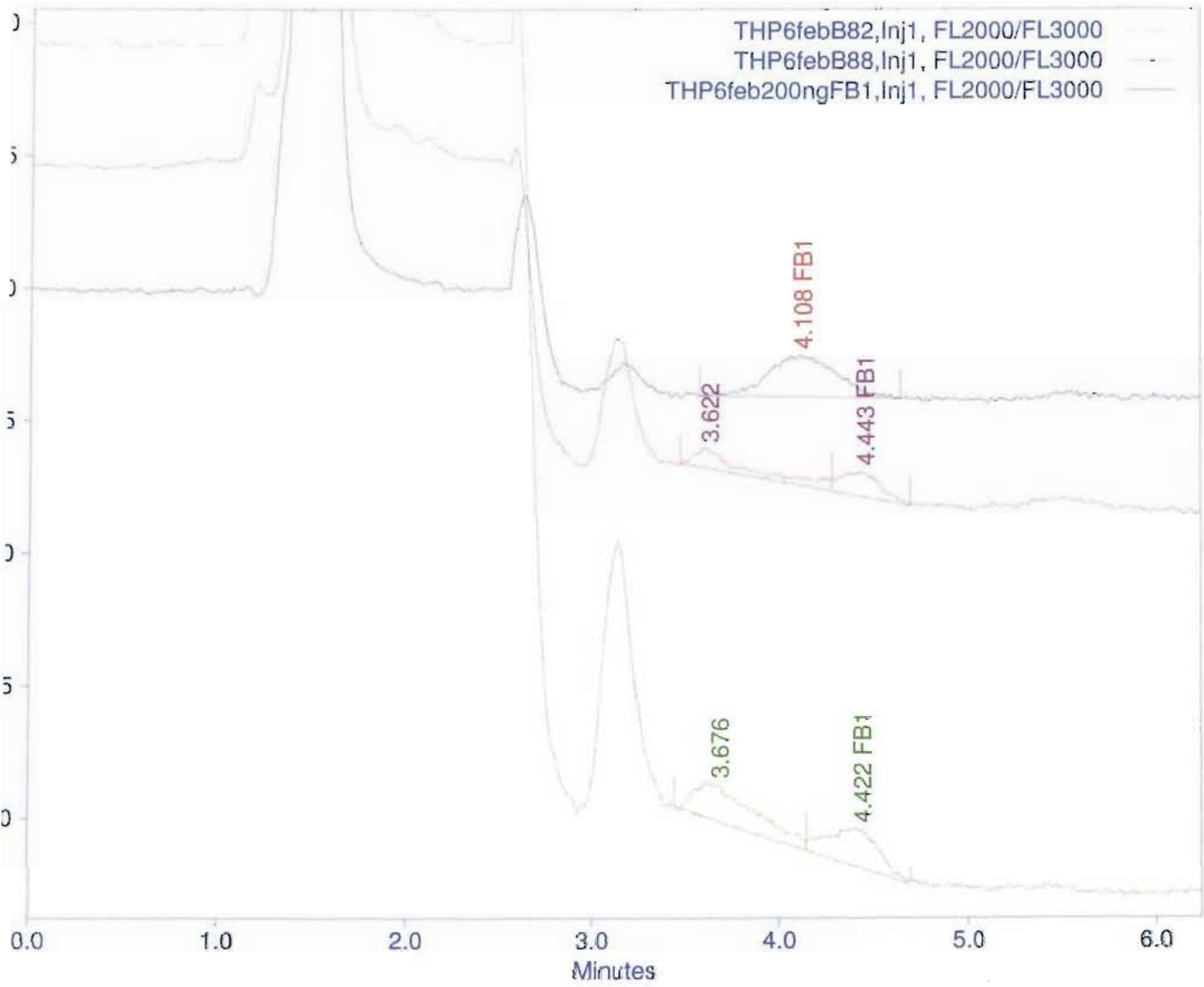

Figure 9.4: High performance liquid chromatograms showing the levels FB_1 retrieved from the sera of two cancer volunteers (green B82 and pink B88 traces), as well as a 200ng.ml^{-1} FB_1 standard (dark blue trace).

cancer versus non-cancer p=0.44). Similar results were found in the Indian sub-group, in that although higher serum levels of FB_1 were detected in the non-cancer subjects (88.2±70.3nM FB_1) than cancer subjects (51.5±25.2nM FB_1), when analysed statistically, they did not differ significantly (Indians, cancer versus non-cancer, p=0.17). This indicates that there was no predominance of exposure to FB_1 in the cancer group over the non-cancer group when analysed in terms of racial classification.

To determine whether any correlation exists between FB_1 serum levels and the serum Sa:So ratios (Table 9.2) in the cancer subjects, a correlation analyses was carried out (Figure 9.5). The correlation coefficient between these variables was -0.23 (R^2=0.053), indicating absence of a correlation between Sa:So ratios and the serum levels of FB_1 in the cancer patients in this study cohort.

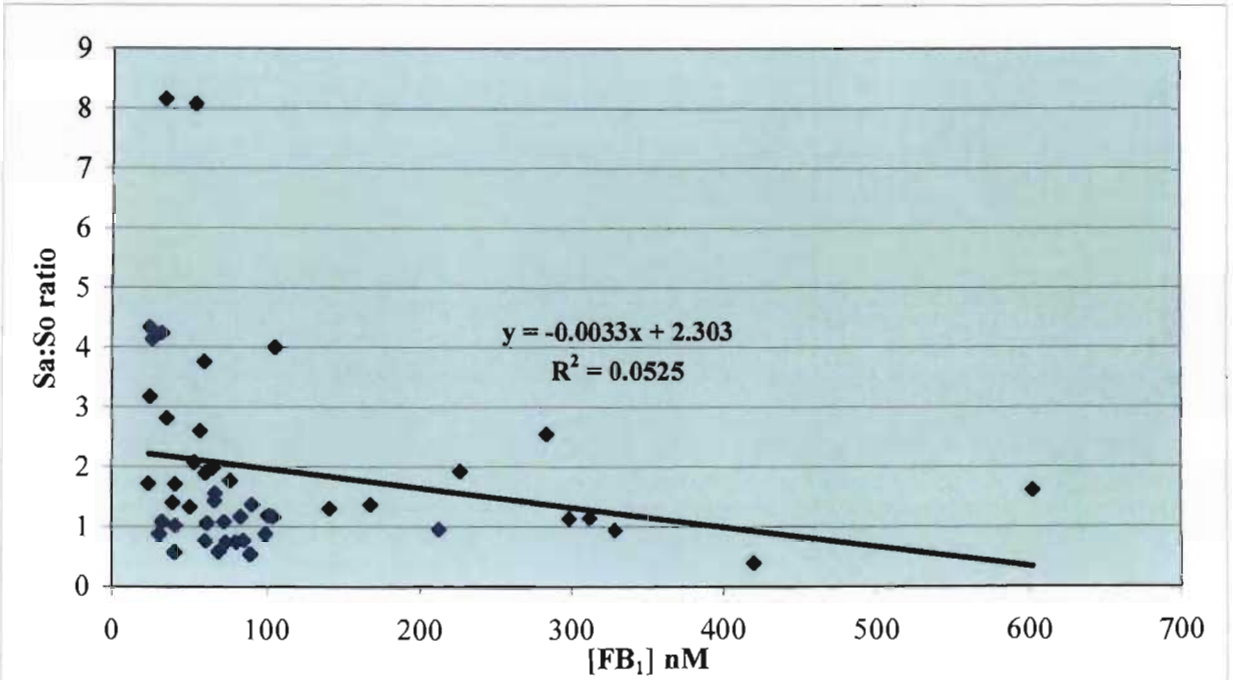

Figure 9.5: Correlation between FB_1 levels and Sa:So ratios in sera of brain cancer subjects

The poor correlation between FB_1 serum levels and the Sa:So ratio is largely due to the fact that FB_1 is poorly absorbed from the GIT, cleared rapidly from circulation in the serum, and excreted primarily in the faeces even after intravenous administration (Bucci *et al.*, 1998). Therefore even though quantitative analyses were done in this study, the results provide more of a qualitative indication of exposure to FB_1. Although an optimised isolation method for FB_1 was applied in this study, direct quantitative correlation

with Sa and So levels would be more applicable to controlled studies where the amount of FB_1 ingested was known or regulated. In humans however, this is not possible, and studies such as this one serve the purpose of elucidating the potential use of Sa:So ratios as a biomarker under real *in vivo* conditions versus *in vitro* laboratory studies.

The serum Sa and So levels, and Sa:So ratios in the Indian, White and African brain cancer and non-cancer subjects are summarized in Table 9.3. The mean serum Sa: So ratio in the brain cancer subjects (n=50) was 1.9±1.7 (range 0.40-8.16), and in the non-cancer subjects (n=21) was 1.7±0.7(range 0.7-3.3). There appeared to be no significant difference between the groups. The Sa:So ratios for the cancer subjects were 1.61±0.9 for the Indians, 1.97±1.1 for the Whites and 2.0±1.9 for the African subjects, which again are not different from data for the respective non-cancer subjects. These analyses indicate that race is not a factor in the variation or determination of the serum Sa:So ratios.

Table 9.3: Summary of serum levels of fumonisin B_1, sphinganine and sphingosine retrieved from non-cancer and brain cancer subjects.

	Mean ± SD				
Healthy volunteers	**Age (years)**	**FB_1 (nM)**	**So (nM)**	**Sa (nM)**	**Sa:So ratio**
Males (n=9)	18.67 ± 0.71	75.56 ± 41.02	129.05 ± 110.30	209.33 ± 289.99	1.41 ± 0.62
Females (n=12)	18.92 ± 0.51	77.33 ± 76.08	48.45 ± 25.90	71.9 ± 29.55	1.63 ± 0.94
All subjects n=(21)	18.81 ± 0.60	76.65 ± 62.10	78.7 ± 78	131.7 ± 185.7	1.7 ± 0.7
African (n=5)	19 ± 1	56.1 ± 39.3	69.9 ± 38.1	75.4 ± 42.6	0.98 ± 0.6
Indian (n=14)	18.7 ± 0.5	88.2 ± 70.3	82.6 ± 97.1	150.6 ± 229	1.87 ± 0.78
White (n=2)	19	47.1 ± 32.2	83.9	92	1.09
Cancer volunteers					
Males (n=27)	29.46 ± 19.74	125.83 ± 143.24	153.17 ± 97.15	259.504 ± 208.22	1.81 ± 1.60
Females (n=23)	35 ± 17.82	86.51± 72.60	212.79 ± 139.44	378.07 ± 350.35	2.09 ± 1.74
All subjects (n=50)	32.006 ± 18.9	107.38 ± 116	180.59 ± 121	316.32 ± 288	1.86 ± 1.67
African (n=33)	28.9 ± 19.7	107 ± 99.16	175.7 ± 124.0	291.3 ± 279	2 ± 1.94
Indian (n=8)	33.5 ± 17.5	51.5 ± 25.2	195.9 ± 141.0	372.3 ± 397.9	1.61 ± 0.88
White (n=9)	42 ± 14.8	158.4 ± 190.5	184.9 ± 101.9	316.32 ± 288	1.97 ± 1.14
Adults (n=35)	41.7 ± 13.6.	123 ± 130	157 ± 107	251 ± 216	1.91 ± 1.78
Children (n=15)	9.5 ± 5.2	71.1 ± 67.84	236 ± 137.48	474 ± 380.20	2.01 ± 1.39
Meningiomas (n=18)	41.44 ± 12.24	103.08 ± 98.10	177.47 ± 121.22	310 ± 258.67	1.71 ± 0.99

Large standard deviations indicate large inter-patient variability in the absolute serum levels of Sa and So. Figures 9.2 and 9.6 present chromatograms of Sa and So retrieved from the sera of three non-cancer volunteers and four brain cancer subjects respectively. The identification of serum Sa and So were confirmed by comparison with the Sa and So standards.

Comparative analyses were also carried out between serum concentrations of Sa, So, Sa: So ratios and FB_1 in adults and children (birth to 18 years) from the cancer group to determine whether age plays a role in these variables. The mean age of the children was 9.5±5.2years, the mean FB_1 sera concentration was 71.1±67.8nM, and the mean sera Sa:So ratio was 2.0±1.4. In the adults (>18 years), the mean age of the subjects was 41.7±13.6 years (Table 9.3). The mean serum FB_1 concentration and Sa:So ratio was 123±130nM, and 1.9±1.8 respectively. Although these results indicate that the adults were exposed to slightly higher levels of FB_1, they were not significantly different ($p=0.15$), and there was no correlation between serum levels of FB_1 and age of the patients (Figure 9.7; $R=0.32$). The Sa:So ratios between the adults (1.91±1.78) and children (2.01±1.39) were also not significantly different ($p=0.86$) within the cancer group.

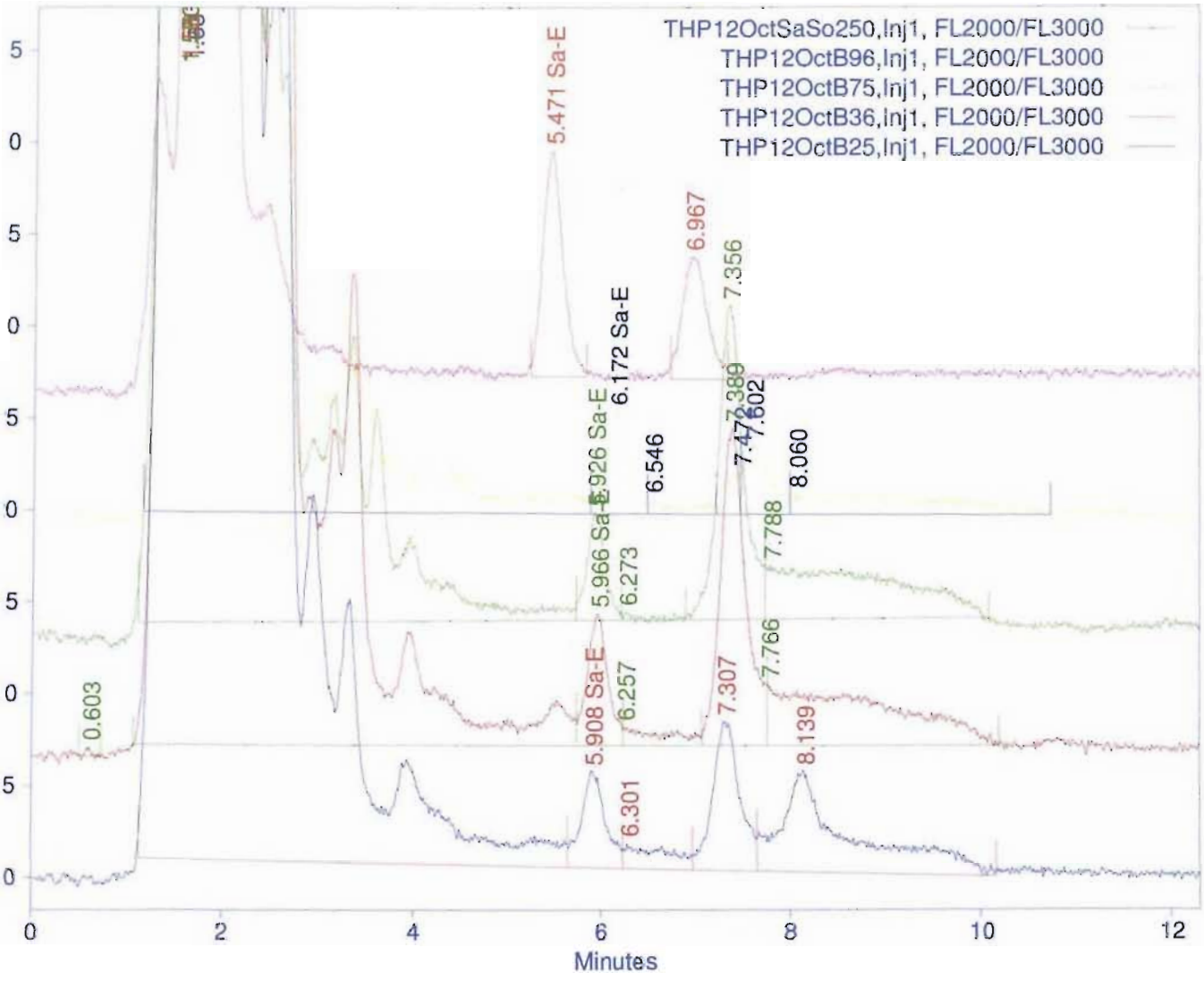

Figure 9.6: High performance liquid chromatograms showing the Sa and So bases retrieved by serum analyses of four brain cancer subjects, as well as a chromatogram of the 250ng.ml^{-1} Sa and So standard (purple trace).

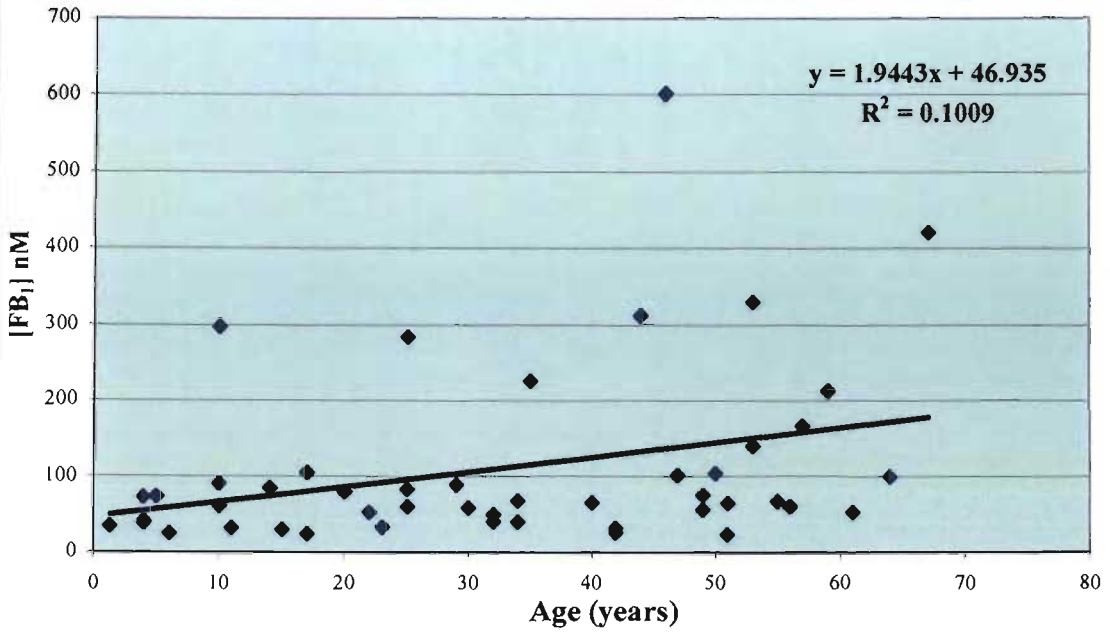

Figure 9.7 : Correlation between age of cancer subjects and serum FB_1 levels

The most prevalent tumour subtype diagnosed in cancer subjects enrolled in this study was the meningioma. Eighteen of the 50 cancer patients (36%) were admitted for removal of meningiomas and their mean age was 41.4 ± 12.2 years (Table 9.3). The mean serum FB_1 concentration in these patients was 103.1 ± 98.1nM FB_1 and the mean serum Sa:So ratio was 1.7 ± 1.0. In comparison to the healthy volunteers, although their mean Sa:So ratio was 1.7 ± 0.7; the serum levels of Sa and So, as well as the serum levels of FB_1 (76.7 ± 62.1) were much higher in the meningioma patients (Table 9.3). However there was no correlation (R = - 0.23) between the serum FB_1 and Sa:So levels in the patients with this tumour subtype (Figure 9.8).

Ramasamy *et al.* (1995) established that FB_1 alters sphingolipid metabolism in endothelial cells from pulmonary arteries, and that FB_1 and D-erythro Sa interferes with the permeability barrier function of these cells. This increase in Sa was attributed to inhibition of CER synthase by fumonisins, and accumulation of this intermediate of *de novo* sphingolipid biosynthesis. Complex sphingolipids have been implicated in cell-cell interaction, as well as cell-extracellular matrix interactions. The blockage of *de novo* sphingolipid synthesis may have weakened intercellular interactions, and affected the barrier function of endothelial cells making the barrier "leaky" (Ramasamy *et al.*, 1995). In addition, complex sphingolipids, as well as So and Sa, affect numerous signal transduction

pathways, some of which have been implicated in the control of endothelial cell permeability (Hoek, 1992).

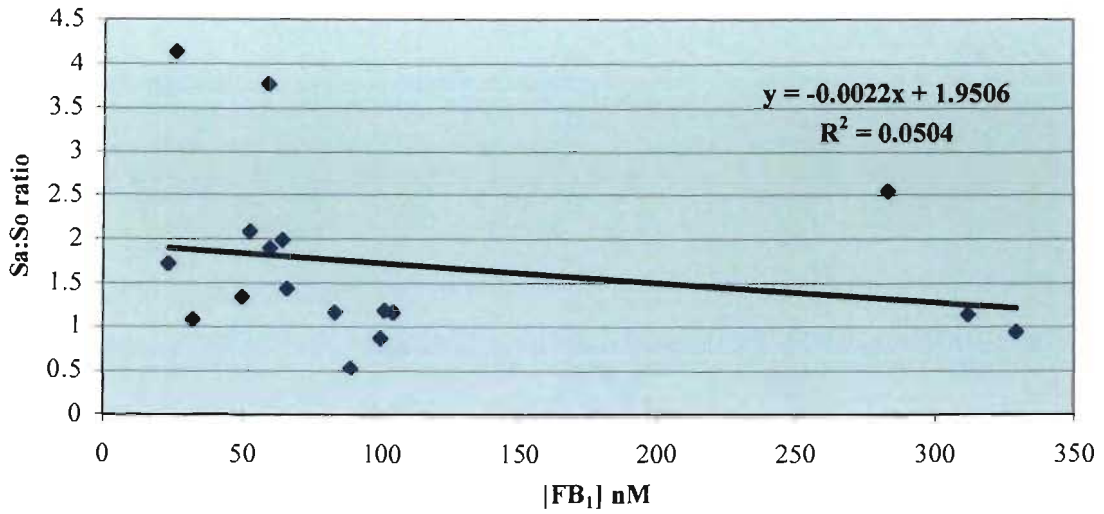

Figure 9.8: Correlation between serum fumonisin B_1 levels and Sa:So ratios in meningioma patients

As sphingoid bases have intrinsic biological activity, and their elevation may have been related to, or contributed to exacerbation of the cancer condition, the serum levels of Sa and So were assessed in relation to the serum levels of FB_1 in the meningioma patients (Figures 9.9 and 9.10).

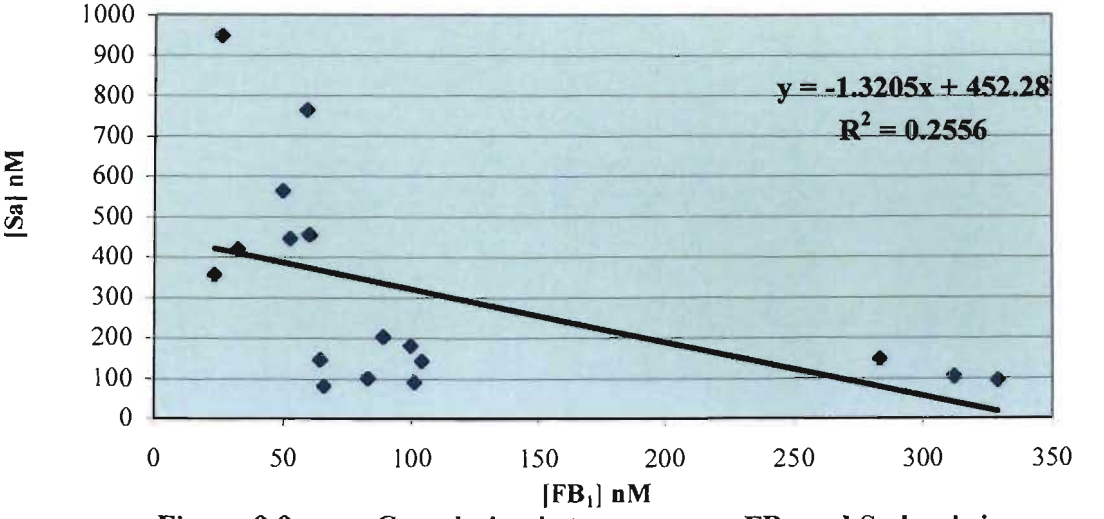

Figure 9.9: Correlation between serum FB_1 and Sa levels in meningioma patients

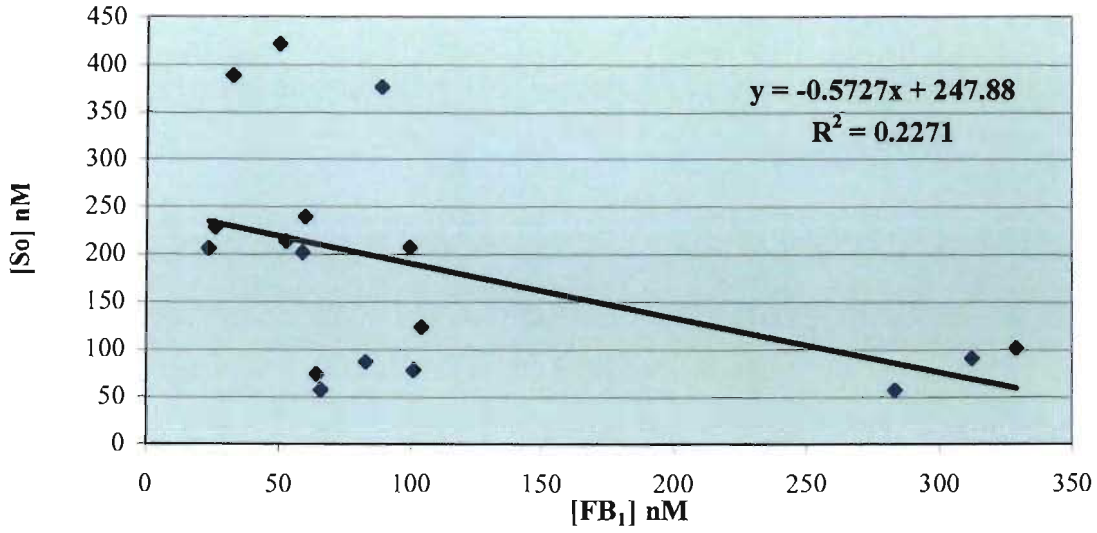

Figure 9.10: Correlation between serum FB_1 and So levels in meningioma patients

No positive correlations however, were noted between serum levels of Sa and FB_1 (R= -0.505; Figure 9.9), nor So and FB_1 (R= -0.48; Figure 9.10) in the meningioma patients. Furthermore, there was no correlation between the serum FB_1 and Sa levels of the 50 brain cancer subjects (R = -0.38; Figure 9.11).

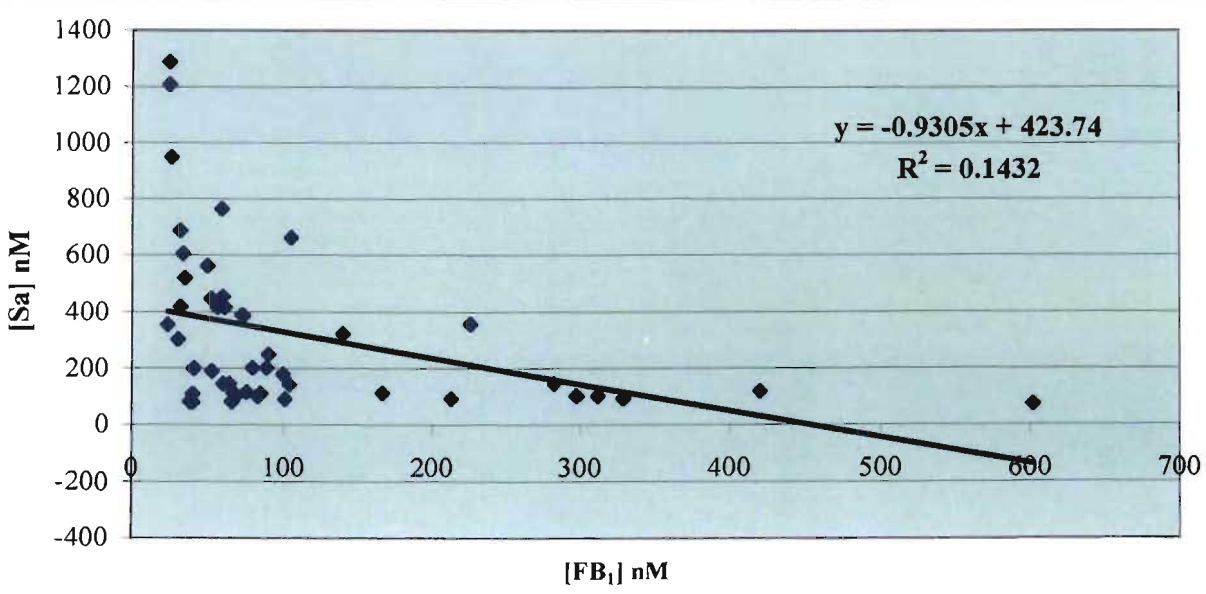

Figure 9.11: Correlation between serum FB_1 and Sa levels in the 50 brain cancer patients

Sphingolipids are integral components of membranes. It would therefore be tempting to speculate that as FB_1 is an inhibitor of sphingolipid metabolism, and that the meninges are membranes that surround the brain; the presence of FB_1 in these patients serum may have disrupted sphingolipid metabolism and endothelial barrier function in the meninges. However, the analytical results of the sera in this study do not provide statistically significant evidence to support this hypothesis.

The serum Sa and So levels, as well as Sa:So ratios for male and female non-cancer subjects are summarized in Table 9.3. The mean serum Sa:So ratio in the healthy male subjects (n=9) was 1.41 ± 0.6 and the serum FB_1 concentration was 75.6 ± 41.0nM (Table 9.3). For the serum samples analysed from non-cancer female subjects (n=12), the Sa:So ratio was 1.6 ± 0.9 and the FB_1 mean concentration was 77.3 ± 76.1nM (n=12). These results indicate that although the absolute amounts of Sa and So were higher in the male non-cancer volunteers, the Sa:So ratios were somewhat higher in female subjects (Table 9.3). As the mean concentrations of FB_1 retrieved from male and female subjects were not significantly different ($p = 0.95$), there was no potential for a correlation of FB_1 levels and So:So ratios, but possibly for gender differences in Sa and So levels alone. Statistical analyses of the healthy male and female Sa:So ratios however indicate no significant differences in this study cohort ($p = 0.63$). The ratios determined overlapped between the sexes as indicated by the large standard deviations calculated, indicating large inter-individual variation (Table 9.3). When the serum samples of the cancer subjects were analysed according to gender, the serum FB_1 levels determined for the females subjects was 86.51 ± 72.60nM FB_1 (Table 9.3). These levels were not significantly different to the serum levels in the healthy females ($p = 0.73$). The mean Sa:So ratio in the female cancer patients ($n = 23$) was 2.09 ± 1.74, and although higher than the serum Sa:So ratio established for female subjects in the healthy group (1.63 ± 0.94) (Table 9.3), this ratio was not significantly different either ($p = 0.43$). The mean serum FB_1 levels in male cancer subjects was 125.83 ± 143.24nM FB_1, and was not significantly different to the serum levels of the healthy male subjects ($p = 0.31$). Comparative analysis of the Sa:So ratios of the cancer and healthy males revealed that these levels did not differ significantly either ($p = 0.56$).

The results of this study are in coherence with Abnet *et al.* (2001a) where no differences between male and female serum sphingolipid concentrations were found.

Castegnaro *et al.* (1998) also reported values for Sa: So ratios in sera from healthy human volunteers from France (eight males and 10 females) and SA (13 females of Asian origin), in which the values ranged from 0.09 to 0.78 and overlapped between the sexes. van der Westhuizen *et al.* (1999) also did not find any significant differences in the Sa:So ratios between males and females within the Transkei region of the Eastern Cape, KZN in SA, the Bomet District in western Kenya, nor between the different regions ($p>0.05$). It was considered possible that the ratio was not sensitive enough to act as a biomarker for fumonisin exposure in humans at the levels of contamination in maize of $580ng.g^{-1}$ in Transkei, $<10ng.g^{-1}$ in KZN and $60ng.g^{-1}$ in Kenya (van der Westhuizen *et al.*, 1999). In urban areas and in developed countries where maize is not the staple diet but merely one item in a mixed diet, intake of fumonisin will be correspondingly reduced depending on the individual consumption patterns. At this level, any increase in the ratio may be masked by the natural variation between and within individuals.

This study assessed the relationship between sphingoid base levels as biomarkers of fumonisin exposure and cancer incidence. No significant association between sphingolipid levels and risk of brain cancer were found from sera analyses for FB_1, Sa and So, nor the Sa:So ratio. In the present study, the serum Sa:So ratio did not prove a potential biomarker to distinguish between brain cancer and non-cancer subjects exposed to FB_1, nor was there sufficient evidence for the use of the Sa:So ratio as a suitable biomarker for susceptibility to brain cancer. Large inter-individual variations in the serum Sa: So ratios made interpretation difficult, and was not considered sensitive enough to act as a biomarker for fumonisin exposure in humans at the levels of exposure through commercially available food products.

These results are supported by findings by Abnet *et al.* (2001b) in a study to determine whether sphingolipids could be used as a biomarker for fumonisin exposure and risk of oesophageal cancer squamous cell carcinoma (OSCC), that although approximately one third of the subjects in that study went on to develop oesophageal cancer between one to six years after the serum was collected, serum sphingolipids did not differ between controls and eventual cases. Collection of serum before diagnosis, as well as the lack of an association between sphingolipid levels and oesophageal cancer incidence allowed the authors to combine the groups for the purposes of another study. Median serum concentrations for the entire study population were 47.3nM (unadjusted) and 52.2nM

(lowess adjusted) for So. No significant associations were found between serum Sa, So or the Sa:So ratio and OSCC incidence in conditional and unconditional logistic regression models with adjustment for age, sex, tobacco use, and alcohol use. This study assessed the relationship between sphingolipid levels, as biomarkers of fumonisin exposure and cancer incidence. No significant association between sphingolipid levels and risk of OSCC were found (Abnet *et al.*, 2001b).

The presence of varying levels of FB_1 in the serum of brain cancer and non-cancer volunteers suggests that it is present in the circulatory system of the general population, and these levels are probably dependent on the level of exposure (Table 9.3). The varying Sa and So levels also indicate great variation between individuals, as most, if not all, tissues have the capacity to synthesize long chain bases *de novo* (Merrill *et al.*, 1985).

Although in past studies attention has been given to the possibility of the formation of fumonisin degradation products, which is likely due to the acidic nature of the stomach and the microbial activity of the GIT, little is known about the GIT absorption of FB_1. A limited amount of FB_1 is absorbed into the bloodstream in its intact form. However, when it loses the tricarballylic side chains by hydrolysis, absorption is enhanced (Hopmans *et al.*, 1997). This may explain the greater toxicity of hydrolysed FB_1 in comparison to FB_1. One school of thought that FB_1 is polyanionic and may decrease its own absorption by binding cations such as sodium, potassium and other large molecules. Polycations have been known to inhibit active transport of sugars and amino acids across the intestinal membrane in rats (Elsenhans *et al.*, 1983). The serum samples in this study were not analysed for the presence of hydrolysed FB_1 products due to the limited volume of blood obtained. It would be interesting in future studies to correlate the percentage of hydrolysed and non-hydrolysed FB_1 in the serum of human subjects.

In this study, due to theatre times and hospitalisation of patients it was not possible to standardise times of blood draw, nor recruit large numbers of brain cancer subjects, both factors that were confounding variables in this study. Fears of Human Immunodeficiency Virus (HIV) testing in clinical settings also prevent the general public from volunteering their blood research for studies such as this. Should future studies be pursued to revisit the use of FB_1 levels and corresponding Sa:So ratios as a biomarker, it would be advisable to recruit larger numbers ($n>200$) of healthy volunteers whose diets could be monitored strictly, where blood draw time would be standardized to specific times of the day so as to

monitor any subtle changes that occur prior to pursuing the link to the aetiology of cancer. Access to larger sample sizes would enable the establishment of credible correlations.

9.4 CONCLUSION

This study reports for the first time matched measurements of Sa:So ratios and FB_1 levels in human serum samples obtained from brain cancer patients and non-cancer volunteers from KZN. Using HPLC, an analytical approach was adopted to isolate and quantify serum levels of FB_1, Sa and So from non-cancer (n=21) and brain cancer (n=50) subjects. Fumonisin B_1 was detected in the serum of both non-cancer (76.7 ± 62.2nM) and brain cancer subjects (107.38 ± 116nM). Considerable overlap in the serum Sa:So ratios also occurred between non-cancer subjects (range 0.7-3.3) and brain cancer subjects (range 0.40-8.16).

The mean serum Sa:So ratio of 21 non-cancer volunteers was 1.7 ± 0.7. Correlation graphs indicated that there was no correlation (R = 0.26) between serum FB_1 levels and Sa:So ratios in the non-cancer subjects. This implies that there is no causal relationship between serum levels of this exogenous sphingolipid inhibitor and inhibition of sphingolipid metabolism in this study population. However non-cancer subjects are equally at risk to the biochemical effects of exposure to this mycotoxin, and this is of growing concern due to the possible side effects of cumulative, and long-term exposure to FB_1.

The mean sera FB_1 level in the brain cancer subjects were 107.4±116nM (range 10.5-298nM) (n=50) and the mean Sa:So ratio (n=50) was 1.9±1.7 (range 0.40-8.16). Correlation analysis of these variables indicated absence of a correlation between serum FB_1 levels and Sa:So ratios (R = -0.23). There was also no correlation between serum levels of FB_1 and age of the patients (R=0.32). Race was not a factor in the variation of sera Sa: So ratios.

Gender-based statistical analyses indicated no significant differences in the non-cancer subjects serum Sa: So ratios in this study cohort either (p = 0.63). In the female brain cancer subjects, the serum FB_1 levels were 86.5 ± 72.6nM FB_1. These levels were not significantly different to the levels in the non-cancer females (p = 0.73). The mean Sa:So ratio in the female cancer patients (n = 23) was 2.1 ± 1.7, and although higher than the

serum Sa:So ratio established for female subjects in the non-cancer group (1.6 ± 0.9), were not significantly different (p = 0.4). Comparative analysis of the Sa:So ratios of the male cancer and non-cancer subjects also revealed that these levels were not significantly different (p = 0.6).

Analyses of the sera of meningioma patients (as this tumour subtype was the most frequently seen in this study), revealed no positive correlations between serum levels of Sa and FB_1 (R = - 0.505), nor So and FB_1 (R= - 0.48). Furthermore, there was no correlation between the serum FB_1 and Sa levels of the 50 brain cancer subjects (R= - 0.38).

A further complication in the potential use of the Sa:So ratio lies in determining the 'normal' levels of Sa and So, since this and previous studies in human and animals have demonstrated considerable inter and intra-individual variation in the Sa: So ratio over time. As individual levels vary widely, repeated serum analyses on an individual may be necessary and this would detract from its usefulness as a biomarker. The sexual differences in the Sa:So ratios, as well as the diet and foods consumed by the subjects prior to testing would also need consideration.

Limiting variables in the study included the sample size; limited volumes of blood and the inability to match all subjects for age and gender. The serum analyses reported in this study reveal that the general public are exposed to FB_1 at varying levels, probably via the ingestion of commercially available foods (although this route could not be verified in this study). A conceptual framework and data are presented that possibly contests the primary use of the Sa:So ratio as a biomarker for a dose response of FB_1-induced inhibition on sphingolipid metabolism, or as a biomarker for brain cancer in human subjects. The potential exists that FB_1 may be a contributing factor by its mere presence in sera, but not a primary cause in the aetiology of brain cancer in the participants in this study, unless it can be located directly within the brain tumour tissue. The analysis of the data from these volunteers from KZN suggests that the serum Sa:So ratio may not be useful as an indicator or biomarker of fumonisin exposure in human subjects.

CHAPTER 10

Ultrastructural and immunochemical analyses of brain carcinomas for fumonisin B_1

10. 1 INTRODUCTION

One of the challenges in environmental health is to attribute a certain health effect to a specific environmental exposure, and to establish a cause-effect relationship. The supposed limited susceptibility of the brain to environmental diseases including cancers, due to the presence of the BBB, increases interest in neurotoxicological studies. This interest stems from the prevalence of these diseases such as cancer regardless of the level of protection of the brain. Diagnoses of neurological disease caused by fungi can be difficult as clinical signs are often ambiguous or similar to those found in other diseases, and histological lesions may be non-specific or absent (Plumlee and Galey, 1994). Therefore, the diagnosis of diseases caused by neurotoxic mycotoxins depends not only on clinical history and lesions, but also on finding the specific mycotoxin in the tissue concerned in association with histopathological changes.

Animal studies have shown that ELEM is characterised by severe oedema and multi-focal liquefactive necrosis predominantly in the white matter of the brain, although the grey matter may also be involved (Marasas *et al.*, 1988a). The causes of ELEM after FB_1 dose may be direct, via the mediated presence of Sa in brain (i.e., by direct inhibition of CER synthase in brain cells), or indirect, via FB_1-induced hepatotoxicity and nephrotoxicity, disruption of barrier function of cultured endothelial cells, and damage to the cerebral blood vessels. Kwon *et al.* (1997a) have shown that small amounts of FB_1 entered brain tissue in developing rats and increased Sa levels, and that plasma Sa elevation due to FB_1 exposure probably did not contribute to the elevation of brain Sa levels. Altered brain Sa levels and Sa: So ratios indicate that sphingolipid metabolism in the CNS of developing rats was vulnerable to FB_1 exposure (Kwon *et al.*, 1997a). Alteration of blood vessels in the CNS and/or disruption of the BBB may have had effects on the transfer of FB_1 or Sa into brain tissue (Kwon *et al.*, 1997b).

Although *F. moniliforme* and fumonisins occur worldwide on maize products, this study was relevant in the South African context since population groups make preferential use of

visibly mouldy maize as an ingredient in the making of traditional home-brewed beers. In addition, studies by Dutton and Kinsey (1995) revealed high incidence of *Fusarium* species of fungi in over 70% in maize and maize containing feeds, drawing attention to the actual and potential presence of fumonisin in the food chain in SA.

In Chapter 9, the analyses of sera from both brain cancer and non-cancer volunteers from KZN suggests that the serum Sa:So ratio may not be ideal as an indicator or biomarker of fumonisin exposure in human subjects. However, it was established that FB_1 was detected in the serum of both non-cancer (76.7±62.2nM) and brain cancer subjects (107.38±116nM). The potential exists that FB_1 may be implicated in the aetiology of brain cancer by its mere presence in sera of brain cancer subjects. In order to test this hypothesis, human brain tumour tissues from the majority of subjects who provided sera for analysis in Chapter 9, and non-tumour tissue specimens were examined to determine whether any association exists between FB_1 presence and human brain cancer. This study was conducted in collaboration with WWH, and the Departments of Neurosurgery and Physiology, UKZN.

Brain tissue specimens were screened for the presence of FB_1 using IHC, employing LM in conjunction with EM, and immuno-electron microscopy. When FB_1 was immunolocalised within necrotic tissue, the histopathology of the tissue was analysed in relation to the localised mycotoxin. Image analysis was also applied for quantitation of FB_1 within brain tissue.

10.2 MATERIALS

Materials used in this chapter were as described in Chapter 6, Section 6.2.1, unless otherwise indicated. In addition, LM materials (e.g., paraffin wax and specimen holders), Poly-L-Lysine, a Pap delimiting pen, aminoethyl carbozole (AEC) chromogen and beem capsules were purchased from Capital Enterprises, SA. All organic solvents were purchased from MERCK. An automatic tissue processor (Shandon) was used to process the tissues for LM at the Department of Anatomical Pathology. A Leica Jung RM2035 rotary microtome was used to section wax-embedded tissue specimens, and a Reichert Ultracut ultramicrotome was used to section resin-embedded sections at the Optics and Imaging Centre, UKZN. The H&E stained sections of the normal and brain tumour tissues were

viewed and photographed on a Zeiss photomicroscope using a Nikon FX camera. A Nikon Optiphot photomicroscope, a Sony 3 charged couple device (CCD) colour video camera and the Kontron Elektronik Imaging System 300 software programme (KS 300) were used for image analysis at the Optics and Imaging Centre, UKZN. The JEOL 1010 TEM was used at the Electron Microscope Unit, UKZN for all electron microscopic analyses.

10.3 METHODS

10.3.1 Collection of specimens

Sixty-three brain tumour tissue biopsies were obtained on surgical removal of the tumours from brain cancer patients examined at WWH, KZN. In addition, 16 non-cancer brain tissue specimens were obtained at autopsies at King Edward VIII Hospital mortuary (Appendix 10.1). Twelve wax-embedded brain tumour specimens were also obtained from the Department of Anatomical Pathology, UKZN. Due to ethical considerations, it was not possible to age or sex match the brain tumour tissue samples analysed with appropriate non-tumour controls.

Specimens were placed into appropriate fixatives to avoid autolysis and bacterial degradation. Fresh specimens were cut into small pieces and immersed in Karnovsky's (1965) fixative (pH 7.2) (Appendix 10.2) in 0.2M sodium cacodylate buffer for TEM. Specimens for ICC were immersed in glutaraldehyde (1%) in phosphate buffer (pH 7.4), and those for LM in 5% formal saline (41% formaldehyde/0.9% sodium chloride (NaCl), 1:8 v/v) dilute formaldehyde (35%) 1:7 in 0.9% NaCl. Specimens were transported to the laboratory in sealed vials in this manner.

Twelve wax-embedded kidney tissue specimens of male Fischer 344 rats fed dietary FB_1 at concentrations ranging from 750 to 25mg.kg^{-1} diets for a period of 21 days were obtained from the MRC, Tygerberg, SA, courtesy of Dr WCA Gelderblom and Prof WFO Marasas. The animal care and use protocol was approved by the Ethics Committee affiliated to the MRC for research undertaken by PROMEC. The selection of rat kidney tissue as a method control was based on the fact that cancer induction by FB_1 was previously investigated by studying the mechanisms involved during cancer initiation and promotion in rat kidney in this species of rat (Gelderblom *et al.*, 1993; 1994). In addition, N2α neuroblastoma cells were grown and treated with FB_1 as described in Chapter 6, Section 6.2.2.1, 6.2.4, and

6.2.6. These cultured cells were also used as method controls in the IHC technique applications.

Both formalin fixed paraffin embedded (FFPE) kidney tissue sections and non-FFPE specimens in the form of the cultured N2α cells, were used as parallel controls in all IHC work to verify specificity and sensitivity of the immunological interactions of the antibodies for FB_1. Since masking of antigenic sites occur with formalin fixation, the positive labelling of the FB_1-treated rat kidney sections verified sensitivity of the method, and the labelling on the FB_1-treated N2α cells verified antibody specificity.

10.3.2 Specimen Preparation

10.3.2.1 Light Microscopy

Brain tissue specimens were processed for LM using conventional techniques. Specimens immersed in 5% "formal saline" (41% formaldehyde/0.9%NaCl, 1:8 v/v = dilute formaldehyde (35%); 1:7 in 0.9% NaCl) were fixed at RT for 12 hours. Samples were orientated and placed in tissue cassettes, dehydrated through a series of ethanol (ethanol 99%), cleared with xylene, and infiltrated with paraffin wax in an automatic tissue processor (Shandon). Specimens were then embedded in cassettes and polymerised at 60°C.

Tissue sections were cut at 2μm thickness using sterile disposable blades on a rotary microtome (Leica Jung, RM2035), and heat fixed onto poly-L-lysine coated glass slides for IHC. These sections were baked on a hot plate at 60°C for 10 min. prior to cooling then dewaxing. Slides for histology were stained routinely with haematoxylin and eosin (H&E) (Humason, 1972).

The procedure employed for IHC is outlined in Table 10.1. All antibodies were diluted to a pre-determined appropriate dilution factor, using a 1% BSA (w/v) in PBS (pH 7.4) solution as the diluent. The use of method controls involved the omission of the primary antibody and its replacement with PBS or with a non-immune serum of the same IgG class. The FB_1-treated and untreated N2α cells (described in Chapter 6) were used as positive and negative controls respectively in conjunction with the FFPE rat kidney tissue specimens obtained from untreated control and FB_1-treated Fischer 344 rats.

The H & E sections of the normal and brain tumour tissues were viewed and photographed on a Zeiss photomicroscope using a Nikon FX camera. The tissue sections used for IHC were viewed on a Nikon Optiphot photomicroscope and the images were captured on a Sony 3CCD colour video camera. Image analysis of the captured images was performed using the KS 300 image analysis system.

Table 10.1: Specimen processing schedule for immunohistochemistry using the peroxidase anti-peroxidase method.

Procedure	Time (min.)
Heat fixed specimens on to slides on a heating tray	10 (at 60°C)
Cooled slides to RT	5
Dewaxed in 100% xylene	2
Dewaxed in 100% xylene	2
Dehydrated in 70% EtOH	2
Dehydrated in 90% EtOH	2
Dehydrated in 100% EtOH	2
Dehydrated in 100% EtOH	2
Drop washed in distilled water (20 ml)	2
Delimited specimen with Pap pen	
Placed in a droplet of distilled water (200 µl)	1
Incubated in 0.5% hydrogen peroxide (H_2O_2) in MeOH (200µl)#	30
Poured off MeOH	
Drop-washed in PBS (pH 7.4)(20ml)	
Immersed specimens in 10mM sodium citrate buffer (pH 6)	20-30 (at 95°C)
Cooled slides to RT in the 10mM sodium citrate buffer (pH 6)	20-30
Drop-washed in PBS (pH 7.4)(20ml)	10
Incubated in 1% BSA in PBS (pH 7.2) (blocking agent) (50µl)#	20
Blotted off excess blocking agent with fibre-free paper	
Placed specimen in primary antibody (mouse anti-FB_1) (1:100) (100µl)#	Overnight incubation, 4°C, 15-16 hours in moist chamber
Drop-washed in PBS (pH 7.4) (20ml)	
Placed in secondary antibody (Goat anti-mouse IgG) (1:200) (100µl)#	120
Drop-washed in PBS (pH 7.4) (10ml)	
Placed in PAP raised in mouse (PAP soluble complex antibody developed in mouse) (1:400) (100µl)#	120
Drop-washed in PBS (pH 7.4)(10ml)	
Stained with DAB (0.5% DAB in 0.01 % H_2O_2) or AEC	3-5min. with checking
Drop-washed with distilled water (20ml)	3
Stained with haematoxylin	3min. with checking
Blued in ammoniated water (1% v/v) or hot water (60°C)	5
Cover-slipped specimens using glycerol jelly	

#During all incubation periods, slides were placed in a humidity chamber to prevent drying of specimens.

10.3.2.2 Evaluation of immunohistochemical staining using image analysis

Using image analysis, quantitative data were generated on the presence of FB_1 from the immuno-stained brain tissue specimens. Initially, tissue sections were examined, and areas of interest were photographed with a Nikon binocular Optiphot photomicroscope using 160 ASA colour film (Eastman-Kodak, USA). Subsequently, all fields of interest were digitised with a 3CCD Sony colour video camera interfaced with the Nikon Optiphot microscope that was linked to the KS300 image analysis system.

Areas of interest were viewed at an initial magnification of 40 times, prior to storage as a digital image (Figure 10.1a). A scale bar was then inserted on a graphics overlay and merged onto the image plane prior to storage as a 24 bit tagged image format. Due to the unavailability of a true colour densitometric setting on the KS300 system used, all images were converted into grey images (Figure 10.1b). A true colour densitometric system would enable one to read the intensity of the DAB or AEC reaction as a range on a colour scale. However, in this system, the intensity of the grey image was represented as numbers ranging from black (0) to white (255). Automatic contrast adjustment of the grey image was performed on all digitised images (Figure 10.1c). All results reflect this uniform contrast enhancement.

The immunoreactive areas were easily detected, appearing dark grey to black on the image. These regions were segmented from the image on the basis of their grey scale. This process created a binary image containing only 2 grey values, 0 and 255, (Figure 10.1c) which defined the immunoreactive area (white) to be analysed. A grey scale value of zero was black and a grey scale value of 255 was white. The grey values in between were displayed in grey increments. Binary images were a necessary transition step from original to the quantitative data, and defined the areas that were to be analysed. Sometimes, filling holes in certain selected regions or deletion of regions in a specified size range was necessary (Figure 10.1d).

The frame area was defined according to the shape and size of the area of interest. Immunoreactive regions were expressed as a percentage of the frame area. For quantitative purposes, the image was geometrically calibrated according to the initial magnification. The immunoreactive regions were expressed as a percentage of the frame area. A record of

measurements was extracted from the binary image according to pre-defined specific features.

To validate the regions measured, a draw mask (segmented areas) of the binary image was superimposed onto the original image plane (Figure 10.1e). Measurement values consisted of the defined measurement parameters as a data-list and were stored in a data base file. The pre-defined measurement parameters and their definitions are listed in Appendix 10.3 (Tables A10.2 and A10.3). The results of image analysis are tabulated in Appendix 10.4 (Table A10.4).

10.3.2.3 Transmission electron microscopy and immuno-electron microscopy

Specimens collected for TEM and ICC were diced into ~1mm^3 pieces using sterile blades. Tables 10.2 and 10.3 outline the specimen processing schedules for TEM and ICC, and differ from the schedules used for the cultured cells in Ch 6. All incubation steps were carried out at RT, unless otherwise indicated. Araldite and Spurr epoxy resins were the embedding media used for TEM and ICC, respectively. During all stages of processing, specimens were kept immersed to ensure complete and effective specimen processing.

Table 10.2: Processing schedule for tissue specimens for transmission electron microscopy.

Procedure	Time (min.)
Fixation in Karnovsky's fixative in 0.2 M sodium cacodylate (5ml)	60
Rinsed in 0.2 M sodium cacodylate buffer (2ml)	10
Rinsed in 0.2 M sodium cacodylate buffer (2ml)	10
Post fixed in 1% osmium tetroxide in 0.2 M sodium cacodylate (4°C)	60
Rinsed in 0.2 M sodium cacodylate buffer (2ml)	10
Rinsed in 0.2 M sodium cacodylate buffer (2ml	10
Dehydrated in 70% EtOH (10ml)	30
Dehydrated in 90% EtOH (10ml)	30
Dehydrated in 100% EtOH (10ml)	30
Dehydrated in 100% EtOH (10ml)	30
Infiltrated with propylene oxide	30
Infiltration with propylene oxide: Araldite resin (1:1) (5ml)	30
Infiltrated specimen with Araldite resin (5 ml)	60 (at 60°C)
Discarded old resin, infiltrated specimen with fresh Araldite resin (5 ml)	60 (at 60°C)
Discarded old resin, infiltrated specimen with fresh Araldite resin (5 ml)	60 (at 60°C)
Embedded specimen in beem capsules with Araldite resin	24-48 hours (at 60°C)

Ultramicrotomy was performed on the specimens fixed for TEM. To ensure that the resin embedded specimens analysed were in the tumour region, semi-thin (1μm) sections were cut with a Reichert Ultracut ultramicrotome using glass knives. Sections were collected onto glass slides, heat-fixed, then stained with 1% Toluidine blue (1%) in a distilled water:acetone (1:1, v/v) solution containing borax (10%, w/v) (Humason, 1972). Specimens were examined on a Nikon Optiphot microscope and areas of interest were selected, trimmed, and sectioned. Sections (50nm) were picked up on copper grids (200 mesh) and stained with uranyl acetate (1%) followed by lead citrate (Reynolds, 1963) (Appendix 6.2) prior to viewing on the JEOL-TEM.

Table 10.3: Processing schedule for tissue specimens for immunocytochemistry.

Procedure	Time (min.)
Fixation of tissue in 1% glutaraldehyde in PBS (pH 7.4) (5ml)	30
Washed specimens in PBS (2 ml)	5
Washed specimens in PBS (2 ml)	5
Dehydrated in 50% EtOH (10ml)	20
Dehydrated in 70% EtOH (10ml)	20
Dehydrated in 90% EtOH (10ml)	20
Dehydrated in 100% EtOH (10ml)	60
Dehydrated in 100% EtOH (10ml)	60
Infiltrated specimen with Spurr epoxy resin: absolute alcohol (1:1) (5 ml)	30
Infiltration of specimen with absolute epoxy Spurr resin	90 (at 60° C)
Infiltration of specimen with absolute Spurr epoxy resin	90 (at 60°C)
Embedded specimen in Spurr epoxy resin	24-48 hours (60°C)

Ultramicrotomy was also performed on the specimens fixed for immuno-electron microscopy, as for the specimens fixed for TEM. For ICC however, following identification of the areas of interest, the fields of interest were located on the block face, and the block trimmed to produce a "mesa" with a trapezoidal shape. Ultra-thin pale-gold sections (50-60 nm) were cut and collected onto uncoated 200 mesh nickel grids prior to immuno-electron labelling. The post-embedding labelling schedule utilised for the immuno-electron localisation of anti-FB_1 antibody was as outlined in Chapter 6, Table 6.3.

The use of method controls involved omission of the primary antibody and its replacement with PBS. The resin embedded FB_1-treated and control N2α cells were used as the positive and negative controls respectively. Specimens were processed for ICC according to the outlined method (Chapter 6, Table 6.3). The primary antibody used was monoclonal mouse

anti-FB_1 and the secondary antibody was goat anti-mouse IgG, conjugated to 10nm gold probes. Following labelling, the specimens were double stained with uranyl acetate and Reynolds' lead citrate for 2-3 minutes respectively (Reynolds, 1963). All specimens were viewed and photographed on the JEOL 1010 TEM. Images were photographed using Kodak fine grain electron sensitive plate film or digitised.

10.4 RESULTS AND DISCUSSION

10.4.1 Light microscopy

Criteria used to classify the neoplasms are based on cytoplasmic features, recognised by LM examination, either with routine stains or by immunological or histochemical techniques separately, or in combination with EM. Histological analyses of H & E stained tissue from normal and the most prevalent brain tumour subtypes analysed in this study are discussed briefly.

10.4.1.1 The blood brain barrier

The CNS differs from other tissues with regard to neoplasia, in that from its well-protected position, it is not easily exposed to the various exogenous physical and chemical agents, which may constitute determining factors in many cancers of epithelia of the body. Tissues of the brain and spinal cord may only be affected by such agents by way of circulating blood.

The capillaries of the CNS had flattened endothelial cells resting on a basement membrane. The endothelial cells were not fenestrated, and were bound together by continuous tight intercellular junctions except in the choroid plexus where this was discontinuous (Figure 10.2). The choroid plexus arises from the walls of the ventricles of the brain, and produces CSF. Each choroid plexus consisted of a mass of capillaries projecting into the ventricle, and by modified ependymal cells that were separated from the delicate underlying capillaries and supporting tissue by a basement membrane. Long bulbous microvilli projected from luminal surfaces of the choroid epithelial cells. The capillaries of the choroid plexus were large, thin-walled and occasionally fenestrated. Continuous tight junctions formed a blood-CSF barrier preventing ingress of almost all other molecules. Glucose (at about 70% plasma concentration) and small amounts of protein are normal constituents of CSF (Burkitt *et al.*, 1993).

Externally, the basement membranes were completely covered by perivascular foot processes of astrocytes. Maintenance of barrier type endothelium appeared to be under the control of astrocyte foot processes. A thin layer of the pia mater extended down into the CNS around small arteries, veins, arterioles and venules, but were absent around capillaries of the CNS. This could potentially be an entry point for xenobiotics to the brain.

The cerebellar cortex formed a series of deeply convoluted folds or folia supported by a branching central medulla of white matter. The cortex consisted of three layers (Figure 10.3a). The outer molecular layer contained relatively few neurons and large numbers of unmyelinated fibres. The inner granular cell layer was extremely cellular, and between the two was a single layer of huge neurons called Purkinje cells (Figure 10.3b). Purkinje cells had large cell bodies, a relatively fine axon extending down through the granular cell layer, and an extensively branching dendritic system that arborised into the outer molecular layer (Figure 10.3b).

10.4.2 Histological analysis of the brain tumour tissues

Starting in the meninges, meningiomas are usually solid masses, and their cells tend not to infiltrate adjacent normal tissue. Histologically, meningothelial meningioma were often characterised by tumour cells that were oval with indistinct borders, often with vacuolated nuclei (Figure 10.13). The specimen shown in Figure 10.4 illustrates the structural pattern of a transitional meningioma and consists of diffuse sheets of spindle-shaped cells. The nuclei of tumour cells were ovoid and uniform, with only an occasional pyknotic form present and their cytoplasm was abundant and eosinophilic. Two rudimentary whorls are visible with the cells arranged circumferentially around a central vascular space (Figure 10.4).

Glioblastoma multiforme is a highly malignant astrocytoma (grade IV). The majority are of astrocytic origin, although some undifferentiated ependymomas and oligodendrocytomas may have a similar histological appearance. These tumours grow rapidly and invade nearby tissue, and contain cells that are very malignant. Glioblastoma multiforme is usually located in the cerebral white matter, but is often deeply seated in the basal ganglia and thalamus (Curan and Jones, 1991). The anaplastic astrocytoma illustrated in Figure 10.5 displayed glioblastomatous transformation. One part of the tumour was a poorly differentiated fibrillary astrocytoma cellular tumour composed of elongated cells. There

were several blood vessels, and the one in the centre shows endothelial cell proliferation. On the right, there is a band of necrosis with palisading of the tumour cells along the margins of necrotic tissue.

The three most common types of pineal region tumours are gliomas, germ cell tumours, and pineal cell tumours. The PNETs usually affect children and young adults, and are usually very malignant. Other PNETs include neuroblastomas, pineoblastomas, medulloepitheliomas, polar spongioblastomas, and ependymoblastomas. Medulloblastomas are the most common PNET. Figure 10.6 illustrates a highly malignant undifferentiated medulloblastoma from the posterior fossa that consists of sheets of elongated cells, with ovoid or round nuclei in which there are very prominent nucleoli. Numerous mitotic figures were visible and many nuclei were pyknotic. No definite rosettes were observed. The stroma was sparse and consisted largely of small blood vessels. The tumour cells had scanty cytoplasm and poorly defined cell boundaries. Some nuclei displayed prominent nucleoli and mitotic activity was high.

Tumours of the choroid plexus are usually located in the fourth ventricle, and less so in the lateral and third ventricles. The specimen in Figure 10.7 is an adenoma of the choroid plexus. This tumour consisted of many papillae, the surface of which was covered with a single layer of columnar epithelial cells. The epithelial cells had strongly eosinophilic cytoplasm and small round nuclei. The smaller papillae had a core consisting of a thin strand of vascular connective tissue. The cores of the larger papillary processes were more fibrous. The structure of the papilloma reflected that of the normal choroid plexus (Figure 10.2).

10.4.2.1 Immunohistochemical analyses of brain tissue specimens

Formalin fixed tissue required an antigen retrieval step before IHC staining could be done due to the formation of methylene bridges during fixation. These bridges that cross-link proteins mask the antigenic sites. In this study, a heat-mediated antigen retrieval method was employed that served to break the methylene bridges, and so expose the antigenic sites in order to allow the antibodies to bind. The concept of recovering lost immuno-reactivity through exposure to heat near the boiling point of water was first met with scepticism as it went against the tenet of protecting proteins from the denaturing effect of heat (Key, 2001). However, Cattoretti and Suurmeijer (1994) were successful when employing a citrate

buffer of pH 6. In this study, sodium citrate buffer (pH 6, Table 10.1) was the antigen retrieval agent of choice, and improved the IHC detection of FB_1 in the FFPE brain tumour tissue sections.

With peroxidase-labelled antibody techniques, the presence of enzymatically active peroxidase, catalase, and haemoprotein in the tissue, that are all capable of reacting with H_2O_2 and reducing DAB, has the ability to confuse the final location of the antigen. This was a problem in the FFPE sections, although much of the native enzyme activity was destroyed during the processing. Blocking the endogenous "peroxidase" with H_2O_2 at the start of the procedure was suggested (Heyderman, 1979), and was found to be effective. This ensured that non-specific binding of the DAB or AEC chromogen to tissue constituents did not produce a false-positive result.

Reagent and tissue controls were necessary for the validation of IHC staining results in the FFPE tissue specimens. The antibody specificity was verified using the FB_1-treated and untreated N2α cells that were not FFPE (Chapter 6; Figures 6.4-6.10). The IHC method specificity was verified with the kidney tissue from FB_1-treated and untreated male Fischer 344 rats. The primary objective of using the rat tissue was to ascertain whether the primary and secondary antibodies were specific for their target antigens within the FFPE tissues following the antigen retrieval step. For this reason the cultured cells could not be used as method controls alone, as they were processed in a dissimilar way, and were neither exposed to formalin fixation nor antigen retrieval. The rat kidney tissues used as method controls where the primary and secondary antibodies were omitted respectively, lacked non-specific binding of the antibodies or the DAB chromogen to tissue constituents (Figures 10.8 and 10.9). The absence of non-immunological FB_1 staining in the untreated control rat kidney tissue therefore further confirmed the specificity of the IHC method applied.

Cancer induction by FB_1 exposure was previously investigated by studying the mechanisms involved during cancer initiation and promotion in rat kidney in the Fischer-344 rats (Gelderblom *et al.*, 1993; 1994). With this in mind, these kidney tissues were obtained from these authors and used as method controls for the IHC method specificity for FB_1. It was understood that with this kidney tissue method control, parallels could not be drawn with regards to the mechanism of cancer induction by FB_1 in these

tissues, as brain and kidney tissues differ significantly in structure and function and their biochemical profiles.

Figure 10.10 illustrates the immunochemical-staining pattern of FB_1 within the kidney of a FB_1-treated Fischer-344 rat, and reveals the localisation of FB_1 in the distal convoluted tubules, and within the lumen and cells of the proximal convoluted tubules (PCT). The results of the present study concur with earlier findings of Gelderblom *et al.* (1993; 1994), who reported that the most prominent toxic lesions by FB_1 in the kidneys were restricted to the tubular epithelium manifesting as necrosis, apoptosis, calcification and the presence of regenerative foci, and scant necrosis in the PCT. Although not an objective, unique to this present study was the direct immunolocalisation of FB_1 in the Fischer 344 rat kidney tissue, unlike in previous studies where the potential presence of FB_1 in the tissue was based on histopathological changes in the tissue following a known exposure to this mycotoxin. The polarity of the FB_1 molecule would enable rapid excretion and therefore it was expected that the kidneys would be at risk. These results support the hypothesis that one of the primary target organs of FB_1 in the rat is the kidney. More importantly for this study is that these results illustrate the immunospecificity of the IHC method.

Human populations differ in their responses to environmental contaminants, and FB_1 exposure in humans is probably exclusively dietary. The severity of health effects depends largely on the magnitude of exposure, and exposed individuals would be expected to vary both on specific health effects, and the degree to which they are affected. The results of the individual IHC analyses of the brain tumour specimens for FB_1 are summarized in Table 10.4. Figures 10.11 and 10.12 are light micrographs of a non-cancer brain specimen that was non-immunoreactive for FB_1, and the method control where the primary antibody was omitted on a brain tumour specimen respectively.

Immunohistochemical analyses of the 76 wax embedded brain tumour specimens revealed FB_1 presence at varying levels in 49 of these specimens (64.47%). Fumonisin B_1 was also minimally detectable in two of the 16 FFPE non-cancer brain specimens.

Table 10.4: Immunohistochemical detection of fumonisin B_1 in brain tumour tissues.

Tumour subtypes/subgroups and IHC positive samples	No. of specimens	Mean Age	Male				Female			
			A[1]		W	C	A		W	C
Meningiomas	23	40.91	6	3	1	1	5	2	2	3
IHC POSITIVE	**18**		**6**	**2**	**0**	**0**	**4**	**2**	**2**	**2**
Glioblastoma multiforme and gliomas	10	14.73	3	2	0	1	1	2	0	1
IHC POSITIVE	**6**		**2**	**1**	**0**	**0**	**1**	**1**	**0**	**1**
Medulloblastoma	9	9.22	8	1	0	0	0	0	0	0
IHC POSITIVE	**7**		**7**	**0**	**0**	**0**	**0**	**0**	**0**	**0**
Astrocytoma	7	16.57	4	0	0	0	1	1	0	1
IHC POSITIVE	**4**		**1**	**0**	**0**	**0**	**1**	**1**	**0**	**1**
Pituitary Adenoma	6	52.6	4	0	0	1	0	0	0	1
IHC POSITIVE	**4**		**3**	**0**	**0**	**1**	**0**	**0**	**0**	**0**
Metastatic adenocarcinoma	4	52.75	1	0	1	1	0	1	0	0
IHC POSITIVE	**3**		**1**	**0**	**0**	**1**	**0**	**1**	**0**	**0**
Craniopharyngioma	2	9.5	1	0	0	0	0	1	0	0
IHC POSITIVE	**2**		**1**	**0**	**0**	**0**	**0**	**1**	**0**	**0**
Posterior fossa tumour	3	12.5	2	1	0	0	0	0	0	0
IHC POSITIVE	**0**	**0**	**0**	**0**	**0**	**0**	**0**	**0**	**0**	**0**
Transphenoidal excision of tumour	2	34.5	0	0	0	0	2	0	0	0
IHC POSITIVE	**0**		**0**	**0**	**0**	**0**	**0**	**0**	**0**	**0**
Cerebellar hemangioblastoma	1	57	1	0	0	0	0	0	0	0
IHC POSITIVE	**1**		**1**	**0**	**0**	**0**	**0**	**0**	**0**	**0**
Choroid plexus papilloma	1	14	1	0	0	0	0	0	0	0
IHC POSITIVE	**1**		**1**	**0**	**0**	**0**	**0**	**0**	**0**	**0**
Pineoblastoma	1	11	0	0	0	0	1	0	0	0
IHC POSITIVE	**1**		**0**	**0**	**0**	**0**	**1**	**0**	**0**	**0**
Neurofibroma	1	30	0	0	0	0	1	0	0	0
IHC POSITIVE	**1**		**0**	**0**	**0**	**0**	1	**0**	**0**	**0**
Plasma cell neoplasm	1	54	0	0	0	0	0	0	1	0
IHC POSITIVE	**1**		**0**	**0**	**0**	**0**	**0**	**0**	**1**	**0**
Acoustic schwannoma	1	51	0	0	0	0	1	0	0	0
IHC POSITIVE	**0**		**0**	**0**	**0**	**0**	**0**	**0**	**0**	**0**
Occipital craniotomy	1	6	0	0	0	0	1	0	0	0
IHC POSITIVE	**0**		**0**	**0**	**0**	**0**	**0**	**0**	**0**	**0**
Left frontal cystic tumour	1	59	1	0	0	0	0	0	0	0
IHC POSITIVE	**0**		**0**	**0**	**0**	**0**	**0**	**0**	**0**	**0**
Suprasellar tumour	1	5	0	0	0	0	1	0	0	0
IHC POSITIVE	**0**		**0**	**0**	**0**	**0**	**0**	**0**	**0**	**0**
Orbital tumour	1	34	0	1	0	0	0	0	0	0
IHC POSITIVE	**0**		**0**	**0**	**0**	**0**	**0**	**0**	**0**	**0**
Total specimens analysed	**76**									
Total positive specimens	**49= 64.5%**									

[1] A=African, I=indian, W= white, C= coloured

Of the 76 brain tumour specimens analysed for presence of FB_1 using IHC, only 38 were matched with serum analyses for FB_1, Sa, So and the Sa: So ratios (Table 10.5). Of the 38 samples, 23 showed presence of FB_1 while 15 did not. The matched mean serum FB_1 concentration in the 23 FB_1 positive tissue specimens was 118.33 ±114.03nM, and for the 15 brain tissue specimens where FB_1 was undetectable, the mean serum FB_1 concentration was 67.46±51.20nM. These values indicate that, although not significantly different ($p=0.11$), the cancer group showing FB_1 presence within the tumour tissue had a higher level of FB_1 in the circulation than the cancer group without FB_1 immunolocalised within tissue. Matched serum samples were not obtained from non-cancer patients from whom brain tissue was obtained, as these were removed at autopsies at King Edward VIII Hospital mortuary. However, the results from Chapter 9 indicate FB_1 was detected in the serum of the non-cancer serum volunteers at a level of 76.7±62.2nM.

The possibility that FB_1 may have been stored in the tissues when ingested via the diet over time in these cancer patients was a factor considered in the present study. A hypothesis exists that on consumption of foods contaminated with *Fusarium* fungi, compounds present in the fungi might alkylate DNA and participate in the induction of tumours (Howard *et al.*, 2001). Support for this hypothesis comes from Bever *et al.* (2000) who reported that the incubation of methanolic extracts of *Fusarium* cultures with DNA in the presence of rat liver S9 proteins resulted in the formation of DNA adducts. The chromatographic characteristics of these unidentified DNA adducts suggest they were hydrophobic (Bever *et al.*, 2000).

In addition, interference with sphingolipid metabolism in response to sustained FB_1 exposure may represent a plausible mechanism by which this mycotoxin may have induced mitogenesis (Yoo *et al.*, 1992; Merrill *et al.*, 1993a; 1993b; Schroeder *et al.*, 1994). Chronic fumonisin induced disruption of sphingolipid metabolism has also been hypothesized to be a contributing factor leading to cellular deregulation and organ toxicity (Merrill *et al.*, 1993c; Riley *et al.*, 1994b; Schroeder *et al.*, 1994; Tolleson *et al.*, 1996a; 1996b; 1999).

Table 10.5: Immunohistochemical detection of FB_1 in human brain tumour tissue specimens with matched serum sphinganine, sphingosine and FB_1 levels.

Sex	Age	Race	Tumour Subtype	Tissue IHC	Serum FB_1 (nM)	Serum So (nM)	Serum Sa (nM)	Serum Sa:So ratio
M	57	A	Cerebellar hemangioblastoma	+	167	83.9	116	1.38
M	14	A	Choroid plexus tumour	+	84.7	148	115	0.78
M	56	A	Excision of tumour	+	60	192	147	0.77
M	1.3	A	Glioblastoma multiforme	+	34.7	185	521	2.82
M	10	A	Medulloblastoma	+	298	92.3	105	1.14
M	40	A	Meningioma	+	65.8	58	83.8	1.44
F	25	A	Meningioma	+	283	58.1	148	2.55
F	42	A	Meningioma	+	25.7	229	949	4.14
F	44	A	Meningioma	+	312	91.6	105	1.15
F	32	A	Meningioma	+	49.6	422	565	1.34
F	47	A	Meningioma	+	101	78.9	93.6	1.19
M	11	A	Occipital tumour	+	31.8	162	689	4.25
F	5	A	Pilocytic astrocytoma	+	73.4	517	387	0.75
M	35	A	Pituitary adenoma	+	226	185	359	1.94
M	21	A	Pituitary Adenoma	+	ND	50.2	88.4	1.76
M	67	A	Pituitary Thoraco adenoma	+	420	299	120	0.4
M	4	A	Posterior fossa tumour with presence of medulloblastoma	+	38.4	60.2	84.5	1.4
F	17	I	Cranial pharyngioma	+	24.2	380	1210	3.18
M	25	I	Meningioma	+	59.7	240	456	1.9
F	64	I	Meningioma	+	99.6	208	182	0.88
F	51	I	Meningioma	+	64.2	74.4	148	1.99
F	42	W	Meningioma	+	32	389	420	1.08
F	61	W	Meningioma	+	52.3	214	448	2.09
	33.5± 20.7				**118.3± 114.0**	**192.1±13 1.98**	**327.8± 302.6**	**1.8±1.0**
M	14	A	Medulloblastoma	-	56.4	56.4	ND	ND
M	23	A	Haemorrhagic lateral ventricle tumour	-	33.4	74.4	60.7	8.16
F	29	A	Meningioma	-	88.8	378	205	0.54
M	59	A	Metastatic cancer. Left frontal cystic tumour	-	213	98.9	95.2	0.96
M	15	A	Pilocytic astrocytoma	-	30.4	345	305	0.88
M	35	I	Meningioma	-	23.7	29.5	ND	ND
F	6	A	Pineoblastoma	-	24.2	297	1290	4.34
F	49	A	Transphenoidal excision of tumour	-	56.3	160	418	2.61
M	34	I	Neurilememmoma	-	39.8	47.9	82.1	1.71
M	10	I	Posterior fossa tumour	-	61.2	393	417	1.06
M	30	W	Meningioma	-	58.8	203	765	3.77
M	51	W	Meningioma	-	23.2	207	357	1.72
M	20	A	Posterior fossa tumour	-	79.7	271	204	0.75
F	25	W	Meningioma	-	83	87.9	103	1.17
F	53	W	Metastatic Carcinoma	-	140	**248**	**325**	1.31
	30.2± 16.6				**67.5± 51.2**	**193.1± 125.1**	**355.9± 340.5**	**2.2±2.1**

Key:

A	I	W	M	F	+	-	ND
African	Indian	White	Male	Female	FB_1 detected	FB_1 not detected	Not Detectable

In this study however, analyses of the matched absolute Sa and So serum levels, do not indicate any major differences between the IHC positive and negative groups. In the FB_1 IHC-positive cancer groups the Sa level was 327.84 ± 302.58nM, and the So levels were 192.1±132nM, and in the FB_1 IHC-negative cancer group, the Sa levels were 355.9±340.5nM and the So levels were 193.1±125.1nM respectively. The mean serum Sa:So ratio in the FB_1 IHC-positive samples was 1.76±1.03, and in the FB_1 IHC-negative group was 2.23±2.13. Tissue Sa and So levels were not assessed in this study.

Since there are intra- and inter-individual differences in levels of exposure to FB_1, as well as in the bioactivity of brain cell types, there was an expected gradient in the intensity of staining for the levels of FB_1 distribution in brain tumour tissue and cells (Figures 10.13 a-c, 10.14). The intensity of FB_1 immunostaining in the brain tissue was considered proportional to the amount of toxin metabolised, ingested, and/or retained by the individual on intermittent dietary exposure. These variations were accompanied by varying serum levels of FB_1, Sa and So in these patients (Table 10.5).

Riley *et al.* (2001) proposed that differences in cell and tissue responsiveness to sphingoid bases, sphingoid base-1-phosphates, and/or CER-mediated effects on proliferation or apoptosis, are likely critical in FB_1 carcinogenicity and tumour promotion. These workers hypothesized that FB_1-induced alterations in sphingolipid signalling pathways lead to altered rates of cell death and regeneration. In certain situations, CER synthase inhibited cells whose DNA is damaged may survive under conditions that would normally lead to their death from CER generated *de novo*. Conversely, inhibition of CER synthase can lead to the accumulation of sphingoid bases and their metabolites, which would also alter rates of cell death and proliferation. Given the minimal evidence for DNA reactivity of fumonisins, the carcinogenic risk from fumonisin may be related to its ability to increase the chance of survival of cells that have been DNA damaged by other means, or related to its ability to stimulate cell division directly. Other possible reasons include its ability to increase regeneration in response to increased cell death, or its potential to

increase the chances of survival of cells whose DNA is damaged through insensitivity to apoptotic effects of disrupted sphingolipid metabolism.

Gelderblom *et al.* (1992; 1994) have indicated that fumonisins appear to be slow cancer initiators, because prolonged exposure of up to 14 days at a relatively high dosage was required to effect cancer initiation. Elsenhans *et al.*(1983) postulated that FB_1 is polyanionic, and may interfere with its own absorption by binding cations such as sodium, potassium and other large molecules. The presence of this mycotoxin in brain tissue in areas where there were no major lesions, as in the two non-cancer brain specimens where FB_1 was detected at very low levels, does not preclude the potential for persistent biochemical dysfunction in the tissue from contributing to brain lesions later on.

The results of the present study concur with the findings of earlier studies by Prelusky *et al.* (1994), who indicate that following ingestion a fraction of FB_1 is absorbed, distributed and remains in tissues for an extended period of time. Ross *et al.* (1993) highlighted that length of exposure to a mycotoxin, level of contamination, individual differences, previous exposure or pre-existing organ impairment may all contribute to the appearance of clinical disease.

The meningiomas were the most common tumour subtype analysed within this study with 36.73% (18 of 49) of all the FB_1 IHC-positive specimens histologically classified as meningiomas (Table 10.4). This tumour subtype was common to subjects in all races and both sexes. These IHC findings are supported by the elevated Sa:So ratios and FB_1 concentrations found in the serum samples from these patients as discussed in Chapter 9. It is documented that FB_1 is a complete carcinogen in that it effects cancer initiation, promotion, and progression (Gelderblom *et al.*, 1991). Although no correlation (R =-0.23) was found to exist between the serum FB_1 and Sa: So serum levels in the patients with this tumour subtype (Chapter 9, Figure 9.8), it is possible that that the presence of this mycotoxin and the serum levels of FB_1 and the sphingoid bases may have contributed to disruption of sphingolipid metabolism in these patients potentially exacerbating, initiating or promoting brain carcinoma formation.

The present study is the first to directly immunolocalise FB_1 in human brain tumour tissue, providing direct evidence that FB_1 crosses the BBB and interacts with the underlying

tissue. The immunolabelled specimens shown in Figures 10.13a-c and 10.14 are meningiomas. With reference to the results of Chapter 9, the level of mean serum level of FB_1 in the patients with meningiomas was 103.07 ± 98.09nM FB_1 and the mean serum Sa: So ratio was 1.71 ± 0.98 (Chapter 9, Table 9.3). Meningiomas arise from the membranes that surround and protect the brain. Brain tissue is rich in complex sphingolipids that serve as important structural components of membranes. The loss of complex sphingolipid biosynthesis induced by FB_1 exposure alters cell behaviour, initiates cellular deregulation, and eventually leads to cell death. The fumonisin-induced increase in free Sa and depletion of complex sphingolipids contribute to inhibition of cell proliferation and increased cell death in some cell types. The consequences of disrupted sphingolipid metabolism are therefore cell type specific. It is possible that inhibition of brain CER synthase by fumonisins and the resultant depletion of sphingolipids may have led to disruption of sphingolipid metabolism, mitogenesis, and subsequent necrosis or malignant transformation.

Cancer promotion by FB_1 may proceed via the induction of a growth differential because this mycotoxin has the potential to both increase the growth rate of pre-cancerous cells and arrest the growth of normal cells (Riley *et al.*, 1994b). The inhibitory effect of FB_1 on cell proliferation appears to be the reason why the fumonisins are slow cancer initiators. A threshold level for cancer initiation exists which, as a function of time, will be determined by the dosage used and the subsequent inhibitory effect on cell proliferation (Gelderblom *et al.*, 1994). Microscopic and other findings suggest that an imbalance between cell loss and replacement develops a condition favourable for carcinogenesis. Gelderblom *et al.* (1988a; 1988b; 1992) reported both tumour promoting and initiating activity of FB_1. These effects can be explained on the basis of sphingolipid metabolism disruption since DNA synthesis in cells is stimulated by the addition of sphingoid bases (Zhang *et al.*, 1990) and by exposure of FB_1 at doses that elevate sphingoid bases (Schroeder *et al.*, 1994).

Defects in cell cycle control have been shown to promote genomic instability and progression to malignancy (Hartwell and Kastan, 1994). The rates of cell proliferation and cell loss, in conjunction with the differentiation status of a tissue, are among the many factors contributing to carcinogenesis. Non-genotoxic chemicals such as FB_1 may affect this balance by increasing proliferation through direct mitogenesis, or through a

regenerative response following loss of cells through cytotoxic (oncotic) or apoptotic necrosis. For a given tissue, disruption of sphingolipid metabolism may cause some cells to die, some cells to cease growing and some to grow faster. If growth arrested cells are selected to enter the cell cycle inappropriately (by passing a cell-cycle checkpoint), increased genomic instability could result and consequently increased cancer risk.

Mitogenic stimulation, which could be supported by food-borne factors, may provide more cells at risk in an enlarged target organ, and also increase cell replication rate. The latter would decrease the time for error-free DNA repair between replication, and increase the potential for any spontaneous chromosome breakage events (and repressor-gene deletion) that may be associated with the replication process (Institute of Food Technologists, 1993). Fumonisins acting as mitogens, could increase the probability or irreversibly lock in a spontaneous genomic error *in vivo* in the brain tissue. It has been proposed that mitogenesis increases cancer risk by increasing the probability of DNA damage being converted to mutations, making DNA more sensitive to being damaged, increasing gross chromosomal alterations, and increasing the expression of oncogenes (Ames and Gold, 1990; Riley *et al.*, 1994b). Fumonisin B_1 may be the first example of an apparently non-genotoxic agent producing tumours through a mode of action involving apoptotic necrosis, atrophy, and consequent regeneration (Dragan *et al.*, 2001).

An indirect effect of FB_1 could be due to disruption of the 'barrier function of endothelial cells, hence damage to the cerebral blood vessels. Ramasamy *et al.* (1995) demonstrated that an elevation of Sa due to FB_1 presence altered sphingolipid biosynthesis and caused disruption of the endothelial barrier function. A disrupted or damaged endothelium increases leakage of plasma components into underlying tissues. Ramasamy *et al.* (1995) further stated that depletion of complex sphingolipids was important in the maintenance of cell communication, and loss of cell-to-cell contact could result. The end result of impaired sphingolipid metabolism and subsequent accumulation of sphingoid bases could be a 'leaky' membrane leading to spilling of vascular fluid into brain and regional tissue damage. The relevance of these findings is important in the current study as FB_1 was localized within brain tumour tissue. In addition, as FB_1 was found in the serum of these patients (Chapter 9), the damaged endothelium may have been a potential route of entry of FB_1 into the brain tissue.

An additional route of FB_1 entry into the brain may be via cerebral vascular endothelial cells that possess a transcellular lipophilic pathway, allowing diffusion of small lipophilic compounds. In addition to this route, specific receptor-mediated transport systems are present for given molecules, like insulin, transferrin, glucose, purines, and amino acids. These transport systems are highly selective and asymmetric. Glucose (at about 70% plasma concentration) and small amounts of protein are normal constituents of CSF, and this could potentially be a vehicle for entry xenobiotics to the brain. Because hydrolysed FB_1 and FB_1-fructose adducts are formed during food processing, Hopmans *et al.* (1997) evaluated the excretion of these products and FB_1 in Fischer-344 rats. Based on the amount of each FB_1-related compound recovered in urine and faeces, it was concluded that hydrolysed FB_1 and the FB_1-fructose adducts were better absorbed than FB_1 (Hopmans *et al.*, 1997). This pathway may also have potentially facilitated entry of FB_1 into the human brain tissue.

With further consideration of the secondary effects of FB_1 exposure of inhibition of sphingolipid metabolism and the consequent increase in the free Sa and So, it must be noted that endothelial cells also have a high affinity receptor, i.e., EDG-1 for So-1-phosphate (Van Brocklyn *et al.*, 1998; Vesper *et al.*, 1999). As So and So-1-phosphate have been shown to stimulate DNA synthesis (Zhang *et al.*, 1990; Zhang *et al.*, 1991), disruption of sphingolipid metabolism by FB_1 in the brain tissues would potentially lead to an increase in free So-1-phosphate. Therefore, there would be further potential for malignant transformation via stimulation of DNA synthesis by its binding to the EDG-1 receptor on the endothelial cells.

Glioblastoma multiforme was the second most common brain tumour subtype analysed using IHC in this study, and 60% (6 of 10) of the specimens analysed in this subgroup showed FB_1 presence (Table 10.5). Kwon *et al.* (2000) assessed the consequences of FB_1 exposure (0.5-75μM) on astrocytes and oligodendrocytes in primary cultures of rat cerebrum, and found that exposure to FB_1 diminished the levels of So at 15 DIV, whereas FB_1 exposed cultures showed significantly increased Sa levels and Sa:So ratios. Also the activity of CNP, an enzyme associated with myelin and oligodendrocytes, was increased in FB_1-treated cultures, suggesting that short-term exposure to FB_1 modified the proliferation of glial cells (Kwon *et al.*, 2000). Glial cells are the cells from which glioblastomas arise, and Kwon *et al.* (2000) have shown direct susceptibility of these cells to FB_1 *in vitro*.

Fumonisin B_1 also displayed epigenetic properties via induction of hypermethylation of DNA, inhibition of protein synthesis and cytotoxic concentrations of FB_1-induced cell cycle arrest in rat C6 glioma cells. This possibly occurred in relation with genotoxic events in the C6 glioma cells (Mobio *et al.*, 2000).

Harel and Futerman (1993) showed that FB_1 (10μM) inhibited axonal growth from hippocampal neurons and decreased cellular sphingolipids. As sphingolipids are structural components of membranes, it may be possible that as FB_1 was directly immunolocalised within these brain tumour specimens, that the increased Sa and So in these regions may have initiated mitogenesis via disruption of sphingolipid metabolism. Schroeder *et al.* (1994) established that FB_1 is mitogenic via accumulation of sphingoid bases, rather than inhibition of complex sphingolipid biosynthesis. Because mitogens can often affect cell transformation, this provides a plausible molecular mechanism to explain the cancer promoting and initiating activity of FB_1, whereby mitogenesis is dependent upon disruption of sphingolipid metabolism and accumulation of sphingoid bases (Schroeder *et al.*, 1994). The observation of mitotic figures in the brain tumour specimens indicate that the presence of high concentrations of free sphingoid bases in these tissues does not preclude cell division, and thus tissue repair processes may have been suppressed. Alternatively, clonal selection may have selected for cells sensitive to the mitogenic effects of elevated free sphingoid bases. Changes in pool size of specific sphingolipids (e.g., SM and CER) which are associated with cellular signalling systems, alter the way extracellular messages are transduced. Systems which are important control points for cellular growth and differentiation may have been disrupted during the interval when repair processes occur, and thus mitogenesis would proceed rapidly (Riley *et al.*, 1994b). The presence of FB_1 in human brain tumour subtypes that arise from cell types used in *in vitro* studies bears further testament to the cancer initiating potential of this mycotoxin *in vivo* and provides a potential mechanism of initiation of the brain tumours.

10.4.3 Image analysis of immunolabelled brain tumour specimens

Although there are three different areas of image analysis, they are not mutually exclusive. These include measuring morphological characteristics of tissues, cells, nuclei or even nucleoli; counting of cell or tissue components; and cytometry and pattern recognition, which measures cytochemical, histochemical and molecular cell or tissue features, such as the DNA content of nuclei, and to classify cells according to the distribution pattern of these features in cells or nuclei (Meijer *et al.*, 1997). In this study, image analysis facilitated the quantitative assessment of the proportion of cells that were positive for FB_1 based on the immunohistochemical staining, as well as the distribution of staining intensities over the tumour tissues. Image analysis was applied in this study to obtain statistically useful information.

Definition of terminology used in image analysis, the steps formulated in the macro drawn up for image analysis of the brain tumour tissue sections, as well as an example of macro utilised for image analysis are outlined in Appendix 10.3. The quantitative results from image analyses of these brain tumour specimens are presented in Appendix 10.4.

In the two non-cancer brain specimens that showed FB_1 presence, the intensity and area of staining was minimal, being limited to five to ten cells in the entire specimen, and consequently these specimens were not statistically analysed. Twenty-two of the specimens that were positively labelled for FB_1, were analysed using image analysis (Appendix 10.4). The remaining positive specimens could not be adequately analysed due to the intensity and area of staining being minimal in a few scattered tumour cells. The selection of the frame measurements was dependent on the size of the specimen, and the areas of interest in the specimen where the stain was localized in the tumour tissue. The area of the frame measurements, which is the area of the specimens analysed, ranged from $21210.17 \pm 99550.15 \mu m^2$ (mean $844475.16 \pm 20479.62\ \mu m^2$).

The range of the field area that represents the area of the specimens that contained FB_1 staining and were analysed statistically, was 819.59 to 10 $426.29 \mu m^2$ (mean: $4475.79 \pm 2383.03\ \mu m^2$). Translated to a percentage of the sample with positive staining, a mean percentage area of all regions in measurement frames was $5.23 \pm 2.25\%$.

In the tumour specimens, the mean grey values, representing the staining intensity of FB_1 immunolocalised in the tissue, varied across all tumours from 96.8 to 211.5 density units (mean: 138.5 ± 29.3). The mean minimum grey value in all regions 27.8 ± 32.7 and the mean maximum grey value in all regions was 236.5 ± 26.5 density units. This was an indication of the upper and lower limits of the staining intensity detected in these tumour specimens. The grey value standard deviation in all regions (mean of 22 samples) was 35.6 ±10.5 density units.

The low transfer of FB_1 to the brain, as indicated by the mean percentage area of FB_1 staining of 5.2 ± 2.3% was probably due to the low lipid solubility of FB_1. Although the quantity of FB_1 localised in the tissue was low, it is an environmental xenobiotic and was not expected to be found in high concentrations, as would be expected for an endogenous compound. In addition, the saturation point of FB_1 on CER synthase may have been reached, inhibiting further FB_1 transport across cell membranes. Of importance however the fact that this compound had the ability to traverse the BBB and enter brain cells, potentially altering normal biochemical and physiological functioning. Not only is FB_1 directly cytotoxic, but also via its inhibition of sphingolipid metabolism may have generated an increase in the tissue levels of cytotoxic sphingoid bases that would have further exacerbated both the direct and indirect toxic effects of FB_1 *in vivo*.

Intra- and inter-individual exposure to FB_1 varies, and this is a likely explanation for its' varying distribution in different areas of tissue. It is possible that the patient who showed FB_1-presence in apparently "normal" tissue was exposed to a higher level of the xenobiotic over an extended period of time, facilitating accumulation of the xenobiotic within the tissues. In addition, the fact that a greater concentration of toxin was localised in the tumour tissues than in normal tissues of two patients, lends support to the hypothesis that FB_1 may play a role in triggering neoplastic transformation in the brain.

10.4.4 Transmission electron microscopy and immunocytochemistry

Transmission electron microscopy of the brain tumour tissue facilitated ultrastructural exploration of these tissues.

10.4.4.1 Transmission electron microscopy of meningiomas

The ultrastructure of the meningiomas reflected the architecture of the cells forming the pia and dura mater. The majority displayed a meningotheliomatous appearance while a few had distinct fibroblastoid characteristics. In meningotheliomatous meningiomas, many cells were large and rounded and contained spherical nuclei with much euchromatin (Figure 10.15). Most of the cytoplasmic organelles were concentrated in the paranuclear region, and many fine filaments occupied most of the cytoplasmic mass. They also consisted of cells with elaborate cytoplasmic extensions. The length, complexity and degree of inter-digitation of these varied, but distinct desmosomes were frequently found between closely apposed cell processes. The densities of cytoplasmic filaments were also variable, and were less prominent in transitional meningiomas that also had relatively short blunt processes, with less inter-digitation than the meningotheliomatous variety.

10.4.4.2 Immunocytochemistry of tumour specimens

Immunoelectron microscopy enabled localisation of the FB_1 antigen with high resolution and specificity at an ultrastructural level. Of the 49 specimens that were positive for FB_1 presence using IHC analyses at the LM level, ten (of the 49) specimens were randomly selected and analysed using immunoelectron microscopy. In these analyses, distinctions were not made between tumour subtypes, age, race or sex of the patients, since this part of the study aimed to determine any possible association with selected organelles in the tumours with FB_1 exposure and subsequent effects. Specificity of the ICC method at the EM level was verified by use of method controls, where absence of immunogold particles binding was observed with omission of the primary antibody.

Considerable data supports the hypothesis that fumonisin-induced disruption of sphingolipid metabolism is important in the cascade of events leading to cellular deregulation (Chapter 2, Table 2.1). Based on the immunochemical localisation of FB_1 in brain tumour specimens at the LM level, a diversity of alterations in cellular regulation was expected due to fumonisin-induced disruption of sphingolipid biosynthesis because these compounds play important roles in cellular structure and function. This was expected due to the potential alteration of the steady-state concentration of many biologically active lipid intermediates and end products, as well as to the direct presence of FB_1. In addition, there

are also several studies that hypothesize fumonisin-induced changes in key enzymes involved in cell cycle regulation, differentiation and/or apoptosis as initial or secondary sites of action (Merrill *et al.*, 1995; 1996a; 1996b; 1997; Riley *et al.*, 1996; Norred *et al.*, 1996; 1998; Wang *et al.*, 1999).

Electron microscopy of the tumour specimens revealed that the neoplastic cells were tightly packed and attached by scattered desmosomes (Figure 10.16). The cytoplasm was abundant and evidence of keratinisation in the cytoplasm was seen, preferentially deposited on the tonofilament bundles. The size of the tumour cells varied considerably, with a large centrally located nucleus in most cells. The nuclei were pleomorphic (Figure 10.15), as in all tumours, and were occasionally hyperchromatic with crenated borders (Figure 10.16). The nuclei of tumour cells contained moderate quantities of heterochromatin, and occasional nucleoli. Nuclear projections and nuclear inclusion bodies were also apparent (Figure 10.19). Some cells were seen in mitosis, with scattered separate chromatin collections.

Irregularity in nuclear form provides an increased area of contact between the nucleus and the cytoplasm, and is considered to denote increased nucleo-cytoplasmic exchanges and heightened metabolic activity (Ghadially, 1982). An inversion in the nucleus to cytoplasm ratio was also evident (Figures 10.15 and 10.16). One or several prominent nuclei were seen in many tumour cells. The nucleoli were variable in size and were often located at the nuclear periphery. Peripheral location of nucleoli was also a feature of FB_1-treated N2α cells (Chapter 6). Enlargement of nucleoli is a characteristic feature of tumour cells. Their large size, indicating rapid RNA turnover, reflects heightened cell replication. In addition, nucleolar margination is considered a sign of increased protein synthesis (Ghadially, 1975).

Gold-labelled FB_1 was present in convoluted, indented and irregular profiles of nuclei (Figure 10.17), in areas of nucleoplasmic clearing, in the nucleoplasm (Figure 10.18), as well as in microsegregated nucleoli. The micrograph shown in Figure 10.19 is of a medulloblastoma, and shows a pyknotic nucleus and lysing nucleoplasm with gold-labelled FB_1 immunolocalised in association with heterochromatin condensation along the periphery of the nucleus. Granules were interspersed with the euchromatin and labelled FB_1 was also found in the nucleoplasm. Sahu *et al.* (1998) have shown that FB_1 induced DNA strand breaks in isolated rat liver nuclei and the potential for having had the same

effect on these cells *in vivo* exists. Similar ultrastructural alterations were observed in the N2α cell line following *in vitro* exposure to FB_1 (Chapter 6). Immunolocalisation of FB_1 in the nuclei of the brain tumour specimens suggests that FB_1 may potentially be both genotoxic and cytotoxic to human brain cells *in vivo*.

Due to the potential for FB_1 by its inhibition of CER synthase to induce accumulation of Sa and So *in vivo*, the effects of these compounds were also considered in terms of their potential role in malignant transformation. Sphingoid bases are found in plasma membranes where they are generated from endogenous CER by ceramidase (Slife *et al.*, 1989). Similar to polyamines, the So molecule has a primary amino group which forms an ionic bond with the oxygen atom of the phosphate group of DNA molecules. This change in the structure of DNA via its interaction with So may have led to alteration of the DNA substrate specificity. Koiv *et al.* (1995) reported that So interacts with DNA in competition for the binding sites with histones, some enzymes, and transcriptional factors and was found to compete with H1 histone for the binding to DNA. The interaction of DNA with So also hinders the ability of DNA to be methylated (Romanenko *et al.*, 1995).

Sphingosine is involved in the control of replication and transcription of DNA through regulation of PKC activity. The reason is that RNA-polymerases and topoisomerase II, which are key enzymes in the activation of the genetic machinery of the cell and histones and proteins of the nuclear matrix, are also substrates of PKC. In addition to PKC, So is known to activate a number of other protein kinases (Pushkareva *et al.*, 1992), such as casein kinase II (McDonald *et al.*, 1991), which is involved in the regulation of DNA synthesis and translocates into the nucleus during replication. Sphingosine located in the nucleus is likely to control the activity of this enzyme. In some cases, So is involved in the regulation of activity of MAP kinases (Coroneos *et al.*, 1996) which transmit signals from receptors of the plasma membrane to transcriptional factors located in the nucleus. The presence of FB_1 in the nuclei of brain tumour cells in this study may have led to disruption of these enzyme functions.

There were moderate numbers of mitochondria present in the cytoplasm of the tumour specimens analysed. The mitochondria varied in size and were pleomorphic (Figures 10.20 and 10.21). Mitochondria with varying numbers of cristae were swollen, and at times

disrupted owing to a flooding of the matrix chamber, as well as the intra-cristal spaces with water. The presence of enlarged mitochondria that had a dense matrix and few, if any, cristae were also seen (Figure 10.21). The paradox of a fast growing tissue with a paucity of mitochondria and/or defective mitochondria may be explained by recalling the historic work of Warburg (1956), which showed the predominance of glycolysis over respiration in the energy metabolism of tumours. Since the enzymes of anaerobic glycolysis occur in the cytoplasmic matrix, and not in the mitochondria, one may argue that a paucity of functioning mitochondrial mass would affect the metabolic activity of a malignant tumour. Thus, there seems a good correlation between what is seen with the EM and the respiratory biochemistry of neoplastic tissues (Ghadially, 1982). However, the immunolocalisation of immunogold-labelled FB_1 in areas of cytoplasmic matrix clearing (Figure 10.21) may also indicate that FB_1 also affects anaerobic glycolysis.

Gold-labelled FB_1 was also localised in elongated (Figure 10.22) and swollen mitochondria (Figure 10.21). Fumonisin B_1 was also immunolocalised within myelin figures that are considered an indication of degenerating mitochondria and of an increase in mitochondrial turnover. The mitochondria of N2α cells exposed to FB_1 showed similar ultrastructural pathology in association with the immunolocalised mycotoxin (Chapter 6). Studies by Rumora *et al.* (2002) showed that on exposure of the RK13 cell line to FB_1, impairment of cell and mitochondrial membrane integrity at nanomolar concentrations occurred. The observations made in the brain tumour tissues concur with the findings of these earlier *in vitro* studies.

The mitochondrial inner membrane consists of about 70% protein and 30% lipid (Mathews and van Holde, 1990). Enzymes of the respiratory chain are firmly embedded in the inner membrane of the mitochondria. The outer membrane contains an attached set of proteins that include enzymes that are involved in amino acid oxidation, fatty acid elongation, membrane phospholipid biosynthesis and enzymatic hydroxylations. The soluble enzymes of the β-oxidation of fatty acids are found in the matrix. This necessitates mechanisms for transporting ions, fatty acids and other organic acids, as well as nucleotides across the inner membrane. Maintenance of respiratory control depends on the structural integrity of mitochondria. Disruption of these organelles causes electron transport to become uncoupled from ATP synthesis. Under these conditions, oxygen uptake proceeds at high rates even in the absence of added ATP. However, synthesis of ATP does not occur

even though electrons are being passed down along the respiratory chain and used to reduce oxygen to water (Mathews and van Holde, 1990). In the present study on brain tumour tissues, disruption of normal mitochondrial structure in association with localised FB_1 may indicate an association with disruption of function. An inadequate supply of ATP reduces cellular functions and biosynthesis, and may eventually cause cell death.

Gold-labelled FB_1 was also immunolocalised within swollen ER in the brain tumour cells, and this may be attributed to the fact that the enzyme CER synthase is located in this cellular organelle. The condensation of serine and palmitoyl-CoA through to the formation of CER takes place in the ER. The binding of FB_1 to CER synthase is the first event in the process of disruption of sphingolipid metabolism. This disruption encompasses all the changes that can occur in the biosynthetic rates and intracellular concentrations of intermediates and end products within both the *de novo* sphingolipid pathway and branch pathways. These include those leading to changes in biosynthesis of glycerolipids and neutral lipids (Riley *et al.*, 2001).

Gold-labelled FB_1 was immunolocalised within the cisternae of the ER (Figure 10.23), in grossly swollen cisternae of the ER (Figure 10.24), and in areas of cytoplasmic lysis (Figure 10.25). These findings are in keeping with studies by Cawood *et al.* (1994) where binding studies in subcellular fractions from rat hepatocytes revealed that ^{14}C-labelled FB_1 bound tightly to microsomal and plasma membrane fractions. Subsequently, Merrill *et al.*(1997) have indicated that FB_1-induced alterations in sphingolipid and glycerophospholipid metabolism result in alterations in phosphorylation status and cell signalling pathways that could contribute to tumour promotion.

A further explanation for finding FB_1 in the ER may be taken from observations of Merrill *et al.* (1993a) who showed that FB_1 might have two modes of interaction with CER synthase. In neuronal cells FB_1 was competitive with both sphingoid base and fatty acyl CoA. The 'Sa-like' domain may interact with the Sa binding-site, and the negatively charged tricarballylic acid groups may interact with the fatty acyl-CoA binding site, by mimicking the polyanionic phosphate groups of the CoA. The ability of FB_1 to interact with both the binding sites might account for its potency. El Bawab *et al.* (2001) have further shown that FB_1 inhibited the CoA-dependent CER synthase activity in rat brain microsomes, and did not inhibit the reverse ceramidase activity purified from rat brain clearly indicating that the two activities represent different enzymes and further attest to

the specificity of FB_1. This provides another potential mode of action of FB_1 in the human brain tissue analysed in this study.

In this study, it was difficult to distinguish between areas of cytoplasmic lysis, or clearing of the matrix and grossly swollen ER (Figures 10.24-10.25). Such cellular abnormalities were also seen in the FB_1-treated N2α cells (Chapter 6). A possible explanation for areas of cytoplasmic lysis in association with immunolocalised FB_1 in many tumour cells is that FB_1 disturbs the integrity of cellular membranes, disrupting the structural integrity of mitochondria and the ER, leading to a subsequent release of enzymes into the cell matrix. Beier *et al.* (1995) found that the amine and carboxylic acid groups in FB_1 are spatially related, suggesting that they have chelating properties, and hence, could cause membrane ion leakage. Yin *et al.* (1998) showed that fumonisins disturb the ordering of membranes, enhance oxygen transport in membranes, increases membrane permeability, promotes free radical intermediate production and accelerates the chain reactions associated with lipid peroxidation. The disruption of membrane structure, the enlargement of the relative oxygen diffusion-concentration products, as well as the enhancement effects on membrane permeability, provide additional insights into potential mechanisms by which fumonisins may have enhanced oxidative stress and cell damage in the brain tumour tissues analysed. This may be the mechanism of action that facilitated entry and action of FB_1 on the brain tissue.

Data exists suggesting that fumonisins cause compositional or oxidative damage to cellular lipids, which in turn causes molecular events culminating in oxidative damage to DNA and other critical macromolecules (Gelderblom *et al.*, 1996a; 1997; Abado-Becognee *et al.*, 1998; Abel and Gelderblom, 1998; Yin *et al.*, 1998; Sahu *et al.*, 1998). In the present study, FB_1 was immunolocalised within cytoplasmic organelles, the cytoplasm and nuclei in tumour tissues and illustrates the ability of FB_1 to traverse cellular membranes, further highlighting potential mechanisms of entry and action of FB_1 in the brain. It is conceivable that the mitogenic, cytostatic, and cytotoxic potential of fumonisin-induced disruption of sphingolipid metabolism may all play some role in the increased cancer risk.

The general expectation for tumours involving multiple events over the lifetime of an individual is that it may be possible only rarely to identify single dietary carcinogenic agents through population studies. Although the exact mechanism of action of FB_1 in the

brain cannot be determined from this study, the immunolocalisation of this mycotoxin in the tumour tissue indicates that the factors listed above may have contributed individually, or in combination to initiate or promote tumour formation and/or progression in the human brain. Although these results reflect carcinogen exposure at the individual level, the impact and actual risk of such an exposure is not yet known, as exposure to carcinogens at a specific time point does not reflect the outcome of cancer in a specific population and vice versa. This data however can be used as part of the exposure assessment in establishing risk assessment models, although the correlation of associated changes, some of which might occur in cellular oncogenes and/or tumour suppressor genes, and the ultimate cancer have not been established unequivocally.

10.5 CONCLUSION

The immunolocalisation of FB_1 in cellular organelles within the brain tumour tissue showing morphological changes suggests that FB_1 may be implicated in the aetiology and exacerbation of the brain cancer condition. In addition, immunolocalisation of FB_1 in cells showing cellular pathology indicates that FB_1 may initiate biochemical and ultrastructural changes that trigger the carcinogenic process. Ultrastructural abnormalities observed in the nucleus and nucleolus might be morphological expressions of biochemical events initiated by FB_1, which may eventually progress to carcinogenesis. Presence of immunogold-labelled FB_1 the ER and mitochondria specifically suggest that FB_1 may be active in association with these cellular organelles as they contain high levels of enzyme systems. The associated ultrastructural abnormalities noted may be a consequence of FB_1 presence.

This IHC and ICC study on the brain tumour tissue highlights the potential for exposure to FB_1 to be implicated in the initiation or exacerbation of the cancer condition, and requires further consideration. From the earlier serum HPLC results of this study where FB_1 was detected in the serum of both non-cancer and cancer subjects (Chapter 9), it was clear that the general population are at risk to the biochemical effects of exposure to this mycotoxin (Chapter 9). However, assumptions that FB_1 presence was a potential inducer of brain cancer could not be made and therefore it had to be localized within the tissue to put forth the hypothesis of a potential cause-effect relationship. This was successfully done within 65% of the brain tumour samples analysed in this study. Fumonisin B_1 was also detected in two non-cancer brain specimens. The differences in response however may have been

attributed to the potential difference in the time scale of exposure or to the presence of FB_1 in the diet of the participant. This was difficult to gauge in the hospital/urban environment, as exposure to this mycotoxin in the normal home environment/diet was unknown.

The potential role of sphingolipids as mediators of fumonisin toxicity is multifaceted, and it is clear that many mechanisms come into play. Fumonisin B_1 effects within the brain and its association with cancer promotion may be related to loss of endothelial cell integrity, and subsequent leakage, increased mitogenesis, loss of cellular membrane integrity as a results of disruption of sphingolipid metabolism, increases in intracellular sphingoid bases, and FB_1 induced alterations in apoptotic pathways. A thorough analysis of the cellular distribution of potential FB_1 susceptible systems is required in search of FB_1-target cell types within the human brain. The differential cellular localisation of xenobiotic metabolising enzymes in the brain may be an important factor in cell-specific toxicity.

Although these findings support the hypothesis that FB_1 may be a potential factor in the aetiology of brain cancer, a larger sample size of both normal and tumour specimens need to be analysed before a direct causative link can be established. In order to establish whether the tissue Sa and So levels were elevated, quantitative evaluation of the levels of Sa and So within the human brain tissue also needs to be considered in relation to FB_1 presence, and whether their levels may be implicated in the initiation, promotion or progression of the cancer condition

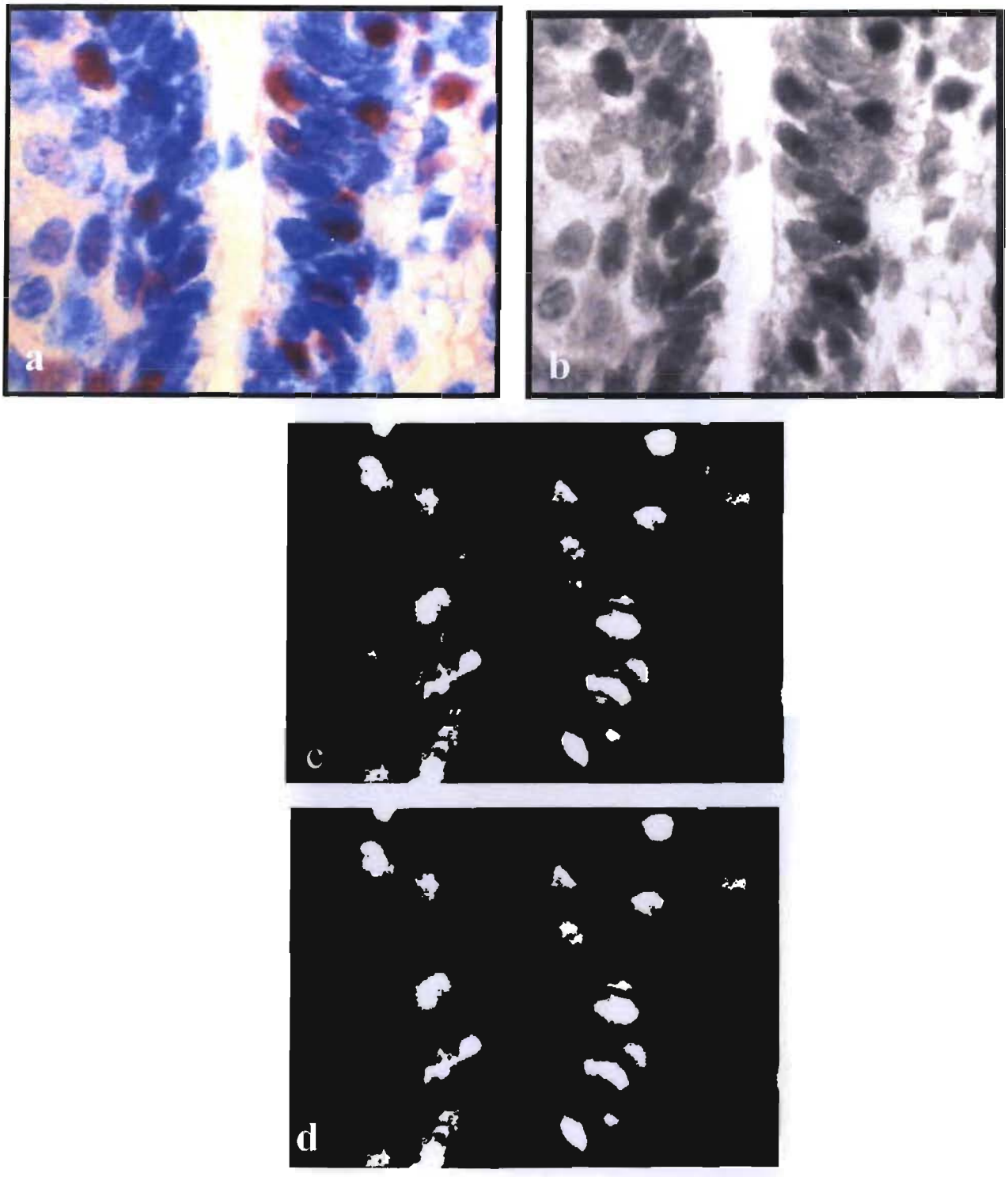

Figures 10.1 a-d: Gallery showing processing of images for analysis where:

(a) is the light microscope image,
(b) is the conversion to grey image,
(c) is the binary image showing segmentation of immuno-reactive regions, and
(d) is the binary image after deletion on the Kontron 300 image analysis system.

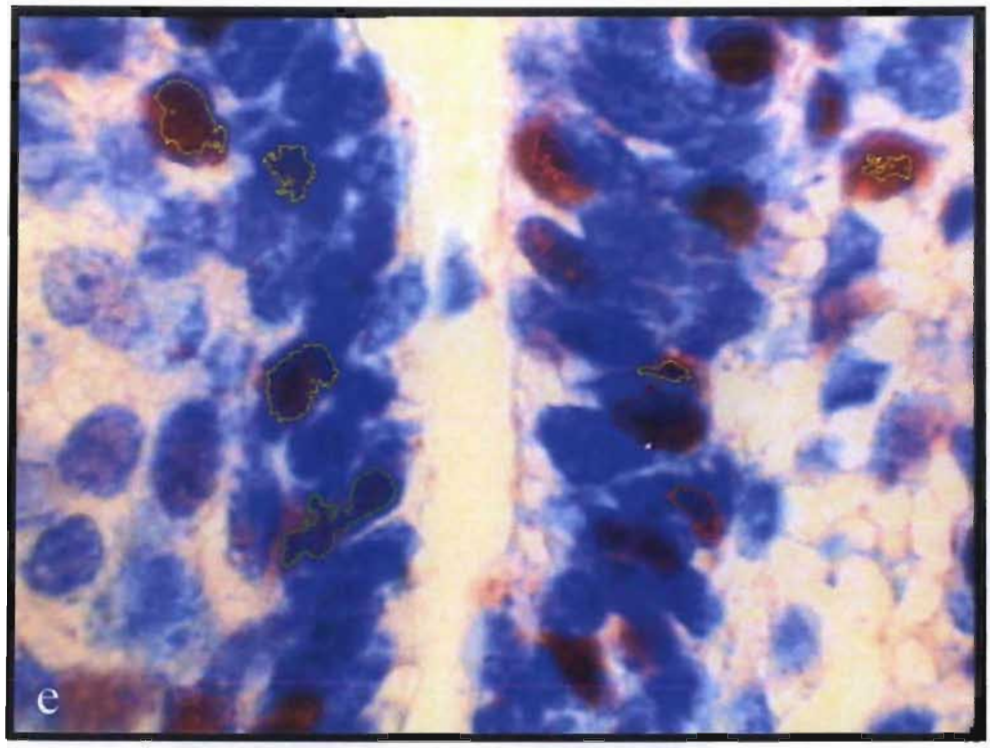

Figure 10.1e: Computed light micrograph to show the areas measured. A mask image overlay (different colours) surrounds the cell with the chromogen. The mask image serves as the region validation check. Each colour in the overlay depicts varying intensity values. Intensity values are expressed on a grey scale.

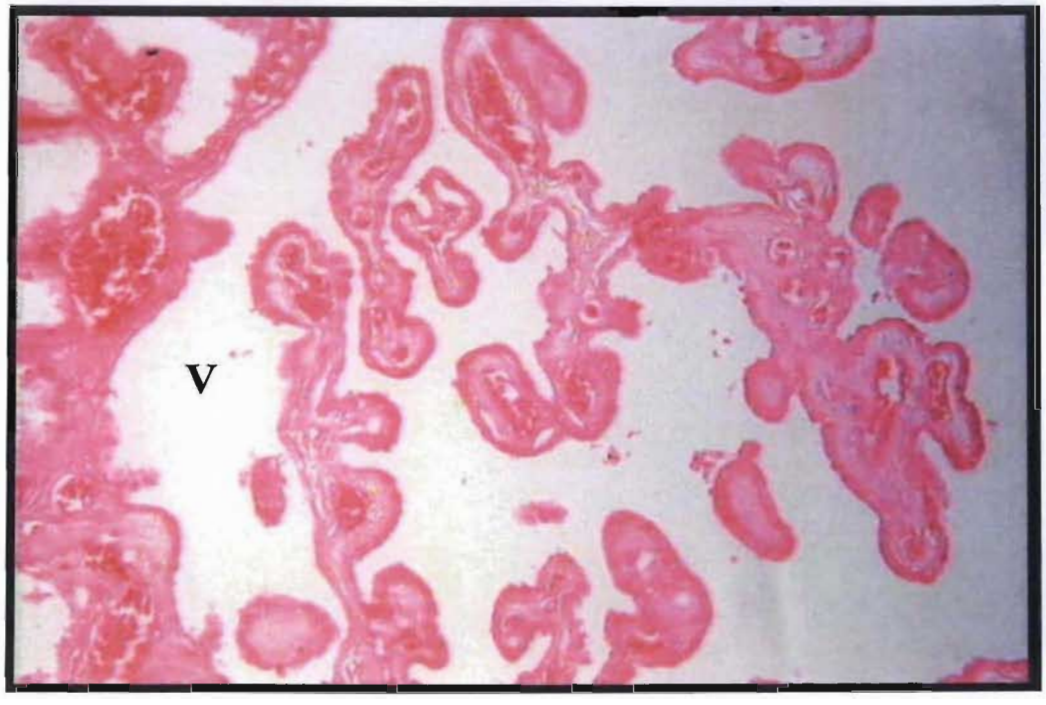

Figure 10.2: Light micrograph of the choroid plexus showing a mass of capillaries projecting into the ventricle (V) of the normal brain (H&E, Magn. X 100).

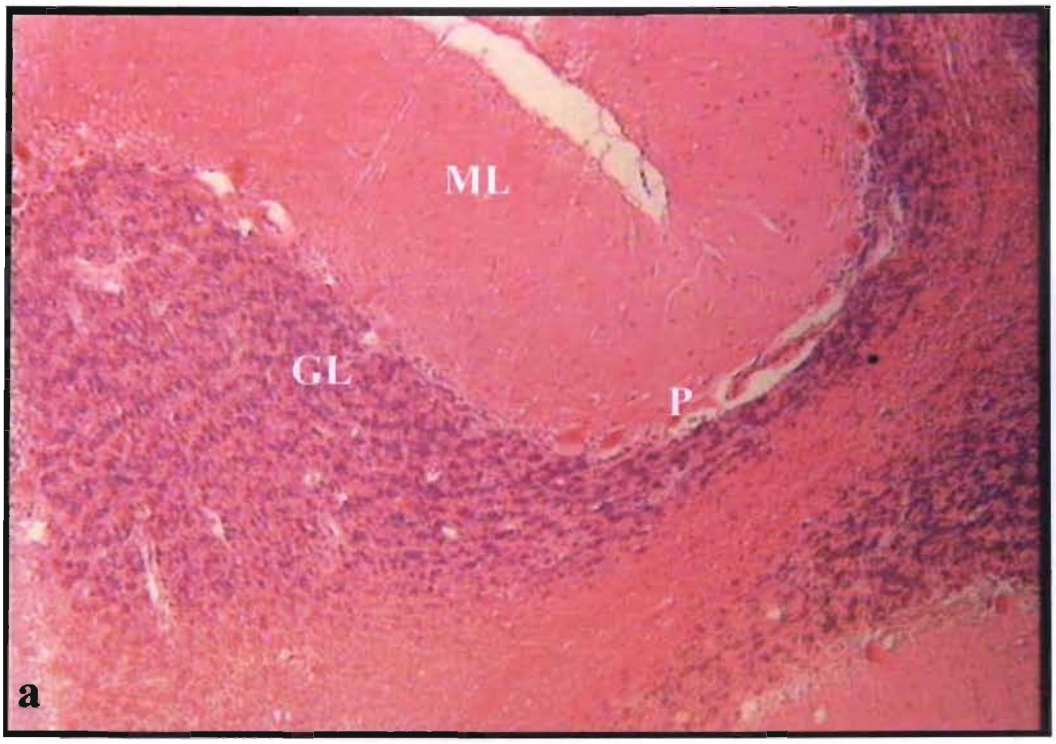

Figure 10.3a: Light micrograph of the cerebellar cortex of the normal brain showing a deeply convoluted fold. The outer molecular layer (ML) contains relatively few neurons and large numbers of unmyelinated fibres, and the inner granular cell layer (GL) is extremely cellular. Between the two is a layer of huge neurons called Purkinje cells (P) (H &E, Magn. X 100).

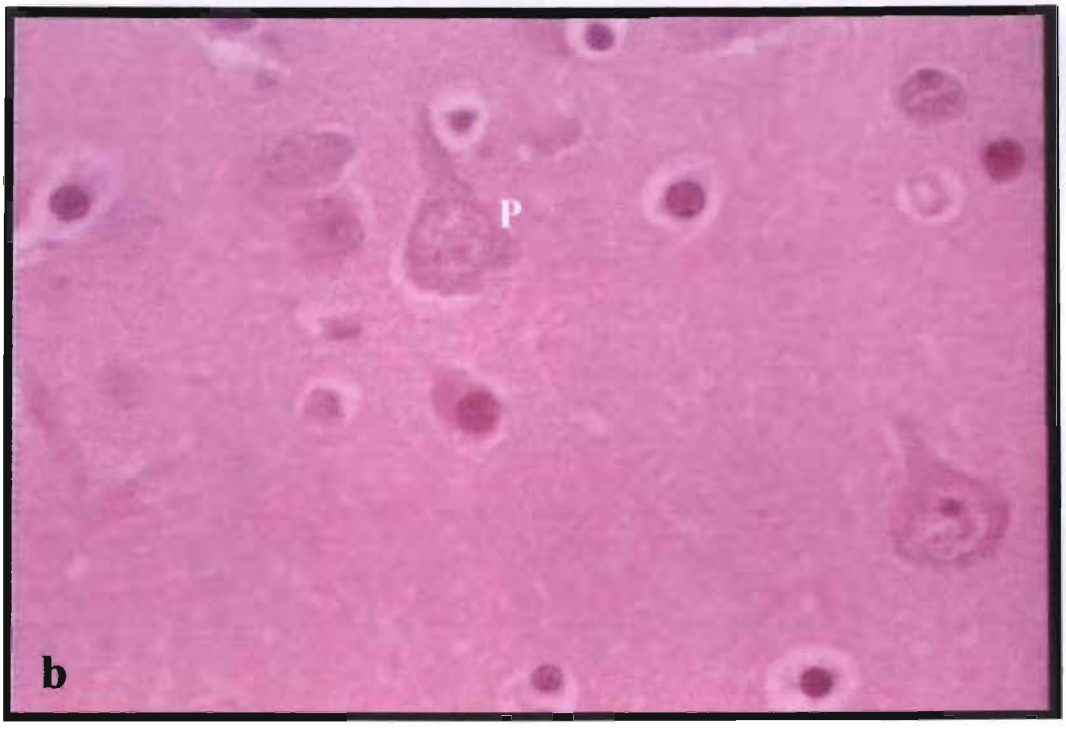

Figure 10.3b: Light micrograph of the Purkinje cells (P) that have very large cell bodies, and relatively fine axon extending down through the granular cell layer (H&E, Magn. X 1 000).

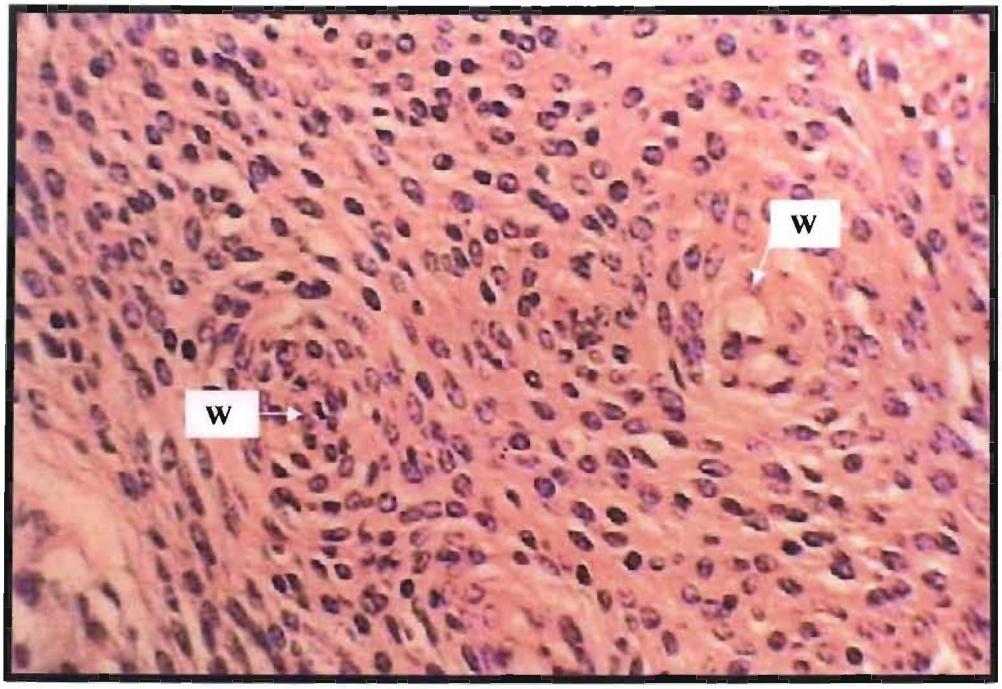

Figure 10.4: Light micrograph of a transitional meningioma consisting of diffuse sheets of spindle cells. Two rudimentary whorls (W) are shown with the cells arranged circumferentially around a central vascular space (H&E, Magn. X 400).

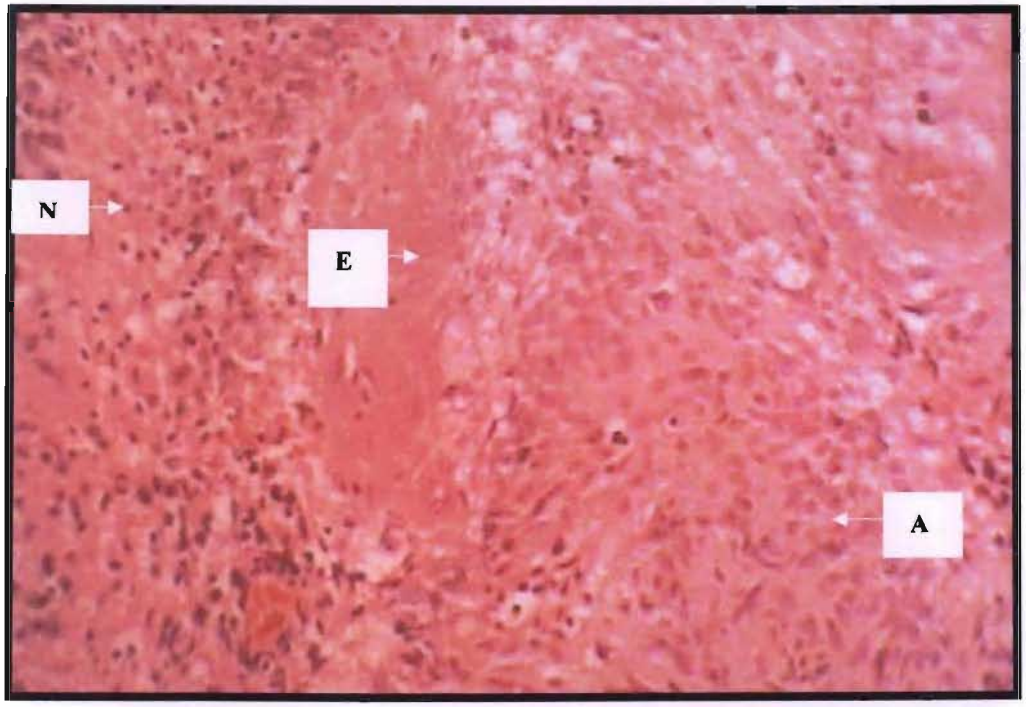

Figure 10.5: Light micrograph of an anaplastic astrocytoma showing glioblastomatous transformation. One part of the tumour is a poorly differentiated fibrillary astrocytoma (A). The blood vessel in the centre is showing endothelial cell proliferation (E). There is also a band of necrosis (N) (H&E, Magn. X 400).

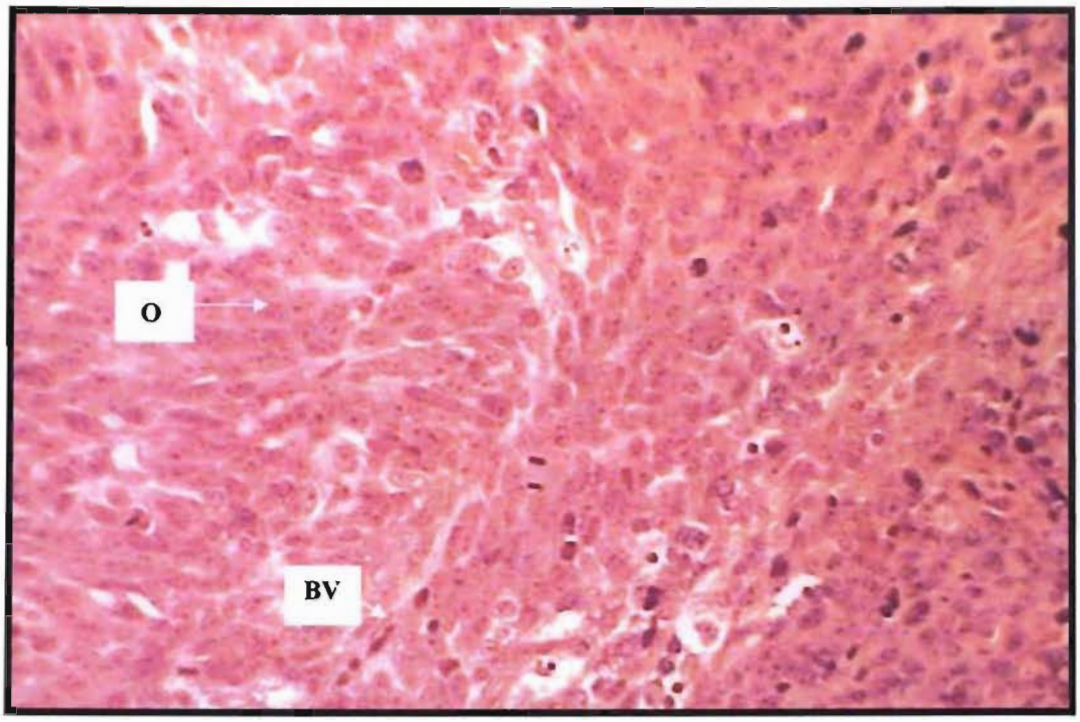

Figure 10.6: Light micrograph of a medulloblastoma from the posterior fossa with ovoid (O) or elongated cells. The stroma is sparse and consists largely of small blood vessels (BV)(H&E, Magn. X 240).

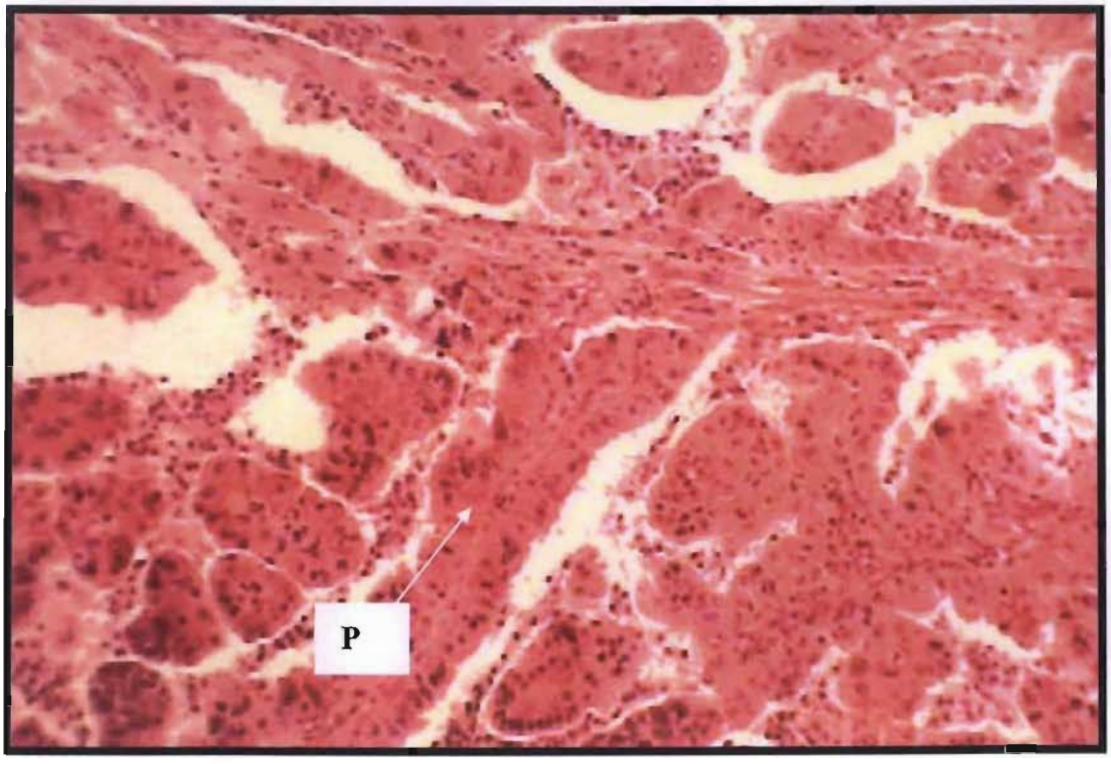

Figure 10.7: Light micrograph of an adenoma of the choroid plexus consisting of numerous papillae (P), the surface of which is covered with a single layer of columnar epithelial cells (H&E, Magn. X 100).

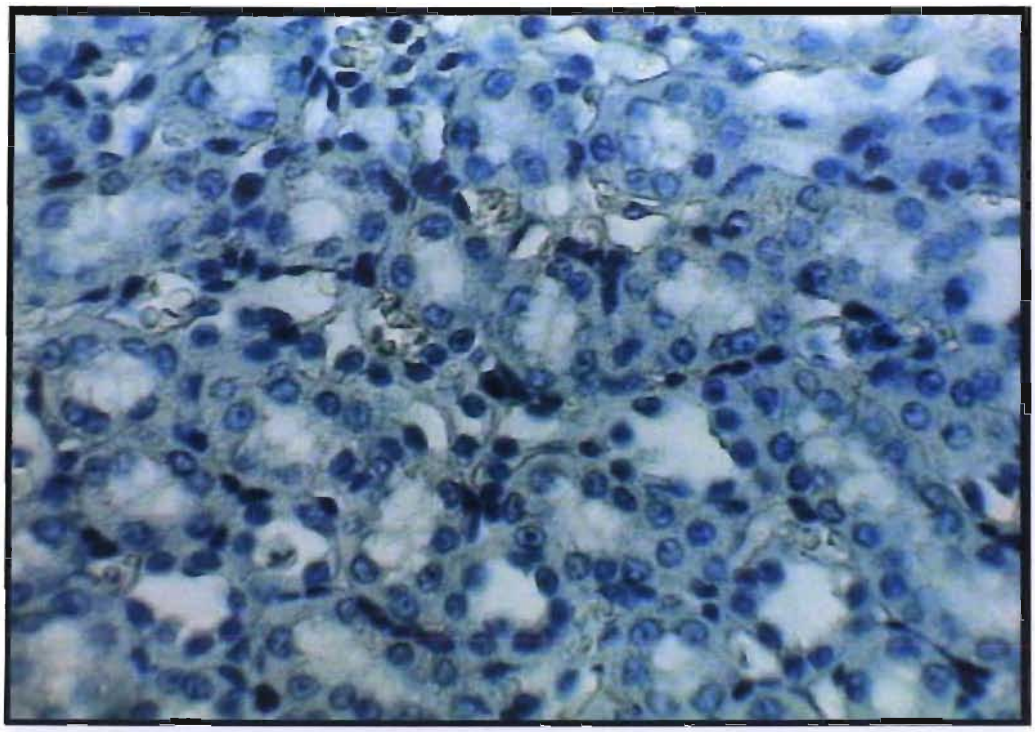

Figure 10.8: Light micrograph of the renal medulla of a FB_1-treated rat kidney used as a negative control in the IHC method, where the primary antibody was omitted. Absence of immunoreactivity indicates the antibody specificity (Magn. X 100).

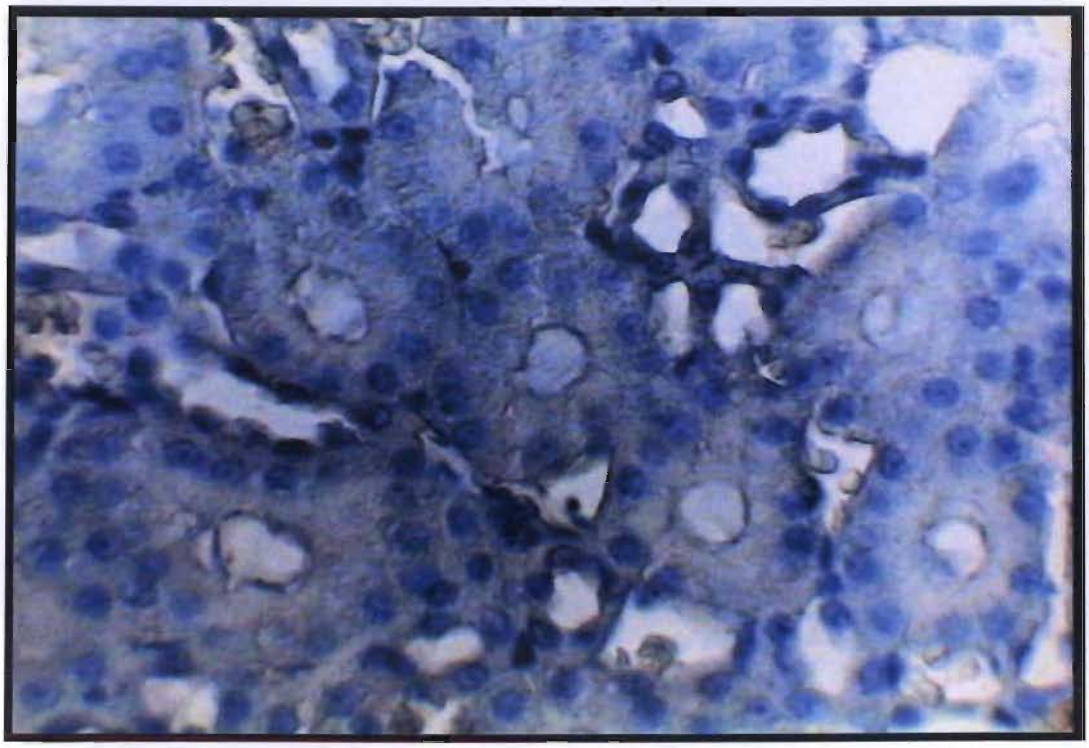

Figure 10.9: Light micrograph of a treated rat kidney where the secondary antibody was omitted during the IHC method application. Absence of immunoreactivity indicates the antibody specificity (Magn. X 400).

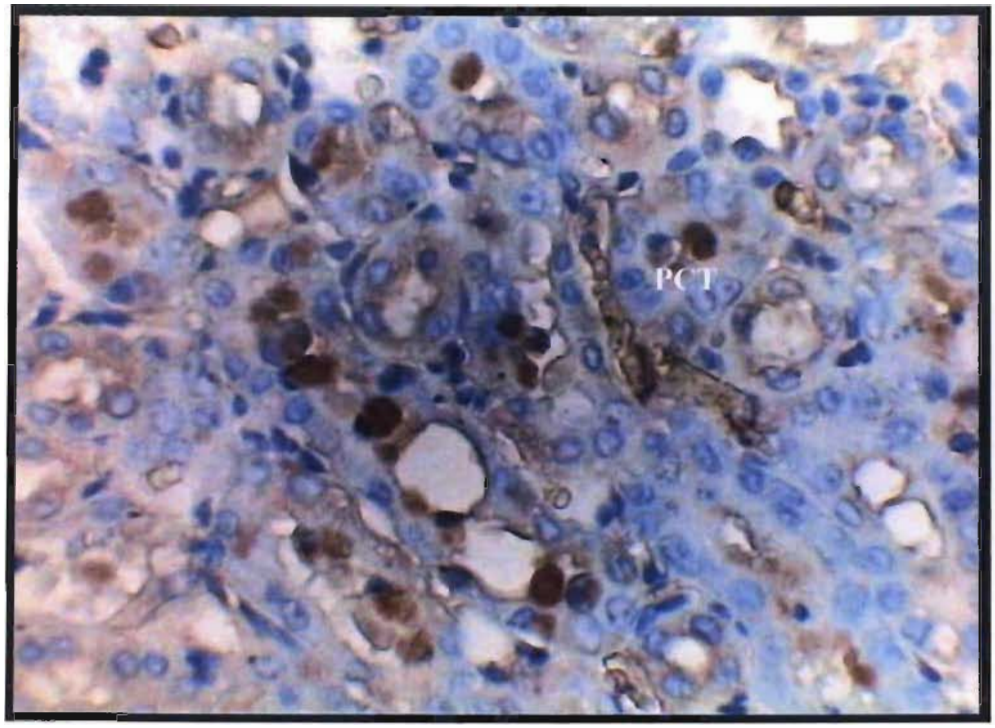

Figure 10.10: Light micrograph of FB_1-treated Fischer 344 rat kidney tissue showing luminal distribution of FB_1 within distal convoluted tubules and within the lumen of the proximal convoluted tubules (PCT) (Magn. X 200).

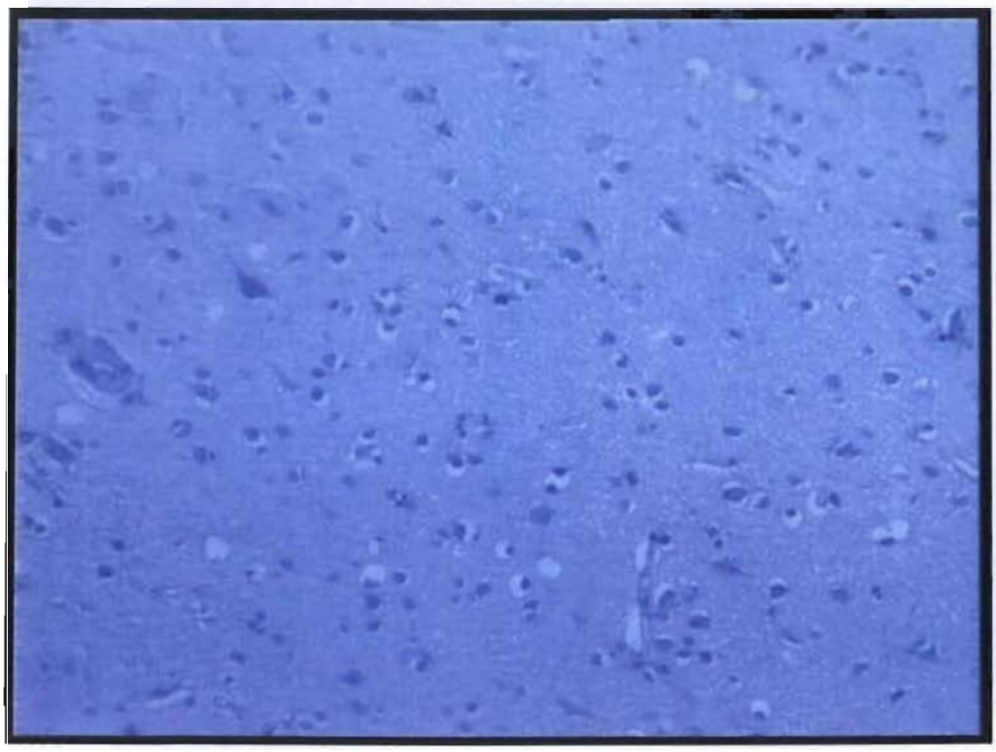

Figure 10.11: Light micrograph of the non-cancer cerebellar cortex showing absence of non-immunological FB_1 staining (Magn. X 100).

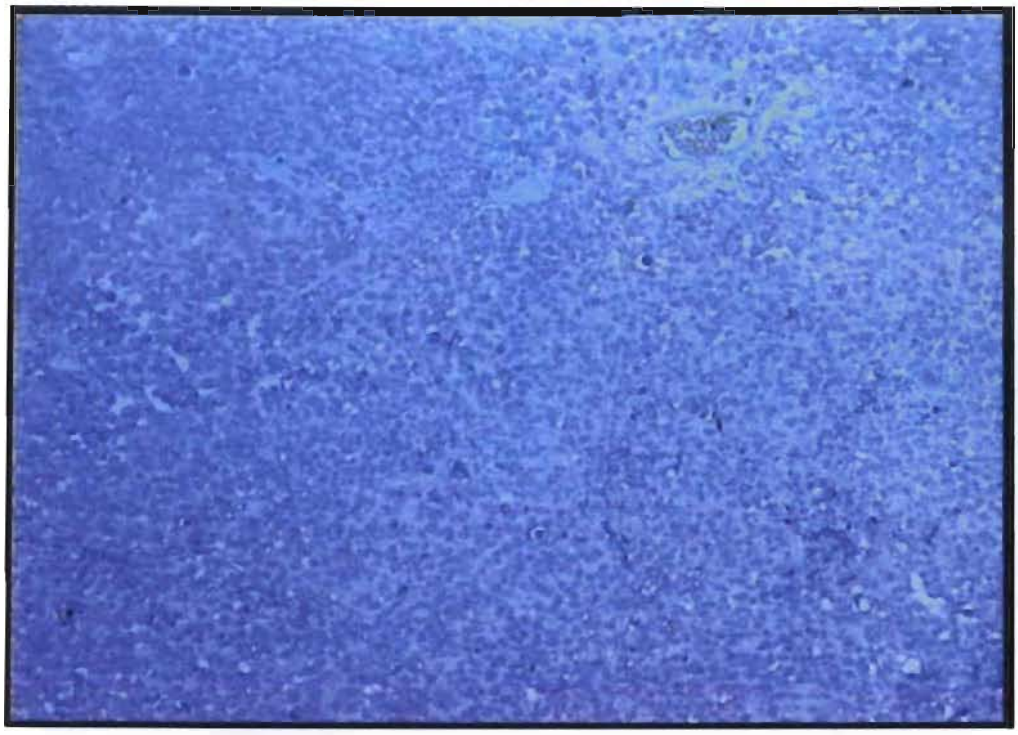

Figure 10.12: Light micrograph of the method control where the primary antibody was omitted showing absence of immunoreactivity in the tumour tissue (Magn. X 40).

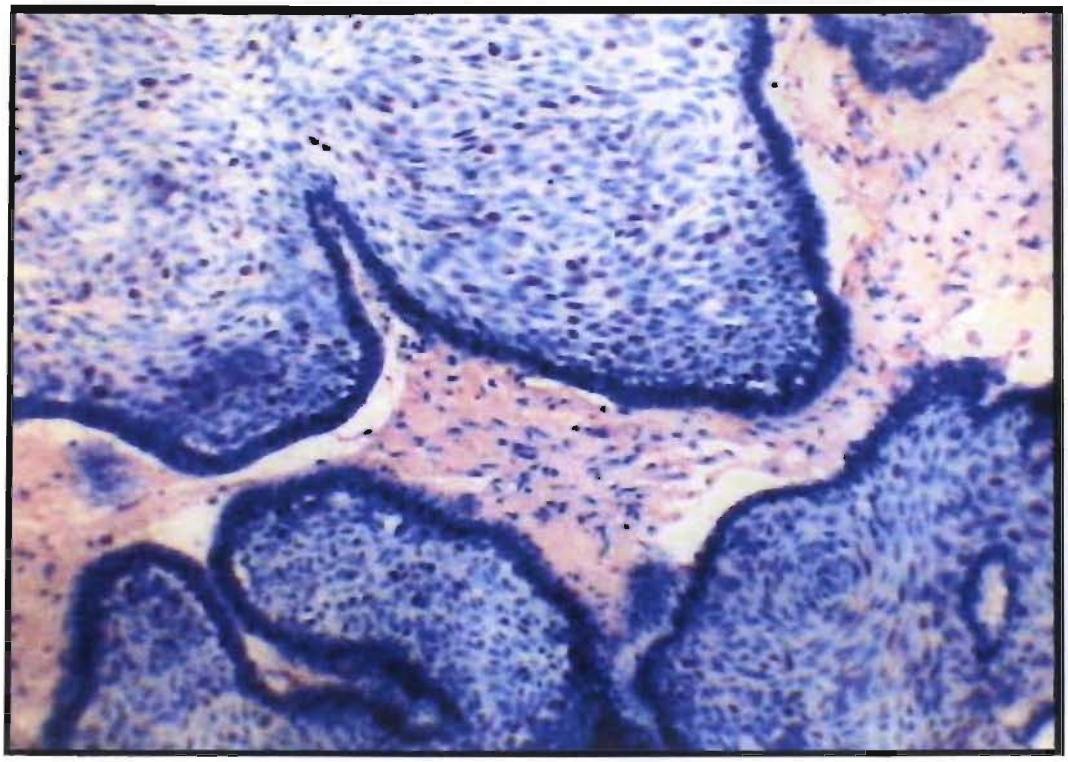

Figure 10.13a: Light micrograph of a meningothelial meningioma showing red AEC chromogen immunoprecipitation in tumour cells within the tissue (Magn. X 100).

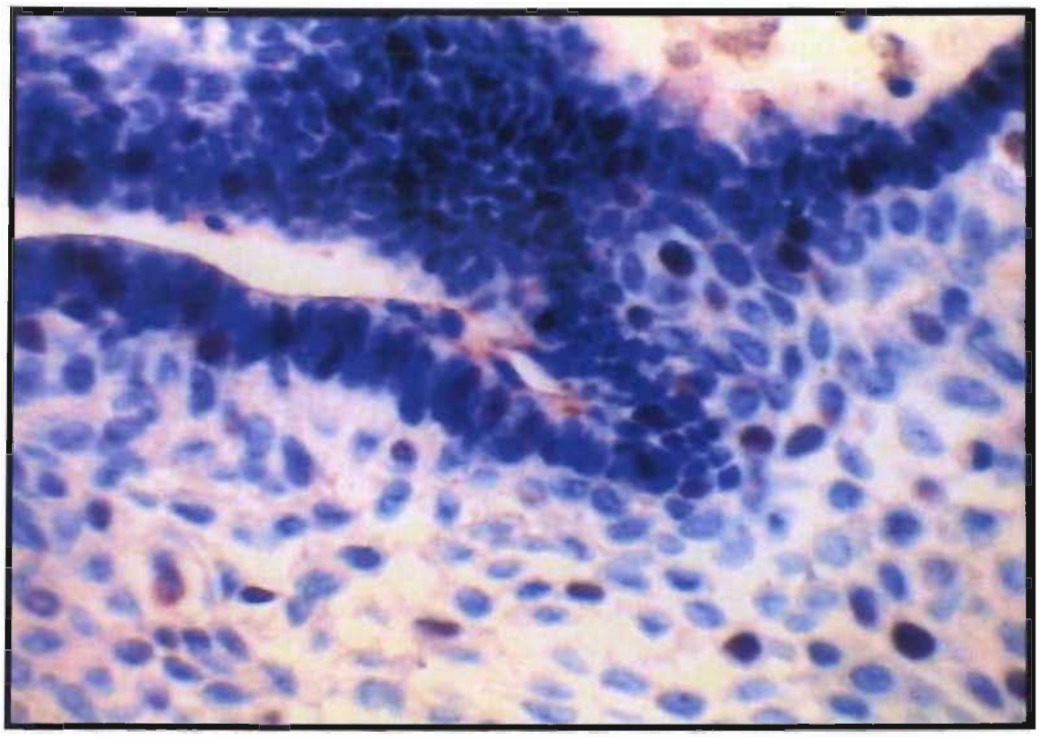

Figure 10.13b: Light micrograph of the meningothelial meningioma showing FB_1 immunoreactivity indicated by the red AEC chromogen (Magn. X 400).

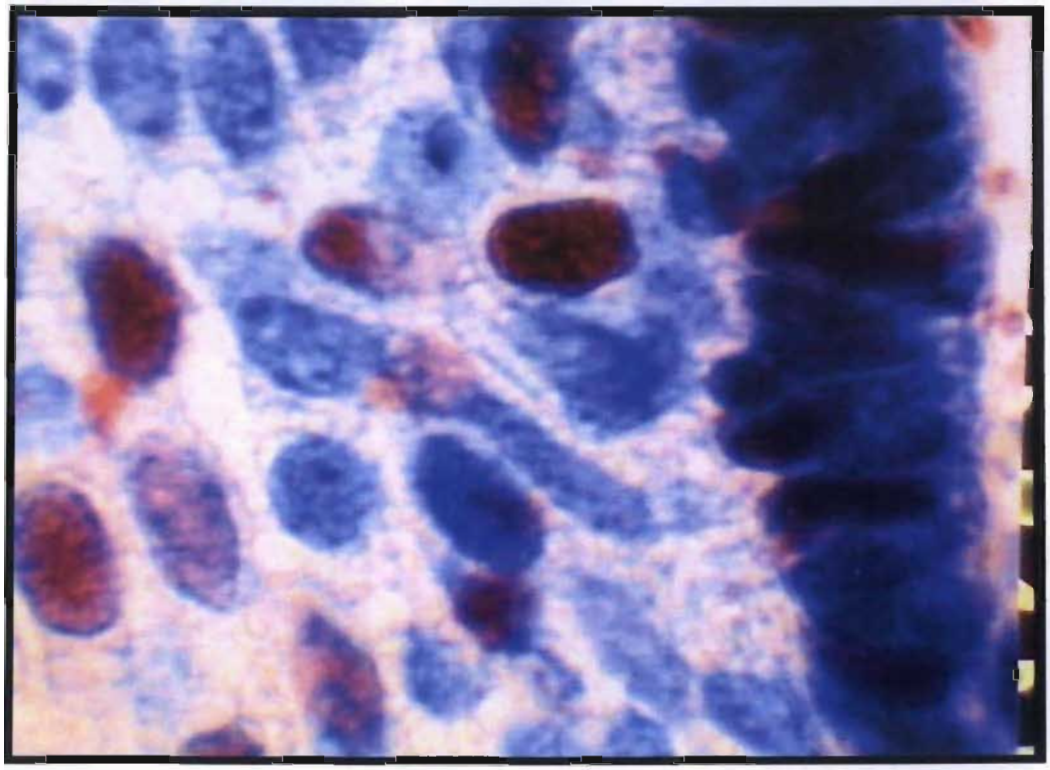

Figure 10.13c: Light micrograph of a meningioma showing varying intensities of the AEC chromogen staining within neoplastic cells with enlarged nuclei (Magn. X 1000).

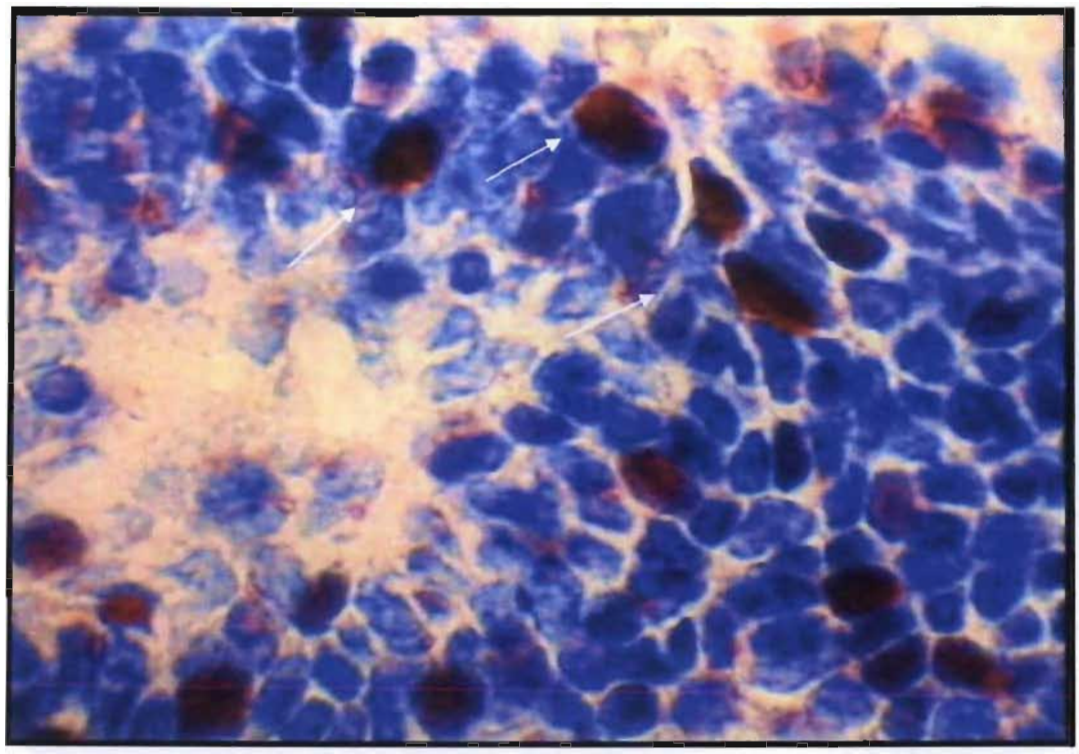

Figure 10.14: Light micrograph of a brain tumour specimen with FB_1 immunoprecipitation in a few cells (red AEC chromogen) (Magn. X 1000).

Figure 10.15: Electron micrograph of a meningioma showing variation of cell size and pyknotic enlarged nuclei (Nu) (Magn. X 2 000).

Figure 10.16: Electron micrograph of a tumour specimen with pleomorphic nuclei (Nu), scattered desmosomes (D) and evidence of keratinisation (K) in the cytoplasm (Magn. X 2 000).

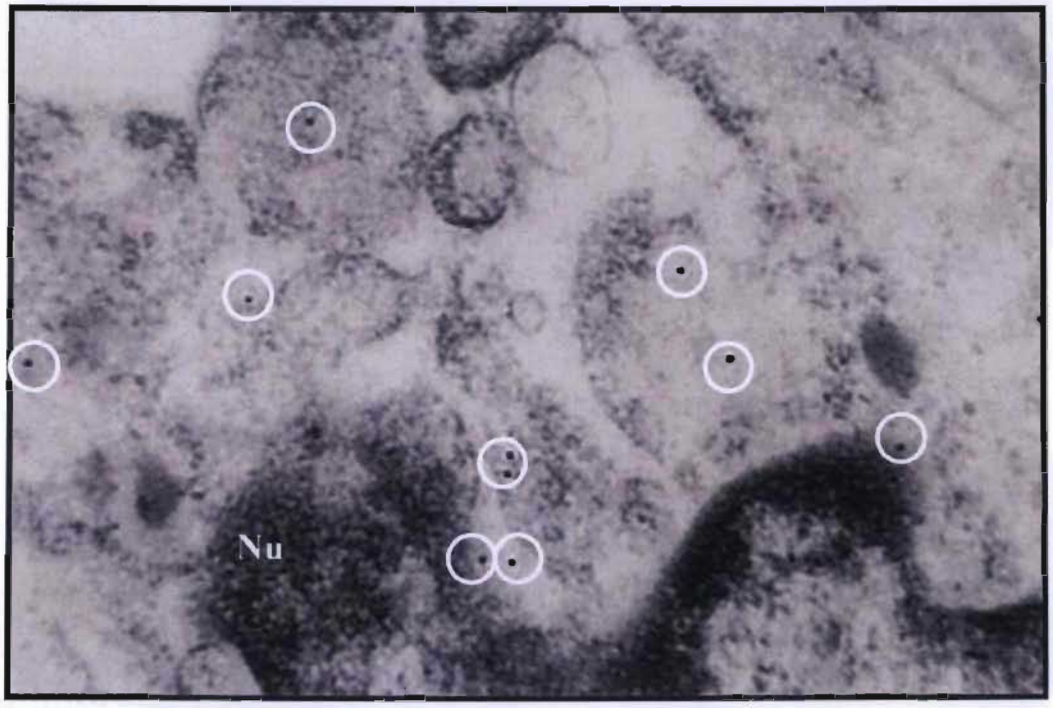

Figure 10.17: Electron micrograph showing a nucleus (Nu) within a tumour specimen with a crenated border and FB_1 immunolocalised on the nuclear membrane and in the cytoplasm (gold probes in circles) (Magn X 25 000).

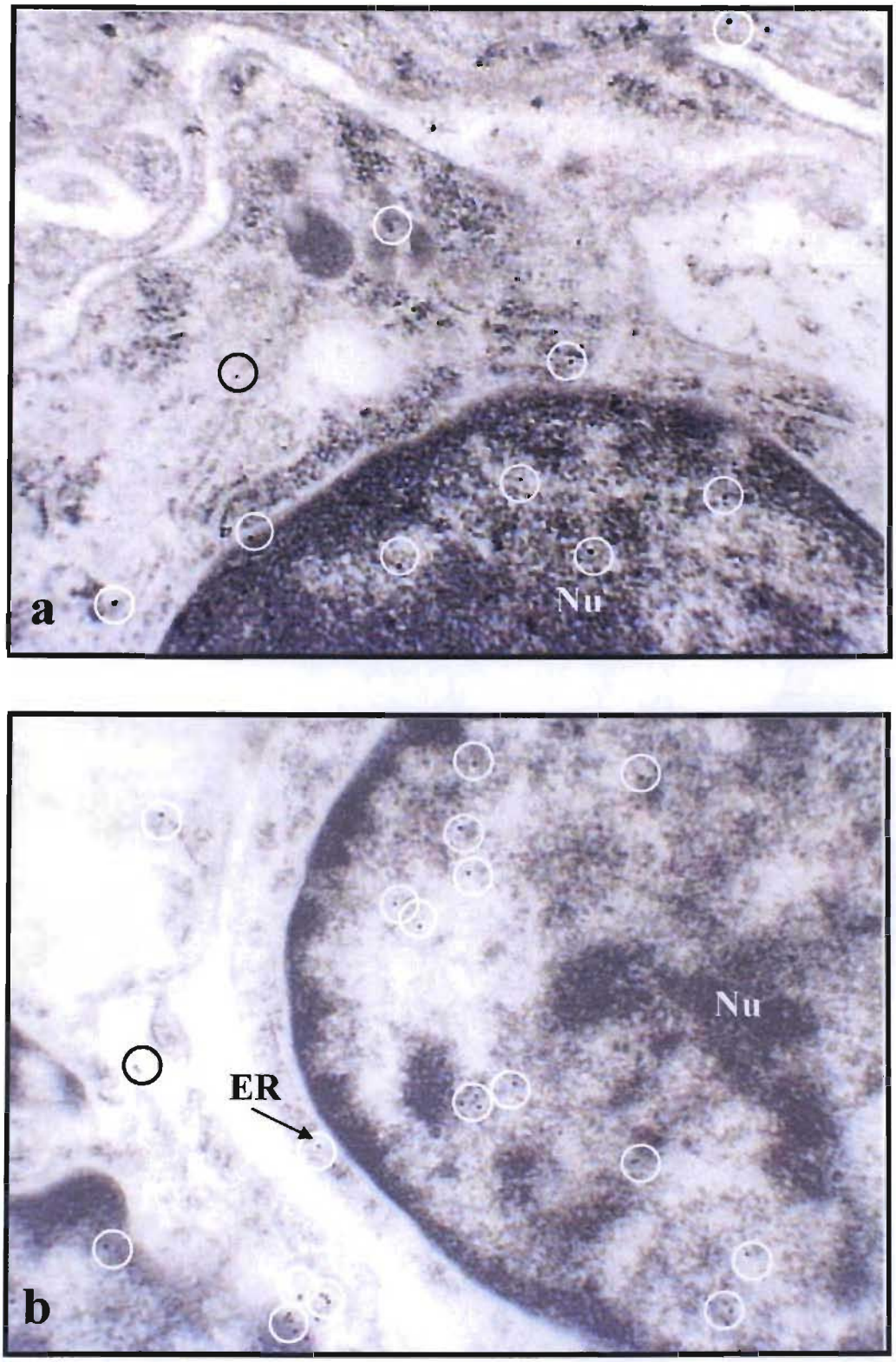

Figures 10.18a and b: Electron micrographs of brain tumour specimens showing nuclei (Nu) with FB_1 immunolocalised on the nuclear envelop and within the nucleoplasm **(a)** (Magn. X 12 000), on the nuclear membrane and in the tumour cell cytoplasm in association with dilated ER **(b)**. Note the gold probes are circled for identification. (Magn. X 25 000).

Figure 10.19: Electron micrograph of a medulloblastoma showing a pyknotic nucleus with gold-labelled FB_1 (gold probes circled) found in association with heterochromatin condensation along the periphery of the nucleus and with granules interspersed within the euchromatin (Magn. X 20 000).

Figure 10.20: Electron micrograph of brain tumour tissue showing FB_1 immunolocalised within a mitochondrion (M) that is closely associated with ER and the nucleus. Note the gold probes are circled. (Magn. X 40 000).

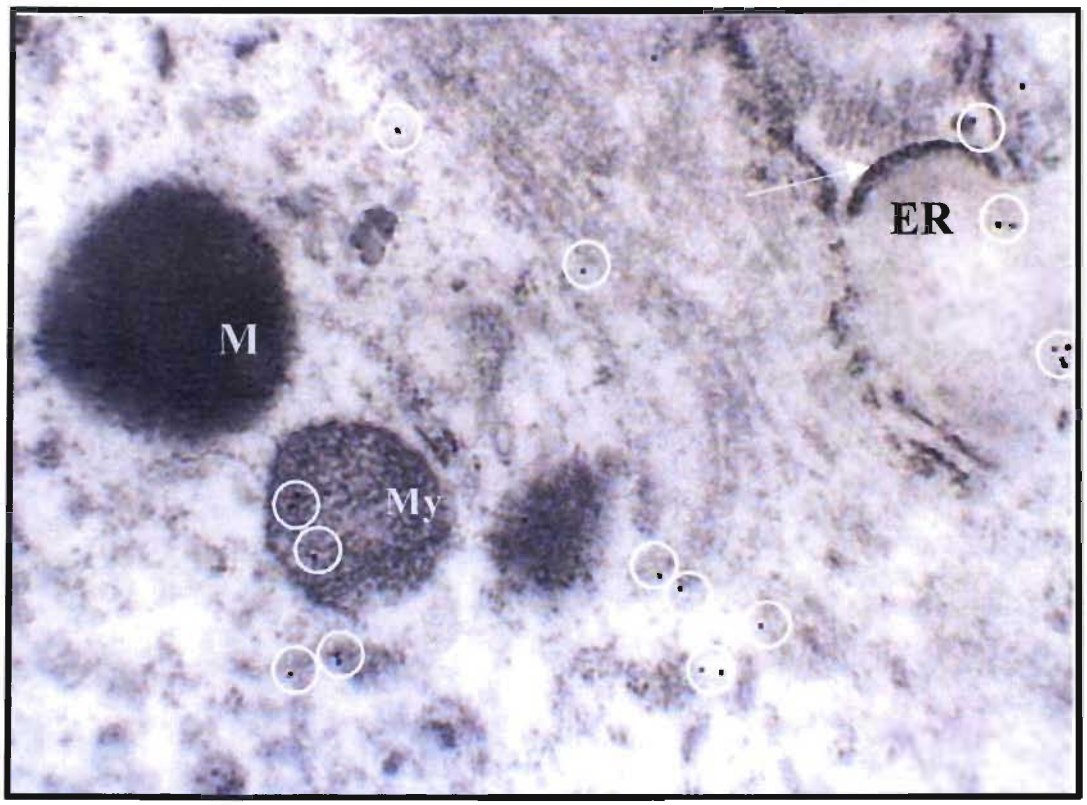

Figure 10.21: Electron micrograph showing immunolabelled FB_1 (gold probes circled) within myelin figures (My), mitochondria (M), cytoplasm and in disrupted ER. (Magn. X 40 000).

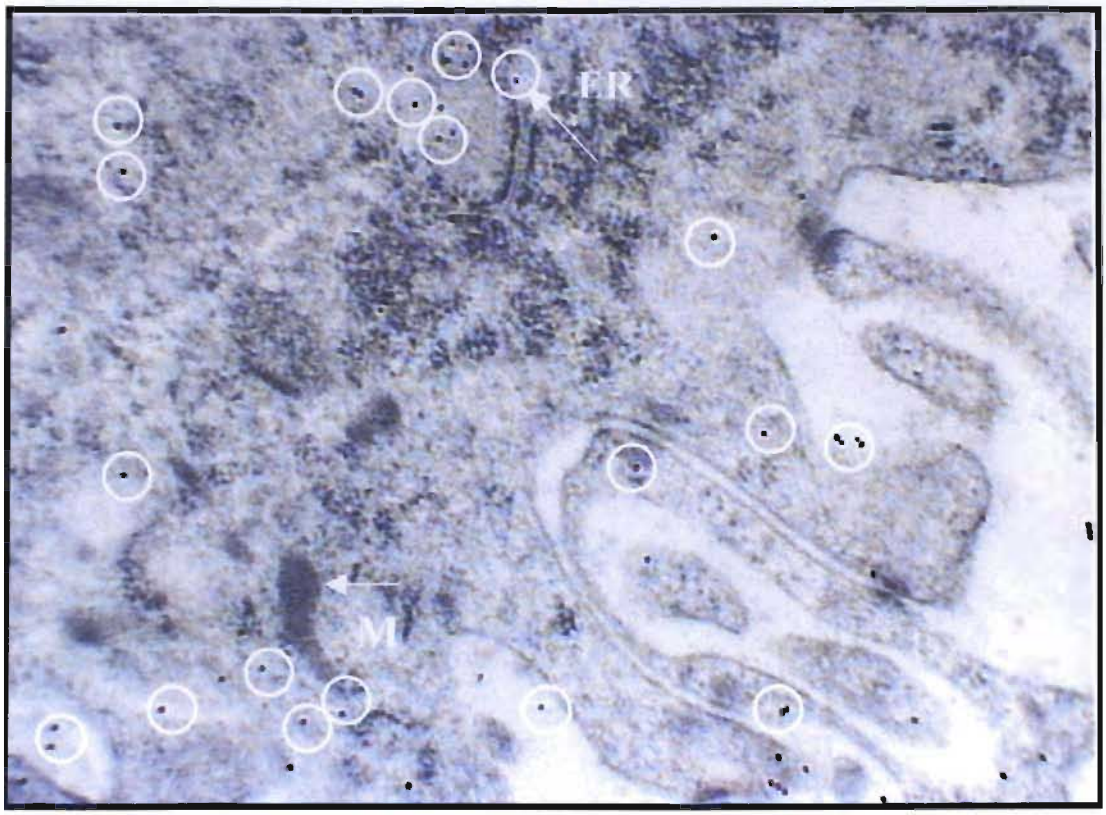

Figure 10.22: Electron micrograph showing FB_1 immunolabelled (gold probes circled) within elongated mitochondria (M) and swollen ER (Magn. X 25 000).

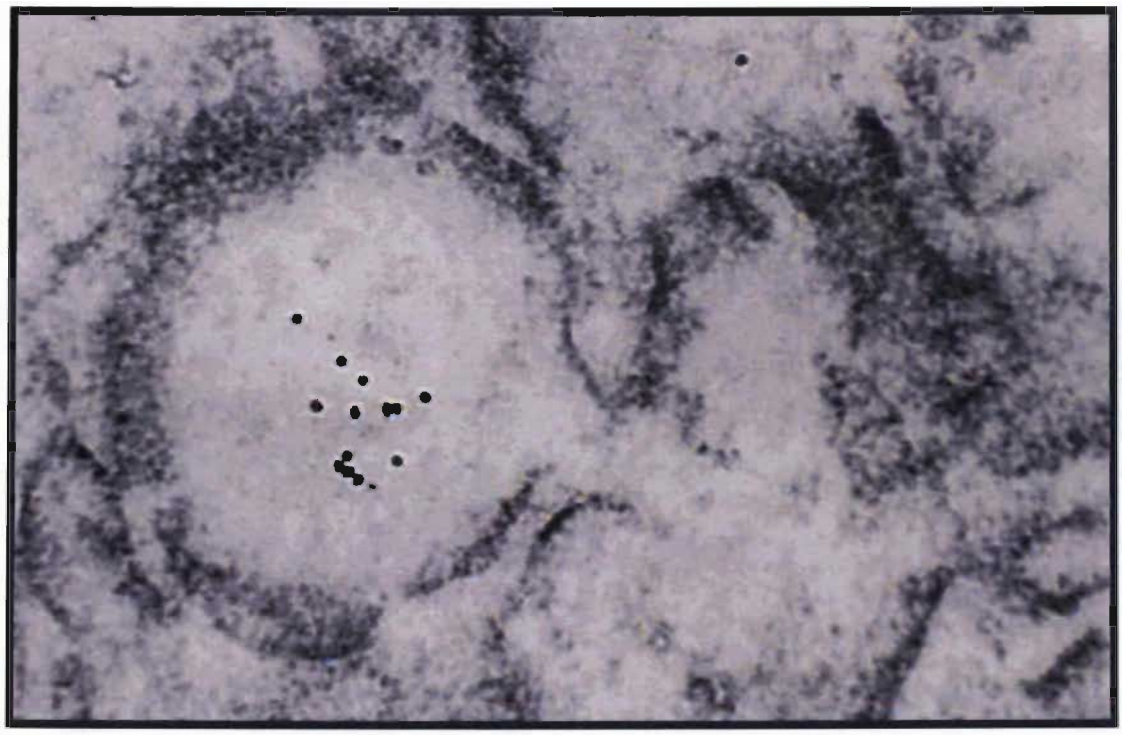

Figure 10.23: Electron micrograph showing immunolabelled FB_1 within swollen disrupted ER (Magn. X 60 000).

Figure 10.24: Electron micrograph showing immunolabelled FB_1 within strands of broken ER and the cytoplasm (Cyt) of a brain tumour cell (Magn. X 60 000).

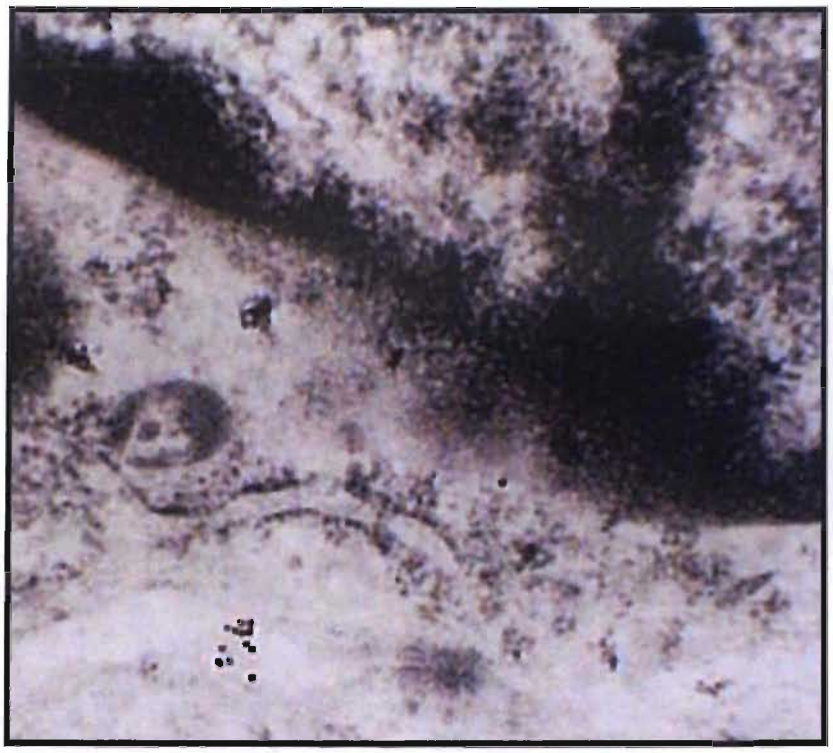

Figure 10.25: Electron micrograph showing immunolabelled FB_1 in association with swollen ER and areas of cytoplasmic lysis (Magn. X 80 000).

CHAPTER 11

Conclusion

Mycotoxicology is a vigorous and eclectic science that has recruited scientists from a wide variety of disciplines. As part of a comprehensive effort to curtail the adverse health effect posed by mycotoxins, substantial international research efforts have been conducted to determine the mechanisms of action of *Fusarium* mycotoxins. The literature review of this study highlighted that although diverse research studies have been directed into the effects of fumonisins on isolated and select cells in the human CNS, no direct links have been established between fumonisin exposure and the incidence of cancer of the brain. This study aimed to address this gap in knowledge within both the *in vitro* and *in vivo* components.

In vitro models in cancer research provide avenues for elucidation of cellular events involved in multistage carcinogenesis. In this study, the N2α neuroblastoma cell line was used to assess chemical toxicity that dealt with mechanistic, cellular and biochemical alterations associated with exposure to certain *Fusarium* mycotoxins and sphingoid bases *in vitro*. Investigations into their interactions with the N2α cells yielded information that would help identify how neuronal cell types might suffer damage as a result of exposure to these compounds *in vivo*. Modern toxicology subscribes to the theory that certain biochemical lesions produced by a compound initiate biological effects or toxic endpoints. The general objective of the *in vitro* cell studies was for elucidation of whether the mycotoxins or their active metabolites reacted with critical cellular molecules, the mode of action of these compounds, and/or for a potential sequence of events initiated by interaction of the mycotoxin or sphingoid base with cellular constituents. These interactions were expected to result in impairment of vital biochemical processes involving these molecules, possibly structurally and functionally altered molecular receptors, and consequent biochemical lesions.

In this study, the characteristics of the mycotoxin-chemical toxicity prediction problem were addressed when the potential for selected *Fusarium* mycotoxins to induce cytotoxicity, apoptosis, growth arrest or necrosis in the N2α mouse neuroblastoma cell line were investigated. For the proper elucidation of the cytotoxicity of *Fusarium* toxins, it was

important to establish whether the observed cellular effects were due to direct interaction of the toxin with the cultured N2α neuroblastoma cells, or whether the toxin interacted with other cellular targets which in turn impaired cell function. Structural and ultrastructural changes that occurred as a result of mycotoxin exposure in the N2α cells were investigated using immunochemical techniques in combination with LM and EM. The *in vitro* effects of FB_1 on sphingolipid metabolism in the N2α cell culture model were also determined by quantitative HPLC analyses of treated N2α cells and CCM for Sa and So levels.

Cytotoxicity is a complex event *in vitro* where its expression may be manifest in a wide spectrum of effects, from simple cell death to complex metabolic aberrations. Viability and cytotoxicity assays have principally been used to enumerate the proportion of live and dead cells in a population. In this study, cell survival, proliferation, and metabolic activity of the N2α cells were determined using the MTT bioassay. Fumonisin B_1, FA, MON, DON, T2 and ZEA, as well as the sphingoid bases Sa and So, induced varying levels of cytotoxicity or mitogenicity in the N2α neuroblastoma cell line following the 48-hour exposure period. As dead cells were unable to metabolise the MTT salt, this factor also facilitated determination of the levels of cell mortality following exposure to these compounds. The experimental evidence indicated that chemical congeners, which seemed to have negligible differences in their molecular structures (e.g., DON and T2; and FB_1, Sa and So), often exhibited large differences in bioactivity and cellular responses. The sphingoid bases were clearly more cytotoxic to this cell line than any of the mycotoxins tested at equivalent concentrations. The MTT assay was useful for quantitative analyses of factor-induced cytotoxicity within a 24-48 hour period of cell culture.

When a cell is exposed to physical stress, biological injury, or deprived of necessary substances, it activates a series of stress responses. With minimal insult, the cell may recover, but with greater insults cell death or apoptosis results, the cell dies and is recycled to its neighbours. If the insult overwhelms a large number of cells then necrosis ensues. In this study, the ApoGlow™ assay was used to determine the effects of FB_1, FA and (FB_1+FA) on the N2α neuroblastoma cell line, and the Jurkat leukaemic suspension cell line. The ApoGlow™ assay was considered expensive, as aside from its high cost, it required specialised equipment for the analyses of data. However, with these confounding variables aside, depending on the cell line analysed and the concentrations of mycotoxin exposure, the ApoGlow™ assay revealed whether the mycotoxins acted antagonistically, in

synergism, or induced some level of cytotoxicity by disruption of cellular metabolism. The assay enabled the determination of whether apoptosis, necrosis, growth arrest, or proliferation occurred when Jurkat and N2α cells were exposed to specific concentrations of FB_1, FA and their combination. The results on the Jurkat cell line indicated the potential effects of these mycotoxins on white blood cells. The effects noted on the N2α cells also provided insight as to how neuronal cells may respond *in vivo* if exposed to these mycotoxins. However, no characteristic or distinct trends were noted in the responses of the N2α and the Jurkat cell lines. This assay indicated that the biochemical events initiated would ultimately lead to cytological manifestations of toxicity. These changes were considered to best be assessed employing microscopical techniques.

In subsequent studies, FM complemented with FCM facilitated quantitative correlative analyses between structural and intracellular biochemical changes that occurred in the N2α cells as a consequence of exposure to mycotoxin or sphingoid bases. The six mycotoxins, and Sa and So, induced varying levels of apoptosis and necrosis in the N2α cells following the 48-hour exposure period. Use of AcO and EtBr, revealed that N2α treated cells were characterized by loss of cell membrane integrity. Significant differences in the staining intensities were evident by comparison of the FB_1, T2 and sphingoid base treated N2α cells with control cells. Staining N2α cells with Rh123 and PI, revealed that visual separation of necrotic and late apoptotic N2α cells was difficult to distinguish using FM. The ZEA-treated N2α cells showed features consistent with the late apoptotic stage, with cytoplasmic condensation or cell shrinkage, as well as the relatively intact cell membrane noted in comparison to DON-treated N2α cells. The DON-treated N2α cells were swollen and displayed compromised plasma membrane integrity indicating possible necrosis. Cells treated with DON also displayed features characteristic of apoptosis, such as membrane blebbing. Cells with decreased Rh123 fluorescence and that were PI positive included necrotic cells, indicated by cellular swelling, and loss of plasma membrane integrity. Variations in N2α cells mitochondrial membrane potential were assessed using JC-1. In MON-exposed N2α cells decreased cytotoxicity was evident in comparison to FA-treated cells. In FB_1-treated N2α cells, large intercellular spaces were indicative of the proportion of cell death induced by FB_1 exposure. Quantitative analyses were carried out using Rh123/PI for FCM analyses.

In most cases, an increase in mycotoxin concentration from 50 to 200μM was paralleled by a decrease in J-aggregate formation, suggesting a decrease in the $\Delta\psi m$. Staining with Rh123/PI indicated whether N2α cells were late apoptotic or necrotic reflected by the levels of PI uptake. With the N2α cells exposed to T2 and DON, staining with Rh123/PI, revealed that the late apoptotic and necrotic N2α cells comprised greater than 80% of the population. Staining with JC-1 however indicated a potential concentration-dependent decrease in viability from 63 to 57% for cells exposed to T2. The viabilities of the N2α cells exposed to DON also varied considerably when the methods were compared. No dose dependent mechanism of cell death was established using either method, as fluctuations were wide. Using Rh123/PI cell viabilities were consistently below 5% at all three levels of exposure.

The FM and JC-1 FCM results correlated well with the MTT assay results. Both the FM and FCM results show that the mycotoxins and sphingoid bases between 50 and 200μM induced varying levels of apoptosis, necrosis, and cytotoxicity on the N2α cells. The Rh123/PI method gave consistently higher levels of compromised cells than the JC-1 method of FCM analyses, and was therefore considered less reliable than JC-1 staining for FCM. Accurate identification and quantification of the mode of cell death occurring in a particular situation is a necessary pre-requisite to understanding the biological processes taking place. This was successfully demonstrated using both FCM and FM in the qualitative and quantitative assessment of the cellular changes following *in vitro* exposure to the selected compounds. As the detection of many mycotoxins by chemical methods is not adequate at present, the feasibility of testing all known mycotoxins chemically is not practical. This tissue culture method in combination with FCM and FM is a potential tool that would be useful in detection of cytotoxicity induced by extracts on whole cells, and the ability of mycotoxin standards to kill particular cell types, provided unbiased interpretation of data was facilitated. Despite the fact that no single method can provide unequivocal quantitative measure of apoptosis in all situations, flow cytometric techniques represent useful tools for biological and clinical studies requiring quantitative information about cell death.

Immunohistochemical and ICC microscopic analyses elucidated the variability that exists with regards to consequences of exposure to a mycotoxin and subsequent cellular sensitivity. The results of FM, FCM, MTT assays, IHC, and ICC correlated well with each

other. The immunolocalisation of T2, ZEA and FB_1 within cellular organelles that showed structural and ultrastructural pathology provided good correlation between potential cause and effect of these mycotoxins. At the LM level, treated cells displayed features of progressive damage leading from gradual retraction of processes, to loss of cytoplasmic volume and complete cell rounding. Some N2α neuroblastoma cells were reduced in size due to cell shrinkage and displayed cytoplasmic condensation. A positive correlation existed between cells that displayed increased intensity of chromogen adhesion, and cells that appeared more compromised by toxin exposure.

At the EM level, microsegregation, and peripheral condensation of the nucleoli were typical features found in association with gold-labelled FB_1 immunolocalised within nucleoli, the nucleoplasm, discontinuous nuclear membranes, and in swollen cellular processes of FB_1-treated N2α cells. Alterations of mitochondrial morphology included markedly swollen mitochondria with circular arrangement of the cristae, disintegration of the internal architecture of mitochondria, and distorted cristae, clearing of the mitochondrial matrix, as well as distortion or disruption of the outer mitochondrial membrane. Gold-labelled FB_1 within elongated and distorted mitochondria, as well as on cristae of mitochondria of the treated cells, indicate direct involvement of FB_1 with these organelles ultrastructural pathology. The ER profiles of FB_1-treated N2α cells were short and discontinuous, with features of dilatation or swelling with occasional vesiculation of cisternae of the ER, in association with immunolabelled FB_1. Gold-labelled FB_1 was localised within areas of cytoplasmic lysis as well as in the surrounding cytoplasm. The immunolocalisation of toxin within cellular organelles that displayed ultrastructural pathology suggested a potential correlation between cause and effect in this neuroblastoma cell line.

Treatment of the N2α cells with ZEA accelerated cell growth at foci, induced giant cell formation, nuclear condensation, peripheral location of nuclei, membrane blebbing, and loss of cell membrane integrity. The cellular target of ZEA appeared cytoplasmic, although nuclear staining was also evident. Extensive cytoplasmic lysis, membrane damage and induction of giant cell formation were features of T2-treated N2α cells. As the IHC staining for T2 seemed predominantly cytoplasmic, it may have altered mitochondrial function in the N2α cells. The N2α cells treated with 100 and 200μM T2 however showed incorporation of toxin into nuclei. The interaction of mycotoxins with cellular macromolecules was viewed as the event initiating the series of observed phenomena.

Lesions occurring in DNA and RNA are of particular significance because they destroy the structural integrity of these informational molecules, and interrupt their biosynthesis and that of proteins and other cellular constituents essential to the viability of the cell.

Biochemical toxicity can be attributed to multi-factorial interactions between biological factors and aspects of chemical structure that partition individual chemicals among mechanistic pathways that govern their activity. Different levels of susceptibility indicate that mycotoxins and sphingoid bases traversed cell membranes and interacted with cellular organelles. The immunolocalisation of FB_1, ZEA and T2 in areas of cellular degeneration, in the nuclei, nucleoli, and mitochondria, ER and in areas of cytoplasmic lysis were considered indicative of sites of toxin interaction and subsequent interference with cellular metabolism. The capacity of a cell to incorporate these mycotoxins and effect cytological changes as a result of this exposure represents a major factor in the initiation of malignant transformation. These *in vitro* studies highlight the potential toxicity of these mycotoxins on neuronal cells, and draws attention to the cytotoxic effects that may be induced *in vivo* and contribute to, or exacerbate the condition of malignant transformation. On the basis of information obtained in these *in vitro* studies, a defined sequence of biochemical events leading to morphological manifestations of toxicity or carcinogenicity could not be constructed. However, results of numerous investigations have revealed general patterns of reactions that are thought to be associated with the toxicity response by virtue of the time course and consistency of their occurrence, and their potential importance in cellular metabolic phenomena.

With the *in vitro* effects of FB_1 on the N2α neuroblastoma cell line documented thus far, it was expected that there would be a modification of sphingolipid metabolism on exposure to FB_1. Quantitative HPLC analyses revealed that exposure to FB_1 caused an increase in intracellular free Sa and depletion of complex sphingolipids in the N2α cell line. Chromatographic analyses of CCM that the N2α cells were cultured in for 72 hours with 50μM FB_1 and 100 μM FB_1 indicate that the N2α cells took up approximately 67% and 76% of the mycotoxin, respectively.

Exposure of the N2α neuroblastoma cell line to FB_1 increases intracellular free Sa and depletion of complex sphingolipids. Determination of levels of total Sa and So from complex sphingolipids in the N2α cells, were facilitated by acid hydrolysis of the cultured

cells. Quantitative results revealed that there was a reduction in the concentrations of Sa from a level of 0.6±0.12μM in control cells, to 0.2±0.09μM in cells exposed to 50μM FB_1 and to 0.2±0.1μM in cells exposed to 100μM FB_1 over the 72 hours incubation period. In terms of So, there was a reduction from 4.9±1.0μM in control cells to 1.0±1.4μM and 1.8±0.5μM in cells exposed to 50μM FB_1 and 100μM FB_1, respectively. These results indicate that there was as reduction in the cellular levels of complex sphingolipids

Determination of the levels of free Sa and So in the N2α cells were facilitated by base hydrolyses. There was a distinct increase in the free Sa:So ratio from 0.52±0.2 in control cells, to 1.14±0.2 in cells exposed to 50μM FB_1. There was a further increase in the Sa:So ratio to 1.4±0.3 in cells exposed to 100μM FB_1. Finally, analysis of the CCM in which the cells were cultured over the 72hour incubation period revealed that the Sa:So ratio in the CCM increased from 1.7±0.3 for controls cells to 2.0±0.2 and 2.50±0.4 for cells exposed to 50μM FB_1 and 100μM FB_1 respectively. Correlation coefficients, R, for the Sa:So ratios to FB_1 in the CCM was 0.75, and for free Sa:So to FB_1 in cells was 0.85. The free Sa:So ratio in cells appear to be a better biomarker than the Sa:So in the CCM.

The conceptual framework, and data presented supports the use of the Sa:So ratio as a biomarker for a dose response of FB_1 on sphingolipid metabolism in N2α cells. This framework is reasonably consistent with observed Sa:So ratios and FB_1 concentrations in the examined cells and culture media, as well as the current literature of FB_1 effects on sphingolipid biosynthesis in cultured cells.

In the clinical component of this study, several analytical methods for FB_1, Sa and So retrieval and quantitation from human sera were assessed. Research on mycotoxins in biological fluids contributes to clarity of the mechanism of health impairment attributable to these compounds and to a possible dose-response relationship. The HPLC analyses of sera described facilitated both qualitative and quantitative assessment of FB_1, Sa and So levels in spiked sera. Extensive optimisation procedures led to reproducible results with high analyte recoveries. Optimal retrieval was achieved with the use of smaller volumes of solvents, increased vortexing times, and triple extraction of protein pellets with methanol for Sa and So. The recoveries of the individual sphingoid bases were considered a function of the volumes and affinities of the solvents used. With FB_1, the mean recovery from spiked human serum samples obtained following optimisation was 95.8% (n=15).

Optimisation of the method also improved detection limits of FB_1 to ~5ng.ml^{-1} at a signal to noise ratio of 5:1.The methods were then considered adequately optimised for use in sera analyses of non-cancer and cancer patients, to establish whether correlations exists between FB_1 exposure, Sa:So ratios and brain cancer.

Matched measurements of Sa:So ratios and FB_1 levels in human serum samples were determined for brain cancer patients and non-cancer volunteers from KZN. The approach used was to isolate and quantify serum levels of FB_1, Sa and So from non-cancer (n=21) and brain cancer (n=50) subjects. Considerable overlap in the Sa:So ratios occurred between subjects in both groups (n=71). Fumonisin B_1 was detected in the serum of both non-cancer and brain cancer subjects. However, no correlation (R = 0.26) existed between serum FB_1 levels and Sa: So ratios in non-cancer, nor the brain cancer subjects (R = - 0.23). This implies absence of a causal relationship between exposure to this exogenous sphingolipid inhibitor and disruption of sphingolipid metabolism in this study cohort.

Gender-specific statistical analyses revealed that there was no significant difference between the non-cancer male and female serum Sa: So ratios in this study cohort (p=0.63). Serum FB_1 levels in the female brain cancer subjects, also did not differ significantly to that of non-cancer females (p=0.73), nor was the mean serum Sa: So ratio in the female cancer patients (2.09±1.74) significantly different (p=0.43) from female subjects in the non-cancer group (1.63±0.94). Furthermore, analysis of the sera Sa: So ratios of the cancer and non-cancer males revealed that these levels did not differ significantly either (p=0.56). Limiting variables in this study included the sample size, limited volumes of blood and the inability to age and sex match all sera samples obtained from the brain cancer subjects.

In the field of mycotoxins, the biomarker approach represents a promising route for evaluation of risk associated with the ingestion of these toxic substances. The data presented in this study however contests the primary use of the Sa: So ratio as a biomarker for a dose response of FB_1 induced inhibition on sphingolipid metabolism, or as a biomarker for brain cancer in human subjects. The potential exists that FB_1 may be a contributing factor in the aetiology of brain cancer by way of its presence in sera. Even in the absence of overt diseases, immuno-modulation associated with mycotoxin exposure have important ramifications and on the health and quality of life of those affected.

The final clinical part of this study dealt with screening human brain tumour and non-tumour tissues using IHC methods to establish whether FB_1 is associated with the cellular pathology of human brain cancer. Seventy-six brain tumour tissue specimens were analysed for FB_1 presence using IHC. Of these, 38 specimens were matched with serum analyses for FB_1, Sa, So, and the Sa: So ratios. Twenty-three of the 38 samples showed presence of FB_1 at the LM level. The matched FB_1 sera analyses of the 23 FB_1 positive tissue specimens indicate that although not significantly different ($p=0.11$); the cancer group with FB_1 within the tumour tissue had higher levels of FB_1 in the circulation than the cancer group without FB_1 immunolocalised within tissue. Fumonisin B_1 was localized within 65% of the tumour samples analysed, and was also detected in two non-cancer brain tissue specimens. Certainly differences in individual absorption and distribution, metabolism and repair all have the potential to influence individual sensitivity to a particular agent. In turn, these specific differences may account for the wide variation in incidence of cancer between and within groups of people.

Experimental studies do not always provide hard experimental data that prove specific cancer-causative factors. Rather they usually provide specific associative hypotheses or 'risk factors' for further study. The IHC and ICC analyses of the brain tumour tissue highlights the potential for exposure to FB_1 to be implicated in the initiation, promotion or exacerbation of the brain cancer condition, and requires further investigation. Immunolocalisation of FB_1 in brain tumour tissue showing morphological changes indicates that FB_1 may be associated with initiation of biochemical and ultrastructural changes that trigger the carcinogenic process. Ultrastructural abnormalities observed in the nucleus and nucleolus might be morphological expressions of biochemical events initiated by FB_1, which may eventually progress to carcinogenesis. Presence of gold-labelled FB_1 in the ER and mitochondria specifically suggests that FB_1 may be active in association with these cellular organelles as they contain high levels of enzyme systems.

Fumonisin B_1 exposure may induce alterations of sphingolipid metabolism and myelin synthesis in the CNS. These alterations may cause along with direct disruption of brain enzyme activity involved in sphingolipid synthesis, damage to myelinating cells. A thorough analysis of the cellular distribution of potential FB_1 susceptible systems is required in search for target cell types in the human brain.

In order to establish a direct causative link between FB_1 presence and brain cancer, a larger sample size of both normal and brain tumour specimens are required. As sphingoid bases are intrinsically cytotoxic, quantitative analyses of the tissue Sa and So levels need to be correlated to tissue FB_1 levels. The elucidation of the biochemical events associated with carcinoma induction by fumonisins would provide insight into the mechanism underlying the carcinogenic process. Considerable experimental data is required in order to relate the biochemical effects of FB_1 directly to the subcellular and cellular events ultimately manifest in toxicity (necrosis) or in tumour induction within the brain.

In this study, a "natural" experiment was exploited. The results are reflected in disease incidence statistics and the challenge was to unravel the pertinent variables. Similarly, just as many experimental designs may be classed as irrelevant to the human situation, so too many manifestational epidemiological associations are unrelated to direct cause. Evaluation on the causal nature of an association is best achieved by means of direct experimentation. Where direct evidence is lacking, evaluation is neither easy nor objective. In this way a variety of corroborative evidence is accumulated which must be evaluated with caution. However laudable caution may be, there comes a point in the accumulation of evidence when it is more prudent to assume that the association is causal until proven otherwise (van Rensburg *et al.*, 1974).

Although the results of IHC analyses reflect FB_1 exposure at the individual level, the impact and actual risk of such an exposure is not yet known, as exposure to a compound at a specific time point does not reflect the outcome of cancer in a specific population and vice versa. The data accumulated in this study does not warrant that FB_1 be classified as a brain carcinogen *in vivo*. However this data may be used as part of the exposure assessment in establishing risk assessment models, although the correlation of associated changes, some of which might occur in cellular oncogenes and/or tumour suppressor genes, and the ultimate cancer has not been established unequivocally.

Currently, the available information on human health effects associated with fumonisins is inconclusive. Further studies on the pathophysiology of fumonisin toxicoses are essential in diagnosis of the disease, establishment of safety parameters and development of control and prevention procedures. Unless systems other than sphingolipid metabolism are discovered affected by fumonisins, the inhibition of CER synthase would be considered the initial step in the toxicity and carcinogenicity of these mycotoxins. This represents only the

starting point for understanding the pathology of these compounds. More must be learned about the cellular consequences of elevations in Sa and various Sa metabolites, and the reductions in key complex sphingolipids caused by fumonisins. Such investigations should provide insight into, not only into the biological role of sphingolipids, but also the mechanism of disease initiation by fumonisins.

Although methods used in this study, such as FM, FCM, IHC, ICC and HPLC have contributed to the elucidation of the mode of action of FB_1 and other mycotoxins studies, some of the most exciting prospects for markers of biological effects or pre-clinical disease arise from tools developed in the field of molecular biology. The major driving force in the development of neoplasia is the interaction of carcinogenic chemicals with the cellular genome of the target cells. The increasing mechanistic understanding of genetic alterations that underlie the progression from initiation to tumour formation has permitted the development of sensitive tests for tumour diagnosis. Studies at the molecular level will complement these studies and provide useful information for the design of remedial measures, and make for better understanding of the mechanism of action of FB_1 and other environmental toxins. The continuing development of molecular epidemiological methods to identify specific mutations in human tumours may at least narrow the list of potential aetiological factors for various human cancers. There is a need to analyse cells and tissues (normal and cancerous) for more than a few sphingoid bases and mycotoxins, if one is to deduce reasonable unambiguous interpretation of experiments on malignant transformation, necrosis, apoptosis or cell cycle arrest.

The history of medicine has clearly recognized that preventative strategies offer the best means of eliminating mortality and morbidity from infections and diseases. Environmentally related diseases are a reality of every day life and in order that people may be rendered more aware of current problems, it is essential that environmental toxicologists remain dedicated to the examination and evaluation of the potential for environmentally induced diseases. The need for prevention of exposure to mycotoxins is certainly relevant in SA where many communities lack modern health care facilities. In SA, the importance of mycotoxins in public health will increase as the available food supplies decreases due to population growth. Opportunities for prevention of fumonisin induced diseases include reducing exposure and interfering with toxicological effects through nutritional intervention. In order to educate people it is necessary to determine the exact association between exposure and disease, establishing reliable and reproducible

indicators of fumonisin exposure and establishing a scientific basis for regulatory guidelines to protect the population from health hazards that are associated with exposure.

Much has been written about coincidence – and many new age philosophers would have one believe that it has mystical meaning. Those more scientifically inclined put coincidence down to statistics. Although FB_1 was immunolocalised in the brain tumour tissues, the postulates required for a proof of a causal relationship in a human brain cancer have not been met. Fumonisins however are a human health hazard and continuous dietary exposure to small amounts could be detrimental. It still has to be shown that risk of brain cancer in a population rises in proportion with the degree of previous exposure to this mycotoxin. This requires quantitative intra- and inter-regional comparisons of exposure and brain cancer risk.

While the condition of all forms of life is of concern, the ultimate effect of environmental degradation is on human health and in this regard; research is undertaken with the intent to serve both the scientific and medical communities by contributing to strategies of disease prevention. Focus is placed on the elucidation of potential carcinogenic stimuli to explain the initiation, promotion, and frequency of cancer. For practicing physicians, environmental related diseases are a reality of everyday life and in order that they might be rendered more aware of current problems, dedication to the examination and evaluation of environmental induced disease is essential

More toxicological research is required to fully define the levels of fumonisins required to affect human health, chemical research to find more rapid and accurate analytical methods, and biochemical research to more fully elucidate the apparent mechanisms of toxicity of fumonisins *in vivo*. This generation of scientists involved in carcinogenesis research will likely see the ultimate rewards: substantial reduction of cancer incidence by prevention of exposure strategies, detection and eradication of early lesions before they become life threatening, and control of more advanced disease from rational treatment are realistic achievements (Yuspa, 2000).

References

Abado-Becognee K, Mobio TA, Ennamany R, Fleurat-Lessard F, Shier WT, Badria F and Creppy EE. 1998. Cytotoxicity of fumonisin B_1: implication of lipid peroxidation and inhibition of protein and DNA syntheses. *Arch Toxicol.* **72**: 233-236.

Abbas HK, Shier WT and Mirocha CJ. 1984. Sensitivity of cultured human and mouse fibroblasts to trichothecenes. *J Assoc Off Anal Chem.* **67(3)**: 607-610.

Abbas HK, Paul RN, Boyette CD, Duke SO and Vesonder RF. 1992. Physiological and Ultrastructural effects of Fumonisin on jimson weed leaves. *Can J Bot.* **70**: 1824-1833.

Abbas HK, Shier WT, Seo JA, Lee YM and Musser S. 1998. Phytotoxicity and cytotoxicity of the fumonisin C and P series mycotoxins from *Fusarium* spp. fungi. *Toxicon.* **36(12)**: 2033-2037.

Abel S and Gelderblom WCA. 1998. Oxidative damage and fumonisin B_1-induced toxicity in primary rat hepatocytes and rat liver *in vivo*. *Toxicology.* **131(2-3)**: 121-131.

Abeywickrama K and Bean GA. 1992. Cytotoxicity of *Fusarium* species mycotoxins and culture filtrates of *Fusarium* species isolated from the medicinal plant *Tribulus terrestris* to mammalian cells. *Mycopathologia.* **120(3)**: 189-193.

Abnet CC, Borkowf CB, Qiao YL, Albert PS, Wang E, Merrill AH Jr., Mark SD, Dong ZW, Taylor PR and Dawsey SM. 2001a. A Cross sectional study of human serum sphingolipids, diet and physiologic parameters. *J Nutr.* **131**: 2748-2752.

Abnet CC, Borkowf CB, Qiao YL, Albert PS, Wang E, Merrill AH Jr., Mark SD, Dong ZW, Taylor PR and Dawsey SM. 2001b. Sphingolipids as biomarkers of fumonisin exposure and risk of esophageal squamous cell carcinomas in China. *Cancer Causes Control.* **12(9)**: 821-828.

Altmann FP. 1976. Tetrazolium salts and Formanzanz. *Progr Histochem Cytochem.* **9**: 1-56.

Ames BN and Gold LS. 1990. Chemical carcinogenesis: Too many rodent carcinogens. *Proc Natl Acad Sci.* **87**: 7772-7776.

Anderson WA. 1969. Nuclear and cytoplasmic DNA synthesis during early embryogenesis of *Paracentrotus lividus*. *J Ultrastruct Res.* **26(1)**: 95-110.

Andreotti PE, Cree IA, Kurbacher CM, Hartman DM, Linder D, Harel G, Gleiberman I, Caruso PA, Ricks SH, Untch M, Sartori C and Bruckner HW. 1995. Chemosensitivity testing of human tumours using a microplate adenosine triphosphate luminescence assay: clinical correlation for cisplatin resistance of ovarian carcinoma. *Cancer Res.* **55**: 5276-5282.

Andrieu-Abadie N, Gouaze V, Salvayre R and Levade T. 2001. Ceramide in apoptosis signaling: relationship with oxidative stresss. *Free Radic Biol Med.* **31(6)**: 717-718.

Ankarcrona M, Dypbukt JM, Bonfoco E, Zhivotovsky B, Orrenius S, Lipton SA and Nicotera P. 1995. Glutamate-induced neuronal death: a succession of necrosis or apoptosis depending on mitochondrial function. *Neuron.* **15(4)**: 961-973.

Aranda M, Pérez-Alzola LP, Ellahueñe MF and Sepúlveda C. 2000. Assessment of *in vitro* mutagenicity in *Salmonella* and *in vivo* genotoxicity in mice of the mycotoxin fumonisin B_1. *Mutagenesis.***15**: 469-471.

Arends MJ, Morris RG and Wyllie AH. 1990. Apoptosis: the role of endonuclease. *Am J Pathol.* **136**:

593-608.

Arends MJ and Wyllie AH. 1991 Apoptosis: mechanisms and role in pathology. *Int Rev Exp Pathol.* **32**: 223-254.

Augerson WS. 2000. A review of the scientific literature as it pertains to Gulf War illnesses [online]. Available from: *http://www.rand.org/publications/MR.hrml* [Accessed 27 August 2002].

Baars AJ, Van Apeldoorn M and Wouters M. 1999. Appendix 1 In: *Toxicology.* Pieters MN, Fiolet DCM and Baars AJ (eds). Deoxynivalenol. Derivation of concentration limits in wheat and wheat containing products. RIVM report 388802008, Rijks Instituut voor Volksgezondheid en Milieu, Bilthoven, The Netherlands.

Bacon CW, Bennett RM, Hinton DM and Voss KA. 1992. Scanning electron microscopy of *Fusarium moniliforme* within asymptomatic maize kernels and kernels associated with equine leukoencephalomalacia. *Plant Disease.* **76(2)**: 144-148.

Bacon CW and Nelson PE. 1994. Fumonisin production in corn by toxigenic strains of *Fusarium moniliforme* and *Fusarium proliferatum. J Food Prot.* **57(6)**: 514-521.

Bacon CW, Porter JK and Norred WP. 1995. Toxic interaction of fumonisin B_1 and fusaric acid measured by injection into fertile chicken egg. *Mycopathologia.* **129(1)**: 29-35.

Ballou LR 1992. Sphingolipids and cell function. *Immunol Today.* **13(9):** 339-341.

Ballou LR, Laulederkind SJF, Rosloniec EF and Raghow R. 1996. Ceramide signalling and the immune response. *Biochim Biophys Acta.* **1301**: 273-287.

Barbieri D, Troiano L, Grassilli E, Agnesini C, Cristofalo EA, Monti D, Capri M, Cossarizza A and Franceschi C. 1992. Inhibition of apoptosis by zinc: a reappraisal. *Biochem Biophys Res Commun.* **187**:1256-1261.

Beasley VR. 1989. Trichothecene mycotoxicosis: Pathophysiologic effects. CRC Press, Boca Raton, Florida, USA.

Becker BA, Pace L, Rottinghaus GE, Shelby R, Misfeldt M and Ross PF. 1995. Effects of feeding fumonisin B_1 in lactating sows and their suckling pigs. *Am J Vet Res.* **56(9)**: 1253-1258.

Beier RC, Elissalde MH and Stanker LH. 1995. Calculated three-dimensional structures of fumonisin B_1, B_2, B_3 and B_4 mycotoxins. *Bull Environ Contam Toxicol.* **54**: 479-487.

Bejaoui K, Wu C, Scheffler MD, Haan G, Ashby P, Wu L, de Jong P and Brown RH Jr. 2001. SPTLC1 is mutated in hereditary sensory neuropathy, type 1. *Nat Genet.* **27(3)**: 261-262.

Bell RM, Hannun YA, and Merrill AH Jr. 1993. In: *Advances in Lipid Research: Sphingolipids and their metabolites.* Academic Press, Orlando, Florida. **26**:69-98.

Bennet JW. 1987. Mycotoxins, mycotoxicoses, mycotoxicology and *Mycopathologia. Mycopathologia.* **100**: 3-5.

Bennett GA and Richard JL. 1994. Liquid chromatographic method for the naphthalene dicarboxaldehyde derivate of fumonisins. *J AOAC Int.* **77**: 501-506.

Bergeron M and Droz B. 1969. Protein renewal in mitochondria as revealed by electron microscope radioautography. *J Ultrastruct Res.* **26(1)**: 17-30.

Berridge MV, Tan AS, McCoy KD and Wang R. 1996. The biochemical and cellular basis of cell proliferation assays that use tetrazolium salts. *Biochemica*. **4**:15-20.

Bever RJ Jr, Couch LH, Sutherland JB, Williams AJ, Beger RD, Churchwell MI, Doerge DR and Howard PC. 2000. DNA adduct formation by *Fusarium* culture extracts: lack of role of Fusarin C. *Chem Biol Interact.* **128**: 141-157.

Bezuidenhout SC, Gelderblom WCA, Gorst-Allman CP, Horak RM, Marasas WFO, Spiteller G and Vleggaar R. 1988. Structure elucidation of the fumonisin mycotoxins from *Fusarium moniliforme*. *Chem Soc Chem Commun.* **11**: 743-745.

Bhat RV, Shetty PH, Amruth RP and Sudershan RV. 1997. A foodborne disease outbreak due to the consumption of moldy sorghum and maize containing fumonisin mycotoxins. *Clin Toxicol.* **35**: 249-255.

Biden P. *pers comm.* 2001. Masters in Medical Science Graduate, University of Natal (now UKZN), Durban, South Africa.

Blank ML, Cress EA, Smith ZL and Snyder F. 1992. Meats and fish consumed in the American diet contain substantial amounts of ether-linked phospholipids. *J Nutr.* **122**: 1656-1661.

Boehringer Mannheim. 1998. *Apoptosis and Cell proliferation*, Second edition. Eisel D, Fertig G, Fischer B, Manzow S and Schmelig K (eds). Germany. pp 27-35.

Bonfoco E, Krainc D, Ankarcrona M, Nicotera P and Lipton SA. 1995. Apoptosis and necrosis: two distinct events induced respectively by mild and intense insults with NMDA or nitric oxide/superoxide in cortical cell cultures. *Proc Natl Acad Sci.* **92**:7162-7166.

Bonsi P, Palmery M and Augusti-Tocco G. 1996. Aflatoxin B_1 cytotoxicity in neurons in culture. *ATLA* **24**: 533-540.

Bose R, Verheij M, Haimovitz-Friedman A, Scotto K, Fuks Z and Kolesnick R. 1995. Ceramide synthase mediates daunorubicin-induced apoptosis: An alternative mechanism for generating death signals. *Cell.* **82**: 404-414.

Bradbury D, Simmons T, Slater K, Crouch S. 2000. Measurement of the ADP: ATP ratio in human leukaemic cell lines can be used as an indicator of cell viability, necrosis and apoptosis. *J Immunol Methods*. **243**:167-190

Branham RDA and Plattner RD. 1993. Isolation and characterization of a new fumonisin from liquid cultures of *Fusarium moniliforme*. *J Nat Prod.* **56**:1630-1633.

Brunner C, Lassmann H, Waehneldt TV, Matthieu JM and Linington C. 1989. Differential ultrastructural localization of myelin basic protein, myelin/oligodendroglial glycoprotein, and 2'3' cyclic nucleotide 3'-phosphodiesterase in the CNS of adult rats. *J Neurochem.* **52**: 296-304.

Bryden WL, Love RJ and Burgess LW. 1987. Feeding grain contaminated with *Fusarium graminearum* and *Fusarium moniliforme* to pigs and chickens. *Aust Vet J.* **64**: 225-226.

Bucci TJ, Hansen DK and LaBorde JB. 1996. Leukoencephalomalacia and hemorrhage in the brain of rabbits gavaged with the mycotoxin fumonisin B_1. *Nat Toxins*. **4**:51-52.

Bucci TJ, Howard PC, Tolleson WH, Laborde JB and Hansen DK. 1998. Renal effects of fumonisin mycotoxins in animals. *Toxicol Pathol.* **26**: 160-164.

Bullerman LB. 1996. Occurrence of *Fusarium* and fumonisins on food grains and in foods. In: *Fumonisins in Foods*. Jackson LS, DeVries JW, and Bullerman LB (eds). Plenum Press, New York. pp 27-38.

Bunner DL and Morris ER. 1988. Alteration of multiple cell membrane functions in L-6 myoblasts by T2 toxin: An important mechanism of action. *Toxicol Appl Pharmacol*. **92(1)**: 113-121.

Burka LT, Doran J and Wilson BJ. 1982. Enzyme inhibition and the toxic action of moniliformin and other vinylogous alpha-ketoacids. *Biochem Pharmacol*. **31(1)**: 79-84.

Burkitt HG, Young B and Heath JW. 1993. *Wheater's Functional Histology: A text and Colour Atlas*. Third edition. Churchill Livingstone, Longman Group Limited, Edinburgh. pp 134-135, 367-373.

Cancer Information Services. 1998. Cancer Association of South Africa. 37a Main Road, Mowbray, PO Box 186, Rondebosch, 7700. Fax: 2721689-1840, Toll free (Republic of South Africa only): 0800-226622.

Casteel SW, Turk JR, Cowart RP and Rottinghaus GE. 1993. Chronic toxicity of fumonisin in weanling pigs. *J Vet Diagn Invest*. **5**: 413-417.

Casteel SW, Turk JR and Rottinghaus GE. 1994. Chronic effects of dietary fumonisin on the heart and pulmonary vasculature of swine. *Fundam Appl Toxicol*. **23**: 518-524.

Castegnaro M, Garren L, Galendo D, Gelderblom WC, Chelule P, Dutton MF and Wild CP. 1998. Analytical method for the determination of sphinganine and sphingosine in serum as a potential biomarker for fumonisin exposure. *J Chromatogr B Biomed Sci*. **720(1-2)**: 15-24.

Castelo MM, Sumner SS, and Bullerman LB. 1998. Occurrence of fumonisins in corn-based food products. *J. Food Prot*. **61(6)**: 704-707.

Cattoretti G and Suurmeijer AJH. 1994. Antigen unmasking on formalin fixed and paraffin-embedded tissues using microwaves: A review. *Adv Antomic Pathol*. **2**:2-9.

Cawood ME, Gelderblom WCA, Alberts JF and Snyman SD. 1994. Interaction of ^{14}C-labelled fumonisin B mycotoxins with primary rat hepatocyte cultures. *Food Chem Toxicol*. **32(7)**:627-632.

Cayama E, Tsuda H, Sarma DSR and Farber E. 1978. Initiation of liver carcinogenesis requires cell proliferation. *Nature*. **275**: 60-61.

Chelule PK, Gqaleni N, Chuturgoon AA and Dutton MF. 2000. The determination of fumonisins B_1 in human faeces: a short-term marker for assessment of exposure. *Biomarkers*. **5(1)**: 1-8.

Chelule PK, Gqaleni N, Dutton MF and Chuturgoon AA. 2001. Exposure of rural and urban populations in KwaZulu-Natal, South Africa to Fumonisin B_1 in Maize. *Environ Health Perspect*. **109(3)**: 253-256.

Chen LB. 1988. Mitochondrial membrane potential in living cells. *Annu Rev Cell Biol*.**4**: 155-181.

Cho S, Dawson PE and Dawson G. 2000. Antisense palmitoyl protein thioesterase 1 (PPT1) treatment inhibits PPT1 activity and increases cell death in LA-N-5 neuroblastoma cells. *J Neurosci Res*. **62(2)**: 234-240.

Chu FS and Li GY. 1994. Simultaneous occurrence of fumonisin B_1 and other mycotoxins in moldy corn collected from the People's Republic of China in regions with high incidence of esophageal cancer. *Appl Environ Microbiol*. **60**: 847-852.

Ciacci-Zanella JR, Merrill AH Jr., Wang E and Jones C. 1998. Characterization of cell cycle arrest by fumonisin B_1 in CV-1 cells. *Food Chem Toxicol.* **36(9-10)**: 791-804.

Ciacci-Zanella JR and Jones C. 1999. Fumonisin B_1, a mycotoxin contaminant of cereal grains, and inducer of apoptosis via the tumour necrosis factor pathway and caspase activation. *Food Chem Toxicol.* **37(7)**: 703-712.

Cifone MG, Roncaioli P, De Maria R, Camarada G, Santoni A, Ruberti G and Testi R. 1995. Multiple pathways originate at the Fas/APO-1 (CD95) receptor: sequential involvement of phosphatidylcholine-specific phospholipase C and acidic sphingomyelinase in the propagation of the apoptotic signal. *EMBO J.* **14(23)**: 5859-5868.

Cohen SM and Ellwein LB. 1990. Cell proliferation in carcinogenesis. *Science.* **249**: 1007-1011.

Cole SPC. 1986. Rapid Chemosensitivity testing on human lung tumour cells using the MTT assay. *Canc Chemother Pharmacol.* **17**: 259-263.

Collins TF, Sprando RL, Hansen DK, Laborde JB, Howard PC and Shackelford ME. 1997. Developmental toxicity of fumonisin B_1 (FB_1) in rats. *Teratology.* **55**: 56-57.

Colvin BM and Harrison LR. 1992. Fumonisin-induced pulmonary edema and hydrothorax in swine. *Mycopathologia.* **117**: 79-82.

Colvin BM, Cooley AJ and Beaver RW. 1993. Fumonisin toxicosis in swine: clinical and pathologic findings. *J Vet Diagn Invest.* **5(2)**: 232-241.

Cornford EM, Pardridge WM, Braun LD and Oldendor WH. 1983. Increased blood brain barrier transport of protein-bound anticonvulsant drugs in the newborn. *J Cereb Blood Flow Metab.* **3**: 280-286.

Coroneos E, Wang Y, Panuska JR, Pempleton DJ and Kester M. 1996. Sphingolipid metabolites differentially regulate extracellular signal-regulated kinase and stress-activated protein kinase cascade. *Biochem J.* **316 (1)**: 13-17.

Cossarizza A, Ortolani C, Forti E, Montagnani G, Paganelli R, Zannotti M, Marini M, Monti D and Franceschi C. 1991. Age-related expansion of functionally inefficient cells with markers of natural killer activity syndrome. *Blood.* 77**(6)**: 1263-1270.

Cossarizza A, Baccarani Contri M, Kalashnikova G and Franceschi C. 1993. A new method for the cytofluorimetric analysis of mitochondrial membrane potential using the J-aggregate forming lipophilic cation 5,5', 6,6'-tetrachloro-1, 1', 3,3'-tetraethylbenzimidazolcarbocyanine iodide (JC-1). *Biochem Biophys Res Commun.* **197**: 40-45.

Coulombe RA Jr. 1993. Biological action of mycotoxins. *J Dairy Sci.* **76(3)**: 880-891.

Coumi N. 2000. The Possible role of Fumonisin B_1 in Pre-Eclampsia. Masters in Medical Science dissertation. University of Natal Medical School (now UKZN), Durban, South Africa.

Counts RS, Nowak G, Wyatt RD, and Schnellmann RG. 1996. Nephrotoxicant inhibition of renal proximal tubule cell regeneration. *Am J Physiol.* **269**: F274-F281.

Cree IA, Pazzagli M, Mini E, Mazzei T, Hunter EMM, Sutherlan LA, Pinzani P, Gerli A and Andreotti PE. 1995. Methotrexate chemosensitivity by ATP luminescence as a measure in human leukaemia cell lines and in breast cancer primary cultures: comparison of the TCA-100 assay with a clonogenic assay. *Anticancer Drugs.* **6(3)**: 398-404.

Crouch SPM, Kozlowski R, Slater KJ and Fletcher J. 1993. The use of ATP bioluminescence as a measure of cell proliferation and cytotoxicity. *J Immunol Methods*. **160**: 81-88.

Cundliffe E, Cannon M and Davies J. 1974. Mechanism of inhibition of eukaryotic protein synthesis by trichothecene fungal toxins. *Proc Natl Acad Sci*. **71**: 30-41.

Curan RC and Jones EL. 1991. Tumours: Structure and Diagnosis. Harvey Milller Publishers, Oxford University Press. pp 76-110.

Dannies PS and Tashjian AH. 1973. Growth hormone and prolactin from rat pituitary tumour cells. In: *Tissue Culture Methods and Applications*. Kruse PF and Patterson MK. (eds). Academic Press, New York. pp 831-852.

Darzynkiewicz Z, Bruno S, Del Bino G, Gorczyca W, Hotz MA, Lassota P and Traganos F. 1992. Features of apoptotic cells measured by flow cytometry. *Cytometry*. **13**: 795-808.

Daskal Y, Prestayko AW and Busch H. 1974. Ultrastructural and biochemical studies of the isolated fibrillar component of nuceoli from Novikoff hepatoma ascites cells. *Exp Cell Res*. **88(1)**: 1-14.

Dawkins JL, Hulme DJ, Brahmbhatt SB, Auer-Grumbach M and Nicholson GA. 2001. Mutataions in SPTLC1 encoding serine palmitoyltransferase, long chain base subunit-1, cause hereditary sensory neuropathy type I. *Nat Genet*. **27(3)**: 309-312.

de Chaves EIP, Bussière M, Vance DE, Campenot RB and Vance JE. 1997. Elevation of Ceramide within Distal Neurites Inhibits Neurite Growth in Cultured Rat Sympathetic Neurons. *J Biol Chem*. **272**: 3028-3035.

de Nijs M. 1998. Public health aspects of *Fusarium* mycotoxins in food in The Netherlands - A Risk Assessment. Wageningen, The Netherlands, Agricultural University, Thesis. pp 140.

de Nijs M, van Egmond HP, Nauta M, Rombouts FM and Notermans SHW. 1998a. Assessment of human exposure to fumonisin B_1. *J Food Prot*. **61**: 879-884.

de Nijs M, Sizoo EA, Vermunt AEM, Notermans SHW and van Egmond H.P. 1998b. The occurrence of fumonisin B_1 in maize-containing foods in the Netherlands. *Food Addit Contam*. **15(4)**: 385-388.

Desjardins AE, Hohn TM and McCormick SP. 1993. Trichothecene biosynthesis in *Fusarium* species: Chemistry, genetics and significance. *Microbiol Rev*. **57(3)**: 595-604.

Diaz GJ and Boermans HJ. 1994. Fumonisin toxicosis in domestic animals: a review. *Vet Hum Toxicol*. **36**: 548-555.

Dobbing J and Sands J. 1979. Comparative aspects of the brain growth spurt. *Early Hum Dev*. **3**: 79-83.

Doko MB and Visconti A. 1994. Occurrence of fumonisins B_1 and B_2 in corn and corn-based human foodstuffs in Italy. *Food Addit Contam*. **11**: 433-439.

Dolbeare F, Gratzner H, Pallavicini M and Gray JW. 1983. Flow cytometric measurement of total DNA content and incorporated bromodeoxyuridine. *Proc Natl Acad Sci USA*. **80(18)**: 5573-5577.

Dombrink-Kurtzman MA, Bennett GA and Richard JL. 1994. An optimized MTT bioassay for determination of cytotoxicity of fumonisins in turkey lymphocytes. *J AOAC Int*. **77(2)**: 512-517.

Doorasamy T. *pers comm*. 2004. Chief Flow cytometry specialist, Inkosi Albert Luthuli central Hospital, Department of Haematology, Durban , South Africa.

Dragan YP, Bidlack WR, Cohen SM, Goldsworthy TL, Hard GC, Howard PC, Riley RT, Voss KA. 2001. Implications of Apoptosis for Toxicity, Carcinogenicity, and Risk Assessment: Fumonisin B_1 as an example. *Toxicol Sci.* **61**: 6-17.

Drury RAB and Wallington EA. 1980. Carleston's histological technique, Fifth edition. Oxford University Press, Oxford. pp 237-245.

Dugyala RR, Sharma RP, Tsunoda M and Riley RT. 1998. Tumor Necrosis Factor-α as a Contributor in Fumonisin B_1 Toxicity. *J Pharmacol Exp Ther.* **285**: 317-324.

Dupuy J, Le Bars P, Boudra H and Le Bars J. 1993. Thermostability of fumonisin B_1, a mycotoxin from *Fusarium moniliforme* in corn. *Appl Environ Microbiol.* **59**: 2864-2867.

Dutton MF, Robertson EJ, Mathews C and Beck BDA. 1993. Occurrence of mycotoxins in maize on a rural area in South Africa and Methods of prevention of contamination and elimination. Proceedings Cereal Science and Technology, Impact on a Changing Africa. ICC International Symposium, Pretoria, pp 823-835.

Dutton MF and Kinsey A. 1995. Occurrence of mycotoxins in cereals and animal feedstuffs in Natal, South Africa 1994. *Mycopathologia.* **131(1)**: 31-36.

Dutton MF and Kinsey A. 1996. A note of the occurrence of mycotoxins in cereals and animal feedstuffs in KwaZulu-Natal, South Africa 1984-1993. *A AfrJ Ani Sci.***26 (2)**: 53-57.

Duvall E, Wyllie AH and Morris RG. 1985. Macrophage recognition of cells undergoing programmed cell death (apoptosis). *Immunology.* **56**: 351-358.

Ehling G, Cockburn A, Snowdon P and Buchhaus H. 1997. The significance of the *Fusarium* toxin deoxynivalenol (DON) for human and animal health. *Cereal Research Commun.* **25**: 433-447.

El Bawab S, Birbes H, Roddy P, Szulc ZM, Bielawska A and Hannun YA. 2001. Biochemical Characterization of the reverse activity of rat brain ceramidase. A CoA independent and Fumonisin B_1-insensitive ceramide synthase. *J Biol Chem.* **276(20)**: 16758-16766.

Elsenhans B, Blume R, Lembcke B, and Caspary WF. 1983. Polycations: a new class of inhibitors for *in vitro* small intestinal transport of sugars and amino acids in the rat. *Biochim Biophys Acta.* **727**: 135-143.

Eriksen GS and Alexander J (eds). 1998. Fusarium toxins in cereals-a risk assessment. Nordic Council of Ministers, Copenhagen, Tema Nord 502. pp 7-27 and 45-58.

Espinosa de los Monteros A, Chiapelli F, Fisher R and De Vellis J. 1988. Transferrin: an early marker of oligodendrocytes in culture. *Int J Dev Neurosci.* **61**:167-175.

European Commission. 2000a. Opinion of the scientific committee on food: Zearalenone [online]. Available from: ***http://www.europa.eu.int/comm/food/fs/sc/scf/out88*** [Accessed 19 August 2002].

European Commission. 2000b. Opinion of the scientific committee on food: T-2 toxin [online]. Available from: ***http://www.europa.eu.int/comm/food/fs/sc/scf/out88*** [Accessed 19 August 2002].

Farber E and Sarma DSR. 1987. Hepatocarcinogenesis: A dynamic cellular perspective. *Lab Invest.* **56**: 2-22.

Farber E, Chen EZY, Harris L, Rinaudo S, Roomi WM, Rotstein J and Semple E. 1989. The biochemical-molecular pathology of the stepwise development of liver cancer. New Insights and problems. In: *Liver Cell Carcinoma.* Bannasch P, Kappler D and Weber G (eds). Kluwer Academic

Publishers. Dorsrcht. pp 273-291.

Farber E. 1990. Clonal adaptation during carcinogenesis. *Biochem Pharmacol.* **39**:1837-1846.

Fazekas B, Bajmocy E, Glavits R, Fenyvesi A and Tanyi J. 1998. Fumonisn B_1 contamination of maize and experimental acute fumonisin toxicosis in pigs. *J Vet Med B.* **45(3)**: 171-181.

Fentie IH and Roisen FJ. 1993. The effects of cytoskeletal altering agents on the surface topography of GM1 in neuro-2A neuroblastoma cell membranes. *J Neurocytol.* **22(6)**: 498-506.

Ferguson SA, Omer VE, Kwon OS, Holson RR, Houston RJ, Rottinghaus GE and Slikker W Jr. 1997. Prenatal fumonisin (FB_1) treatment in rats results in minimal maternal or offspring toxicity. *Neurotoxicology.* **18**: 561-569.

Fernandez-Pol JA, Hamilton PD and Klos DJ. 1982. Correlation between the loss of the transformed phenotype and an increase in superoxide dismutase activity in a revertant subclone of sarcoma virus-infected mammalian cells. *Cancer Res.* **42**: 609-617.

Fernandez-Pol JA. 1991. Modulation of EGF receptor protooncogene expression by growth factors and hormones in human breast carcinoma cells. *Crit Rev Oncog.* **2**: 173-185.

Fernandez-Pol JA 1992. Growth factors, oncogenes, anti-oncogenes and aging. In: *Geriatric Oncology.* Balducci L, Lyman GH, Ershler WB (eds). JB Lippincott Co., Philadelphia. pp 60-75.

Fernandez-Pol JA, Klos DJ and Hamilton PD. 1993. Cytotoxic activity of Fusaric acid on human adenocarcinoma cells in tissue culture. *Anticancer Res.* **13(1)**: 57-64.

Flavahan NA and Vanhoutte PM. 1995. Endothelial cell signalling and endothelial cell dysfunction. *Am J Hypertens.* **8**: 28S-41S.

Floyd RA. 1990. Role of oxygen free radicals in carcinogenesis and brain ischemia. *FASEB J.* **4**: 2587-2597.

Flynn TJ, Pritchard D, Bradlaw J, Eppley R and Page S. 1996. *In vitro* embryotoxicity of fumonisin B_1 evaluated with cultured postimplantation staged rat embryos. *In Vitro Toxicology.* **9**: 271-279.

Flynn TJ, Stack ME, Troy AL and Chirtel SJ. 1997. Assessment of the Embryonic Potential of the Total Hydrolysis Product of Fumonisin B_1 Using Cultured Organogenesis-staged Rat Embryos. *Food Chem Toxicol.* **35**: 1135-1141.

Fowler BA, Lucier GW and Hayes AW. 1989. Organelles as tools in toxicology. In: *Principles and methods of toxicology.* Hayes AW (ed) Raven Press Ltd., New York. pp 815-835.

France-Lanord V, Brugg B, Michel PP, Agid Y and Ruberg M. 1997. Mitochondrial free radical signal in ceramide-dependent apoptosis: a putative mechanism for neuronal death in Parkinson's disease. *J Neurochem.* **69(4)**: 1612-1621.

Francis K, van Beek J, Canova C, Neal JW, and Gasque P. 2003. Innate immunity and brain inflammation: the key role of complement. *Exp Rev Mol Med.* **5**: 1-19.

Freshney RI. 1983. In: *Culture of Animal cells: A manual of Basic Technique.* Liss AR (ed). New York. pp 39-78, 119-128.

Frisch SM and Francis H. Disruption of epithelial cell-matrix interactions induces apoptosis. *J Cell Biol.* **124**: 619-626.

Furuya S, Ono K and Hirabayashi Y. 1995. Sphingolipid biosynthesis is necessary for dendrite growth and survival of cerebellar Purkinje cells in culture. *J Neurochem.* **65**: 1551-1561.

Furuya S, Mitoma J, Makino A and Hirabayashi Y.1998. Ceramide and its interconvertible metabolite sphingosine function as indispensable lipid factors involved in survival and dendritic differentiation of cerebellar Purkinje cells. *J Neurochem.* 71(1): 366-77.

Futerman AH, Boldin S, Brann AB, Schwarz A and Zisling R. 1998. Regulatory roles for sphingolipids in the growth of polarized neurons. In: *Sphingolipids as signaling modulators in the nervous system.* Ledeen RW, Hakomori S-I, Yates AJ, Schneider JS and Yu RK (eds). *Ann New York Acad Sci.* **845**: 176-187.

Galvano F, Campisis A, Russo A, Galvano G, Palumbo M, Renis M, Barcellona ML, Perez-Polo JR and Vanella A. 2002. DNA damage in astrocytes exposed to FB_1. *Neurochem Res.* **27(4)**: 345-351.

Gathercole PS, Thiel PG and Hofmeyr JHS. 1986. Inhibition of pyruvate dehydrogenase complex by moniliformin. *Biochem J.* **233**: 719-723.

Gaver RC and Sweeley CC. 1965. Methods for Methanolysis of Sphingolipids and direct determination of Long-Chain bases by Gas Chromatography. *J Am Oil Chem Soc.* **42**: 295-298.

Gelderblom WCA, Jaskiewicz K, Marasas WFO, Thiel PG, Horak RM, Vleggaar R and Kriek NPJ. 1988a. Fumonisins-Novel mycotoxins with cancer-promoting activity produced by *Fusarium moniliforme. Appl Environ Microbiol.* **54**: 1806-1811.

Gelderblom WCA, Jaskiewicz K, Marasas WFO, Thiel PG, Horak RM, Vleggaar R and Kriek NPJ. 1988b. Cancer-promoting potential of different strains of *Fusarium moniliforme* in a short-term cancer initiation/promotion assay. *Carcinogenesis.* **9**: 1405-1409.

Gelderblom W, Marasas W, Thiel P, Semple E and Farber E. 1989. Possible non-genotoxic nature of active carcinogenic components produced by *Fusarium moniliforme. Proc Am Assoc Cancer Res.* **30**: 144.

Gelderblom WCA and Snyman SD. 1991. Mutagenicity of potentially carcinogenic mycotoxins produced by *Fusarium moniliforme. Mycotoxin Res.* **7**: 46-52.

Gelderblom, WCA, Kriek NPJ, Marasas WFO and Thiel PG. 1991. Toxicity and carcinogenicity of the *Fusarium moniliforme* metabolite, fumonisin B_1 in rats. *Carcinogenesis.* **12**: 1247-1251.

Gelderblom WCA, Semple E, Marasas WFO, and Farber E. 1992. The cancer-initiating potential of fumonisin B mycotoxins. *Carcinogenesis.* **13**: 433-437.

Gelderblom WCA, Cawood ME, Snyman SD, Vleggaar R and Marasas WFO. 1993. Structure-activity relationships of fumonisins in short-term carcinogenesis and cytotoxicity assays. *Food Chem Toxicol.* **31**: 407-414.

Gelderblom WCA, Cawood ME, Snyman SD, and Marasas WFO. 1994. Fumonisin B_1 dosimetry in relation to cancer initiation in rat liver. *Carcinogenesis.* **15**: 209-214.

Gelderblom WCA, Snyman SD, Abel S, Lebepe-Mazur S, Smuts CM, van der Westhuizen L and Marasas WFO. 1995a. Hepatotoxicity and carcinogenicity of the fumonisins in rats: A review regarding mechanistic implications for establishing risk in humans. In: *Fumonisins in Food.* Jackson L, DeVries JW and Bullerman LB (eds). New York, Plenum Press. pp 279-296.

Gelderblom WCA, Snyman SD, van der Westhuizen L and Marasas WFO. 1995b. Mitoinhibitory effect of fumonisin B_1 on rat hepatocytes in primary culture. *Carcinogenesis.* **16**: 625-631.

Gelderblom WCA, Snyman SD, Lebepe-Mazur S, van der Westhuizen L, Kriek NPJ and Marasas WFO. 1996a. The cancer-promoting potential of fumonisin B_1 in rat liver using diethylnitrosamine as a cancer initiator. *Cancer Lett.* **109**: 101-108.

Gelderblom WCA, Smuts CM, Abel S, Snyman SD, Cawood MA, van der Westhuizen L and Swanevelder S. 1996b. Effect of fumonisin B_1 on protein and lipid synthesis in primary rat hepatocytes. *Food Chem Toxicol.* **34**: 361-369.

Gelderblom WCA, Smuts CM, Abel S, Snyman SD, van der Westhuizen L, Huber WW and Swanevelder S. 1997. Effect of fumonisin B_1 on the levels and fatty acid composition of selected lipids in rat liver, *in vivo*. *Food Chem Toxicol.* **35**: 647-656.

Gelderblom WC, Seier JV, Snijman PW, Van Schalkwyk DJ, Shephard GS and Marasas WF. 2001. Toxicity of Culture Material of *Fusarium verticillioides* strain MRC 826 to nonhuman Primates. *Environ Health Perspect.* **109(2)**: 267-276.

Gennero I, Fauvel J, Nieto M, Cariven C, Gaits F, Briand-Mesange F, Chap H and Salles JP. 2002. Apoptotic Effect of Sphingosine 1-phosphate and increased Sphingosine 1-phosphate hydrolysis on Mesangial cells cultured at low cell density. *J Biol Chem.* **277(15)**: 12724-12734.

Gerlier D and Thomasset N. 1986. Use of MTT colorimetric assay to measure cell activation. *J Immunol Meth.* **94**: 57-63.

Ghadially FN. 1975. *Ultrastructural Pathology of the cell. A text and Atlas of Physiological and Pathological Alterations in cell fine structure*. Butterworths, London.

Ghadially FN. 1982. *Ultrastructural Pathology of the Cell and Matrix: A Text and Atlas of Physiological and Pathological Alterations in the Fine Structure of Cellular and Extracellular Components*, Second edition. William Clowes Ltd., Butterworths, London.

Ghadially FN. 1985. *Diagnostic Electron Microscopy of Tumours*, Second edition. Butterworths, London. pp 25-62.

Gillard BK, Harrell RG and Marcus DM. 1996. Pathways of glycosphingolipid biosynthesis in SW13 cells in the presence and absence of vimentin intermediate filaments. *Glycobiology.* **6(1)**: 33-42.

Goel S, J Schumacher, SD Lenz and BW Kemppainen. 1995. Effects of *Fusarium moniliforme* isolates on sphingolipid levels in horses. *Toxicologist.* **15**:290 (Abstract number 1556).

Goers J. 1993. *Immunochemical techniques: Laboratory manual.* Academic Press Inc., California. pp 107-115.

Goodman Y and Mattson MP. 1996. Ceramide protects hippocampal neurons against excitotoxic and oxidative insults, and amyloid β-peptide toxicity. *Neurochem.* **66(2)**: 869-872.

Gorman AM, Samali A, McGowan AJ, Cotter TG. 1997. Use of flow cytometry techniques in studying mechanisms of apoptosis in leukemic cells. *Cytometry.* **29**: 97-105.

Gumprecht LA, Marcucci A, Weigel RM, Vesonder RF, Riley RT, Showker JL, Beasley VR, and Haschek WM. 1995. Effects of intravenous fumonisin B_1 in rabbits: nephrotoxicity and sphingolipid alterations. *Nat Toxins.* **3**: 395-403.

Gumprecht LA, Beaslet VR, Weigel RM, Parker HM, Tumbleson ME, Bacon CW, Meredith FI and Haschek WM. 1998. Development of fumonisin-induced hepatoxicity and pulmonary edema in orally dosed swine: morphological and biochemical alterations. *Toxicol Pathol.* **26(6)**: 777-788.

Gyongyossy-Issa MIC and Khachatourians GG. 1984. Interaction of T2 toxin with murine lymphocytes. *Biochim Biophys Acta*. **803:** 197-202.
Hakomori S. 1990. Bifunctional role of glycosphingolipids. Modulators for transmembrane signalling and mediators for cellular interactions. *J Biol Chem*. **265**:18713-18716.

Hall FL, Fernyhough P, Ishii DN and Vulliet PR. 1988. Suppression of nerve growth factor-directed neurite outgrowth in PC 12 cells by sphingosine, an inhibitor of protein kinase C. *J Biol Chem*. **263(9)**: 4460-4466.

Halliwell B and Gutteridge JMC. 1990. Role of free radicals and catalytic metal ions in human disease: an overview. *Methods Enzymol*. **186(B)**: 1-85.

Hanada K, Nishijima M, and Akamatsu Y. 1990. A temperature-sensitive mammalian cell mutant with thermolabile serine palmitoyltransferase for the sphingolipid biosynthesis. *J Biol Chem*. **265**: 22137-22142.

Hanada K, Nishijima M, Kiso H Jr, Hasegawa A, Fujita S, Ogawa T and Akamatsu Y. 1992. Sphingolipids are essential for the growth of Chinese hamster ovary cells: Restoration of the growth of a mutant defective in sphingoid base biosynthesis by exogenous sphingolipids. *J Biol Chem*. **267**: 23527-23533.

Hanada K, Izawa K, Nishijima M and Akamatsu Y. 1993. Sphingolipd deficiency induces hypersensitivity of CD14, a glycosylphosphatidylinositol-anchored protein to phosphoinositol specific phospholipase. *J Biol Chem*. **268:** 13820-13823.

Hanelt M, Gareis M, Kollarczik B. 1994. Cytotoxicity of mycotoxins evaluated by the MTT-cell culture assay. *Mycopathologia*. **128**:167-174.

Hannun YA, Loomis CR, Merrill AH Jr and Bell RM. 1986. Sphingosine inhibition of protein kinase C activity and dibutyrate binding *in vitro* and in human platelets. *J Biol Chem*. **261(27)**: 12604-12609.

Hannun YA and Bell RM. 1989. Functions of sphingolipids and sphingolipid breakdown products in cellular regulation. *Science*. **243**: 500-507.

Hannun YA, Merrill AH Jr. and Bell RM. 1991. Use of sphingosine as an inhibitor of protein kinase C. *Meth Enzymol*. **201**: 316-328.

Hannun YA. 1994. The sphingomyelin cycle and the second messenger function of ceramide. *J Biol Chem*. **269(5)**: 3125-3128.

Hannun YA and Obeid LM. 1995. Ceramide; an intracellular signal for apoptosis. *Trends Biochem Sci*. **20**: 73-77.

Hannun YA, Luberto C and Argraves KM. 2001. Enzymes of sphingolipid metabolism: from modular to integrative signalling. *Biochemistry*. **40(16)**: 4893-4903.

Hannun YA and Obeid LM. 2002. The ceramide-centric universe of lipid mediated cell regulation: Stress encounters of the lipid kind. *J Biol Chem*. **277(29)**: 25847-25850.

Harel R and Futerman AH. 1993. Inhibition of sphingolipid synthesis affects axonal outgrowth in cultured hippocampal neurons. *J Biol Chem*. **268**: 14476-14481.

Hartwell LH and Kastan MB. 1994. Cell cycle control and cancer. *Science*. **266**: 1821-1828.

Haschek WM, Smith CW, Bacon CW, Meredith F and Constable PD. 1995. Fumonisins decrease

pulmonary clearance of particulates in pigs. *Vet Pathol.* **32**: 558-563.

Haschek-Hock WMC, Constable PD and Tumbleson ME. 1998. Fumonisin-induced endothelial and hemodynamic changes in porcine edema. FEDRIP database, National Technical Information Service (NTIS).

Henderson GI, Perez T, Schenker S, Mackins J and Anthony AC. 1995. Maternal to fetal transfer of 5-methyltetrahydrofolate by the perfused human placental cotyledon: evidence for a concentrative role by placental folate receptors in fetal folate delivery. *J Lab Clin Med.* **126**: 184-203.

Hennig B, Shasby DM, Fulton AB and Spector AA. 1984. Exposure to free fatty acid increases the transfer of albumin across cultured endothelial monolayers. *Arteriosclerosis.* **4**: 489-497.

Heyderman E. 1979. Immunoperoxidase techniques in histopathology: applications, methods and controls. *J Clin Pathol.* **32**: 971-978.

Hidaka H, Nagatsu T, Takeya Y, Takeuchi T and Suda H. 1969. Fusaric acid, a hypotensive agent produced by fungi. *J Antibiot.* **22(5)**: 228-230.

Hidari KI-PJ, Ichikawa S, Fujita T, Sakiyama H and Hirabayashi Y. 1996. Complete removal of sphingolipids from the plasma membrane disrupts cell to substratum adhesion of mouse melanoma cells. *J Biol Chem.* **271**: 14636-14641.

Higashi T, Isomoto A, Tyuma E, Kakishita E, Uomoto M and Nagai K. 1985. Quantitative and continuous analysis of ATP release from blood platelets with firefly luciferase luminescence. *Thromb Haemost.* **53(1)**: 65-69.

Hoek JG. 1992. Intracellular signal transduction and the control of endothelial permeability. *Lab Invest.* **67:** 1-4.

Hoekstra D and Kok JW. 1992. Trafficking of glycosphingolipids in eukaryotic cells; sorting recycling of lipids. *Biochim Biophys Acta.* **1113 (3-4)**: 277-294.

Holt PS and Deloach JR. 1988. Cellular effects of T-2 mycotoxin on two different cell lines. *Biochim Biophys Acta.* **971**: 1-8.

Holt PS, Buckley S, Norman JO and Deloach JR. 1988. Cytotoxic effect of T-2 mycotoxin on cells in culture as determined by rapid colorimetric bioassay. *Toxicon.* **26**: 549-558.

Holt PS, Buckley S and Deloach JR. 1989. Detection of the lethal effects of T-2 toxin on cells using a rapid colorimetric viability assay. *Toxicol in Vitro.* **3**: 311-316.

Hopmans EC, Hauck CC, Hendrich S and Murphy PA. 1997. Excretion of fumonisin B_1, hydrolyzed fumonisin B_1, and the fumonisin FB_1-fructose adduct in rats. *J Agric Food Chem.* **45**: 2618-2625.

Horbach GJMJ and De Groene EM. 1995. New Molecular techniques to Monitor *In Vitro* Toxicity: Transgenic Cell line and Changes in Gene Function and Expression: Useful tools in Toxicity Testing? *Toxic in Vitro.* **9(4)**: 509-512.

Howard PC, Churchwell MI, Couch LH, Marques MM, and Doerge DR. 1998. Formation of N-(carboxymethyl) fumonisin B_1 following the reaction of fumonisin B_1 with reducing sugars. *J Agric Food Chem.* **46**: 3546-3557.

Howard PC, Eppley RM, Stack ME, Warbritton A, Voss KA, Lorentzen RJ, Kovach RM and Bucci TJ. 2001. Fumonisin B_1 carcinogenicity in a two-year feeding study using F344 rats and B6C3F1 mice. *Environ Health Perspect.* **109(2)**: 277-282.

Hsia CC, Wu JL, Lu XQ and Li YS. 1988. Natural occurrence and clastogenic effects of nivalenol, deoxynivalenol, 3-acetyl-nivalenol, 15, acetyl-deoxynivalenol, and zearalenone in corn from a high-risk area of oesophageal cancer. *Cancer Detect Prev.* **13**: 79-86.

Hsieh DPH. 1987. Mode of Action of Mycotoxins. In: *Mycotoxins in Food.* Krogh P (ed). Academic Press, Cambridge. Chapter 7. pp 149-176.

Huang C, Dickman M, Henderson G and Jones C. 1995. Repression of protein kinase C and stimulation of cyclic AMP response elements by fumonisin, a fungal encoded toxin which is a carcinogen. *Cancer Res.* **55(8)**: 1655-1659.

Humason G. 1972. *Animal tissue techniques.* Third Edition, WH Freeman and Company, San Fransisco.

Humpf HU, Schmelz EM, Meredith FI, Vesper H, Vales TR, Menaldino DS, Liotta DC and Merrill AH Jr. 1998. Acylation of naturally occurring and synthetic 1-deoxysphinganines by ceramide synthase: Formation of N-palmitoyl-aminopentol produces a toxic metabolite of hydrolyzed fumonisin, AP1, and a new category of ceramide synthase inhibitor. *J Biol Chem.* **273(30)**: 19060-19064.

Humphreys SH, Carrington C and Bolger M. 1997. Fumonisin risk scenarios. *Toxicologist.* **36**: 170-174.

Hunot S, Brugg B, Ricard D, Michel PP, Muriel MP, Ruberg M, Faucheux BA, Agid Y and Hirsch EC. 1997. Nuclear translocation of NF-kappa B is increased in dopaminergic neurons of patients with Parkinson Disease. *Proc Natl Acad Sci USA.* **94(14)**: 7531-7536.

Institute of Food Technologists. 1993. Expert Panel on Food Safety and Nutrition, Office of Scientific Public Affairs: Scientific Status Summary. Potential Mechanisms for Food Related Carcinogens. Food Technology. pp 105-118.

International Agency for Research on Cancer. 1993a. Monographs on the Evaluation of Carcinogenic Risks to Humans In: *Some naturally occurring substances, food items and constituents, heterocyclic aromatic amines and mycotoxins.* Lyon. World Health Organisation. **56**: 397-333.

International Agency for Research on Cancer. 1993b. Monographs on the Evaluation of Carcinogenic Risk to Humans. Toxins derived from *Fusarium moniliforme*: Fumonisins B_1 and B_2 and fusarin C. In: *Some naturally occurring substances: Food items and constituents, heterocyclic aromatic amines and mycotoxins.* Lyon, World Health Organisation. **56**: 445-466.

Iverson F, Amstrong C, Nea E, Truelove J, Fernie S, Scott PM, Stapley R, Hayward S and Gunner S. 1995. Chronic feeding study of deoxynivalenol in B6C3F1 male and female mice. *Teratogen Carcinogen Mutagen.* **15**: 283-306.

Jacobs LS and Kester M. 1993. Sphingolipids as mediators of effects of platelet-derived growth factor in vascular smooth muscle cells. *Am J Physiol.* **265(3 pt 1)**: C740-C747.

Jacobsen BJ, Bowen KL, Shelby RA, Dienar UL, Kempainen BW and Floyd J. 1993. Mycotoxins and mycotoxicoses [online]. Available from: *http://www.aces.edu/department/ipm/mandm.html.* [Accessed 04 July 2002].

Jaffe EA. 1987. Cell biology of endothelial cells. *Hum Pathol.* **18(3)**: 234-239.

Jarvis WD, Kolesnick RN, Fornari FA Jr., Traylor RS, Gewirtz DA and Grant S. 1994. Induction of apoptotic DNA damage and cell death by activation of the sphingomyelin pathway. *Proc Natl Acad Sci USA.* **91(1)**: 73-77.

Jarvis WD, Fornari FA Jr, Traylor RS, Martin HA, Kramer LB, Erukulla RK, Bittman R and Grant S. 1996. Induction of apoptosis and potentiation of ceramide mediated cytotoxicity by sphingoid bases in human myeloid leukaemia cells. *J Biol. Chem.* **271(14)**: 8275-8284

Jarvis WD and Grant S. 1998. The role of ceramide in the cellular response to cytotoxic agents. *Curr Opin Oncol.* **10(6)**: 552-559.

Jaskiewicz K, Marasas WFO, and Van der Walt FE. 1987. Oesophageal and other main cancer patterns in four districts of Transkei, 1981-1984. *S Afr Med J.* **72**: 27-30.

Javed T, Dombrink-Kurtzman MA, Richard JL, Bennett GA, Cote LM and Buck WB. 1995. Sero-hematologic alterations in broiler chicks on feeds amended with *Fusarium proliferatum* culture material or fumonisin B_1 and moniliformin. *J Vet Diagn Invest.* **7(4)**: 520-526.

Jeckel D, Karrenbauer A, Birk R, Schmidt RR and Wieland F. 1990. Sphingomyelin is synthesized in the *cis* Golgi. *FEBS Lett.* **261(1)**: 155-157.

Jeckel D, Karrenbauer A, Burger KNJ, van Meer G and Wieland F. 1992. Glucosylceramide is synthesized at the cytosolic surface of various Golgi subfractions. *J Cell Biol.* **117(2)**: 259-267.

Jensen RG and Newburg DS. 1995. Bovine milk lipids. In: *Handbook of Milk Composition.* Jensen RG (ed), Academic Press, New York. pp 543-575.

Johnson PF and McKnight SL. 1989. Eukaryotic transcriptional regulatory proteins. *Annu Rev Biochem.* **58**: 799-839.

Jone E, Erickson L, Trosko JE and Chang CC. 1987. Effect of biological toxins on gap-junctional intercellular communication in Chinese hamster V79 cells. *Cell Biol Toxicol.* **3**: 1-15.

Jones C, Ciacci-Zanella JR, Zhang Y, Henderson G and Dickman M. 2001. Analysis of fumonisin B_1-induced apoptosis. *Environ Health Perspect.* **109(2)**: 315-320.

Kang YK and Alexander JM. 1996. Alterations of the glutathione redox cycle status in fumonisin B_1-treated pig kidney cells. *J Biochem Toxicol.* **11**: 121-126.

Karnovsky MJ. 1965. A formaldehyde glutaraldehyde fixative of high molarity: for use in electron microscopy. *J Cell Biol.* **27**: 127-139.

Kellerman TS, Marasas WFO, Pienaar JG, and Naudé TW. 1972. A mycotoxicosis of Equidae caused by *Fusarium moniliforme* Sheldon. *Onderstepoort J Vet Res.* **39**: 205-208.

Kellerman TS, Marasas WFO, Thiel PG, Gelderblom WCA, Cawood M and Coetzer JAW. 1990. Leukoencephalomalacia in two horses induced by oral dosing of fumonisin B_1. *Onderstepoort J Vet Res.* **57**: 269-275.

Kemshead JT. 1985. Neuroblastoma and Glioblastoma Antigens. In: *Immunological Studies of Brain cells and Functions.* Spastics International Medical Publications. Adinolfi M and Bignami A (eds). Oxford, Blackwell Scientific Publications Ltd. Philadelphia. JB Lippincott Co. Research Monograph **6**: 27-47.

Kerr JFR, Wyllie AH and Currie AR. 1972. Apoptosis: a basic biological phenomenon with wide ranging implications in tissue kinetics. *Br J Cancer.* **26**: 239-257.

Key M. 2001. Antigen Retrieval. In: *Handbook of immunochemical staining methods*, Third edition. Boenisch T, Farmilo AJ, Stead RH, Key M, Welcher R, Harvey R, Atwood KN (eds). DAKO

Corporation: California, USA. 23-25.

Khachatourians GG. 1990. Metabolic effects of trichothecene T-2 toxin. *Can J Physiol Pharmacol.* **68(7)**: 1004-1008.

Kharlamov A, Guidotti A, Costa E, Hayes R and Armstong D. 1993. Semi-synthetic sphingolipids prevent protein kinase C translocation and neuronal damage in the perifocal area following photochemically induced thrombotic brain cortical lesion. *J Neurosci.* **13**: 2483-2494.

Kiessling KH. 1986. Biochemical mechanism of action of mycotoxins. *Pure Appl Chem.* **58**: 327-38.

Knasmüller S, Bresgen N and Kassie F. 1997. Genotoxic effects of three *Fusarium* mycotoxins fumonisin B_1, moniliformin and vomitoxin in bacteria and in primary cultures of rat hepatocytes. *Mutat Res.* **391(1-2)**: 39- 48.

Koiv A, Palvimo J and Kinnunen PK. 1995. Evidence for ternary complex formation by histone H1, DNA and liposomes. *Biochemistry.* **34(25)**: 8018-8027.

Kolesnick RN and Krönke M. 1998. Regulation of ceramide production and apoptosis. *Annu Rev Physiol.* **60**: 643-665.

Kravtsov VD, Greer JP, Whitlock JA and Koury MJ. 1998. Use of the microculture kinetic assay of apoptosis to determine chemosensitivities of leukaemias. *Blood.* **92**: 968-980.

Kriek NPJ, Kellerman TS and Marasas WFO. 1981. A comparative study of the toxicity of *Fusarium verticillioides* (= *F. moniliforme*) to horses, primates, pigs, sheep and rats. *Onderstepoort J Vet Res.* **48**: 129-131.

Kroemer G, Zamzani N and Susin SA. 1997. Mitochondrial control of apoptosis. *Immunol Today.* **18**: 44-51.

Kuiper-Goodman T, Scott PM, McEwen NP, Lambert GA and Ng -W. 1996. Approaches to the assessment of fumonisins in corn-based foods in Canada. *Adv Exp Med Biol.* **392**: 369-393.

Kurbacher CM, Cree IA, Bruckner HW, Brenne U, Kurbacher JA, Muller K, Ackermann T, Gliste TA, Wilhelm LM, Engel H, Mallman PK and Andreotti PE. 1998. Use of an *ex vivo* ATP luminescence assay to direct chemotherapy for recurrent ovarian cancer. *Anti-Cancer Drugs.* **9**:51-57.

Kwon O-S, Schmued LC and Slikker WS Jr. 1997a. Fumonisin B_1 in developing rats alters brain sphinganine levels and myelination. *Neurotoxicology.* **18**: 571-580.

Kwon O-S, Sandberg JA and Slikker WS Jr. 1997b. Effects of fumonisin B_1 treatment on blood-brain barrier transfer in developing rats. *Neurotoxicol Teratol.* **19**: 151-155.

Kwon O-S, Newport GD and Slikker WS Jr. 1998. Quantitative analysis of free sphingoid bases in the brain and spinal cord tissues by high performance liquid chromatography with a fluorescence detection. *J ChromatogrB Biomed Sci Appl.* **720(1-2)**: 9-14.

Kwon O-S, Slikker W Jr. and Davies. 2000. Biochemical and morphological effects of fumonisin B_1 on primary cultures of rat cerebrum. *Neurotoxicol Teratol.* **22**: 565-572.

LaBorde JB, Terry KK, Howard PC, Chen JJ, Collins TFX, Shackelford ME and Hansen DK. 1997. Lack of embryotoxicity of fumonisin B_1 in New Zealand white rabbits. *Fundam Appl Toxicol.* **40**: 120-128.

Lacey SW, Sanders JM, Rothberg KG, Anderson RGW and Kamen BA. 1989. Complementary DNA for the folate binding protein correctly predicts anchoring to the membrane of glycosyl-phosphotidylinositol. *J Clin Invest.* **84**: 715-720.

Larocca JN, Farooq M and Norton WT. 1997. Induction of oligodendrocyte apoptosis by C2-ceramide. *Neurochem Res.* **22(4)**: 529-534.

Leatherhead Food Research Association. 2002. Mycotoxins [online]. Available from: *http://www.leatherheadfood.html* [Accessed 15 September 2002].

Leatherman DL and Middlebrook JL. 1993. Effect of emetine on T-2 toxin-induced inhibition of protein synthesis in mammalian cells. *J Pharmacol Exp Ther.* **266**: 741-748.

Leduc EH, Bernhard W and Tournier P. 1966. Cyclic appearance of atypical mitochondria containing DNA fibres in cultures of an adenovirus 12- induced hamster tumor. *Exp Cell Res.* **42(3)**: 597-616.

Leist M, Single B, Castoldi AF, Kuhnle and Nicotera P. 1997. Intracellular Adenosine Triphosphate (ATP) concentration: a switch in the decision between apoptosis and necrosis. *J Exp Med.* **185(8)**: 1481-1486.

Lemasters JJ, Nieminen A-L, Qian T, Trost LC, Elmore SP, Nishimura Y, Crowe RA, Cascio WE, Bradham CA, Brenner DA and Herman B. 1998. The mitochondrial permeability transition in cell death: a common mechanism in necrosis, apoptosis and autophagy. *Biochim Biophys Acta.* **1366**: 177-196.

Lemmer ER, Gelderblom WC, Shephard EG, Abel S, Seymour BL, Cruse JP, Kirsch RE, Marasas WF and Hall PM. 1999. The effects of dietary iron overload on fumonisin B_1-induced cancer promotion in the rat liver. *Cancer Lett.* **146(2)**: 207-215.

Lim CW, Parker HM, Vesonder RF and Haschek WM. 1996. Intravenous fumonisin B_1 induces cell proliferation and apoptosis in the rat. *Nat Toxins.* **4**: 34-41.

Lopez-Mediavilla C, Orfao A, Gonzales M and Medina JM. 1989. Identification by flow cytometry of two distinct rhodamine-123-stained mitochondrial populations in rat liver. *FEBS Lett.* **254**: 115-120.

LumiTech™. 1999. ApoGlow- High Throughput Apoptosis Assay Kit. Lumitech Ltd., Nottingham Business Park, City Link, Nottingham, NG24LA, United Kingdom.

Machlin LJ and Bendich A. 1987. Free radical tissue damage: protective role of antioxidant nutrients. *FASEB J.* **1**: 441-445.

Makaula NA, Marasas WFO, Venter FS, Badenhorst CJ, Bradshaw D and Swanevelder S. 1996. Oesophageal and other cancer patterns in four selected districts of Transkei, Southern Africa: 1985-1990. *Afr J Health Sci.* **3**:11-15.

Mandala SM, Thornton R, Tu Z, Kurtz MB, Nickels J, Broach J, Menzeleev R and Spiegel S. 1998. Sphingoid base 1-phosphate phosphatase: A key regulator of sphingolipid metabolism and stress response. *Proc Natl Acad Sci USA.* **95**: 150-155.

Mandon E, van Echten G, Birk R, Schmidt RR and Sandhoff K. 1991.Sphingolipid biosynthesis in cultured neurons. Down regulation of serine palmitoyltransferase. *Eur J Biochem.* **198(3)**: 667-674.

Mandon EC, Ehses I, Rother J, van Echten G and Sandhoff K. 1992. Subcellular localization and membrane topology of serine palmitoyltransferase, 3-dehydrosphinganine reductase, and sphinganine *N*-acyltransferase in mouse liver. *J Biol Chem.* **267(16)**: 11144 -11148.

Mangoura D and Dawson G. 1998. Programmed cell death in cortical chicken embryo astrocytes is associated with activation of protein kinase PK 60 and ceramide formation. *J Neurochem.* **70**: 130-138.

Maragos CM and Richard JL. 1994. Quantitation and stability of fumonisins B_1 and B_2 in milk. *J AOAC Int.* **77(5)**: 1162-1167.

Marasas WFO, Kellerman TS, Pienaar JG and Naudé TW. 1976. Leukoencephalomalacia: A mycotoxicosis of Equidae caused by *Fusarium moniliforme* Sheldon. *Onderstepoort J Vet Res.* **43**: 113-122.

Marasas WFO, Van Rensburg SJ and Mirocha CJ. 1979a. Incidence of *Fusarium* species and the mycotoxins, deoxynivalenol and zearalenone, in corn produced in esophageal cancer areas in Transkei. *J Agric Food Chem.* **27**: 1108-1112.

Marasas WFO, Kriek NPJ, Wiggins VM, Steyn PS, Towers DK and Hastie TJ. 1979b. Incidence, geographic distribution and toxigenicity of *Fusarium* species in South African corn. *Phytopathology.* **69**: 1181-1185.

Marasas WFO, Wehner FC, Van Rensburg SJ and Van Schalkwyk DJ. 1981. Mycoflora of corn produced in human oesophageal cancer areas in Transkei, Southern Africa. *Phytopathology.* **71**: 792-796.

Marasas WFO, Nelson PE, and Toussoun TA. 1984. Toxigenic *Fusarium* species: identity and mycotoxicology. The Pennsylvania State University Press, Pennsylvania. pp 216- 328.

Marasas WFO, Kellerman TS, Gelderblom WCA, Coetzer JAW, Thiel PG and Van der Lugt JJ. 1988a. Leukoencephalomalacia in a horse induced by fumonisin B_1 isolated from *Fusarium moniliforme*. *Onderstepoort J Vet Res.* **55**: 197-203.

Marasas WFO, Jaskiewicz K, Venter FS and Van Schalkwyk DJ. 1988b. *Fusarium moniliforme* contamination of maize in oesophageal cancer areas in Transkei. *S Afr Med J.* **74**: 110-114.

Marasas WFO. 1993. Occurrence of *Fusarium moniliforme* and fumonisins in maize in relation to human health (Editorial). *S Afr Med J.* **83**: 382-383.

Marasas WFO, Thiel PG, Gelderblom WCA, Shephard GS, Sydenham EW and Rheeder JP. 1993. Fumonisins produced by *Fusarium moniliforme* in maize: Foodborne carcinogens of Pan African importance. *Afr Newslett Occup Health Saf.* **2/93** (suppl): 11-18.

Marasas WFO. 1994. Foodborne disease handbook: Diseases caused by viruses, parasites, and fungi. Hui YM, Gorham JR, Murrell KD and Cliver DO (eds). New York, Marcel Dekker. **2**: 521-573.

Marasas WFO. 1996. Fumonisins: history, world-wide occurrence and impact. In: *Fumonisins in Food.* Jackson LS, De Vries JW and Bullerman LB. (eds). Plenum Press, New York, pp 1-18.

Marasas WFO. 1997. Risk assessment of fumonisins produced by *Fusarium moniliforme* in corn. *Cereal Res Commun* **25**: 399-406.

Marchetti P, Castedo M, Susin SA, Zamzami N, Hirsch T, Macho A, Haeffner A, Hirsch F, Geuskens M and Kroemer G. 1996. Mitochondrial permeability transition is a central coordinating event of apoptosis. *J Exp Med.* **184(3)**: 1155-1160.

Martinou JC. 1999. Apoptosis: Key to the mitochondrial gate. *Nature.* **399(6735)**: 411-412.

Martinova EA and Merrill AH Jr. 1995. Fumonisin B_1 alters sphingolipid metabolism and immune

function in BALB/c mice: Immunological responses to fumonisin B_1. *Mycopathoogia.* **130(3)**: 163-170.

Mathews CK and van Holde KE. 1990. *Biochemistry.* Benjamin Cummings Publishing Company Inc., Redwood City. pp 298-336.

Mathias S, Pena LA and Kolesnick RN. 1998. Signal Transduction of stress via ceramide. *Biochem J.* **335**: 465-480.

Mattson MP, Barger SW, Furukawa K, Bruce AJ, Wyss-Coray T, Mark RJ and Mucke L. 1997. Cellular signaling roles of TGF β, TNF α and β APP in brain injury responses and Alzheimer's disease. *Brain Res Rev.* **23(1-2)**: 47-61.

McDonald OB, Hannun YA, Reynolds CH and Sahyoun N. 1991. Activation of casein kinase II by sphingosine. *J Biol Chem.* **266(32)**: 21773-21776.

Medlock KA and Merrill AH Jr. 1988. Inhibition of serine palmitoyltransferase *in vitro* and long-chain base biosynthesis in intact Chinese hamster ovary cells by β-chloroalanine. *Biochemistry.* **27(18)**: 7079-7084.

Meijer GA, Belien JAM, van Diest PJ and Baak JPA. 1997. Image analysis in clinical pathology. *J Clin Pathol.* **50**: 365-370.

Meivar-Levy I and Futerman AH. 1999. Up-regulation of neutral glycosphingolipid synthesis upon long-term inhibition of ceramide synthesis by fumonisin B_1. *J Biol Chem.* **274**: 4607-4612.

Mekhancha-Dahel C, Lafarge-Fraysinnet C and Fraysinnet C. 1990. Immunosuppressive effects of four trichothecene mycotoxins. *Food Addit Contam.* 7: S94-S96.

Meldolesi J, Clementi F, Chiesara E, Conti F and Fanti A. 1967. Cytoplasmic changes in rat liver after prolonged treatment with low doses of ethionine and adenine: An Ultrastructural and biochemical study. *Lab Invest.* 17:265-267.

Merrill AH Jr .1983. Characterization of serine palmitoyltransferase activity in Chinese hamster ovary cells. *Biochim Biophys Acta.* **754**: 284-291.

Merrill AH Jr., Nixon DW and Williams RD. 1985. Activities of serine palmitoyltransferase (3-ketosphinganine synthase) in microsomes from different rat tissues. *J Lipid Res.* **26**: 617-622.

Merrill AH Jr and Wang E. 1986. Biosynthesis of long chain (sphingoid) bases from serine by LM cells. Evidence for introduction of the 4-trans-double bond after *de novo* biosynthesis of N-acylsphinganine(s). *J Biol Chem.* **261(8)**: 3764-3769.

Merrill AH Jr., Wang E, Mullins RE, Jamison WC, Nimkar S and Liotta DC. 1988. Quantitation of free sphingosine in liver by high-performance liquid chromatography. *Anal Biochem.* **171(2)**: 373-381.

Merrill AH Jr and Stevens VL. 1989. Modulation of protein kinase C and diverse cell functions by sphingosine- a pharmacologically interesting compound linking sphingolipids and signal transduction. *Biochim Biophys Acta.* **1010(2)**: 131-139.

Merrill AH Jr and Jones DD. 1990. An update of the enzymology and regulation of sphingomyelin metabolism. *Biochim Biophys Acta.* **1044(1)**: 1-12.

Merrill AH Jr. 1991. Cell regulation by sphingosine and more complex sphingolipids. *J Bioenerget Biomembr.* **23(1)**: 83-104.

Merrill AH Jr, Hannun YA and Bell RM. 1993a. Sphingolipids and their metabolites in cell regulation. In: *Advances in lipid research: Sphingolipids and their metabolites.* Bell RM, Hannun YA and Merrill AH Jr. (eds). Orlando, Florida, Academic Press. **25**: 1-24.

Merrill AH Jr, van Echten G, Wang E and Sandhoff K. 1993b. Fumonisin B_1 inhibits sphingosine (sphinganine) N-acyltransferase and *de novo* sphingolipid biosynthesis in cultured neurons *in situ*. *J Biol Chem.* **268(36)**: 27299-27306.

Merrill AH Jr, Wang E, Gilchrist DG and Riley RT. 1993c. Fumonisins and other inhibitors of *de novo* sphingolipid biosynthesis. *Adv Lipid Res.* **26**: 215-234.

Merrill AH Jr, Wang E, Schroeder JJ, Smith ER, Yoo H-S and Riley RT. 1995. Disruption of sphingolipid metabolism in the toxicity and carcinogenicity of fumonisins. In: *Molecular approaches to food safety issues involving toxic microorganisms.* Eklund M, Richard J and Mise K (eds). Fort Collins, Colorado, Alaken Press. pp 429-443.

Merrill AH Jr and Sweeley CC. 1996. Sphingolipid metabolism and cell signalling. In: *Biochemistry of Lipids, Lipoproteins, and Membranes.* Vance DE and Vance J (eds). Elsevier Science Publishers, Amsterdam, The Netherlands. **31**: 309-338.

Merrill AH Jr, Schmelz EM, Wang E, Dillehay DL, Rice LG, Meredith F, Riley RT. 1996a. Importance of sphingolipids and inhibitors of sphingolipid metabolism as components of animal diets. *J Nutr.* **127(5)**: 830S-833S.

Merrill AH Jr, Wang E, Vales TR, Smith ER, Schroeder JJ, Menaldino DS, Alexander C, Crane HM, Xia J, Liotta DC, Meredith FI and Riley RT. 1996b. Fumonisin toxicity and sphingolipid biosynthesis. *Adv Exp Med Biol.* **392**: 297-306.

Merrill AH Jr, Schmelz EM, Dillehay DL, Spiegel S, Shayman JA, Schroeder JJ, Riley RT, Voss KA, and Wang E. 1997. Sphingolipids-the enigmatic lipid class: biochemistry, physiology, and pathophysiology. *Toxicol Appl Pharmacol.* **142(1)**: 208-225.

Merrill AH Jr, Sullards MC, Wang E, Voss KA and Riley RT. 2001. Sphingolipid metabolism: roles in signal transduction and disruption by fumonisins. *Environ Health Perspect.* **109(2)**: 283-289.

Merrill AH Jr. 2002. *De Novo* sphingolipid biosynthesis: A Necessary, but dangerous pathway. *J Biol Chem.* **277(29)**: 25843-25846.

Michel C, van Echten-Deckert G, Rother J, Sandhoff K, Wang E and Merrill AH Jr. 1997. Characterization of ceramide synthesis. A dihydroceramide destaurase introduces the 4,5-trans-double bond of sphingosine at the level of dihydroceramide. *J Biol Chem.* **272(36)**: 22432-22437.

Migliorati G, Nicoletti I, Pagliacci MC, D'Adamio L and Riccardi C. 1993. Interleukin-4 protects double -negative and CD4 single-positive thymocytes from dexamethasone-induced apoptosis. *Blood.* **81**:1352-1358.

Mirocha CJ, Gilchrist DG, Shier WT, Abbas HK, Wen Y and Vesonder RF. 1992. AAL toxins, fumonisins (biology and chemistry) and host-specificity concepts. *Mycopathologia.* **17**: 47-56.

Mobio TA, Anane R, Baudrimont I, Carratu M-R, Shier TW, Dano SD, Ueno Y and Creppy EE. 2000. Epigenetic Properties of Fumonisin B_1: Cell Cycle arrest and DNA base modification in C6 glioma cells. *Toxicol Appl Pharmacol.* **164**: 91-96.

Monnet-Tschudi F, Zurich MG, Pithon E, van Melle G and Honegger P. 1995. Microglial

responsiveness as a sensitive marker for trimethyltin (TMT) neurotoxicity. *Brain Res.* **690**: 8-14.

Monnet-Tschudi F, Zurich MG and Honegger P. 1996. Comparison of the developmental effects of two mercury compounds on glial cells and neurons in aggregate cultures of rat telencephalon. *Brain Res.* **741**: 52-59.

Monnet-Tschudi F, Zurich MG, Olivier S, Matthieu JM, Honegger P, and Schilter B. 1999. The naturally occurring food mycotoxin fumonisin B_1 impairs myelin formation in aggregating brain cell culture. *Neurotoxicology.* **20**: 41-48.

Mossman T. 1983. Rapid colorimetric assay for cellular growth and survival: Application to proliferation and Cytotoxicity assays. *J Immunol Meth.* **65**: 55-63.

Munibazi C and Bullerman LB. 1996. Molds and mycotoxins in foods in Burundi. *J Food Prot.* **59**: 869-875.

Munkvold G. 1996. Effect of processing on fumonisin content of corn. *Adv Exp Med Biol.* **392**: 323-334.

Munkvold GP, McGee DC and Carlton WM. 1997. Importance of different pathways for maize kernel infection by *Fusarium moniliforme. Phytopathology.* **87(2)**: 209-217.

Munsch N and Muller WE. 1980. Effects of T2 toxin on DNA polymerases and terminal deoxynucleotidyltransferase of Molt4 and Nu8 cell lines. *Immunopharmacology.* **2(4)**: 313-318.

Musser SM and Plattner RD. 1997. Fumonisin composition in cultures of *Fusarium moniliforme*, *Fusarium proliferatum*, and *Fusarium nygami. J Agric Food Chem.* **45**:1169-1173.

Nagatsu T, Hidaka H, Kuzuya H, Takeya K and Umezawa H. 1970. Inhibition of dopamine beta-hydroxylase by fusaric acid (5-butylpibolinic acid) *in vitro* and *in vivo. Biochem Pharmacol.* **19(1)**: 35-44.

Nair MG. 1998. Fumonisins and Human Health. *Ann Trop Paediatri.* **18 (Suppl)**: S47-S52.

Nakamura S, Kozutsumi Y, Sun Y, Miyake Y, Fujita T, and Kawasaki T. 1996. Dual role of sphingolipids in signalling of the escape from and onset of apoptosis in a mouse cytotoxic T-cell line, CTLL-2. *J Biol Chem.* **271**: 1255-1257.

Nan X, Meehan R and Bird A. 1993. Dissection of the methyl CpG binding domain from the chromosomal protein MeCp2. *Nucleic acid Res.* **21**: 4886-4892.

Nass MMK, Nass S and Afzelius BA. 1965. The general occurrence of mitochondrial DNA. *Exp Cell Res.* **37**: 516-522.

Nelson PE, Plattner RD, Shackelford DD and Desjardins AE. 1991. Production of fumonisins by *Fusarium moniliforme* strains from various substrates and geographic areas. *Appl Environ Microbiol.* **57(8)**: 2410-2412.

Nicoletti I, Migliorati G, Pagliacci MC, Grignani F and Riccardi C. 1991. A rapid and simple method for measuring thymocytes apoptosis by Propidium iodide staining. *J Immunol Methods.* **139**:271-279.

Nishizuka Y. 1988. The molecular heterogeneity of protein kinase C and its implications for cellular regulation. *Nature.* **334**: 661-665.

Nishizuka Y, Shearman MS, Oda T, Berry N, Shimomura T, Asaoka C, Ogita K, Kikkawa U, Kishimoto A, Kose A, Sato N and Tanaka C. 1991. Protein kinase C family and nervous function. *Prog Brain Res.* **89**: 125-141.

Norred WP, Bacon CW, Porter JK and Voss KA. 1990. Inhibition of protein synthesis in rat primary hepatocytes by extracts of *Fusarium moniliforme*-contaminated corn. *Food Chem Toxicol.* **28**: 89-94.

Norred WP, Bacon CW, Plattner RD and Vesonder RF. 1991. Differential Cytotoxicity and Mycotoxin Content Among Isolates of *Fusarium moniliforme*. *Mycopathologia.* **115**: 37-43.

Norred WP, Plattner RD, Vesonder RF, Bacon CW and Voss KA. 1992a. Effects of selected secondary metabolites of *Fusarium moniliforme* on unscheduled synthesis of DNA by rat primary hepatocytes. *Food Chem Toxicol.* **30**: 233-237.

Norred WP, Wang E, Yoo H, Riley RT and Merrill AH Jr. 1992b. *In vitro* toxicology of fumonisins and the mechanistic implications. *Mycopathologia.* **117(1-2)**: 73-78.

Norred WP. 1993. Fumonisins-mycotoxins produced by *Fusarium moniliforme*. *J Toxicol Environ Health.* **38**: 309-328.

Norred WP, Riley RT, Meredith FI, Bacon CW and Voss KA. 1996. Time- and dose-response effects of the mycotoxin, fumonisin B_1 on sphingoid base elevation in precision-cut rat liver and kidney slices. *Toxicol In Vitro.* **10**: 349-358.

Norred WP, Plattner RD, Dombrink-Kurtzman MA, Meredith FI, Riley RT. 1997. Mycotoxin-induced elevation of free sphingoid bases in precision-cut rat liver slices: Specificity of the response and structure-function relationships. *Toxicol Appl Pharmacol.* **147**: 63-70.

Norred WP, Voss KA, Riley RT, Meredith FI, Bacon CW and Merrill AH Jr. 1998. Mycotoxins and health hazards: Toxicological aspects and mechanism of action of fumonisins. *J Toxicol Sci.* **23 (2)**: 160-164.

Obeid LM, Linardic CM, Koralak LA and Hannun YA. 1993. Programmed cell death induced by ceramide. *Science.* **259(5102)**: 1769-1771.

Oettle'AG. 1965. The aetiology of primary carcinoma of the liver in Africa: A critical appraisal of previous ideas with an outline on the Mycotoxin hypothesis. *S Afr Med J.* **39**:817-825.

Ohnishi M and Fujino Y. 1982. Sphingolipids in immature and mature soybeans. *Lipids.* **17**: 803-810.

Ohta H, Yatomi Y, Sweeney EA, Hakomori S-I and Igarashi YA. 1994. Possible role of sphingosine in induction of apoptosis by tumour necrosis factor α in human neutrophils. *FEBS Lett.* **355**: 267-270.

Oldham JW, Allred LE, Milo GE, Kindig O and Capen CC. 1980. The toxicological evaluation of mycotoxins T-2 and T-2 tetraol using normal human fibroblasts *in vitro*. *Toxicol Appl Pharmacol.* **52(1)**: 159-168.

Osweiler GD, Ross PF, Wilson TM, Nelson PE, Witte ST, Carson TL, Rice LG and Nelson HA. 1992. Characterization of an epizootic of pulmonary edema in swine associated with fumonisin in corn screenings. *J Vet Diagn Invest.* **4**: 53-59.

Pace JG. 1983. Effect of T2 mycotoxin on rat liver mitochondria electron transport system. *Toxicon.* **21(5)**: 675-680.

Pace J and Watts M. 1989. Hepatic subcellular distribution of [3H] T2 toxin. *Toxicon.* **27**: 1307-1311.

Palanee T. 1998. The Immunolocalisation of Aflatoxin B_1 in lung carcinomas. Masters in Medical Science dissertation, University of Natal, Medical School (now UKZN), Durban, South Africa.

Palanee T, Dutton MF and Chuturgoon AA. 2000. Cytotoxicity and Aflatoxin B_1 and its chemically synthesised epoxide derivative on the A549 human epithelioid lung cell line. *Mycopathologia.* **151**:155-159.

Paris F, Grassme' H, Cremesti A, Zager J, Fong TM, Haimovitz-Friedman F, Fuks Z, Gulbin E and Kolesnick R. 2001. Natural ceramide reverses Fas resistance of acid sphingomyelinase (1/1) hepatocytes. *J Biol Chem.* **276(11)**: 8297-8305.

Park DL, Rua SM Jr, Mirocha CJ, Abd-Alla ES and Weng CY. 1992. Mutagenic potential of fumonisin contaminated corn following ammonia decontamination procedure. *Mycopathologia.* **117(1-2)**: 105-108.

Patel S, Hazel CM, Winterton AGM and Mortby E. 1996. Survey of ethnic foods for mycotoxins. *Food Addit Contam.* **13**: 833- 841.

Patel S, Hazel CM, Winterton AGM and Gleadle AE. 1997. Surveillance of fumonisins in UK maize-based foods and other cereals. *Food Addit Contam.* **14**:187-191.

Perry DK and Hannun YA. 1998. The role of ceramide in cell signaling. *Biochim Biophys Acta.* **1436**: 233-243.

Pinelli E, Poux N, Garren L, Pipy B, Castegnaro M, Miller DJ and Pfohl-Leszkowicz A. 1999. Activation of mitogen-activated protein kinase by fumonisin B_1 stimulates cPLA2 phosphorylation, the arachidonic acid cascade and cAMP production. *Carcinogenesis.* **20**: 1683-1688.

Pitt JI, Bas'ilico JC, Abarca ML and Lopez C. 2000. Mycotoxins and toxigenic fungi. *Med Mycol.* **38(1)**: 41- 46.

Plattner RD, Weisleder D, Shackelford DD, Peterson R, and Powell RG. 1992. A new fumonisin from solid cultures of *Fusarium moniliforme*. *Mycopathologia.* **117**: 23-28.

Plattner RD. 1995. Detection of fumonisins produced in *Fusarium moniliforme* cultures by HPLC with electrospray MS and evaporative light scattering detectors. *Nat Toxins.* **3**:294-298.

Plumlee KH and Galey FD. 1994. Neurotoxic Mycotoxins: A review of Fungal toxins that cause neurological disease in large animals. *J Vet Med.* **8(1)**: 49-54.

Pohland AE. 1994. Worldwide occurrence of fumonisins. In: *The Toxicology Forum.* Caset Association Ltd., Fairfax, VA. pp 186-196.

Polak JM and van Noorden S. 1986. Immunocytochemistry-Modern methods and applications, Second Edition. John Wright and Sons Ltd., Bristol. pp 146-166.

Porter JK, Bacon CW, Wray EM and Hangler WM Jr. 1995. Fusaric acid in *Fusarium moniliforme* cultures, corn and feeds toxic to livestock and neurochemical effects in the brain and pineal glands of rats. *Nat toxins.* **3(2)**: 91-100.

Pouly S, Storch MK, Matthieu JM, Lassmann H, Monnet-Tschudi F and Honegger P. 1997. Demyelination induced by protein kinase C-activating tumor promoters in aggregating brain cell cultures. *J Neurosci Res.* **49**: 1-12.

Prelusky DB, Trenholm HL and Savard ME. 1994. Pharmacokinetic fate of ^{14}C-labelled fumonisin B_1 in swine. *Nat Toxins.* **2(2)**: 73-80.

Prelusky DB, Trenholm HL, Rotter BA, Miller JD, Savard ME, Yeung JM and Scott PM. 1996. Biological fate of fumonisin B_1 in food-producing animals. In: *Fumonisins in Food*. Jackson LS, De Vries JW, and Bullerman LB (eds). Plenum Press, New York. pp 265-278.

Puranam KL, Guo WX, Qian WH, Nikbakht K and Boustany RM. 1999. CLN3 defines a novel anti-apoptotic pathway operative in neurodegeneration and mediated by ceramide. *Mol Genet Metab*. **66:** 294-308.

Pushkareva MYu, Khan WA, Alessenko AV, Sahyoun N and Hannun YA. 1992. Sphingosine activation of protein kinases in Jurkat T cells. *In vitro* phosphorylation of endogenous protein substrates and specificity of action. *J Biol Chem*. **267(21)**: 15246-15251.

Qureshi MA and Hagler WM Jr. 1992. Effect of fumonisin-B_1 exposure on chicken macrophage function *in vitro*. *Poult Sci*.**71**: 104-112.

Radin NS, Shayman JA and Inokuchi J. 1993. Metabolic effects of inhibiting glucosylceramide synthesis with PDMP and other substances. *Adv Lipid Res*. **26**:183-213.

Radin NS. 1994. Glucosylceramide in the nervous system: a mini review. *Neurochem Res*. **19**:533-540.

Rafai P, Bata A, Vanyi A, Papp Z, Brydl E, Jakab L, Tuboly S and Tury E. 1995. Effects of various levels of T-2 toxin on the clinical status, performance and metabolism of growing pigs. *Vet Rec*. **136(19)**: 485-489.

Ramasamy S, Boissonneault GA, Decker EA and Henning B. 1991. Linoleic acid-induced endothelial cell injury: Role of membrane bound enzyme activities and lipid oxidation. *J Biochem Toxicol*. **6**: 29-35.

Ramasamy S, Wang E, Hennig B and Merrill AH Jr. 1995. Fumonisin B_1 alters sphingolipid metabolism and disrupts the barrier function of endothelial cells in culture. *Toxicol Appl Pharmacol*. **133(2)**: 343-348.

Ramljak D, Calvert RJ, Wiesenfeld PW, Diwan BA, Catipovic B, Marasas WFO, Victor TC, Anderson LM and Gelderblom WCA. 2000. A potential mechanism for fumonisin B_1-mediated hepatocarcinogenesis: cyclin D1 stabilization associated with activation of Akt and inhibition of GSK-3 beta activity. *Carcinogenesis*. **21**: 1537-1546.

Reddy L. 1999. Quantitative determination of fumonisins and related metabolites and their establishment in biological fluids. Masters in Medical Science dissertation, University of Natal, Medical School (now UKZN), Durban, South Africa.

Reubel GH, Gareis M and Amselgruber WM. 1987. Cytotoxicity evaluation of mycotoxins by an MTT-bioassay. *Mycotoxin Res*. **3**: 85-96.

Reubel GH, Gareis M and Amselgruber WM. 1989. Effects of *Fusarium* mycotoxin zearalenone and deoxynivalenol on the mitochondrial methylthiazoltetrazolium-cleavage activity of monolayer cells. *Toxicol in vitro*. **3**: 311-16.

Reynolds ES. 1963. The use of lead citrate at high pH as an electron opaque stain in electron microscopy. *J Cell Biol*. **17**: 208-212.

Rheeder JP, Marasas WFO, Thiel PG, Sydenham EW, Shephard GS and Van Schalkwyk DJ. 1992. *Fusarium moniliforme* and fumonisins in corn in relation to human esophageal cancer in Transkei. *Phytopathology*. **82**: 353-357.

Riboni L, Prinetti A, Bassi R, Caminiti A and Tettamanti G. 1995. A Mediator Role of Ceramide in the

Regulation of Neuroblastoma Neuro2α Cell Differentiation. *J Biol Chem.* **270**: 26868-26875.

Rice-Evans C and Burbon R. 1993. Free radical-lipid interactions and their pathological consequences. *Prog Lipid Res.* **32**: 71-110.

Richard JL, Meerdink G, Maragos CM, Tumbleson M, Bordson G, Rice LG and Ross PF. 1996. Absence of detectable fumonisins in the milk of cows fed *Fusarium proliferatum* (Matsushima) Nirenberg culture material. *Mycopathologia.* **133**: 123-126.

Riley RT, An N-Y, Showker JL, Yoo H-S, Norred WP, Chamberlain WJ, Wang E, Merrill AH Jr, Motelin G, Beasley VR and Haschek WM. 1993. Alteration of tissue and serum sphinganine to sphingosine ratio: An early biomarker of exposure to fumonisin-containing feeds in pigs. *Toxicol Appl Pharmacol.* **118**: 105-112.

Riley RT, Voss KA, Yoo HS, Gelderblom WCA and Merrill AH Jr. 1994a. Mechanism of fumonisin toxicity and carcinogenesis. *J Food Prot.* **57**: 638-645.

Riley RT, Hinton DM, Chamberlain WJ, Bacon CW, Wang E, Merrill AH Jr and Voss KA. 1994b. Dietary fumonisin B_1 induces disruption of sphingolipid metabolism in Sprague-Dawley rats: A new mechanism of nephrotoxicity. *J Nutr.* **124(4)**: 594-603.

Riley RT, Wang E and Merrill AH Jr. 1994c. Liquid chromatographic determination of sphinganine and sphingosine: use of the free sphinganine to sphingosine ratio as a biomarker for consumption of fumonisins. *J AOAC Int.* **77**: 533-540.

Riley RT, Wang E, Schroeder JJ, Smith ER, Plattner RD, Abbas H, Yoo HS and Merrill AH Jr. 1996. Evidence for disruption of sphingolipid metabolism as a contributing factor in the toxicity and carcinogenicity of fumonisins. *Nat Toxins.* **4**: 3-15.

Riley RT, Showker JL, Owens DL and Ross PF. 1997. Disruption of sphingolipid metabolism and induction of equine leukoencephalomalacia by *Fusarium* proliferatum culture material containing fumonisin B_1 or B_3. *Environ Toxicol Pharmacol.* **3**: 221-228.

Riley RT, Voss KA, Norred WP, Wang E, and Merrill AH Jr. 1998. Fumonisins: mechanism of mycotoxicity. *Rev Méd Vét.* **149**: 617-626.

Riley RT, Voss KA, Norred WP, Bacon CW, Meredith FI and Sharma RP. 1999. Serine palmitoyltransferase inhibition reverses anti-proliferative effects of ceramide synthase inhibition in cultured renal cells and suppresses free sphingoid base accumulation in kidney of BALBc mice. *Environ Toxicol Pharmacol.* 7: 109-118.

Riley RT, Enongene E, Voss KA, Norred WP, Meredith FI, Sharma RP, Spitsbergen J, Williams DE, Carlson DB and Merrill AH Jr. 2001. Sphingolipid Perturbations as mechanisms for fumonisin carcinogenesis *Environ Health Perspect.* **109(2)**: 301-308.

Rimando AM and Porter JK. 1997. Fusaric acid increases melatonin levels in the weanling rat and pineal cell cultures. *J Toxicol Environ Health.* **50(3)**: 275-284.

Rizzo A, Atroshi F, Ahotupa M, Sankari S and Elovaara E. 1994. Protective effect of antioxidants against free radical-mediated lipid peroxidation induced by DON or T-2 toxin. *J Vet Med.* **A41**: 81-90.

Robb J, Norval M and Neill WA. 1990. The use of tissue culture for the detection of mycotoxins (Letter). *Appl Microbiol.* **10**:161-165.

Robertson PL, Du Bois M, Bowman PD and Goldstein GW. 1985. Angiogenesis in developing rat brain: An *in vivo* and *in vitro* study. *Dev Brain Res.***23**: 219-223.

Robinson KM and Gregory MA. 1977. Ultrastructural features of cultured carcinoma of the oesophagus cells. *Proc Electron Microsc Soc South Afr.* 7:125-126.

Rodriguez-Lafrasse C, Rousson R, Pentchev PG, Louisot P and Vanier MT. 1994. Free Sphingoid bases in tissue from patients with type C Niemann-Pick disease and other lysosomal storage disorders. *Biochem Biophys Acta.* **1226**: 138-144.

Romanenko EB, Alessenko AV and Vanyushin BF. 1995.Effect of sphingomyelin and anti-oxidants on the *in vitro* and *in vivo* DNA methylation. *Biochem Mol Biol Int.* **35**: 87-94.
Roomi MW, Ho RK, Sarma DSR and Farber E. 1985. A common biochemical pattern in preneoplastic hepatocytes nodules generated in four different modles in rat. *Cancer Res.* **45**: 564-571.

Rosenstein Y and Lafarge-Frayssinet C. 1983. Inhibitory effect of Fusarium T-2 toxin on lymphoid DNA and protein synthesis. *Toxicol Appl Pharmacol.* **70(2)**: 283-288.

Ross PF, Ledet AE, Owens DL, Rice LG, Nelson HA, Osweiler GD and Wilson TM. 1993. Experimental equine leukoencephalomalacia, toxic hepatosis, and encephalopathy caused by corn naturally contaminated with fumonisins. *J Vet Diagn Invest.* **5**: 69-74.

Rother J, Van Echten G, Schwarzmann G and Sandhoff K. 1992. Biosynthesis of sphingolipids: Dihydroceramide and not sphinganine is desaturated by cultured cells. *Biochem Biophys Res Commun.* **189**: 14-20.

Rotter BA, Thompson BK and Clarkin S and Owen TC. 1993. Rapid colorimetric bioassay for screening of *Fusarium* mycotoxins. *Nat toxins.* **1**:303-307.

Rotter BA, Thompson BK, Prelusky DB, Trenholm HL, Stewart B, Miller JD and Savard ME. 1996. Response of growing swine to dietary exposure pure fumonisin B_1 during an eight-week period: Growth and clinical parameters. *Nat Toxins.* **4**: 42-50.

Rouleau J, MacLeod AR and Szyf M. 1995. Regulation of the DNA methyltransferase by the Ras-AP-1 signaling pathway. *J Biol Chem.* **270(4)**: 1595-1601.

Rumora L, Kovacic S, Rozgaj R, Cepelak I, Pepeljnjak S and Zanic Grubisic T. 2002. Cytotoxic and genotoxic effects of fumonisin B_1 on rabbit kidney RK13 cell line. **76(1)**: 55-61.

Sack RL and Goodwin FK. 1974. Inhibition of dopamine β-hydroxylase in manic patients. A clinical trial and fusaric acid. *Arch Gen Psychiatry.* **31(5)**: 649-654.

Sahu SC, Eppley RM, Page SW, Gray GC, Barton CN and O'Donnell MW. 1998. Peroxidation of membrane lipids and oxidative DNA damage by fumonisin B_1 in isolated rat liver nuclei. *Cancer Lett.* **125**: 117-121.

Sandhoff K, Kolter T, Van Echten-Deckert G. 1998. Sphingolipid metabolism. Sphingoid analogs, sphingolipid activator proteins, and the pathology of the cell. *Ann N Y Acad Sci.* **845**:139-151.

Sato G, Augusti-Tocco G, Posner M and Kelly P. 1970. Hormone secreting and hormone-responsive cell cultures. *Recent Prog Horm Res.* **26**:539-546.

Saunders NR and Mollgard K. 1984. Development of the blood brain barrier. *J Dev Physiol.* **6**: 45-47.

Schmelz EM, Dombrink-Kurtzman MA, Roberts PC, Kozutsumi Y, Kawasaki T, and Merrill AH Jr. 1998. Induction of apoptosis by fumonisin B_1 in HT29 cells is mediated by the accumulation of endogenous free sphingoid bases. *Toxicol Appl Pharmacol.* **148**: 252-260.

Scholfield C. *pers comm.* 2002. LumiTech™ consultant. Lumitech Ltd. Nottingham Business Park. City Link, Nottingham, NG24LA, United Kingdom. (Now with Cambrex™).

Schroeder JJ, Crane HM, Xia J, Liotta DC and Merrill AH Jr. 1994. Disruption of sphingolipid metabolism and stimulation of DNA synthesis by fumonisin B_1: A molecular mechanism for carcinogenesis associated with *Fusarium moniliforme*. *J Biol Chem.* **269(5)**: 3475-3481.

Schwarz A, Rapaport E, Hirschberg K and Futerman H. 1995. A regulatory role for sphingolipids in neuronal growth: Inhibition of sphingolipid synthesis and degradation have opposite effects on axonal branching. *J Biol Chem.* **270**: 10990-10998.
Schwarz A and Futerman AH. 1998. Inhibition of sphingolipid syntheis, but not degradation, alters the rate of dendrite growth in cultured hippocampal neurons. *Dev Brain Res* .**108**:125-130.

Schwarzmann G and Sandhoff K. 1990. Metabolism and intracellular transport of glycosphingolipds. *Biochemistry.* **29**: 10865-10871.

Scott PM, Delgado T, Prelusky DB, Trenholm HL and Miller JD.1994. Determination of fumonisins in milk. *J Environ Sci Health.* **B29**: 989-998.

Scott PM and Lawrence GA. 1995. Analysis of beer for fumonisins. *J Food Prot.* **58**:1379-1382.

Seddon IR, Smith TK and de Lange CFM. 1997. *Fusarium* mycotoxins in weaner and starter pigs. *Ontario Swine Research Review.* pp 21-23.

Shapiro HM. 1985. *Practical Flow Cytometry.* Alan R Liss (ed.) New York.

Sharma RP, Dugyala RR and Voss KA. 1997. Demonstration of *in situ* Apoptosis in mouse liver and kidney after short-term repeated exposure to fumonisin B_1. *J Comp Pathol.* **117**: 371-381.

Shelby RA, Zhang D, Dalrymple LW. 1995. Using Brine shrimp bioassay to measure cytotoxicity of *Fusarium* toxins. *Phytopathology.* **85(10)**: 1208-1211.

Shephard GS, Sydenham EW, Thiel PG and Gelderblom WCA. 1990. Quantitative determination of fumonisins B_1 and B_2 by high-performance liquid chromatography with fluorescence detection. *J Liq Chromatogr.* **13**: 2077-2087.

Shephard GS, Thiel PG and Sydenham EW. 1992. Determination of fumonisin B_1 in plasma and urine by high performance liquid chromatography. *J Chromatogr.* **574**: 299-304.

Shephard GS, Thiel PG, Sydenham EW, Vleggaar R and Alberts JF. 1994a. Determination of the mycotoxin fumonisin B_1 and identification of its partially hydrolysed metabolites in the faeces of non-human primates. *Food Chem Toxicol.* **32(1)**: 23-29.

Shephard GS, Thiel PG, Sydenham EW and Alberts JF. 1994b. Biliary excretion of the mycotoxin fumonisin B_1 in rats. *Food Chem Toxicol.* **32**: 489-491.

Shephard GS, Thiel PG, Stockenstrom S and Sydenham EW. 1996a. Worldwide survey of fumonisin contamination of maize and corn-based products. *J AOAC Int.* **79**: 671-687.

Shephard GS, van der Westhuizen L, Thiel PG, Gelderblom WCA, Marasas WFO and van Schalkwyk DJ. 1996b. Disruption of sphingolipid metabolism in non-human primates consuming diets of fumonisin-containing *Fusarium moniliforme* culture material. *Toxicon.* **34**: 527-534.

Shephard GS. 1998. Chromatographic determination of the fumonisin mycotoxins. *J Chromatogr A.* **815**: 31-39.

Shephard GS and van der Westhuizen L. 1998. Liquid chromatographic determination of sphinganine/ sphingosine ratio in serum. *J Chromatogr B Biomed Sci Appl.* **710 (1-2)**: 219-222.

Shephard GS, Thiel PG, Sydenham EW, Savard ME, Snijman PW and Vleggaar R. 1998. Toxicokinetics of fumonisin B_1 and B_2: comparative studies in rats and non-human primates. In: *Mycotoxins and Phycotoxins-Developments in Chemistry, Toxicology and Food Safety.* Miragalia M, Van Egmond H, Brera C and Gilbert J. (eds). Alaken Inc, Fort Collins, CO, USA. pp 517-522.

Sheu CW, Rodriguez I, Eppley RM and Lee JK. 1996. Lack of transforming activity of fumonisin B_1 in BALB/3T3 A31-1-1 mouse embryo cells. *Food Chem Toxicol.* **34**: 751-753.

Shier WT, Abbas HK and Mirocha CJ. 1991. Toxicity of mycotoxins fumonisin B_1 and B_2 and *Alternaria alternata* f. sp. *lycopersici* toxin (AAL) in cultured mammalian cells. *Mycopathologia.* **116**: 97-104.

Shifrin VL and Anderson P. 1999. Trichothecene mycotoxins trigger ribotoxic stress response that activates c-Jun N-terminal kinase and p38 mitogen-activated protein kinase and induces apoptosis. *J Biol Chem.* **274**: 13985-13992.

Shimizu S, Eguchi Y, Kamiike W, Itoh Y, Hasegawa J, Yamabe K, Otsuki Y, Matsuda H and Tsujimoto Y. 1996a. Induction of apoptosis as well as necrosis by hypoxia and predominant prevention of apoptosis by Bcl-2 and Bcl- xL. *Cancer Res.* **56**: 2161-2166.

Shimizu S, Eguchi Y, Kamiike W, Waguri S, Uchiyama Y, Matsuda H and Tsujimoto Y. 1996b. Bcl-2 blocks loss of mitochondrial membrane potential while ICE inhibitors act at a different step during inhibition of death induced by respiratory chain inhibitors. *Oncogene.* **13**: 21-29.

Simmons TD. 1999. Mitochondrial biochemistry and its role in apoptosis. M Phil to PhD tranfer report. Faculty of Life Sciences, Nottingham Trent University, England, United Kingdom.

Simons K and van Meer G. 1988. Lipid sorting in Epithelial cells. *Biochemistry.* **27(17)**: 6197-6202.

Sitas F and Pacella R. 1994. Cancer in South Africa, 1989. Johannesburg: The Natal Witness Printing and Publishing Company.

Sitas F, Madhoo J and Wessie J. 1998. Incidence of Histologically diagnosed Cancer in South Africa, 1993-1995. Johannesburg. National Cancer Registry of South Africa. pp 29-58.

Slater TF, Sawyer B and Straubli U. 1963. Studies on succinate tetrazolium reductase systems III. Points of coupling of four different tetrazolium salts. *Biochim Biophys Acta.* **77**:383-393.

Slife CW, Wang E, Hunter R, Wang S, Burgess C, Liotta DC and Merrill AH Jr. 1989. Free sphingosine formation from endogenous substrates by a liver plasma membrane system with a divalent cation dependence and a neutral pH optimum. *J Biol Chem.* **264**: 10371-10377.

Smith ER and Merrill AH Jr. 1993. Altering *de novo* sphingolipid biosynthesis affects phospholipid profiles in J744 macrophages. *FASEB J.* **7**: A173 (Abstract 1001).

Smith ER, Jones PL, Boss JM and Merrill AH Jr. 1997. Changing J774A.1 Cells to New Medium Perturbs Multiple Signaling Pathways, including the Modulation of Protein Kinase C by Endogenous Sphingoid Bases. *J Biol Chem.* **272(9)**: 5640-5646.

Smith GW, Constable PD and Haschek WM. 1996. Cardiovascular responses to short-term fumonisin exposure in swine. *Fundam Appl Toxicol.* **33**:140-148.

Smith GW, Constable PD, Tumbleson ME, Rottinghaus GE and Haschek-Wanda M. 1999. Sequence of cardiovascular changes leading to pulmonary edema in swine fed culture material containing fumonisin. *Am J Vet Res.* **60**: 1292-1300.

Smith JE and Moss MO. 1985. Mycotoxins: Formation, Analysis and Significance. New York. USA. John Wiley and Sons. pp 1-148.

Smith JS and RA Thakur. 1996.Occurrence and fate of fumonisins in beef. In: *Fumonisins in Food.* Jackson LS, DeVries JW and Bullerman LB (eds). Plenum Press, New York. *Adv Exp Med Biol.* **392**: 39-55.

Smith TK and MacDonald EK. 1991. Effects of fusaric acid onbrain regional neurochemistry and vomiting behaviour in swine. *J Anim Sci.* **69(5)**: 2044-2049.

Smith TK, McMillen EG and Castillo JB. 1997. Effect of feeding blends of fusarium mycotoxin-contamination grains containing deoxynivalenol and fusaric acid on growth and feed consumption of immature swine. *J Anim Sci.* **75(8)**: 2184-2191.

Smith TK and Seddon IR. 1998. Synergism demonstrated between fusarium mycotoxins. *Feedstuffs*. pp 12-17.

Snyman, C. 1993. In: *An Introduction to Immunocytochemistry.* Multicopy, University of Natal, Durban, South Africa. Wolfe-Coote SA (ed). pp 1-35.

Solfrizzo M, Avantaggiato G and Visconti A. 1997. *In vivo* validation of the sphinganine/sphingosine ratio as a biomarker to display fumonisin ingestion. *Cereal Res Commun.* **25**: 437-441.

Spiegel S, Oliviera A and Carlson RO. 1993. The role of sphingosine in cell growth regulation and transmembrane signalling. *Adv Lipid Res.* **25**:105-129.

Spiegel S and Merrill AH Jr. 1996. Sphingolipid metabolism and cell growth regulation: A state of the art review. *FASEB J.* **10(12)**: 1388-1397.

Spiegel S, Yamada KM, Hom BE, Moss J and Fishman PH. 1986. Fibrillar organization of fibronectin is expressed co-ordinately with cell surface gangliosides in a variant murine fibroblast. *J Cell Biol.* **102(5)**: 1898-1906.

Spyker JA. 1975. Assessing the impact of low level chemicals on development: behavioral and latent effects. *Fed Proc.* **34**: 1835-1844.

Stevens VL, Nimkar S, Jamison WC, Liotta DC and Merrill AH Jr. 1990. Characteristics of the growth inhibition and cytotoxicity of long-chain (sphingoid) bases for Chinese hamster ovary cells: Evidence for an involvement of protein kinase C. *Biochim Biophys Acta.* **1051(1)**: 37-45.

Stevens VL and Tang J. 1997. Fumonisin B_1-induced sphingolipid depletion inhibits vitamin uptake via the glycosylphosphatidylinositol-anchored folate receptor. *J Biol Chem.* **272**: 18020-18025.

Stockenström S, Sydenham EW and Thiel PG. 1994. Determination of fumonisins in corn: Evaluation of two purification procedures. *Mycotoxin Res.* **10**: 9-14

Strum JC, Swenson KI, Turner JE and Bell RM. 1995. Ceramide triggers meiotic cell cycle progression in *Xenopus* oocytes. A potential mediator of progesterone-induced maturation. *J Biol Chem.* **270**: 13541-13547.

Sun TSC and Stahr HM. 1993. Evaluation and application of a bioluminescent bacterial genotoxicity test. *J Assoc Off Anal Chem Int.* **76**: 893-898.

Susin SA, Zamzami N and Kroemer G. 1998. Mitochondria as regulators of apoptosis: doubt no more. *Biochim Biophys Acta.* **1366(1-2)**: 151-165.

Suzuki A, Iwasaki M, Kato M and Wagai N. 1997. Sequential operation of ceramide synthesis and ICE cascade in CPT-11-initiated apoptotic death signaling. *Exp Cell Res.* **233**: 41-47.

Sweeley CC. 1991. Sphingolipids. In: *Biochemistry of lipids, lipoproteins and membranes.* Vance DE and Vance JE (eds). Amsterdam, Elsevier Science Publishers. pp 327-361.

Sweeney EA, Sakakura C, Shirahama T, Masamune A, Ohta H, Hakomori S and Igarashi Y. 1996. Sphingosine and its methylated derivative N, N'-dimethylsphingosine (DMS) induce apoptosis in a variety of human cancer cell lines. *Int J Cancer.* **66**: 358-366.

Sydenham EW, Thiel PG, Marasas WFO, Shephard GS, Van Schalkwyk DJ and Koch KR. 1990a. Natural occurrence of some *Fusarium* mycotoxins in corn from low and high esophageal cancer prevalence areas of the Transkei, Southern Africa. *J Agric Food Chem.* **38**: 1900-1903.

Sydenham EW, Gelderblom WCA, Thiel PG and Marasas WFO. 1990b. Evidence for the natural occurrence of fumonisin B_1, a mycotoxin produced by *Fusarium moniliforme*, in corn. *J Agric Food Chem.* **38**: 285-290.

Sydenham EW, Shephard GS, Thiel PG, Marasas WFO and Stockenström S. 1991. Fumonisin contamination of commercial corn-based human foodstuffs. *J Agric Food Chem.* **39**: 2014-2018.

Sydenham EW, Shephard GS and Thiel PG. 1992. Liquid Chromatographic Determination of Fumonisins B_1, B_2 and B_3 in Foods and Feeds. *J Assoc Off Anal Chem.* **75(2)**: 313-318.

Sydenham EW, Shephard GS, Thiel PG, Stockenstrom S and Snijman PW. 1996. Liquid chromatographic determination of fumonisins B_1, B_2 and B_3 in corn: AOAC-IUPAC collaborative study. *J AOAC Int.* **79(3)**: 688-696.

Tanaka C and Saito N. 1992. Localization of subspecies of protein kinase C in the mammalian central nervous system. *Neurochem Int.* **21**: 499-512.

Telles-Pupulin AR, Salguiero-Pagadigorria CL, Bracht A and Ishii-Iwamoto EL. 1998. Effects of Fusaric Acid on rat liver mitochondria. *Comp Biochem Physiol C Pharmacol Toxicol Endocrinol.* **120(1)**: 43-51.

Thiel PG. 1978. A molecular mechanism for the toxic action of moniliformin, a mycotoxin produced by *Fusarium moniliforme*. *Biochem Pharmacol.* **27(4)**: 483-486.

Thiel PG, Marasas WFO, Sydenham EW, Shephard GS and Gelderblom WCA. 1992. The implications of naturally occurring levels of fumonisins in corn for human and animal health. *Mycopathologia.* **117**: 3-9.

Thiel PG, Sydenham EW, Shephard GS and van Schalkwyk DJ. 1993. Study of reproducibility characteristics of a liquid chromatographic method for the determination of fumonisins B_1 and B_2 in corn: IUPAC collaborative study. *J AOAC Int.* **76(2)**: 361-366.

Thompson WL, Wannemacher RW Jr. 1984. Detection and quantitation of T-2 toxin with a simplified protein synthesis inhibition assay. *Appl Environ Microbiol.* **48(6)**: 1176-80.

Thompson WL and Wannemacher RW Jr. 1986. Structure-function relationships of 12,13-epoxy trichothecene mycotoxins in cell culture: Comparison of whole animal lethality. *Toxicon.* **24**: 985-994.

Tolleson WH, Dooley KL, Sheldon WG, Thurman JD, Bucci TJ, and Howard PC. 1996a. The mycotoxin fumonisin induces apoptosis in cultured human cells and in liver and kidneys of rats. *Adv Exp Med Biol.* **392**: 237-250.

Tolleson WH, Melchior WB Jr, Morris SM, McGarrity LJ, Domon OE, Muskhelishvili L, James SJ and Howard PC. 1996b. Apoptotic and anti-proliferative effects of fumonisin B_1 in human keratinocytes, fibroblasts, esophageal epithelial cells and hepatoma cells. *Carcinogenesis.* **17**: 239-249.

Tolleson WH, Couch LH, Melchior WB, Jenkins GR, Muskhelishvili M, Muskhelishvili L, McGarrity LJ, Domon O, Morris SM and Howard PC. 1999. Fumonisin B_1 induces apoptosis in cultured human keratinocytes through sphinganine accumulation and ceramide depletion. *Int J Oncol.* **14(5)**: 833-843.

Tornaletti S and Pfeifer GP. 1995. Complete and tissue independent methylation of CpG sites in the p53 gene: Implications for mutations in human cancers. *Oncogene.* **10**: 1493-1499.

Trump BF, Jesudasan ML and Jones RT. 1978. Ultrastructural features of Diseased cells. In: *Diagnostic Electron Microscopy.* Trump BF and Jones RT (eds). John Wiley and Sons, New York. **1**: 1-89.

Trusal LR and O'Brien JC. 1986. Ultrastructural effects of T-2 toxin mycotoxin on rat hepatocytes *in vitro*. *Toxicon* **24**: 481-488.

Tryphonas H, Iverson F, Ying So EA, MgGuire PF, O'Grady L, Clayson DB and Scott PM. 1986. Effects of deoxynivalenol (Vomitoxin) on the humoral and cellular immunity of mice. *Toxicol Lett.* **30**: 137-150.

Tseng TC, Tu JC and Soo LC.1995. Natural occurrence of mycotoxins in *Fusarium* infected beans. *Microbios.* **84**: 21-28.

Tsujimoto Y. 1997. Apoptosis and necrosis: intracellular ATP level as a determinant for cell death modes. *Cell Death Different.* **4**: 429-434.

Tsunoda M, Sharma RP and Riley RT. 1998. Early fumonisin B_1 toxicity in relation to disrupted sphingolipid metabolism in male BALB/c mice. *J Biochem Mol Toxicol.* **12**: 281-289.

Ueno Y. 1983. General toxicology. In: *Developments in Food Science IV Trichothecenes, chemical, biological and toxicological aspects.* Ueno Y (ed). Amsterdam, Elsevier. pp 135-146.

Ueno Y, Umemori K, Niimi E, Tanuma S, Nagata S, Sugamata M, Ihara T, Sekijima M, Kawai K, Ueno I and Tashiro F. 1995. Induction of apoptosis by T-2 toxin and other natural toxins in HL-60 human promyelotic leukemia cells. *Nat Toxins.* **3**: 129-137.

United States National Toxicology Program. 1982. National Toxicology Program technical report on the carcinogenesis bioassay of zearalenone (CAS No. 17924-92-4) in F344/N rats and B6C3F1 mice (feed study). Research Triangle Park, North Carolina, US Department of Health and Human Services, National Toxicology Program (NTP –81-54; NIH Publication. No. 83-1791).

United States National Toxicology Program. 1999. National Toxicology Program technical report on the toxicology and carcinogenesis studies of fumonisin B_1 (CAS No. 116355-83-0) in F344/N rats and B6C3F1 mice (feed studies). Research Triangle Park, North Carolina, US Department of Health and Human Services, National Toxicology Program (NTP TR 496; NIH Publication. No. 99-3955).

Vaccarino F, Guidotti A and Coasta E. 1987. Ganglioside inhibition of glutamine-mediated protein kinase C translocation in primary cultures of cerebellar neurons. *Proc Natl Acad Sci USA.* **84**: 8707-8711.

Van Brocklyn JR, Lee MJ, Menzeleev R, Olivera A, Edsall L, Cuvillier O, Thomas DM, Coopman PJP, Thanagada S, Liu CH, Hla T and Spiegel S. 1998. Dual actions of sphingosine-1-phosphate: extracellular through the Gi-coupled receptor Edg-1 and intracellular to regulate proliferation and survival. *J Cell Biol.* **142**: 229-249.

van der Westhuizen L, Shephard GS, Snyman SD, Abel S, Swanevelder S and Gelderblom WCA. 1998. Inhibition of sphingolipid biosynthesis in rat primary hepatocyte cultures by fumonisin B_1 and other structurally related compounds. *Food Chem Toxicol.* **36(6)**: 497-503.

van der Westhuizen L., Brown NL., Marasas WFO, Swanevelder S and Shephard GS. 1999. Sphinganine/Sphingosine ratio in plasma and urine as a possible Biomarker for Fumonisin exposure in Humans in rural areas in Africa. *Food Chem Toxicol.* **37(12)**: 1153-1158.

van der Westhuizen L, Shephard GS and van Schalkwyk DJ. 2001. The effect of a single gavage dose of fumonisin B_1 on the sphinganine and sphingosine levels in vervet monkeys. *Toxicon.* **39(2-3)**: 273-281.

van Echten G, Birk R, Brenner-Weiss G, Schmidt RR and Sandhoff K. 1990. Modulation of sphingolipid biosynthesis in primary cultured neurons by long chain bases. *J Biol Chem.* **265(16)**: 9333-9339.

van Echten-Deckert G, Zschoche A, Bär T, Schmidt RR, Raths A, Heinemann T and Sandhoff K. 1997. *cis*-4-Methylsphingosine Decreases Sphingolipid Biosynthesis by Specifically Interfering with Serine Palmitoyltransferase Activity in Primary Cultured Neurons. *J Biol Chem.* **272**: 15825-15833.

van Echten-Deckert G, Giannis A, Schwarz A, Futerman AH and Sandhoff K. 1998. 1-Methylthiodihydroceramide, a Novel Analog of Dihydroceramide, Stimulates Sphinganine Degradation Resulting in Decreased *de Novo* Sphingolipid Biosynthesis. *J Biol Chem.* **273**: 1184-1191.

van Rensburg SJ, van der Walt , Purchase IF, Pereira Coutinho L and Markham R. 1974. Primary liver cancer rate and aflatoxin intake in a high cancer area. *S AfrMed J.* **48(60)**: 2508A-2508D.

van Rensburg SJ , Bradshaw ES, Bradshaw E and Rose EF. 1985. Oesophageal cancer in Zulu men, South Africa: a case control study. *Br J Cancer.* **51(3)**: 399-405.

Van Veldhoven PP and Mannaerts GP. 1991. Subcellular localization and membrane topology of sphingosine-1-phosphate lyase in rat liver. *J Biol Chem.* **266(19)**: 12502-12507.

Vaux DL. 1993 Toward the understanding of the molecular mechanisms of physiological cell death. *Proc Natl Acad Sci USA.* **90**: 786-789.

Vermes I, Haanen C and Reutelingsperger CPM. 1998. Molecular biology of apoptosis and programmed cell death. In: *Free Redicals and Molecular Biology of Human Diseases*. Arumoma O and Halliwell B. (eds). OICA International, Saint Lucia. pp 225.

Vermes I, Haanen C and Reutelingsperger CPM. 2000. Flow Cytometry of Apoptotic cell death. *J Immunol Methods.* **243**: 167-190.

Vesonder RF, Gasdorf H and Peterson RE. 1993. Comparison of cytotoxicities of *Fusarium* metabolites and *Alternaria* metabolite AAL-toxin to cultured mammalian lines. *Arch Environ Contam Toxicol.* **24**. 473-477.

Vesper H, Schmelz E-M, Nikolova-Karakashian MN, Dillehay DL, Lynch DV and Merrill AH Jr. 1999. Sphingolipids in Food and the Emerging Importance of Sphingolipids to Nutrition. *J Nutr.* **129**: 1239-1250.

Visconti A, Minervini F, Lucivero G and Gambatesa V. 1991. Cytotoxic and immunotoxic effects of *Fusarium* mycotoxins using rapid colorimetric bioassay. *Mycopathologia*. **113**:181-186.

Visconti A, Doko MB, Schurer B and Boenke A. 1993. Intercomparison study for the analysis of fumonisins B_1 and B_2 in an unknown solution. In: *Proceedings of the UK Workshop on Occurrence and Significance of Mycotoxins*. Scudamore K (ed). Slough, United Kingdom, Ministry of Agriculture, Fisheries and Food, Central Science Laboratory. pp 200-202.

Von Milczewskis KE. 1987. Toxicity of epoxy trichothecenes in cultured mammalian cells. *Mycotoxin Res.* **3**: 69-76.

Vorhees CV. 1992. Developmental Neurotoxicity. In: *Neurotoxicology*. Tilson HA and Mitchell CL (eds). Raven Press, New York. pp 295-329.

Voss KA, Plattner RD, Bacon CW, and Norred WP. 1990. Comparative studies of hepatotoxicity and fumonisin B_1 and B_2 content of water and chloroform/methanol extracts of *Fusarium moniliforme* strain MRC 826 culture material. *Mycopathologia*. **112**: 81-92.
Voss KA, Chamberlain WJ, Bacon CW and Norred WP. 1993. A preliminary investigation on renal and hepatic toxicity in rats fed purified fumonisin B_1. *Nat Toxins*. **1**: 222-228.

Voss KA, Bacon CW, Norred WP, Chapin RE, Chamberlain WJ, Plattner RD and Meredith FI. 1996a. Studies on the reproductive effects of *Fusarium moniliforme* culture material in rats and the biodistribution of [^{14}C] fumonisin B_1 in pregnant rats. *Nat Toxins*. **4**: 24-33.

Voss KA, Riley RT, Bacon CW, Chamberlain WJ and Norred WP. 1996b. Subchronic toxic effects of *Fusarium moniliforme* and fumonisin B_1 in rats and mice. *Nat Toxins*. **4**: 16-23.

Voss KA, Riley RT, Bacon CW, Meredith FI and Norred WP. 1998. Toxicity and sphinganine levels are correlated in rats fed fumonisin B_1 (FB_1) or hydrolyzed FB_1. *Environ Toxicol Pharmacol.* **5**: 101-104.

Voss KA, Porter JK, Bacon CW, Meredith FI and Norred NP. 1999. Fusaric acid and modification of the subchronic toxicity to rats of fumonisins in *F. moniliforme* culture material. *Food Chem Toxicol.* **37(8)**: 853-861.

Vudathala DK, Prelusky DB, Ayround M, Trenholm HL, and Miller JD. 1994. Pharmacokinetic fate and pathological effects of ^{14}C-fumonisin B_1 in laying hens. *Nat Toxins*. **2(2)**: 81-88.

Walsh SW. 1994. Lipid Peroxidation in pregnancy. *Hyper Preg*. **3(1)**: 1-32.

Walum E, Hansson E and Harvey AL. 1990. *In vitro* testing of neurotoxicity. *ATLA*.**18**: 153-179.

Wang E, Norred WP, Bacon CP, Riley RT and Merrill AH Jr. 1991. Inhibition of sphingolipid biosynthesis by fumonisins: Implications for diseases associated with *Fusarium moniliforme*. *J Biol Chem*. **266 (22)**: 14486-14490.

Wang E, Ross PF, Wilson TM, Riley RT and Merrill AH Jr. 1992. Increases in serum sphingosine and sphinganine and decreases in complex sphingolipids in ponies given feed containing fumonisins, mycotoxins produced by *Fusarium moniliforme*. *J Nutr*. **122(8)**: 1706-1716.

Wang E, Riley RT, Meredith FI and Merrill AH Jr. 1999. Fumonisin B_1 consumption by rats causes reversible, dose-dependent increases in urinary sphinganine and sphingosine. *J Nutr*. **129(1)**: 214-220.

Wang H, Jones C, Ciacci-Zanella J, Holt T, Gilchrist DG and Dickman MB. 1996. Fumonisins and *Alternaria alternata* lycopersici toxins: sphinganine analog mycotoxins induce apoptosis in monkey

kidney cells. *Proc Natl Acad SciUSA*. **93**: 3461-3465.

Warburg O. 1956. The metabolism of Tumors (English Translation). *Science* (Lond). **123**:309-314.

Wattenberg EV, Badria FA and Shier WT. 1996. Activation of mitogen-activated protein kinase by the carcinogenic mycotoxin fumonisin B_1. *Biochem Biophys Res Commun*. **227**: 622-627.

Weibking TS, Ledoux DR, Bermudez AJ, Turk JR and Rottinghaus GE. 1993. Effect of feeding *Fusarium moniliforme* culture material containing known levels of fumonisin B_1 on the young broiler chick. *Poult Sci*. **72(3)**: 456-466.

Wilson BJ and Maronpot RR. 1971. Causative fungus agent of leukoencephalomalacia in equine animals. *Vet Rec*. **88(19)**: 484-486.

Wilson E, Wang E, Mullins RE, Uhlinger DJ, Liotta DC, Lambeth JD and Merrill AH Jr. 1988. Modulation of the free sphingosine levels in human neutrophils by phorbol esters and other factors. *J Biol Chem*. **263**: 9304-9309.

Wilson TM, Ross PF, Owens DL, Rice LG, Green SA, Jenkins SJ and Nelson HA. 1992. Experimental reproduction of ELEM-A study to determine the minimum toxic dose in ponies. *Mycopathologia*. **117**: 115-120.

Witty JP, Bridgham JT and Johnson AL. 1996. Induction of apoptotic cell death in hen granulosa cells by ceramide. *Endocrinology*.**137**: 5269-5277.

Wyllie AH, Kerr JF and Currie AR. 1980. Cell death: the significance of apoptosis. *Int Rev Cytol*. **68**:251-306.

Yang G-H, Jarvis BB, Chung Y-J and Pestka JJ. 2000. Apoptosis induction by satratoxins and other trichothecene mycotoxins: Relationship to ERK, p38 MAPK, and SAPK/JNK activation. *Toxicol Appl Pharmacol*. **164**:149-160.

Yarom R and Yagen B. 1986. T-2 toxin effect on the ultrastructure of myocardial micro-vasculature. *J Exp Path*. **67**: 55-63.

Yeung JM, Wang H-Y and Prelusky DB. 1996. Fumonisin B_1 induces protein kinase C translocation via direct interaction with diacylglycerol binding site. *Toxicol Appl Pharmacol*. **141**: 178-184.

Yike I, Allan T, Sorenson WG and Dearborn DG. 1999. Highly sensitive protein translation assay for trichothecene toxicity in Airborne particulates: Comparison with cytotoxicity assays. *Appl Environ Microbiol*. **65(1)**: 88-94.

Yin J-J, Smith MJ, Eppley RM, Page SW and Sphon JA. 1996a. Effects of fumonisin B_1 on oxygen transport in membranes. *Biochem Biophys Res Commun*. **225(1)**: 250-255.

Yin J-J, Smith MJ, Eppley RM, Troy AL, Page SW, and Sphon JA. 1996b. Effects of fumonisin B_1 and (hydrolyzed) fumonisin backbone AP1 on membranes: A spin-label study. *Arch Biochem Biophys*. **335**: 13-22.

Yin J-J, Smith MJ, Eppley RM, Page SW, and Sphon JA. 1998. Effects of fumonisin B_1 on lipid peroxidation in membranes. *Biochim Biophys Acta*. **1371(1)**: 134-142.

Yoo HS, Norred WP, Wang E, Merrill AH Jr and Riley RT. 1992. Fumonisin inhibition of *de novo* sphingolipid biosynthesis and cytotoxicity are correlated in LLC-PK1 cells. *Toxicol Appl Pharmacol*. **114**: 9-15.

Yoo HS, Norred WP, Showker J and Riley RT. 1996. Elevated sphingoid bases and complex sphingolipid depletion as contributing factors in fumonisin-induced cytotoxicity. *Toxicol Appl Pharmacol.* **138(2)**: 211-218.

Yoshizawa T, Yamashita A and Luo Y. 1994. Fumonisin occurrence in corn from high- and low-risk areas for human esophageal cancer in China. *Appl Environ Microbiol.* **60**: 1626-1629.

Yu CH, Lee YM, Yun YP and Yoo HS. 2001. Differential effects of fumonisin B_1 on cell death in cultured cells: the significance of the elevated sphinganine. *Arch Pharm Res.* **24(2)**: 136-143.

Yuspa SH. 2000. Overview of carcinogenesis: past, present and future. *Carcinogenesis.* **21(3)**: 341-344.

Zamzami N, Marchetti P, Castedo M, Zanin C, Vayssiere J-L, Petit PX and Kroemer G. 1995a. Reduction in mitochondrial potential constitutes and early irreversible step of programmed lymphocyte death *in vivo*. *J Exp Med.* **181**: 1661-1672.

Zamzami N, Marchetti P, Castedo M, Decaudin D, Macho A, Hirsch T, Susin SA, Petit PX, Mignotte B and Kroemer G. 1995b. Sequential Reduction of Mitochondrial Transmembrane Potential and Generation of Reactive Oxygen Species in Early Programmed Cell Death. *J Exp Med.* **182**: 367-377.

Zhang H, Buckley NE, Gibson K and Spiegel S. 1990. Sphingosine stimulates cellular proliferation via a protein kinase C-independent pathway. *J Biol Chem.* **265(1)**: 76-81.

Zhang H, Desai NN, Olivera A, Seki T, Brooker G and Spiegel S. 1991.Sphingosine-1-phosphate, a novel lipid, involved in cellular proliferation. *J Cell Biol.* **114(1)**: 155-167.

APPENDIX 1:

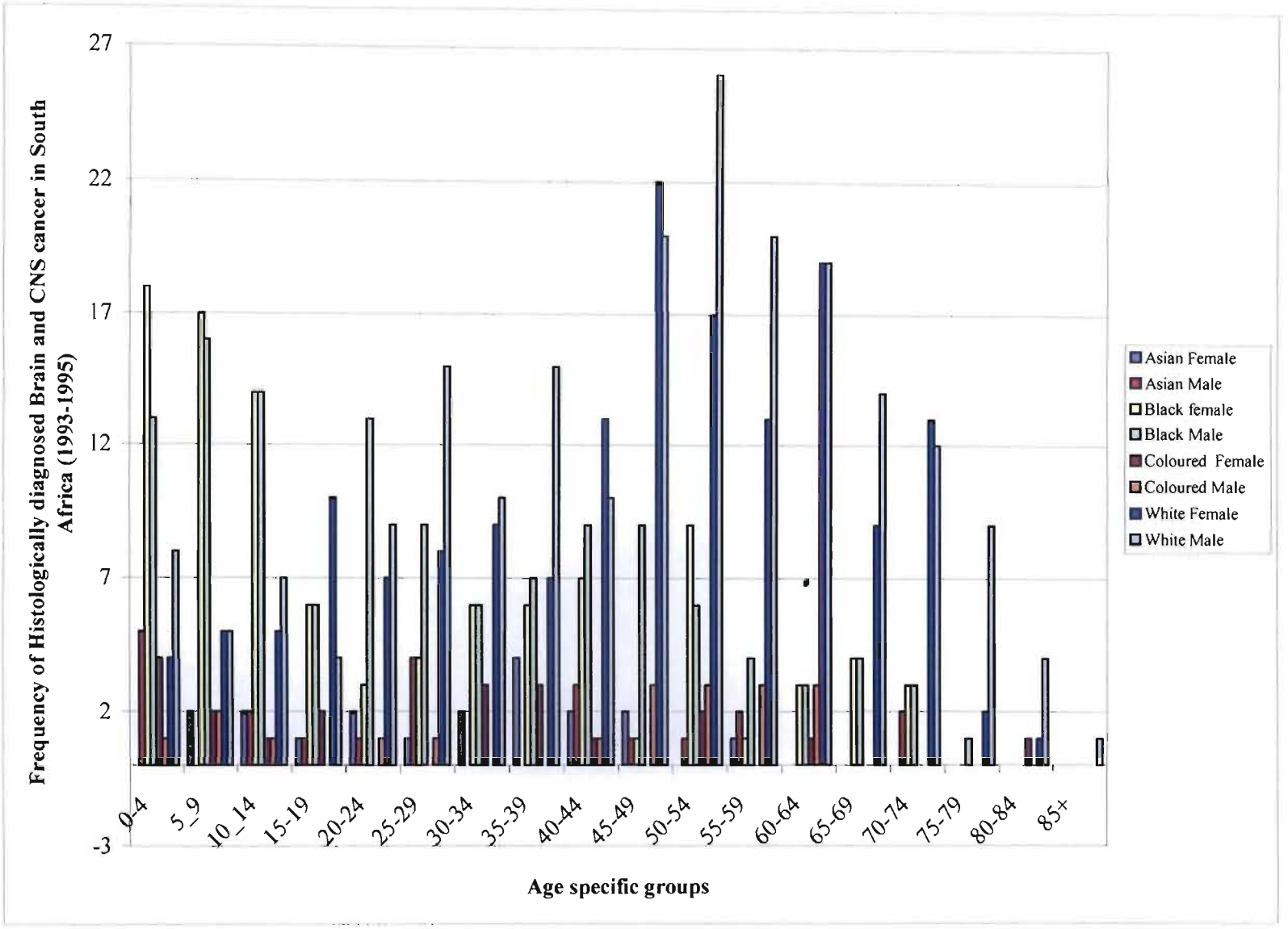

Figure A1.1: Frequency of histologically diagnosed brain and central nervous system cancer in South Africa (1993-1995) (Sitas *et al.*, 1998).

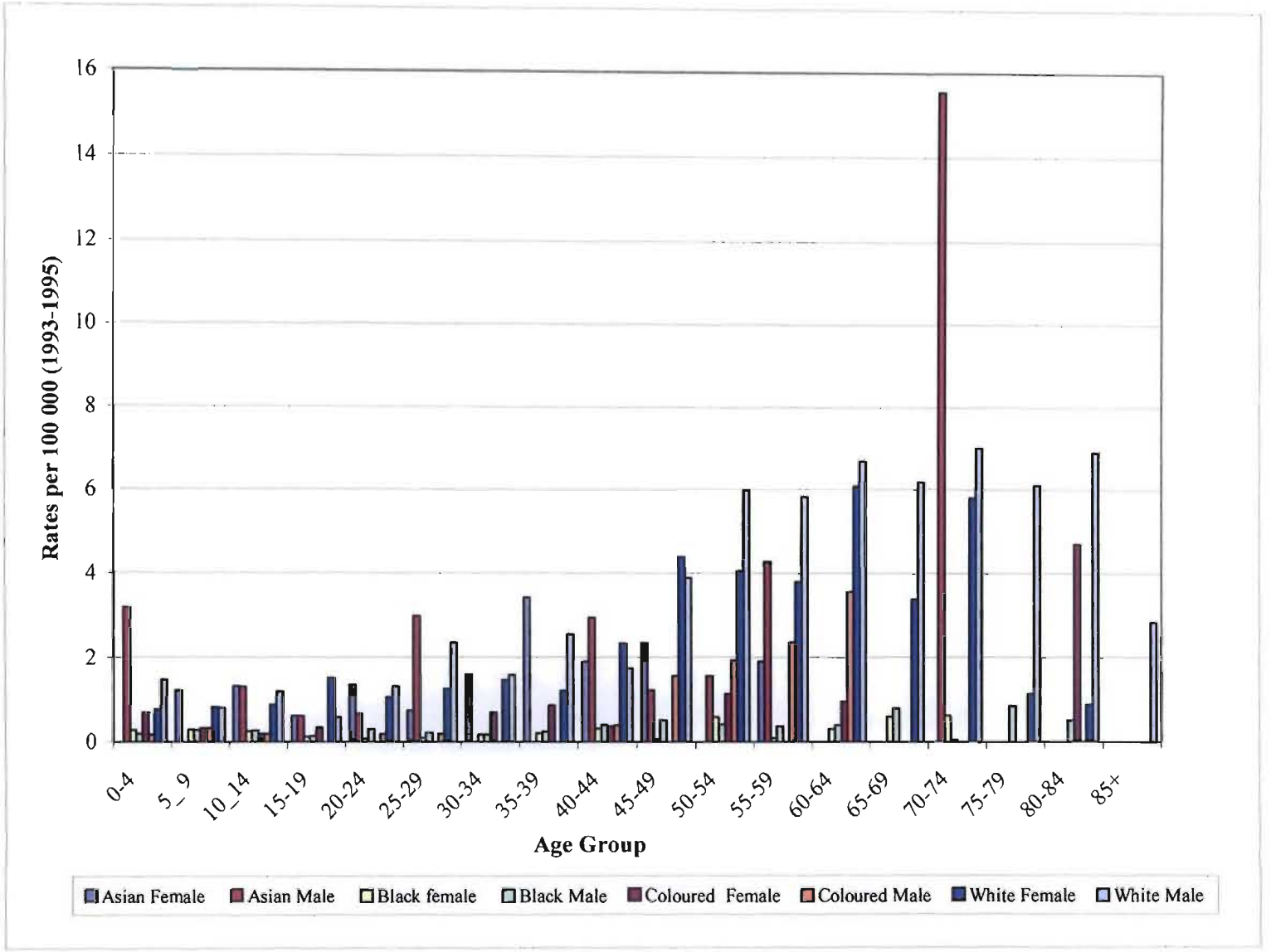

Figure A1.2 : Age specific brain and central nervous system cancer rates per 100 000(1993-1995) (Sitas *et al.*, 1998).

APPENDIX 2

Table A2: Major divisions of the nervous system.

<table>
<tr><td colspan="4">THE NERVOUS SYSTEM</td></tr>
<tr><td colspan="2">CENTRAL NERVOUS SYSTEM</td><td colspan="2">PERIPHERAL NERVOUS SYSTEM</td></tr>
<tr><td>Brain contained within the cranium</td><td>Spinal cord lodged in the vertebral canal</td><td colspan="2">Ganglia and peripheral nerves that lie outside the brain and spinal cord</td></tr>
<tr><td colspan="2" rowspan="2"> 
</td><td>Somatic Subsystem includes sensory neurons of the dorsal root and cranial ganglia that innervate the skin, muscles and joints</td><td colspan="2">Autonomic Subsystem includes the motor system for the viscera , the smooth muscles and exocrine glands. It in turn consists of three segregated subdivisions:-</td></tr>
<tr><td>Provides sensory information to the CNS about muscle and limb position and the environment</td><td>Sympathetic Nervous System
Participates in the response of the body to stress</td><td>Parasympathetic Nervous System
Acts to conserve the body's resources and restore homeostasis</td><td>Enteric Nervous System
Controls function of smooth muscle of the gut</td></tr>
</table>

APPENDIX 3

Table A3: ADP: ATP ratios of Jurkat cells treated with FB_1, FA and (FB_1+FA) over 22.5 hours.

	ADP:ATP ratios			
Conc. µg/ml	Control	FB_1	FA	FB_1+FA
1.56	0.27	0.59	0.26	0.64
3.15	0.264	0.45	0.61	0.58
6.25	0.301	0.50	0.361	0.49
12.5	0.25	0.592	0.298	0.54
25	0.28	0.439	0.342	0.547
50	0.28	0.60	0.435	0.477
100	0.37	0.33	0.22	0.542
200	0.34	0.27	0.33	0.30
400	0.4	0.21	0.443	0.397
800	0.28	0.17	1.279	0.75

Key :

APOPTOSIS	NECROSIS	PROLIFERATION	GROWTH ARREST

APPENDIX 4

Table A4: ADP: ATP ratios of the N2 α neuroblastoma cells treated with FB_1, FA and (FB_1+FA) over 24 hours.

	ADP: ATP ratio			
Conc µg/ml	Control	FB_1	FA	FB_1+FA
2	0.31	0.38	0.352	0.30
4	0.11	0.479	0.45	0.31
8	0.37	0.33	0.422	0.5027
16	0.31	0.416	0.412	0.4238
32	0.33	0.385	0.373	0.5001
64	0.29	0.446	0.341	0.5106
128	0.39	0.508	0.31	0.5959
256	0.41	0.434	0.70	0.73
512	0.42	0.578	0.77	0.71
1000	0.51	0.602	0.79	0.5371

Key:

APOPTOSIS	NECROSIS	PROLIFERATION	GROWTH ARREST

APPENDIX 5

Preparation of 0.5M Tris stock solution

Dissolved 60.6g Tris-[hydroxymethyl]-aminomethane (molecular weight 121.12 in 800 ml distilled water. Adjusted pH to 7.2 with concentrated HCl (40 ml) and then adjusted final volume to 1000 ml.

Preparation of 0.05M (50 mM) Tris-HCl buffer

Diluted 0.5 M Tris stock solution 1:10 (v/v) with 0.85% physiological saline (0.15M NaCl) (i.e. 8.764 g NaCl in 1000 ml water). Then made up :

1. 0.02% BSA in 0.05 M Tris (500 ml)(i.e., 0.1g BSA in 500ml 0.05M Tris). Adjusted pH to 7.2 with concentrated HCl.
2. 1% BSA in 0.05 M Tris (20 ml)(i.e., 0.2 g BSA in 20 ml, 0.05 M Tris). Adjusted pH to 8.2 with 1M NaOH.

APPENDIX 6

Appendix 6.1

Method of preparation of Uranyl acetate

A saturated solution of 50:50 EtOH:water with uranyl acetate (421.15 g/ml) was prepared in a 5 ml tube. The mixture was allowed to settle for 4 hours, then centrifuged for 15 minutes to pellet any particles in the suspension immediately before use.

Appendix 6.2

Method of preparation of Lead Citrate

Materials

2.66 g Lead nitrate

3.52 g Sodium citrate

60 ml water

16 ml 1N Sodium hydroxide

Method

The lead nitrate was dissolved in 60 ml water. Sodium citrate was added to the solution and a precipitate formed. The mixture was left to stand at RT for 30 min. After 30 min., the 16 ml 1N Sodium hydroxide was added and the solution turned clear. The stain was then filtered and stored at 4°C until use.

APPENDIX 7

Appendix 7.1

Table A7: Recoveries of Fumonisin B_1 from spiked sera samples.

Specimen (replicates)	0.5 ml serum spiked with	FB_1 recovered per ml serum (ng/ml)	% FB_1 recovered
1	200ng FB_1	393.47	98.37
2		378.86	94.7
3		409.65	102.4
4		472.17	118
n=4		**413.54±41.06**	**103.37±10.25**
1	300ng FB_1	500.49	83.41
2		649.66	108.276
4		535.97	89.33
5		548.48	91.413
6		526.02	87.67
n=5		**552.12±57.30**	**92.02±9.55**
1	400ng	749.79	93.72
2		727.5	90.9
3		671.84	83.9
4		817.32	102
5		758.38	94.79
6		688.27	86.03
n=6		**735.52±52.48**	**91.89±6.53**

Appendix 7.2

Preparation of Alkaline water

0.1ml 2M NH_4OH was diluted in 250ml deionised water, pH 8.5-9.2. The solution was prepared fresh daily.

APPENDIX 8

Appendix 8.1

Aqueous methanolic HCl (1M HCl) for acid hydrolysis of complex sphingolipids was prepared immediately before use by mixing 8.6ml concentrated HCl with 9.4ml H_2O, and bringing it to a 100ml volume with MeOH.

Saturated methanolic KOH was prepared by dissolving 30g KOH in 100ml MeOH, and filtering through Whatman No 2 paper.

Appendix 8.2

Table A8.1: Recoveries of Fumonisin B_1 from culture media following the 72 hours exposure to N2α cells.

Treatment/replicates	FB_1 recovered from the CCM (μM)	% FB_1 recovered from CCM	% FB_1 taken up by the N2α cells
50μM FB_1			
1	21.7	43.3	56.7
2	19.2	38.3	61.7
3	16.2	32.4	67.6
4	11.8	23.6	76.4
5	12.8	25.6	74.5
Mean±SD	16.3±4.2	32.6±8.3	67.4±8.3
100μM FB_1			
1	23.9	23.9	76.1
2	24.1	24.1	75.9
3	23.0	23.0	77.00
4	21.9	21.9	78.1
5	22.9	22.9	77.1
6	26.6	26.6	73.4
Mean±SD	23.76±1.61	23.76±1.61	76.24±1.61

Appendix 8.3

Table A8.2: Total sphinganine and sphingosine levels in the N2α cell line following treatment for 72 hours: acid hydrolysis of cells.

Treatment	So (μM)	Sa (μM)	Sa: So ratio
Control			
1	4.6	0.52	0.11
2	6.02	0.62	0.10
3	4.00	0.76	0.19
Mean±SD	4.89±1.03	0.64±0.12	0.13±0.05
50μM FB_1			
1	2.56	0.26	0.10
2	0.19	0.11	0.59
3	0.24	0.1	0.39
Mean±SD	0.99±1.35	0.15±0.09	0.16±0.25
100μM FB_1			
1	1.55	0.20	0.13
2	2.32	0.32	0.14
3	1.39	0.199	0.145
Mean±SD	1.75±0.5	0.24±0.07	0.138±0.01

Appendix 8.4

Table A8.3: Free sphingosine and sphinganine levels in N2α cells after treatment with Fumonisin B_1 for 72 hours: base hydrolysed extracts of the N2α cell line.

Treatment	So (nM)	Sa (nM)	Sa:So Ratio
Control			
1	30.33	16.71	0.55
2	36.60	11.51	0.31
3	42.24	29.28	0.69
Mean±SD	36.39±5.96	19.17±9.14	0.52±0.19
50 μM FB_1			
1	53.30	54.03	1.01
2	60.28	63.61	1.06
3	47.13	64.13	1.36
Mean±SD	53.57±6.58	60.59±5.68	1.14±0.19
100μM FB_1			
1	47.21	53.22	1.13
2	43.93	78.02	1.78
3	49.68	64.05	1.29
Mean±SD	46.94±2.88	65.10±12.43	1.40±0.33

Appendix 8.5

Table A8.4: Sphinganine and sphingosine analyses of the culture media following exposure of N2α cells to 50 and 100μM fumonisin B_1 over 72 hours.

Treatment/replicates	So (nM)	Sa(nM)	Sa:So ratio
Control			
1	24.8	38.2	1.54
2	25.4	45.8	1.80
3	48	63.9	1.33
4	21.9	40.6	1.85
5	18.5	39.2	2.12
Mean±SD	27.72±11.66	45.54±10.67	1.73±0.30
50μM FB_1			
1	18.9	42	2.22
2	22.9	42.9	1.87
3	33	65.7	1.99
4	29.9	56.4	1.89
5	27.2	51.6	1.897
Mean±SD	26.38±5.59	51.72±9.87	1.97±0.15
100μM FB_1			
1	27.3	56.1	2.055
2	27.5	62.4	2.27
3	25.2	59	2.34
4	23.2	65.3	2.82
5	29.9	89.7	3
Mean±SD	26.62±2.54	66.5±13.43	2.50±0.40

APPENDIX 9

Appendix 9.1

Key used for all relevant tables in this appendix:

A	I	W	M	F	-	ND
African	Indian	White	Male	Female	Serum insufficient for analyses	Not Detectable

Table A9.1: Determination of the serum concentrations of sphinganine, sphingosine and fumonisin B_1 in the serum of 21 non-cancer subjects.

Age	Race	Sex	FB_1(nM)	So (nM)	Sa (nM)	Sa:So ratio
18	A	F	20.1	18	ND	ND
19	I	F	22.3	-	-	-
19	I	F	24.1	57.7	80	1.4
19	W	F	24.4	-	-	-
19	I	F	46.3	35.2	79	2.2
19	I	F	60.7	29.9	81	2.7
20	A	F	66	50.9	88	1.7
19	W	F	69.8	83.9	92	1.1
19	I	F	74.2	22.8	76	3.3
19	I	F	106	26.1	40	1.5
19	A	F	118	73.2	88	1.2
18	I	F	296	86.8	95	1.1
FEMALES						
18.9±0.5			**77.3±76.1**	**48.5±25.9**	**71.9±29.6**	**1.6±0.9**
18	I	M	22.5	129	91	0.71
18	A	M	26	119	102	0.86
19	I	M	41.2	47.9	84	1.75
20	A	M	50.3	88.2	99	1.12
19	I	M	91.6	47.2	79	1.67
19	I	M	95.2	343	801	2.33
18	I	M	106	-	-	-
18	I	M	122	-	-	-
19	I	M	127	-	-	-
MALES						
18.7±0.71			**75.8±41.0**	**129.1±110.3**	**209.3±289.99**	**1.41±0.65**
ALL SUBJECTS						
18.81±0.60			**76.65±62.11**	**78.68±77.99**	**123.44±182.42**	**1.55±0.82**

Appendix 9.2

Table A9.2: Determination of the concentrations of sphinganine, sphingosine and fumonisin B_1 in the serum of 16 non-cancer subjects.

Age	Race	Sex	FB_1(nM)	So (nM)	Sa (nM)	Sa:So
18	A	F	20.1	18	ND	ND
18	A	M	26	119	102	0.86
18	I	F	296	86.8	95	1.09
18	I	M	22.5	129	91	0.71
19	A	F	118	73.2	88	1.20
19	I	F	24.1	57.7	80	1.39
19	I	F	60.7	29.9	81	2.71
19	I	F	46.3	35.2	79	2.24
19	I	F	74.2	22.8	76	3.33
19	I	F	106	26.1	40	1.53
19	I	M	41.2	47.9	84	1.75
19	I	M	91.6	47.2	79	1.67
19	W	F	69.8	83.9	92	1.1
19	I	M	95.2	343	801	2.34
20	A	F	66	50.9	88	1.73
20	A	M	50.3	88.2	99	1.12
18.9±0.6			**75.5±66.3**	**78.7±77.99**	**131.67±185.72**	**1.65±0.73**

APPENDIX 10

Appendix 10 .1

Table A10.1: List of non-cancer brain specimens obtained at autopsies at King Edward VIII hospital mortuary.

Non-Cancer Subjects	Age	Race	Sex	Cause of death
1	65	A	M	Motor vehicle accident (MVA)
2	65	A	M	Gun shot wound
3	45	A	F	MVA
4	64	A	F	Diabetic
5	9	A	F	MVA
6	25	A	M	Gun shot wound in chest
7	35	A	M	Stabbed in chest
8	35	A	M	Gunshot wound in abdomen
9	28	A	M	Multiple stab wound n chest
10	49	A	M	Tuberculosis (TB)
11	Unknown	A	F	MVA
12	Unknown	A	M	MVA
13	Unknown	A	F	MVA
14	Unknown	A	M	MVA
15	36	A	F	Hepatitis / TB
16	43	A	F	Cardiac failure

Appendix 10.2

Karnovsky's fixative

2g	paraformaldehye
25ml	distilled water
1-3 drops	1M NaOH
10 ml	glutaraldehyde (25% stock)
12 ml	0.2M sodium cacodylate buffer
25 mg	Calcium chloride

Method to make Karnovsky's fixative (50 ml, pH 7.2)

The paraformaldehyde was dissolved in tepid water (i.e., water that was not allowed to boil). Then 1-3 drops of 1M NaOH were added until the fluid started to clear. Undiluted glutaraldehyde and the 0.2M sodium cacodylate buffer were then added. Finally, calcium chloride was added. The fixative was then filtered and the pH adjusted to pH 7.2. The solution was allowed to fix for 1hr at 4°C, and then used as required.

Appendix 10.3

Table A10.2: Definition of terminology used in image analysis.

1	FLD COUNT	Number of measured regions
2	FLDAREA	Area of all regions
3	FLDAREAP(%)	Percentage area of all regions in measurement frames
4	FRAME AREA (μm^2)	Area of measurement frame
5	FRAME AREA1 ($pixels^2$)	Unscaled area of the measurement frame
6	FLDMEAND	Mean grey value of all regions
7	FLDSTDD	Grey value standard deviation in all regions
8	FLDMIND	Minimum grey value in all regions
9	FLDMAXD	Maximum grey value in all regions

Table A10.3: Steps formulated in the macro drawn up for image analysis of the brain tumour tissue sections.

1. imgdelete 1
2. Gclear 0
3. Tvlive
4. Tvinput 1
5. MS marker 1,100.00,0.00,37,46,9,3,2
6. Gmerge1,255
7. ImgRGB2grey 1,2
8. Normalise 2,3,5
9. Dislev 3,4,10,129,1
10. Binscrap 4,5,0,100,0
11. Mssetgeom
12. Msframe
13. MSsetfeat "FIELDFEAT'
14. MSsetfeat "DRAWFEAT'
15. Msmeasmask 5,1,"database", 0,2,10
16. Msdrawmask 5,1
17. Imgdisplay 1
18. Gmerge 1,255

Appendix 10.4

Table A10.4: Image analysis of brain tumour specimens.

No	FLDAREA /μm^2	FLDAREAP /%	FRAMEAREA /μm^2	FRAMEAREA1 /pixel^2	FLDMEAND /grey	FLDSTDD /grey	FLDMIND /grey	FLDMAXD /grey
1	5544.74	6.66	83202.63	369725	104.08	21.21	75	176
2	3672.4	5.97	61534.57	412850	211.54	42.16	81	254
3	7317.83	7.35	99550.15	442368	97.55	23.03	1	170
4	10426.29	10.47	99550.15	442368	116.54	25.28	10	203
5	5276.04	7.45	70780.46	314525	138.31	30.95	71	234
6	7527.79	7.56	99550.15	442368	111.74	26.94	1	196
7	819.59	1.74	47173.17	209622	162.18	20.36	89	237
8	6333.28	6.75	93882.54	417183	120.67	28.05	2	229
9	5939.24	6.45	92108.78	409301	120.31	27.88	2	225
10	1522.84	2.04	74618.06	331578	178.96	38.2	51	254
11	5001.95	5.66	88297.29	392364	129.09	24.7	3	244
12	1287.67	6.07	21210.17	94251	120.56	33.15	1	254
13	4179.2	4.2	99550.15	442368	96.84	41.55	1	251
14	1809.99	1.87	96973.91	430920	118.73	42.57	1	254
15	5488.71	5.66	96973.91	430920	122.28	40.67	1	254
16	5351.21	5.67	94297.06	419025	157.86	51.91	1	254
17	2586.15	4.13	62573.28	278055	157.9	54.06	5	254
18	3578.57	3.59	99550.15	442368	134.72	50.55	1	254
19	2909.76	3.25	89426.09	397380	164.98	52.67	47	254
20	1473.78	1.54	95883.59	426075	154.39	34.36	60	244
21	5227.66	5.45	95883.59	426075	164.01	36.05	54	254
22	5192.78	5.42	95883.59	426075	163.99	36.07	54	254
	4475.794091	**5.23%**	**84475.15636**	**381716.5455**	**138.5104545**	**35.56227273**	**27.81818182**	**236.5**
	2383.034465	**2.248770564**	**20479.62867**	**88384.36932**	**29.32650491**	**10.52198421**	**32.74379093**	**26.4858**